U.PORTO

FEUP FACULDADE DE ENGENHARIA
UNIVERSIDADE DO PORTO

TRANSITION ZONES IN RAILWAY TRACKS

An experimental and numerical study on the structural behaviour

ANDRÉ LUÍS MARQUES PAIXÃO

Dissertation submitted to the Faculty of Engineering of University of Porto
in partial fulfilment of the requirements for the degree of
DOCTOR OF PHILOSOPHY IN CIVIL ENGINEERING

Supervisor: Eduardo Manuel Cabrita Fortunato (Senior Research Officer, LNEC; Visiting Associated Professor, FEUP)

Co-Supervisor: Rui Artur Bártolo Calçada (Full Professor, FEUP)

LABORATÓRIO NACIONAL DE ENGENHARIA CIVIL
REFER EPE
FCT Fundação para a Ciência e a Tecnologia
MINISTÉRIO DA EDUCAÇÃO E CIÊNCIA
POPH PROGRAMA OPERACIONAL POTENCIAL HUMANO
QREN QUADRO DE REFERÊNCIA ESTRATÉGICO NACIONAL
UNIÃO EUROPEIA Fundo Social Europeu

DECEMBER 2014

Ao meu avô António Francisco

Abstract

The railway track continually degrades over its life cycle. This has negative consequences for maintenance and availability of the lines and is particularly evident at locations with abrupt changes in the track's support conditions, such as transition zones to bridges or other structures. To mitigate this problem, modern lines comprise specifically designed backfills with high-performance geomaterials to provide an adequate approach to the structures. However, the problem of track degradation at transition zones is far from being completely solved.

The research presented in this Thesis aimed at providing insight into the structural behaviour of transition zones using a novel and integrated approach to investigate the problem, contributing to an efficient management of railway assets, in the context of the life-cycle cost reduction paradigm of the railway system, in particular, the railway track.

In the scope of a research project involving LNEC, FEUP and REFER, a 30 km-long railway line is used as case study and its construction is followed up closely. Laboratorial characterisation of bound and unbound granular material used in transition zones is carried out, in particular using cyclic load triaxial tests on large specimens. Thorough *in situ* characterisation of the track substructure is performed, including specific *portancemètre* surveys at transition zones. The deformation of the backfill of a transition zone case study to a bridge is monitored using different techniques, including sub-horizontal inclinometers installed during construction. The results obtained regarding the substructure at transition zones indicate that the design of the backfills was successful in minimizing settlements and achieving a gradual stiffness increase at the approach to the structures. The analysis of the evolution of the geometric quality of the line evidenced higher degradation rates at some transition zones and other track singularities, mostly associated with abrupt changes in the track substructure.

To fill the gap between experimental and numerical studies, extensive field measurements are presented and used to calibrate and validate FEM models that consider the relevant track components of the superstructure and substructure. The models also account for the dynamic train-track interaction and are very accurate in reproducing the measurements. The experimental works comprised dynamic

track characterisation with receptance tests and a new approach using the light falling weight deflectometer. Innovative solutions for transition zones, such as under sleeper pads (USP), are also analysed in detail in specific case studies of transition zones to underpasses. The experimental results evidenced the increase in the vertical stiffness of the track at the approach to structures, which could suggest the amplification of the dynamic track-interaction. However, because the design of the backfills provides a smooth stiffness variation and the track evidenced a very good track quality, the simulations indicated limited dynamic amplifications of the train loads in the tested scenarios. As regards USP, simulations suggested a beneficial contribution to reduce track degradation rates, but a careful design is required to prevent excessive dynamic amplifications when trains enter or exit sections of the track with USP.

Later, the effect of the differential settlements on the dynamic response of the train-track system at the approach to structures is investigated. To that aim, comprehensive parametric studies using numerical simulations are carried out. The results of the simulations are integrated and used to establish performance indicators that affect the train-track interaction, based on the length and amplitude of track defects. A novel approach is then presented and applied to the line under study, in an attempt to associate the results of the parametric studies with locations denoting rapid track degradation or other critical scenarios. Tools and actions are suggested to Railway Infrastructure Managers to monitor the performance of transition zones and for a more efficient management of the infrastructure.

Key-words: railway track; transition zones; backfill design and construction; degradation of the track geometric quality; *in situ* characterisation; cyclic load triaxial tests; instrumentation and monitoring; under sleeper pads (USP); numerical modelling; dynamic train-track interaction.

Resumo

A via-férrea degrada-se continuamente ao longo do seu ciclo de vida útil. Este aspeto tem consequências negativas para a manutenção e disponibilidade das linhas e é particularmente evidente em locais com alterações bruscas das condições de apoio da via, tais como zonas de transição para pontes e outras obras-de-arte. Para atenuar esse problema, as ferrovias modernas incluem estruturas em aterro concebidas para proporcionar uma adequada aproximação às obras-de-arte, utilizando geomateriais de elevado desempenho, usualmente designados "blocos técnicos". No entanto, o problema da degradação da via nestas zonas de transição não está ainda completamente resolvido.

No contexto do atual paradigma de redução de custos do ciclo de vida das infraestruturas de transporte, a investigação apresentada nesta Tese visa aprofundar o conhecimento sobre o comportamento estrutural de zonas de transição, utilizando uma abordagem inovadora e integrada para analisar o problema, contribuindo para uma gestão mais eficiente dos ativos do sistema ferroviário, em particular a via-férrea.

No âmbito de um projeto que envolveu o LNEC, a FEUP e a REFER, foi acompanhada a construção de uma linha férrea com 30 km de extensão. Procedeu-se à caracterização laboratorial de materiais naturais britados ligados e não ligados utilizados nas zonas de transição, nomeadamente recorrendo a ensaios triaxiais cíclicos sobre provetes de grandes dimensões. Foi realizada uma extensa caracterização *in situ* da subestrutura da via, incluindo campanhas específicas realizadas com o equipamento portancemètre em zonas de transição. Foram monitorizadas as deformações do aterro de um caso de estudo de zona de transição para uma ponte utilizando diferentes técnicas, o recurso a inclinómetros sub-horizontais instalados durante a construção. Os resultados obtidos sobre a subestrutura nas zonas de transição indicam que a conceção destas estruturas foi bem sucedida, minimizando os assentamentos e conferindo um aumento gradual da rigidez vertical na aproximação às obras-de-arte. A análise da evolução da qualidade geométrica da via evidenciou taxas de degradação mais elevadas em algumas zonas de transição e em outras singularidades, principalmente associadas a alterações bruscas verificadas na subestrutura da via.

Para aproximar os estudos numéricos dos trabalhos experimentais, foram desenvolvidos e apresentados extensos trabalhos de campo cujos resultados foram utilizados na calibração e validação de modelos MEF que incluem os elementos relevantes da superestrutura e da subestrutura. Estes modelos também consideram a interação dinâmica veículo-via e são muito precisos na reprodução das medições efetuadas. Os trabalhos experimentais consistiram na caracterização dinâmica da via, recorrendo a ensaios de recetância e a uma nova abordagem usando o defletómetro de impacto portátil. Também foram analisadas em detalhe soluções inovadoras para zonas de transição, como as palmilhas sob as travessas (usualmente designados *under sleeper pads*, USP) em casos de estudo específicos de zonas de transição para passagens inferiores. Os resultados experimentais evidenciaram um aumento na rigidez vertical da via na aproximação às obras-de-arte, o que poderia sugerir a amplificação da interação dinâmica veículo-via. No entanto, devido à existência de uma variação gradual da rigidez vertical conferida pelos aterros de transição e à boa qualidade geométrica da via, as simulações indicaram amplificações dinâmicas limitadas nos cenários testados. Quanto à utilização de USP, as simulações apontam para uma contribuição benéfica na redução de taxas de degradação da via, no entanto, é necessário garantir o adequado dimensionamento destas para minimizar amplificações dinâmicas da solicitação dos veículos que se podem desenvolver na entrada e saída das secções de via com USP.

Posteriormente foi investigado o efeito dos assentamentos diferenciais, que ocorre na aproximação às obras-de-arte, sobre a resposta dinâmica do sistema veículo-via. Para tal, recorreu-se a simulações numéricas em estudos paramétricos exaustivos. Os resultados das simulações foram integrados e utilizados para estabelecer indicadores de desempenho que afetam a interação veículo-via, com base no comprimento e amplitude dos defeitos da via. Foi apresentada e aplicada à linha em estudo uma nova abordagem, numa tentativa de associar os resultados dos estudos paramétricos aos locais da via que evidenciavam degradação mais acelerada ou a outras situações críticas. São sugeridas ferramentas e ações para os gestores das infraestruturas ferroviárias, visando a monitorização do desempenho de zonas de transição e promovendo uma gestão mais eficiente da infraestrutura.

Palavras-chave: via-férrea; zonas de transição; conceção e construção de blocos técnicos; degradação da qualidade geométrica da via; caracterização *in situ*; ensaios triaxiais cíclicos; instrumentação e monitorização; palmilhas sob as travessas; modelação numérica; interação dinâmica veículo-via.

Acknowledgements

This Thesis would not have been possible without the guidance and help of several individuals and institutions to whom I owe much gratitude and, therefore, I am pleased to convey my sincere thanks in this modest acknowledgment:

To my Supervisor, Professor Eduardo Fortunato, for the opportunity to carry out this research and for his invaluable contribution to the Thesis. His overwhelming dedication to railway research, the availability for discussion with constructive criticism and the high standards he passed on to me are profoundly acknowledged. I will always have those and other valuable lessons in mind.

To my Co-Supervisor, Professor Rui Calçada, for his permanent support and motivation throughout the research, for his lessons and insight into various aspects of railway dynamics and for the opportunity to interact and collaborate with other members of the railway research group in FEUP.

To Cristina Alves Ribeiro for the long hours of discussion on railway transition zones, for the introduction to the numerical techniques developed in her PhD thesis and for sharing some codes.

To Nuno Pinto for his companionship during track monitoring works and his tireless dedication put into developing the measuring systems, even in the most adverse situations we shared in the field.

To LNEC's Technical Officer Rui Coelho for the relentless availability, skill, optimism and companionship during almost all experimental works in the field.

To Carlos Albuquerque for the generous sharing since the very beginning of this peculiar path, resulting in a thriving friendship.

To all other colleagues from FEUP, in particular, Joel Malveiro, Aires Colaço, Andreia Meixedo, Cristiana Bonifácio for the availability and willingness during the experimental works in the track.

To LNEC and to the Transportation Department, in the name of its Director, Principal Research Officer António Lemonde de Macedo, for the opportunity that was provided and for all the conditions and means available. I am also thankful to the Geotechnique Department, in the name of its Director, Principal Research Officer Laura Caldeira, for the equipment and means available for the field works.

To FEUP, for the conditions and means available to perform the experimental works on the tracks and the numerical modelling, as well as the support for the international dissemination of some results. I am also grateful for the knowledge shared by the Professors of my Doctoral Programme's courses.

To *Fundação para a Ciência e a Tecnologia* for the PhD grant [SFRH/BD/75821/2011], funded by *Programa Operacional Potencial Humano* of QREN Portugal 2007-2013 and by the national budget through the MCTES.

To REFER, EPE, for funding the research project "*Avaliação do comportamento das zonas de transição na via-férrea da Variante de Alcácer*" and to Eng.º José Carlos Clemente, Eng.ª Alexandra Borges and Eng.ª Andreia Grossinho for the launch and coordination of the project. Also to Eng.º Pedro Gaiato, Eng.º Jonatas Marques and the members of the ROS team, particularly Carlos Oliveira, for the support and interest demonstrated during the experimental works in the track.

To Geocontrole, especially to José Carlos Correia for the practical lessons on cyclic load triaxial tests.

To Mota-Engil Engenharia, for the availability to perform characterisation tests on the tracks.

To all friends from LNEC, in particular Carlos, Sandra and Francesca for the motivation and sharing during this journey, and to all members of the Transportation Department, especially the support of Simona Fontul.

To my dearest friends, unfortunately fewer and fewer remaining in Portugal, but still very close and essential to recharge energies at crucial moments. Thank you Miranda and Rui.

Last but not least, to my closest family. My parents for everything they have provided and the precious values they have passed on to me. My beloved Inês and Vicente, while waiting for Teresa, for the patience, continuous support and joyful moments we shared.

Contents

Chapter 1

Introduction 1

1.1 Background and motivation to the present study 1

1.2 Aim of the research and expected contributions 5

1.3 Thesis Outline 7

Chapter 2

The railway track and its behaviour 9

2.1 The structure of the railway track 9

2.1.1 Components of the superstructure of ballasted tracks 12

2.1.2 The substructure of ballasted tracks 14

2.2 Mechanical degradation of railway tracks 14

2.2.1 The importance of the vertical stiffness of the track 18

2.2.2 Permanent track settlements 23

2.3 The geometric quality of the track 26

2.3.1 Assessing the track geometric quality 26

2.3.2 Track maintenance 33

2.4 Track structural analysis 35

2.4.1 General aspects 35

2.4.2 Advanced numerical methods 36

2.5 Characterisation of materials and assessment of track behaviour 38

2.5.1 In situ characterisation of the track behaviour 39

2.5.2 Laboratorial characterisation of track components and geomaterials 44

2.5.3 Physical modelling of the structure 45

Chapter 3

Transition zones to railway structures 47

3.1 Introduction 47

3.2 General aspects 48

3.3 The problem at transition zones to bridges and other structures 50

3.4 Countermeasures for transition zones 54

3.4.1 Wedge-shaped backfills for transition zones 59

3.4.2 Under sleeper pads 64

3.5 A review on numerical modelling of transition zones 66

3.5.1 General aspects 66

3.5.2 Previous numerical works 69

3.5.3 Comparison summary of numerical approaches to study transition zones 82

3.6 Final Remarks 84

Chapter 4

The *Alcácer* bypass and its transition zones 87

4.1 Introduction 87

4.2 General aspects of the *Alcácer* Bypass 88

4.3 The track platform 90

4.4 Transition zones and other singularities 96

4.5 Traffic 101

4.6 Analysis of the track geometry 103

4.6.1 The inspection vehicle 103

4.6.2 General aspects of the track quality 103

4.6.3 Standard Deviation of the Longitudinal Level 108

4.7 Case Study of the construction of a transition zone 116

4.7.1 General aspects of the transition zone case study 116

4.7.2 Characterisation of the backfill materials using cyclic load triaxial testing 119

4.7.3 In situ characterisation of the layers 129

4.7.4 Monitoring backfill settlements 134

4.7.5 Evolution in track geometry 150

4.8 Concluding remarks 151

Chapter 5

Numerical modelling and experimental validation of transition zones 153

5.1 Introduction 153
5.2 Case study 1 - dynamic train-track interaction at transitions to underpasses 154
5.2.1 Description of the transition zones to the underpasses 154
5.2.2 Characterisation of the substructure and superstructure of the track 158
5.2.3 Monitoring track behaviour during train passage 163
5.2.4 Description of the models 177
5.2.5 Model calibration 182
5.2.6 Validation of the model with experimental data 187
5.2.7 Analysis of the train-track interaction 193
5.2.8 Optimisation of the design of the transition zone with USP 198
5.3 Case study 2 - dynamic train-track interaction at the transition zone to a bridge 201
5.3.1 Description of the transition zone case study 201
5.3.2 Characterisation of the track 202
5.3.3 Track monitoring during train passages 204
5.3.4 Description of the model 209
5.3.5 Model calibration 213
5.3.6 Validation with experimental measurements 214
5.3.7 Simulation analysis of train-track interaction 216
5.4 Concluding remarks 218

Chapter 6

Numerical simulations of transition zones with uneven rail profiles 221
6.1 Introduction 221
6.2 Description of the numerical model 222
6.3 Influence of the bump settlement profiles on the train-track interaction 224
6.3.1 Preliminary simulations with uniform settlement of the backfill 224
6.3.2 Simplification of the train model 229
6.3.3 Influence of different bump profiles at the backfill 230
6.4 Influence of the dip settlement profiles on the train-track interaction 238
6.4.1 The viaduct over the EN120 238
6.4.2 Measurements of accelerations inside the car body 240
6.4.1 Validation of the numerical accelerations inside the car model 243
6.4.2 Simulations of the train-track dynamic interaction 246
6.5 Comprehensive parametric study on the influence of the shape of dip profiles in the train-track interaction 256

6.5.1 Initial considerations *256*
6.5.2 Results and discussion *257*
6.5.3 Establishing performance indicators *269*
6.6 Concluding Remarks 271

Chapter 7

Integrated analysis of field data and numerical results 273
7.1 Scope 273
7.2 Advanced characterisation of the longitudinal level 275
7.2.1 Average longitudinal level considering wavelength ranges D1 and D2 ..... *275*
7.2.2 Analysis of the longitudinal level by means of spectrograms *276*
7.2.3 Analysis of the longitudinal level based on a range of chords and the respective amplitudes at mid-chord *280*
7.3 Comparison of the longitudinal level defects with the numerical results from Chapter 6 284
7.3.1 Overlay plots of chord length vs amplitude at mid-chord *284*
7.3.2 Analysis of the locations that suggest scenarios of lower performance of the track *289*
7.4 Assessment of the track degradation at singularities of the track 295
7.5 Proposed methods to monitor the performance of transition zones and promoting early detection of critical situations 307
7.6 Concluding remarks 309

Chapter 8

Conclusions and Future Work 311
8.1 Conclusions and Achievements 311
8.2 Perspectives for Future Work 314

References 317

Annex A 335

List of Figures

Figure 1-1. Comparison of transport performance by mode and respective CO_2 emissions in EU-28 countries (EC, 2014). 2
Figure 1-2. Recent evolution of the performance of passenger and freight transport in EU-28 countries (EC, 2014)....2
Figure 1-3. Examples of abrupt changes in the track support conditions – transition zones: a) embankment-bridge transition (Photo: © Bombardier); b) transition between different track configurations (Ochoa de Olza Galé, 2007); c) successive transitions between track on bridge and track in tunnel (Photo: © THSR)....4
Figure 2-1. Aspects of the components that comprise the ballasted track: a) track frame (rails, fastenings, rail pads, sleepers) and ballast; b) substructure of the track on embankment; c) final aspect of the track. 10
Figure 2-2. Schematic cross section of the ballasted track (UIC, 2008b). 10
Figure 2-3. Schematic representation of the vertical load transfer (Esveld, 2001). 11
Figure 2-4. Different configurations of ballastless track: 1) rails supported by sleepers placed on concrete or asphalt layer; 2) rails directly fixed to the concrete slab; 3) rail embedded in a concrete slab (Quante, 2001)....12
Figure 2-5. Details of ballasted tracks: a) wheelset and track frame with standard gauge (Esveld, 2001); b) fastening systems pre-installed on monoblock concrete sleepers. 13
Figure 2-6. Simplified representation of the normal railway track deterioration process (adapted from Selig & Waters, 1994; Esveld, 2001).....15
Figure 2-7. Schematic diagram of the recursive and increasing non-uniform degradation process of railway tracks. 17
Figure 2-8. Influence of different aspects on the deterioration of the track quality, for different track categories (after UIC, 2008a).....19

Figure 2-9. Influence of variations in the characteristics of the components of the track on the track modulus (Li & Selig, 1995). 20
Figure 2-10. Non-linear behaviour of the track and its components: a) examples of measured static force-deflection curves of the track (Fröhling *et al.*, 1996); b) load curves on rail pads at different temperatures (Carrascal *et al.*, 2007); c) variations of the resilient modulus (*E*) of granular material under different stress levels (mean stress, *p*) (Fortunato, 2005). 21
Figure 2-11. Continuous track stiffness measurement (speed of 20 km/h and excitation frequency 5.7 Hz): a) abrupt stiffness variation at the approach to a bridge (Dahlberg, 2004); b) influence of the thickness of the layers; the red dashed line represents the depth of the clay layer in the subgrade (Berggren, 2005).....22
Figure 2-12. Stress-strain diagram of a granular material under repeated loading (Allaart, 1992); σd - deviatoric stress; $\varepsilon 1$ - axial deformation. 24
Figure 2-13. Permanent settlements: a) due to the accumulation of traffic of a track on a sandy subgrade (Selig & Waters, 1994); b) embankments for HSL in Spain (adapted from Melis Maynar, 2006).....25
Figure 2-14. Schematic representation of the various settlement components of the substructure that contribute to the permanent settlement of railway tracks (UIC, 2008b). 25
Figure 2-15. Schematic representation of geometric track parameters (after Zwanenburg, 2009). 28
Figure 2-16. Excitation of the train-track system: a) relation between the type and the wavelength of the defects and respective excitation frequencies (Esveld, 2001); b) receptance curve of a track (denoting the track flexibility in the frequency domain) with the identification of the resonance frequencies (after Dahlberg, 2003). 30
Figure 2-17. General aspect of a maintenance composition with tamping machine, followed by a dynamic stabiliser (a) and detail of the tamping tines penetrating the ballast layer (b) [Photos: Plasser & Theurer]. 33
Figure 2-18. Schematic representation of an infinite beam supported on elastic medium: *P* is the axle load; *x* is the axle position; *y* is the rail deflection; *k* is the foundation coefficient; *EI* is the bending stiffness of the rail (adapted from Esveld, 2001). 35
Figure 2-19. Comparison of the results obtained with different numerical models: MULTA, PSA, ILLITRACK (Adegoke *et al.*, 1979).....37
Figure 2-20. Aspects of railway track numerical modelling: a) simple beam-spring model (Dahlberg, 2003); b) three-dimensional modelling of the track with a more detailed representation of the components and layers (symmetry with respect to the centre line) (Lundqvist *et al.*, 2006).....38
Figure 2-21. Aspects of non-destructive tests for the characterisation of track support layers: a) falling weight deflectometers; b) plate load tests; c) *portancemètre*.....39

Figure 2-22. Receptance curves of numerical models evidencing the influence of the track substructure in the dynamic behaviour (v_s is the wave propagation speed) (Knothe & Wu, 1998). 40
Figure 2-23. Aspects of receptance test on the track (Alves Ribeiro, 2012): a) instrumented hammer and accelerometers on the rails and sleepers; b) examples of successive receptance functions obtained on the same position. 41
Figure 2-24. Vibration modes and respective resonance frequency ranges commonly found in ballasted tracks (after De Man, 2002). 41
Figure 2-25. Rolling Stiffness Measurement Vehicle: a) aspect of the modified structure; b) working principle (Berggren, 2010). 42
Figure 2-26. Track instrumentation: a) welding strain gauges on the rail web to assess dynamic loads from the vehicles (Alves Ribeiro *et al.*, 2010); b) accelerometers fixed to the rail and sleeper (Kaynia *et al.*, 2005b); c) geophone and LASED-based displacement transducer (Lozano del Moral & Cuéllar, 2009); d) transducers to measure relative displacements between the rail and sleepers and between the sleeper and the capping layer (Kaynia *et al.*, 2005b). 43
Figure 2-27. Cyclic load triaxial tests on specimens of unbound granular material: a) model of the behaviour of granular materials (Werkmeister *et al.*, 2001); b) aspect of large specimen with local instrumentation (Fortunato, 2005).....45
Figure 2-28. Aspects of physical models built in laboratories: a) full model of the track constructed in CEDEX, Spain; b) GRAFT II in Heriot Watt University, UK (Percival *et al.*, 2013); c) partial model with half sleeper (INNOTRACK, 2006); d) small scale model (Al-Shaer *et al.*, 2008). ..46
Figure 3-1. Discontinuities in the track support conditions: a) example of sucessive changes in the substructure; b) schematic representation of the variations in the vertical stiffness of the track (adapted from Frühauf *et al.*, 2008). 49
Figure 3-2. Numerical results of the dynamic amplification due to track degradation with the number of load cycles at transition zones (after Alves Ribeiro, 2012). 50
Figure 3-3. Schematic representation and respective examples of excessive uneven rail profiles: a) dip (photo: ATSB, 2014); b) bump (photo: Read & Li, 2006). 51
Figure 3-4. Schematic representation of causes for rapid track degradation at transition zones.....52
Figure 3-5. Track defect at the approach to structues: a) example of uneven rail profile (Read & Li, 2006); b) excessive depth of ballast to account for backfill settlements (Melis Maynar, 2006)..53
Figure 3-6. Factors that affect the performance of approaches to road bridges (Briaud *et al.*, 1997)....53
Figure 3-7. Wedge-shaped backfill at the approach to a bridge (adapted from ERRI, 1999). 54
Figure 3-8. Reinforcement of backfill soils: hole boring (a) for vertical stone columns (b) (Li *et al.*, 2010); drilling of inclined holes (c) and grouting operations (d) (Moreno *et al.*, 2005).....56

Figure 3-9. Structural countermeasures at transition zones: a) ballast reinforcement with polyurethane (Woodward *et al.*, 2011); b) side walls at a ballast/slab track transition (Costa D'Aguiar *et al.*, 2013); c) ballasted/slab track transition to a HSL bridge in China with auxiliary rails (Hao *et al.*, 2009); d) auxiliary rails at a ballasted/slab track transition to a tunnel in Spain (Ochoa de Olza Galé, 2007).....58
Figure 3-10. Schematic design of wedge-shaped transition zones for various railway infrastructure managers (see Table 3-1). 60
Figure 3-11. Construction aspects of transition zones: a) example of an abutment providing very limited access to compaction equipment; b) compaction of the CBM inside the abutment walls.64
Figure 3-12. Under sleepers pads (USP): a) schematic representation (Loy, 2008); b) example of application (Riessberger, 2010). 64
Figure 3-13. Comparison between the evolution of the geometric quality of railway stretches with and without USP in the Austrian network (adapted from Schilder, 2006). 65
Figure 3-14. Schematic representation of numerical models using: a) beam and spring-damper elements (Calçada, 1995); b) plane elements; c) 3D solid elements (Alves Ribeiro, 2012).....68
Figure 3-15. The stochastic track model used by Oscarsson (2001). The variables that were taken as stochastic (rail pad stiffness, ballast stiffness, ballast-subgrade mass, and sleeper spacing) are denoted k_p, k_b, M_b and L, respectively. 70
Figure 3-16. Schematic representation of the model that was considered by Hunt (1997).....71
Figure 3-17. Maximum interaction forces between the wheel and the rail, depending on the speed of the train and the magnitude of the geometric defect (Lei & Mao, 2004).....72
Figure 3-18. Numerical study by Namura and Suzuki (2007): a) schematic representation of the model; b) vertical accelerations measured in the axle box of a train running at 300 km/h (after applying a low-pass filter with cut-off frequency of 30 Hz).....72
Figure 3-19. Aspects of the numerical study by Banimahd and Woodward (2007a): a) view of the mesh; b) dynamic amplification factors due to a track defect with different geometries. 73
Figure 3-20. Aspect of the three-dimensional numerical model of the transition between two different subgrades (Alves Ribeiro *et al.*, 2009): a) detail of the bogie and wheel-rail contact; b) general view of the mesh. 74
Figure 3-21. Train-track interaction forces (1st axle) over a transition zone with abrupt stiffness variation in the subgrade (Alves Ribeiro *et al.*, 2009). 74
Figure 3-22. Aspects of the numerical model by Nicks (2009): a) general aspect; b) detail of the bogie.75
Figure 3-23. Aspects of 3D models of transition zones: a) to a box culvert on soft soils (Coelho, 2011); b) to a bridge with slab track (Shan *et al.*, 2013). 76

Figure 3-24. Results of wheel-rail contact forces at sections with unsupported sleepers: a) due to different gap depths for trains speeds of 324 km/h (Lundqvist & Dahlberg, 2005); b) influence of the train speed and the depth of the gap (Zhang *et al.*, 2008).....77
Figure 3-25. Representations of the numerical models developed by Varandas (2013): a) beam-spring-damper model; d) variation of the resilient modulus in a transvers view; c) example of the deformed shape of the transition zone under the wheel loads.....78
Figure 3-26. Numerical studies on USP: a) wheel-rail interaction contact after optimisation of USP stiffness (Lundqvist *et al.*, 2006); b) 3D model with USP with variable stiffness properties (Witt, 2008).....80
Figure 3-27. Aspects of numerical modelling using the DEM: a) network of contact forces between the sleepers and the ballast (Lobo-Guerrero & Vallejo, 2006); b) three-dimensional modelling of ballast tamping (Azéma, 2007);.....81
Figure 3-28. Aspects of a numerical model of a short transition zone using the DEM (Chen & McDowell, 2014): a) general view; b) example of contact force distribution. 82
Figure 4-1. *Alcácer* bypass: a) location of the by-pass; b) schematic representation of the layout adapted from REFER (2010). 88
Figure 4-2. Standard track cross-section on embankment.....89
Figure 4-3. Aspects of the track during construction: a) layers of the substructure; b) components of the superstructure; c) concrete monoblock sleepers with fastening system and rail pads; d) fastening of the rail and application of pre-load; e) aspect of the track before cleaning the excess of ballast and establishing the final geometry of the track.....89
Figure 4-4. Location of the structures where USP were installed.....90
Figure 4-5. Aereal views of the track platform at the end of the 1st stage of construction of *Alcácer* bypass (REFER, 2010).....91
Figure 4-6. Requirements of the layers for track on embankments.....92
Figure 4-7. Grading envelopes and some required properties: a) UGM and capping material; b) sub-ballast. 92
Figure 4-8. Typical evolution of PSD curves of the granite (a) and the limestone (b) obtained before and after compaction; evolution of methylene blue values (c). 93
Figure 4-9. Evolution of the cumulative distribution functions of $EV2$ measured with the *Portancemêtre* on top of the sub-ballast layer. 94
Figure 4-10. Daily precipitation and average daily temperature (source:snirh.pt).....94
Figure 4-11. Deformation modulus E_{V2} obtained in PLT tests and in the 3rd *portancemètre* survey.....95
Figure 4-12. Overlay of the values of E_{V2} and satellite view of the track (imagery: © 2014 Google). PS - road overpass; PH – culvert; PI – underpass; BT1 and BT2 – Technical blocks. 96

Figure 4-13. Examples of track singularities in the *Alcácer* bypass (REFER, 2010): a) construction of the backfill to a viaduct; b) construction of a road underpass; c) final aspect of a culvert. 97
Figure 4-14. Technical blocks type 1 (a) and 2 (b) (REFER, 2006): 1-ballast; 2-sub-ballast; 3-capping; 4-cement bond mixture (CBM) with binder content (BC) of 5%; 5-unbound granular material (UGM); 6-embankment with soils. 98
Figure 4-15. Deformation modulus E_{V2} obtained with *portancemètre* and location of track singularities. 100
Figure 4-16. The *Alfa Pendular* train: a) general aspect; b) schematic representation of the axle arrangement (in m) and respective load estimates (in kN).....101
Figure 4-17. Intercity passenger train: a) general aspect; b) schematic representation of the axle arrangement (in m) and respective load estimates (in kN).....102
Figure 4-18. Coal freight train with double traction (two CP locomotives of series 4700) transporting about 25 cars: a) general view of the locomotives; b) rear wagons; c) schematic representation of the axle arrangement (in m) and respective load estimates (in kN).....102
Figure 4-19. REFER's inspection vehicle: a) general view; b) detail of the inertial box mounted on the bogie frame. 103
Figure 4-20. Track geometry parameters (in mm) regarding the surveys carried out in March 2011 (red) and July 2013 (black), and respective Alert Limit values by REFER (dashed lines). 106
Figure 4-21. Aspects of the breather switch on the bridge: a) fixed and sliding rails; b) gap between sections of the deck. 107
Figure 4-22. Power Spectral Density (PSD) of some track geometry parameters, regarding the survey carried out in July 2013.....107
Figure 4-23. Average longitudinal level of the left and right rails (LL), in the wavelength ranges D1 and D2, regarding the surveys carried out in May 2011 (red) and July 2013 (black).....108
Figure 4-24. Cumulative distribution functions of $SDLL, D1$; REFER's Alert Limit; Track Quality Classes according to EN 13848-6 for train speeds between 160 and 230 km/h (CEN, 2014)...109
Figure 4-25. Standard deviation of the longitudinal level of each rail, $SDLL, D1$, regarding the surveys carried out between May 2011 and July 2013. 110
Figure 4-26. Average standard deviation of the longitudinal level (D1), $SDLL, D1$ regarding the surveys carried out between May 2011 and July 2013. 111
Figure 4-27. Evolution (May 2011 to July 2013) of the standard deviation of the longitudinal level (D1) of each rail, $SDLL, D1$, at three transision zones with wedge-shaped backfills type BT1.112
Figure 4-28. Evolution of the cumulative distribution functions of $SDLL, D1$: a) BT1; b) BT2; c) changes in the substructure; Track Quality Classes according to EN 13848-6 for train speeds between 160 and 230 km/h. 114

Figure 4-29. Estimated deterioration rates in mm/MGT. 116
Figure 4-30. Aspects of the southern approach to the bridge over Sado river. 117
Figure 4-31. Design of the wedge-shaped backfill of the transition zone case study. 117
Figure 4-32. Three-dimensional representation of the wedge-shaped backfill: a) abutment structure; b) abutment and CBM wedge; c) UGM wedge; d) final representation of the structure. 118
Figure 4-33. Aspects of the cyclic load triaxial tests: a) preparation of the specimens; b) instrumented specimen before testing; c) aspect of the triaxial apparatus. 120
Figure 4-34. Stress paths applied to the specimens. 120
Figure 4-35. Example of axial (a) and radial (b) deformations calculated from the measurements performed during the tests. 121
Figure 4-36. Results of E_r for different stress paths: a) granite (sub-ballast); b) limestone (capping and UGM). 122
Figure 4-37. E_r obtained for the two UGM (p_{max} = 250 kPa; q_{max} = 500 kPa): a) influence of w-wOPM; b) influence of D_c. 123
Figure 4-38: Classification of UGM according to EN 103286-7. 124
Figure 4-39: Results of E_r on CBM material for different stress paths. 126
Figure 4-40: Comparison of E_r values of the CBM for different curing times: a) *BC* = 3%; b) *BC* = 1%.126
Figure 4-41: Permanent axial deformation for $1x10^6$ load cycles (p_{max} = 40 kPa and q_{max} = 75 kPa). .127
Figure 4-42. Permanent axial deformation for 20 000 cycles in different stress paths. 128
Figure 4-43. Aspects of the compaction of the layers using heavier (a) and lighter (b) compaction equipment. 129
Figure 4-44. Compaction control results (D_c) obtained with nuclear gauge and respective diference to optimum water content value (w-w_{OPM}): a) CBM; b) UGM and capping; c) sub-ballast. 130
Figure 4-45. Location of alignments 1 to 3 in the backfill and respective *portancemètre* results. 131
Figure 4-46. Aspects of the p*ortancemètre* surveys (a and b) and PLT tests (c) on the backfill. 132
Figure 4-47. E_{V2} results with the *Portancemètre*: a) on capping and embankment near the transition zone; b) gradual stiffness increment measured on the sub-ballast layer at an adjacent transition zone. 133
Figure 4-48. Schematic diagrams of the inclinometer system: a) calculation principle of the vertical displacements; b) casing with one exit only (Slope Indicator, 2006). 135
Figure 4-49. Schematic representation of the inclinometers inside the backfill: a) longitudinal view; b) three-dimensional translucent view. 136
Figure 4-50. Aspects of the installation of the inclinometer system during construction of the backfill: a) location of the inclinometers; b) view of the openings in the abutment backwall; c) laying the

casing segments with geotextiles protecting the joints; d) installation of the pulley and return tube; e) covering the inclinometer with backfill material. 137
Figure 4-51. Ends of the inclinometers: a) opening of the inclinometer 1 on the abutment wall during the tests with the dummy probe; b) manouvering the probe inside inclinometer 2 with the return cable; c) detail of the dead-end pulley (Sisgeo); d) detail of the casing opening with the return cable. 138
Figure 4-52. Details of the protective geotextile to prevent fines from obstructing the interior of the casing: a) joint between two casing segments; b) pulley at the end of the casing. 138
Figure 4-53. Aspects of the installation of inclinometer 1: a) additional protection with geotextile and sand; b) pouring the with hydraulic fill under the abutment. 139
Figure 4-54. Aspects of the inclinometer probe (Sinco, Slope Indicator, model 50302910): a) schematic representation; b) view of the probe.....140
Figure 4-55: Reference positions of inclinometers 1 and 2 measured in March 2011. 141
Figure 4-56: Measurement of internal displacements of the backfill in inclinometers 2 (a) and 1 (b).142
Figure 4-58: Interfaces of wedges of the backfill with different materials: a) CBM and UGM; b) UGM and embankment with soils. 142
Figure 4-59. Layout of the survey points on the approach to the bridge: a) plan view; b) aerial view during contruction; c) track cross section. 144
Figure 4-60. Survey points: a) detaild view; b) installation on the sleeper's end; c) levellig survey...145
Figure 4-61. Aspects of the geodetic reference mark R1: a) detailed view; b) location. 145
Figure 4-62. Reference profile of the survey points on the sleepers and sub-ballast at the transition zone. 146
Figure 4-63. Displacements of the survey points on the sub-ballast layer: a) points PN1 to PN7; b) points PP1 to PP7. 146
Figure 4-64. Displacements of the survey points on the sleepers' ends: a) points TN1 to TN7; b) points TP1 to TP7. 147
Figure 4-65. Estimate of the vertical deformation of the ballast (Ni = TNi - PNi; Pi = TPi - PPi). 149
Figure 4-66. Longitudinal level measurements at the transition zone (σ denotes standard deviation).150
Figure 5-1. View of the underpasses UP1 (a) and UP2 (b). 155
Figure 5-2. Track plan view and longitudinal profile of transition zones at UP1 and UP2. 156
Figure 5-3. Schematic track cross-sections from S1 to S4 (see location in Figure 5-2).....157
Figure 5-4. Grading envelopes of granular materials. 157
Figure 5-5. Some aspects of the USP preparation. 158
Figure 5-6. Deformation modulus obtained with the *portancemètre* at the transitions to UP1 (above) and UP2 (below). 159

Figure 5-7. Light falling weight deflectometer tests. 160
Figure 5-8. View of the track receptance test. 160
Figure 5-9. Impulse time history (a) and frequency content (b); respective acceleration response in time and frequency domains (c and d). 161
Figure 5-10. Receptance functions obtained in each section 162
Figure 5-11. Location of the transducers at UP1 (a) and UP2 (b). 163
Figure 5-12. Schematic representation of the rail extensometry: a) shear rosette; b) full Wheatstone bridge; c) installed setup. 164
Figure 5-13. Track instrumentation: a) strain gauges on the rail web; b) displacement transducers along the transition zone; c) detail of the PSD on the rail; d) rail-sleeper relative displacement transducer; e) general view of the transducers. 165
Figure 5-14. Schematic representation of the data acquisition system. 166
Figure 5-15. Passenger tilting train configuration (in m) and approximate axle loads (in kN). 167
Figure 5-16. Dynamic wheel loads: a) example of a time history; b) distribution of peak loads. 168
Figure 5-17. Signature $S0\lambda$ of the *Alfa Pendular*. 169
Figure 5-18. Comparison between frequency content of the rail shear strain and the train signature (S_0). 169
Figure 5-19. Time histories and frequency contents of rail displacements measured in sections S1 to S4. 170
Figure 5-20. Average peak vertical displacements of the rail for each train crossing UP1 (a) and UP2 (b). 171
Figure 5-21. Estimated values of vertical track stiffness along transitions: a) to UP1; b) to UP2. 173
Figure 5-22. Time history and frequency contents of rail pad deformation. 174
Figure 5-23. Time history and frequency contents of accelerations measured on sleepers at different distances from the box culvert wall (see Figure 5-11). 175
Figure 5-24. Average bogie peak acceleration values at UP1 and UP2. 176
Figure 5-25. Comparison of frequency contents up to 50 Hz. 177
Figure 5-26. Models of the transition zones and details of the finite element mesh. 178
Figure 5-27. Aspects of the vehicle model: a) view of the components of the primary suspension; b) model of one of the 12 bogies of the train (see parameters in Table 5-5). 181
Figure 5-28. Schematic diagram of the procedure adopted for the calibration and validation of the numerical models. 182
Figure 5-29. Reduced models used in the calibration: a) detailed views of the meshes; b) example of the vertical displacement contours after static calibration. 184

Figure 5-30. Experimental and numerical receptance curves for sections S1 to S4 after dynamic calibration.....186
Figure 5-31. Comparison of rail displacements at S1: numerical results against field measurements.188
Figure 5-32. Comparison of rail displacements at S2: numerical results against field measurements.189
Figure 5-33. Comparison of rail displacements at S3: numerical results against field measurements.189
Figure 5-34. Comparison of rail displacements at S4: numerical results against field measurements.190
Figure 5-35. Comparison of rail-sleeper relative displacements: numerical results against field measurements.....190
Figure 5-36. Numerical results and field measurements of the vertical accelerations of the sleeper near S1. 191
Figure 5-37. Numerical results and field measurements of the vertical accelerations of the sleeper near S2. 192
Figure 5-38. Numerical results and field measurements of the vertical accelerations of the sleeper near S3. 192
Figure 5-39. Numerical results and field measurements of the vertical accelerations of the sleeper near S4. 193
Figure 5-40. Frequency content of numerical results and field measurements of the vertical accelerations of the sleepers.....194
Figure 5-41. Vertical displacement of the 1st axle of the train crossing transition zones UP1 and UP2.195
Figure 5-42. Interaction forces between the 1st axle of the train and the rails.....196
Figure 5-43. Maximum rail seat loads on the transition zones to UP1 and UP2.....196
Figure 5-44. Axle's vertical displacements (a) and sleeper's vertical acceleration (b) considering the effect of a 12-bogie train model or the superimposition of the effect of 12 times one bogie spaced in time.....199
Figure 5-45. Vertical displacement of the 1st axle of the train crossing transition zones UP1 and UP2, including the improved design of UP1.....199
Figure 5-46. Interaction forces between the 1st axle of the train and the rails, including the improved design of UP1.....200
Figure 5-47. Maximum rail seat loads on the transition zones to UP1 and UP2, including the improved design of UP1.....200
Figure 5-48. General views of transition zone during the construction of the backfill and in operation.201
Figure 5-49. Schematic longitudinal profile and plan view of the transition zone.....202
Figure 5-50. Track cross sections on earthworks and on the bridge (REFER, 2006). 202
Figure 5-51. Light falling weight deflectometer tests. 204

Figure 5-52. Track instrumentation: a) general aspect of the site; b) strain gauges; c) fibre optic rail pad sensor (installation during construction and final aspect); d) LASER-PSD system; e) LVDT transducer; f) MEMS accelerometer; g) piezoelectric accelerometer. 205
Figure 5-53. Differences in shear forces between sections 1 and 2. 206
Figure 5-54. Measured dynamic wheel loads of the *Alfa Pendular* and expected values. 206
Figure 5-55. Vertical loads transferred to the rail pad, calculated using the strain gauges (R_{strain}) and the rail pad load sensor (R_{rpad1}).....207
Figure 5-56. Median values of the peak vertical accelerations of the sleepers (f<80Hz). 209
Figure 5-57. Vertical rail-sleeper relative displacements. 209
Figure 5-58. Model of the transition zone: a) complete view; b) details of the mesh; c) schematic representation considering the thickness values assigned to the plane-stress elements. 210
Figure 5-59. Aspects of the vehicle model: a) identification of the components of the primary and secondary suspensions; b) model of one of the 6 coaches (see parameters in Table 5-9). 212
Figure 5-60. Rail displacements at position 5 (x = -4.5 m), on the bridge. 213
Figure 5-61. Rail displacements at position 1 (x = 41.1 m), in plain track. 214
Figure 5-62. Rail displacements at position 2 (x = 14.7 m), on the UGM. 215
Figure 5-63. Rail displacements at position 4 (x = 0.9 m), on the CBM.....215
Figure 5-64. Rail-sleeper relative displacements at x = 22.2 m. 215
Figure 5-65. Vertical loads transferred to the rail pads at x = 26.4 m. 216
Figure 5-66. Vertical sleeper accelerations at x =18.6 m and x =26.4 m. 216
Figure 5-67. Numerical train-track interaction forces (a) and vertical axle displacements (b). 217
Figure 6-1. Schematic representation of the numerical model (a), and detailed aspects of the track on the backfill (b) and on the bridge (c).....223
Figure 6-2. Backfill settlements: a) schematic representation; b) detail of the top nodes of the ballast layer moved downwards by δmax. 224
Figure 6-3. Vertical displacements of the first axle along the transition zone due to diffferent settlement values. 225
Figure 6-4. Vertical displacements of the rail at x = 0.9 m, due to the first six axles of the train. 225
Figure 6-5. Influence of the settlement of the backfill on the train-track interaction force. 226
Figure 6-6. Influence of the train's direction in the: a) vertical axle displacements; b) train-track normal interaction force. 227
Figure 6-7. Vertical accelerations of the coach, a) and b), and vertical coach-bogie interaction forces, c) and d), obtained at the leading and rear bogies of the 1st coach, considering: no differential settlements (in green) and 15 mm settlement from trains running from the the abutment to the bridge (in red) or from the bridge to the abutment (in black). 228

Figure 6-8. Vertical axle displacements (a) and train-track interaction forces (b) of the 5th and 21st axles of 6-car and 2-car models. 229
Figure 6-9. Replication of the results of a 2-car train model in order to simulate the effect of a full train. 230
Figure 6-10. Schematic representation of the bump profile shapes U, W, S and G. 231
Figure 6-11. Backfill bump profiles and consequent positions of the sleeper....232
Figure 6-12. Location of hanging sleepers and respective gap sizes in unloaded conditions. 232
Figure 6-13. Unloaded rail position (dashed lines) and vertical axle displacements of the 5th axle (solid lines)....233
Figure 6-14. Positive and negative peaks of the vertical acceleration of the first 8 axles. 234
Figure 6-15. Peak variations of the dynamic train-track interaction force. 235
Figure 6-16. Frequency content of the interaction force of the 5th axle. 236
Figure 6-17. Peak contact forces between sleepers and ballast layer. 237
Figure 6-18. Peak vertical accelerations of the sleepers, along the transition zone. 237
Figure 6-19. Plan and longitudinal views of the design of the viaduct over EN 120 (REFER, 2006). 238
Figure 6-20. Aspects of the construction of the viaduct over road N120 (REFER, 2010): a) before the construction of the viaduct and respective technical blocks; b) before laying the track; c) after its conclusion (imagery: © 2012 Nokia, © 2012 Microsoft). 239
Figure 6-21. Location of the accelerometers inside the coach car (a and b) and schematic representation of the orientation of the accelerometers' axes *x*, *y* and *z* (image: www.mathworks.com). 242
Figure 6-22. Summary of the parametric results. 243
Figure 6-23. Settlement profile applied in the numerical model (a) and longitudinal level of the rail at the approach to the viaduct (b). 244
Figure 6-24. Comparison of experimental and numerical vertical accelerations, obtained inside the coach car. 244
Figure 6-25. Frequency content of the numerical (a) and experimental (b) vertical accelerations, obtained inside the coach car. 245
Figure 6-26. Notation of rotary vehicle motions (Popp & Schiehlen, 2010). 246
Figure 6-27. Hypothetical dip settlement profiles. 246
Figure 6-28. Dip settlement profiles and actual rail revel ($LLD1 + D2$): change in dip amplitude (left); change in dip length (right). 248
Figure 6-29. Backfill settlement profiles and consequent positions of the sleeper (in unloaded conditions)....248
Figure 6-30. Location of hanging sleepers (markers) and respective gap sizes in unloaded conditions.249

Figure 6-31. Unloaded rail position (dashed lines) and vertical displacements of the 1st axle (solid lines).....249
Figure 6-32. Unloaded rail position (dashed lines) and vertical displacements of the 5th axle (solid lines).....249
Figure 6-33. Peak vertical displacements of the first eigth axles. 250
Figure 6-34. Vertical acceleration of the 1st axle.....250
Figure 6-35. Vertical acceleration of the 5th axle. 251
Figure 6-36. Positive and negative peaks of the vertical acceleration of the first 8 axles.....251
Figure 6-37. Normal train-track interaction force 1st axle.....252
Figure 6-38. Normal train-track interaction force 5th axle.....252
Figure 6-39. Peak variations of the dynamic train-track interaction force. 252
Figure 6-40. Vertical acceleration inside the 2nd coach car at the alignments with the leading and rear bogies. 253
Figure 6-41. Positive and negative peaks of the vertical acceleration inside the first two coach cars, at the alignments with the respective leading (1 and 3) and rear bogies (2 and 4). 253
Figure 6-42. Peak contact forces between each sleeper and the ballast layer. 255
Figure 6-43. Peak vertical accelerations of the sleepers, along the transition zone. 255
Figure 6-44. Combinations of kA and kL (a) and respective amplitudes and lengths of the dip (b)....256
Figure 6-45. Overlay with the 100 profiles considered in the parametric study. 257
Figure 6-46. Peak axle displacements: a) obtained with axle nr. 1; b) considering all axles. 258
Figure 6-47. Peak accelerations on the 1st axle: a) positive values; b) negative values. 258
Figure 6-48. Peak axle accelerations, considering all axles: a) positive values; b) negative values. ...258
Figure 6-49. Peak axle accelerations ($m/s2$), considering all axles: a) positive values; b) negative values. 259
Figure 6-50. Peak interaction force on the 1st axle: a) positive values; b) negative values. 259
Figure 6-51. Peak interaction force, considering all axles: a) positive values; b) negative values. 260
Figure 6-52. Peak dynamic coefficients (Q_{dyn} / Q_{sta}), considering all axles: a) maximum values; b) minimum values. 260
Figure 6-53. Peak car body accelerations at the alignment with the bogies: a) positive values; b) negative 261
Figure 6-54. Peak car body accelerations ($m/s2$) at the alignment with the bogies: a) positive values; b) negative values.....261
Figure 6-55. Settlement profiles of cases 10, 21 and 93.....262
Figure 6-56. Time histories of the sleeper-ballast contact forces near the dip ceter line in cases 10, 21 and 93: a) to c) sleepers *n*-11 to *n*+12; d) to f) sleepers *n*+1, n and *n*+1.....263

Figure 6-57. Summary of the sleeper-ballast contact forces under the 1st bogie of the vehicle, for three example cases (10, 21 and 93). 264
Figure 6-58. Schematic representation of load redistribution on a track section with hanging sleepers.264
Figure 6-59. Number of sleepers that are initially hanging (a) and have peak loads lower than 5 kN (b).265
Figure 6-60. Number of sleepers with peak loads higher than 100 kN. 265
Figure 6-61. Maximum sleeper-ballast contact force: a) 3D surface; b) contour lines (kN).....266
Figure 6-62. Peak sleeper accelerations: a) positive values; b) negative values. 267
Figure 6-63. Peak sleeper accelerations in m/s^2: a) positive values; b) negative values. 267
Figure 6-64. Peak sleeper accelerations (f < 80 Hz): a) positive values; b) negative values. 268
Figure 6-65. Peak sleeper accelerations in m/s^2 (f < 80 Hz): a) positive values; b) negative values. ..268
Figure 6-66. Summary of the parametric results. 270
Figure 7-1. Hypothetical longitudinal track profiles derived from simple sine functions, in the wavelength range between 3 m and 25 m: a) shorter track segment of 12 m; b) longer track segment of 35 m using the same sine functions as in (a). 274
Figure 7-2. Longitudinal level (average of left and right rails) considering wavelength ranges D1 and D2 (3 m to 70 m). 276
Figure 7-3. Spectrograms of the longitudinal level of the track: a) representation of spatial frequencies, ξ, up to 1 m^{-1}; b) content for spatial frequencies between 0.33 m^{-1} and 0.014 m^{-1}. 277
Figure 7-4. Comparison of the wavelength content of the longitudinal level and relevant aspects of the track substructure (continues). 278
Figure 7-5. Schematic representation of the calculation procedure to determine the amplitude at mid point of the chords.....280
Figure 7-6. Example of the application of the method to a portion of the track at 26.32 km mark: a) measuring mid-chord amplitudes of the longitudinal level; b) chord lengh vs mid-chord amplitude representation. 281
Figure 7-7. Two representations of the density of occurences: a) 3D surface; b) scatter plot (the size of the dots is proportional to the root square of the number of occurences). 282
Figure 7-8. Occurrences corresponding to track segments of about 5 km. 283
Figure 7-9. Overlay of the contour lines of the positive peak (a) and negative peka (b) axle accelerations (m/s^2) obtained in section 6.5.3 and the measured track defects. 285
Figure 7-10. Overlay of the contour lines of the numerical maximum (a) and minimum (b) dynamic coefficients (Q_{dyn} / Q_{sta}) obtained in section 6.5.3 and the measured track defects. 285
Figure 7-11. Overlay of the contour lines of the numerical maximum vertical accelerations inside the *Alfa Pendular* car body (m/s^2) obtained in section 6.5.3 and the measured track defects. 286

Figure 7-12. Overlay of the contour lines of the numerical maximum sleeper-ballast contact force (kN) obtained in section 6.5.3 and the measured track defects. 286
Figure 7-13. Overlay of the contour lines of the numerical positive peak (a) and negative peak (b) sleeper accelerations (m/s^2) after applying a low-pass filter with cut-off frequency of 80 Hz (see section 6.5.3) and the measured track defects. 287
Figure 7-14. Overlay of the results in Figure 7-7 with the summary of the numerical results obtained in section 6.5.3. 288
Figure 7-15. Examples of rail profiles with the same amplitude (at mid-chord) for a given chord length. 289
Figure 7-16. Longitudinal level measurements at the transition zone. 290
Figure 7-17. Locations that may be causing lower passenger comfort. 291
Figure 7-18. Locations that may be causing the increase of track degradation rates (continues). 292
Figure 7-19. Average standard deviation of the longitudinal level (D1), $SDLL$, D1, between 0.5 and 10 km, calculated with moving window of 10 m (a) and 75 m (b), regarding the surveys carried out between May 2011 and July 2013 and evolution between the first and last surveys, $\Delta SDLL$, D1.297
Figure 7-20. Average standard deviation of the longitudinal level (D1), $SDLL$, D1, between 10 and 20 km, calculated with moving window of 10 m (a) and 75 m (b), regarding the surveys carried out between May 2011 and July 2013 and evolution between the first and last surveys, $\Delta SDLL$, D1.298
Figure 7-21. Average standard deviation of the longitudinal level (D1), $SDLL$, D1, between 20 and 28.4 km, calculated with moving window of 10 m (a) and 75 m (b), regarding the surveys carried out between May 2011 and July 2013 and evolution between the first and last surveys, $\Delta SDLL$, D1. 299
Figure 7-22. Values of the $SDLL$, D1 and $\Delta SDLL$, D1 obtained at the underpasses at: a) 4.590 km mark (UP1) and b) 22.842 km mark (UP2). 301
Figure 7-23. Average standard deviation of the longitudinal level D1, $SDLL$, D1, at the South approach to the Sado bridge, calculated with moving window of 10 m and 75 m, regarding the surveys carried out between May 2011 and July 2013 and evolution between the first and last surveys, $\Delta SDLL$, D1. 302
Figure 7-24. Average standard deviation of the longitudinal level D1, $SDLL$, D1, at the Viaduct over EN120, calculated with moving window of 10 m and 75 m, regarding the surveys carried out between May 2011 and July 2013 and evolution between the first and last surveys, $\Delta SDLL$, D1. 303
Figure 7-25. Cumulative distribution functions of $SDLL$, D1 (May 2011 and July 2013 surveys), calculated with moving windows of 10 m and 75 m, and representative points corresponding to different types of track singularities: a) Technical Blocks type 1 (BT1); b) Technical Blocks type 2 (BT2); c) culverts without technical blocks (no BT); d) rail expansion joints. 305

List of Tables

Table 2-1. Excitation frequencies depending on the wavelength of the defect and train speed. 29
Table 3-1. Comparison of different examples of transition zones for HSL (see Figure 3-10). 61
Table 3-2. Summary comparison of numerical models to study transition zones. 83
Table 4-1. Some requirements and obtained values on the materials applied in the sub-ballast and capping layers. 92
Table 4-2. Track singularities with wedge-shaped backfill type BT1 (Figure 4-14a) 98
Table 4-3. Track singularities with wedge-shaped backfill type BT2 (Figure 4-14b). 99
Table 4-4. Track singularities (PH or PF) without wedge-shaped backfill (no BT). 99
Table 4-5. Track geometry limits (in mm) for train speed of 220 km/h. 104
Table 4-6. State conditions of CBM specimens tested regarding the resilient behaviour. 125
Table 4-7. ε_1^p accumulated between 3000 and 5000 cycles. 128
Table 4-8. Summary of requirements and results of compaction control. 130
Table 5-1. Characteristics of the under sleeper pads, provided by the manufacturer, CDM. 158
Table 5-2. Average peak absolute rail displacements and vertical track stiffness estimates. 172
Table 5-3. Average peak acceleration values for bogie passages (f<80Hz). 176
Table 5-4. Properties of the track materials after calibration. 179
Table 5-5. Characteristics of the bogie model (see Figure 5-27) (adapted from Alves Ribeiro, 2012; Ribeiro *et al.*, 2013). 181
Table 5-6. Calibration of material properties. 185
Table 5-7. Comparison of field and numerical track resonant frequencies ft and frp (in Hz). 187
Table 5-8. Summary of peak vertical displacements of the rail (mm). 207
Table 5-9. Characteristics of the coach model (see Figure 5-59) (adapted from Alves Ribeiro, 2012; Ribeiro *et al.*, 2013). 212
Table 6-1. Recommended levels of comfort (CEN, 2005). 228

Table 6-2. Description of the MEMS 3-axis accelerometers of the smartphones. 241
Table 6-3. Designation of the profiles and values of the parameters kA and kL. 247
Table 7-1. Locations of higher concentration of track defects and with higher amplitudes that suggest higher degradation – see Figure 7-18 (continues). 294
Table 7-2. Summary of the main aspects that affect the performance of transition zones and possible actions to monitor and detect the early development of critical situations. 309

Chapter 1

Introduction

1.1 Background and motivation to the present study

The continuous growth of the world population and the intensive use of automobiles or other fossil-based motorised vehicles have been placing an increased burden on modern societies, resulting in traffic congestions, affecting public health and causing negative environmental and climate impacts. It is considered that railway transport, integrated in a planned and efficient transport network, can contribute to mitigate some of these aspects. The low-friction surface on which the trains run makes railway transport one of the most energy-efficient means of land transportation and with very low CO_2 emissions (Figure 1-1).

The EU strategy presented in the new White Paper on Transport for 2050 (EC, 2011) states that the EU policy to increase competitiveness and economic growth (supported in social, environmental and territorial sustainability) is oriented to the development of green and sustainable transport systems, encouraging a modal shift towards rail freight and passenger transport. This paradigm is also clear in the strategic agenda of the European Rail Research Advisory Council (ERRAC, 2007, 2011) and in the Trans-European Transport Network (TEN-T) program 'core network' by 2030 (EC, 2005, 2013a, b). The continuous relevance given to projects related to rail transport, particularly the expansion of the European rail network for high-speed railways and the cross-border projects for rail freight corridors is very noticeable. In Portugal, these policies are reflected in the document "*PETI3 + Plano Estratégico dos Transportes e Infraestruturas Horizonte 2014-2020*" (SEITC, 2014), presented by the Portuguese Government. Over the past few decades, similar initiatives have helped to promote rail transport in Europe, both in the transportation of passengers and goods. However, the recent global financial crisis and subsequent factors seem to have affected all modes of transport, interrupting that general increasing trend in railway transport (Figure 1-2).

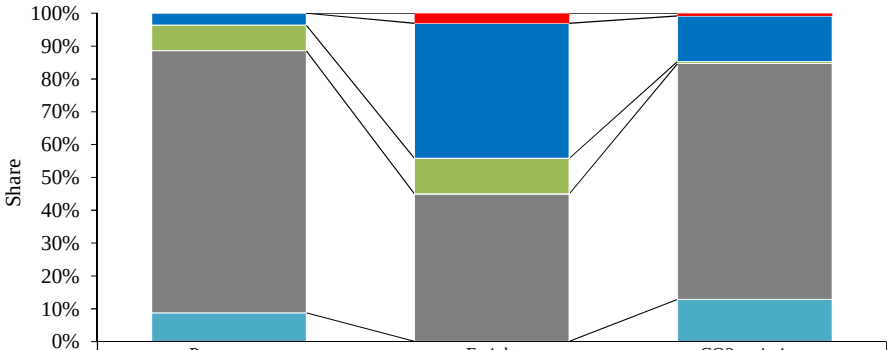

	Passengers (billion passenger-km)	Freight (billion tonne-km)	CO2 emissions (million tonnes)
Other	0	115	9.2
Total navigation	238	1551	161.5
Railways	512	407	7
Road transportation	5265	1693	833.3
Total civil aviation	577	3	149.3

Figure 1-1. Comparison of transport performance by mode and respective CO_2 emissions in EU-28 countries (EC, 2014).

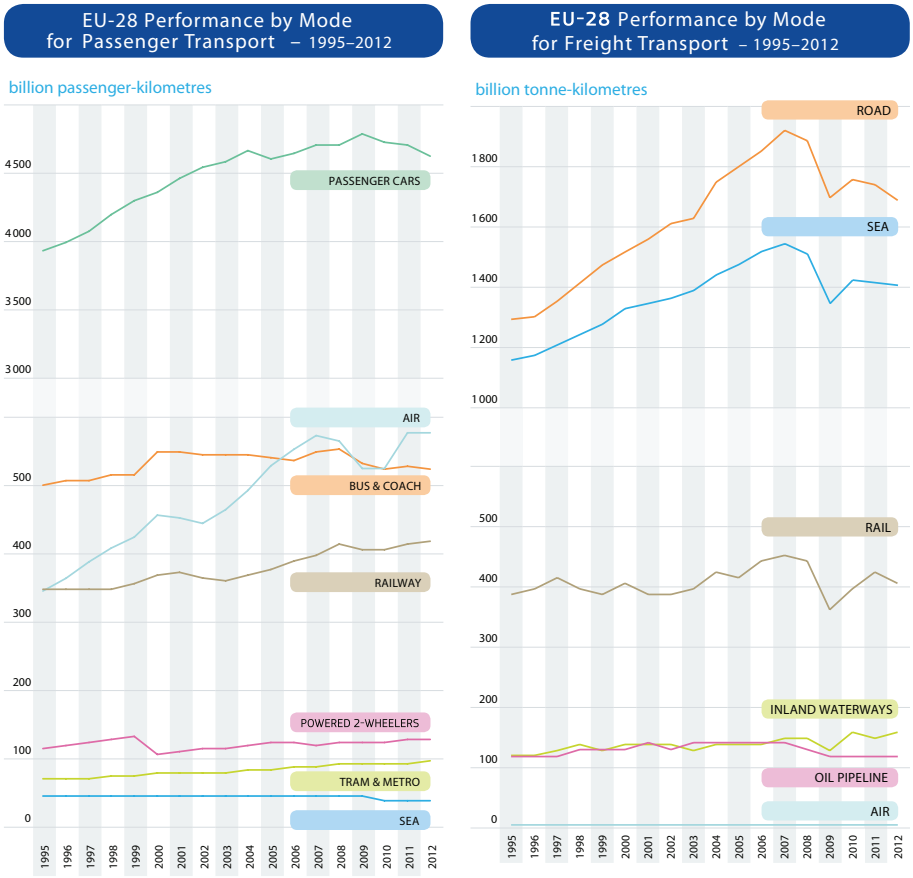

Figure 1-2. Recent evolution of the performance of passenger and freight transport in EU-28 countries (EC, 2014)

The competitiveness in the field of transport systems and the increasing requirements on the rail transport, especially with regard to safety, quality of service and increased economic and environmental efficiency have contributed to the optimisation of railway track systems.

Furthermore, over the past decades, various aspects of the railway infrastructure have evolved to respond to the ambitions for higher speeds of passenger trains and heavier axle loads of freight trains than in the past. However, despite the efforts that have been developed, there may still be significant scope for technological progress in several critical aspects of this type of transport infrastructure. Thus, taking into account the current paradigm of sustainable development, the optimisation of design and operation of the subsystem "railway track" are issues of great relevance.

Track maintenance and renewal activities are of utmost importance to railway infrastructure managers, due to the high costs and disruptions that it induces in the operation of this transport system.

In this context it should be mentioned the recent trend of applying advanced analytical tools for railway infrastructure management, such as RAMS (Reliability, Availability, Maintainability and Safety) and LCC (Life Cycle Cost) analysis tools (CEN, 1999; Patra, 2007), towards providing strategies for optimising maintenance operations and reducing the life cycle cost of this transport system. These tools provide means to evaluate the performance of the railway and are important contributes to the decision-making process in railway infrastructure management.

It is known that the railway track continually degrades over its life-cycle (Selig & Waters, 1994; Esveld, 2001). Changes in the track alignment give rise to variations in the dynamic axle load of the trains, which then accelerate track degradation, with consequences for maintenance and availability of the lines. This behaviour is particularly evident at some critical locations that are associated with abrupt changes in the track configuration, such as transitions zones to bridges or other structures. In order to mitigate this problem, careful design and construction is required, for which several recommendations have been suggested in the past (ERRI, 1999). However, studies based on the maintenance records of existing high-speed lines have shown that the problem of track degradation associated with such transition zones is not yet solved (López Pita *et al.*, 2006).

Despite past efforts by the scientific and technical community, to understand the mechanisms leading to a rapid degradation in some critical locations of the track and to predict and minimize its negative effects, particularly in areas of abrupt changes of support conditions of the structure (Figure 1-3), it seems to be consensual that these phenomena are far from being fully understood.

a) b) c) 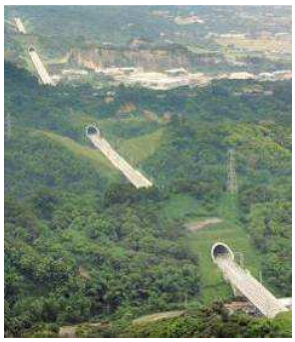

Figure 1-3. Examples of abrupt changes in the track support conditions – transition zones: a) embankment-bridge transition (Photo: © Bombardier); b) transition between different track configurations (Ochoa de Olza Galé, 2007); c) successive transitions between track on bridge and track in tunnel (Photo: © THSR).

Among the numerous studies conducted over the past decades, only a few reverted into meaningful conclusions about the complex behaviour of the railway track and sometimes the scientific explanations that were found were not sufficient to justify some of the anomalies regarding its structural behaviour. Perhaps for this reason, most of the methods available for predicting the track degradation consist of empirical approaches (Dahlberg, 2001). Often, these do not take into account the influence of some important variables such as environmental factors, characteristics of the materials of the superstructure and substructure of the track, or the influence of the dynamic train-track interaction caused by geometric defects of the track and abrupt variation of its vertical stiffness.

Although it has been acknowledged since long ago the importance of the geometric quality of the track and its support conditions, these issues are areas of research for which it is necessary to direct additional efforts in order to obtain further insight into behaviour of the track infrastructure.

Despite the fact that there are several methods to model the behaviour of the track and ideas on how to mitigate the effects at locations evidencing rapidly increasing track degradation rates, it has been very difficult to assess the adequacy of such ideas, either due to the lack of means, or due to difficulties relating to the operation of the infrastructure itself.

Thus, in order to contribute to the sustainability of rail infrastructures, it is considered appropriate to develop studies on the rational design of such structures, in order to minimize its life-cycle costs.

In this context, it seems of great interest to evaluate the performance of track locations evidencing abrupt changes in the support conditions that are normally associated with rapidly increasing track degradation rates and to study the suitability of non-traditional structural solutions, especially in

transition zones between embankments and civil engineering structures (e.g. bridges, viaducts, underpasses, culverts and other structures).

For this purpose, in the studies presented in this thesis it was intended to carry out the analysis of the behaviour of such transition zones in service, particularly those on which there was available information concerning the materials that were applied and the construction processes that were used. In particular, various locations were characterised, instrumented and monitored in a recent railway line in Portugal, particularly the bypass between *Pinheiro* station and the 94 km mark of the Southern Main Line, usually referred to as "*Alcácer* bypass".

In fact, the data that was available on the *Alcácer* bypass, in particular with regard to the characterization of the track platform, provided a solid basis for the subsequent development of studies. These concern the monitoring of structures, such as transition zones, as well as the analysis of the track's behaviour in service.

Moreover, the integral construction of a new infrastructure of this kind in Portugal was a singular event that provided exclusive conditions for the instrumentation and monitoring works of the behavior of the railway track. Furthermore, local geological typology and geotechnical conditions of this infrastructure ensured relative homogeneity throughout the line, regarding the foundation properties. These conditions contributed significantly to the reduction of the influence of other external factors that normally hinder similar studies in other works with different conditions, such as in the cases of track renewal works or lines crossing quite different foundation conditions.

1.2 Aim of the research and expected contributions

The main objective of the research presented in this thesis is to contribute to a deeper understanding of the structural behaviour of specific locations in railway tracks that often evidence rapidly increasing degradation rates and are associated with abrupt changes in the track support conditions, such as in transition zones. The studies aim at providing insight into the behaviour of railway tracks considering the dynamic train-track interaction, thus to improve the design of the infrastructure and to contribute to an efficient management of the railway assets, within the scope of the life-cycle cost reduction paradigm. To achieve those goals, this thesis focuses on the following specific objectives:

- Characterise the materials and layers of the track substructure at transition zones by means of laboratorial studies on geomaterials using advanced approaches that include cyclic loading triaxial tests and by experimental works comprising instrumentation of the backfills for long-term monitoring using sub-horizontal inclinometers and topographic levelling surveys;

- Develop a method to analyse and compare successive track geometry data obtained with inspection vehicles and integrate the results with the information from the design and with other results that were obtained during construction;
- Characterise the track in service at transition zones using advanced non-destructive approaches, such as the receptance tests to evaluate the dynamic response of the track in the frequency domain and a novel approach to assess the support conditions of the sleepers using the Light Falling Weight Deflectometer (LFWD);
- Monitor the structural response of the track using a wide range of instrumentation techniques and measuring systems as trains pass by at different transition zones, including locations where innovative track elements – particularly under sleeper pads (USP) - were installed and tested;
- Apply and further develop numerical models that use novel techniques and take into account the dynamic train-track interaction to analyse the structural behaviour of transition zones, followed by the calibration of those models using the information obtained in field characterisation tests and by the respective validation using the data from track monitoring campaigns;
- Perform parametric analysis using the above numerical modelling technique to assess the influence of different configurations of longitudinal rail profiles at transition zones on the train-track interaction;
- Develop a framework to integrate the results obtained in the numerical studies with the data from the track inspection vehicles and other information obtained in the field, aiming at identifying scenarios that suggest higher risk of derailment, higher degradation rates and lower passenger comfort.

Regarding the work that is presented, the data that was obtained and how the studies were conducted, particularly the integrated approach considering the physical and mechanical characteristics of the structures, the boundary conditions and the loadings acting on the structures, it is considered that a set of substantial information was obtained regarding the track subsystem. This information contributes to extend the knowledge on the response of the transition zones, bearing in mind the assessment of the performance of these structures. Furthermore, the resulting knowledge may be used to design and build efficient transition zones with better long-term performance and to develop methods that anticipate and contribute to mitigate the development of increasing degradation rates of the geometric quality of the track. The research work above is expected to contribute to the following areas:

- Improve the ability to monitor and assess the behaviour of the track during construction and in service under passing trains;
- Provide insight into the behaviour of the elements that comprise the transition zones and, consequently, on the design, construction and behaviour of those elements;
- Make use numerical models that consider the dynamic train-track interaction to contribute to a more efficient design of some critical locations of the railway track;
- Extend the knowledge on the influence of abrupt variations of the track support conditions and uneven rail profiles in the dynamic train-track interaction;
- Provide more information out of the data from the track inspection vehicles, thus allowing a systematic assessment of the evolution of the track degradation and promoting an early detection of critical situations that can affect the normal operation of the line;
- Establish performance indicators that may be considered to detect situations denoting higher risk of derailment, lower passenger comfort and early development of increasing degradation rates, thus contributing to the efficient management of the railway infrastructure and reducing its life-cycle costs.

1.3 Thesis Outline

This thesis consists of eight chapters. Chapter 2 provides a brief overview of the main aspects that characterise and govern the behaviour of railway track structures and presents a short review on past research studies that are relevant for the works developed in this thesis.

Chapter 3 presents a review on railway transition zones, focusing on the design of backfills constructed at the approach to bridges, viaducts or other civil engineering structures. A brief review is also presented regarding past numerical modelling studies on transition zones.

Chapter 4 describes general aspects of the track and traffic of the *Alcácer* bypass and presents the analysis of the physical and mechanical characteristics of the geomaterials and layers of the track platform. A transition zone case study at the approach to a bridge is analysed in detail, including the laboratorial characterization of geomaterials and *in situ* mechanical characterisation of the layers.

Chapter 5 addresses dynamic numerical analyses of the train-track interaction at two case studies in the *Alcácer* bypass. Experimental validation of the numerical models is carried out using track monitoring results under passing trains. Track characterisation using non-destructive tests is also

presented and analysed. The influence of under sleeper pads at transition zones is discussed in the first case study, based on the experimental and numerical results.

Chapter 6 focuses on the influence of the settlement profiles in the train-track system using numerical simulations of transition zones with uneven rail profiles. Parametric studies comprising dynamic analyses were performed to simulate different settlement scenarios. Based on the results, performance indicators were established that may provide useful information for railway infrastructure managers.

Chapter 7 presents an application of a framework to integrate the numerical results from Chapter 6 with the data obtained in the field (including the track geometry data), in an attempt to identify locations in the track that might be experiencing a decrease in performance.

Lastly, in Chapter 8, major conclusions and recommendations for future work are summarised.

Chapter 2

The railway track and its behaviour

2.1 The structure of the railway track

For railway vehicles to operate in adequate safety and quality conditions, it is necessary that the actions imposed on the track and that the motion experienced by passengers or goods remain below a certain acceptable threshold. The structural optimisation of railway tracks can be summarised as the process in which the above conditions are maintained at the lowest possible life cycle cost of the infrastructure and providing maximum availability of the railway line for train operation. To achieve this goal, the structural configurations of the railway track have been evolving over the years. However, the ballasted track remains the most common structural configuration and significant improvements have been introduced in its design and, especially, in its maintenance procedures.

In general, the ballasted track is made up of rails, fasteners, rail pads, sleepers, layers of granular material (Figure 2-1), supported on a foundation (embankment or cutting) or on civil engineering structures (for example, bridges, viaducts, tunnels, among others). With regard to the definitions of the various components of the track, it may be adopted the nomenclature used in Code 719R (UIC, 2008b), developed by the *Union Internacionale des Chemins de Fer* (UIC), as shown in Figure 2-2.

Normally, the rails are fixed to the sleepers and these are supported on the ballast layer. This set of components is usually given the designation of “superstructure” (Figure 2-2). It should be noted that the inclusion of ballast layer in the definition of superstructure is not consensual in the literature. Sometimes, it may be used the term "track frame" to refer to the set of rails, sleepers and fastening systems (Figure 2-1a).

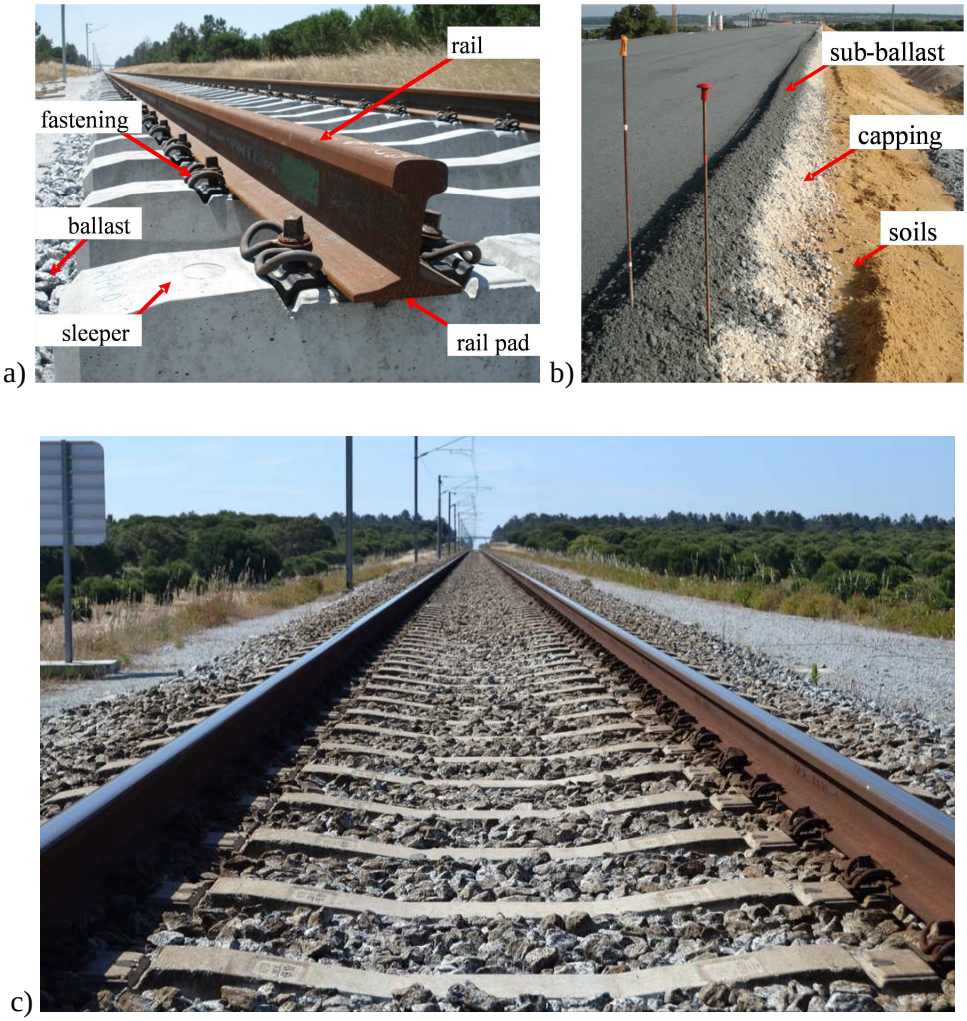

Figure 2-1. Aspects of the components that comprise the ballasted track: a) track frame (rails, fastenings, rail pads, sleepers) and ballast; b) substructure of the track on embankment; c) final aspect of the track.

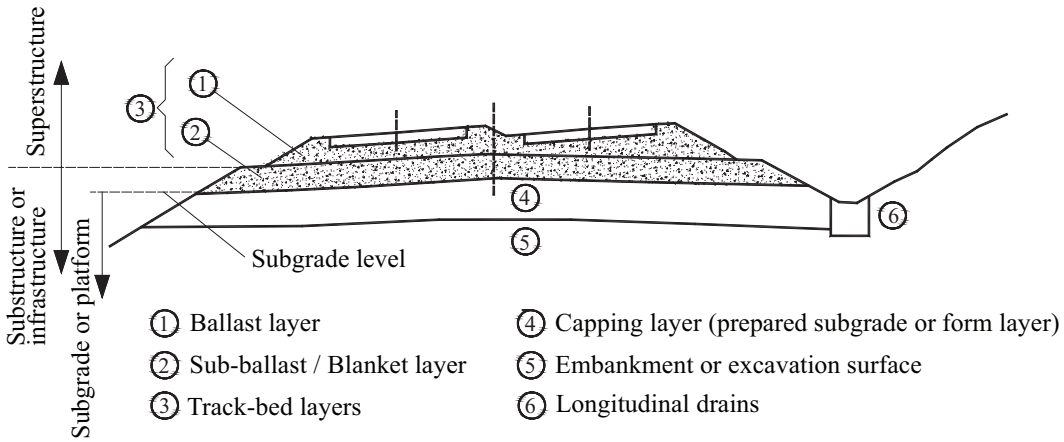

Figure 2-2. Schematic cross section of the ballasted track (UIC, 2008b).

The superstructure rests, naturally, on the track "substructure" (Figure 2-2) which consists in superimposed supporting layers with different properties and functions (Selig & Waters, 1994). In recent railway lines for high performance, the superstructure may comprise, among other layers, the sub-ballast and the capping (Figure 2-1b).

In addition to providing guidance to the wheels of the vehicles, another main function of the railway track is to provide a rapid reduction with depth of the vertical loads of the vehicles acting on the rail down to the layers below and to the foundation (Figure 2-3). Indeed, after a few meters in depth, the effect of the load due to traffic becomes practically negligible (Selig & Waters, 1994). To obtain an adequate structural behaviour of the track during its life cycle, the loads transferred in depth should be compatible with the bearing capacity of the underlying components and layers, so that the materials may undergo linear elastic or resilient behaviour (Jardine, 1992; Gomes Correia, 2004; Burrow *et al.*, 2007a), thus limiting permanent deformations that contribute to deteriorate the track quality.

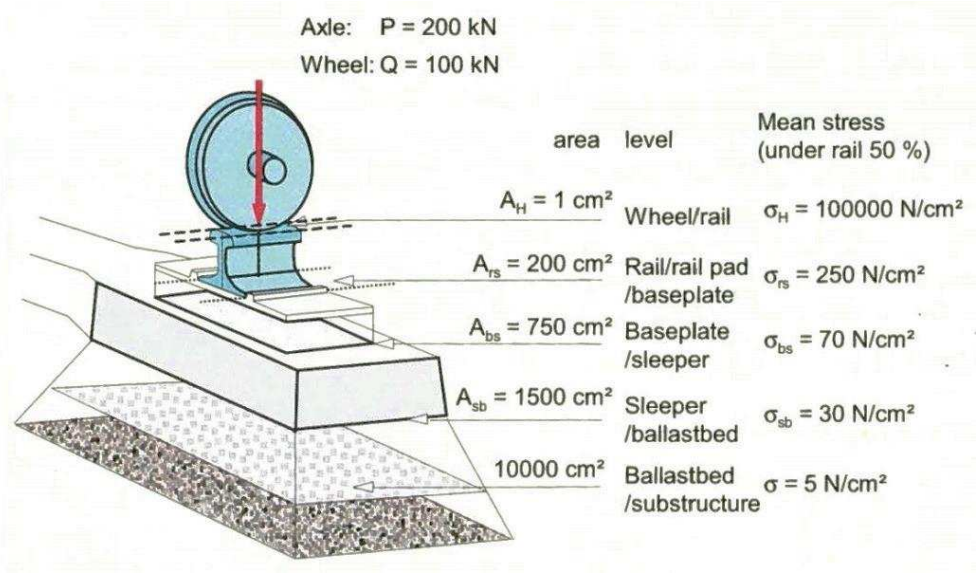

Figure 2-3. Schematic representation of the vertical load transfer (Esveld, 2001).

The geometrical, physical and mechanical characteristics of the superstructure and substructure depend on the type of railway operation it is intended. Thus, railway lines can be classified considering aspects related to: their configuration; the amount of traffic; the speed of operation; the type of platform, among other aspects. Different design methods of the trackbed and subgrade layers have been applied by railway infrastructure managers to account for some of these aspects (Burrow *et al.*, 2007a; UIC, 2008b).

In recent decades there has been a rising increase in the construction of railway lines using less conventional track configurations (Figure 2-4), particularly in high-speed lines (HSL) in some Asian (Japan, China, Taiwan) and European countries (Germany, The Netherlands) (Paixão & Fortunato, 2009b). In general, these structures are referred to as "ballastless track" configurations, in that the ballast layer in replaced by a concrete slab ("slab track") or by other material such as an asphalt layer. Some studies support that these structural configurations perform better than the ballasted track and evidence lower life cycle costs, particularly in HSL and in lines with significantly more traffic (Paixão *et al.*, 2009).

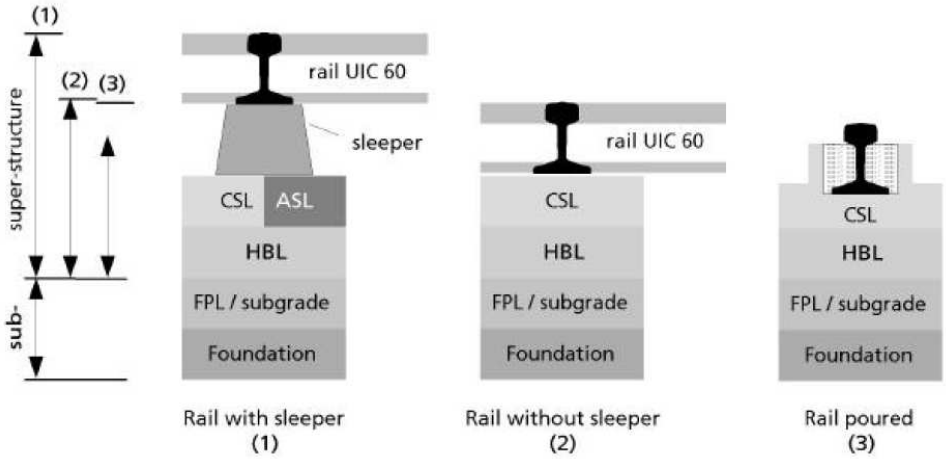

CSL - Concrete Supportive Layer; ASL - Asphalt Supportive Layer; HBL - Hydraulically-Bonded Layer; FPL - Frost Protection Layer.

Figure 2-4. Different configurations of ballastless track: 1) rails supported by sleepers placed on concrete or asphalt layer; 2) rails directly fixed to the concrete slab; 3) rail embedded in a concrete slab (Quante, 2001).

2.1.1 Components of the superstructure of ballasted tracks

The rails may be considered as the most representative components of the railway track and they have a primary role to provide wheel-rail guidance mechanisms. This function is mainly ensured by the shape of the rail head, the conicity of the wheels and the flanges of the wheels (Figure 2-5a).

From a structural point of view, these components also have the function to sustain and transfer the vertical, lateral and longitudinal loads of the vehicles to the underlying components/layers of the track, as well as the loads resulting from thermal actions.

In what regards the fastening systems, they must ensure proper positioning of the rails on the sleepers, regardless of the expected vertical, lateral and longitudinal loads. Modern fastening systems for

concrete sleepers normally have appropriate resilient components – the rail pads (Figure 2-5b) – to provide additional elasticity to the track.

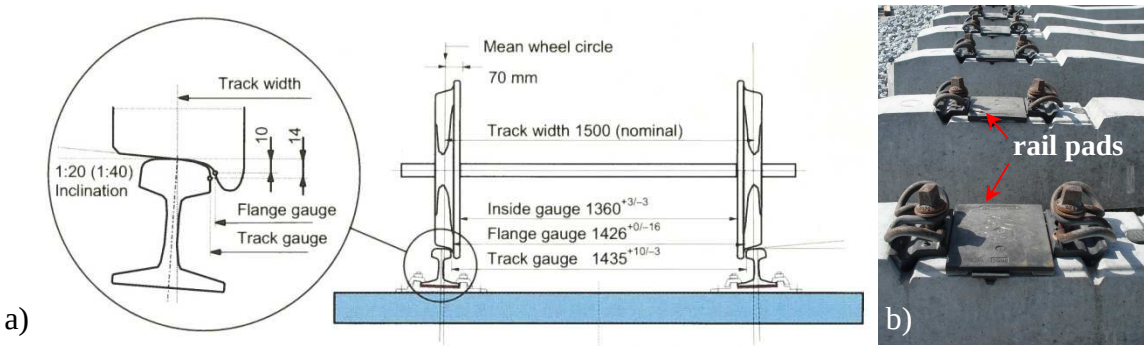

Figure 2-5. Details of ballasted tracks: a) wheelset and track frame with standard gauge (Esveld, 2001); b) fastening systems pre-installed on monoblock concrete sleepers.

In most track configurations, the rails rest on sleepers, which have the function to attenuate and distribute the loads from the rails to the ballast layer. The sleepers also play an important role in the stability of the track due to their weight (normally between 250-400 kg) and to the fact they are interlocked in the ballast layer, thus allowing the track to withstand the usual lateral forces produced by running vehicles and due to buckling resulting from thermal variation induced on the rails. The sleepers are also largely responsible for ensuring the correct inclination of the rails and the relative position between the two rails (Figure 2-5a).

The ballast is formed by a layer of coarse granular material and the interaction between the hard particles provides high resistance to compression to the layer. As mentioned earlier, the ballast allows partial embedding of the sleepers (Figure 2-1c), largely contributing to the stability of the track frame. The sleepers apply large loads on the ballast layer (e.g. vertical pressures of about 300 kPa, see Figure 2-3) that has the function to spread and reduce the loads transferred to the layers bellow. The ballast layer also provides important resilient properties to the track, adding vertical elasticity and capacity to attenuate vibrations resulting from the passage of vehicles. Another important function of the ballast layer is related to its significant contribution to the drainage of the track, because it allows the percolation of water between its particles.

Given that the ballast is constituted by particles with similar dimensions, its granular structure can be easily rearranged, which facilitates maintenance works and consequently enables to restore adequate

geometrical quality of the track. This feature also provides greater ease in placement and removal of ballast material or other track components.

2.1.2 The substructure of ballasted tracks

The sub-ballast also has the function to reduce the loads resulting from the vehicles by spreading and transferring them, at acceptable levels, to the layers below. Although the ballast and the sub-ballast share this function, the sub-ballast must provide a more efficient and economic approach to reduce the stresses onto the subgrade than the alternative of increasing the thickness of the ballast layer (Fortunato, 2005). To that aim, the aggregates and the construction process of the sub-ballast layer need to comply with specific requirements. The separation between the ballast and the foundation, conferred by sub-ballast layer, aims primarily: i) to avoid the wear of the platform due to the mechanical action of the ballast particles; ii) prevent inter penetration of material into the layers; iii) and prevent the rise of fine soil particles from foundation that can contaminate the ballast layer (ballas foulling). In addition to protect against the freezing and thawing cycles, the sub-ballast also serves as a waterproofing and draining layer that prevents the rise of the water and contributes to direct the rainfall-runoff to the drainage systems.

It is considered that the track subgrade consists of all the layers of the substructure, natural or constructed for the purpose that rest below the sub-ballast layer. The capping layer (or blanket, form layer) is normally assumed to be the most superficial part of the subgrade. The upper layers of the subgrade have the following functions: enable adequate compaction of the sub-ballast material; provide support conditions to the overlying layers and accommodate the stresses transmitted by the upper layers; spread and transfer the loads to the layers below at lower stress levels; allow for adequate drainage in eventual rise of water levels. To that aim, the layers must consist of good quality materials, following more demanding compaction and bearing capacity requirements than those required for the underlying subgrade materials.

2.2 Mechanical degradation of railway tracks

Consider a hypothetical situation of a straight railway line section, having an initial geometry without apparent defects, comprising layers that provide excellent support conditions, components denoting uniform characteristics throughout its length and vehicles with wheelsets without defects. This is an ideal situation for railway operation from the point of view of the optimisation of maintenance costs. In this scenario, except from the influence of the variability of external actions, it would be expected a uniform wear and degradation of the track throughout its length. Moreover, the track would settle evenly rather than forming localised irregularities in the positioning the rails (geometric defects).

However, due to the intrinsic variability of the characteristics of the materials, the different support conditions of the track, the small initial imperfections in the rail positioning and the variability of the dynamic loads applied by the vehicles (Prud' Homme, 1970; Esveld, 2001; Hawari, 2007), the track tends to deteriorate more rapidly at some locations, promoting the development of differential track settlements. In practice, the development of defects and settlements (i.e., the degradation of the railway track) is not uniform either in space or in time.

It can be considered that the degradation of the geometric quality of the railway track results from the deterioration processes that take place both in the superstructure (rails, rail pads, sleepers and ballast layer) and in the underlying layers (e.g. sub-ballast, capping and other subgrade layers).

Within the scope of this thesis, particular attention will be given to the degradation component of the geometric quality of the railway track resulting from the accumulation of plastic deformations of the layers, a process which in practice results into permanent settlements that cause transversal and longitudinal levelling defects.

As mentioned in the literature (Selig & Waters, 1994; Profillidis, 1995; Esveld, 2001; López Pita, 2006), the normal process of degradation of the geometric quality of the track can be divided into two stages (eventually three). Firstly, after construction or renovation of the line, a rapid degradation is verified that stabilises after the passage of the first thousands of train axles. Afterwards, there is a stage of linear degradation with time (or traffic) at lower and rather constant rates. An eventual third phase corresponds to a rapid increase in the degradation rates of the track, when it becomes paramount to intervene with maintenance or rehabilitation works (Figure 2-6).

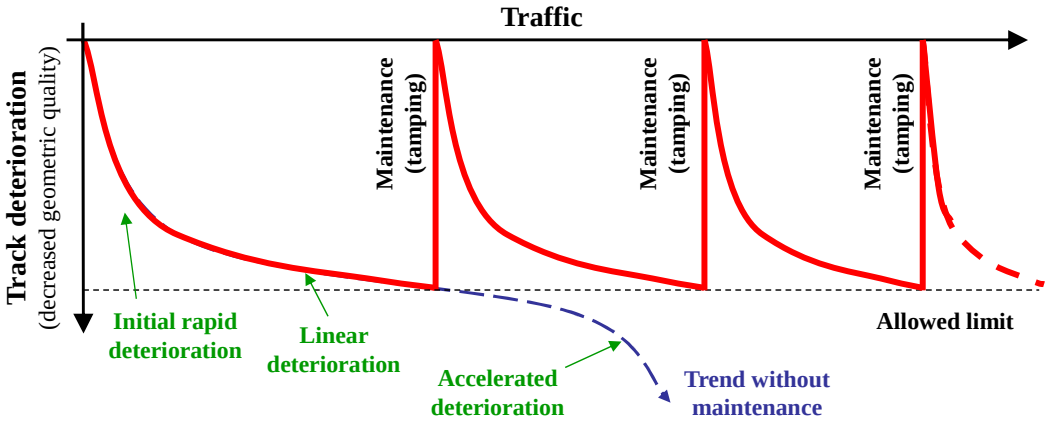

Figure 2-6. Simplified representation of the normal railway track deterioration process (adapted from Selig & Waters, 1994; Esveld, 2001).

In general, the complex mechanisms that cause further degradation of the geometric quality of tracks built on layers of granular material, such as the ballast and sub-ballast layers, are a consequence of the following (Figure 2-7):

- When vehicles run on the tracks, the existence of defects in their wheelsets, the geometric irregularities of the rails and the variations in the track support conditions - primarily related to the variations in the vertical stiffness of the track - induce the amplification of the dynamic components of the axle loads and can trigger and foment the degradation of the track.
- Also due to the process described in the previous point, with the accumulation of loading cycles, the components and layers of the track undergo inelastic (plastic) deformations, accumulating plastic strains and causing the formation or the increase of irregularities in the geometry of the track (Selig & Waters, 1994; Fröhling, 1997; Dahlberg, 2001; Ubalde *et al.*, 2007). For example, after the initial process of stabilisation and as the degradation of the ballast layer progresses, the particles become rounder and smaller due to abrasion and fragmentation. Consequently, a contamination process of the ballast by fine particles may be triggered, reducing the mechanical properties and the drainage capacity of this layer. Due to the above aspects, the track may tend to degrade faster at some locations, causing slight redistributions in the load transfer to the track components, which can lead to further degradation in adjacent areas and to the development of more differential settlements.
- The additional and increasing defects of the track and the accumulation of settlements resulting from this process induce a subsequent increase of the dynamic interaction forces between the vehicle and the track. Thus, the geometric quality of the track may deteriorate further, leading to a continuously increasing degradation process.

In addition, geotechnical failure mechanisms in the substructure tend to lead to critical situations that eventually compromise the normal operation of railway tracks. Selig and Waters (1994) identified the following main failure mechanisms: i) excessive progressive settlement from repeated traffic loading; ii) consolidation settlement and massive shear failure under the combined weights of the train, track structure, and soils; iii) progressive shear failure from repeated wheel loading; iv) shrinking and swelling from moisture change; v) frost heave and thaw softening; and vi) subgrade attrition. These geotechnical failure mechanisms must be prevented during the life cycle of the infrastructure. Thus, adequate design of the subgrade and proper maintenance of the superstructure is required to avoid excessive stress levels on the bottom layers. Unforeseen rehabilitation works in the substructure are extremely costly, complex, limit the track availability and disturb the normal train operation.

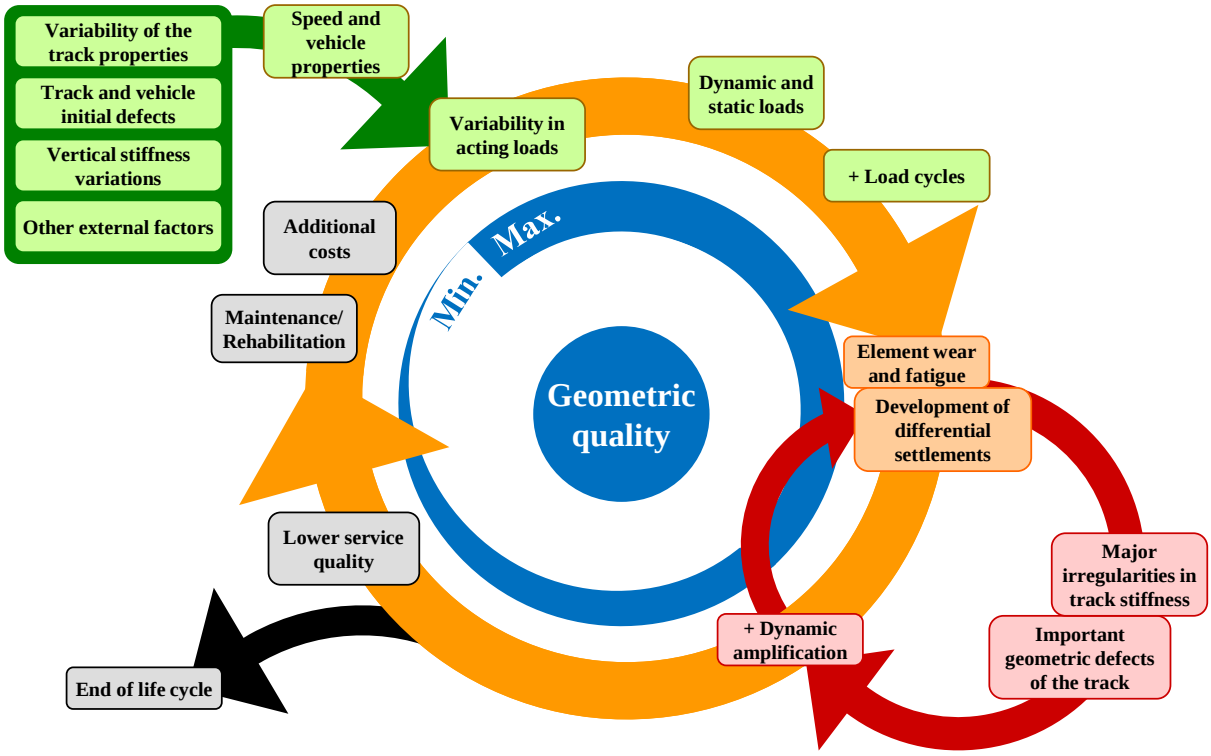

Figure 2-7. Schematic diagram of the recursive and increasing non-uniform degradation process of railway tracks.

In normal conditions, the track degradation rates are influenced by several factors such as:

i) The amount of traffic running on the track - corresponds to the number of load cycles.

ii) The load amplitude caused by the vehicles - particularly the vertical component of the axle load acting on the rails, which comprises the static and dynamic load components. Among other factors, the dynamic component depends on the speed of the vehicle, its unsprung mass (e.g, wheelsets and non-suspended motor components), the existence of defects on the surface of the vehicle's wheels, the vertical stiffness of the track and the geometric quality of the track, as suggested by the formulation proposed by Prud'Homme (1970):

$$Q_d = Q_s + 2\sigma_{\Delta Q} \tag{2-1}$$

Where:

$$\sigma_{\Delta Q} = \sqrt{\sigma_{\Delta QUS}^2 + \sigma_{\Delta QS}^2} \tag{2-2}$$

$$\sigma_{\Delta QUS} = 0.45 \frac{V}{100} b\sqrt{m_{US}K} \quad (2\text{-}3)$$

$$\sigma_{\Delta QS} \approx (0.11\ to\ 0.16) Q_s \quad (2\text{-}4)$$

- Q_s and Q_d are, respectively, the static and dynamic vertical components of the load applied by a given wheel;
- $\sigma_{\Delta QUS}$ and $\sigma_{\Delta QS}$ are, respectively, the standard deviations of the dynamic overloads due to the unsprung masses and sprung masses (bogie frames, carbody and remaining components) of the vehicles;
- V is the train running speed;
- b is a parameter that depends on the irregularities of the rail surface;
- m_{US} is the unsprung mass of the vehicle;
- K is the vertical stiffness of the track.

iii) The quality of the construction and of the materials used in the track - factors such as resiliency and the robustness of the superstructure components; the vertical stiffness of the track; the degree of compaction of the support layers; and drainage conditions can influence the structural behaviour of the track over time.

iv) Other external causes, such as: the action of erosive agents; excessive temperature variations; the amount of rainfall that influences the water content of the soils; frequency of maintenance operations, in particular tamping.

An analysis conducted by experts under a UIC study (2008a) on the quantification of the influence of different aspects that contribute to the degradation of the geometric quality of the railway (with the exception of the influence of vehicles and erosive agents) allowed to summarise the information presented in Figure 2-8. In this figure, it is noted the overall large contribution that is attributed to factors related to aspects of the substructure, independently of the category of lines. This highlights the importance of the substructure to the performance of railway tracks, in general.

2.2.1 The importance of the vertical stiffness of the track

The vertical stiffness of the track - or simply “track stiffness”, using the nomenclature of the European Technical Specifications for Interoperability (CE, 2011) - is an important indicator of the structural behaviour of the railway track (Sussmann *et al.*, 2001). The track stiffness reflects the overall resistance of the infrastructure against vertical deformations, when loaded. It can be defined as the ratio between the load applied by a wheel on the rail and the maximum vertical displacement of the track, measured at the top of the same rail.

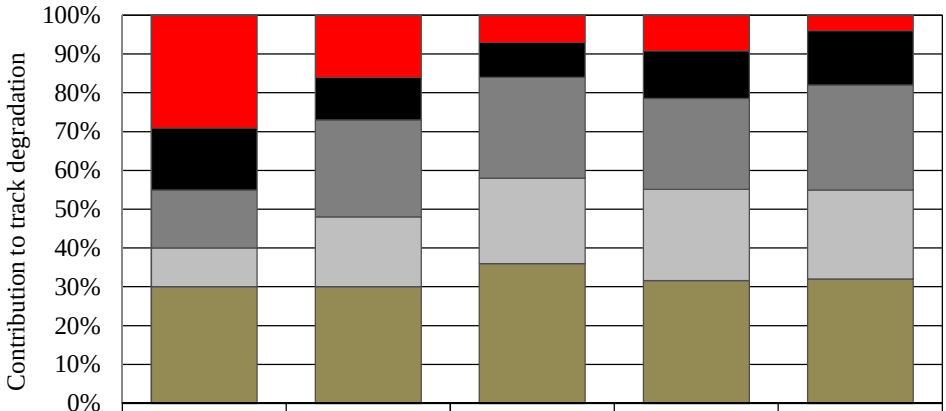

	Purpose built HSL (V≥250 km/h)	Specially upgraded HSL (V=200 km/h)	Conventional lines (rebuilt)	Conventional lines	Classical old lines (poor conditions)
Rail surface	29%	16%	7%	9%	4%
Track components	16%	11%	9%	12%	14%
Ballast	15%	25%	26%	23%	27%
Drainage	10%	18%	22%	23%	23%
Substructure	30%	30%	36%	31%	32%

Figure 2-8. Influence of different aspects on the deterioration of the track quality, for different track categories (after UIC, 2008a).

The track stiffness is usually expressed in kN/mm and has a different physical meaning than other parameters often used in structural analyses of the railway tracks. The ballast coefficient (in kN/m^3), the track modulus (in kN/m^2) and the equivalent stiffness coefficient (also in kN/mm) used in the discrete support models are examples of such parameters, and they all are interconnected as described by Teixeira (2003). The *in situ* measurement of some of these parameters is not consensual in the field of railway engineering, as discussed by Kerr (2000). These parameters depend on the stiffness of the various components and layers of the track, from the soils in the foundation, up to the rail, as evidenced in Figure 2-9.

The track stiffness influences its bearing capacity (a structural characteristics used in pavement engineering that is related to the ability to support the actions of upcoming traffic) and its dynamic behaviour under running vehicles. In a way, considering the influence that the track stiffness has on the amplitude of the dynamic component of the loads from the vehicles, it becomes partially responsible for triggering and determining the degradation rates of the geometric quality. Therefore, the track stiffness has an important aspect regarding its long-term performance and maintenance costs, according to what has been highlighted in the past (Prud' Homme, 1970) and in relatively recent studies (Sussmann *et al.*, 2001; Teixeira, 2003; Hunt & Wood, 2005; Berggren, 2009).

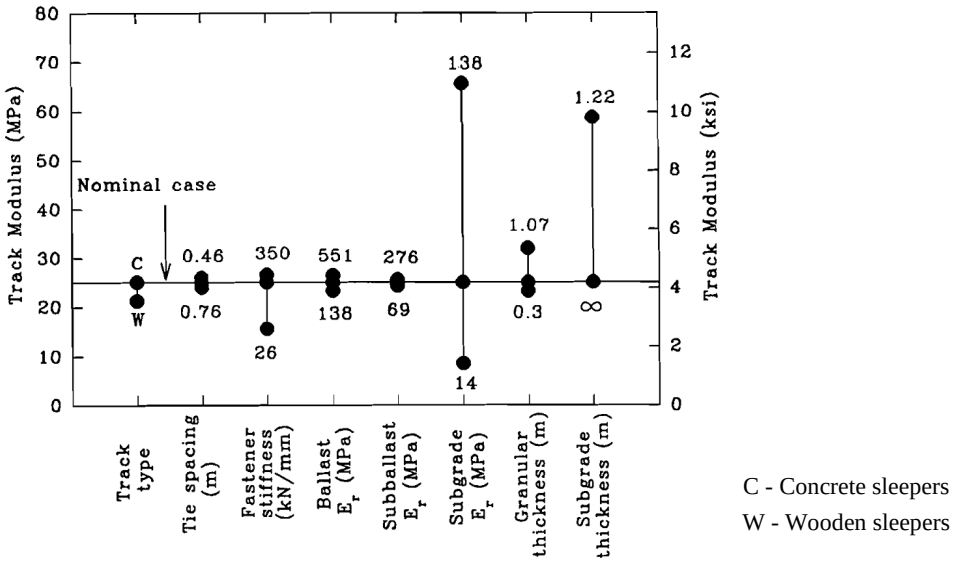

Figure 2-9. Influence of variations in the characteristics of the components of the track on the track modulus (Li & Selig, 1995).

A track characterised by a low vertical stiffness may undergo considerable vertical deformation, given the high loads acting on the rails. Furthermore, the dissipated energy resulting from rail traffic in this hypothetical situation would have a significant economic impact due to the additional traction energy that would be required to move the trains on the rails.

In contrast, excessively stiff track can lead to increased dynamic interaction forces between the wheel and the rail, accelerating the wear and fatigue of the various components that constitute the track and vehicles. Higher track stiffness also causes greater interaction forces between the sleepers and the ballast, hence causing more degradation and transferring greater stress levels onto the underlying layers.

In general, there is uninterrupted oscillation of the track stiffness throughout the length of a line, as evidenced by several studies (Fröhling, 1997; Oscarsson, 2001; Berggren, 2009) (Figure 2-10). Among the factors that contribute to fluctuations of the track's vertical stiffness, the following may be highlighted: i) variability of environmental conditions (Liegner, 2004; Fortunato, 2005); ii) the constructive approach adopted for the support layers; iii) and the intrinsic variability of the physical and mechanical characteristics of the materials that comprise these layers and the foundation of the track (Fortunato, 2005). For example, the stiffness of the rail pads is strongly influenced by the preload and by temperature variations (Wu & Thompson, 1999; De Man, 2002; Carrascal *et al.*, 2007)

(Figure 2-10b) and the response of the support layers is clearly non-linear under vertical loads (Lekarp *et al.*, 2000a; Sussmann *et al.*, 2001; Fortunato, 2005), as shown in Figure 2-10c.

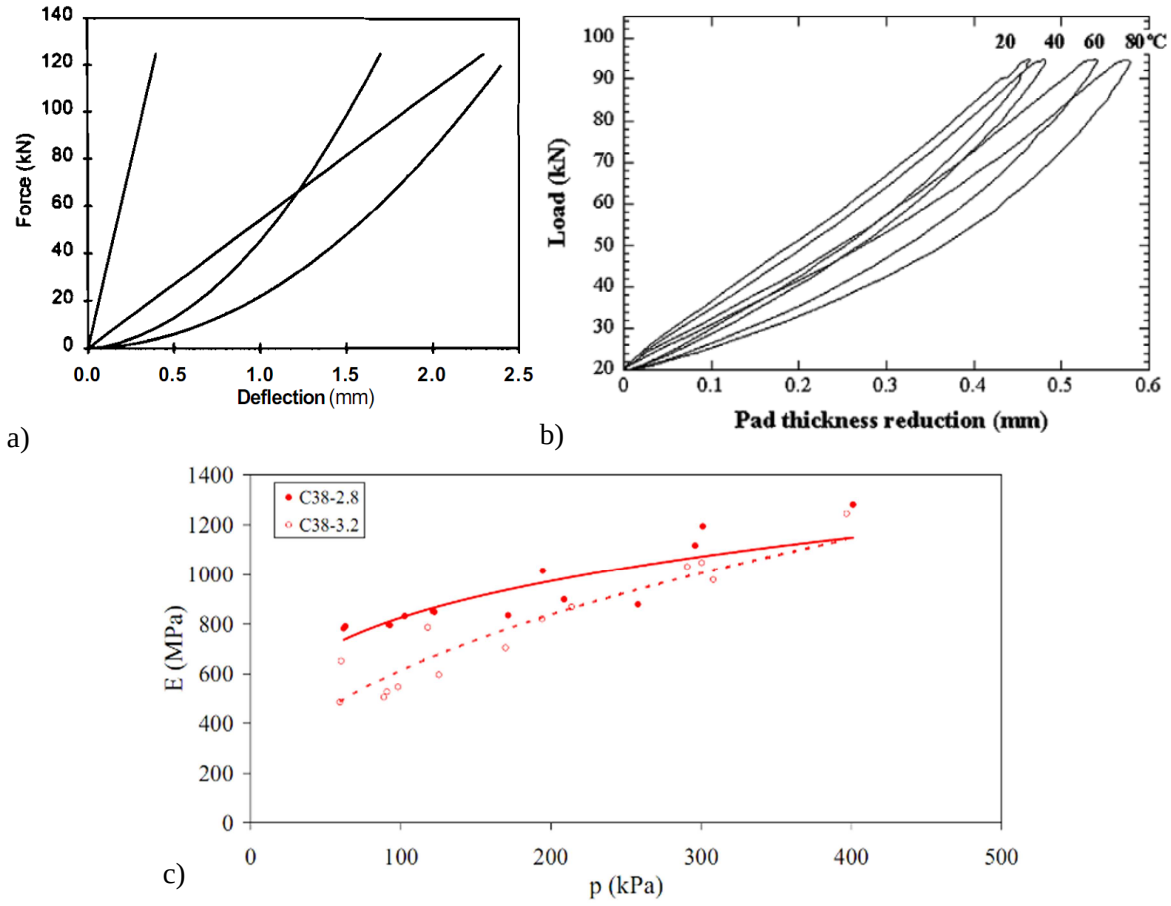

Figure 2-10. Non-linear behaviour of the track and its components: a) examples of measured static force-deflection curves of the track (Fröhling *et al.*, 1996); b) load curves on rail pads at different temperatures (Carrascal *et al.*, 2007); c) variations of the resilient modulus (E) of granular material under different stress levels (mean stress, p) (Fortunato, 2005).

Variations in the vertical stiffness can be associated with changes in the configurations of the track, for example: i) the transitions between earthworks and civil engineering structures (e.g. bridges, viaducts and tunnels) (Figure 2-11a); ii) variation of the characteristics of the layers of the substructure along a line (Figure 2-11b); iii) or varying properties of the components of the superstructure.

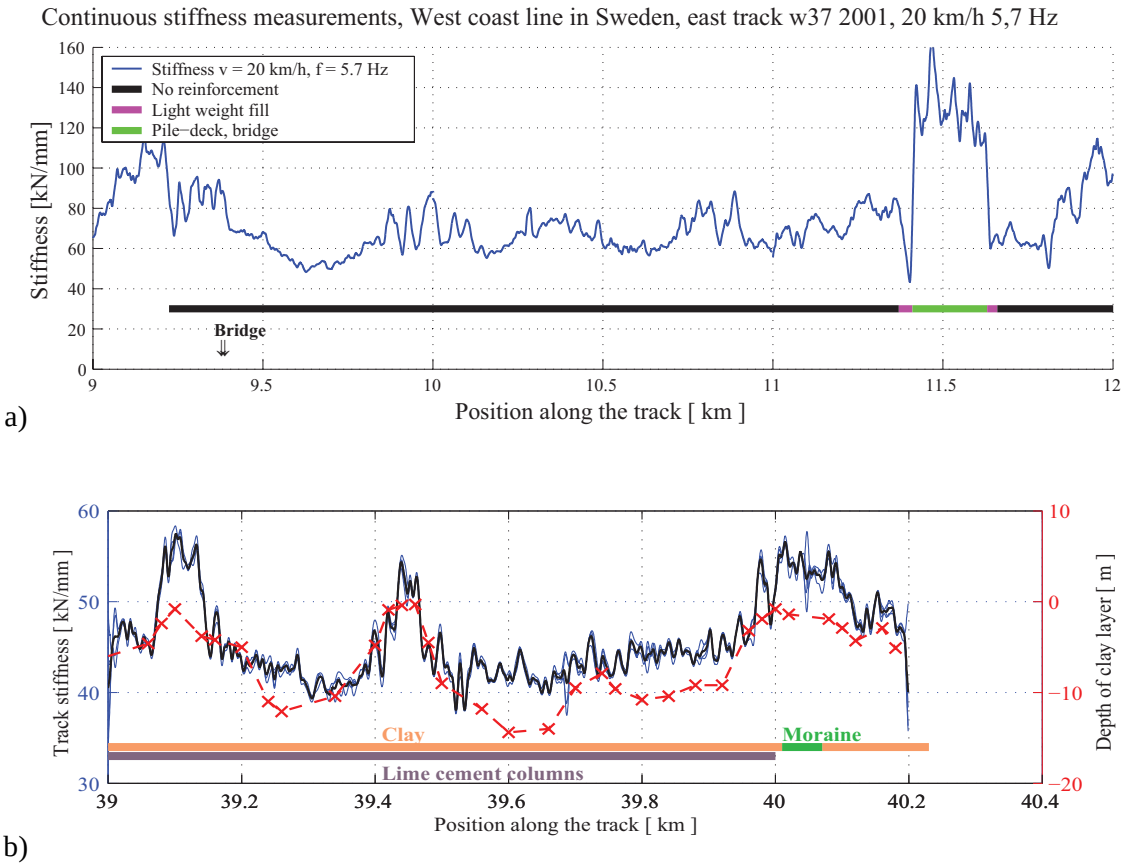

Figure 2-11. Continuous track stiffness measurement (speed of 20 km/h and excitation frequency 5.7 Hz): a) abrupt stiffness variation at the approach to a bridge (Dahlberg, 2004); b) influence of the thickness of the layers; the red dashed line represents the depth of the clay layer in the subgrade (Berggren, 2005).

Following what was mentioned earlier, one of the most relevant aspects of the variability of the vertical stiffness it is its negative influence to induce variations in the dynamic loads of the vehicles, triggering and fomenting the development of track defects. Moreover, apart from this aspect, these irregularities induce unwanted vibrations in vehicles and on the track. In most cases, the variation in vertical stiffness with low wavelength is mostly of random nature along the track. Variations of vertical stiffness with larger wavelengths induce lower frequency oscillations in the vehicle, which contribute negatively to passenger comfort and can generate unwanted vibrations in the surrounding area to the track (Dahlberg, 2010).

As of the 70's and following the studies by Prud'Homme (1970, 1976) for the design of HSL between Paris and Lyon, more relevance was given to aspects related to the track vertical stiffness. Some

authors have discussed and demonstrated the importance of the magnitude of the track stiffness and its variability in the maintenance of railway tracks (López Pita *et al.*, 2004; Berggren, 2009).

For example, the EUROBALT II project (Dahlberg, 2004) aimed to optimise the total cost of the life cycle of ballasted railway tracks. Some of the objectives of this project were to identify the most important parameters that should be monitored in order to detect defects early and the parameters that could be controlled to reduce degradation rates. It was concluded that the vertical stiffness, the displacement of the sleepers and the settlements of the various layers are the most important parameters that influence the behaviour of the track. A study by Teixeira (2003), based on the optimisation of maintenance and energy dissipation costs in a railway line, proposed an optimal range between 70 to 80 kN/mm for the vertical stiffness.

Banverket, the former Swedish railway infrastructure manager, promoted various studies concerning the behaviour of the track, including the development of a vehicle that allows to perform continuous measurements of the vertical stiffness (Berggren, 2005, 2009). This approach aims at anticipating eventual maintenance operations and reducing its costs, thereby contributing to the optimisation of the network management.

In view of the knowledge that was acquired in the past, softer rail pads have been used in recent railway lines (compared with those used in conventional tracks or in the first HSL) with the aim to reduce the vertical stiffness of the track and thus contribute to the reduction of maintenance costs.

Despite being acknowledged the importance of the track stiffness - justifying the inclusion of this parameter in the Technical Specifications for Interoperability of the trans-European network (CE, 2011) - there is no regulation that establishes the requirements for its amplitude or variability along the track. However, if the construction or rehabilitation of the layers of the tracks follows the requirements established in the Code 719R, appropriate levels of track stiffness may be achieved (UIC, 2008b).

2.2.2 Permanent track settlements

In ballasted railway tracks laid on earthworks, the degradation of the geometric quality of the track is often associated with the development of permanent differential settlements. Typically, these are a consequence of the accumulation of plastic deformations resulting from the deformation or degradation of the support layers and foundation.

Due to the resilient behaviour of the granular materials in the upper layers of the track, the deformation suffered by these materials is almost completely recovered after each load cycle. However, in each load cycle small plastic deformations remain (Figure 2-12). The accumulation of

these small plastic deformations, after a considerable number of load cycles, contributes to the deformations of the track that, eventually, may become incompatible with the normal train operation. During the first load cycles, the rate of the plastic deformations decreases significantly and in the following cycles the behaviour of the materials is almost independent of the loading history, provided that the material is not subjected to higher stress levels (Lackenby, 2006). Otherwise, for increasing stress levels and more demanding stress paths, it is known that the permanent deformation of aggregates mainly depends on the initial density of the material and the loading history.

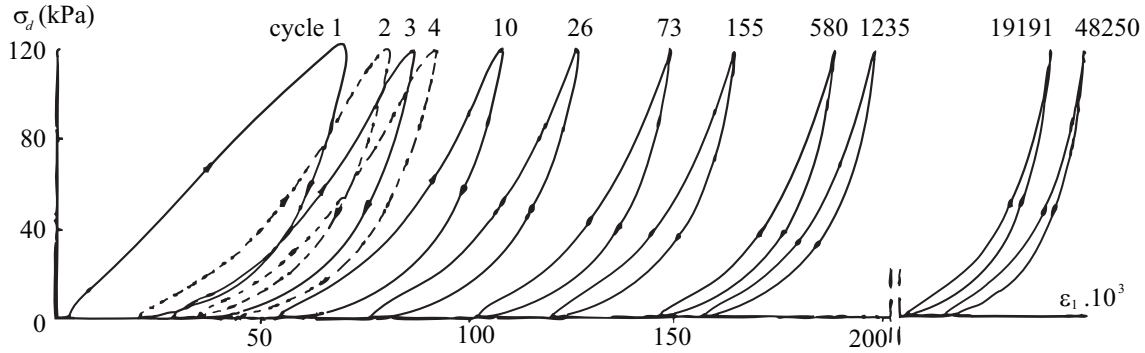

Figure 2-12. Stress-strain diagram of a granular material under repeated loading (Allaart, 1992); σ_d - deviatoric stress; ε_1 - axial deformation.

It is verified that for normal railway tracks, supported on foundations with adequate bearing capacity and after the initial stabilisation of the layers, the ballast is the layer that contributes mostly to the degradation of the geometric quality, in particular, the area affected by tamping actions (Selig & Waters, 1994) (Figure 2-13a). In some situations, the permanent settlements suffered by the material of the embankment and of the natural soils can be equally relevant, as in the examples shown in Figure 2-13b.

The settlements due to the substructure may be associated with the behaviour of compacted soils (variation of volume by collapse, deformation due to creep, consolidation and even due to compaction because of the cyclic loading of the vehicles) and due to the natural soils (Figure 2-14). The sum of these contributions may reach values of the order of tens of centimetres (Melis Maynar, 2006), as seen in Spanish HSL, especially in some rather high embankments (Figure 2-13b). Nevertheless, the reesults do not suggest a clear link between the embankment height and the settlement amplitude.

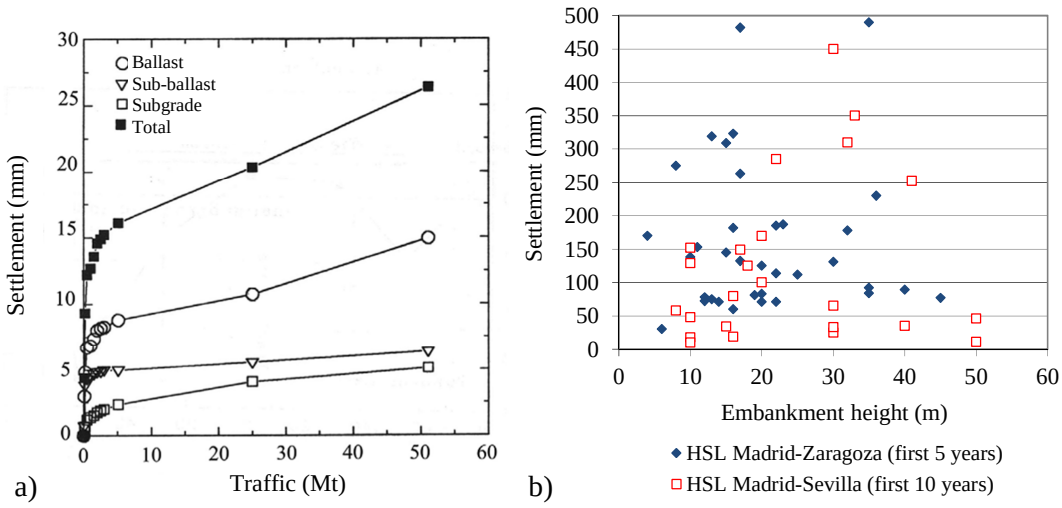

Figure 2-13. Permanent settlements: a) due to the accumulation of traffic of a track on a sandy subgrade (Selig & Waters, 1994); b) embankments for HSL in Spain (adapted from Melis Maynar, 2006).

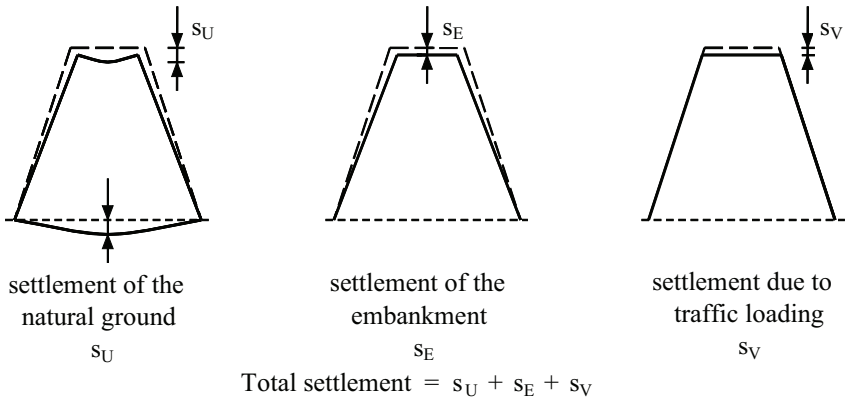

Figure 2-14. Schematic representation of the various settlement components of the substructure that contribute to the permanent settlement of railway tracks (UIC, 2008b).

It is important to note that when absolute settlements occur, typically, there are also significant differential settlements. These effects mainly increase vertical accelerations in the carbodies of the running vehicles, having a negative impact on passenger comfort and, ultimately, may compromise safe train operation.

As discussed previously, in response to this behaviour of the track, railway infrastructure managers need to carry out maintenance operations to restore an adequate level of track geometric quality. It should be noted again that frequent implementation of these interventions is often undesirable because

it is costly, affects the normal operations of vehicles and accelerates the degradation of the ballast material (Selig & Waters, 1994).

In these circumstances, studies have been developed and many degradation models have been proposed to predict the long-term behaviour of railway lines and to enable a more efficient management of the railway infrastructure (Sussmann *et al.*, 2001; Dahlberg, 2004; Zoeteman & Esveld, 2004; Vale, 2010).

2.3 The geometric quality of the track

Since the dawn of the railways, and especially with the advent of high-speed lines, railway infrastructure managers give special attention to the geometric quality of the tracks. The correct positioning of the rails is critical to ensure safe transport of goods and passengers and provide adequate service level quality.

The actual geometry of a particular railway line corresponds to its theoretical position that was established in the design, plus the geometry defects. Given the behaviour of the track and the external loads acting on the structure, such as those resulting from the successive passage of vehicles and varying environmental conditions, the magnitude of the track geometric defects tends to increase with time.

Apart from issues related to transport safety, it is necessary to ensure a desired level of service quality. In the case of passenger transport, it is essential to ensure an adequate level of comfort that can be achieved by limiting the accelerations felt by the passengers inside the coach cars. It is precisely on this point that the geometrical quality of the track has a great importance, in that the accelerations measured inside the vehicles, in general, tend to increase with the magnitude of the tracks defects.

2.3.1 Assessing the track geometric quality

The assessment of the geometric quality of railway lines consists of measuring specific parameters that characterise the geometry of the track and quantifying the incidence of situations where the values of those different parameters deviate from a given tolerance. Following this approach, indexes are calculated representing the geometric quality regarding each geometric parameter or a combination of different parameters. To promote the railway interoperability between European countries, there has been a tendency to standardise the methods to measure the geometry of the tracks and the criteria for the geometric quality levels, as is evident by the European standard series EN 13848.

2.3.1.1 Measuring the track geometry

For several decades, the detection of geometric defects in the track was based on visual inspections using simple methods and means. Following the technological evolutions, various railway infrastructure managers started using sophisticated equipment that allowed the direct assessment of the geometry of the track (performing measurements of the position of the rail) at low running speeds. Some of the advanced equipment consisted of railway cars dedicated to assess different aspects of the track and circulating at commercial speeds.

With the increase in railway traffic, the advent of high-speed railways and the subsequent increasing demands for track geometric quality, there was a need to develop advanced systems allowing a faster and more efficient detection of geometric defects of the track, without direct contact with the rail. At present, in high performance railway lines, inspection vehicles are used that were specifically designed and dedicated to this function and, in general, can run at speeds above 160 km/h. With this type of vehicles, it is possible to perform track measurements more frequently, evaluate the influence of track defects at greater speeds, increase track availability and obtain information for a more efficient management of the infrastructure. Among other features, to calculate the geometric profile of the rails, these vehicles make use of optical measurement systems (normally comprising LASER transducers) that continuously determine the relative distance between the rails and a reference position in the inspection vehicle. In addition, such contactless measuring techniques usually are complemented by inertial measurement systems (comprising orthogonally positioned accelerometers) to calculate the dynamic displacements of the reference position of that optical system by means of double integration in time of the measured accelerations. In particular, these contact-less measuring technics are important for detecting long wavelength defects of the track, which are relevant for passenger comfort in high-speed transport.

2.3.1.2 Relevant geometric parameters of the track

Commonly, a set of parameters are considered to assess how the actual position of the rails diverges from their established theoretical position. The differences between these two positions are called geometric irregularities or defects in the track and, usually, periodic inspections of the railway track are carried out to detect these defects. Some of the most commonly used parameters to characterise the geometric quality of railway tracks are listed below, according to EN 13848-1 (CEN, 2003) as depicted in Figure 2-15:

- Track gauge – distance between the gauge faces of the two adjacent running rails measured, normally at about 14 mm below the running surface.

- Cross level – the difference in height (cant) of the adjacent running tables computed from the angle between the running surface and a horizontal reference plane;
- Longitudinal level - deviation in the direction perpendicular to the running surface of consecutive running table levels on any rail, expressed as an excursion from the mean vertical position (reference line), covering the wavelength ranges;
- Alignment – deviation in the transverse direction of consecutive positions on any rail, expressed as an excursion from the mean horizontal position (reference line) covering different wavelength ranges;
- Twist – the algebraic difference between two cross levels taken at a defined distance apart, usually expressed as a gradient between the two points of measurement.

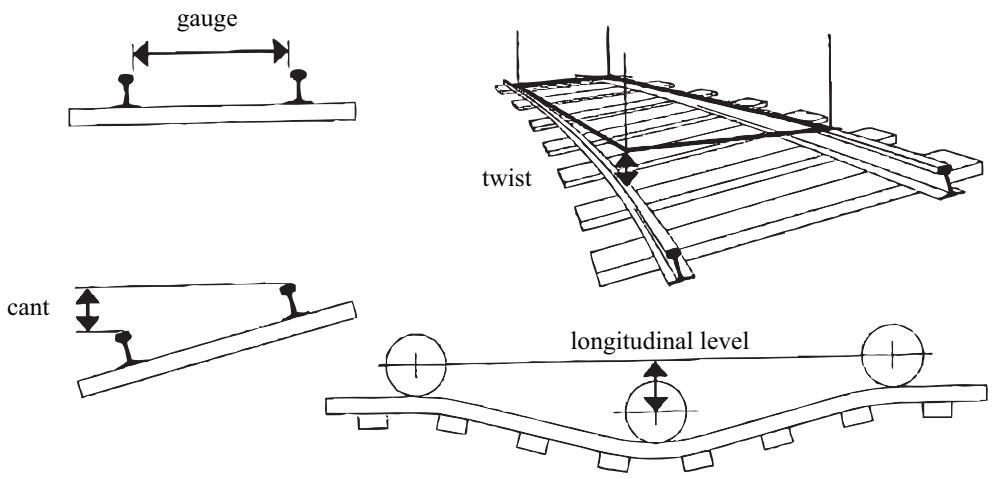

Figure 2-15. Schematic representation of geometric track parameters (after Zwanenburg, 2009).

The defects in the longitudinal level entail greater relevance in the context of this thesis due to their effects on the interaction between the vehicles and the track and on the negative contribution to the degradation of the track. Depending on the wavelength of the defects and on the speed of the vehicles, the train-track system is excited by different frequencies, according to the following expression:

$$f = \frac{v}{\lambda} \tag{2-5}$$

Where f is the excitation frequency of the train-track system (Hz), v is the vehicle speed (m/s) and λ is the wavelength of the track defect (m).

Generally, the closer the excitation frequencies are from the natural vibration frequencies of the vehicle-track system (including its components), the higher the effects of the dynamic interaction between the vehicle and the track. As an example, Table 2-1 shows some values of excitation frequencies depending on the running speed of the vehicle and on the wavelength of the defect.

Table 2-1. Excitation frequencies depending on the wavelength of the defect and train speed.

Running speed							
(km/h)	100	150	200	250	300	350	400
(m/s)	27.8	41.7	55.6	69.4	83.3	97.2	111.1
λ (m)	Excitation frequency (Hz)						
0.1	277.8	416.7	555.6	694.4	833.3	972.2	1111.1
3	9.3	13.9	18.5	23.1	27.8	32.4	37.0
25	1.1	1.7	2.2	2.8	3.3	3.9	4.4
75	0.4	0.6	0.7	0.9	1.1	1.3	1.5

The longitudinal level defects denoting relatively very small wavelengths (λ < 3 m) can induce significant variations in dynamic loads of the vehicles. These effects are normally associated with the following aspects (Figure 2-16a): rail corrugation; wheels with rolling defects; uneven or poorly support conditions of the sleepers on the ballast layer (a phenomenon usually referred to as "hanging sleepers"); poorly executed welds and joints in the rails. The excitation caused by these types of defects is characterized by frequencies above 20 Hz and can have negative repercussions in resonant vibration of unsprung masses of the vehicles (e.g. wheelsets, axle boxes) and the track itself (Figure 2-16b). This type of excitation promotes the rapid degradation of the track and rolling stock.

Track defects with wavelengths between 3 m < λ < 25 m (normally denoted as short wavelength range) are typically associated with resonance phenomena in semi-suspended masses (for example, the bogie and its components) and some components comprising the suspended mass of the vehicle (e.g. the car body). As indicated in Figure 2-16, the suspended mass of vehicles is excited at frequencies between 0.7 and 50 Hz. Consequently, this type of defects reduces passenger comfort level and increases track and vehicle degradation rates.

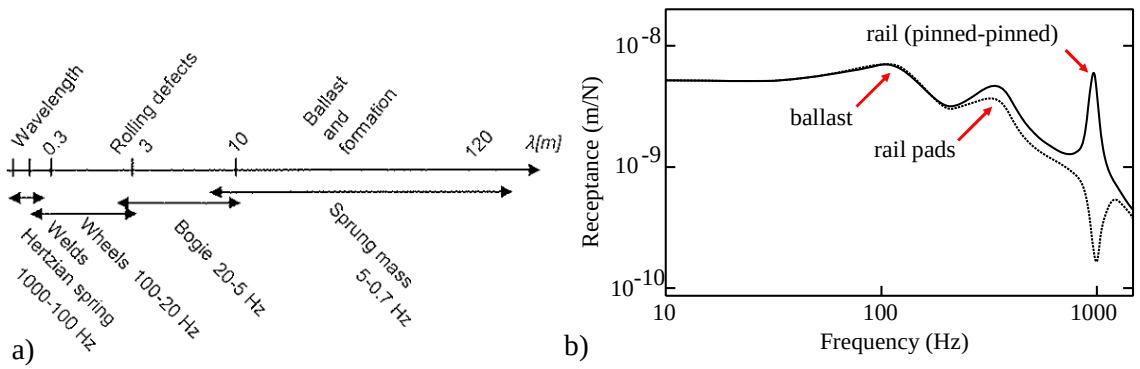

Figure 2-16. Excitation of the train-track system: a) relation between the type and the wavelength of the defects and respective excitation frequencies (Esveld, 2001); b) receptance curve of a track (denoting the track flexibility in the frequency domain) with the identification of the resonance frequencies (after Dahlberg, 2003).

Some defects in the longitudinal level are related to the development of differential settlements that are caused by the variation in the degree of compaction of the ballast layer and in the characteristics of the subgrade that are found along the line. They are characterized by wavelengths of about 7 to 20 m (ERRI, 1975) and can reach amplitudes of several centimetres. In general, the standard deviation of the longitudinal level of a new line in good condition, in the short wavelength range, is around 0.4 to 0.5 mm (UIC, 2008a).

As regards defects with greater wavelengths (λ > 25 m), the effects can lead to resonance of the suspended masses, particularly in trains running at high speeds, and significantly affect passenger comfort.

Advanced methods for the characterisation of the geometric quality of the tracks may also be used. These include: spectral analysis of the defects that relate the amplitudes of the defects with their wavelength; probability distribution functions, correlating wave amplitudes with the probabilities of occurrence; and spatial distribution functions relating frequency and amplitude of the wave with spatial coordinates (Ubalde, 2004; Berawi, 2013). In particular, the Power Spectral Density (PSD) of a given signal denotes its energy in relation to frequency for a given track geometry parameter measured over a given track section. For a track geometric parameter x, the most commonly used formula to calculate the PSD is given by (CEN, 2014):

$$S_{xx}(v) = \lim_{\lambda \to \infty} \frac{1}{\lambda} \bar{X}(v) X(v) \tag{2-6}$$

Where:

λ is the wavelength and ν the respective spatial frequency;

$X(\nu) = \int_{-\infty}^{+\infty} x(\lambda) e^{-i2\pi\nu\lambda} d\lambda$ is the Fourier transformation of $x(\lambda)$;

$\bar{X}(\nu)$ is the complex conjugate of $X(\nu)$.

The PSD curves can be of help for characterising the geometric quality over a section of track or a line for vehicle manufacturers to have a better knowledge of the quality of the track the vehicles will run on and for infrastructure managers to know which defect wavelengths are present on the track. Repetitive defects, such as welds, normally are evidenced by the existence of peaks in the PSD curves. Recent studies have focused on the use of PSD analysis to be implemented by railway infrastructure managers to improve maintenance policies (Berawi, 2013).

2.3.1.3 Geometric quality indexes and intervention levels

Among other aspects, the management of maintenance operations is governed by the level of degradation of the geometric quality of the track. Thus, it is necessary to analyse the records of the inspection vehicles and assess the geometric quality of the track in order to classify the track in quality levels and act accordingly.

Various approaches are currently used by infrastructure managers across the world to classify the quality of the track geometry, termed Track Quality Class in (CEN, 2014). This assessment is based on indexes (commonly designated Track Quality Index - TQI) which reflect the quality of the track calculated using an algorithm that combines the influence of one or a set of geometric parameters. These parameters are related to either isolated track defects or the variance of a given parameter over a specific length of track.

There are a few European and national standards related to track geometry that establish levels of quality and limit values for different geometric parameters of the track, which are relevant to railway lines in Portugal, in particular the EN 13848 series, the Technical Specifications for Interoperability (TSI) and REFER's Technical Instruction VIA 018 - *Tolerâncias dos parâmetros geométricos da via* (REFER, 2009). Three action levels are normally considered regarding the geometric quality in European lines (CE, 2008; CEN, 2008):

- IAL - Immediate Action Limit (formerly denoted as Safety Limit in some documents): refers to the value, which, if exceeded, requires taking immediate measures to reduce the risk of

derailment to an acceptable level. This can be done either by closing the line, reducing speed or by correction of track geometry;

- IL - Intervention Limit: refers to the value, which, if exceeded, requires corrective maintenance in order that the immediate action limit shall not be reached before the next inspection;
- AL - Alert Limit: refers to the value, which, if exceeded, requires that the track geometry condition is analysed and considered in the regularly planned maintenance operations.

Unlike IAL level, which takes into account the track/vehicle interaction, as well as the risk of unexpected events, the intervention and alert limits are mainly linked with maintenance policy (CEN, 2008). For each of these levels, limit values are established for the different parameters of track geometry presented in section 2.3.1.2, which depend on the train speed category. The EN 13484-5 (CEN, 2008) enforces the requirements of the various geometric parameters regarding the IAL action level and recommends a set of tolerance ranges for IL and AL action levels.

The TSI establishes IAL limits for twist, gauge and cant, but not for longitudinal level and alignment. The EN 13848-5 mentions that for lines covered by the high-speed infrastructure TSI, the requirements stated in the HS INS TSI prevail (CE, 2008). The parameters not covered by the TSI need to be compliant with the EN 13848-5. The IAL limits in the TSI are slightly more restrictive than in EN 13848-5. The Portuguese regulation (REFER, 2009) specifies the IL and AL limits, which are in agreement with the range of values suggested in EN 13848-5.

A different classification from levels IAL, IL and AL used in Europe was established by UIC SC 7 G Working Group 'Geometric Parameters', also into three groups: QN1, QN2 and QN3. This classification is taken into consideration in UIC 518 OR (UIC, 2009a) and in EN 14363 (CEN, 2005) in the classification of railway lines used in tests for acceptance of railway vehicles. The classification comprises slightly different categories of speed and different limit values, but the definition of QN1 and QN2 are quite similar to AL and IL, respectively. The definition of level QN3 is different from AIL in that it reflects the most unfavourable maintenance condition but still acceptable for operation.

The former version of the TSI used the classification QN1-QN3, but after the revision it only uses the classification of EN 13848-5 (IAL, IL and AL). It also dropped limits for longitudinal level and alignment.

2.3.2 Track maintenance

The measurement and analysis of the geometric parameters of the track allows evaluating the quality of the construction, of the maintenance and renewal works, as well as the performance of the railway track in service. Besides these aspects, the assessment of geometrical quality also plays a fundamental role in planning and managing maintenance operations by railway infrastructure managers. Usually, the maintenance planning of European railway infrastructure managers is especially oriented by the analysis of the longitudinal level in shorter wavelengths (UIC, 2008a). This approach is based on the analysis of isolated defects as well as on the analysis of the standard deviation of this parameter in a particular stretch of line, typically 200 m long. Due to the rather complex and unpredictable nature of the evolution of the geometric defects, in general, two types of maintenance approaches are considered by railway infrastructure managers (Esveld, 2001; Kobbacy & Murthy, 2008): preventive and corrective maintenance actions.

As regards normal maintenance operations, several types of equipment that have specific functions are used, which have a main objective to correct the track position, tamp the ballast layer and re-establish its cross-section.

Heavy mechanised maintenance equipment is used to restore the track geometric quality, meeting the tolerances established for the various geometric parameters (Figure 2-17): tamping machines; ballast regulators, stabilisers, rail-grinding machines, ballast cleaners, among others. According to the data collected by various European railway infrastructure managers (UIC, 2008a), about a third of the total length of the main lines is submitted to such operations each year.

a) b)

Figure 2-17. General aspect of a maintenance composition with tamping machine, followed by a dynamic stabiliser (a) and detail of the tamping tines penetrating the ballast layer (b) [Photos: Plasser & Theurer].

The tamping and levelling operations of the track consist of successive elevation of the rail and of a small group of sleepers to a desired position, followed by compaction of ballast layer in the area where the track frame was lifted. The compaction of this layer is achieved by a robust mechanism of slender metal spikes, called tamping tines, which are introduced in the ballast layer, on both sides of the rails (Figure 2-17b). When introduced into the ballast layer, the tamping tines apply a simultaneous action of compression and vibration, which enables the rearrangement of the ballast particles under the sleepers and promotes the compaction of the ballast layer. These equipment were introduced in the 60's and since then their manufacturers have been implementing successive improvements.

Immediately after tamping the track, it is observed that the ballast layer does not evidence compaction conditions suitable for the normal train operation. The elevation of the track frame, the insertion of the tamping tines and the compression and vibration actions cause a derangement of the particles of the ballast layer. In practice, it appears that tamping operations drastically reduce the lateral resistance of the track itself. Therefore, dynamic stabilisation of the track is a common procedure to restore or recover part of the lateral resistance of the railway track. This type of operation consists in applying horizontal vibrations on the track in order to rapidly achieve the desired degree of compaction of the ballast, equivalent to that resulting from the passage of about 100 000 tonnes of traffic. Studies on the evaluation of the contribution of dynamic stabilisation to the durability of the geometric quality of the track indicate that this procedure does not produce clear benefits for the reduction of the degradation rates of the geometric quality (UIC, 2008a). Despite these findings, it seems to be consensual that any contribution to increase the structural stability of the track can bring benefits in terms of maintaining its geometric quality.

In high performance railway tracks, grinding operations are of particular relevance with regard to the preventive maintenance approach. These operations may be implemented independently of tamping operations and consist in the removal of a thin surface layer of the rail by abrasive elements. These actions aim to remove small surface irregularities of the rail and minimise the development of corrugation defects, thus contributing to the conservation of the track's geometric quality. In addition to dealing with the defects of the rails, this type of operation has benefits in reducing maintenance costs, reducing emitted noise and increasing passengers' comfort.

Despite the complex systems and the high-performance machinery that has been developed, the intensive use of these equipment is still not sufficient to restore the geometric quality that the track evidences in its initial installation. For this reason, considering for the life cycle of these infrastructures, it appears to be of utmost importance that the initial installation of the track shall be guided by tight requirements of geometric quality.

2.4 Track structural analysis

2.4.1 General aspects

The design of the layers of railway track has traditionally been based on empirical methods rather than following analytical or mechanistic approaches. Throughout history, the thicknesses of the ballast and sub-ballast layers have been determined based on experience and on past practices, according to the usual procedures of the various railway infrastructure managers.

It can be considered that the vertical dynamic actions are a basic parameter for the design of support layers, as well as other components of the track. The actions caused by the passage of the vehicles interacting with the track are relatively difficult to evaluate. Various methods were presented in the past to estimate the vertical loads and some are well known and documented in the literature (Profillidis, 1995; Mira *et al.*, 1999; Esveld, 2001; López Pita, 2006), as that of Prud'Homme (1970) presented earlier in section 2.2. Many of these methods are only rough approximations and, simply, consist in determining a dynamic amplification coefficient that is applied to the static loads of the axles.

One of the first approaches developed with the aim of assessing how the vehicle loads were transferred to the track structure was proposed by Winkler in 1867 with the introduction of a model of an infinite beam embedded in elastic medium (Figure 2-18).

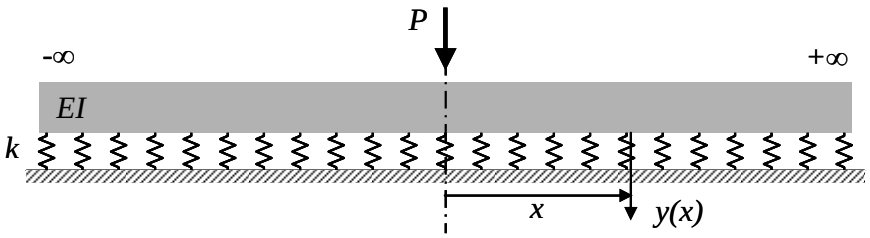

Figure 2-18. Schematic representation of an infinite beam supported on elastic medium: *P* is the axle load; *x* is the axle position; *y* is the rail deflection; *k* is the foundation coefficient; *EI* is the bending stiffness of the rail (adapted from Esveld, 2001).

Over the following decades, various methods using this approach were developed and improved to evaluate the deformations and stress levels at various depths of the track, mostly comprising an empirical or semi-empirical approach (López Pita, 2006). In the second half of the 20th century, with the dawn of high-speed railway services, there was a need to reassess the design methods of railway tracks and evaluate the extent to which old practices were adequate to this new type of transport with

more demanding requirements. Taking advantage of the existing knowledge concerning the behaviour of road pavements and design methods, some railway infrastructure managers incorporated some of this information into their design regulations. Old classic design methods were somewhat replaced with newer approaches such as multi-layered elastic models. Consequently, catalogues of track configurations were adopted by several railway infrastructure managers. Among other aspects, this new design paradigm also highlighted the need to provide a number of intermediate layers to allow for the stress reduction with depth down to the layers below.

Since the use of computers with increased capacity, advanced numerical methods become very useful to provide insight into the track behaviour and to investigate particular aspects of the track response. Currently, continuous element methods (e.g., Finite Element Method - FEM, Finite Difference Method - FDM) are extensively used in the analysis of numerous railway aspects. More recently, advances in numerical models in discontinuous media (Bobet *et al.*, 2009), such as the Discrete Element Method - DEM, appear to have great potential for the study of tracks comprising granular material.

2.4.2 Advanced numerical methods

Aiming at contributing to the optimisation of the design of track configurations, with respect to its mechanical and geometrical characteristics, advanced numerical models have been used with increasing complexity, thus achieving a better representation and understanding of the track behaviour, as well as of its components.

The rise of advanced numerical methods have been particularly suitable for modelling the geometry and boundary conditions of the structure, the characteristics of the various materials that make up the system and the actions. Moreover, they allowed the introduction of different constitutive laws, such as non-linear and/or plastic formulations to represent the material behaviour. Over the past decades, several models have been used to study the behaviour of the track under vertical loads imposed by trains (Tarabji & Thompson, 1976; Prause & Kennedy, 1977; Adegoke *et al.*, 1979; Chang *et al.*, 1980; Sauvage & Larible, 1982; Huang *et al.*, 1984). In these studies, the results were somewhat different from each other, as evidenced in Figure 2-19.

In part, the differences that have been observed between the results obtained with the numerical modelling are due to different simplifications adopted to represent the track geometry, the different formulations to simulate the behaviour of the materials and the adopted numerical methods to solve the problem.

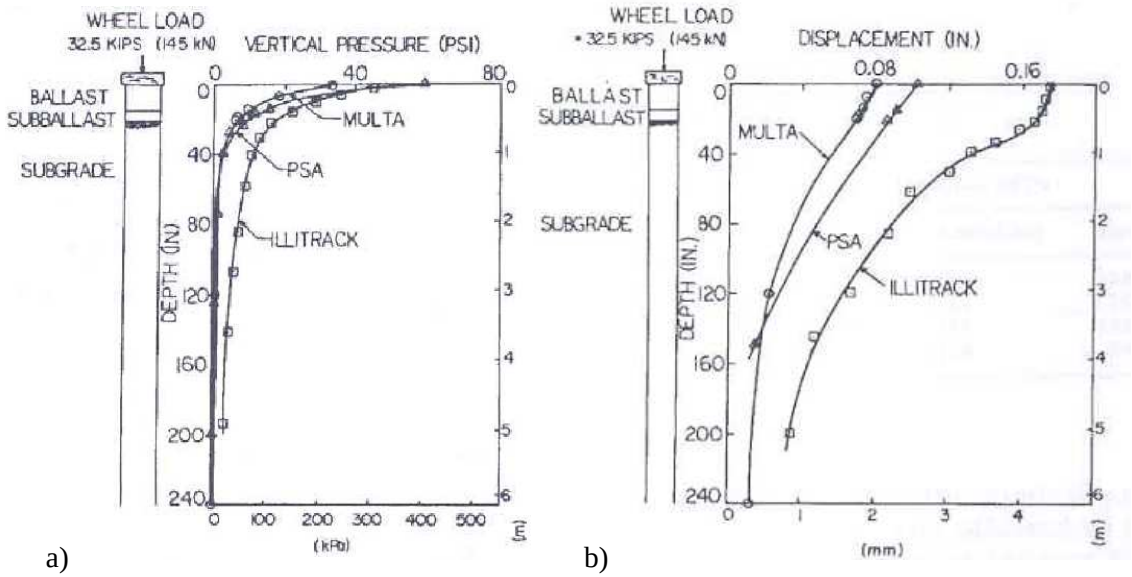

Figure 2-19. Comparison of the results obtained with different numerical models: MULTA, PSA, ILLITRACK (Adegoke *et al.*, 1979).

Developments in numerical modelling have allowed obtaining results closer and closer to reality. The intensive use of these methods allowed the development of several parametric studies, as well as, building diagrams that describe the relationships between the relevant variables (ERRI, 1983; Li & Selig, 1998; Mira *et al.*, 1999). Some of these results have been used to develop procedures for design of support layers of the track, for example, the UIC Code 719R (2008b).

Additionally, following the advances in the understanding of the behaviour of geomaterials (Lekarp *et al.*, 2000a, b), such information was possible to be incorporated into more sophisticated numerical models (Suiker, 2002; Fortunato & Resende, 2006; Paixão & Fortunato, 2009a), allowing to simulate the nonlinear elastic response of the materials and the development of plastic deformation in the support layers. The results obtained taking into account the different formulations of material behaviour can be significantly different.

Considering the increasing speeds of railway vehicles and the importance of this factor in the response of the train-track system, advances have been observed in numerical methods to perform dynamic simulations of the interaction between vehicles and the track. Most numerical studies found in the literature that take into account the train-track interaction, consider the linear elastic behaviour of the materials and study the problem in the frequency or time domains. An extensive review on the evolution of train-track interaction models and its application can be found in Popp *et al*. (1999; 2005), Dahlberg (2003), Ferreira (2008) and Vale (2010). Over the last decades, a large range of numerical

models for dynamic analysis have been developed from simple approaches of beams on elastic foundation models (Figure 2-20a) to more advanced three-dimensional models, representing the track components and layers with more detail (Figure 2-20b).

The complex numerical models that consider the dynamic behaviour of the train-track system are of special interest in scope of this thesis. These approaches can contribute to the understanding of the track behaviour, in particular in areas evidencing abrupt changes in vertical stiffness and accelerated degradation.

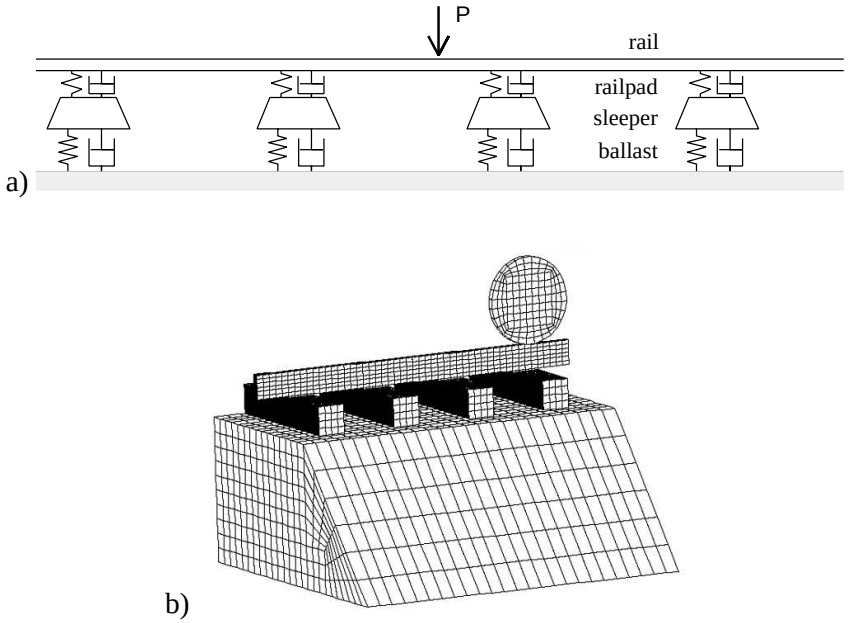

Figure 2-20. Aspects of railway track numerical modelling: a) simple beam-spring model (Dahlberg, 2003); b) three-dimensional modelling of the track with a more detailed representation of the components and layers (symmetry with respect to the centre line) (Lundqvist *et al.*, 2006).

2.5 Characterisation of materials and assessment of track behaviour

To fully benefit from structural numerical models, it is necessary to have adequate information concerning the behaviour of the materials. In addition, it is important to evaluate the response of the structures to the actions in order to assess the suitability of those models.

The information on the performance of the track and the behaviour of the materials should result from characterisation works that can be developed in laboratory testing, with *in situ* testing and with monitoring campaigns. If possible, this characterisation should be developed both at the superstructure and substructure levels of the track.

2.5.1 In situ characterisation of the track behaviour

The *in situ* characterisation of the behaviour of the substructure can be carried out during construction, preferably using non-destructive testing (Fortunato, 2005; Burrow *et al.*, 2007b; Puppala, 2008), using various techniques such as falling weight deflectometers (Figure 2-21a), plate load tests (Figure 2-21b) and the *portancemètre* (Figure 2-21c).

a) b) c)

Figure 2-21. Aspects of non-destructive tests for the characterisation of track support layers: a) falling weight deflectometers; b) plate load tests; c) *portancemètre*.

In general, these tests consist of applying a vertical load (static or dynamic impulse) on top of the layers to be studied and measuring the resulting deflection at the surface. The results obtained with these tests allow for the assessment of the stiffness of the layers, a parameter that is correlated to the deformation modulus, associated with a particular testing method. Some authors (Fortunato, 2005) highlight the fact that the measurement of the vertical deformation of the substructure layers, can vary significantly at a given location depending on the testing method that is used.

The *in situ* geophysical characterisation methods, for example the Surface Wave Methods (SWM), are less common characterisation alternatives that, due to their non-destructive and expeditious application, are also relevant for the characterisation of large structures with linear development, such as railway infrastructures (Fortunato, 2005; Alves Costa, 2011).

As regards the track structure as a whole (substructure and superstructure), its response also depends on the characteristics of the acting loads, such as the amplitude and loading frequency. It responds in a wide range of frequencies depending on its configuration and characteristics of the components/layers (Esveld, 2001; De Man, 2002) (see also Figure 2-16): i) the low frequency range (about 0-40 Hz) is normally governed by the physical and mechanical properties of the substructure; ii) the mid frequency range (about 40-400 Hz) depends on the properties of the components of the superstructure,

excluding the rail; iii) the high frequency range (400-1500 Hz) is normally governed by the properties of the rail and sleeper spacing.

The response of the track to different frequencies can be assessed by means of transfer functions (frequency response functions) that correlate the frequency content of load impulses with the frequency content of the track response, for example, in terms of displacements, velocities or accelerations, that correspond, respectively, to the receptance (Figure 2-22), admittance (or mobility) and inertance functions (De Man, 2002). The receptance function is normally considered in the dynamic characterisation of the track and can be described as:

$$H_{wF}^2(f) = \frac{S_{ww}(f)}{S_{FF}(f)} \tag{2-7}$$

Where: f is the vibration frequency (Hz); $H_{wF}(f)$ is the complex transfer function from force to displacement (m/N); $S_{ww}(f)$ and $S_{FF}(f)$ are the autospectra of the displacements (m^2s) and of the force (N^2s), respectively, which can be obtained by means of Discrete or Fast Fourier Transform (DFT/FFT) of discrete time recordings.

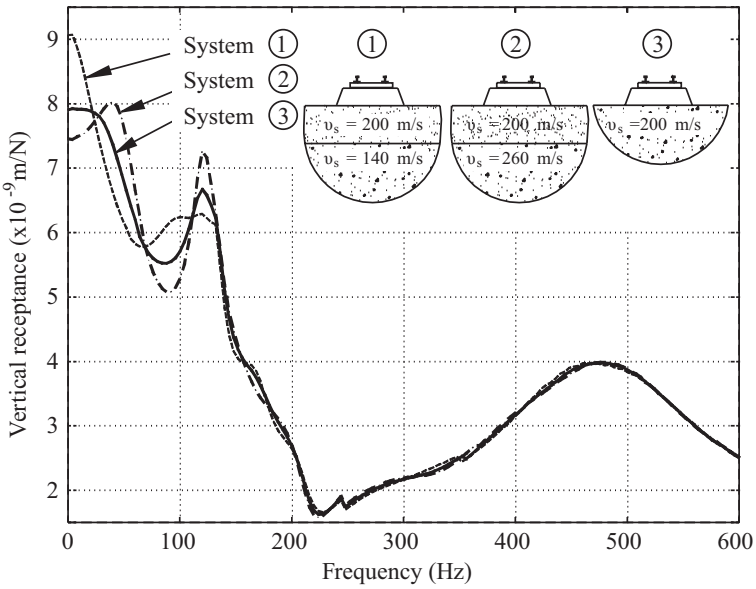

Figure 2-22. Receptance curves of numerical models evidencing the influence of the track substructure in the dynamic behaviour (v_s is the wave propagation speed) (Knothe & Wu, 1998).

Receptance tests are normally performed on the track using instrumented impact hammers with load transducers and using accelerometers on the rails and sleepers (Figure 2-23). The test makes it possible

to determine the track flexibility in the frequency domain and estimate the resonance frequency of the principal track vibration modes that are schematically depicted in Figure 2-24.

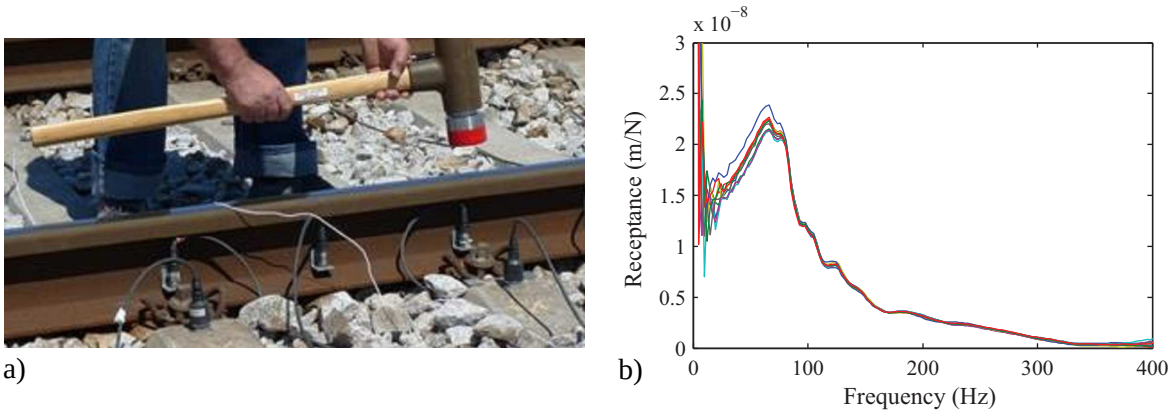

Figure 2-23. Aspects of receptance test on the track (Alves Ribeiro, 2012): a) instrumented hammer and accelerometers on the rails and sleepers; b) examples of successive receptance functions obtained on the same position.

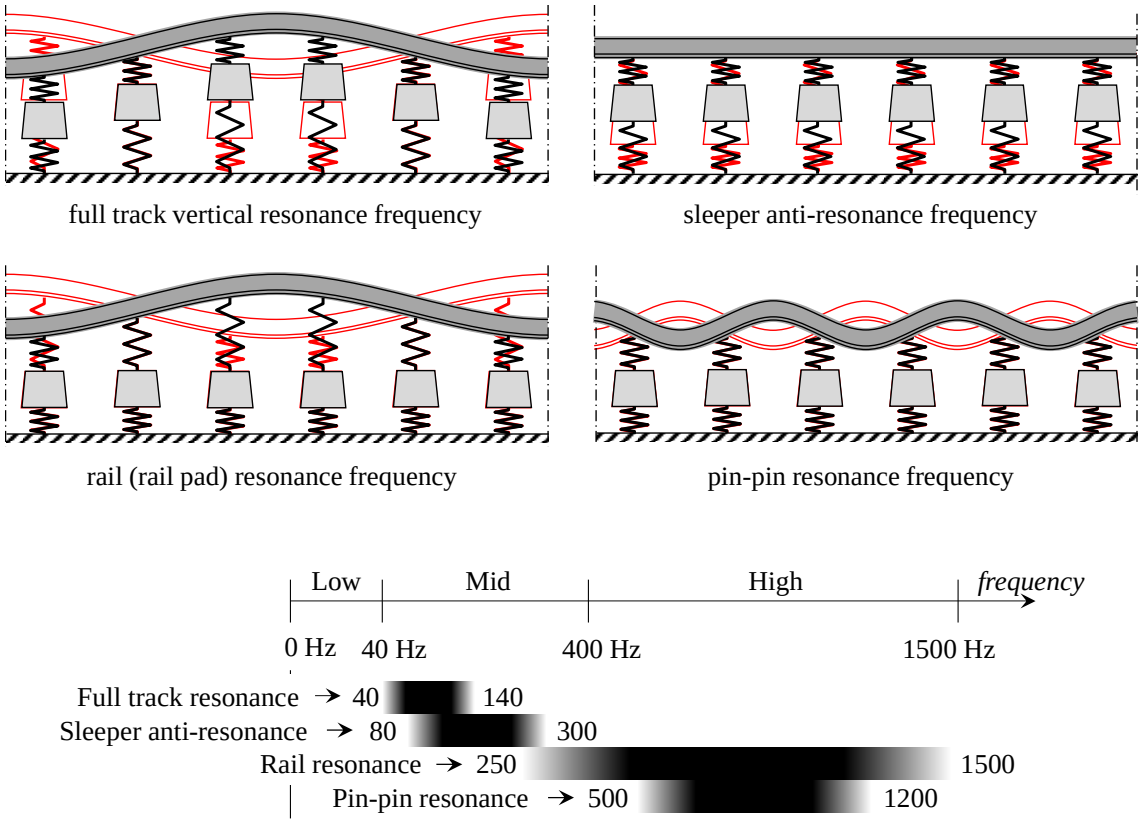

Figure 2-24. Vibration modes and respective resonance frequency ranges commonly found in ballasted tracks (after De Man, 2002).

The determination of the stiffness of the layers under variable loading amplitudes and frequencies, using several characterisation methods and for different state conditions of the geomaterials, allows to assess the quality of the layers and track components and to obtain relevant parameters for numerical modelling, providing insight into the behaviour of the track (Alves Ribeiro, 2012).

Regarding additional *in situ* characterisation methods of the railway track, there have been important advances in measuring techniques of the vertical stiffness of the track. Some approaches uses prototypes vehicles that vertically excite the track while running at moderate velocities and evaluate the respective track response (Berggren, 2005; INNOTRACK, 2008; Berggren, 2009; Hosseingholian *et al.*, 2009; With & Bodare, 2009; Quibel *et al.*, 2010). One method that uses a modified vehicle developed in Sweden (Berggren, 2005, 2009) consists of a two-axle wagon with a static load of 180 kN which was modified with the installation of two masses of 4000 kg on the vertical alignment of one of the axles (Figure 2-25). Hydraulic actuators mounted on the vehicle force these masses to oscillate at frequencies between 3 and 50 Hz, thus allowing for maximum dynamic load amplitudes of 60 kN. Using the data from load transducers and accelerometers positioned on the loaded wheelset, it is possible to estimate the vertical stiffness of the track.

a)

b) 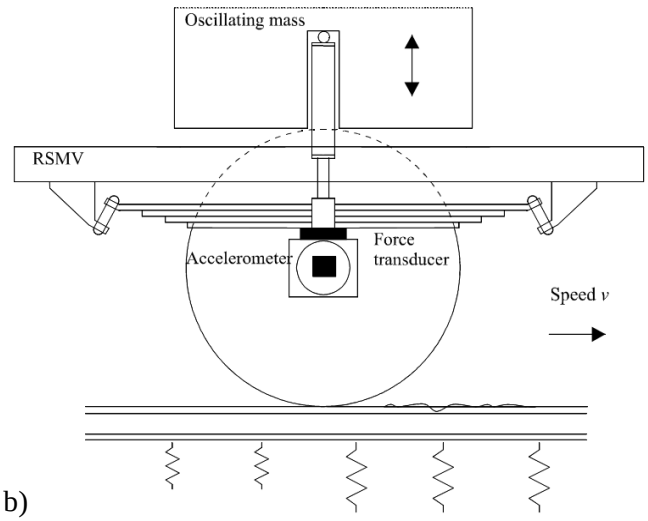

Figure 2-25. Rolling Stiffness Measurement Vehicle: a) aspect of the modified structure; b) working principle (Berggren, 2010).

To evaluate the dynamic performance of the railway system, it is essential to monitor the behaviour of the track and of the vehicles, as well as the interaction between the two. In this context, several

experimental studies focusing on the track stiffness and on the train-track interaction have been developed in the past years (Kaynia *et al.*, 2005b; Suzuki *et al.*, 2005; Kaynia & Clouteau, 2007; Cuéllar *et al.*, 2009; Lozano del Moral & Cuéllar, 2009; Coelho *et al.*, 2011; Alves Ribeiro, 2012; Pinto *et al.*, 2013). In general, these studies comprise significant instrumentation works of the track components, in order to characterise the behaviour of the track during the passage of the trains by measuring several physical parameters using: strain gauges on the rail web to determine dynamic wheel loads acting on the rail and rail seat loads (Figure 2-26a); accelerometers (Figure 2-26b) and geophones (Figure 2-26c) to evaluate the motion of different track components; displacement transducers to determine relative and absolute displacements of the various track components (Figure 2-26d).

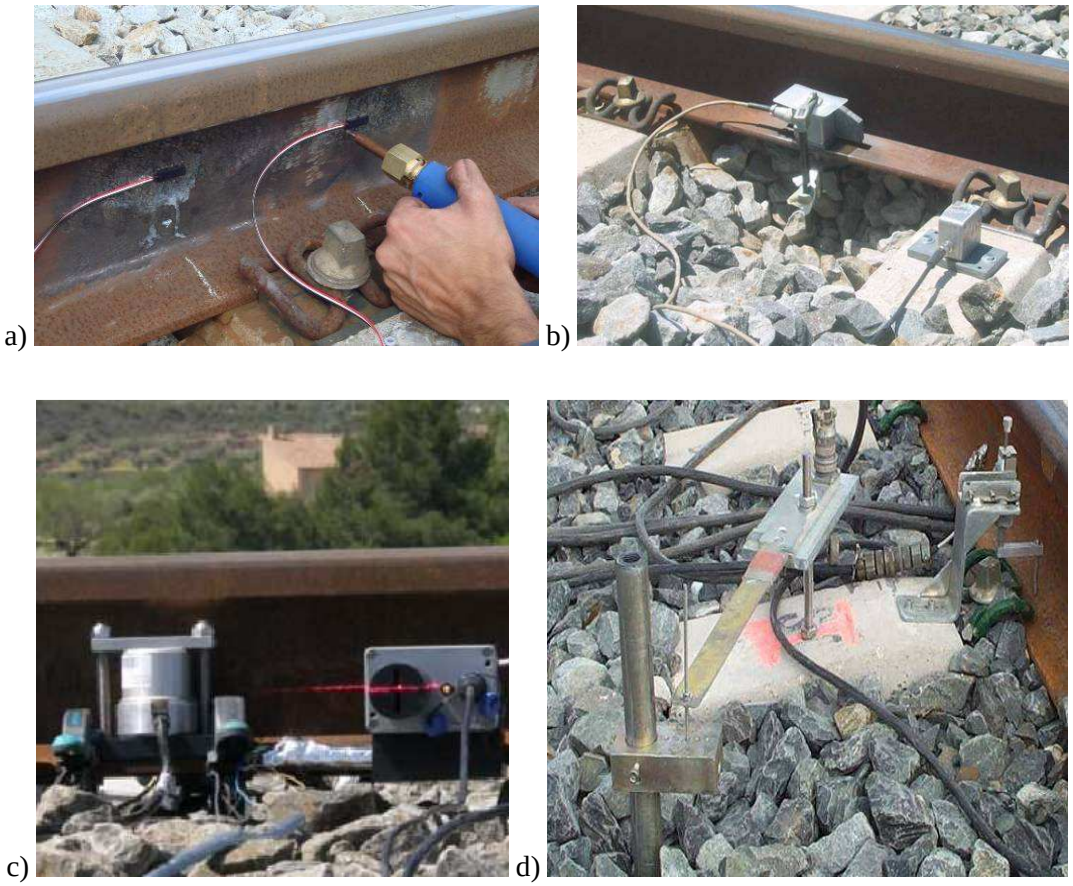

Figure 2-26. Track instrumentation: a) welding strain gauges on the rail web to assess dynamic loads from the vehicles (Alves Ribeiro *et al.*, 2010); b) accelerometers fixed to the rail and sleeper (Kaynia *et al.*, 2005b); c) geophone and LASED-based displacement transducer (Lozano del Moral & Cuéllar, 2009); d) transducers to measure relative displacements between the rail and sleepers and between the sleeper and the capping layer (Kaynia *et al.*, 2005b).

As regards the study of the long term behaviour of railway tracks on earth structures, the methods used in the observation of embankments (Fortunato et al., 2000; Pardo de Santayana et al., 2006) may be of particular interest in monitoring permanent settlements of the track structure. Topographic surveys and inclinometers have traditionally been used to monitor the evolution of permanent settlements in earth structures. These systems can be applied in transport infrastructures for the same purpose (Machan & Bennett, 2008).

2.5.2 Laboratorial characterisation of track components and geomaterials

Given the large contribution of resilient components of the superstructure (rail pads and, eventually, under sleeper pads and ballast mats) in the dynamic behaviour of the track and its vertical stiffness, the laboratory characterisation of the behaviour of these components may be particularly relevant (Carrascal *et al.*, 2007; UIC, 2009b). The characterisation of physical and mechanical properties of these components is essential to predict the behaviour of the track and obtain relevant information for application in numerical models.

As regards the aggregates used in the track layers, the laboratorial characterisation of these materials has been preferably carried out using a cyclic load triaxial testing on cylindrical samples (Werkmeister *et al.*, 2001; Suiker *et al.*, 2005; Indraratna *et al.*, 2010). The resilient and permanent deformation of these materials depend on many factors, both intrinsic and external parameters including the water content conditions and the stress level acting on the material (Lekarp *et al.*, 2000a, b; Fortunato, 2005). Using this type of laboratory testing it is possible, albeit with some limitations, to simulate the conditions to which the materials are submitted in the track and reproduce the long-term behaviour of the layers, by applying a large number of load cycles on properly instrumented specimens (Figure 2-27). Among other aspects, these tests allow the establishment of models to simulate the resilient behaviour (Boyce, 1980) and the permanent deformation (Gidel *et al.*, 2001), thus to predict the behaviour and performance of different railway track configurations. However, although it is possible to obtain relevant information using such laboratorial characterisation, this approach is not used often because there are difficulties associated with the duration of the tests (particularly when studying the permanent deformation of the materials) and the specificities of the method (Brecciaroli & Kolisoja, 2006).

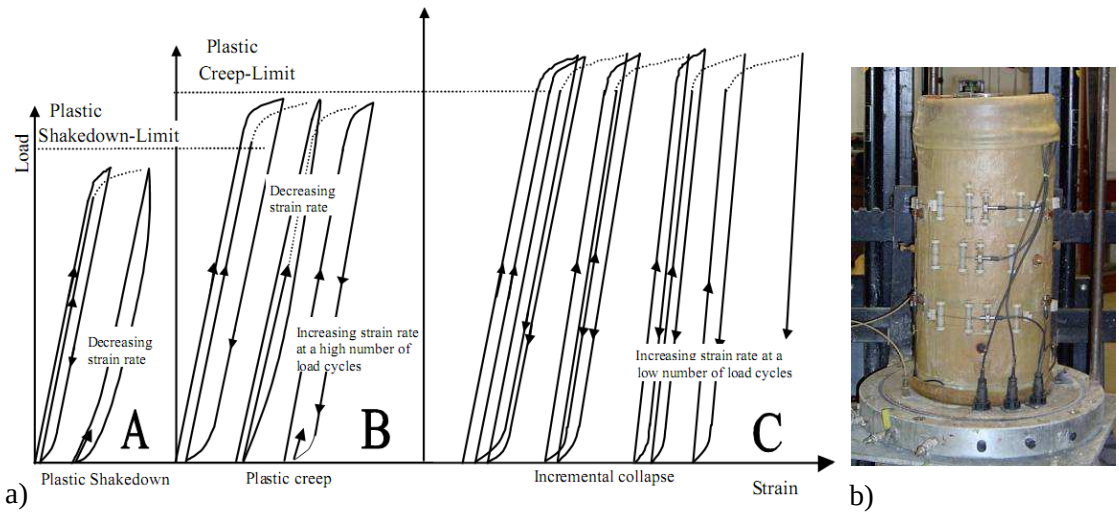

Figure 2-27. Cyclic load triaxial tests on specimens of unbound granular material: a) model of the behaviour of granular materials (Werkmeister *et al.*, 2001); b) aspect of large specimen with local instrumentation (Fortunato, 2005).

2.5.3 Physical modelling of the structure

Over the years, there have been several attempts to reproduce the structure of the railway, its foundation and the dynamic loads imposed by trains in laboratory. Recent and relevant examples of full track physical models include the one built by the *Centro de Estudios y Experimentation of Public Works* (CEDEX) in Spain (Figure 2-28a) within the scope of the European project SUPERTRACK (Kaynia *et al.*, 2005a) and the "Geopavement & Railway. Accelerated Fatigue Testing" (GRAFT I and II) (Figure 2-28b) built by the Heriot Watt University in the United Kingdom (Kennedy *et al.*, 2012; Percival *et al.*, 2013). The results obtained with these physical models have permitted to validate innovative technologies for railway track configurations as well as to validate and calibrate some numerical models.

Other research teams have developed studies using partial models of the track, similar to that shown in Figure 2-28c to analyse the specific aspects of its behaviour (Indraratna & Salim, 2005; INNOTRACK, 2006; Thom, 2006; Baessler, 2008; Powrie & Le Pen, 2008). Evidently, these partial models have the advantage of mobilising fewer resources but their applicability may be limited because they cannot fully reproduce the behaviour of the track. Reduced models of the railway track have also been developed in the past, for example by the *Laboratoire Central des Ponts et Chaussées* (LCPC) in France (Al-Shaer *et al.*, 2008), using a reduced scale model of 1 to 3 to study the dynamic behaviour of the track (Figure 2-28d). This study emphasised that the dynamic behaviour of the railway can be quite distinct from its static behaviour and the vertical stiffness of the railway can vary

substantially with the accumulation of load cycles. The vertical acceleration measured on the sleepers and in the ballast layer can be used as indicators for predicting the evolution of these settlements.

Figure 2-28. Aspects of physical models built in laboratories: a) full model of the track constructed in CEDEX, Spain; b) GRAFT II in Heriot Watt University, UK (Percival *et al.*, 2013); c) partial model with half sleeper (INNOTRACK, 2006); d) small scale model (Al-Shaer *et al.*, 2008).

Finally, compared to *in situ* characterisation methods, laboratory physical modelling has several advantages with regard to repeatability and reproducing different settings. However, some aspects that characterise the complex behaviour of the track, for example the density of the ballast layer, are hardly adequately reproduced in the laboratory, which in some circumstances may affect the validity of the results obtained in laboratory.

Chapter 3

Transition zones to railway structures*

3.1 Introduction

The initial geometry of the railway track degrades throughout its life cycle. Changes in the track alignment give rise to dynamic axle load variations, accelerating the track degradation, with consequences in maintenance and availability of the line. This behaviour is particularly evident at some critical locations that are associated with abrupt changes in track vertical stiffness, such as transitions to bridges or other civil engineering structures (e.g. viaducts, underpasses, culverts, tunnels). In order to mitigate the problem, careful design and construction is required, for which several recommendations have been suggested. However, studies based on the maintenance records of existing high-speed railway lines (HSL) have shown that track degradation associated with stiffness variations are far from being solved.

This chapter presents a review on railway transition zones, focusing on the designs of backfills at the approach to civil engineering structures and between different track configurations, for example, between ballasted track to slab track. A brief state-of-the-art is also presented focusing on the numerical modelling of railway tracks at transition zones, addressing different studies and highlighting the respective advantages and disadvantages.

* This chapter has the contribution of the following journal articles:

- **Paixão, A.; Fortunato, E. & Calçada, R.** (2013) *Design and construction of backfills for railway track transition zones*; Proceedings of the Institution of Mechanical Engineers, Part F: Journal of Rail and Rapid Transit;
- **Fortunato, E.; Paixão, A. & Calçada, R.** (2013) *Railway Track Transition Zones: Design, Construction, Monitoring and Numerical Modelling*; The International Journal of Railway Technology; Vol. 2; n.º 4; p. 33-58; 2049-5358;

3.2 General aspects

The experience of the railway industry shows that in normal ballasted railway tracks, resting on foundations with adequate bearing capacity and after the initial stabilisation of the supporting layers, it is the ballast layer that contributes most significantly to the degradation of the geometric quality of the track (Selig & Waters, 1994; UIC, 2008a). When necessary and in response to this track behaviour, railway infrastructure managers carry out maintenance operations to restore adequate quality levels of track geometry. To enable more efficient management of railway operation, studies have been developed and several empirical relationships using simplistic approaches have been proposed to predict the track degradation behaviour (ORE, 1970; Dahlberg, 2001).

One of these approaches has been presented by Fröhling (1998) and suggests an expression for the track settlement that relies on field measurements and on a numerical model considering the train-track dynamic interaction, aiming at contributing to a better understanding of the relationship between the spatial variation of the track stiffness and its deterioration. Among other aspects, the validated mathematical model considers the dynamic vehicle loading and non-linear, spatially varying track stiffness. The suggested expression has the following form:

$$\varepsilon_{N_i} = \left[\left[K_1 + K_2\left(\frac{k_{2mi}}{K_3}\right)\right]\frac{P_{dyn}}{P_{ref}}\right]^w logN \tag{3-1}$$

Where:

- ε_{N_i} is the ballast permanent deformation;
- k_{2mi} is the measured average track stiffness at a particular sleeper;
- K_1 and K_2 define a linear approximation between the deviator stress and the track stiffness as calculated with the a numerical model;
- K_3 is the constant factor by which the calculated track stiffness differs from the measured track stiffness;
- P_{dyn} and P_{ref} are the dynamic and reference wheel loads, respectively;
- w is a calibration exponent and N is the number of loading cycles.

In the study resulting from the application of this model, it was concluded that the spatial variation of the track vertical stiffness contributes significantly towards the track deterioration, both in terms of differential track settlements and increased dynamic wheel loads.

The experience regarding the operation of conventional or high-speed railway lines evidences that, at some locations, the degradation process of the track is clearly faster than normal and the

empirical degradation relationships to predict settlements no longer seem to apply. At these locations, maintenance operations are required more often to re-establish proper geometric quality of the track and to maintain adequate passenger comfort and safety levels, thus affecting normal operation of the railway lines. Moreover, these locations usually correspond to specific singularities in the track, which in general evidence vertical stiffness discontinuities (see Figure 3-1) associated with changes in the track superstructure (rail, fastening system, sleeper, ballast, switches, rail expansion joints) or in the substructure, such as at the approaches to bridges (Berggren, 2009; Dahlberg, 2010b). In the literature, the stretches of railway track where these changes occur are commonly designated “Transition Zones”.

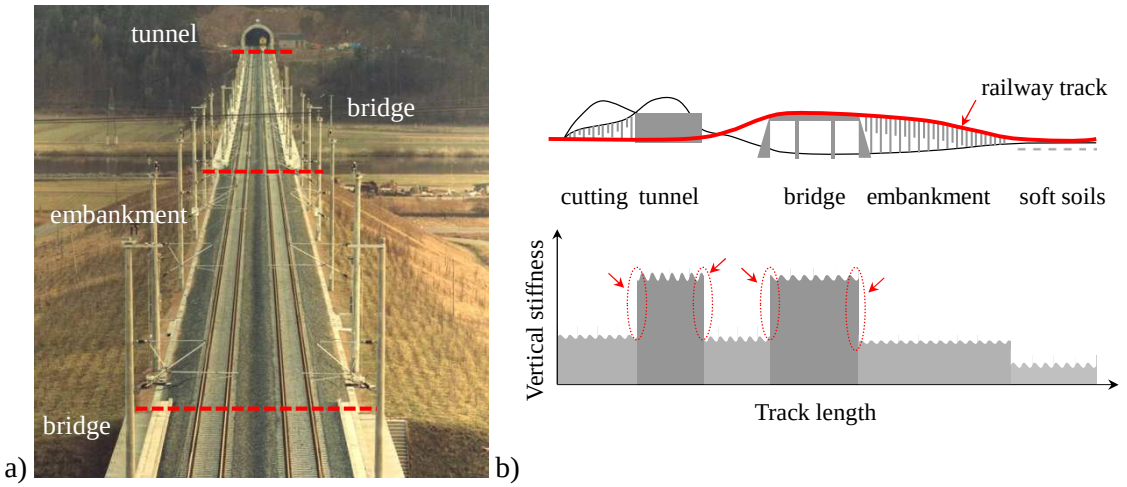

Figure 3-1. Discontinuities in the track support conditions: a) example of sucessive changes in the substructure; b) schematic representation of the variations in the vertical stiffness of the track (adapted from Frühauf *et al.*, 2008).

Situations of rapid track degradation at transition zones have been reported in studies developed in Spain on the analysis of the data from maintenance operations between 1992 and 2002 in the Madrid-Seville HSL (Ubalde, 2004). The analysis of the results showed that maintenance works at transition zones to bridges or to culverts were up to three or six times more frequent, respectively, when compared with open track. Earlier European studies pointed out that maintenance frequency at these locations may be five times higher and unit costs twice as high, because standard maintenance procedures cannot be applied (ERRI, 1999).

3.3 The problem at transition zones to bridges and other structures

Already in the 70's some European authors addressed the negative aspects of the track behaviour at transition zones. The causes were reported to be related to: i) variations in the track vertical stiffness; ii) displacements and rotations of the bridge deck; iii) differential settlements at the transition zone. It was also noted that all these aspects contributed to the increment of the dynamic load of the trains (Eisenman & Leykauf, 1977). More recently, as referred to in the literature and as evidenced with field measurements, important amplifications of the dynamic loads of the trains have been identified at these zones (Figure 3-2), in particular, vertical wheel-rail interaction forces (Namura & Suzuki, 2007; Plotkin & Davis, 2008; Dahlberg, 2010b; Alves Ribeiro, 2012; Banimahd *et al.*, 2012).

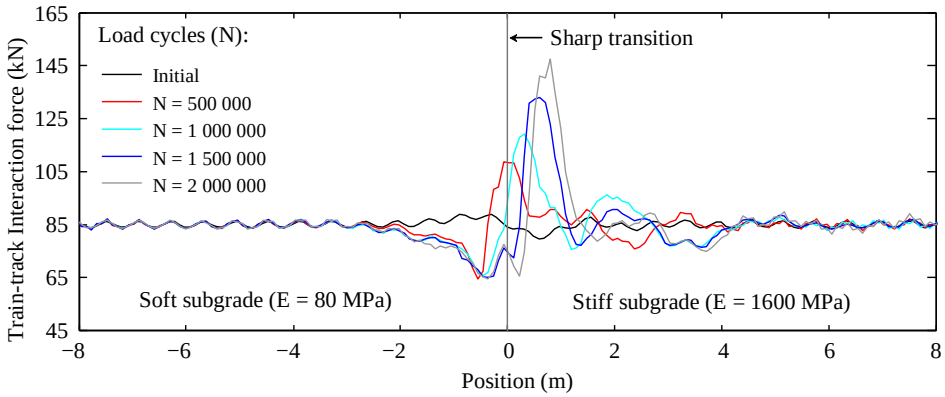

Figure 3-2. Numerical results of the dynamic amplification due to track degradation with the number of load cycles at transition zones (after Alves Ribeiro, 2012).

Severe cases of accelerated degradation can be caused by various factors and amplified by their combination, as observed recurrently at transitions between embankments and structures. Despite all the studies that were developed and probably due to the complexity of the problem, there is not an overall consensus on the main factors that trigger the deterioration of the track at transition zones, forming the well-known “dip” and “bump” longitudinal rail profiles (Figure 3-3).

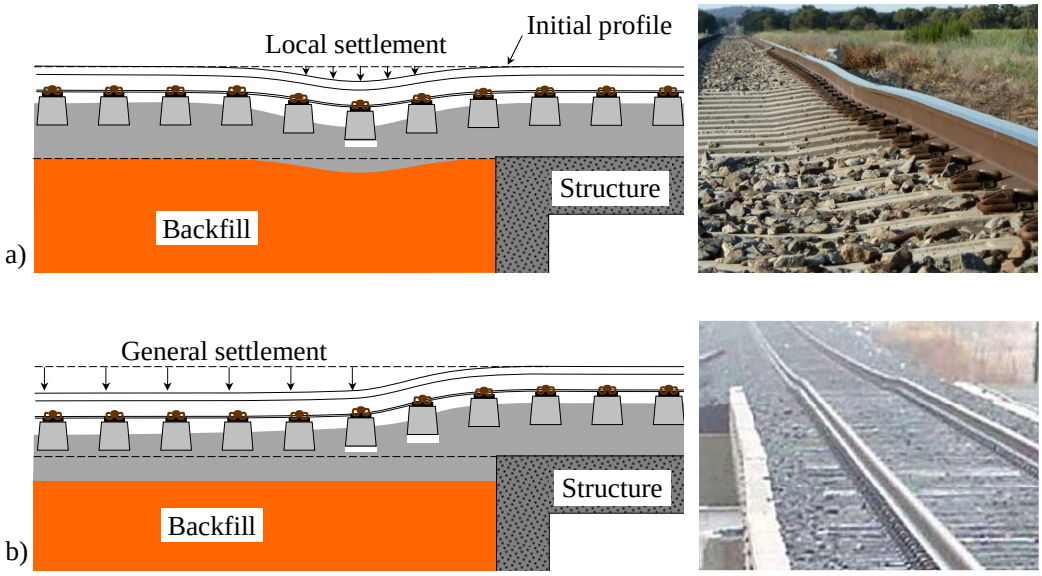

Figure 3-3. Schematic representation and respective examples of excessive uneven rail profiles: a) dip (photo: ATSB, 2014); b) bump (photo: Read & Li, 2006).

Although the sources of the problem are yet to be fully understood, it has been attributed to two main factors (ERRI, 1999; Dahlberg, 2010b; Banimahd *et al.*, 2012):

a) Rapid variations in track stiffness, due to different mechanical characteristics of the materials in the superstructure or substructure (Figure 3-4a). This causes differential elastic track deflections which result in increasing dynamic loads that can trigger localised degradation (Figure 3-2);
b) Important differential settlements of the track and its foundation (considering that no significant settlements are expected in the abutments or other structures) yield longitudinal level defects and also increase the dynamic loads and cause further damage (Figure 3-4b). The differential settlements are largely caused by the plastic behaviour of geomaterials, particularly the ballast layer, under the action of cyclic loads of trains, but also due to the consolidation of the track substructure (Selig & Waters, 1994). This factor can lead to severe cases of geometry defects at the approaches to the structures, with the deterioration of support conditions for a few sleepers at the transition, as depicted in Figure 3-4b. In fact, unsupported sleepers can also be regarded as localised abrupt reduction of track stiffness, thus aggravating even more the difference between the track stiffness on embankment and on bridge, and further increasing the track degradation rate (Lundqvist & Dahlberg, 2005; Varandas, 2013).

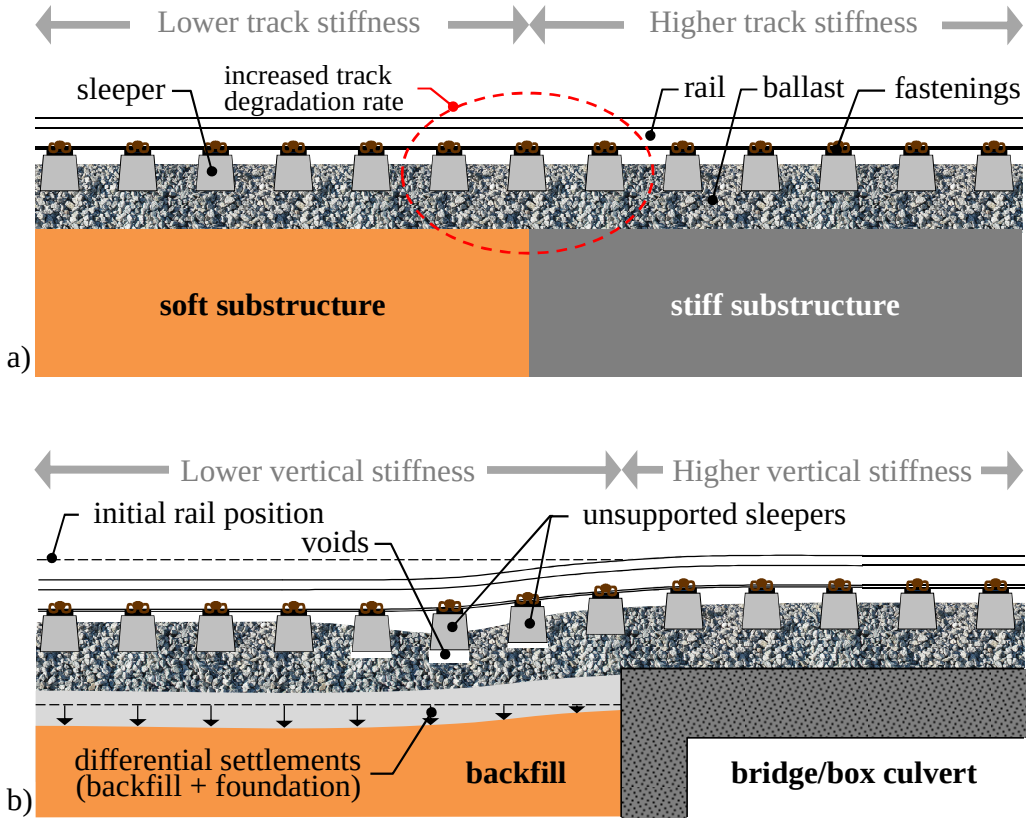

Figure 3-4. Schematic representation of causes for rapid track degradation at transition zones.

These two factors can severely amplify the dynamic train-track interaction if the transition zone is not properly designed or/and the track is poorly maintained. In such scenarios, the train wheels and the track degrade at a faster rate, the levels of passenger comfort decrease and the risk of derailment may arise (Li & Davis, 2005; Namura & Suzuki, 2007; Dahlberg, 2010b; Banimahd *et al.*, 2012).

Normally, to address this problem (Figure 3-5a), railway infrastructure managers carry out costly maintenance operations, adding more ballast and tamping the track in order to re-establish its adequate geometry (ERRI, 1999; Ubalde, 2004; López Pita *et al.*, 2006; Nicks, 2009). However, these operations reduce the track availability, moreover, it is known that frequent tamping operations increase the ballast degradation rate and the excessive depth of the ballast layer (Figure 3-5b) may reduce the lateral resistance of the track (Esveld, 2001; Melis Maynar, 2006).

a) b)

Figure 3-5. Track defect at the approach to structues: a) example of uneven rail profile (Read & Li, 2006); b) excessive depth of ballast to account for backfill settlements (Melis Maynar, 2006).

Over the past decades, several studies have focused on transition zones to structures in order to understand the processes involved in accelerated track degradation and to minimise its negative effects (ERRI, 1999; Kaynia *et al.*, 2005a; Read & Li, 2006; Plotkin & Davis, 2008; Cuéllar *et al.*, 2009; Nicks, 2009; Alves Ribeiro, 2012). Briaud et al. (1997) identified some mechanisms that limit the performance of these zones in road infrastructures, as summarised in Figure 3-6.

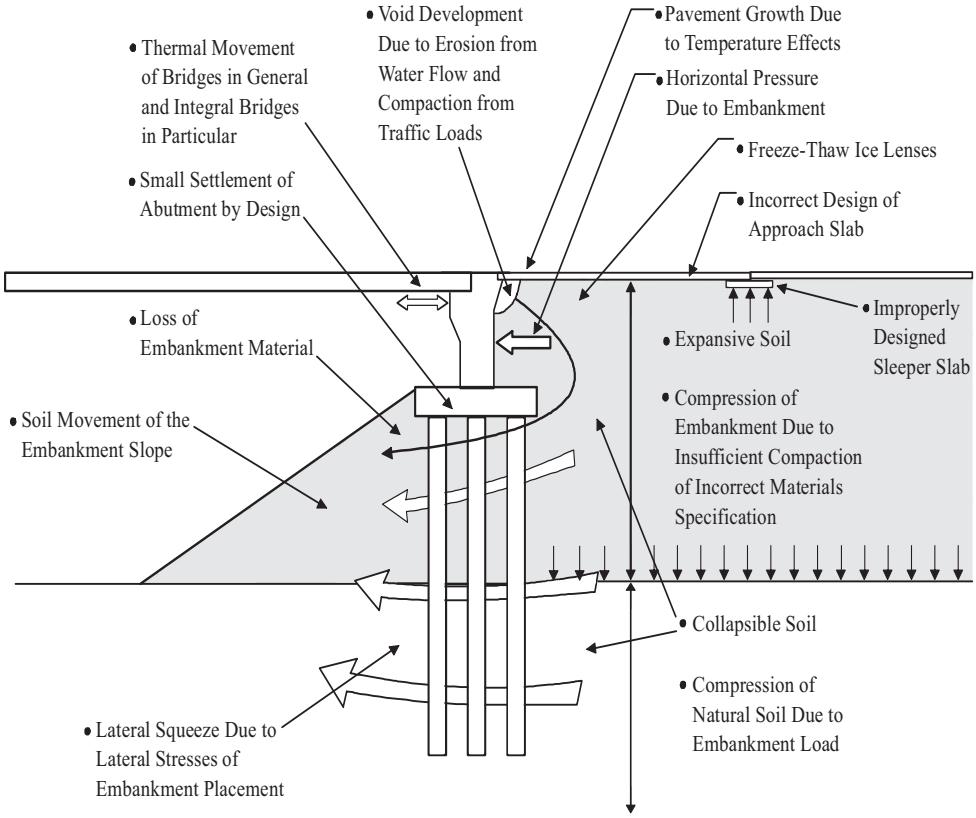

Figure 3-6. Factors that affect the performance of approaches to road bridges (Briaud *et al.*, 1997).

3.4 Countermeasures for transition zones

Several railway entities have identified the above problems and have suggested constructive measures to control the rapid degradation of the track, to smooth the abrupt stiffness transitions and to minimise differential settlements (UIC, 2008b). Most of the recent designs for transition zones between embankments and bridges or other civil engineering structures have in common a wedge-shaped backfill with well-compacted layers made of bound and unbound granular material (Figure 3-7). Other structural solutions have also been implemented such as transition slabs, or track resilient components, like soft rail pads or under sleeper pads (Dahlberg, 2010b).

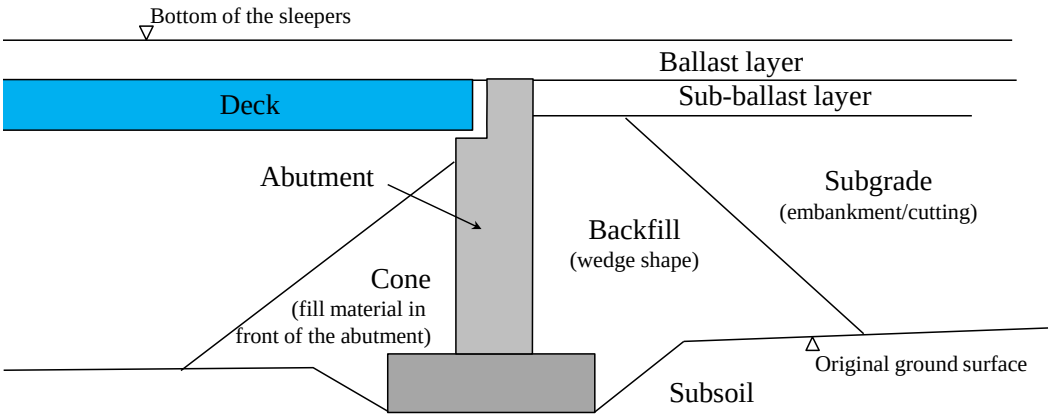

Figure 3-7. Wedge-shaped backfill at the approach to a bridge (adapted from ERRI, 1999).

The former Japanese National Railways (JNR) was one the first to incorporate wedge-shaped transition zones in the backfills of bridge abutments for HSL. In the 70's, French railways recommended wedges built with cement bound granular mixtures. Around that time, soil-cement mixtures were also applied in the top layers of the transition zones in the Roma-Florence HSL, for lengths of about 20 m on the backfill.

Many studies have followed over the last decades, focusing on understanding the causes and suggesting solutions to minimise the negative aspects of transitions. In the late 90's the former European Rail Research Institute (ERRI) promoted a joint project to carry out a study on the state of the art and eventually to prepare guidelines for design, construction and maintenance of transition zones between embankments and bridges (ERRI, 1999). The study focused on various aspects of transition zones, from the point of view of railway, bridge and geotechnical engineering. A review of the technical specifications and current practices in construction was discussed and examples of transition designs applied by various railway infrastructure managers

were presented and compared. In recent studies, some authors suggest that the design of transition zones should be based primarily on minimising potential track faults and permanent deformation of the substructure in the transition zone, rather than just simply providing a smoother track stiffness variation (Banimahd *et al.*, 2012). In fact, problems related to the substructure behaviour are hard to identify and can be far more difficult to solve than the alternative approach of frequently lifting the rails and adding more ballast under the sleepers.

Currently, it is common practice to construct wedge-shaped backfills at approaches to bridge, to underpasses or to culverts in HSL. In general, the construction of these wedges-shaped structures follows specific geometries and comprises well-compacted layers of selected granular materials. In addition to reducing differential settlements, the wedge shaped backfills materialise a gradual transition of vertical stiffness between the embankment, built with traditional geomaterials, and the structure. With this objective, the materials applied in the wedges usually show higher deformation moduli and are less sensitive to plastic deformations than the geomaterials generally applied in embankments. For that reason, layers of unbound granular material (UGM) and cement bound granular mixtures (CBM) are frequently applied in backfills (ERRI, 1999). In some countries, these structures are called "technical blocks" (*Blocs Techniques* in France; *Bloco Técnico* in Portugal) or "transition wedges" (*Cuñas de Transición* in Spain) (UIC, 2008b).

Despite the efforts that were undertaken in the past to minimise the negative effects that arise in these locations and although it is widely recognised the need to include a stretch that provides a smooth stiffness transition, in general, transition zones continue to exhibit poor performance. Actually, at present days, a great amount of maintenance effort is still spent at these locations, with negative consequences in terms of costs, track availability and restrictions in train operations. Innovative designs for transition zones continue being suggested by researchers and by the railway industry to solve this problem (Woodward *et al.*, 2012; Costa D'Aguiar *et al.*, 2013).

Frequently, the poor performance of these structures results from faulty execution of the backfill, in particular, the use of less suitable materials, inadequate compaction of the layers and poor drainage conditions (Li & Davis, 2005). This situation is common in both old and new railway lines, aimed at high performance. With regard to road infrastructures, severe situations are also commonly reported, though repair operations seem to be easier to carry out in general, with additional layers of asphalt concrete.

Several methods for rehabilitation and improvement of the performance of these zones have been proposed to address specific problems. Some of the suggested solutions are primarily to improve the track foundation, particularly to increase its bearing capacity and to control settlements (ERRI, 1999; Moreno *et al.*, 2005; Cuéllar *et al.*, 2009; Nicks, 2009; Li *et al.*, 2010; Woodward *et al.*, 2012):

i) Replacement of existing geomaterials in the backfill with other natural material with better mechanical properties;
ii) Application of geosynthetics (geotextiles, geogrids, geomembranes or geocells);
iii) Soil stabilisation or reinforcement of the trackbed layers with binders (lime, cement or bitumen);
iv) Construction of reinforced concrete transition slabs under the track;
v) Execution of piles (steel, reinforced concrete, gravel or wooden) (Figure 3-8a and b);
vi) Injection of cement grout into the backfill (Figure 3-8b and c).

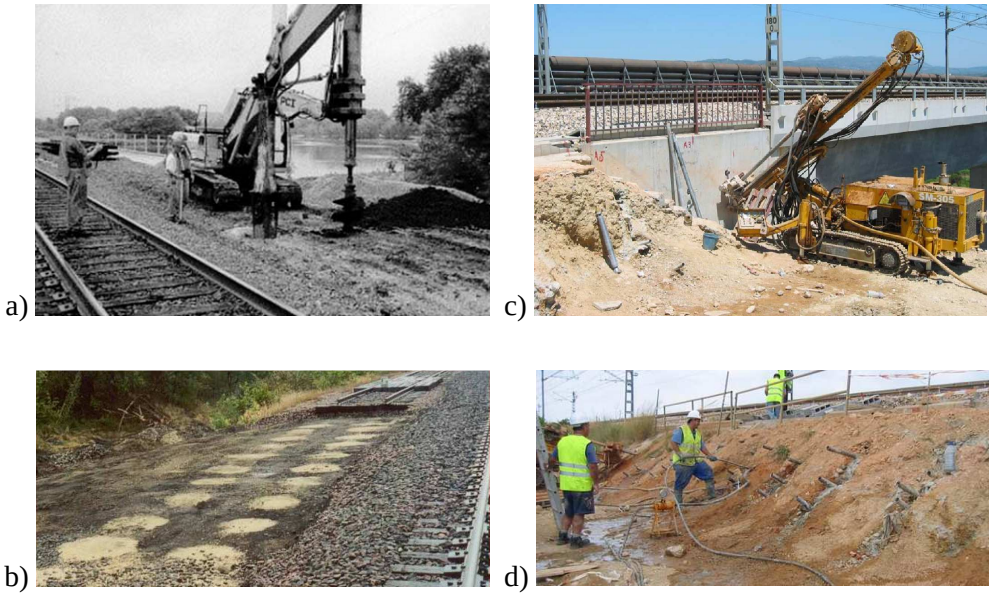

Figure 3-8. Reinforcement of backfill soils: hole boring (a) for vertical stone columns (b) (Li *et al.*, 2010); drilling of inclined holes (c) and grouting operations (d) (Moreno *et al.*, 2005).

Read and Li (2006) presented an overall review on solutions and construction measures for transition zones. In most cases, these interventions concern transitions for freight railway lines, which had to face higher axle loads and increasing annual tonnage, or transitions for which no

wedge shaped backfills with better characteristics similar to those implemented at present days had been foreseen.

Recent experimental studies have been developed in order to understand the problem and to contribute to the minimisation of maintenance efforts at these zones (Coelho et al., 2011; Luomala & Nurmikolu, 2012). Numerical models have also been intensively used in other studies to address various aspects of transition zones (Hunt, 1997; Lei & Zhang, 2010; Alves Ribeiro, 2012; Banimahd et al., 2012; Chen, 2013; Shi et al., 2013; Varandas, 2013), which will be addressed in more detail in section 3.5.

Considering the high occurrence of abrupt stiffness transitions along railway lines and the limitations of the solutions that have been implemented, some authors highlight that further research is still required to better understand the problems at transition zones (Banimahd *et al.*, 2012).

With regard to experimental studies, in general, these involve *in situ* measurements of rail and sleeper displacements and accelerations using dedicated transducers (Coelho *et al.*, 2011; Luomala & Nurmikolu, 2012; Shi *et al.*, 2013), as well as dynamic axle loads using strain gauges placed on the rail web or using instrumented vehicles with continuous measuring systems (Namura & Suzuki, 2007; Cuéllar *et al.*, 2009; Lozano del Moral & Cuéllar, 2009; Alves Ribeiro, 2012). As expected, higher deflections of the rail were generally observed for the track on embankment, when compared with track on backfill, which evidence the increasing track stiffness from earthworks to bridge. Important wheel/rail dynamic interaction forces have also been identified in some studies (Namura & Suzuki, 2007; Plotkin & Davis, 2008).

As regards the transition between embankments and other structures, such as tunnels, or between different types or railway track, there are some situations where it is necessary to achieve a gradual change in stiffness and to obtain a good compatibility in terms of structural behaviour. In the particular case of transitions between ballasted and slab track (a frequent situation in recent high speed lines with long tunnels and/or viaducts), a good performance can be achieved by using some of the following constructive measures (Peña Peña, 2003; Namura & Suzuki, 2007; Watanabe *et al.*, 2011; Muramoto *et al.*, 2012; Woodward *et al.*, 2012; Costa D'Aguiar *et al.*, 2013):

i) Placement of a layer of track component with gradually increasing stiffness from ballasted track to slab track;

ii) Adoption of more adjustable and resilient fastening systems with specific rail pad stiffness;

iii) Ballast compaction and agglutination by injecting of a binder (Figure 3-9a) - it is also possible to build ballast side walls immediately after the end of the slab to improve the ballast confinement (Figure 3-9b);

iv) Use of larger and heavier sleepers on the ballasted side (Figure 3-9c), with a roughened bottom face, and with smaller spacing between them;

v) Extension of the lower cement bound mixture layer from the slab track to ballasted track, replacing the sub-ballast layer;

vi) Including an additional pair of inner rails fixed to the sleepers, thus providing greater bending stiffness to the track frame (Figure 3-9c and d).

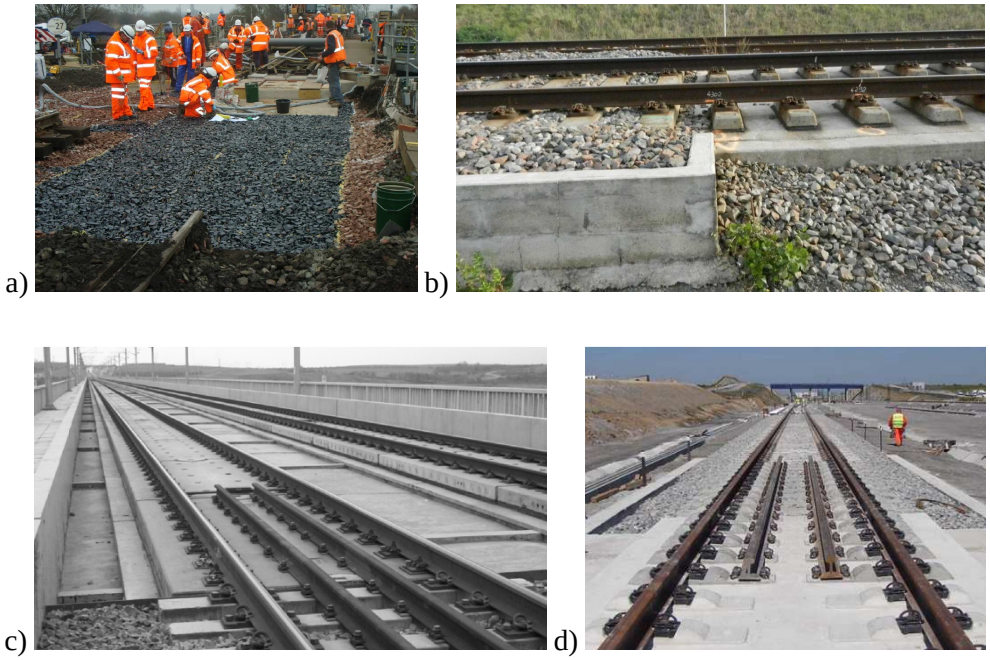

Figure 3-9. Structural countermeasures at transition zones: a) ballast reinforcement with polyurethane (Woodward *et al.*, 2011); b) side walls at a ballast/slab track transition (Costa D'Aguiar *et al.*, 2013); c) ballasted/slab track transition to a HSL bridge in China with auxiliary rails (Hao *et al.*, 2009); d) auxiliary rails at a ballasted/slab track transition to a tunnel in Spain (Ochoa de Olza Galé, 2007).

These constructive measures for transitions between ballasted and slab tracks have been proven by experience, some of theme following an empirical approach, allowing to conclude that the minimisation of the problem may involve the combination of two or more measures presented

above. Some of these solutions can be equally interesting to minimise the negative effects observed at some transitions to bridges, underpasses or culverts.

Numerical studies suggest using under sleeper pads (USP) in ballasted track transitions (Hunt, 1997; Lundqvist *et al.*, 2006; Dahlberg, 2010b), because USP reduce sleeper-ballast contact stresses, slow track degradation and can be used to control stiffness variations (Johansson *et al.*, 2008; UIC, 2009; Schneider *et al.*, 2011). Some studies highlight that the stiffness of the USP should be carefully determined as well as its conjugation with the rail pad stiffness (Johansson *et al.*, 2008) while others were inconclusive or did not recommend the use of USP in transition zones (Insa *et al.*, 2013). The use of USP at transition zones will be addressed in more detail in section 3.4.2 and Chapter 5 as a case study at the transition to an underpass.

3.4.1 Wedge-shaped backfills for transition zones

Studies regarding measurements of the track modulus at transition zones with a train loading vehicle evidenced that CBM material seems to provide better gradual stiffness variations at bridge approaches, as compared to hot-mix asphalt or geocell trackbed reinforcements (Li & Davis, 2005).

In general, the current practice for transitions to bridge abutments, to underpasses or to culverts in HSL comprises the construction of wedge-shaped backfills as mentioned earlier. Normally, the backfill is composed of two main parts (Figure 3-10):

i) a wedge with layers of cement bound granular mixture (CBM) next to the structure walls;
ii) a wedge with layers of selected unbound granular material (UGM).

Some designs also comprise treated/reinforced layers and/or increment of thickness of the upper layers at the approach to the structure, as will be described below. Other materials are also suggested for the abutment backfill base (AB) under the wedge-shaped CBM.

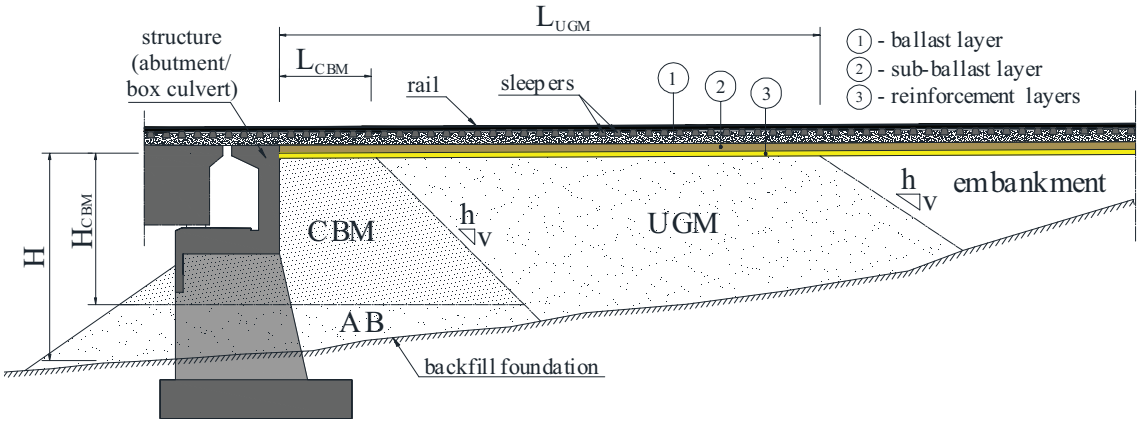

Figure 3-10. Schematic design of wedge-shaped transition zones for various railway infrastructure managers (see Table 3-1).

Over the last decades, designs for transition zones of HSL have evolved. Table 3-1 provides a comparison between transition zones designs for which the authors were able to find relevant information.

Although not discussed here in detail, some railway infrastructure managers establish slightly different geometries for the transition zones depending on the following factors (SNCF, 2002; GIF, 2004b; RFI, 2005): i) the height of the backfill (H); ii) if the structure was constructed before or after the embankment; iii) type of structure (open or closed abutment, shallow or buried underpass or culvert).

The transition designs that were analysed share some similarities:

i) A backfill with layers of selected materials extending out up to about 20 m from the structure wall and ending in a wedge-shaped fill with slope between 3:2 and 2:1 (h:v), thus providing a gradual transition to the embankment;
ii) Next to the structure walls, a wedge-shaped fill with 1:1 slope using layers of CBM is generally applied with binder content (*BC*) of about 3-5%;
iii) Well-compacted layers of UGM are usually applied in the wedge-shape fill between the CBM wedge and the embankment;
iv) Drainage elements between the CBM wedge and the structure are specified in the design.

Table 3-1. Comparison of different examples of transition zones for HSL (see Figure 3-10).

Aspects of the transition zone	France (SNCF, 2001, 2002; UIC, 2008b)	Germany* (DB AG, 1995; UIC, 2008b)	Italy (RFI, 2005)
foundation of the backfill	stripped or treated natural ground	$E_{V2} \geq$ 45MPa	N/I
AB (material between backfill foundation and CBM wedge)	if H < 3 m: only CBM 3 < H < 10 m: UGM below 3m H > 10 m: selected material PS: 0/100 below 10m	same as CBM	if H≥4: UGM; else: same as CBM
Aspects of the wedge-shape fill using cement bound granular mixtures (CBM):			
L_{CBM} (m)	1	≥1.5	1
H_{CBM} (m)	3	≥3	if H>4; 3 m else; H
slope (h:v)	1:1	≥1:1	1:1
BC (%)	3	2.5-3	3-5
Dc (%)	N/A	≥98 OP	≥95 OPM
other aspects	PS: 0/31.5	PS: 0/32 the top 0.5m is UGM $E_{V2} \geq$ 80MPa	prepared in plant only R_c > 3-7 MPa R_{it} > 0.2 MPa
Aspects of the wedge-shape fill using selected unbound granular material (UGM):			
L_{UGM} (m)	5	≥20	≥8
slope (h:v)	3:2	≥2:1	2:1
Dc (%)	N/A	≥100 OP	≥98 OPM
other aspects	$E_{V2} \geq$ 150MPa PS: 0/20 to 63 $\rho_d/\rho_s \geq$ 80%	PS: 0/45	$E_{V2} \geq$133MPa *CBR* ≥ 50
Aspects of the upper layers:			
reinforcement layer (e.g. capping, frost protection)	PS: 0/31.5 *BC* = 3% for a length of 10 m	frost protection layer over embankment	CBM *e* = 20 + UGM *e* = 20 + CBM *e* = 20
sub-ballast layer		stabilised with binder over 10 m with *e*=50	bituminous layer; *e* = 12
ballast layer	former TGV transition zones included variation in thickness	N/I	+15% thickness transition along 3 m, over the backfill

Notes: *different geometries for the transition are established for lines with slower speeds; E_{V2} - deformation modulus obtained in the 2nd load of the plate load test (AFNOR, 2000; DIN, 2012); E_{vd} – dynamic deformation modulus (FGSV Verlag GmbH, 2012); N/A - not applicable; N/I - no information; H and L – see Figure 3-10; *BC* - Binder content; *Dc* - Degree of compaction; OP and OPM - Optimum Proctor and Optimum Proctor Modified test compaction conditions; PS – min./max. particle size in mm; R_c and R_{it} – compressive and indirect tensile strength of CBM; *CBR* – Californian Bearing Ratio; *e* - layer thickness in cm.

Table 3-1 (continued). Comparison of different examples of transition zones for HSL (see Figure 3-10).

Aspects of the transition zone	Spain (GIF, 2004a, b; UIC, 2008b)	Japan (RTRI, 2007) (Tatsuoka *et al.*, 2005)	China (Hao *et al.*, 2009)	Portugal[+] (considered in Chapter 4)
foundation of the backfill	specific geometry of the relief	depends on design	concrete or gravel at the abutment base $E_{vd} \geq 30$MPa	N/I
AB (material between backfill foundation and CBM wedge)	same as CBM	same as CBM	same as CBM	same as CBM
Aspects of the wedge-shape fill using cement bound granular mixtures (CBM):				
L_{CBM} (m)	3	≥2	3-5	3
H_{CBM} (m)	H	H	H	H
slope (h:v)	1:1	1.15:1	2:1 to 5:1	1:1
BC (%)	>3	4	3	5
Dc (%)	≥95 OPM	≥95 OPM	≥95 OP	≥98 OPM
other aspects	prepared in plant only $E_{V2} \geq 160$MPa	PS: 0/37.5 $R_c > 2$ MPa geogrids with 0.3m spacing	inverted wedge is used $E_{vd} \geq 50$ MPa	PS: 0/31.5 $R_c > 1$ MPa $R_{it} > 0.25$ MPa
Aspects of the wedge-shape fill using selected unbound granular material (UGM):				
L_{UGM} (m)	20	N/I	N/A	20
slope (h:v)	3:2	N/I	N/A	3:2
Dc (%)	≥95 OPM	N/I	N/A	≥95 OPM
other aspects	$E_{V2} \geq 80$MPa	N/I	N/A	PS: 0/31.5
Aspects of the upper layers:				
reinforcement layer (e.g. capping, frost protection)	UGM *e* = 40 to 60; no capping on top of CBM	N/I	treated granular material with BC=5% Dc=97% OP	same as CBM or UGM, respectively
sub-ballast layer	*e* = 30	N/I	$E_{vd} \geq 55$MPa	*e* = 30
ballast layer	+5 cm thickness transition along 3 m, at the CBM	N/I	N/I	*e* = 30

Notes: [+]case study addressed to in Chapter 4; E_{V2} - deformation modulus obtained in the 2nd load of the plate load test (AFNOR, 2000; DIN, 2012); E_{vd} – dynamic deformation modulus (FGSV Verlag GmbH, 2012); N/A - not applicable; N/I - no information; H and L – see Figure 3-10; *BC* - Binder content; *Dc* - Degree of compaction; OP and OPM - Optimum Proctor and Optimum Proctor Modified test compaction conditions; PS – min./max. particle size in mm; R_c and R_{it} – compressive and indirect tensile strength of CBM; *e* - layer thickness in cm.

The Japanese innovative transition solution comprises geogrid reinforcements mostly due to seismic risk in Japan (Tatsuoka *et al.*, 2005). Some railway infrastructure managers establish localised cemented/treated layers of sub-ballast or capping at the approach to the structure, or bituminous sub-ballast layer on top of CBM layers interposed with UGM layers, as suggested in

Italy (RFI, 2005). Additionally, some specifications comprise designs for transition zones with excessive skew (SNCF, 2002; GIF, 2004b; UIC, 2008b).

Most railway infrastructure managers establish minimum reference values for the deformation modulus measured *in situ* during construction, on top of the layers, as performance based requirements. The E_{V2} modulus, obtained in the second load of the plate load test (AFNOR, 2000; DIN, 2012), or the E_{vd} dynamic modulus (FGSV Verlag GmbH, 2012), obtained with the light falling weight deflectometer, are commonly used as reference parameters. It is assumed that higher deformation modulus values are related to good performance of the layers, both in terms of resilient behaviour and susceptibility to permanent deformation. It should be noted that the measured moduli (E_{V2} and E_{vd}) depend on the resilient modulus of the materials comprising the various underlying layers.

Thus, it is clear that the application of selected materials in different sections of transition zones, complying with established requirements, must be specified precisely. Moreover, the engineering disciplines involved in the railway project ought to think through the design of transition zones together with the aim to:

i) Facilitate execution of earthworks, for example assuring that the geometry of abutment simplifies compaction of the backfill layers, avoiding situations as the one depicted in Figure 3-11a;
ii) Provide a smooth stiffness transition considering the train speeds, the deformability of the materials applied in the backfills and the stiffness of the track resilient elements (in particular, the rail pads);
iii) Minimise long-term settlement resulting from the behaviour of both the substructure and the superstructure of the track.

Regarding the construction of the layers in the transition zone (embankment soils, UGM and CBM) it is necessary to implement a quality assurance process and tight quality control procedures. Good compaction of the layers is required taking into account the thickness, the water content during compaction of the materials, the compaction equipment used plus the number of roller passes. Adequate compaction equipment is crucial bearing in mind the constraints to use heavy compaction near the structure walls and in less accessible places of the backfill (Figure 3-11). Aspects of the CBM need to be established in detail, such as the binder content and if it is mixed in place or in plant, regarding the need to achieve a good homogeneity of the mixture. It is noted that mix in place is rejected by some railway infrastructure managers.

a) 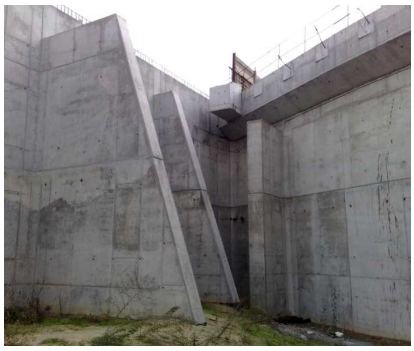 b)

Figure 3-11. Construction aspects of transition zones: a) example of an abutment providing very limited access to compaction equipment; b) compaction of the CBM inside the abutment walls.

3.4.2 Under sleeper pads

Under sleeper pads (USP) are less conventional railway track components made of materials with resilient properties (polyurethane rubber and/or polyethylene), normally 7 to 10 mm thick, embedded or glued to the underside of concrete sleepers (Figure 3-12).

a) 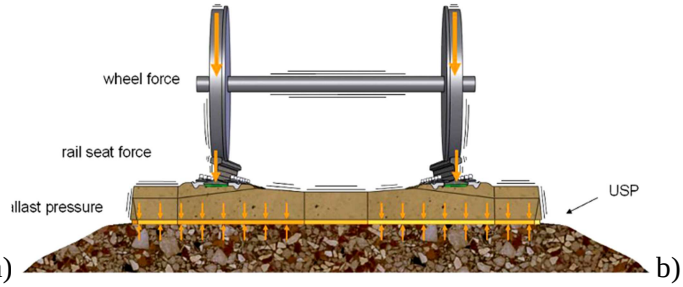

b) 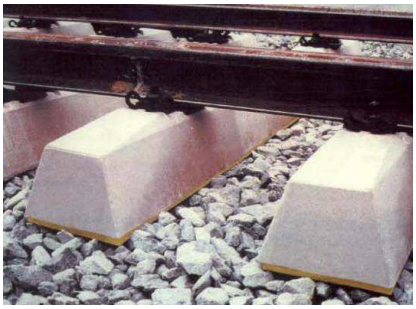

Figure 3-12. Under sleepers pads (USP): a) schematic representation (Loy, 2008); b) example of application (Riessberger, 2010).

From 2005 to 2009, a UIC research project on “Under Sleeper Pads” (UIC, 2009) was developed involving thirteen European railway infrastructure managers. An overall positive experience using USP was reported, considering various beneficial aspects to the track system. Due to the resilient properties of these elements, USP allow for the reduction of the vertical stiffness of the track. This increase in resiliency results from the deformation of USP at the

contacts with the angularities of the ballast particles. A significant increase in the contact area is established between the sleeper and the ballast; hence, it is achieved a reduction in stress concentrations under the sleepers and improved stress distribution to the ballast layer. Consequently, reduced deterioration of sleepers and ballast particles can be expected as well as slower degradation of the geometric quality of the track, as depicted in Figure 3-12. In the figure, the rapid decrease in the standard deviation of the curves results from track maintenance operations.

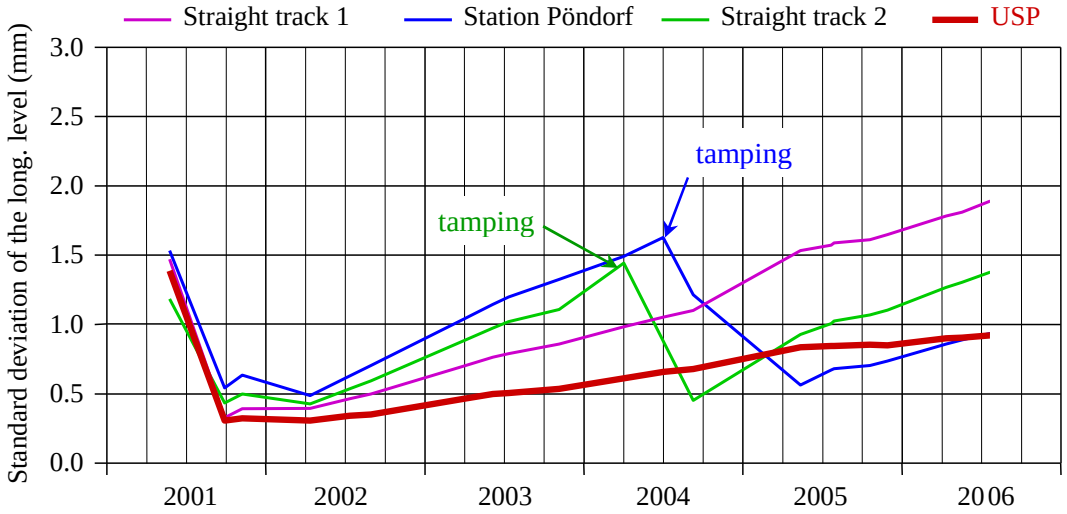

Figure 3-13. Comparison between the evolution of the geometric quality of railway stretches with and without USP in the Austrian network (adapted from Schilder, 2006).

This aspect seems to contribute to decrease the degradation rate of the track geometry. In the framework of the UIC project, as reported by Schneider *et al.* (2011), measurements of track geometry evidenced that track settlements increased with time at a faster rate for tracks without USP, when compared with adjacent sections with USP.

Other relevant and positive aspects of USP reported in the UIC study include the following: i) possibility to reduce the depth of the ballast layer; ii) lower deterioration of the sleepers; iii) attenuation of noise and vibrations; iv) cost-effective alternative to under ballast mats for vibration control in the frequency ranges above 40-50 Hz. Different participants involved in the UIC study reported opposite conclusions as to whether USP reduce the lateral resistance of the track (UIC, 2009).

Although the UIC study (2009) reported an overall beneficial influence of USP at localised discontinuities of track stiffness, further information on the use of USP at transition zones are still scarce to non-existent.

Most studies on the analysis of the influence of USP in the dynamic behaviour of transition zones are based on numerical simulations. Using such tools, recent studies point out the benefit of using USP to enhance track behaviour, especially in what regards the control of vertical stiffness of the track and reduction of train-track interaction forces (Lundqvist *et al.*, 2006; Johansson *et al.*, 2008; Witt, 2008; Insa *et al.*, 2012; Insa *et al.*, 2013), as will be discussed in section 3.5.2.

In the context of the research project INNOTRACK, Lozano del Moral and Cuéllar (2009) reported some results of *in situ* measurements at a transition zone with USP on a high-speed railway bridge. The stiffness of the track was two times higher on the abutment than on the backfill. Track stiffness increments of about 40% were also reported for trains travelling from open track to track with USP at the approach to the bridge, but no significant difference was observed for trains travelling in the opposite direction.

Despite these numerical and field studies and the option of some railway infrastructure managers to install USP in slab tracks, little is still known about its actual benefit on transition zones. Aiming to contribute to a better understanding of the influence of USP at transition zones, a case study comprising a transition zone to an underpass with USP will be analysed in more detail in Chapter 5.

3.5 A review on numerical modelling of transition zones

3.5.1 General aspects

Despite the past efforts of the railway industry and research institutions, the behaviour of the train-track system at transition zones is not completely clear (Kaynia *et al.*, 2005a; Täljsten *et al.*, 2007; Costa D'Aguiar *et al.*, 2013). The numerical tools can provide a significant contribution to understanding and predicting the behaviour of the track in situations of accelerated degradation due to: abrupt variations in the vertical stiffness of the track; uneven rail profiles; hanging sleepers; rail expansion joints and switches. In recent decades, various numerical models have been developed to study and to understand the behaviour of the track at transition zones. With that objective, numerical techniques - such as the finite element method

(FEM) - have been extensively used to perform dynamic structural analyses in order to simulate the effects caused by the passage of trains, but only a few performed adequate calibration and validation of the models with experimental measurements. Considering that at transition zones the track's support conditions change in space and in time, the problem is generally studied in the time domain. The models have been developed with different levels of complexity in terms of:

- Extension of the track and dimensions of the represented medium;
- Degree of discretisation of the medium;
- Dynamic aspects of the problem and the numerical method used to solve it;
- Aspects of the vehicle's behaviour;
- Representation of the vehicle-track interaction;
- Consideration of different support conditions found at transition zones, that result in variations of the vertical stiffness of the track;
- Longitudinal rail profile defects or differential settlements;
- Sleeper-ballast interaction allowing the development of hanging sleepers;
- Simulating resilient and permanent deformation behaviour of the geomaterials in the track's support layers.

In general, it is possible to divide the models found in the literature into three large groups to study transition zones (Figure 3-14): 1) models that only use linear elements, that is, beams and spring-damper elements; 2) models that use plane elements; 3) and three-dimensional element models.

The first group is the simplest, because in those models the track is modelled using linear elements. The rails are considered as beams on discrete viscoelastic supports (such as the parallel spring-damper Kelvin-Voigt model). Normally, one layer of these viscoelastic elements is used to model the rail pads and one or more layers are used to model the trackbed, as depicted in Figure 3-14a. Sleepers are normally considered as rigid bodies with mass and inserted between the rail pads and the trackbed. These models typically require reduced computational effort but are difficult to calibrate and to apply to complex geometries, such as transitions with wedge-shaped backfills. Moreover, the stresses, the deformations and the propagation of vibrations in the trackbed layers that result from train's loads, are not adequately reproduced.

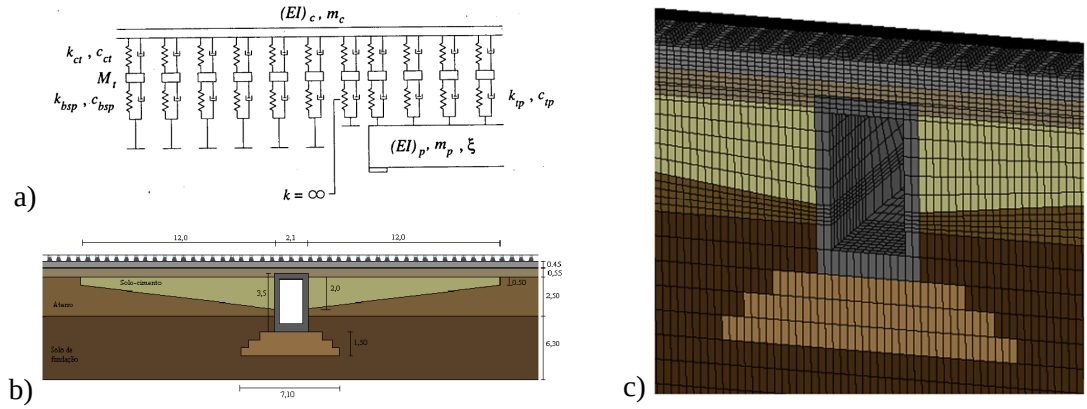

Figure 3-14. Schematic representation of numerical models using: a) beam and spring-damper elements (Calçada, 1995); b) plane elements; c) 3D solid elements (Alves Ribeiro, 2012).

The models that use plane elements, as the one presented in Figure 3-14b, are less common and regard a simplified and innovative approach to address the problem. They also comprise linear elements and spring-dampers to model the rail and the rail pads, but they use plane-stress elements to model the trackbed layers (Alves Ribeiro, 2012). This approach allows a more realistic representation of the geometry and behaviour of the layers. Moreover, the elastic parameters that usually define the behaviour of the materials can be considered directly in the model. On the other hand, they require more computational effort due to the increased number of degrees of freedom and generally require proper calibration of the thickness of the plane-stress elements. This is the numerical technique that will be adopted in chapters 5 and 6 of this thesis.

The models of the last group use solid three-dimensional elements and are generally more complex than the previous ones. They allow a better representation of the geometry of the track and substructure (Figure 3-14c), as well as the behaviour in the three dimensions, which facilitates the introduction of material parameters. However, they require a high computational effort and longer calculation times, in part, due to the very large number of degrees of freedom.

In the above modelling approaches, it can be important to represent with some accuracy the behaviour of the vehicles, of the track and the dynamic interaction between the two, depending on the type of problem to be studied. An extensive review on the development of models of vehicle-track interaction and its application can be found in Popp et al. (1999; 2005), Dahlberg (2003) and Ferreira (2008). In this sense, the use of complex numerical models that consider the dynamic interaction of vehicle-track system is especially valuable to the work to be developed, since they can provide insight in the behaviour of critical railway track sections such as

transition zones. It should be noted that in these dynamic analyses on a finite domain, viscous boundaries are generally required to account for the unwanted reflection of elastic waves at the boundaries of the model.

Other modelling technics were not mentioned above, such as the analytical models and those that use the discrete element method (DEM). The first ones assume a continuously supported beam and are very limited when it comes to reproducing the track's behaviour. Concerning the DEM approach, it is expected that such models may prove to be extremely useful to study transition zones in the near future, particularly in what regards the interaction between the sleepers and the ballast grains. However, it still may not be an adequate numerical approach to study large segments of the track, such as transition zones, due to the complexity it involves and the significant computation effort it requires.

3.5.2 Previous numerical works

As discussed earlier, the vertical stiffness of the track can have an irregular spatial distribution that influences the interaction between the vehicle and the track. Some authors have proposed to study the influence of the variations in the vertical stiffness on the structural behaviour of the train-track system using simple numerical models. Early studies showed that the stiffness of the track subgrade has a fundamental contribution to the vertical stiffness. In studies conducted in the rail research centre of CHARMEC, Sweden, various statistical and mathematical tools were applied to the numerical modelling of the interaction between the vehicle and the track (Oscarsson, 2001, 2002; Andersen & Nielsen, 2003; Nielsen & Oscarsson, 2004). These studies aimed at understanding the influence of the variation of the stiffness of the track elements on the interaction between these two systems. In one of these studies (Oscarsson, 2001, 2002), it was analysed in detail the influence of the variability of the characteristics of the track components on the contact forces between the wheel and the rail, on the amplitude of the vertical acceleration of wheelsets and on the displacements of the sleepers. In particular, it was studied the influence of the following parameters (Figure 3-15): i) stiffness of the rail pads and of the ballast; ii) the equivalent dynamic mass of the ballast-subgrade system; iii) and the spacing between sleepers. It was found that the stiffness of the rail pads was the parameter that most influenced the variation of the contact force between the wheel and the rail and the acceleration of the wheelsets. Furthermore, it was concluded that the displacement of the sleepers was mainly influenced by the stiffness of the ballast layer. Field monitoring campaigns and laboratory tests developed in the scope of these studies allowed to successfully calibrate and validate the models that were developed.

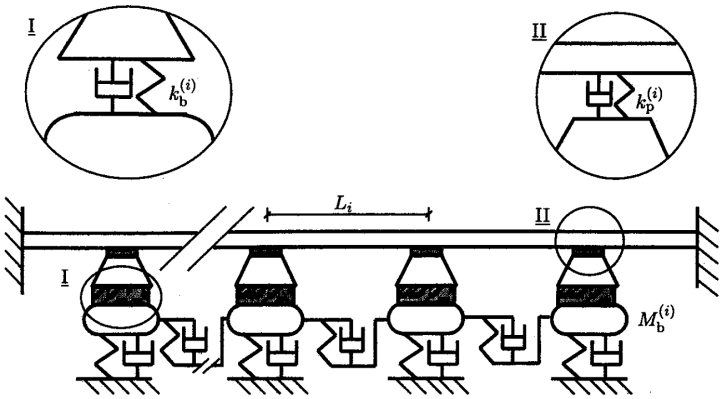

Figure 3-15. The stochastic track model used by Oscarsson (2001). The variables that were taken as stochastic (rail pad stiffness, ballast stiffness, ballast-subgrade mass, and sleeper spacing) are denoted k_p, k_b, M_b and L, respectively.

Concerning the study of transition zones, a few numerical approaches were based on continuous beam models. Some authors (Andersson & Dahlberg, 1998) evidenced the importance of the unevenness of the track vertical stiffness that is normally observed in these locations, in that it causes important variation in the train-track contact forces. They also found that these forces tend to increase with the speed of the vehicles, with the variation in the vertical stiffness of the track and with the amplitude of track defects.

Other numerical studies developed at the Delft University of Technology (Schooleman, 1996; Esveld, 2001) to simulate transitions between two zones with different vertical stiffness and with differential settlements also revealed similar conclusions. Different levels of acceleration and load amplification were verified in the two zones, depending on the differential of the vertical stiffness of the track, on the speed of the vehicles and on the amplitude of the differential settlements. A parametric study by Schooleman (1996) focused on establishing maximum amplitudes of differential settlements to avoid passenger discomfort in high speed trains by limiting the maximum vertical acceleration inside the car bodies to 1 m/s^2. Different track bum profiles were compared in dynamic analyses and it was concluded that aspects related to differential settlements at transition zones seem to be more critical than changes in the vertical stiffness of the track.

Hunt (1997) studied the long-term behaviour of transitions with stiffness variations and differential settlements using a beam-spring model (Figure 3-16) and considering the dynamic train-track interaction for different types of train models. Although the numerical model was

relatively simple, the study seems to encompass a very good understanding of main mechanisms that affect the performance of transition zones.

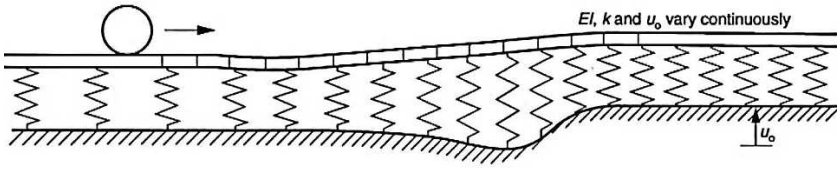

Figure 3-16. Schematic representation of the model that was considered by Hunt (1997).

Considering a foundation with elastic behaviour and using a beam-spring-damper model, Lai and Mao (2004) studied the variations of the accelerations of the vehicles and the train-track interaction forces when the vehicles crossed the transition zones at different speeds. In the analysis, different bump profiles were considered by the introduction of a track section with a slight gradient (Figure 3-17). Given the relatively high bending stiffness of the rails, it appears that the profiles considered in the study do not quite reproduce real uneven longitudinal profiles of the track – normally, the rails may evidence a smooth and wavy shape, rather than a series of line segments. Nevertheless, the study highlighted that uneven rail profiles had greater influence in the amplification of contact forces and accelerations on the rail and body cars, in comparison with the influence of the variations in the vertical stiffness of the track.

Other authors (Namura & Suzuki, 2007; Kang *et al.*, 2008) used beam-spring-damper models, with train-track interaction, to study the transition between ballasted and slab tracks (Figure 3-18a). They aimed at determining the resilient properties of the track components in transition zones to achieve an adequate dynamic behaviour. The study by Namura and Suzuki (2007) considered both the variations in the stiffness of the subgrade and the track defects, such as irregularities and the presence of hanging sleepers. One of the relevant aspects of this study was that the model was validated using measurements of wheel loads and accelerations in the axle box (Figure 3-18b).

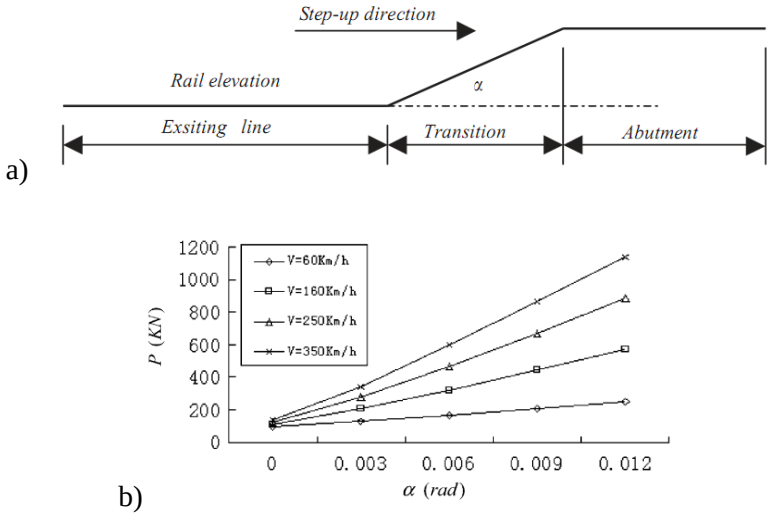

Figure 3-17. Maximum interaction forces between the wheel and the rail, depending on the speed of the train and the magnitude of the geometric defect (Lei & Mao, 2004).

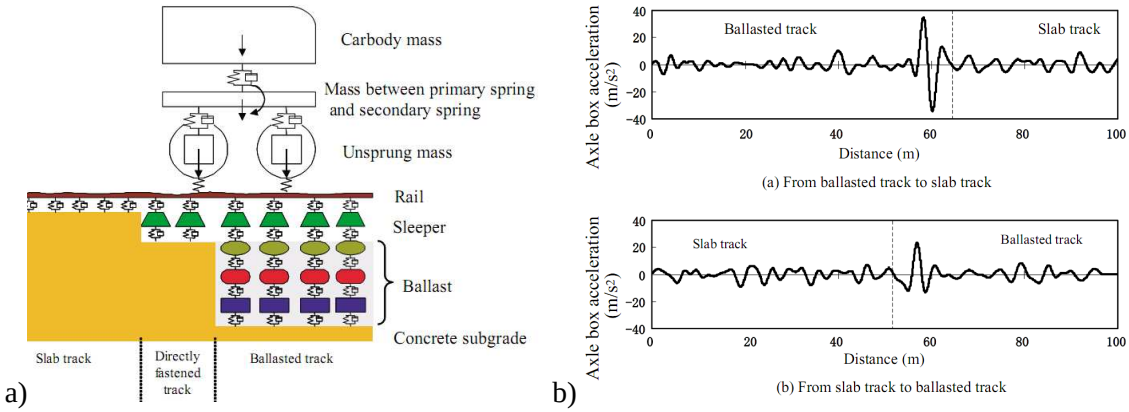

Figure 3-18. Numerical study by Namura and Suzuki (2007): a) schematic representation of the model; b) vertical accelerations measured in the axle box of a train running at 300 km/h (after applying a low-pass filter with cut-off frequency of 30 Hz).

Probably due to higher computational capabilities and the more efficient numerical techniques that were developed, in the last decades, some authors opted to use complex three-dimensional dynamic models in order to evaluate the performance of transition zones (Banimahd & Woodward, 2007a; Alves Ribeiro *et al.*, 2009; Hao *et al.*, 2009; Dahlberg, 2010a).

Advanced numerical studies were developed at the Heriot Watt University, Edinburgh, on transition zones using three-dimensional coupled train-track models, considering explicit methods to numerically integrate the differential equations of motion of the vehicle-track system

(Banimahd & Woodward, 2007a; Banimahd *et al.*, 2012). Among other aspect, parametric studies were carried out on the influence of the length of the transition zone and of the train speed in the displacements of the rail, the rail-wheel interaction forces and the accelerations of the car body. Track defects were considered and hanging sleepers were modelled as local soft support conditions. A particular aspect of this study was that it considered the non-linear resilient behaviour of the geomaterials.

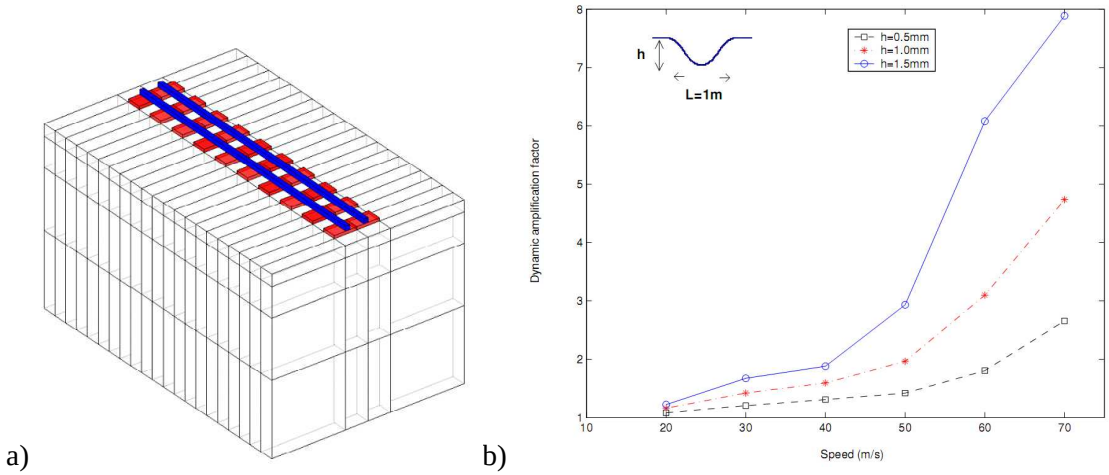

Figure 3-19. Aspects of the numerical study by Banimahd and Woodward (2007a): a) view of the mesh; b) dynamic amplification factors due to a track defect with different geometries.

In another study (Alves Ribeiro *et al.*, 2009) also using an explicit time integration scheme, different scenarios of abrupt variations of track vertical stiffness were studied, referring to different levels abrupt changes in the elastic modulus of the track subgrade. The scenarios referred to three distinct situations in which the elastic modulus of the subgrade of a track section was, respectively, 5, 10 or 20 times higher than the subgrade in the adjacent section of the track (Figure 3-20). Acceleration values, displacements and interaction forces between the wheel and the rail (Figure 3-21) on two axles of a bogie were investigated, obtained for each of those scenarios and for different vehicle speeds. It was concluded that the increase in speed and higher stiffness amplitudes between the two subgrades (in this case, the Young modulus of the materials) significantly increased the interaction forces between the wheel and the rail. The model developed in this study also allowed to identify cases of loss of contact between the sleeper and the ballast layer, a situation that was observed in some scenarios.

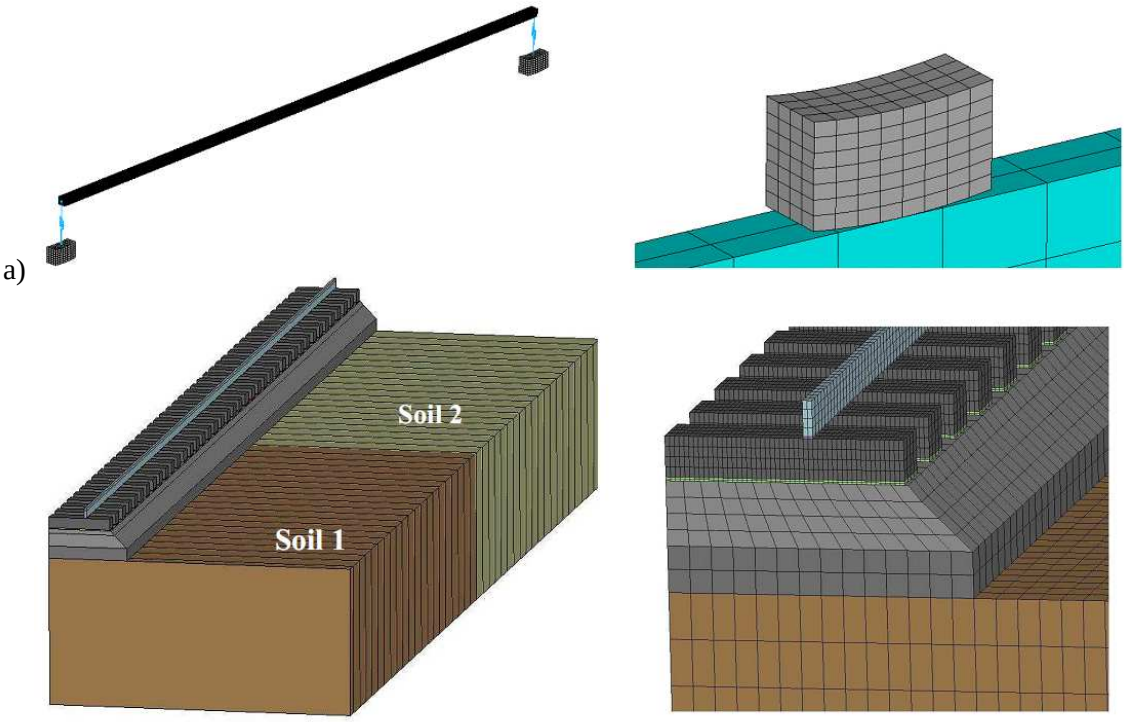

Figure 3-20. Aspect of the three-dimensional numerical model of the transition between two different subgrades (Alves Ribeiro *et al.*, 2009): a) detail of the bogie and wheel-rail contact; b) general view of the mesh.

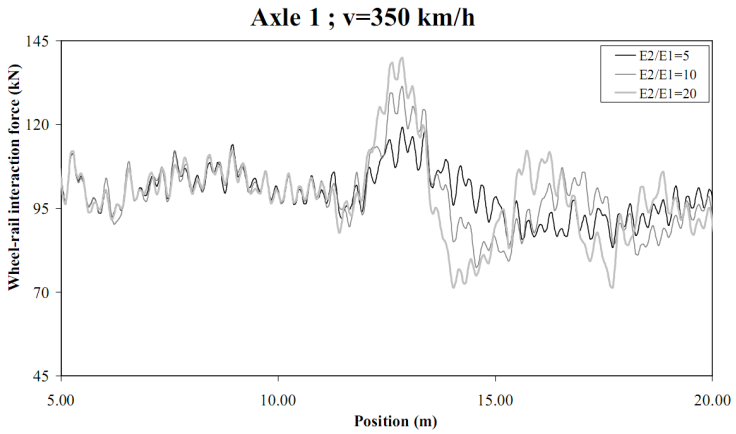

Figure 3-21. Train-track interaction forces (1st axle) over a transition zone with abrupt stiffness variation in the subgrade (Alves Ribeiro *et al.*, 2009).

Later, considering the results of the three-dimensional models, Alves Ribeiro (2012) developed a numerical approach to study transition zones using 2D models with plane-stress elements to simulate the sleepers and the geomaterials. The modelling approach considered the dynamic train-track interaction and it was calibrated using those 3D models and validated with field

measurements. In addition, in the scope of her PhD works, the author developed a procedure that included settlement laws to simulate the permanent deformation of the geomaterials in order to predict the long-term evolution of transition zones (see earlier Figure 3-2). One of the main findings was that hanging sleepers have a significant negative impact on the track degradation and strongly influence its dynamic behaviour.

Based on an initial survey on the problems that affect transition zones of railway lines in the Unites States of America, Nicks (2009) carried out an extensive parametric study regarding the influence of the configuration of the track bump and dip and of the train speed in the magnitude of the dynamic load of the trains, among other aspects. A three-dimensional model with train-track interaction was considered, using explicit time integration. The model comprised a very detailed bogie, the track components, the embankment, the foundation and the bridge with a fairly high level of detail (Figure 3-22). Analysing the mesh that was used for the bogie, it seems that the high discretisation of some components may have been unnecessary, particularly because the study focused on the dynamic behaviour of the transition zone, rather than on specific aspects of the vehicle.

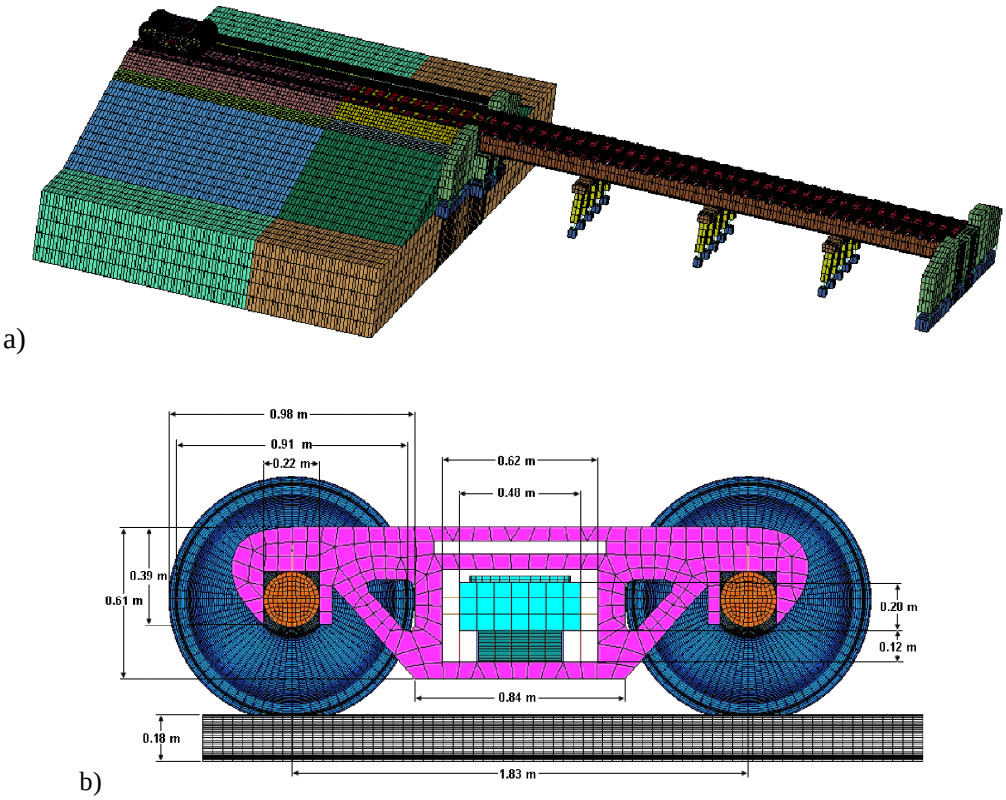

Figure 3-22. Aspects of the numerical model by Nicks (2009): a) general aspect; b) detail of the bogie.

A few authors also developed dynamic analysis using three-dimensional models to study transition zones but without considering the train-track interaction, probably because the studies focused on other relevant aspects such as the groundwater flow, the non-linear behaviour of the geomaterials or simply because of the increased computational effort was considered too high. In his PhD works, Coelho (2011) developed a detailed 3D dynamic model of a transition zone on soft soils, using implicit time integration, considering the track components, the embankment, a box culvert and the foundation (Figure 3-23a), but without the train-track interaction. The works were validated with field measurements and it was highlighted that problems at transition zones seem to be primarily caused by differential settlements, rather than stiffness transition. This finding appears to be particularly relevant in that case study because the track evidenced severe problems of differential settlements due to the poor bearing conditions of the soft soils that are normally found in The Netherlands. The author also reported that hanging sleepers strongly influenced the track behaviour and the results of the numerical study did not recommend transition slabs for that case study.

Recent studies used similar numerical approaches (3D model using implicit time integration without train-track interaction) to compare two configurations of wedge-shaped backfills at the approach to bridges for high-speed trains in China, in terms of reducing stresses and displacements on the rail and subgrade (Shan *et al.*, 2013). The study focused on the transition between ballasted track on the embankment and slab track on the bridge and used a detailed 3D mesh of the track, embankment and bridge (Figure 3-23b). However, it did not account for track defects and it was not validated with field measurements.

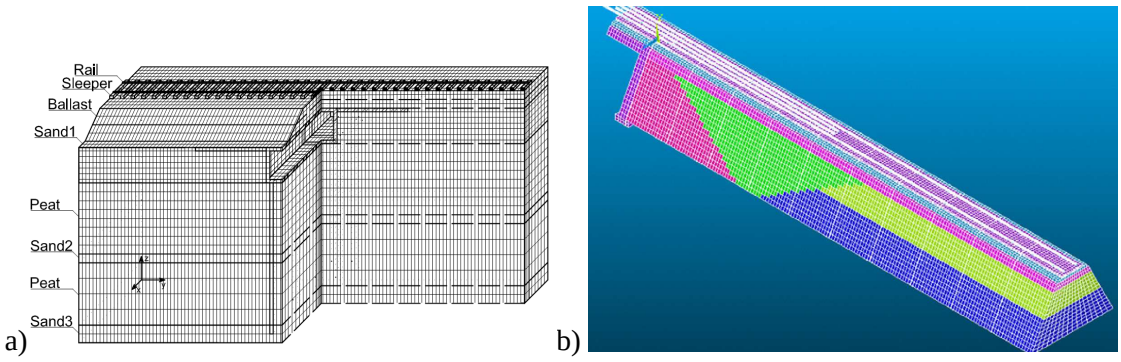

Figure 3-23. Aspects of 3D models of transition zones: a) to a box culvert on soft soils (Coelho, 2011); b) to a bridge with slab track (Shan *et al.*, 2013).

Some authors (Gallego Giner *et al.*, 2011), considered static 3D models of portions of the transition zones to develop an innovative method to support the design of wedge-shaped backfills. The numerical approach also accounted for the elastoplastic behaviour of the geomaterials using the Drucker-Prager yield criterion. In normal conditions and under the successive load cycles of the trains, the geomaterials in the track undergo very small permanent deformations compared with the respective resilient deformation in each load cycle. Thus, in this study, the consideration of the elastoplastic behaviour of the materials induced larger vertical deformations of the track, which may have influenced the correct assessment of the vertical stiffness, thus affecting the design method that was proposed.

The particular problem of unsupported (or hanging) sleepers has been the subject of several numerical modelling studies (Lundqvist, 2005; Lundqvist & Dahlberg, 2005; Zhang *et al.*, 2008; Bezin *et al.*, 2009; Zhu *et al.*, 2010), which highlighted the correlation between this phenomenon and the abrupt change in the vertical stiffness of the track. In general, these studies showed the influence of the size of the gap under the sleeper in the dynamic amplification of the wheel-rail interaction forces, as shown in Figure 3-24.

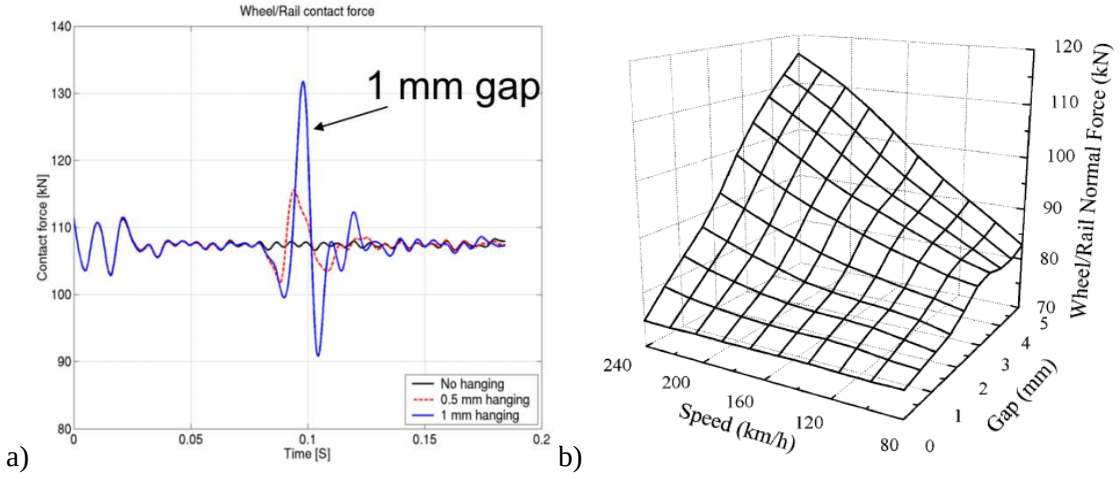

Figure 3-24. Results of wheel-rail contact forces at sections with unsupported sleepers: a) due to different gap depths for trains speeds of 324 km/h (Lundqvist & Dahlberg, 2005); b) influence of the train speed and the depth of the gap (Zhang *et al.*, 2008).

In the PhD works by Varandas (2013), different numerical models were developed to investigate the behaviour of a faulty transition zone to a box culvert on very soft soils - the same case study by Coelho (2011). Firstly, a dynamic beam-spring-damper model with train-track

interaction was developed and validated with field data (Figure 3-25a). A method was proposed to model the sleeper-ballast contact using a non-linear relationship that allowed to account for hanging sleepers. The study highlighted the negative impact of hanging sleepers on the dynamic behaviour of the train-track system at the transition zone. Using a ballast settlement law and considering the cumulative traffic, it was successful in predicting the long-term behaviour of the transition zone case study that evidenced an excessive number of hanging sleepers (Varandas *et al.*, 2014). In the scope of the same research works, the author developed a three-dimensional model using explicit time integration (without train-track interaction) that considered the non-linear sleeper-ballast interaction, the hanging sleepers and the non-linear resilient behaviour of the geomaterials (Figure 3-25b) using constitutive laws derived from cyclic load triaxial tests. With this approach, it was possible to model the problem in more detail and provide insight into the response of the geomaterials and into the behaviour of that particular transition zone (Figure 3-25c).

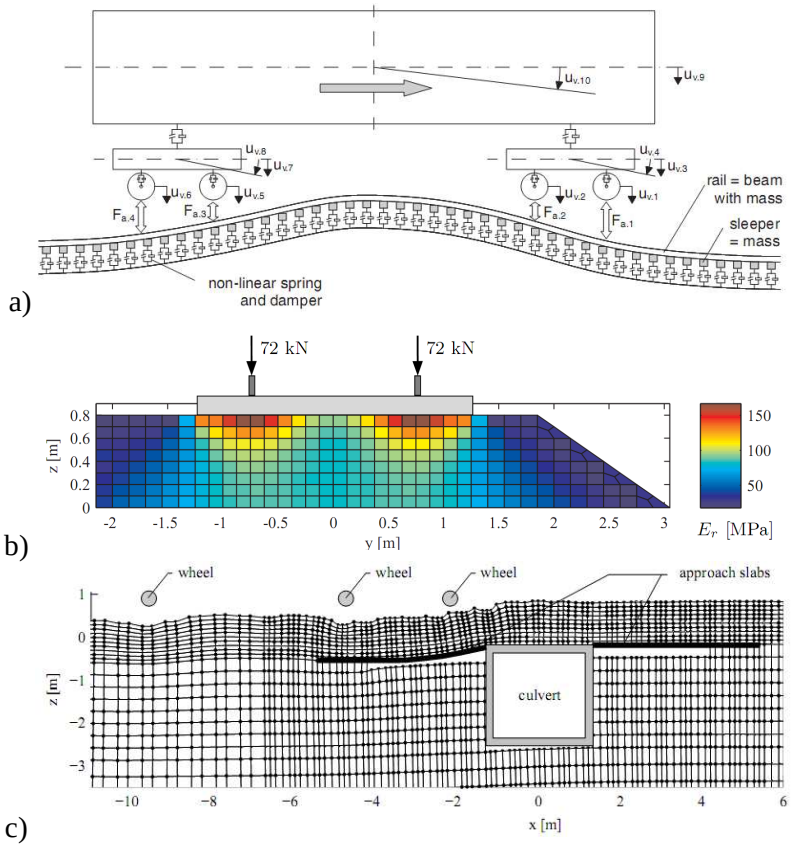

Figure 3-25. Representations of the numerical models developed by Varandas (2013): a) beam-spring-damper model; d) variation of the resilient modulus in a transvers view; c) example of the deformed shape of the transition zone under the wheel loads.

It was compared the results considering the geomaterials with non-linear elastic behaviour (using a k-θ law (Lekarp *et al.*, 2000)) with those obtained from the modelling with linear resilient behaviour. An interesting finding was that when the ballast layer was considered to have linear elastic behaviour with a Young Modulus (E) of 130 MPa, the results of the global response of the track were somewhat similar to those with the non-linear behaviour.

Other numerical studies on the dynamic behaviour of the track have investigated the importance of under sleeper pads (USP) in mitigating the negative dynamic effects arising when vehicles cross singularities of the track with abrupt changes in vertical stiffness (Dahlberg, 2010a). The approach of these studies was to use complex mathematical methods to determine the most suitable stiffness to assign to these resilient components, and to provide a smooth stiffness transition, thus establishing the most appropriate levels of vertical stiffness to implement in the transitions.

In one of those studies, developed at the Institute of Technology of Linköping University (Lundqvist *et al.*, 2006), three-dimensional numerical models were used to model situations of abrupt variation in the vertical stiffness of the track, considering the wheel-rail interaction and using explicit time integration. Optimisation algorithms were used to adjust the stiffness of the USP, aiming to reduce the variations of the interaction force between the wheel and the rail (Figure 3-26a). It was concluded that the optimal stiffness transition depended on the direction of the train; however, the behaviour of the track was not particularly affected by this aspect. It was also reported that even without optimizing the stiffness of the USP at transition zones, it was possible to achieve considerable reductions in the dynamic component of the interaction forces between the wheels and the rails just by providing a simple and gradual variation in stiffness. This study was partially developed in the scope of the well-known European research project SUPERTRACK (Kaynia *et al.*, 2005b).

Another study carried out in that university (Witt, 2008), aimed at assessing the benefit of the introduction of the USP to protect the ballast by reducing the loads action on that layer. Comparing different levels of stiffness of the USP (Figure 3-26b), it was found that the use of more resilient USP would reduce the maximum vertical loads acting on the ballast layer by about 60%. However, the results of numerical analyses performed in this study - where it was considered the variability of the subgrade stiffness along the track - it was concluded that the use of softer USP presents an important negative aspect associated with the increased variability of the contact forces between the wheels and the rails.

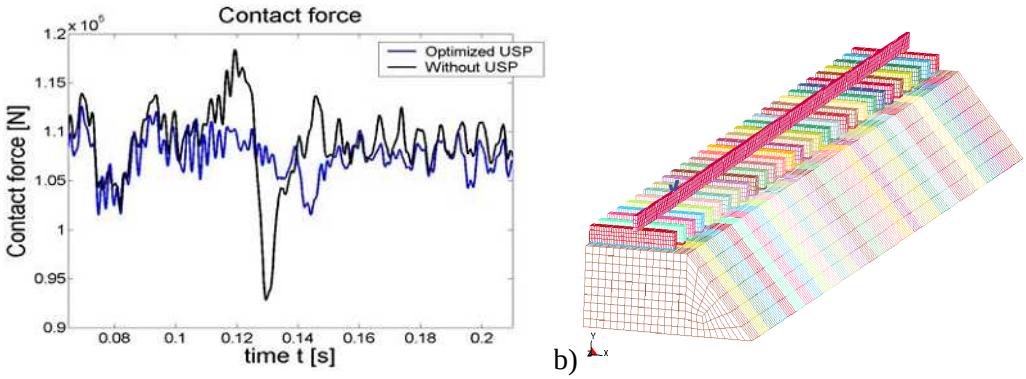

Figure 3-26. Numerical studies on USP: a) wheel-rail interaction contact after optimisation of USP stiffness (Lundqvist *et al.*, 2006); b) 3D model with USP with variable stiffness properties (Witt, 2008).

At Chalmers University of Technology, Sweden, another numerical study (Johansson *et al.*, 2008) was developed to investigate the dynamic behaviour of the track with USP. Two numerical models were used and calibrated with *in situ* measurements. Each model was more suitable for a specific range of frequencies to study the effects of different parameters that were considered in the study. It was found that USP are especially influential in the dynamic interaction behaviour between the vehicle and the train in the frequency range 0-250 Hz. The study reported that softer USP were more suitable for reducing stress at the interface between the sleeper and the ballast layer. Stiffer USP, or ballasted track without USP, were adequate to minimise stresses due to the bending of the rails and vibrations in the sleepers and rails.

Although quite complex numerical models have been developed, there is still no satisfactory way to adequately simulate the behaviour of the ballast layer and its interaction with other components of the track, using only the traditional approach of continuous elements methods such as the Finite Element Method (FEM) or the Finite Difference Method (FDM). Using these methods carries some disadvantages related to the difficulties in implementing suitable constitutive laws to represent the behaviour of the material, as well as representing the intrinsically discontinuous behaviour of ballast particles. However, using continuous element methods may be relevant in situations in which the track system is analysed as a whole, but not necessarily, when studying the behaviour of the ballast layer in detail.

In view of the developments in computational performance and in the available numerical tools, at present day it is possible to make use of specific numerical techniques to reproduce with

more accuracy the behaviour of granular materials, but at the expense of a significant amount of computational effort. One of these numerical techniques is the Discrete Element Method (DEM). In some situations, the DEM is an attractive alternative to continuous methods, in that it allows a better understanding of the behaviour of the ballasted tracks, given that the geometrical discontinuities and rearrangement of the particles can effectively be modelled (Figure 3-27).

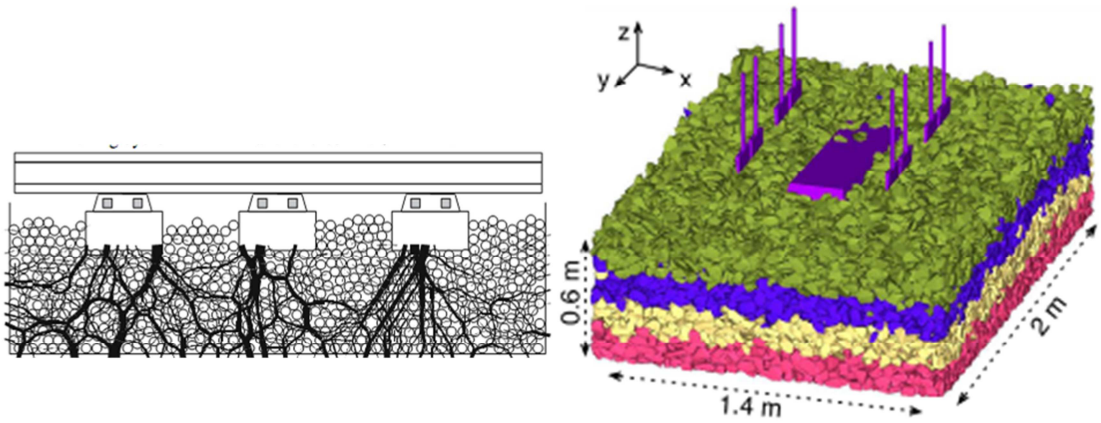

a) b)

Figure 3-27. Aspects of numerical modelling using the DEM: a) network of contact forces between the sleepers and the ballast (Lobo-Guerrero & Vallejo, 2006); b) three-dimensional modelling of ballast tamping (Azéma, 2007);.

Some authors have pointed out the relevance of using DEM to model the ballast cyclic loading tests. However, some aspects like how the particles are modelled (Azéma, 2007; Lu & McDowell, 2007) and how fragmentation is considered (Hossain *et al.*, 2007; Karrech, 2007) are still open to discussion.

A recent study (Chen, 2013; Chen & McDowell, 2014) considered a very simplified transition zone in 3D using the DEM, aiming at providing a more realistic representation of the sleeper-ballast interaction. The study considered both the variations in the track vertical stiffness and the development of settlements at the sleeper base, resulting from the ballast grain flow. Smooth and abrupt stiffness transition zones were compared in this 3-sleeper long model (Figure 3-28) and the reinforcement with geogrid was analysed. Train loads acting on the track were modelled as 90º out-of-phase sinusoidal loads applied on the sleepers, thus without considering the train-track interaction. The study evidenced that a gradual variation in the stiffness of the subgrade reduced track degradation rates and placing geogrid in the ballast layer was not effective.

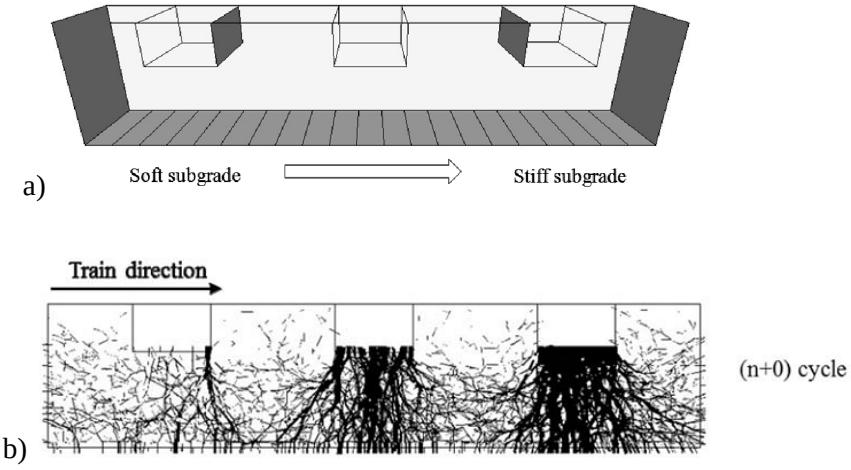

Figure 3-28. Aspects of a numerical model of a short transition zone using the DEM (Chen & McDowell, 2014): a) general view; b) example of contact force distribution.

Currently, DEM has the disadvantage of requiring significant computation resources. In addition, there is still limited experience in using this method to solve problems related to railway track.

3.5.3 Comparison summary of numerical approaches to study transition zones

Considering the abrupt variations in the track's support conditions at transition zones, the train-track interaction is an aspect of the dynamic modelling that is usually necessary to take into account. Depending on the purpose of each study, some considered the train-track interaction using a more detailed model of the train (with axles, primary and secondary suspensions, and bogies and car bodies), while others only considered the train wheels. However, some studies found in the literature did not account for these aspects and the trains were simulated as moving loads. Others also did not take into account the dynamic component of the problem.

Table 3-2 presents a summary comparison between the features of some relevant models found in the literature that focused on transition zones. The studies were chronologically ordered and pertinent innovations are pointed out.

Table 3-2. Summary comparison of numerical models to study transition zones.

Reference of the numerical study	3D model	Dynamic analysis	Train-track interaction	Foundation elements	Track faults / bump profile	Hanging sleepers	Long-term behaviour	Validation with field data	Introduced innovation
(Hunt, 1997)	-	●	●	-	●	-	●	-	Both stiffness variations and evolution of bump profile
(Lei & Mao, 2004)	-	●	●●	-	○	-	-	-	Parametric study on length and severity of bump profile
(Lundqvist *et al.*, 2006); (Witt, 2008)	●	●	○	-	-	●	-	-	3D dynamic model with wheel-rail interaction; stiffness optimisation algorithm
(Banimahd & Woodward, 2007a); (Banimahd *et al.*, 2012)	●	●	●	●	●	○	-	-	3D model with both stiffness variations and bump profile
(Namura & Suzuki, 2007)	-	●	●●	-	●	●	●	●	Validation of model with field data
(Li & Wu, 2009)	-	●	●●	-	-	-	-	-	Parametric study of transitions to floating slab track
(Alves Ribeiro *et al.*, 2009)	●	●	●	●	-	-	-	-	More realistic 3D bogie-track interaction; trackbed layers
(Nicks, 2009)	●	●	●	●	●	●	-	○	Detailed 3D dynamic model of backfill, track, bridge and bogie; some field validation
(Coelho, 2011)	●	●	-	●●	●	●	-	●	Extensive validation; groundwater flow
(Gallego Giner *et al.*, 2011)	●	-	-	●	-	-	-	-	Detailed static 3D; method for backfill design
(Varandas *et al.*, 2011; Varandas *et al.*, 2014)	-	●	●●	-	●●	●●	●	●	Non-linear sleeper-ballast contact; method to predict long term settlements at transition
(Alves Ribeiro *et al.*, 2008); (Alves Ribeiro, 2012)	-	●●	●	●●	-	●	●	●	Detailed 2D model; calibrated and validated using 3D models and field data
(Varandas, 2013)	●	●	-	●	●●	●●	-	●	3D non-linear sleeper ballast interface; Non-linear resilient behaviour of geomaterials
(Insa *et al.*, 2013)	●	○	○	●	-	-	-	-	Detailed static 3D + uncoupled vehicle model for dynamics
(Shan *et al.*, 2013)	●	●	-	●	-	-	-	-	Detailed 3D dynamic model of backfill, bridge and track
(Chen, 2013) (Chen & McDowell, 2014)	○	○	-	-	-	-	○	-	Discrete Element Method in 3D in 3-sleeper long model

Key: "-" aspect is not included/accounted for; "○" simplified/alternative approach is considered; "●" aspect is considered; "●●" aspect is considered in a more elaborate/accurate way than others.

Considering the studies mentioned in Table 3-2, some common findings and conclusions can be highlighted as follows:

- Increasing train speeds amplify the effects at transition zones in terms of: train-track interaction forces, displacements, velocities, accelerations on the track and train, loads acting on the ballast and on subjacent trackbed layers.
- Considering a perfectly horizontal rail profile, higher variations in the train-track interaction forces occur when trains run from softer to stiffer track support conditions (as in transitions from embankments to bridges), when compared with plain track with relatively constant vertical stiffness.
- A smooth stiffness transition, provided by wedge-shaped backfills, may substantially reduce the negative effects caused by the passage of trains.
- Abrupt stiffness transitions can initiate track degradation at transition zones, but the problem only becomes significant due to the development of bumps and/or dips in the longitudinal rail profile at the approach to the structure. That faulty rail profile eventually leads to hanging sleepers, which have a severe effect on track degradation.
- Due to the low resonant vertical frequency of the suspension of the car boxes, passenger comfort is not significantly affected in most situations, except in severe situations of differential settlements.
- Some technical solutions may be suitable to minimise the problems at transition zones, such as: wedge-shaped backfills with specific geometries and material properties; additional pair of rails; under sleeper pads; backfill reinforcement using grout, vertical rods or geogrids.

3.6 Final Remarks

In this chapter, it was presented a short review on transition zones for conventional and high-speed railway lines (HSL), including a discussion on the design of wedge-shaped backfills and other less conventional structural solutions. It has been reported that the main cause of the problems observed at transition zones lies in the abrupt variations of track vertical stiffness and in differential settlements that occur between the backfill and the structures. In addition to dealing with the almost inevitable degradation at the superstructure, particularly at the ballast layer, efforts should also be put in mitigating the problem that arises from the poor performance of the substructure.

A brief state-of-the-arte on the numerical modelling of transition zones was also presented comparing different modelling techniques and highlighting the advantages and disadvantages of each numerical approach.

For a proper modelling of dynamic train-track system, numerical models need to take into account not only relevant aspects of vehicle-track interaction and the track irregularities, but also the behaviour of the various layers that comprise the track substructure. As noted by Banimahd and Woodward (2007b), the simplest models do not allow for adequate reproduction of these problems and may not be suitable for studying specific effects on some components of the railway track. Not only because some models have a reduced level of discretisation, but also because they cannot properly reproduce the complex behaviour of the track that depends, among other aspect, on the non-linear variation of the stiffness, on the geometry of the structure and on the loading history (Chang *et al.*, 1980).

However, the consideration of non-linear behaviour of the materials that comprise the layers of the track in the three-dimensional dynamic analyses with train-track interaction makes the resolution of the numerical problem very time consuming, requiring a large computational effort and a very cautious analysis of the results.

Thus, it seems that it is necessary to continue to improve the numerical techniques in order to reproduce, as close as necessary, the actual behaviour of the structures, concerning the physical constraints and providing efficient analysis.

Taking into account the various studies that were presented, it may be considered that the accelerations on the axles of the vehicles, the contact forces between wheel and rail, as well as the acceleration levels inside the vehicle body can be used as performance indicators of the dynamic behaviour of transition zones. The results of some studies (Namura & Suzuki, 2007; Alves Ribeiro, 2012) suggest that some of these indicators may play an important role in monitoring the performance of transition zones in actual railway lines.

Chapter 4

The *Alcácer* bypass and its transition zones*

4.1 Introduction

This chapter presents a brief description of the *Alcácer* bypass that is a recent railway line built in Portugal for mixed traffic and allows for maximum train speeds of 220 km/h. Considering the characteristics of the line, it was used to study the behaviour of transition zones in the scope of a research project, as mentioned earlier.

After the description of the line, results regarding the track platform are presented and discussed in terms of the requirements for the physical and mechanical characteristics of the geomaterials and layers. A general description of the transition zones and other singularities of the line is presented. A brief characterisation of the traffic is also provided.

Then, the construction of a transition zone case study is analysed in detail. Results of conventional laboratorial and cyclic load triaxial testing on granular materials and *in situ* mechanical characterisation of the layers are presented. Relevant aspects regarding the construction are addressed and discussed.

* Part of this chapter is based on the following articles:

- **Paixão, A.; Fortunato, E. & Calçada, R.** (2013) *Design and construction of backfills for railway track transition zones*; Proceedings of the Institution of Mechanical Engineers, Part F: Journal of Rail and Rapid Transit;
- **Fortunato, E.; Paixão, A. & Fontul, S.** (2012a) *Improving the use of unbound granular materials in railway sub-ballast layer*; Advances in Transportation Geotechnics II; Hokkaido University, Japan; 10-12 Sep. 2012; pp. 522-527;

4.2 General aspects of the *Alcácer* Bypass

The *Alcácer* bypass (*Variante de Alcácer*, in Portuguese) is a railway stretch, about 28.98 km long, that was recently built in the scope of the modernisation of the Portuguese Southern Main Line between about kilometre markers 59.0 and 94.5 (Figure 4-1). It is located between the south end of the *Pinheiro* station and the branch line of *Somincor*. The position reference system that is used in this work is the same that was established in the design (REFER, 2006), which starts at kilometre zero (at the south end of *Pinheiro* station) and ends after about 29 km.

The line allows for mixed traffic, with maximum axle loads of 25 t, in a single railway track with broad (Iberian) gauge of 1.668 m, using continuously welded UIC60E1 rails and 2.6 m long monoblock concrete sleepers (SATEPOR TBMP 02), spaced 0.6 m. The sleepers have the particularity of being compatible with the Standard gauge (1.435 m). The fastening system is Vossloh W14 with elastomer rail pads Zw700/148/165 (static stiffness of 50-70 kN/mm, measured between 18 and 68 kN, as provided by the manufacturer). Figure 4-2 shows a schematic representation of the standard cross-section of the track on embankment.

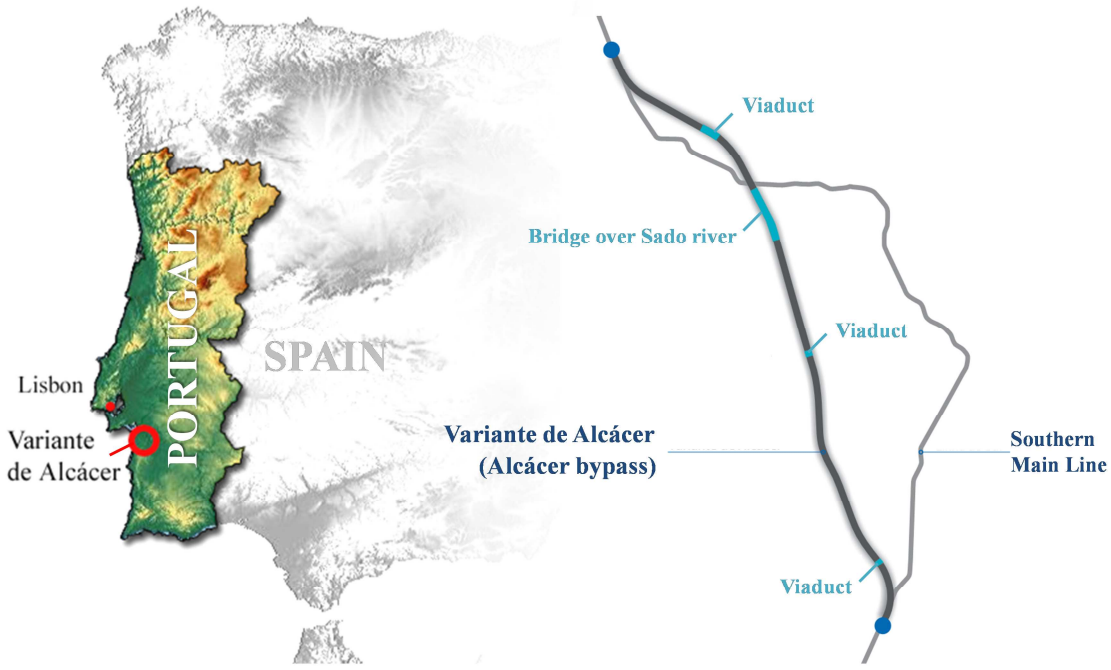

Figure 4-1. *Alcácer* bypass: a) location of the by-pass; b) schematic representation of the layout adapted from REFER (2010).

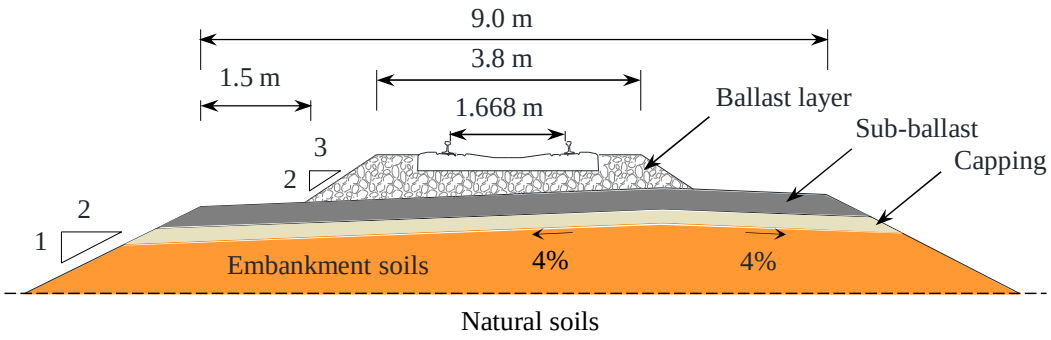

Figure 4-2. Standard track cross-section on embankment.

Figure 4-3 shows some aspects of the layers and components of the track substructure and superstructure during construction.

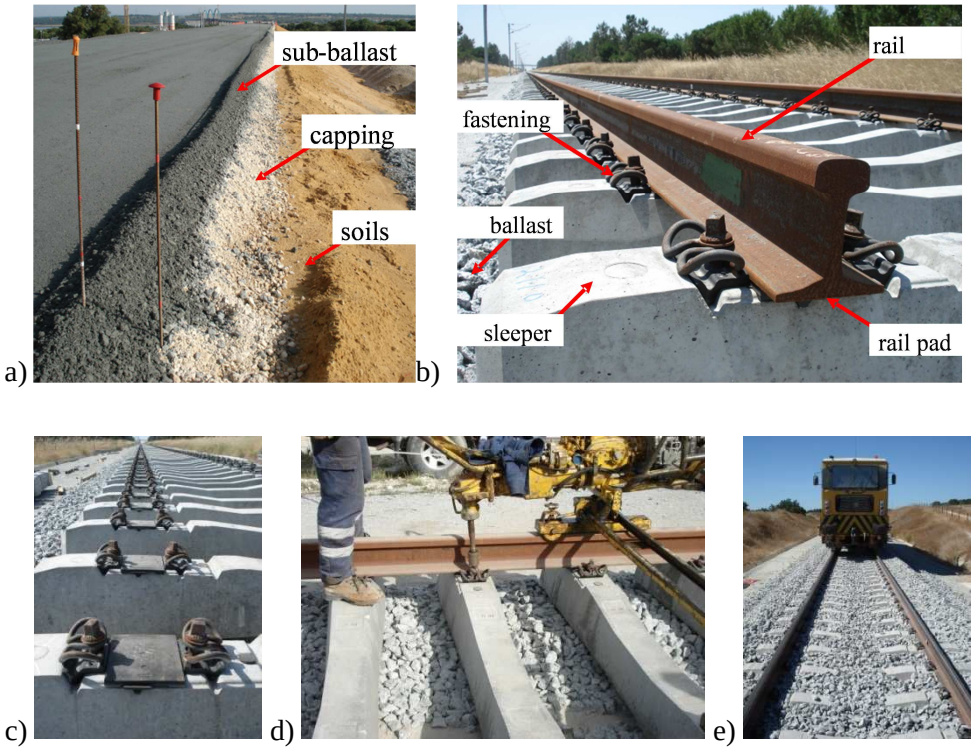

Figure 4-3. Aspects of the track during construction: a) layers of the substructure; b) components of the superstructure; c) concrete monoblock sleepers with fastening system and rail pads; d) fastening of the rail and application of pre-load; e) aspect of the track before cleaning the excess of ballast and establishing the final geometry of the track.

Under sleeper pads (USP) were installed, as trial tests, in a few sleepers during construction at the approach to the structures identified Figure 4-4. This was an initiative to investigate the use of USP (provided by CDM, Portugal, Lda) at transition zones in the scope of the research project mentioned earlier.

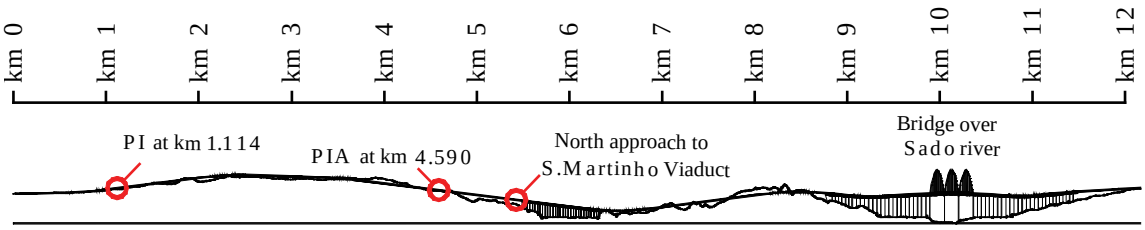

Figure 4-4. Location of the structures where USP were installed.

The 1st stage of the construction - mainly comprising earthworks and structures, excluding the prominent new bridge over Sado river (Figure 4-1) - begun in February 2007 and was concluded in October 2008. The 2nd stage was divided in sub-stages related to the construction of the bridge over Sado river and its approach viaducts, the laying of the track and the construction of the electrification, signalling and telecommunication systems (REFER, 2010). The by-pass was officially opened to traffic in December 12th, 2010. However, in October 28th 2010, passenger and freight trains started using it temporarily (with speeds limited to 60 km/h) as an alternative to the old line that went out of service due to the derailment of a coal freight train at the approach to the old railway bridge over Sado river.

4.3 The track platform

In general, the track platform was constructed on gypsum-clay geologic formations from the Tertiary, Mio-Pliocene (namelly, *Algeruz/Monte do Pinheiro* and *Marateca* formations) with the lithology predominantly comprising sands and seldomly silts and clays. At the south of the Sado river, between 11.275 and 17.700 km marks, dune sands from the Quaternary (Holocene) are found. Throughout the line, the first layers of natural soils consisted of silty sand and organic material, reaching sometimes several meters deep. In general, the relief is not very pronounced, leading to excavations and embankments with heights rarely exceeding 5 m. Figure 4-5 presents aspects of the track platform at the end of the 1st stage.

Figure 4-5. Aereal views of the track platform at the end of the 1st stage of construction of *Alcácer* bypass (REFER, 2010).

The design of the track substructure followed the recommendations of Code 719R (UIC, 2008b). Due to the impracticality to obtain soil type QS3, the capping layer was constructed with a thickness of 0.20 m (Figure 4-6), using well-graded crushed limestone aggregate. The minimum degree of compaction, D_c, was 97% of the Optimum Modified Proctor (OPM) value, in order to obtain a deformation modulus (E_{V2}) of at least 80 MPa on top of the layer, in the second cycle of the plate load test. The calculation of E_{V2}, following the French AFNOR procedure (2000), considers the well-known Boussinesq solutions for a 0.6 m diameter circular rigid load plate applying a pressure of 200 kPa on a homogenous, isotropic and linearly elastic half space. The capping layer was placed on a subgrade characterised by $E_{V2} \geq 60$ MPa and a minimum degree of compaction of 95% OPM. The design of the sub-ballast layer was in accordance with the Technical Instruction IT.GEO.006 (REFER, 2007) and established a minimum thickness of 0.30 m. It was established a minimum degree of compaction of D_c = 98% OPM and a minimum value of the deformation modulus of $E_{V2} \geq 120$ MPa, measured at the top of the layer. Figure 4-8 shows the envelopes of the particle size distribution (PSD) established in the design and additional requirements for the materials. During construction, samples for laboratory testing of sub-ballast and capping were collected from stockpile and from the layers, before and after compaction. Among other physical characteristics, PSD, Los Angeles, micro-Deval and methylene blue tests were performed on 45 granite and on 67 limestone samples. Table 4-1 presents average values obtained in the tests and the respective design requirements.

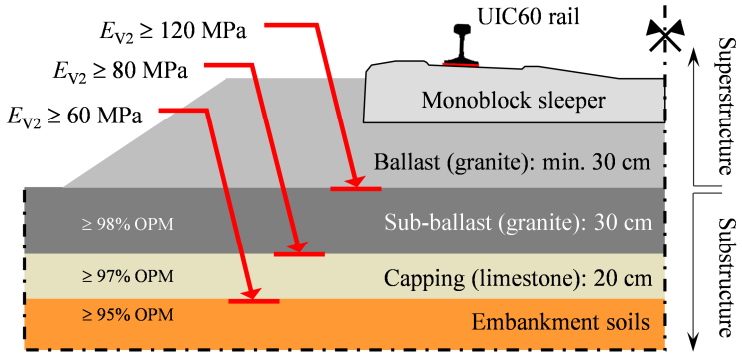

Figure 4-6. Requirements of the layers for track on embankments.

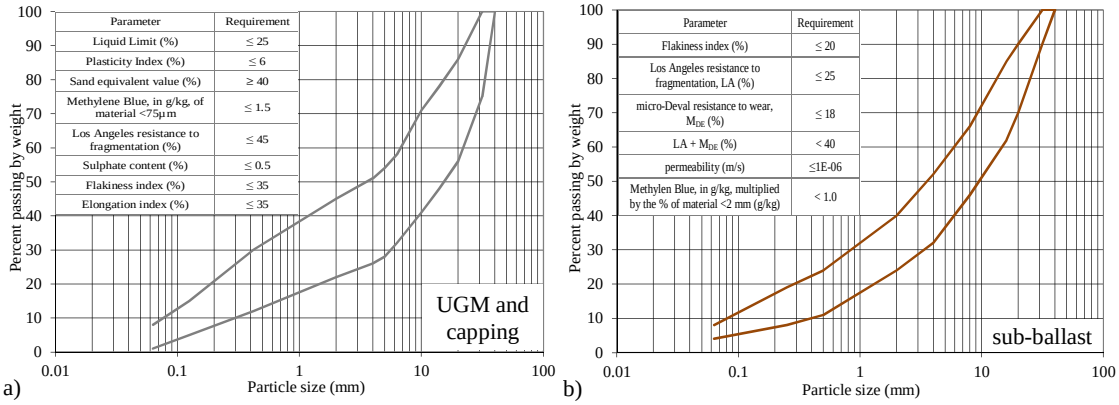

Figure 4-7. Grading envelopes and some required properties: a) UGM and capping material; b) sub-ballast.

Table 4-1. Some requirements and obtained values on the materials applied in the sub-ballast and capping layers.

Parameters	Sub-ballast (granite)			Capping (limestone)		
	Requirements	Results		Requirements	Results	
	REFER (2007)	$\bar{x}$	CV	REFER (2006)	$\bar{x}$	CV
Los Angeles	LA ≤ 25	23	0.03	LA ≤ 45	27	0.01
Micro-Deval	MDE ≤ 18	5	0.08	-	12	0.03
Los Angeles + Micro-Deval	LA+MDE < 40	28	0.03	-	39	0.01
Methylene blue value times % passing sieve 2 mm (g/kg)	MB ≤ 1	0,35	0,58	MB ≤ 4	0,75	0,17
Dc_{OPM} (%)	≥ 98	99,4	0,01	≥ 97	98,7	0,01

$\bar{x}$ – average value; CV – coefficient of variation.

In Figure 4-8a and b, examples of PSD curves obtained before and after compaction are presented. From the analysis of the curves, minor changes are noticed for both materials, which

denotes the good quality of the materials. Together with the percentage of fine particles, the MB value of the aggregate is an adequate parameter to assess the influence of the water content (w) on the aggregate behaviour. From the analysis of Figure 4-8c it can be concluded that the MB values obtained on limestone samples were higher than those obtained on granite samples (it was only possible to compare results obtained before compaction with those of 12 tests carried out after compaction). Although during the construction process, an evolution of this parameter has been observed in both materials, such evolution was not very relevant and it was still possible to meet the design requirements.

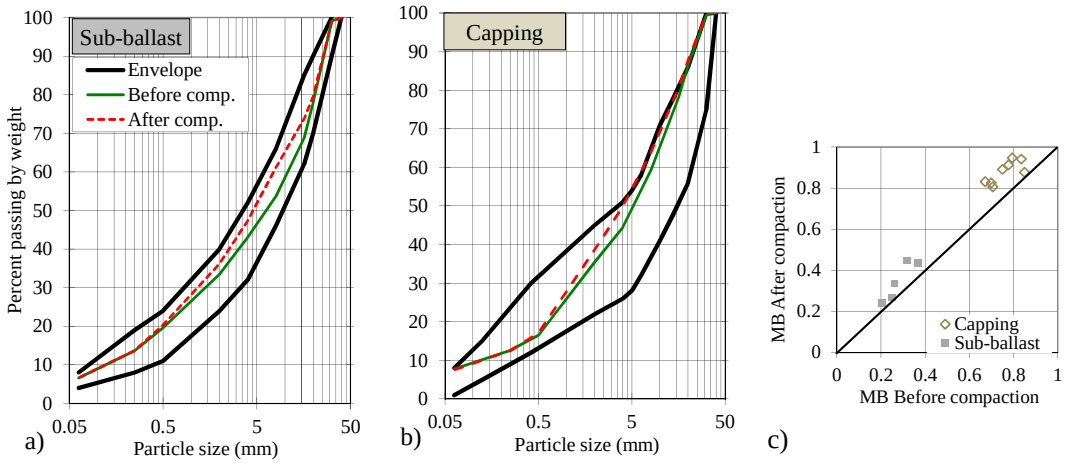

Figure 4-8. Typical evolution of PSD curves of the granite (a) and the limestone (b) obtained before and after compaction; evolution of methylene blue values (c).

It is known that performance characterisation of geomaterials and layers is essential for the prediction of their behaviour. Therefore, the traditional mechanical and physical characterisation of materials was completed with *in situ* loading tests. The performance-based specifications related to transport infrastructure are usually based on minimum deformation modulus evaluated through non-destructive tests on different layers. To this end, following IT.GEO.006 (2007) and according to Code 719R (UIC, 2008b), 174 plate load tests (PLT) were performed on the sub-ballast surface, between June and October 2008, as the layer was being concluded. The majority of the results of the PLT tests were between 120 and 250 MPa, with an average value of 205 MPa, thus complying with the minimum limit of 120 MPa.

Measurements with the *portancemètre* equipment (Quibel, 1999) were also performed. This non-destructive loading equipment consists of a rolling vibrating wheel that allows for continuous stiffness measurement and respective values of deformation modulus. It performs a swift measurement, enabling an overall view of the variation of the modulus along the line and

giving an average value at about every 1.0 m. Figure 4-9 shows the cumulative distribution of the results of the three *portancemètre* surveys performed over the entire length of the sub-ballast layer that were carried out in the following dates: i) November 2008; ii) December 2008; and iii) March 2010. The results only regard track sections on earthworks given that the track on structures did not comprise sub-ballast layer.

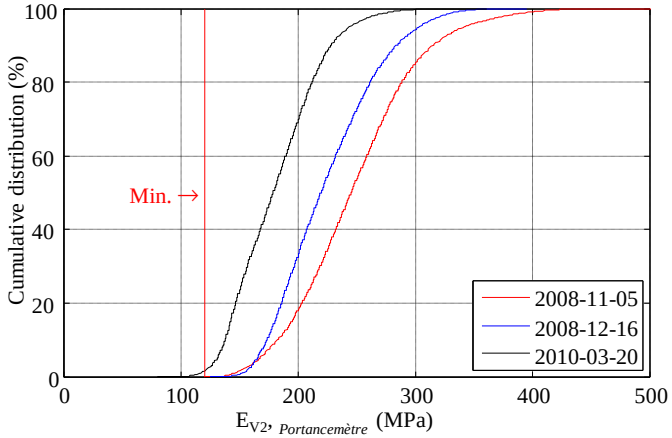

Figure 4-9. Evolution of the cumulative distribution functions of E_{V2} measured with the *Portancemêtre* on top of the sub-ballast layer.

Although, in general, the measured values were always higher than the limit set in the design (120 MPa), a significant reduction in E_{V2} was verified when, due to rainfall that occurred during the rainy season, the average value of the water content increased from 3.7% (in 2008-11-05) to 4.7% (in 2010-03-20). This influence of the water content on the behaviour of the aggregates is well-known and documented in the literature (Paute *et al.*, 1994; Fortunato, 2005). Figure 4-10 shows the available data regarding the daily precipitation from the two weather stations nearest to the railway bypass (*Montevil* and *Comporta*), including the average daily temperatures (reported by the *Comporta* station). The results confirm the rainier winter of 2010, compared with the same period of 2008.

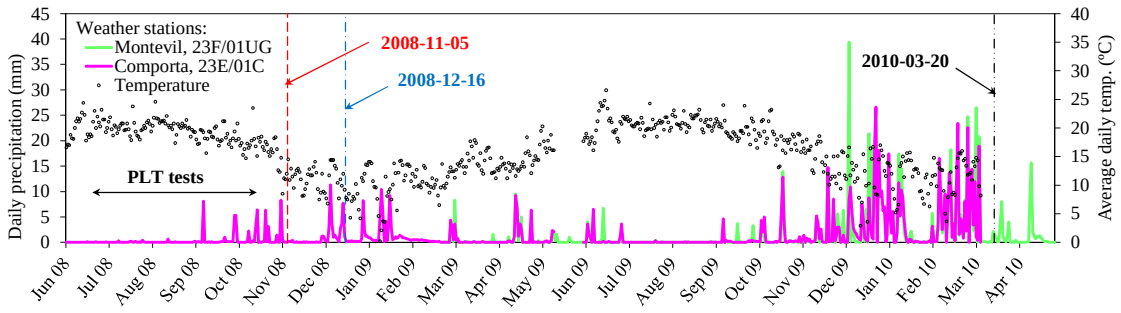

Figure 4-10. Daily precipitation and average daily temperature (source:snirh.pt).

Figure 4-11 presents the values of the E_{V2} obtained in 174 PLT tests and the results of the 3rd *portancemètre* survey on the sub-ballast layer, along with other physical characteristics of the platform. It is visible that the values of the PLT were generally higher than those obtained with the *portancemètre*. Again, this difference seems to be explained by the influence of the water content of the geomaterials, considering that the PTL were performed during a very dry period with almost no precipitation and with high temperatures (Figure 4-10). In addition, it is observed that the section of the track between 11.8 km and 16.5 km marks showed the most significant differences. This is probably related to the fact that the PLT tests in that stretch of the track were performed firstly, in late June 2008 and early July, during some of the hottest days of that summer and before the short periods of rain in August and September (Figure 4-10).

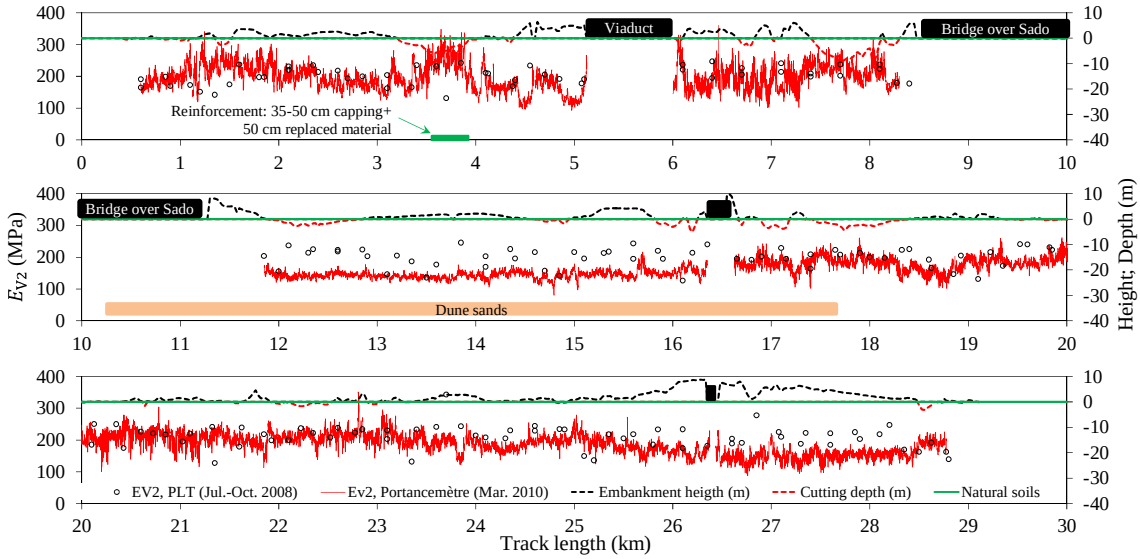

Figure 4-11. Deformation modulus E_{V2} obtained in PLT tests and in the 3rd *portancemètre* survey.

A more detailed analysis of the values obtained with the *portancemètre* evidenced a spatial variation of E_{V2} at the approach to some structures (bridges, viaducts, underpasses, culverts). To carry out this analysis, a georeferenced representation method was developed in the context of this study that enables overlaying multiple levels of information, namely: the physical characteristics of the infrastructure; the results of the quality control during construction; and the information obtained from the monitoring of the railway line in operation.

The method was developed in MATLAB environment to post process the available data and it makes use of the function `plot_google_map.m`*. In Figure 4-12, an example is presented with the variation of E_{V2} in a stretch where there are different track configurations. It appears that the values of E_{V2} increase at the approach to viaducts and underpasses or over buried structures that have technical blocks. These structures were designed to produce a gradual variation of stiffness in these areas, as discussed in Chapter 3. In the cutting section between about 3.5 km and 4 km marks, it was necessary to strengthen the foundation of the track. It is visible that this reinforcement yielded higher values of E_{V2} in that stretch.

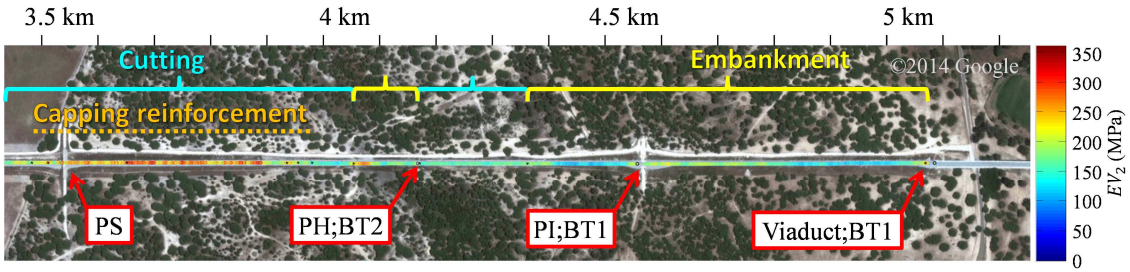

Figure 4-12. Overlay of the values of E_{V2} and satellite view of the track (imagery: © 2014 Google). PS - road overpass; PH – culvert; PI – underpass; BT1 and BT2 – Technical blocks.

4.4 Transition zones and other singularities

The track layout of the *Alcácer* bypass intersects existing infrastructures and natural obstacles such as rivers and streams. The design established different structures to account for these obstacles and for other constrains, in particular:

- A bridge over Sado river, with the respective north and south approach viaducts;
- Two viaducts over the streams of *São Martinho* and *Água Cova*;
- A viaduct over the national road N120;
- 7 road overpasses – PS (*Passagem Superior*);
- Two road underpasses – PI (*Passagem Inferior*);
- 6 agricultural underpasses – PIA (*Passagem Inferior Agrícola*);
- 4 fauna underpasses – PF (*Passagem de fauna*);
- 37 culverts - PH (*Passagem Hidráulica*);

* The function `plot_google_map.m` was developed by Zohar Bar-Yehuda and is available at the MATLAB Central File Exchange on-line library (File ID: #27627):
http://www.mathworks.com/matlabcentral/fileexchange/27627-plot-google-map

The structures mentioned above can be considered as track singularities because they entail sudden variations in the track support conditions. Considering the variations that occur in the track substructure between embankments and cuttings or in sections of the track with reinforcement in the substructure, these locations may also be considered as track singularities – more than 80 situations were identified corresponding to such scenarios. Switches and rail expansion joints are also examples of track singularities in that they are associated with variations in the configuration of the track superstructure. In the *Alcácer* bypass, switches can be found at the end of the line, where it merges with the old line, and rail expansion joints can be found on the bridge over Sado river (at km marks 8.790, 8.835, 9.600, 10.125, 10.170, 10.890 and 10.928), mainly to avoid excessive stresses on the rails due to the longitudinal displacements of the bridge.

a) b) c)

Figure 4-13. Examples of track singularities in the *Alcácer* bypass (REFER, 2010): a) construction of the backfill to a viaduct; b) construction of a road underpass; c) final aspect of a culvert.

At the transition zones of some singularities, particularly at the approaches to bridges, viaducts, underpasses and culverts, wedge-shaped backfills were established in the design and were constructed following specific requirements, as discussed in Chapter 3. The design established two types of wedge-shaped backfills (Figure 4-14) - also designated “Technical Blocks” in some countries (*Blocs Techniques* in France; *Bloco Técnico* in Portugal): 1) Technical Blocks Type 1 at the approach to larger structures (bridges, viaducts and underpasses); 2) Technical Blocks Type 2 at the approach to some culverts that were placed at a relatively shallow depth in the embankments (less than about 1.5 m from the base of the ballast layer).

Tables 4-2 and 4-3 present the lists of the transition zones to bridges or viaducts, or over underpasses and culverts, and that include wedge-shaped backfills type BT1 and BT2, respectively. Table 4-4 provides the list of culverts that the design did not establish wedge-shaped backfills (no BT) because they were at a depth greater than about 1.5 m from the base of the ballast layer.

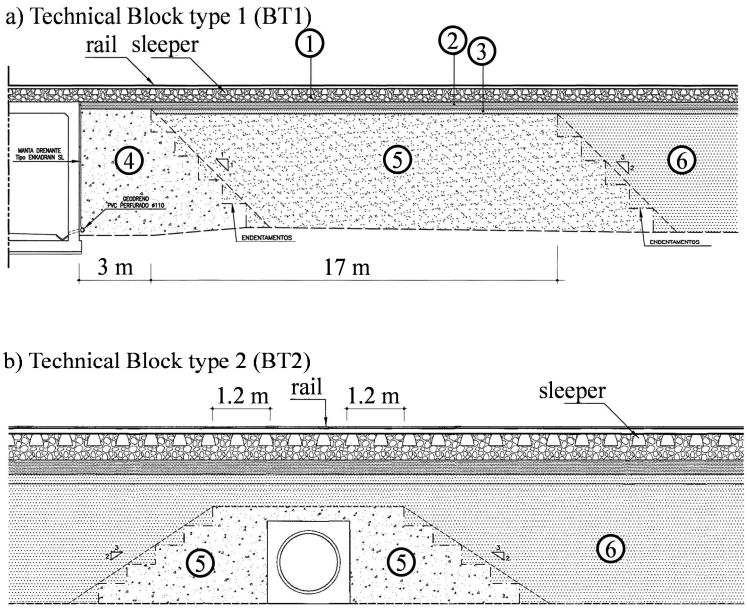

Figure 4-14. Technical blocks type 1 (a) and 2 (b) (REFER, 2006): 1-ballast; 2-sub-ballast; 3-capping; 4-cement bond mixture (CBM) with binder content (BC) of 5%; 5-unbound granular material (UGM); 6-embankment with soils.

Table 4-2. Track singularities with wedge-shaped backfill type BT1 (Figure 4-14a).

Location (km)	Structure
1.114	Road underpass, PI
4.590	Agricultural underpass, PIA
5.142	North approach to the viaduct over S. Martinho stream
5.994	South approach to the viaduct over S. Martinho stream
6.463	Agricultural underpass, PIA
8.312	North approach to the bridge over Sado river
11.268	South approach to the bridge over Sado river
15.671	Agricultural underpass, PIA
16.352	North approach to the viaduct over Água Cova stream
16.623	South approach to the viaduct over Água Cova stream
18.859	Agricultural underpass, PIA
22.842	Agricultural underpass, PIA
23.889	Road underpass, PI
26.378	North approach to viaduct over EN120
26.430	South approach to viaduct over EN120
26.987	Agricultural underpass, PIA

Table 4-3. Track singularities with wedge-shaped backfill type BT2 (Figure 4-14b).

Location (km)	Structure and diameter (Ø)	Location (km)	Structure and diameter (Ø)
0.324	Culvert, PH 0.1, Ø=1.0 m	21.153	Culvert, PH 21.1, Ø=1.0 m
1.244	Culvert, PH 1.1, Ø=1.2 m	22.593	Culvert, PH 22.1, Ø=1.0 m
1.975	Culvert, PH 1.3, Ø=1.0 m	22.705	Culvert, PH 22.2, Ø=1.2 m
4.181	Culvert, PH 4.1, Ø=1.0 m	23.055	Culvert, PH 23.1, Ø=1.0 m
12.960	Fauna underpass, PF 12.1, Ø=1.2 m	23.178	Culvert, PH 23.2, Ø=1.0 m
13.400	Fauna underpass, PF 13.1, Ø=1.0 m	24.535	Culvert, PH 24.1, Ø=1.0 m
13.820	Culvert, PH 13.2, Ø=1.0 m	24.690	Culvert, PH 24.2, Ø=1.0 m
14.025	Fauna underpass, PF 14.1, Ø=1.0 m	25.076	Culvert, PH 25.1, Ø=1.0 m
17.290	Box culvert, PH 17.1, 1.5x1.0 m	25.539	Culvert, PH 25.3, Ø=1.2 m
20.546	Culvert, PH 20.1, Ø=1.2 m	28.407	Box culvert, PH 28.1, 1.5x1.0 m
20.781	Culvert, PH 20.2, Ø=1.2 m		

Table 4-4. Track singularities (PH or PF) without wedge-shaped backfill (no BT).

Location (km)	Structure and diameter (Ø)	Location (km)	Structure and diameter (Ø)
1.595	Culvert, PH 1.2, Ø=1.0 m	8.127	Culvert, PH 8.1, Ø=1.0 m
2.584	Culvert, PH 2.1, Ø=1.0 m	15.275	Fauna underpass, PF 15.1, Ø=1.0 m
2.939	Culvert, PH 2.2, Ø=1.0 m	19.117	Culvert, PH 19.1, Ø=1.2 m
4.583	Culvert, PH 4.2, Ø=1.0 m	21.765	Box culvert, PH 21.2, 1.5 x 1.0 m
4.787	Culvert, PH 4.3, Ø=1.0 m	23.653	Culvert, PH 23.3, Ø=1.2 m
6.188	Culvert, PH 6.1, Ø=1.2 m	25.363	Culvert, PH 25.2, Ø=1.0 m
6.330	Culvert, PH 6.2, Ø=1.0 m	25.880	Culvert, PH 25.4, Ø=1.2 m
6.932	Culvert, PH 6.3, Ø=1.0 m	26.685	Culvert, PH 26.1, Ø=1.0 m
7.138	Culvert, PH 7.1, Ø=1.2 m	27.047	Culvert, PH 27.1, Ø=1.0 m
7.220	Culvert, PH 7.2, Ø=1.2 m	27.494	Culvert, PH 27.2, Ø=1.0 m

Figure 4-15 shows the distribution of the track singularities along the line, as well as the values of the E_{V2} obtained with the *portancemètre* (March 2010) on the sub-ballast layer throughout the line and other physical characteristics of the line. It is visible that near some singularities there seems to be a rapid variation of E_{V2}, generally, increasing as approaching the structures. As mentioned earlier, these results are a consequence of the wedge-shaped backfills that were constructed in those transition zones. This aspect will be addressed in detail in the case study presented in 4.7. Additionally, in Annexes A, detailed results of the E_{V2} are presented for each track singularity of the railway bypass.

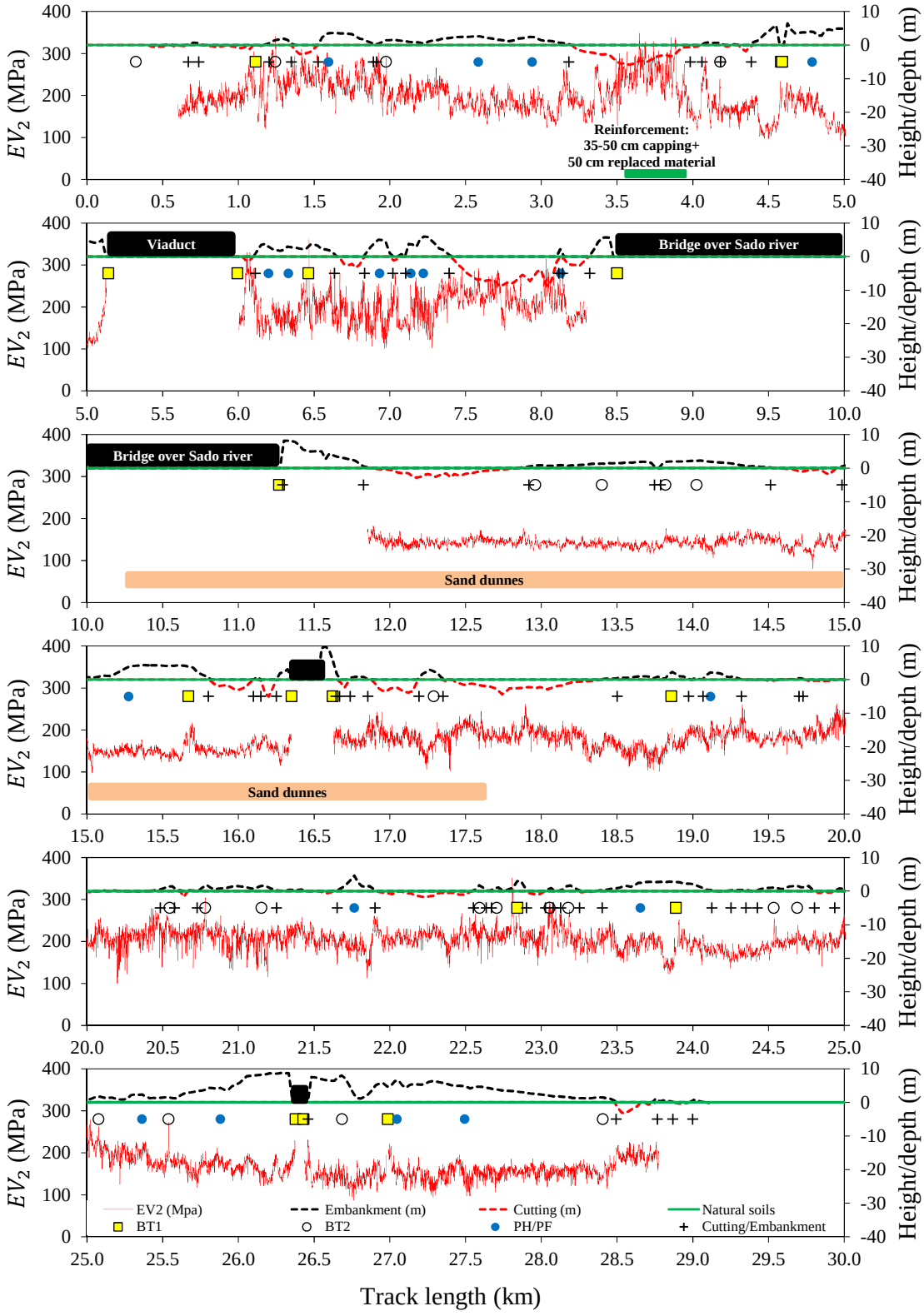

Figure 4-15. Deformation modulus E_{V2} obtained with *portancemètre* and location of track singularities.

4.5 Traffic

As mentioned earlier, the line allows for mixed traffic and different services have been in operation since the inauguration. The main train services are described below.

The *Alfa Pendular* (Figure 4-16) is the fastest passenger service in the Portuguese network. It consists of a 6-coach tilting passenger train (similar to ETR 401 pendolino) travelling at maximum speed of 220 km/h, taking less than 8 min to go through the *Alcácer* bypass. In normal conditions, there are two daily trains in each direction connecting Lisbon and Algarve with very few stops.

a)

b)

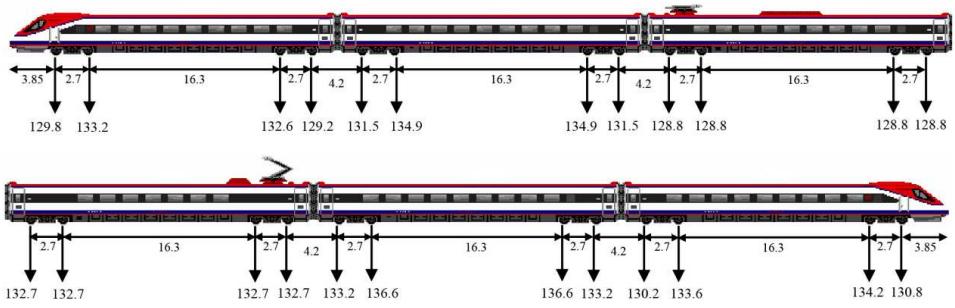

Figure 4-16. The *Alfa Pendular* train: a) general aspect; b) schematic representation of the axle arrangement (in m) and respective load estimates (in kN).

The second fastest passenger service is the *Intercidades* (Intercity express) which consists of one electric locomotive (recently the CP 5600 by Siemens; formerly also the CP 1900) and 3 to 6 refurbished coach cars (Corail-like), depending on the expected number of passengers. In the first years, these trains still used the old line to serve the city of Alcácer do Sal. But since December 2011, after a major revision on the national railway services, that stop was cancelled and the *Intercidades* was allowed to use the *Alcácer* bypass. Initially the trains were only allowed to travel at maximum speed of 160 km/h, but after a recent update on the coache's

bogies, the *Intercidades* has had the maximum speed increased to 200 km/h. Normally, there are 3 daily *Intercidades* in each direction, connecting Lisbon and Algarve.

a)

b)

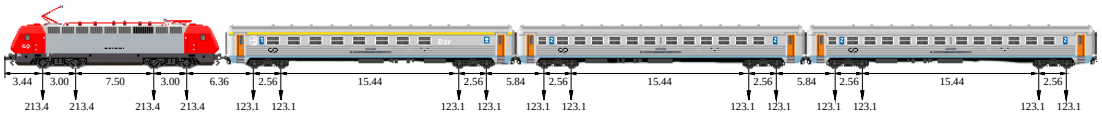

Figure 4-17. Intercity passenger train: a) general aspect; b) schematic representation of the axle arrangement (in m) and respective load estimates (in kN).

The freight traffic in the bypass accounts for the transport of a variety of goods, such as coal, ore, liquid fuels, wood, aggregates, containers, mostly originated or destined to the deep-water port of Sines. Normally, there are about 15 to 20 freight trains each day running at speed of about 80 km/h to 100 km/h. Trains transporting the coal from the port of Sines to Pego powerplant (Figure 4-18) are the longest and heaviest freight trains using the *Alcácer* bypass.

a)

b)

c)

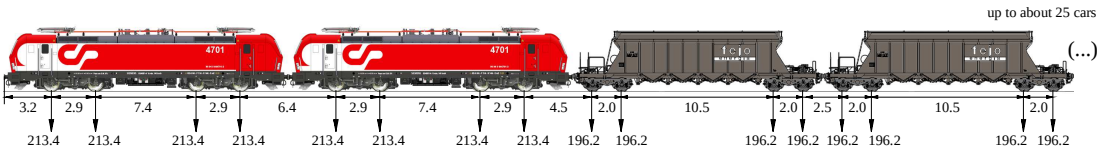

Figure 4-18. Coal freight train with double traction (two CP locomotives of series 4700) transporting about 25 cars: a) general view of the locomotives; b) rear wagons; c) schematic representation of the axle arrangement (in m) and respective load estimates (in kN).

The type of traffic and the number of trains has not been constant in the last year in the *Alcácer* bypass. Estimates based on observations and on reports by REFER suggest that, in the last 4 years, the annual gross tonnage has varied from about 6 to 8 million gross tonnes (MGT). In total, since the inauguration to July 2013, it is estimated that the accumulated tonnage was about 16.6 MGT.

It should be mentioned that the design of the track layout accounts for a possible increase of passenger train speeds up to 250 km/h for the *Alfa Pendular* and 220 km/h for the intercity.

4.6 Analysis of the track geometry

4.6.1 The inspection vehicle

Currently REFER uses a self-propelled inspection vehicle, a Plasser&Theurer EM-120 (Figure 4-19), running at a maximum speed of 120 km/h on broad gauge tracks (Iberian gauge). The vehicle and the inspection systems have been updated and upgraded in recent years. The vehicle allows the evaluation of all track geometric parameters using an inertial system, rail profile wear and corrugation with independent laser systems, catenary static geometric parameters and also track gauge with a laser system, plus ballast contamination with ground penetration radar (Alves & Vieira, 2014). Measurements of the short-wave defects of the track (< 1 m) and surveys to detect unsupported sleepers are only performed occasionally in the Portuguese network.

a) b)

Figure 4-19. REFER's inspection vehicle: a) general view; b) detail of the inertial box mounted on the bogie frame.

4.6.2 General aspects of the track quality

There are two main regulations that apply to the track of the *Alcácer* bypass in terms of its geometric quality, namely the EN 13848 series and the Technical Instruction VIA 018 (REFER, 2009). The EN 13848, Part 5: Geometric quality levels (CEN, 2008) establishes the Alert Limits

(AL) and the Intervention Limits (IL), while REFER's standard establishes the Immediate Action Limits (IAL). These three classifications are related to different levels of track degradation and were described in Chapter 2. Table 4-5 shows the limit values for the different geometric parameters, considering the maximum speed of 220 km/h in the *Alcácer* bypass for the passenger-tilting train *Alfa Pendular*.

Table 4-5. Track geometry limits (in mm) for train speed of 220 km/h.

Standard	IT VIA 018 (REFER, 2009)		EN 13848-5 (CEN, 2008)
Parameter	AL	IL	IAL
Alignment D1, LA_{D1} $^{+}$	±8	±9	±12
Alignment D2, LA_{D2} $^{+}$	±15	±17	±24
Standard deviation of LA_{D1}	1.1	n.a.	n.a.
Long. Level D1, LL_{D1} $^{+}$	±12	±14	±20
Long. Level D2, LL_{D2} $^{+}$	±20	±23	±33
Standard deviation of LL_{D1}	1.9	n.a.	n.a.
Twist (base-length 3 m) $^{+}$	±9	±12	*
Gauge[1]	-4/+20	-5/+23	-7/+28
Mean gauge (over 100 m)[1]	-3/+16	-4/+18	-5/+20

D1 - denotes defects within the wavelength range between 3 and 25 m; D2 - denotes defects within the wavelength range between 25 and 70 m; $^{+}$ difference to the peak value; [1] difference to the nominal value; * depends on the track layout and base-length, among other factors.

The surveys in the *Alcácer* bypass were performed about 2 to 4 times each year and measurements of the geometric parameters of the track were recorded at every 25 cm, thus each survey normally had more than 100 000 readings of each geometric parameter. Considering the significant amount of data to be analysed, a code was developed in MATLAB to post process the information from the inspection vehicle. The post processing of the data was a key aspect so that the results from different surveys could be compared against each other, thus making it possible to study the evolution of the track geometry. This is mainly because the records of the surveys of the inspection vehicle normally do not match exactly with each other along the line. Thus, a code was developed to account for this aspects and it basically performs the following tasks: a) reorders and crops the records if necessary to analyse the same length of the track in all surveys; b) removes any existing offsets and performs slight adjustments in the spatial sampling frequency if necessary; c) applies a general resampling to the data (yet using the same spatial

frequency of 1/0.25 m) so that the successive readings in a given location of the track obtained in different surveys share exactly the same position in the database.

In the calculation of average values and standard deviations of the geometric parameters, instead of dividing the length of the track in independent stretches with 200 m, it was considered a moving window of 200 m to analyse the data. This decision aimed at providing a better assessment of the track geometry at transition zones, considering that the length of these structures stretches up to about a few dozens of meters. Using the adopted method, values (averages and standard deviations of the parameters) were calculated at every 0.25 m of the track, and each value was calculated considering a window that included the previous 100 m and the next 100 m, i.e. each value was assigned to the respective centre of a 200 m-window. If this method had not been adopted, the influence of a given transition zone to the geometric parameters could be reflected separately in two different stretches of 200 m.

Figure 4-20 shows some results regarding the track measurements performed at about 120 km/h by the REFER's inspection vehicle in the surveys of March 2011 and July 2013. The results denote the average of the left and right rails, when applicable.

It can be concluded that more than 28 months after the track was opened to traffic, the track quality is still very good and none of the Alert Limits had been reached yet. The results regarding the left and right rails were quite similar along the track for the various parameters, thus not evidencing a preferential side of track degradation. It is observed some evolution in a few parameters, particularly, the standard deviation of the longitudinal alignment and level, as well as the track gauge. It seems that the standard deviation of the alignment will be the first parameter to reach the respective value of the Alert Limit at around 8.8 km mark, certainly caused by the rail expansion joints (the breather switches) on the bridge over Sado river (Figure 4-21).

The Power Spectral Density of the track parameters over a given track section is another useful tool to analyse the track geometry. Among other aspects, it allows identifying repetitive defects with similar wavelengths, such as welds, which are evidenced by peaks in the Power Spectral Density curve. Figure 4-22 shows the Power Spectral Density curves of the longitudinal alignment, *LA* (D1 and D2), longitudinal level, *LL* (D1 and D2), twist and gauge, calculated for the entire length of the bypass, with regard to the respective spatial wavelength.

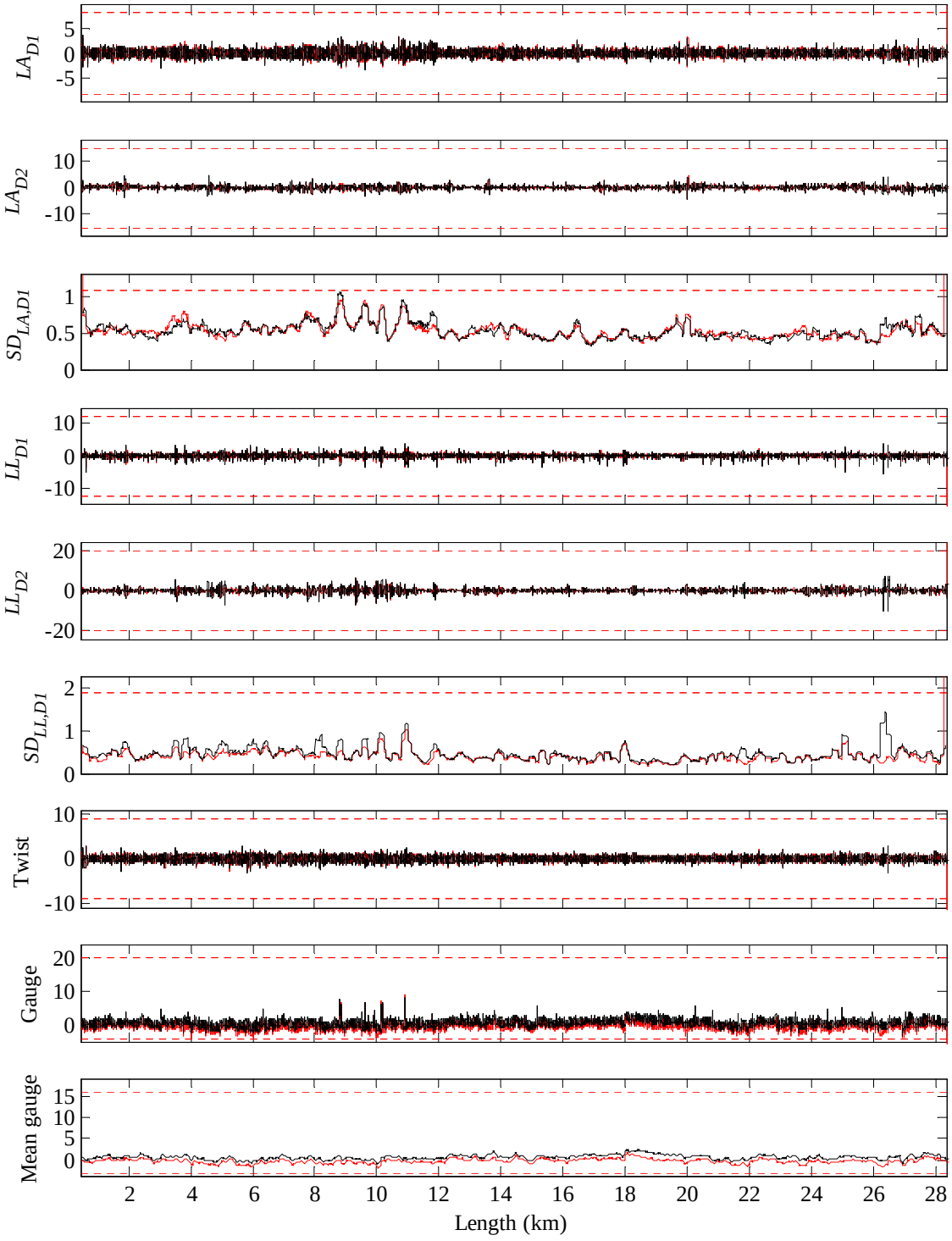

Figure 4-20. Track geometry parameters (in mm) regarding the surveys carried out in March 2011 (red) and July 2013 (black), and respective Alert Limit values by REFER (dashed lines).

a) b)

Figure 4-21. Aspects of the breather switch on the bridge: a) fixed and sliding rails; b) gap between sections of the deck.

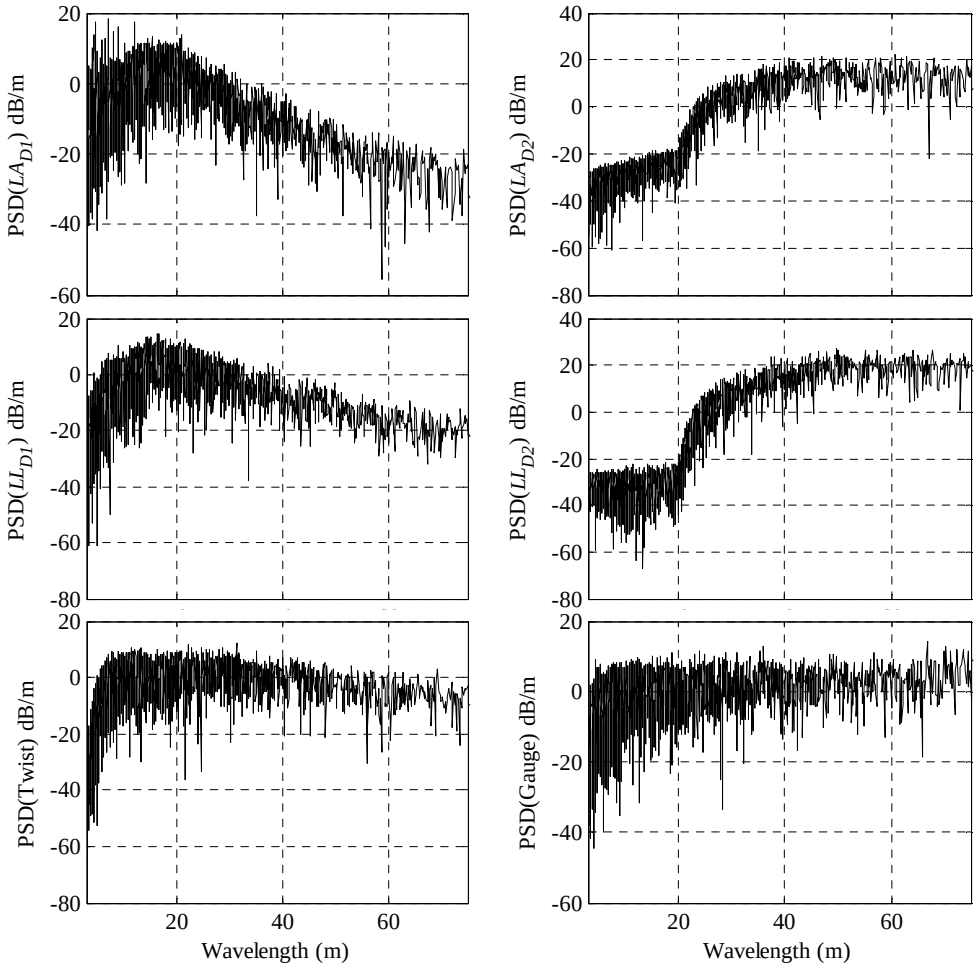

Figure 4-22. Power Spectral Density (PSD) of some track geometry parameters, regarding the survey carried out in July 2013.

As was expected, the Power Spectral Density curves of the *LL* and *LA* that regard D1 evidence more energy content in the respective wavelength range (3 to 25 m), and, in the same way, D2 denotes higher content for wavelengths above 25 m. Although the different parameters show some variability, there does not seem to be any prominent peak that might indicate repetitive track defects, which suggests the defects that were developed so far are mostly of random nature. The variability in the results is probably because the entire length of the track was considered in the analysis, thus not only reflecting the variability in the geometry, but also the influence of different track configurations (substructures) and the intrinsic variability of the mechanical characteristics of the materials.

Considering that the works in this thesis mainly address the vertical behaviour of the track, in the subsequent sections, focus will be given to the longitudinal level. In general, this is the parameter that most influences the dynamic interaction between the vehicles and the track. In addition, given the very good track quality of the line, none of the extreme values of isolated defects on the longitudinal level (either D1 or D2) has been reached (Figure 4-23). Therefore, particular attention will be paid to the evolution of the standard deviation of the longitudinal level in the wavelength range of D1 along the track because this parameter is normally used to assess the overall track quality and to plan early maintenance operations.

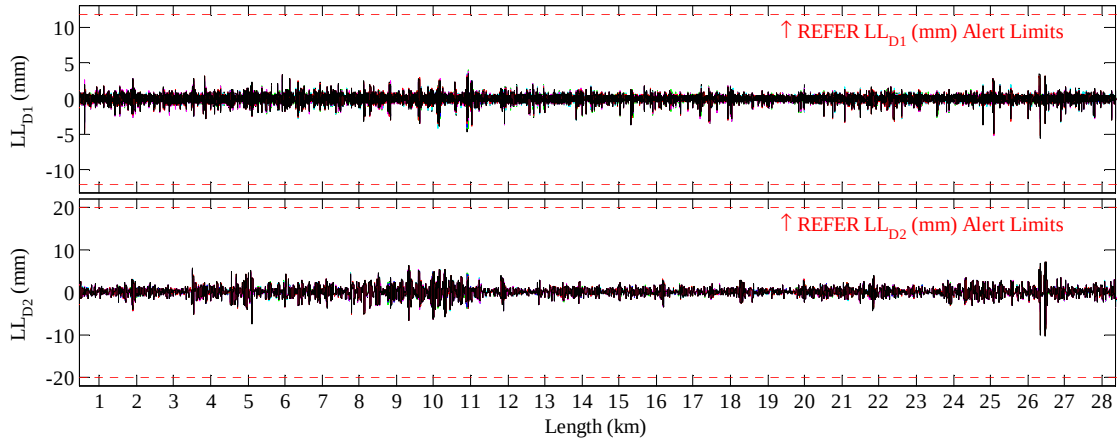

Figure 4-23. Average longitudinal level of the left and right rails (*LL*), in the wavelength ranges D1 and D2, regarding the surveys carried out in May 2011 (red) and July 2013 (black).

4.6.3 Standard Deviation of the Longitudinal Level

The standard deviation of the longitudinal level was calculated using a moving window of 200 m and compared between different surveys from May 2011 to July 2013. Figure 4-24

shows the cumulative distribution functions of the average values of the standard deviation of the longitudinal level of the left and right rails ($\overline{SD}_{LL,D1}$), considering the wavelength range D1 (3 m and 25 m). In the figure, it was included the Alert Limit of 1.9 mm established by REFER for this geometric parameter (REFER, 2009), as well as the Track Quality Class limits (A to E), mentioned in EN 13848-6 (CEN, 2014) for train speeds between 160 and 230 km/h. According to the norm, these five class limits are used to classify the track quality in decreasing order, from A to E, and for five speed ranges.

In the figure, the cumulative distribution curves tend to move to the right because the track degrades with the accumulated traffic. When the line was opened to traffic, about 96% of its length had levels of $\overline{SD}_{LL,D1}$ belonging to Track Quality Class A, about 3% to Class B and less than 2% to Class C. After 28 months, the percentage of track with Class A was reduced to 85%, Class B increased to 8%, Class C increased less than 6% and about 1% belonged to Class D. Nevertheless, all sections of the track were still well below REFER's Alert Limit of $\overline{SD}_{LL,D1}$ = 1.9 mm during that period. From the analysis, it was also verified that when the line was open to traffic the mean value of $\overline{SD}_{LL,D1}$ was about 0.38 mm and after 28 months it increased to 0.42 mm. These results are in agreement with the range of values of 0.4-0.5 mm normally found in recently constructed lines (UIC, 2008a).

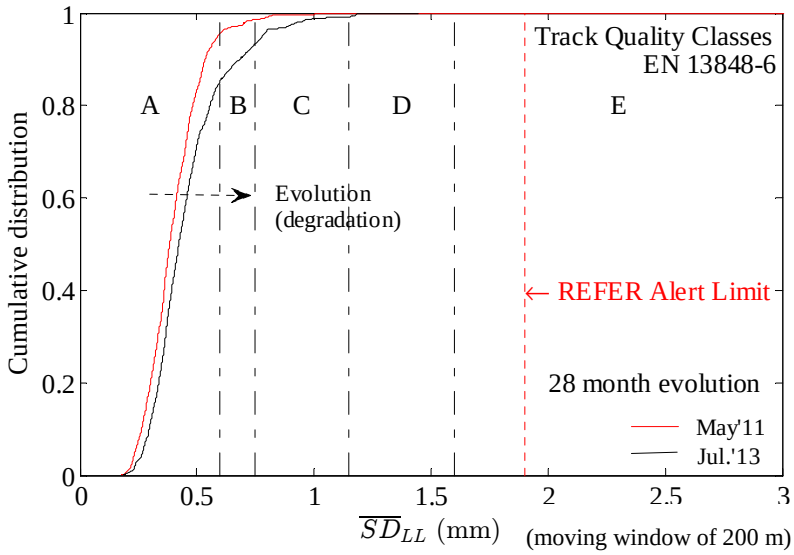

Figure 4-24. Cumulative distribution functions of $\overline{SD}_{LL,D1}$; REFER's Alert Limit; Track Quality Classes according to EN 13848-6 for train speeds between 160 and 230 km/h (CEN, 2014).

Figure 4-25 presents the standard deviation of the longitudinal level of the left and right rails ($SD_{LL,D1}$) obtained throughout the length of the line, considering the same wavelength range and all the surveys between May 2011 and July 2013.

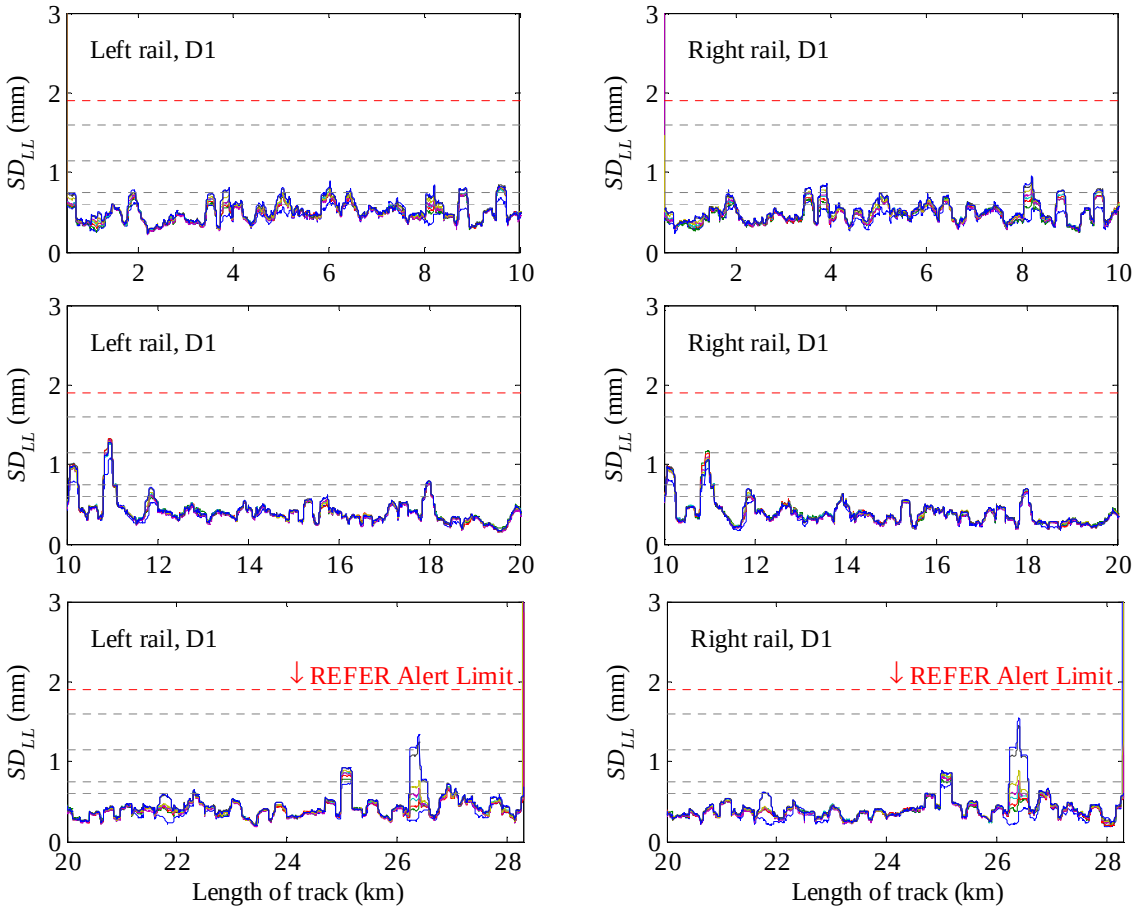

Figure 4-25. Standard deviation of the longitudinal level of each rail, $SD_{LL,D1}$, regarding the surveys carried out between May 2011 and July 2013.

The figure evidences that most sections of the line remain in classes A and B and do not exhibit significant evolution. The sections of the track that evidence higher evolution seem to be the same in the successive surveys, reaching classes C and D in a few sections in the survey performed in July 2013.

Figure 4-26 presents the average values of the two rails that were presented in Figure 4-25 and also shows the location of relevant track singularities (discussed in section 4.4), identified with vertical lines in the figure, namely: i) transition zones to bridges, viaducts and underpasses with wedge-shaped backfills type 1 (BT1 in Figure 4-14a); ii) transition zones to culverts with wedge-shaped backfills type 2 (BT2 in Figure 4-14b); iii) transition zones to buried culverts without wedge-shaped backfills (no BT); iv) track expansion joints on the bridge (EJ).

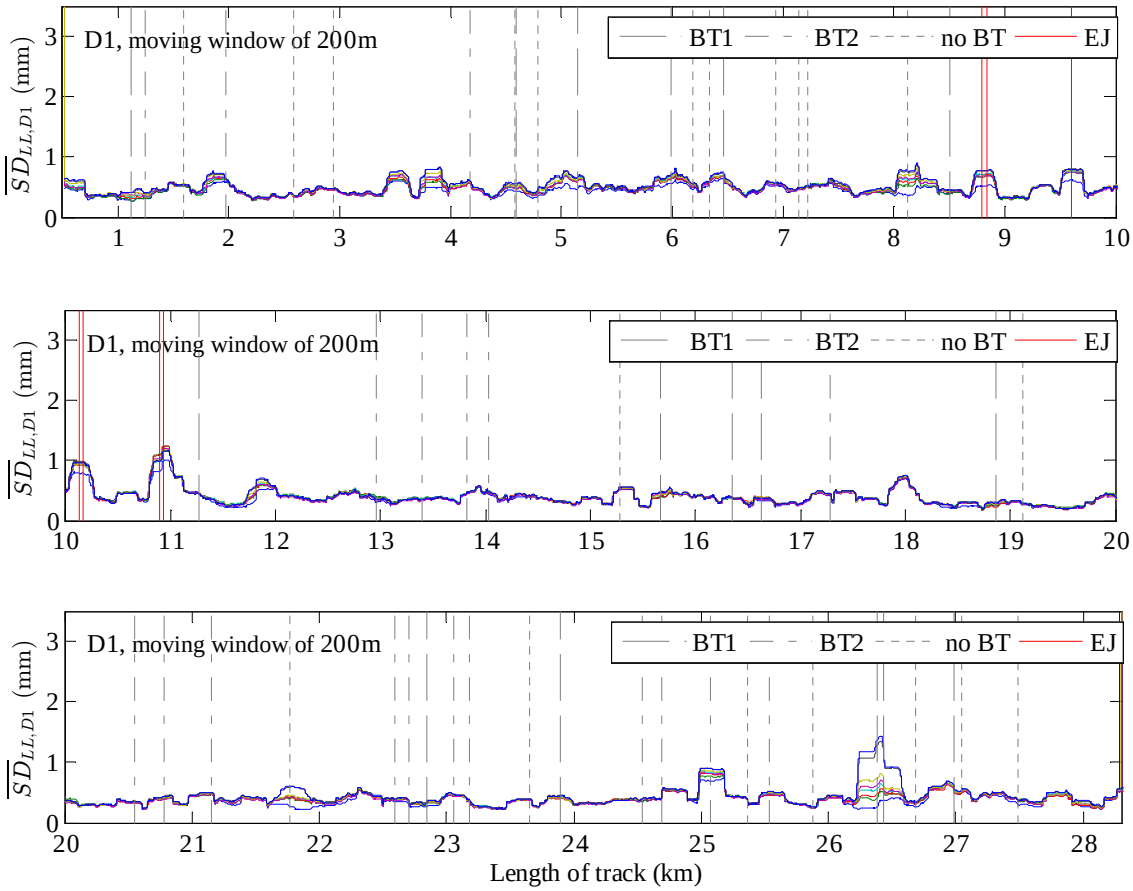

Figure 4-26. Average standard deviation of the longitudinal level (D1), $\overline{SD}_{LL,D1}$ regarding the surveys carried out between May 2011 and July 2013.

The figure evidences that, in general, the values of the standard deviation of the longitudinal level were rather stable in this period, but some stretches evidenced a faster increase, which is related to higher track degradation rates. Looking closely at the figure, it is verified that some of these stretches are coincident with the areas around the track singularities, for example: the culvert without technical block (no BT) at about 8.1 km mark; the seven expansion joints of the bridge (EJ), located between about 8.7 km and 11.0 km marks; the culvert without technical block (no BT) at about 21.8 km mark; the culvert with wedge-shaped backfill type 2 (BT2) at about 25.1 km mark; and the viaduct over N120 at about 26.4 km mark.

However, other sections were identified also showing relatively rapid degradation rates that, initially, were not associated with track singularities, in particular, at about km marks 3.5, 3.7, 5.0 and 11.9. The first two locations (3.5 and 3.7 km marks) seem to be associated with the reinforcement in the substructure that was required due to the poor bearing capacity of the foundation, which was identified earlier in Figure 4-12. The second location (at 5.0 km mark) appears to be related to the north approach to the viaduct over *São Martinho* stream (also

identified in Figure 4-12). The last example (at 11.9 km mark) is coincident with a transition embankment/cutting (the highest and longest embankment in the bypass located at the south approach to the bridge) and with the area where the earthworks from stages 1 and 2 meet.

Therefore, all the locations denoting higher track degradation seem to the related to the presence of some kind of track singularity, either be it an approach to a structure, changes in the substructure or specific track components such as rail expansion joints, which were identified in section 4.4.

In Figure 4-27 a close up of the results from Figure 4-25 is presented regarding the location of three transition zones with wedge-shaped backfills type BT1: i) the south approach to the bridge over Sado river; ii) the underpass at km mark 22.842; and iii) the viaduct over road N120. A detailed analysis of the track geometry at each of the singularities identified in the *Alcácer* bypass is presented in Annex A.

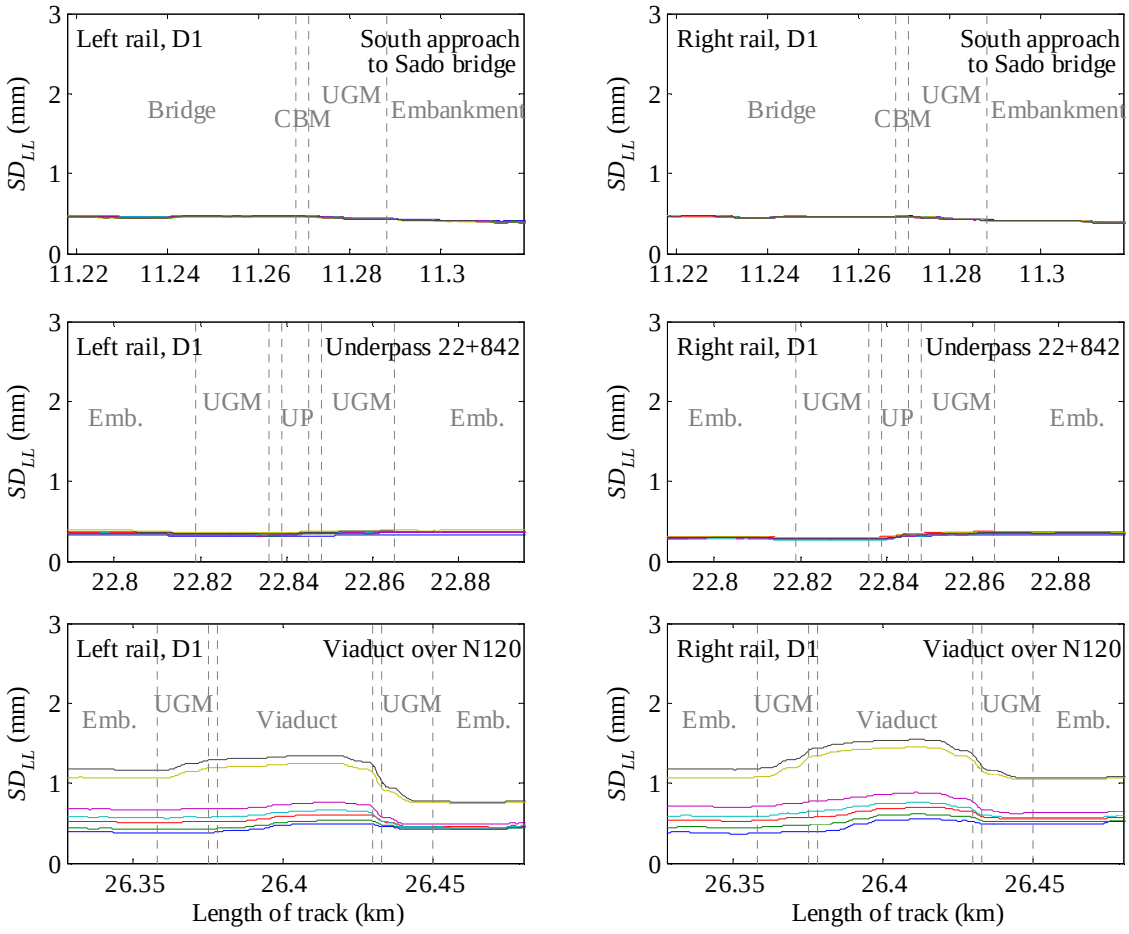

Figure 4-27. Evolution (May 2011 to July 2013) of the standard deviation of the longitudinal level (D1) of each rail, $SD_{LL,D1}$, at three transision zones with wedge-shaped backfills type BT1.

The results in Figure 4-27 evidence the very good track quality and minor evolution of the parameter $SD_{LL,D1}$ at the approaches to the bridge and to the underpass. However, at the approach to the viaduct over N120, there seems to be an important evolution in $SD_{LL,D1}$. Considering that the three cases comprised transition zones with wedge-shaped backfills type BT1, following the same specifications, these findings suggest that the construction of wedge-shaped backfills, by itself, cannot solve all the problems associated with transition zones to structures.

To investigate the connection between the evolution of the standard deviation of the longitudinal level and the presence of singularities in the track, cumulative curves were plotted with the identification of the track sections that had track singularities, such as: a) transition zones to structures with BT1 (Figure 4-28a); b) transition zones to structures with BT2 (Figure 4-28b); and c) other changes in the substructure including embankment/cutting transitions and subgrade reinforcements (Figure 4-28c). The markers in the curves are the representative points of the $\overline{SD}_{LL,D1}$ values corresponding to the singularities calculated as the maximum value of $\overline{SD}_{LL,D1}$ in a range of 100 m from its location. It should be noted that the average distance between the singularities from the same type is about 1490 m, and they distance from each other is at least 200 m, with the exception of three transition zones of type BT2 located between km marks 22.593 and 24.690. This ensures that in the following figures, almost all the markers correspond to a specific singularity of that type, which is represented by one value of $\overline{SD}_{LL,D1}$ that is not shared with nearby singularities of that type.

In Figure 4-28, the markers towards the right represent singularities with larger variability in the longitudinal level in a range of 100 m, which is associated with larger defects in that area. The higher the marker is in the curve, the greater the standard deviation is in that area, with respect to the rest of the line. The majority of the transition zones with BT1 (Figure 4-28a) and BT2 (Figure 4-28b) fall in the upper half of the curves, meaning that the value of $\overline{SD}_{LL,D1}$ in that area is higher than the mean value of the line. In what regards other changes in the substructure (Figure 4-28c), the markers are quite dispersed in the curves, although the density of markers appears to be greater in the upper part of the curves.

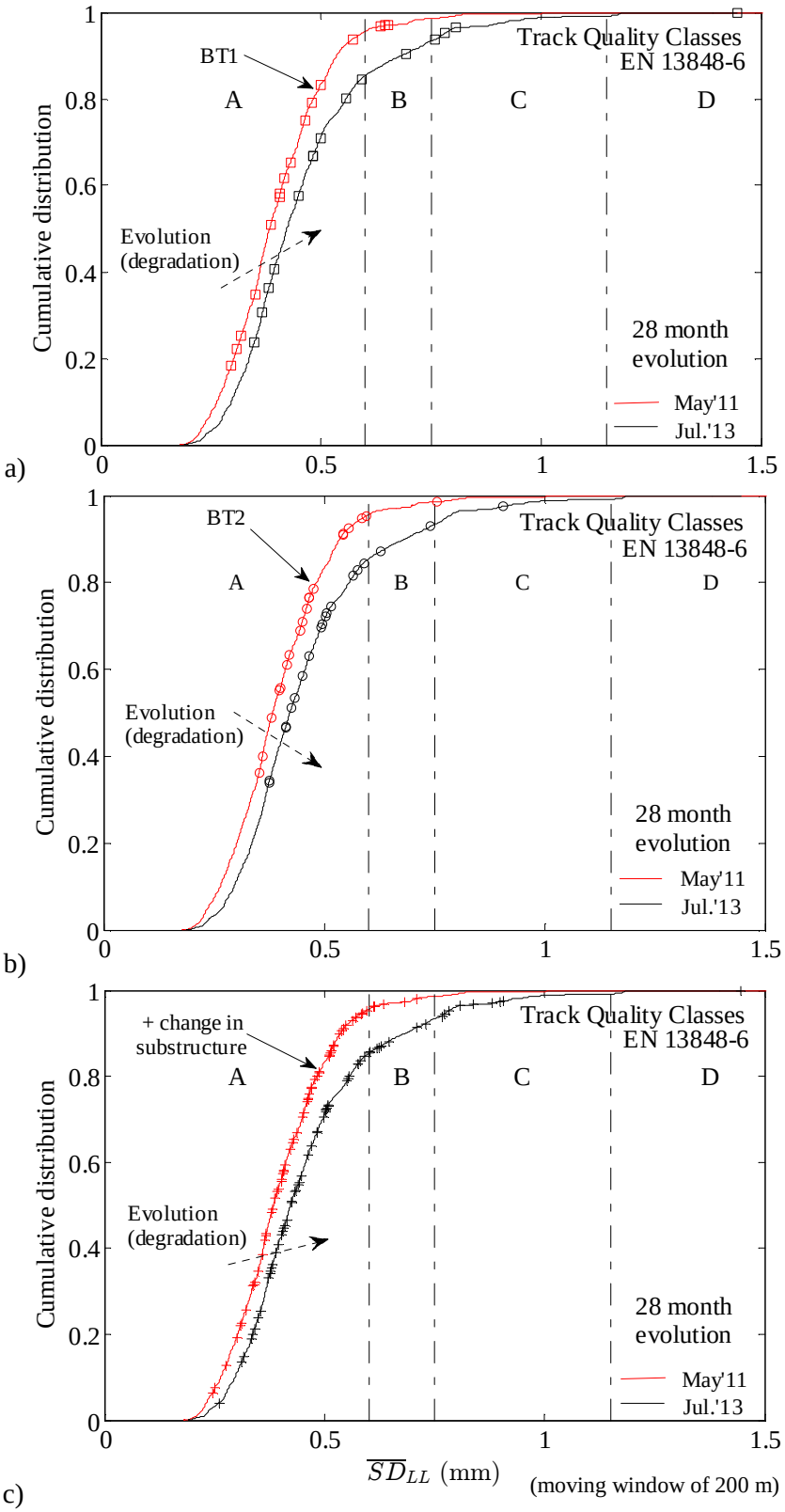

Figure 4-28. Evolution of the cumulative distribution functions of $\overline{SD}_{LL,D1}$: a) BT1; b) BT2; c) changes in the substructure; Track Quality Classes according to EN 13848-6 for train speeds between 160 and 230 km/h.

Analysing the evolution between the two curves, the more a marker moves towards the right, the greater the track degradation between the two surveys in that area. Normally, points do not move towards the left – it would represent an increase in the track geometric quality, which may occur after maintenance operations. There were no reports of track maintenance operations during that period. The more a marker moves upwards, the greater the relative track degradation between the two surveys in that area, with respect to the average degradation that occurred in the rest of the line, i.e., the track degrades faster than the average if the marker moves upwards with higher amplitude.

Points moving upwards and to the right mean that the track section had higher track degradation and at a higher rate, between the surveys, comparing with the average values. This seems to be the case of transition zones to bridges, viaducts and underpasses – the wedge-shaped backfills of type BT1 in Figure 4-28a. Markers denoting areas with transition zones to culverts with BT2 (Figure 4-28b) generally moved downwards and to the right which means lower track degradation during that period, although most markers were in upper half of the curve the initial survey, as mentioned above. Considering the evolution of the markers in Figure 4-28c, the general trend is clearly towards the right and slightly upwards, though it is not fully clear due to the large number of points that make it difficult to read the evolution of each marker.

Considering the total traffic of about 17 MGT between May 2011 and July 2013 mentioned earlier, Figure 4-29 shows estimates of the deterioration rates observed over the entire length of the *Alcácer* bypass.

It is visible that while most part of the line shows a degradation rate within the normal range of 1 to 2 mm/100 MGT found in the literature (Esveld, 2001), some sections showed higher rates with a maximum at about 7 mm/100 MGT, which corresponds to the section of the track near the viaduct over the road N120. That particular transition zone will be analysed in Chapter 6 in more detail. The reference values of 1 to 2 mm/100 MGT refer to normal degradation rates between two maintenance operations and only account for normal track conditions: quick settlements and the well-known rapid deterioration of track immediately after tamping are not considered. This partially explains some differences in the results because of those two factors: i) the line is very recent, thus the ballast may be experiencing the initial rapid deterioration; ii) considering the early age of some embankments, it is possible that some settlement may occur at the substructure, thus affecting the track geometry.

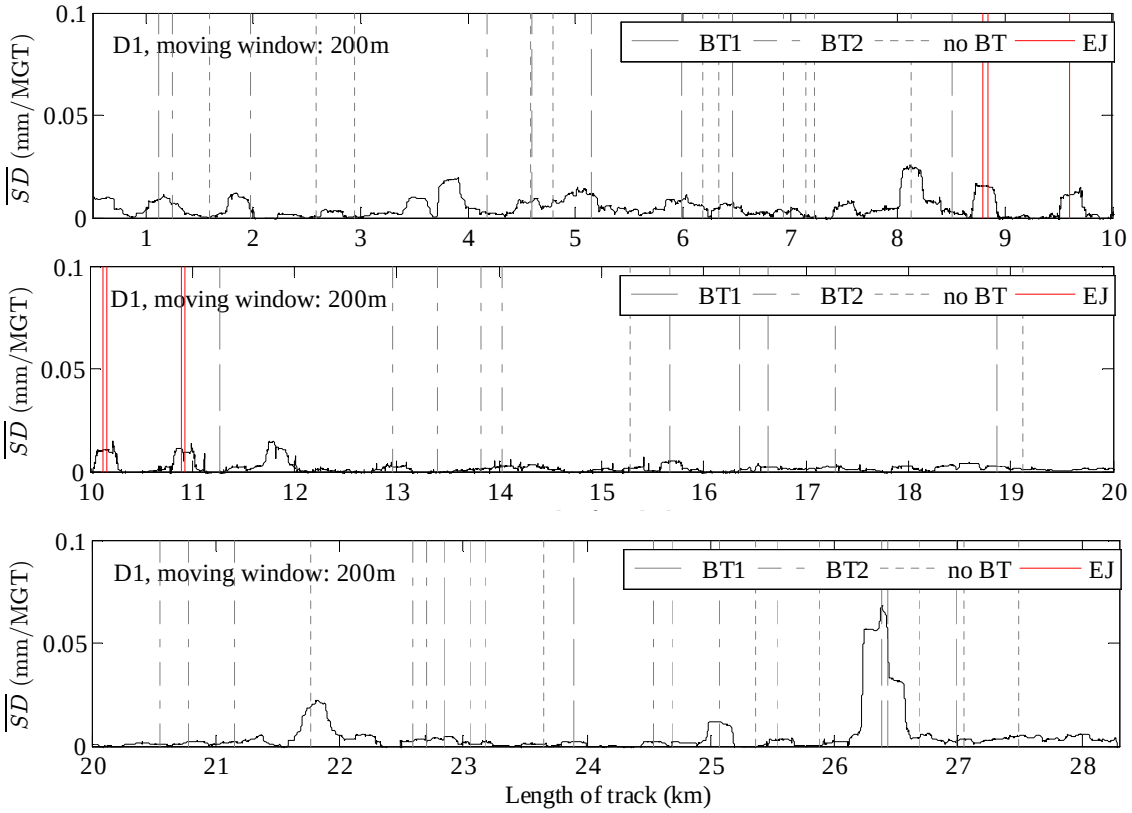

Figure 4-29. Estimated deterioration rates in mm/MGT.

4.7 Case Study of the construction of a transition zone

4.7.1 General aspects of the transition zone case study

The study presented herein regards the construction of the transition zone at the south approach to the railway bridge over Sado river (Figure 4-30). In Figure 4-31, a general drawing for the design of the transition zone case study is presented. The characteristics of the transition zone, namely the aspects of the wedge-shaped backfill, are the same as those described in Chapter 3, (see Table 3.1). It comprises a backfill with a smaller wedge-shaped transition made of CBM layers, followed by larger wedge of UGM layers providing the transition to the embankment. The design did not establish changes in the track superstructure at the transition zone. It is worth noting that the abutment type is open, about 9 m high, with two central columns supporting the cap beam, where the end of the bridge deck rests. The abutment has two relatively large wingwalls on the sides, both featuring one counterfort in the backfill. The abutment rests on a large footing covering all its structure, which is supported on pile foundations. Figure 4-32 shows schematic three-dimensional representations of the transition zone.

Figure 4-30. Aspects of the southern approach to the bridge over Sado river.

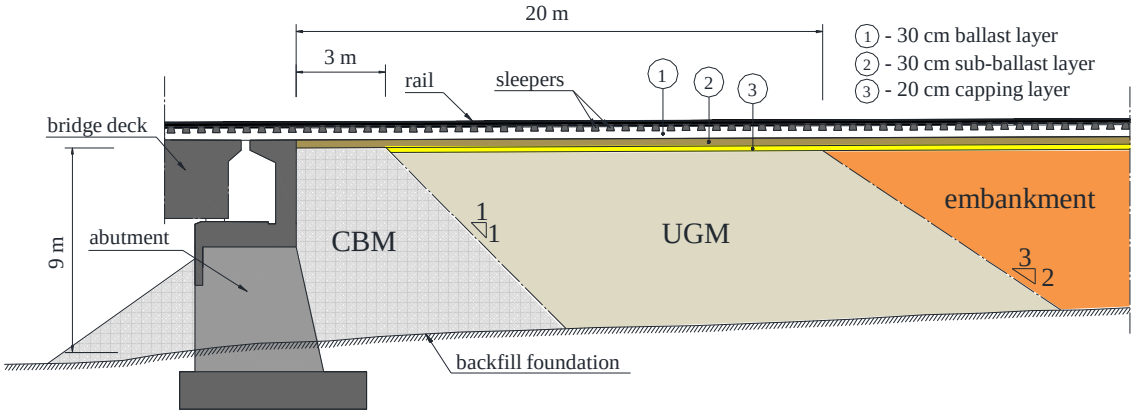

Figure 4-31. Design of the wedge-shaped backfill of the transition zone case study.

The limestone aggregate described earlier was used in the wedge-shape UGM and in the capping layer. The sub-ballast layer was constructed with the granite aggregate to comply with the demanding requirements of the Los Angeles test resistance to fragmentation, as addressed in section 4.3.

Regarding the CBM, a mix in plant of the previous limestone aggregate was used with Binder Content (*BC*) of 5% by weight (Portland cement). As mentioned in Chapter 3, a minimum compressive strength (R_c) of 1 MPa was required for specimens after curing for 7 days. The minimum indirect tensile strength (R_{it}) required after curing for 60 days was 0.25 MPa. Laboratorial tests showed that the mixture complied with the requirements: average R_c values of 9.7 MPa and R_{it} values of 1.3 MPa were obtained (Paixão & Fortunato, 2010; Paixão *et al.*, 2011).

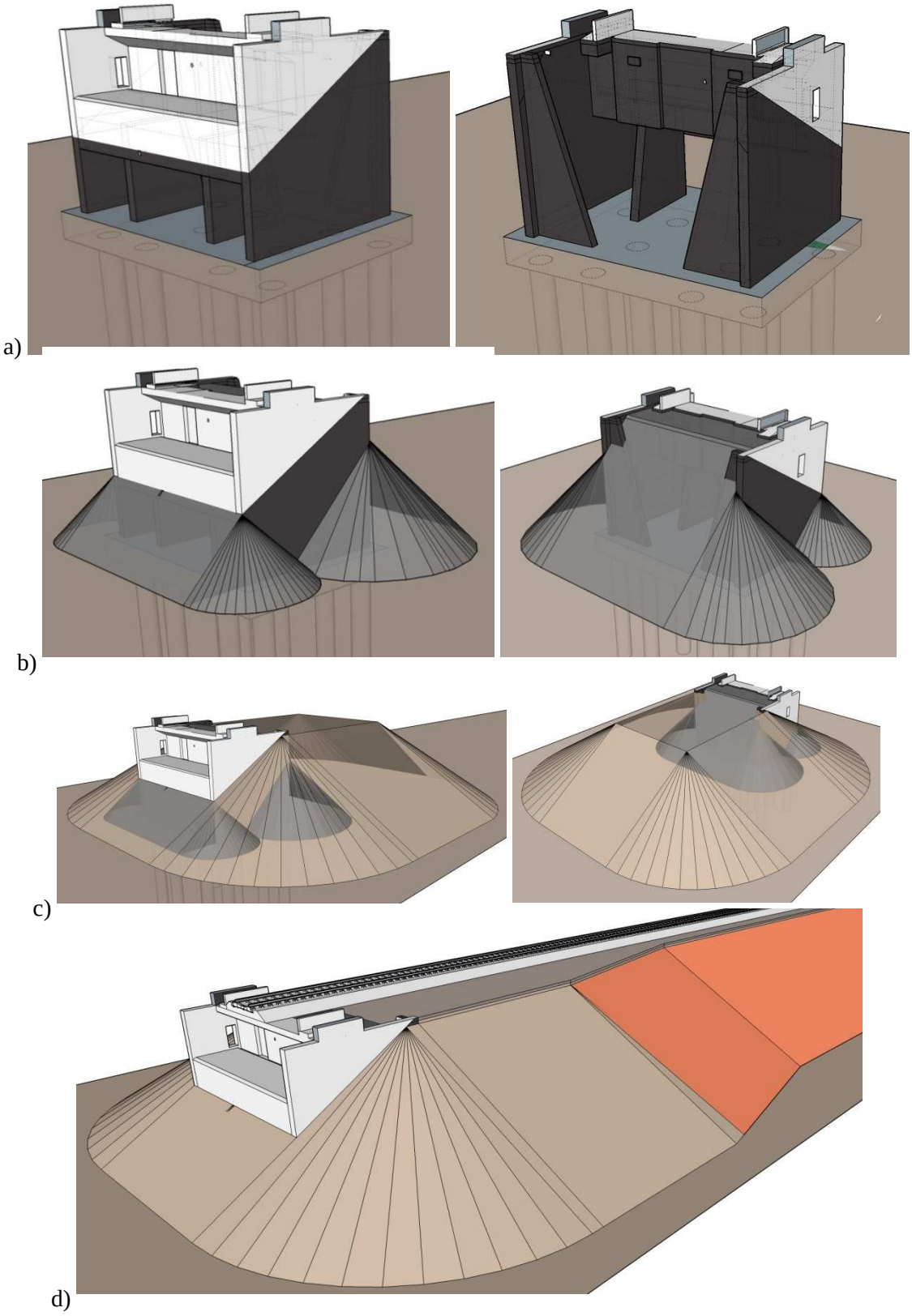

Figure 4-32. Three-dimensional representation of the wedge-shaped backfill: a) abutment structure; b) abutment and CBM wedge; c) UGM wedge; d) final representation of the structure.

4.7.2 Characterisation of the backfill materials using cyclic load triaxial testing

In general, unbound granular materials applied in roads and railways show non-linear resilient behaviour, depending on the applied stress level, the degree of compaction and water content, among other factors (Lekarp *et al.*, 2000). Aiming at characterizing the materials applied in the transition zone for a mechanistic design approach, additional laboratorial tests were developed, in particular cyclic load triaxial tests, to assess the resilient and long-term behaviour of these materials for different state conditions and stress paths (Gomes Correia, 2004). The characterisation of the geomaterials using this advanced laboratorial testing also aimed at providing relevant information to be considered in the calibration of the numerical models, as will be discussed in Chapter 5. These tests were not established in the design nor where there minimum requirements for the parameters related to their resilient and permanent deformation behaviour. Nevertheless, the results of the cyclic load triaxial tests allowed ranking the aggregates based on their resilient modulus (E_r) and susceptibility to permanent deformation according to EN 13286-7 (CEN, 2004).

4.7.2.1 Resilient behaviour

Cyclic load triaxial tests were performed on large specimens (200 mm diameter by 400 mm high - Figure 4-33) using the full grain sizes of the aggregates and following the EN 13286-7. Although when the railway line is in operation the aggregates in the substructure, undergo cyclic loads with relatively low stress levels, during construction they are subject to much severe conditions that result from transport to the site, compaction with heavy rollers and traffic by heavy construction vehicles. Thus, the resilient behaviour was characterised using Method A (variable confining pressure) - High Stress Level procedure, established in EN 13286-7.

The cyclic triaxial load test system that was used (Fortunato *et al.*, 2012b) comprised the following aspects (Figure 4-33):

- a triaxial cell for specimens of 200 mm diameter and 400 mm high, with the possibility of placing internal instrumentation, in particular, load and pressure cells and LVDT displacement transducers;
- a system to generate and apply axial loads up to 100 kN, using a frame as reaction;
- a system to generate and apply confining pressure;
- control systems for applied axial (σ_1) and confining pressures ($\sigma_2 = \sigma_3$);
- local axial displacement transducers: three internal transducers to measure axial displacements (fixed inside the specimen and spaced 120° along the perimeter) and three internal transducers to measure perimetral displacements (to allow the calculation

of radial deformation); one transducer to measure axial displacements of the loading rod;

- a signal conditioning system;
- a system for the acquisition and processing of the data with graphical interface for the operator.

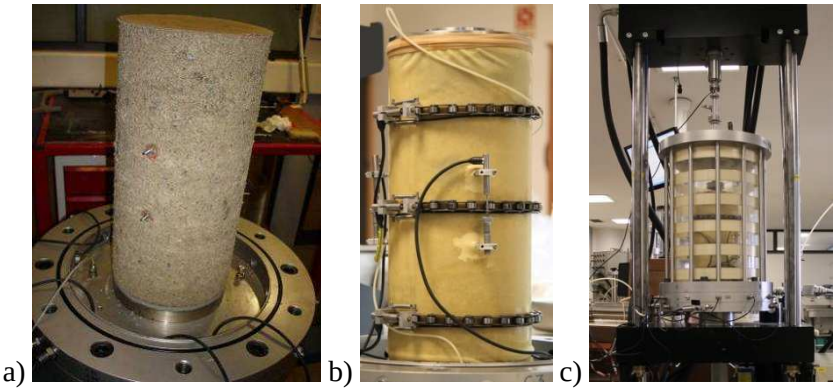

Figure 4-33. Aspects of the cyclic load triaxial tests: a) preparation of the specimens; b) instrumented specimen before testing; c) aspect of the triaxial apparatus.

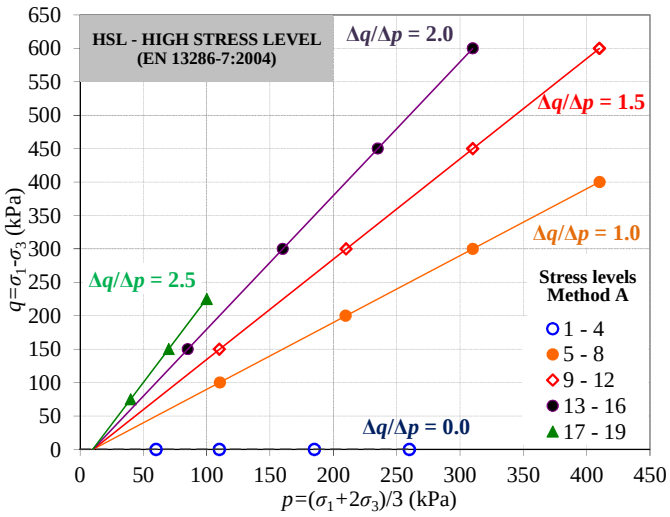

Figure 4-34. Stress paths applied to the specimens.

The procedure consisted of two main stages: i) conditioning of each specimen with 20 000 load cycles with a maximum mean stress ($p = 1/3(\sigma_1 + 2\sigma_3)$) of p_{max} = 310 kPa and a maximum deviatoric stress ($q = \sigma_1 - \sigma_3$) of q_{max} = 600 kPa; ii) a series of cyclic loadings along different stress paths (Figure 4-34).

The specimens were prepared by vibrocompaction with different values of water content (w) and degree of compaction (D_c). A load frequency of 1 Hz was applied and radial and axial

deformations were measured through local instrumentation using small submersible LVDT (Figure 4-33b and Figure 4-35). The system that was used allows the axial and radial strains to be recorded with a resolution of at least 1×10^5 on the central part of the specimen, ensuring negligible interference with the behaviour of the material to be tested.

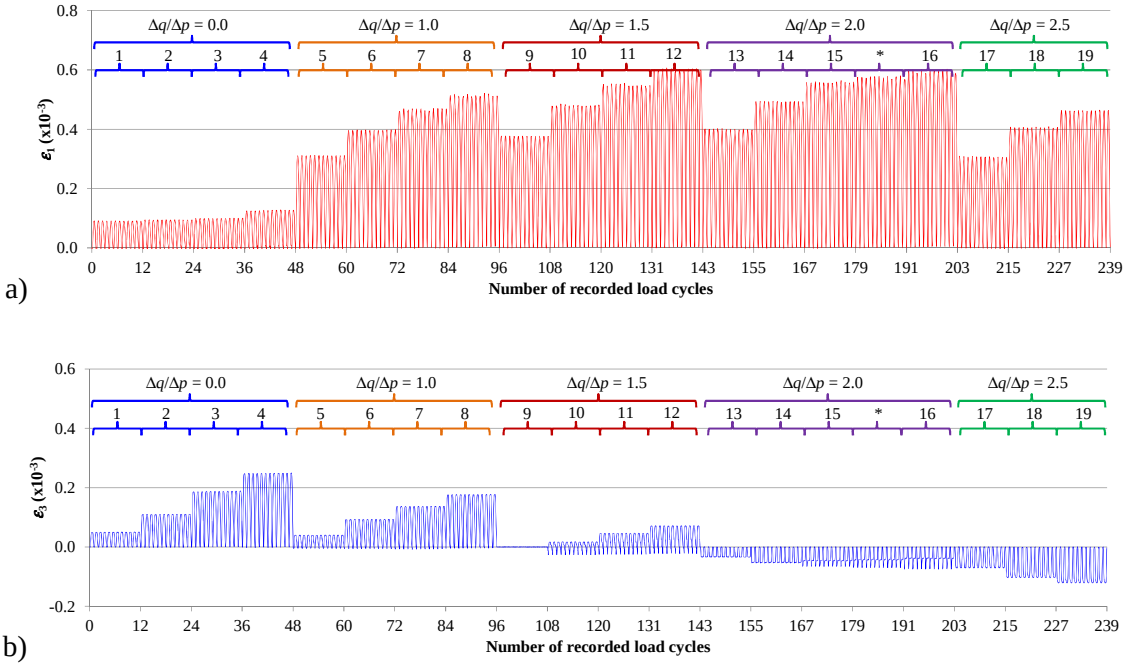

Figure 4-35. Example of axial (a) and radial (b) deformations calculated from the measurements performed during the tests.

Considering that the triaxial tests were performed with variable confining pressure, the resilient modulus (E_r) and the Poisson's ratio (ν) were calculated using the following expressions (Lekarp *et al.*, 2000):

$$E_r = \frac{\Delta(\sigma_1 - \sigma_3)\Delta(\sigma_1 + 2\sigma_3)}{\varepsilon_1\Delta(\sigma_1 + \sigma_3) - 2\varepsilon_3\Delta\sigma_3} \tag{4-1}$$

$$\nu = \frac{\Delta\sigma_3\varepsilon_1 - \Delta\sigma_1\varepsilon_3}{\varepsilon_1\Delta(\sigma_1 + \sigma_3) - 2\varepsilon_3\Delta\sigma_3} \tag{4-2}$$

The results evidenced the typical non-linear behaviour of these materials with the stress level in that the obtained E_r values increased with the mean stress, as reported by other authors (Gomes Correia, 2004). This behaviour was more evident in specimens with higher E_r, considering the same stress level. $E_r = k_1\theta^{k_2}$ curves provided a good estimate (see Figure 4-36 where, for

example, "G96.3; -3.7" denotes a granite specimen (G), with D_c = 96.3%, regarding maximum density obtained by vibrocompaction, and a deviation from the reference value of the optimum water content (w_{OPM}) of -3.7%), with the coefficient of determination (R^2) greater than 0.95 in most cases. It also seems that, in general, lower w and higher D_c lead to higher E_r, for the same stress level.

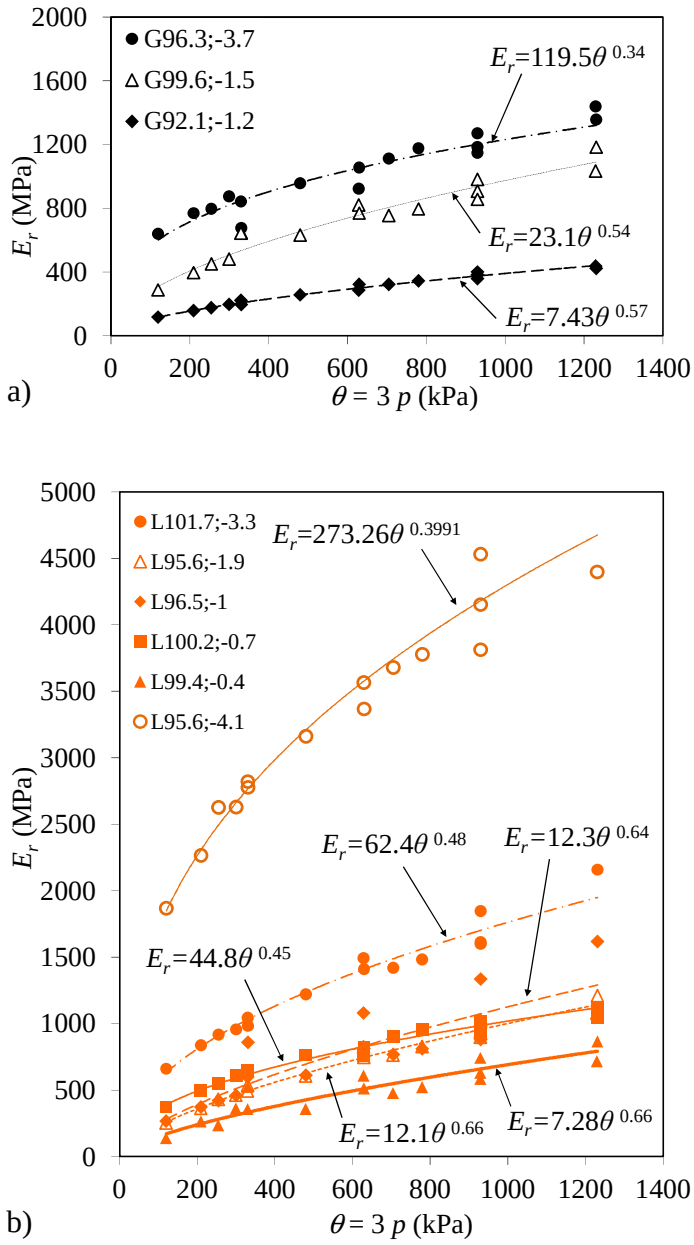

Figure 4-36. Results of E_r for different stress paths: a) granite (sub-ballast); b) limestone (capping and UGM).

This conclusion is most evident when considering the E_r obtained in the stress path established for the determination of the characteristic resilient modulus ($p_{max} = (\sigma_1 + 2\sigma_3)/3 = 250$ kPa and $q_{max} = (\sigma_1 - \sigma_3) = 500$ kPa), as presented in Figure 4-37.

The E_r values obtained for limestone (capping and UGM) are close to or greater than those obtained with the granite (sub-ballast), in similar state conditions. For that stress level, limestone E_r ranged from about 500 to 4000 MPa and the granite between 350 and 1200 MPa. Earlier studies reported similar conclusions and resilient modulus ranging from 300 to 1000 MPa were observed for well graded crushed aggregates, adequate for unbound layers, in similar stress paths and state conditions (Balay *et al.*, 1998). One of the limestone specimens that was tested (L95.6;-4.1) revealed very high resilient modulus, comparing with the other limestone specimens. These results were probably caused by the very low water content (w-w_{OPM} = -4.1%) of that specimen.

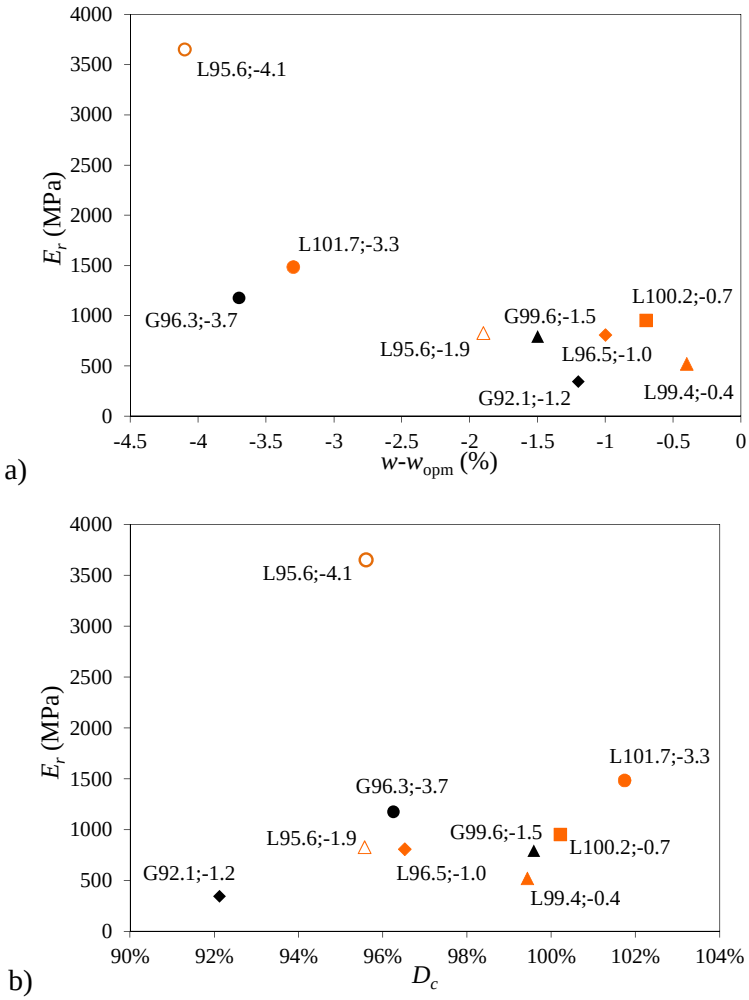

Figure 4-37. E_r obtained for the two UGM (p_{max} = 250 kPa; q_{max} = 500 kPa): a) influence of w-wOPM; b) influence of D_c.

The materials can be ranked by the following parameters (CEN, 2004): 1) the characteristic resilient modulus, E_{rc}, obtained on specimens with D_c = 97% and w = w_{OPM} -2%, for the stress path mentioned above; 2) the characteristic permanent axial strain (ε_1^c), in the same state conditions, calculated during the conditioning of the specimens (p_{max}=310 kPa and q_{max}=600 kPa). Considering that samples L95.6;-1.9 and G99.6;-1.5 exhibit state conditions nearest to the required, E_{rc} values were 814 MPa and 790 MPa and ε_1^c values were 1.25x10^{-3} and 1.36x10^{-3}, respectively. Therefore, the materials exhibit excellent performance and can be ranked as class C1 (Figure 4-38).

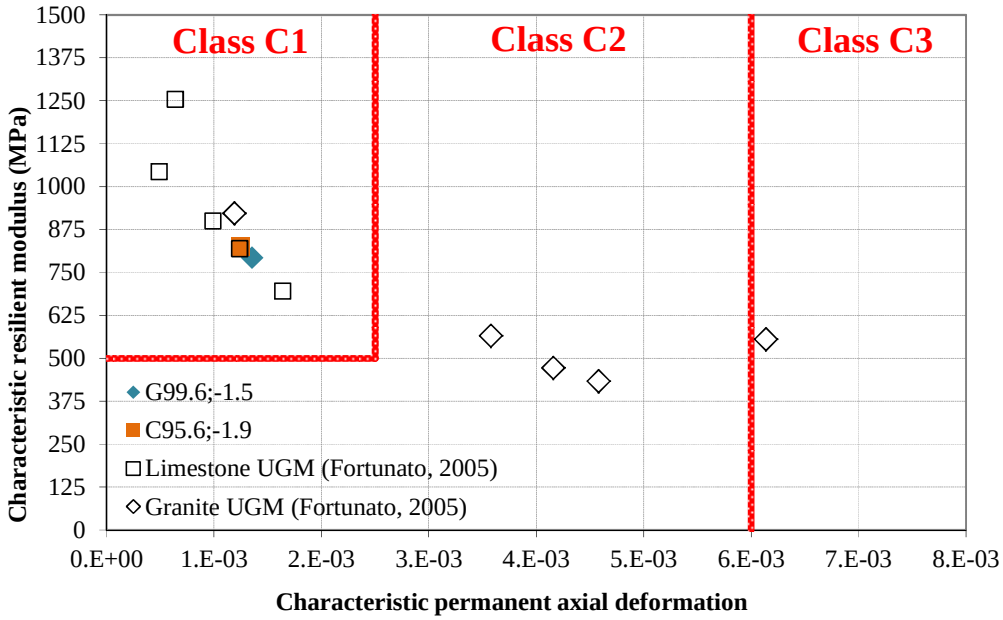

Figure 4-38: Classification of UGM according to EN 103286-7.

Cyclic load triaxial tests were also performed on specimens of CBM to study its resilient behaviour and assess the influence of the Binder Content (BC) on the response of the material. Although the EN 13286-7 is not specific for bound aggregates, the same method was adopted here to be coherent with the study of the unbound materials and so that a direct comparison was possible, in terms of values of E_r.

A set of specimens was prepared with the state conditions described in Table 4-6, with respect to the Optimum Modified Proctor compaction reference values, considering values of BC of 1%, 3% and 5%. These specimens were tested at 60 days of curing.

Table 4-6. State conditions of CBM specimens tested regarding the resilient behaviour.

Material	Specimens	D_c (%)	w - w_{OPM} (%)
Limestone CBM with BC=1% (L1)	L1;100.0;-1.7	100.0%	-1.7
	L1;102.1;-0.7	102.1%	-0.7
Limestone CBM with BC=3% (L3)	L3;96.2;-1.3	96.2%	-1.3
	L3;96.7;-1.5	96.7%	-1.5
	L3;99.3;-1.3	99.3%	-1.3
Limestone CBM with BC=5% (L5)	L5;98.6;-1.9	98.6%	-1.9
	L5;104.8;-1.8	104.8%	-1.8

Figure 4-39 shows the E_r values obtained with the CBM specimens and the best fitting curves $E_r = k_1\theta^{k_2}$ for each group with different values of BC (1%, 3% and 5%). The results evidence a strong influence of the value of BC in the resilient modulus. Moreover, considering the tested range of values of D_c and w-w_{OPM}, the behaviour of the CBM does not seem to be very influenced by the water content or the degree of compaction of the mixture. In proportion, and comparing with the unbound materials, the CBM seems to be less influenced by the stress level, particularly for higher values of BC. The obtained results of E_r fall into ranges of values reported in the literature for this type of materials (Jofré Ibáñez & Ruiz Rubio, 2009).

During the first stage of these tests, additional specimens were prepared to be tested later to study the influence of curing time. The specimens were kept in controlled humidity and temperature conditions to preserve the initial state conditions and avoid excessive evaporation. Despite all the efforts it was not possible to test CBM specimens with BC = 5%. Figure 4-40 evidences that the stiffness of the CBM material (with BC = 3% and 1%) increases with curing time. Results of unbound limestone aggregate are also provided for comparison. Regarding the specimens with BC = 3% it appears that the resilient values more than double after about 14 months and the material get less sensitive to the stress level. The CBM with BC = 1% in Figure 4-40b also denotes an increase of stiffness with the curing time, yet less pronounced.

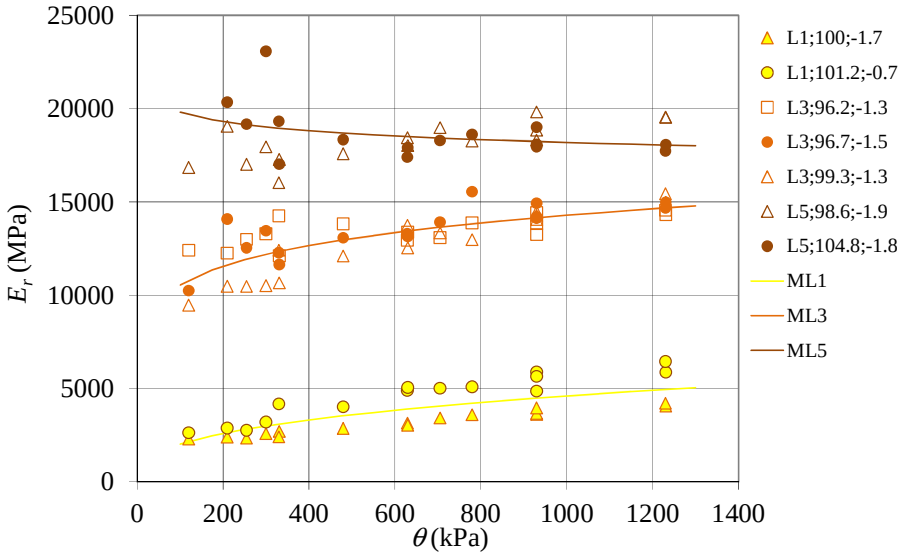

Figure 4-39: Results of E_r on CBM material for different stress paths.

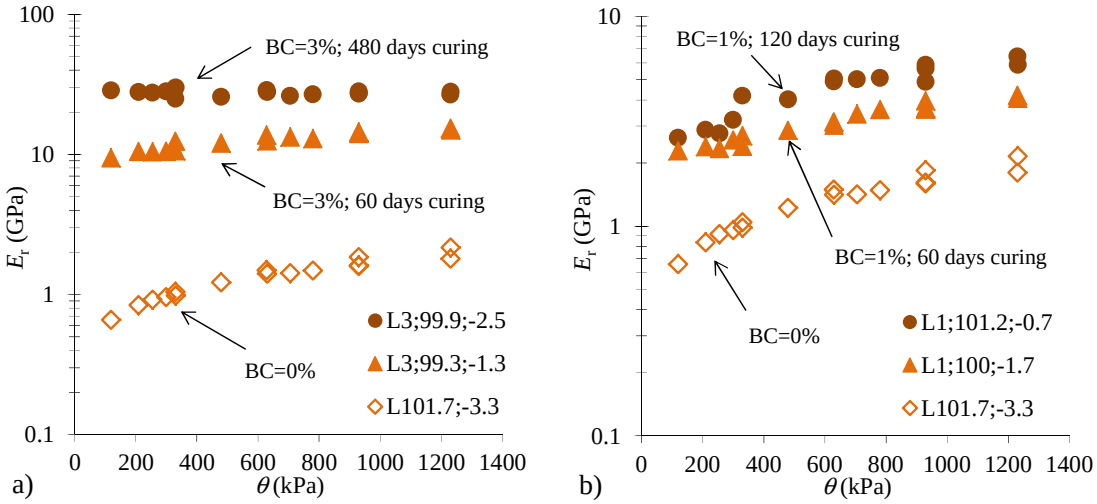

Figure 4-40: Comparison of E_r values of the CBM for different curing times: a) *BC* = 3%; b) *BC* = 1%.

In general, it was noted that the E_r values of the bound and unbound granular materials that were tested denoted a wide range of variability, depending on different factors, mainly: the stress path and the water content for the unbound material applied in the sub-ballast, in the capping and in the UGM; the curing time and binder content regarding the material of the CBM. In particular, the E_r values ranged from about 100 to 4000 MPa, regarding the unbound material, and between about 15 to 25 GPa, regarding the CBM with *BC* = 5%.

4.7.2.2 Permanent deformation of unbound materials

Subsequently, a study on the permanent axial strain (ε_1^p) of both materials, for 10^6 load cycles, was carried out under a single stress path, established in order to simulate the conditions imposed in service to the sub-ballast (p_{max} = 40 kPa and q_{max} = 75 kPa). To this end, a limestone and a granite specimen (L97.0;-0.8, G95.8;-1.6) were prepared to achieve D_c = 97% and w-w_{OPM} between 1% and 1.5%.

As presented in Figure 4-41, ε_1^p values increased rapidly at the beginning of the tests, but after 10^6 cycles, they were similar for both materials. However, comparing the evolution at the end of each test, it can be observed that the granite ε_1^p growth rate was significantly higher (4.2×10^{-7}/cycle) than the limestone ε_1^p growth rate (1.2×10^{-7}/cycle).

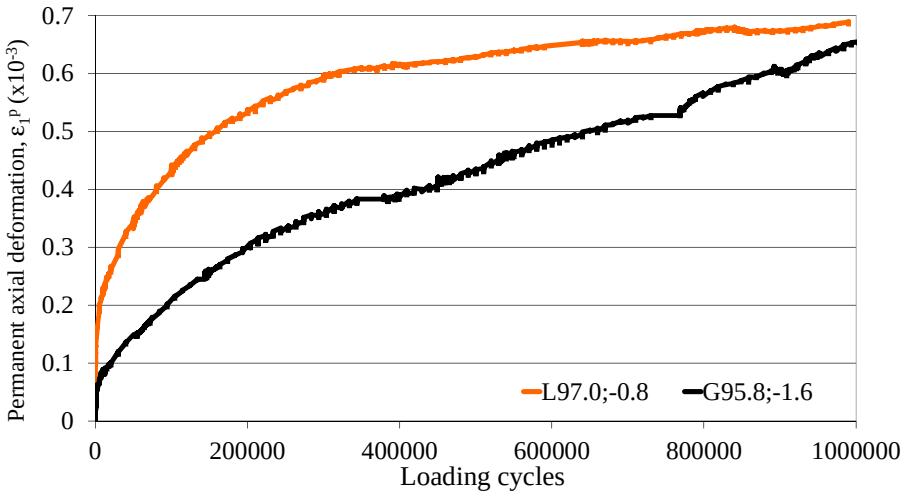

Figure 4-41: Permanent axial deformation for 1x10^6 load cycles (p_{max} = 40 kPa and q_{max} = 75 kPa).

Considering the ε_1^p values obtained during the conditioning process described in 4.7.2.1 (specimens to study the resilient behaviour), and the ones obtained at 20 000 cycles during the permanent deformation study, it is possible to conclude that the applied stress path has a great influence on the ε_1^p (Figure 4-42).

It should be mentioned that it was not possible to carry out laboratorial dynamic tests on the materials for frequencies similar to those resulting from train passages. However, some studies on similar materials have concluded that the frequency of the load cycles does not seem have

significant influence on the behaviour of granular materials, up to about 20 Hz (Boyce, 1980; Gomes Correia, 1985).

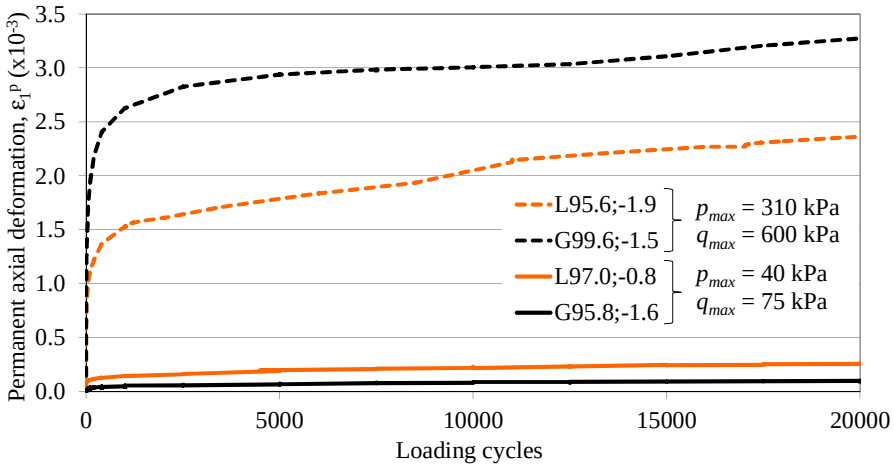

Figure 4-42. Permanent axial deformation for 20 000 cycles in different stress paths.

Regarding the *Shakedown* concept (Werkmeister, 2003), in particular the strain values suggested for Plastic Shakedown Limit (PSL = 0.0045%) and Plastic Creep Limit (PCL = 0.04%), Table 4-7 presents the accumulated ε_1^p between 3000 and 5000 load cycles.

For the higher stress level, the obtained values were similar in both materials and were between the values proposed for PCL and PSL (CEN, 2004). For the lower stress level, and objectively, a stress path closer to the one imposed to the sub-ballast layer during its life cycle, the values obtained for both materials were lower than the proposed value for PSL.

Table 4-7. ε_1^p accumulated between 3000 and 5000 cycles.

Specimen	p_{max}; q_{max} (kPa)	$\varepsilon_1{}^p{}_{5000} - \varepsilon_1{}^p{}_{3000}$ (%)
L95.6;-1.9	310; 600	0.01266
G99.6;-1.5	310; 600	0.01122
L97.0;-0.8	40; 75	0.00276
G95.8;-1.6	40; 75	0.00087

Given the ε_1^p values accumulated between 3000 and 5000 load cycles, particularly for the lower stress level, makes it possible to admit that the granitic material reveals a better performance

than the limestone. However, an overall analysis taking into account what has been presented earlier, make it possible to conclude that: a) during the conditioning of the specimens to characterise the resilient behaviour, both ε_1^p and its growth rate at the end of the conditioning were higher for all granite specimens; b) during the study of the permanent deformation after 10^6 load cycles, although the granite showed a slightly lower ε_1^p value at the end of the test, the ε_1^p growth rate of the granite was about 3.5 times greater than the one obtained in the limestone specimen.

4.7.3 In situ characterisation of the layers

During construction, the CBM and UGM wedges of this transition zone were compacted in layers of 30 cm using 11 ton single drum roller (Figure 4-43a). At some locations of the CBM backfill, smaller roller or manual compaction equipment was required (Figure 4-43b). The capping was compacted in a single 20 cm layer and the sub-ballast in two layers of 15 cm each.

Minimum degrees of compaction (D_c) were established for the layers (Table 4-8), regarding Modified Proctor compaction reference values, in terms of maximum dry density (ρ_{dOPM}) and optimum water content (w_{OPM}). The compaction control tests of each layer comprised measurements with the nuclear density gauge, calibrated using the sand replacement method. Table 4-8 shows average D_c and water content (w) values, the respective coefficients of variation (CV) and median w-w_{OPM} values. From the analysis of the results, an overall good compliance with the minimum D_c requirements is observed. Figure 4-44 shows the distribution of the results of the compaction control quality on the layers of CBM, UGM, capping and sub-ballast.

a) b)

Figure 4-43. Aspects of the compaction of the layers using heavier (a) and lighter (b) compaction equipment.

Table 4-8. Summary of requirements and results of compaction control.

	Min. D_c (%)	ρ_{dOPM} (g/cm^3)	w_{OPM} (%)	Number of tests	Average D_c (%)	CV_{Dc} (%)	Average w (%)	CV_w (%)	Median w-w_{OPM}
CBM	98	2.22	6.8	15	100.5	1.9	6.8	11.4	0.1 %
UGM and capping layer	95	2.23	5.6	159	99.2	1.7	5.9	16.1	0.4 %
Sub-ballast	98	2.33	5.8	54	99.3	0.9	5.2	13.4	-0.9 %

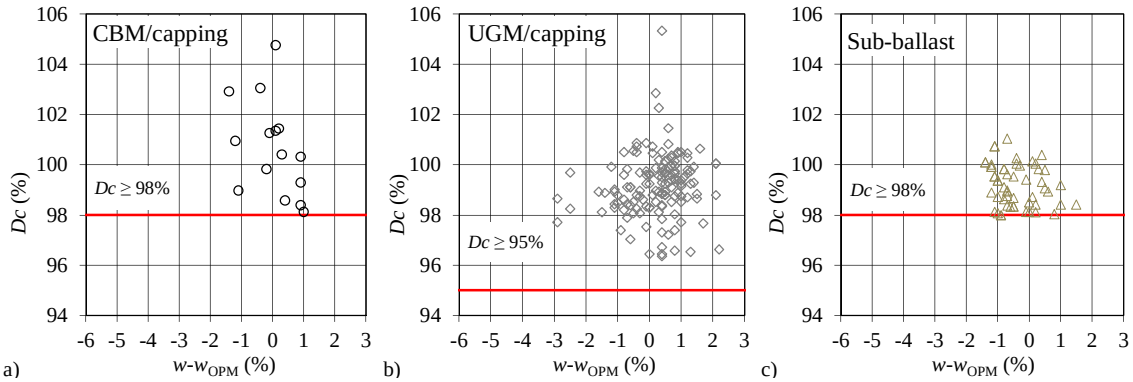

Figure 4-44. Compaction control results (D_c) obtained with nuclear gauge and respective diference to optimum water content value (w-w_{OPM}): a) CBM; b) UGM and capping; c) sub-ballast.

In addition to the compaction control, measurements of the deformation modulus, E_{V2}, of the layers were also carried out by means of the plate load test, PLT (AFNOR, 2000). Measurements with the *portancemètre* equipment were also performed (Quibel, 1999).

After construction of the abutment, but prior to the construction of the wedge-shaped transition, *Portancemètre* measurements were performed on top of the backfill foundation. The measured E_{V2} values ranged from 50 to 120 MPa, along alignment 1 (Figure 4-45a and b). It is interesting to note the higher values near the abutment. A probable cause for this fact is the presence of the abutment's footing which is very stiff. Although minimum values for E_{V2} on the foundation were not specified, it can be verified that the results are higher than the minimum values suggested by other Railway Infrastructure Managers for the construction of transition zones, as mentioned in Chapter 3.

To characterise the wedge-shaped transitions, measurements of the deformation modulus using the *portancemètre* were also carried out during construction of the backfill at two intermediate

levels (Figure 4-46a and b), along alignments 2 and 3 (Figure 4-46c and s), respectively located at 6.0 m and 2.5 m below rail level.

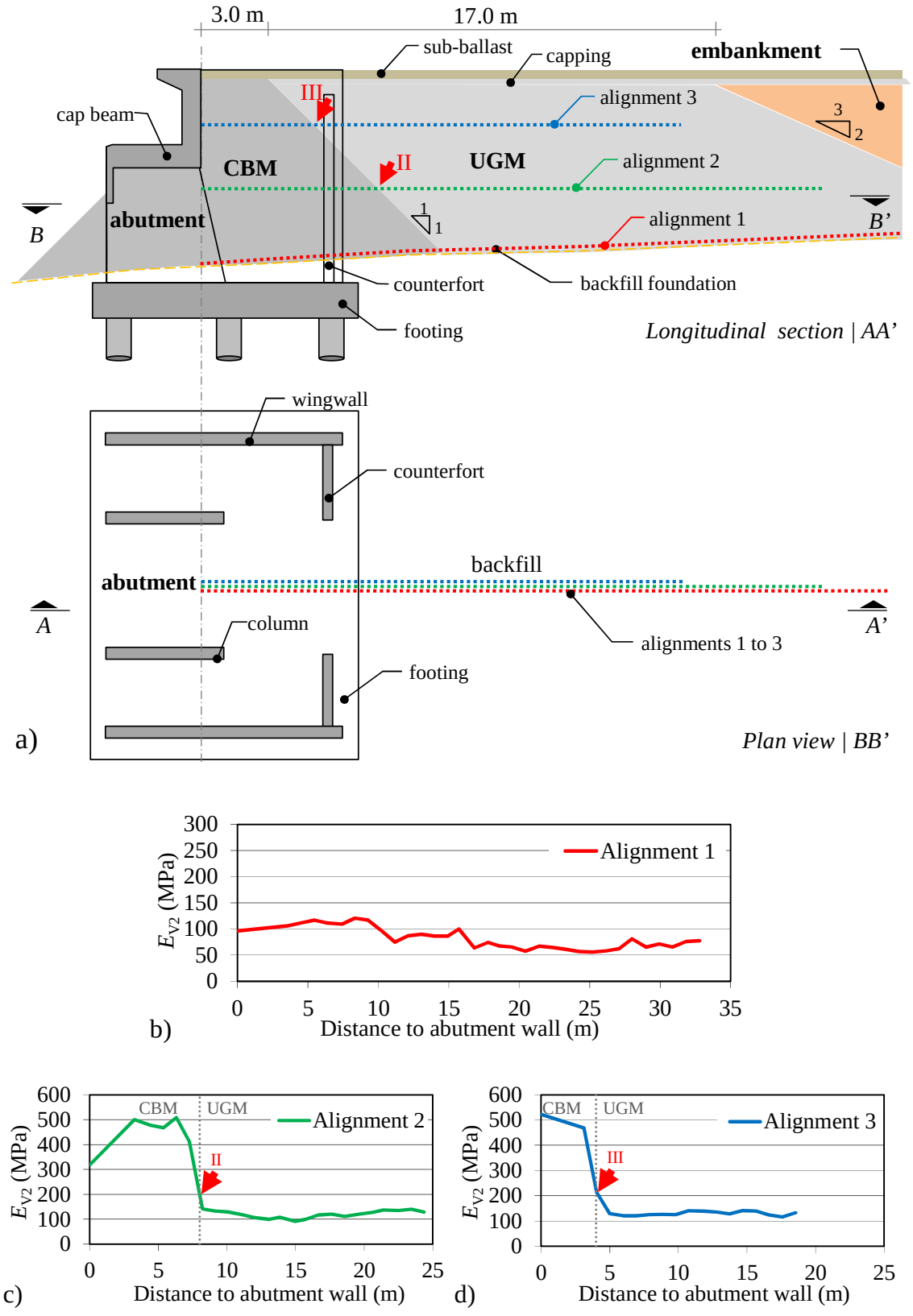

Figure 4-45. Location of alignments 1 to 3 in the backfill (a) and respective *portancemètre* results (b to d).

Considering the *portancemètre* measurements, higher E_{V2} values were obtained on the CBM layers, when compared with the ones at adjacent UGM layers: about 500 MPa against about 120 MPa. The higher stiffness on the CBM layers was expected, considering the well-known effect of cement binders in the mechanical properties of aggregate mixtures (Xuan *et al.*, 2012), as demonstrated earlier. Moreover, as presented in 4.7.2.1 and also reported in the literature, the mechanical behaviour of these mixtures strongly depends on the curing time. For that reason, considering that both *Portancemètre* measurements on CBM layers were performed as early as one day after laying the previous 60 cm of CBM, higher E_{V2} values could have been measured after longer curing periods. This observation is based on the fact that the stiffness of bounded materials can increase with time due to the continuing hydration of the cement phase (Kolias & Williams, 1984; Kongsukprasert & Tatsuoka, 2007). Possibly, in that scenario, the vertical stiffness of the backfill could have been closer to that of the abutment and bridge, thus contributing to soften the stiffness transition. It is also interesting to note the relatively lower values obtained at the beginning of alignment 2 (Figure 4-45c) near the abutment wall (around 300 MPa), when compared with other measurements on the same CBM layer. This may be due to poor compaction at that location, namely, it was found impractical to adequately compact the layers bellow the abutment's cap beam (see Figure 4-45). Despite this observation, no apparent influence was verified at alignment 3, next to the abutment wall.

a) b)

c) 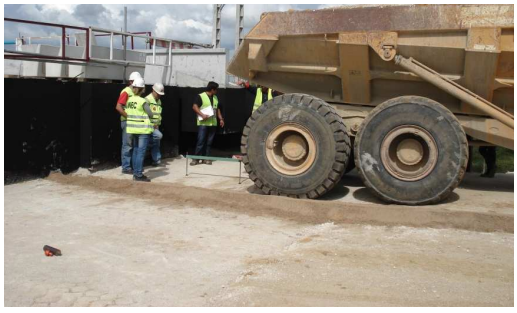

Figure 4-46. Aspects of the p*ortancemètre* surveys (a and b) and PLT tests (c) on the backfill.

As mentioned earlier, in addition to *Portancemètre* measurements, PLT were also performed along the transition zone (Figure 4-46c). One PLT was performed on the CBM, obtaining E_{V2} = 521 MPa. On UGM layers two PLT were performed, resulting in E_{V2} values of 156 and 135 MPa. A good agreement is observed when comparing the PLT values with the earlier *Portancemètre* results on the intermediate layers of both CBM and UGM wedges.

At the UGM wedge, E_{V2} values of 210 and 232 MPa were obtained with PLT on the capping and sub-ballast, respectively, denoting slightly higher values than usually found on these layers, in open track.

On the earthworks adjacent to the transition zone, it was also possible to carry out *Portacemètre* measurements on the uppermost layer of the embankment and on the capping. Figure 4-47a illustrates 10 m moving averages of E_{V2} measurements obtained with *Portancemètre* in nearby earthworks. Values between 75 and 105 MPa were obtained on the top layer of the embankment. As regards the capping layer, values between 90 and 125 MPa were obtained. These values were lower than the E_{V2} modulus obtained on the capping at the transition zone (210 MPa). This difference was certainly due to the presence of the stiffer materials under that layer, comprising the wedge-shape transition. Away from the bridge, weaker embankment soils were present beneath the capping, thus resulting in lower E_{V2} values.

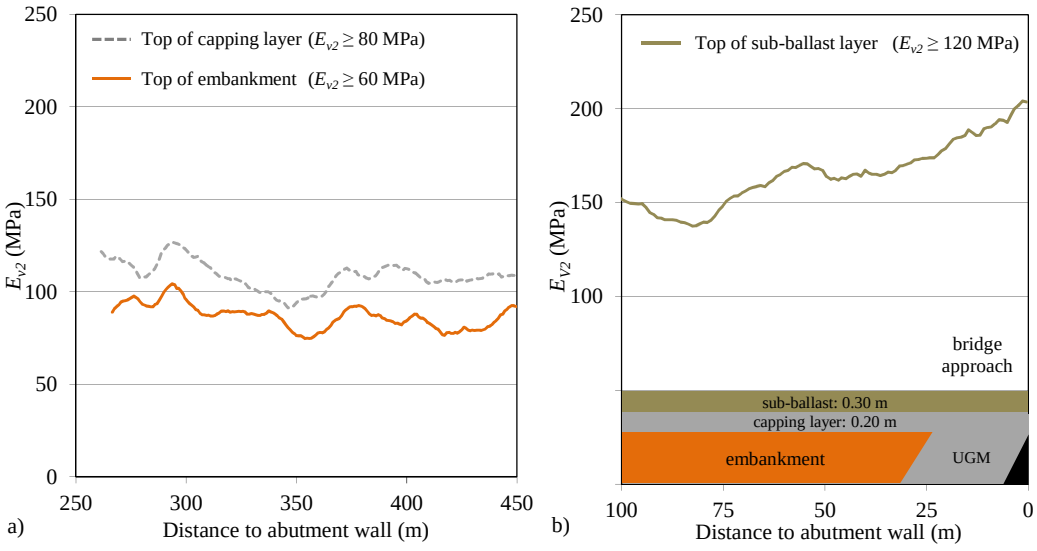

Figure 4-47. E_{V2} results with the *Portancemètre*: a) on capping and embankment near the transition zone; b) gradual stiffness increment measured on the sub-ballast layer at an adjacent transition zone.

Unfortunately, it was not possible to carry out *Portancemètre* measurements on top of the finished sub-ballast layer at the case study transition zone before the track was laid. Nevertheless, it was possible to perform *Portancemètre* measurements at another transition zone to a bridge of the same railway project that was constructed by the same contractor, using the same materials and equipment, and following the same requirements. The gradually stiffness increment at that transition zone is quite evident (Figure 4-47b). It can be observed a stiffness increment of about 40% along 75 m, at the bridge approach. However, it should be noted that, among other aspects, the stiffness of the backfill of the two transition zones can be influenced by different construction and compaction conditions.

Although *Portancemètre* and PLT results performed on the layers bellow the sub-ballast indicate relatively sharp stiffness transition from the UGM to the CBM wedge (Figure 4-45), E_{V2} values presented in Figure 4-47b, measured on the sub-ballast, point towards a smoother stiffness transition. This observation seems to indicate that the sub-ballast layer has a significant influence in levelling the sharp variations of the equivalent elastic modulus measured at the surface of a multi-layer structure (in the present case expressed in terms of E_{V2}). On one hand, the sub-ballast contributes to increase the substructure stiffness on embankment soils and on the UGM wedge. On the other, it seems to reduce the higher stiffness values observed on the CBM wedge.

Taking into consideration that the track superstructure remains the same throughout the line, it is expected that the adopted transition design may provide a smooth track stiffness transition, measured on the superstructure. Gradual stiffness transitions at bridge approaches with CBM have also been measured using specific modified loading vehicles, as reported by other authors (Li & Davis, 2005).

4.7.4 Monitoring backfill settlements

In order to assess the long-term behaviour of this transition zone, in terms of the vertical deformation of the backfill, different and complementary approaches were used in this case study, namely: i) sub-horizontal inclinometers installed inside the backfill; ii) topographic surveys of the track's longitudinal profile.

4.7.4.1 Vertical deformation of embankments using inclinometers

The instrumentation of embankments using inclinometers is a method often used to measure and monitor vertical and/or horizontal displacements in geotechnical structures, including transport infrastructures (Machan & Bennett, 2008; Abu-Farsakh & Chen, 2014). In the case of sub-

horizontal installation of inclinometer systems, it is possible to calculate profiles of vertical displacements in the embankments in sub-horizontal alignments. The working principle consists in measuring the variation in inclination of the casings that constitute the inclinometers. To that aim, a probe is inserted inside the inclinometer casings and runs through its entire length to perform successive measurements of the angle of tilt of the casing segments (Figure 4-48).

Normally, the measurements are performed at every 0.50 m inside the casing using probes with servo-accelerometer sensors at both ends. The successive readings of the angle of tilt along the inside of the casing allow determining it's the longitudinal profile.

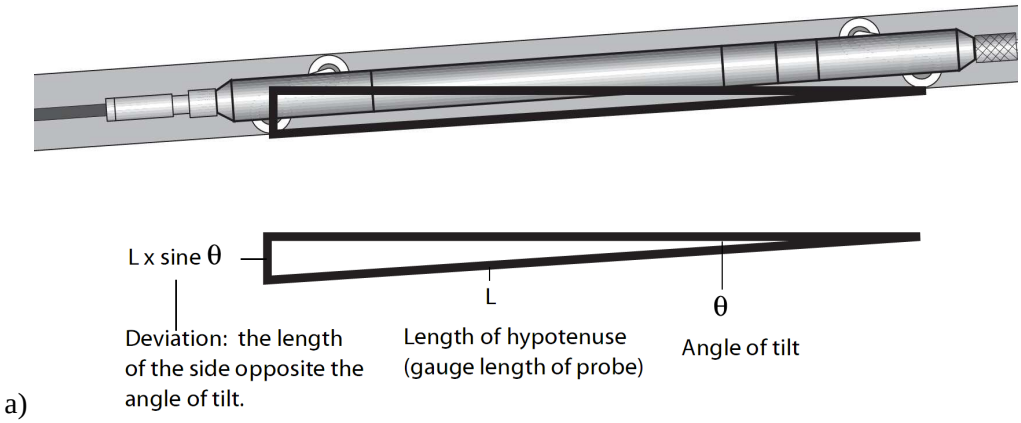

Figure 4-48. Schematic diagrams of the inclinometer system: a) calculation principle of the vertical displacements; b) casing with one exit only (Slope Indicator, 2006).

Given a reference profile of the casing, it is possible to determine the subsequent vertical displacements of the tube relative to that reference profile, by comparing the readings of inclinations made in these two campaigns. The relative vertical displacement, δ_z, of a given section can be calculated using the following expression:

$$\delta_z = L \times \left(sin\theta_i - sin\theta_{ref}\right) \tag{4-3}$$

Where:

L – is the distance between the two sensors located at both ends of the inclinometer probe;

θ_{ref} and θ_i – are the angles of tilt of the reference position and the position in study, respectively.

In order to reduce reading errors, the measurements are normally made twice inside the casing: after performing the first measurements along the casing, the probe is inserted again for a second round of measurements but in inverted position, i.e. with the probe's ends in opposite position.

In this case study, an innovative application of two sub-horizontal inclinometer systems was developed and implemented during construction of that backfill in April 2010 (Figure 4-49 and Figure 4-50). The inclinometers (1 and 2) were installed parallel to the track's alignment, at depths of about 6.2 m and 2.5 m from the rail level, respectively. Each inclinometer comprises about eighteen 3.0 m-long casing segments in aluminium (with nominal diameter of 76 mm), corresponding to a casing with total length of about 54 m.

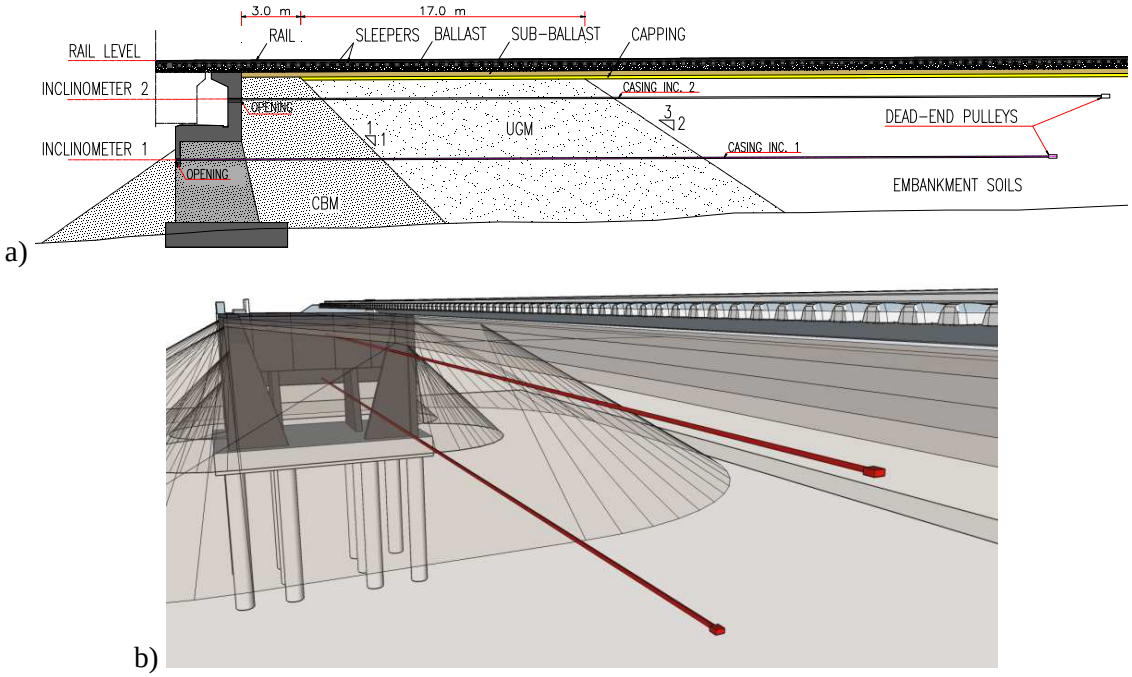

Figure 4-49. Schematic representation of the inclinometers inside the backfill: a) longitudinal view; b) three-dimensional translucent view.

Initially, it was necessary to make two openings in the abutment backwall to account for the access to the inclinometers (Figure 4-50b). The ends of the inclinometers opposite to the abutment (that are inside the embankment soils) remained inaccessible after construction. Thus,

because the inclinometers only have one opening, it was necessary to place a dead-end pulley (Figure 4-50d) at the end of each inclinometer so that a return cable could be installed to manoeuvre the inclinometer probe (Figure 4-51).

The casings and the return tubes were installed as the embankment was reaching the respective installation levels of inclinometers 1 and 2. To ensure the correct installation of the casings, it was necessary that the layers with the different materials of the wedge-shaped backfill were at the same level prior to the installation (Figure 4-50c to e). The installation of each inclinometer consisted of placing the casings inside a longitudinal trench, about 50 cm wide and 30 cm deep that was opened in the backfill (Figure 4-50). To make the trench surface more even and to adequately support the casings, a layer of sand was placed under the inclinometers.

Figure 4-50. Aspects of the installation of the inclinometer system during construction of the backfill: a) location of the inclinometers; b) view of the openings in the abutment backwall; c) laying the casing segments with geotextiles protecting the joints; d) installation of the pulley and return tube; e) covering the inclinometer with backfill material.

a) b) 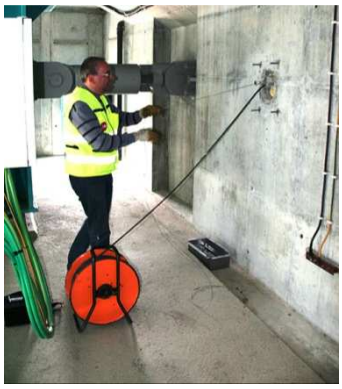

c) d)

Figure 4-51. Ends of the inclinometers: a) opening of the inclinometer 1 on the abutment wall during the tests with the dummy probe; b) manouvering the probe inside inclinometer 2 with the return cable; c) detail of the dead-end pulley (Sisgeo); d) detail of the casing opening with the return cable.

In order to prevent fines of the embankment soils from entering the casings and obstructing the inclinometers, the joints of the casings and the pulleys were wrapped around with geotextile as depicted in Figure 4-52.

Figure 4-52. Details of the protective geotextile to prevent fines from obstructing the interior of the casing: a) joint between two casing segments; b) pulley at the end of the casing.

After placing the casings inside the trench, it was filled with sand up to the same height of the existing layer. To avoid changes in the position of the casings and to prevent them from damaging during the construction of the subsequent layers, the first layers of material placed on top of the inclinometers were compacted carefully with manual equipment only.

During the installation of the inclinometers, one of the most critical aspects was the execution of the interface between the abutment and the casings. Because the abutment is a very stiff structure and it is not expected to undergo significant settlements, it was necessary to ensure that the open ends of the inclinometers were allowed to settle and rotate relatively to the abutment. As shown above in Figure 4-51, the access to the inclinometers is located at the front of the abutment.

With regard to the lower inclinometer 1, it was installed below the abutment seat (Figure 4-50b). Due to difficulty access to this area, it was decided to fill part of the volume under the abutment seat with hydraulic fill and concrete filling (C12/15). Thus, to ensure that the inclinometer would function adequately in this area, it was protected with more geotextile and with additional volume of sand (Figure 4-53).

a) b) 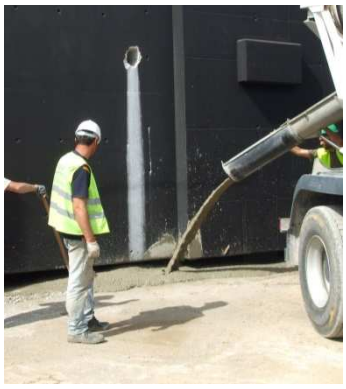

Figure 4-53. Aspects of the installation of inclinometer 1: a) additional protection with geotextile and sand; b) pouring the with hydraulic fill under the abutment.

The inclinometer probe (Sinco, Slope Indicator – see Figure 4-54) has a resolution of about 0.02 mm per 500 mm (Slope Indicator, 2006). In the manufacturer's website, the technical note

"Accuracy of Inclinometers"* describes a method to estimate a conservative value of the total error of the readings that was derived empirically from a large number of datasets. It mentions that the total error is the sum of the systematic and random errors, which depend on the number of readings (n). The random error is estimated to be $0.1778\sqrt{n}$ (mm) and the systematic error $0.127\,n$ (mm). Considering that the method adopted in the this study eliminates the systematic errors of the readings, the conservative value of the total random errors were estimated to be about 1.84 mm for the total number of 107 reading in each inclinometer (corresponding to about 0.03 mm per meter of length of the inclinometer casing).

a)

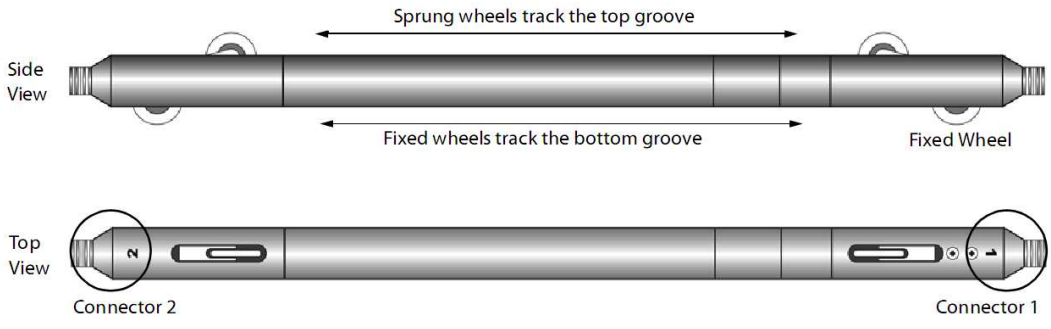

b)

Figure 4-54. Aspects of the inclinometer probe (Sinco, Slope Indicator, model 50302910): a) schematic representation; b) view of the probe.

Figure 4-55 shows the profiles of the inclinometers 1 and 2 measured in May 2010 after the conclusion of the backfill (about 5 months before opening the line to traffic in October 2010), which were considered as a reference position.

* http://www.slopeindicator.com/support/inclinometers/technote-inclin-accuracy.html

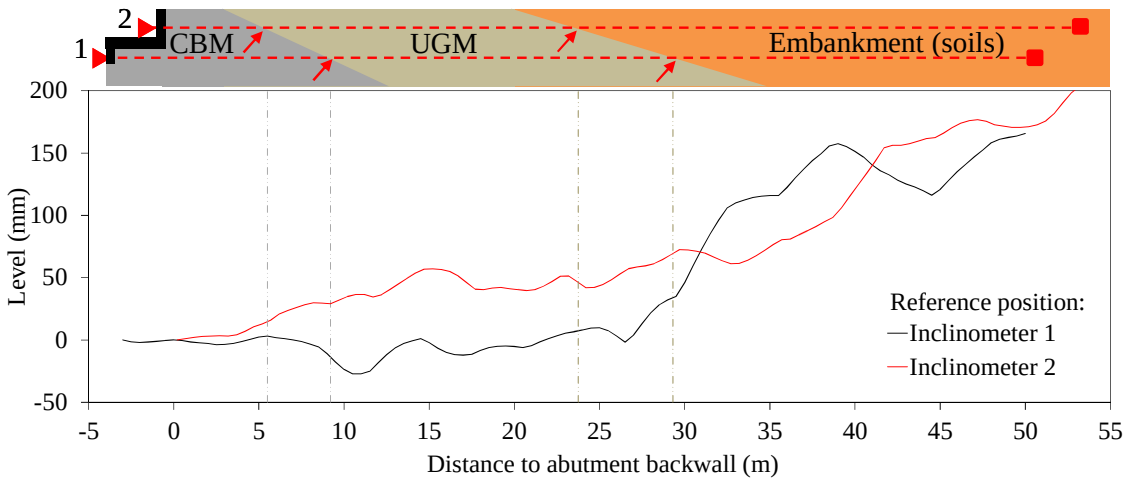

Figure 4-55: Reference positions of inclinometers 1 and 2 measured in March 2011.

Figure 4-56 shows the evolution in the vertical deformation of the backfill layers in the longitudinal alignments of inclinometers 1 and 2. The results evidence that a significant part of the settlements developed in the first 10 months after the conclusion of the backfill, whereas during the following 19 months smaller deformations were observed in both inclinometers. As would be expected, negligible settlements were observed in the CBM wedge, considering the low susceptibility of that material to permanent deformation. After the first 10 months, the maximum settlements were about 7 mm and 9 mm regarding inclinometers 1 and 2, respectively, and occurred at the end of the wedge-shaped backfill, at the transition between the UGM material and the embankment with soils. In general, greater evolution of settlements was detected in this area on both inclinometers. This was probably due to geometry of the wedge-shaped backfill that made it more difficult to compact the layers at the interface between different materials (Figure 4-57).

Between months 10 and 29, settlements in inclinometer 1 seem to have stabilised, particularly in the CBM and UGM wedges, and the section of the embankment with soils showed a slight increase in settlements by about 2 to 3 mm. In general, the alignment of inclinometer 2 appears to have undergone a greater evolution in settlements. The section on the UGM wedge showed settlement increments up to about 3 mm and the soils on the embankment appear to have undergone a general uniform settlement of about 3 mm. The larger evolution observed in inclinometer 2 in this period, comparing with inclinometer 1, was probably because inclinometer 2 was installed about one month after inclinometer 1, thus the layers under inclinometer 1 had more time to settle before that period. Other factors that may have influenced

the results were the different volumes of material under each inclinometer deforming at different rates, as well as different volumes of material on top of them, corresponding to different loads acting on the deformation of the earth structure.

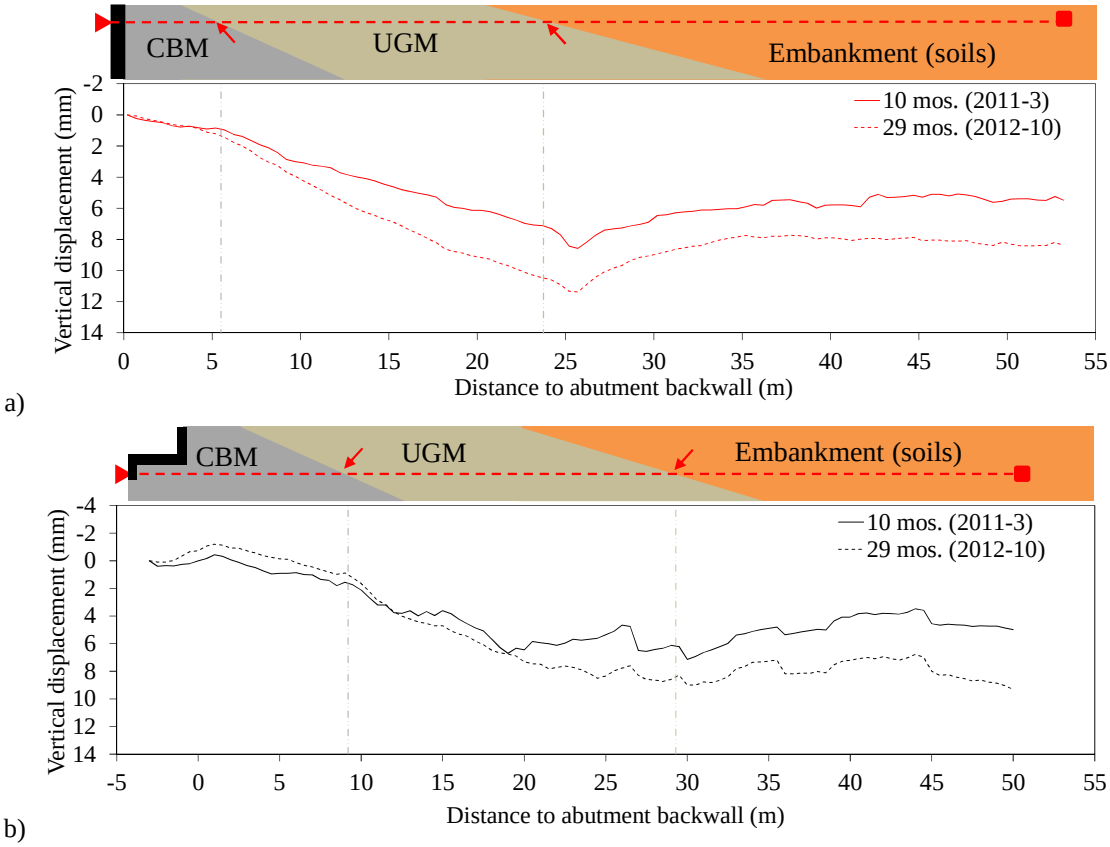

Figure 4-56: Measurement of internal displacements of the backfill in inclinometers 2 (a) and 1 (b).

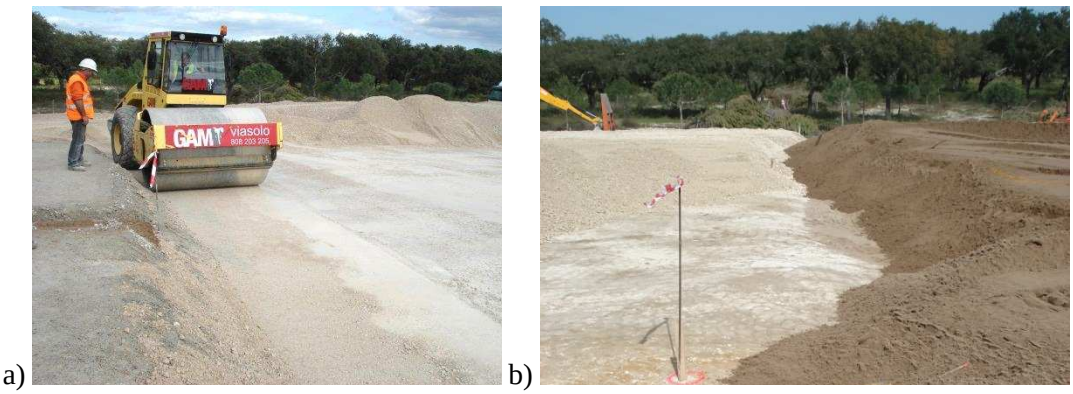

Figure 4-57: Interfaces of wedges of the backfill with different materials: a) CBM and UGM; b) UGM and embankment with soils.

It is also worth noting that a local elevation of the position of the casing of the inclinometer 1 was observed in the CBM (Figure 4-56b). Although the displacements were very small and fairly close to the range of the reading error with the equipment, this movement may have been caused because, in that section, the segments of the inclinometer casing were installed under the abutment (Figure 4-53), in a location with limited access where the hydraulic fill was poured. The absence of adequate compaction in that location may have allowed the casing segments to undergo an upward mechanism movement that resulted from the downward displacements that were developed in the adjacent area of the backfill, away from the abutment.

Additional measurements of the inclinometers' positions were carried out over the following years. The differences between these successive measurements and those of month 29 were within the range of the measurement errors (about 0.03mm/m), therefore they were not presented here for easier interpretation of the results. This indicates that the backfill has practically stabilised since month 29 (October 2012) and no significant settlements were observed since that reading, with the line in operation.

These findings evidenced that these types of earth structures undergo faster settlement rates in earlier ages, as is normally observed in other earth structures (Clements, 1984; Fortunato & Veiga Pinto, 1997b, a; Soriano & Sanchez, 1999; Rodríguez *et al.*, 2000; Pardo de Santayana *et al.*, 2006). Moreover, it shows that, in this case, to further minimise in influence of post-construction settlements in the longitudinal level of the track at the transition zone, the track and its substructure should be left to rest at least one year (if possible two years) before establishing the final geometry of the track. This conclusion seems to be particularly relevant to be considered in the design and construction of other railway lines and transport infrastructures that include similar transition zones to structures in order to assure that the deformation of these earth structures does not compromise the final longitudinal level of the superstructure.

4.7.4.2 Surface settlements with precise levelling

In order to monitor the surface settlements in various positions of the backfill, vertical displacements were measured with topographic surveys (precise levelling).

During construction, various sets of surveying points were installed at the transition zone, forming seven main transverse alignments, spaced of 10 m apart, as depicted in Figure 4-58. The system of surveying points comprises (Figure 4-59):

i) two longitudinal alignments of seven concrete blocks installed on the sub-ballast, on each side of the track, with one survey point each (PN1 to PN7 and PP1 to PP7);

ii) two longitudinal alignments of seven survey points each, located at the sleepers' ends (TN1 to TN7 and TP1 to TP7).

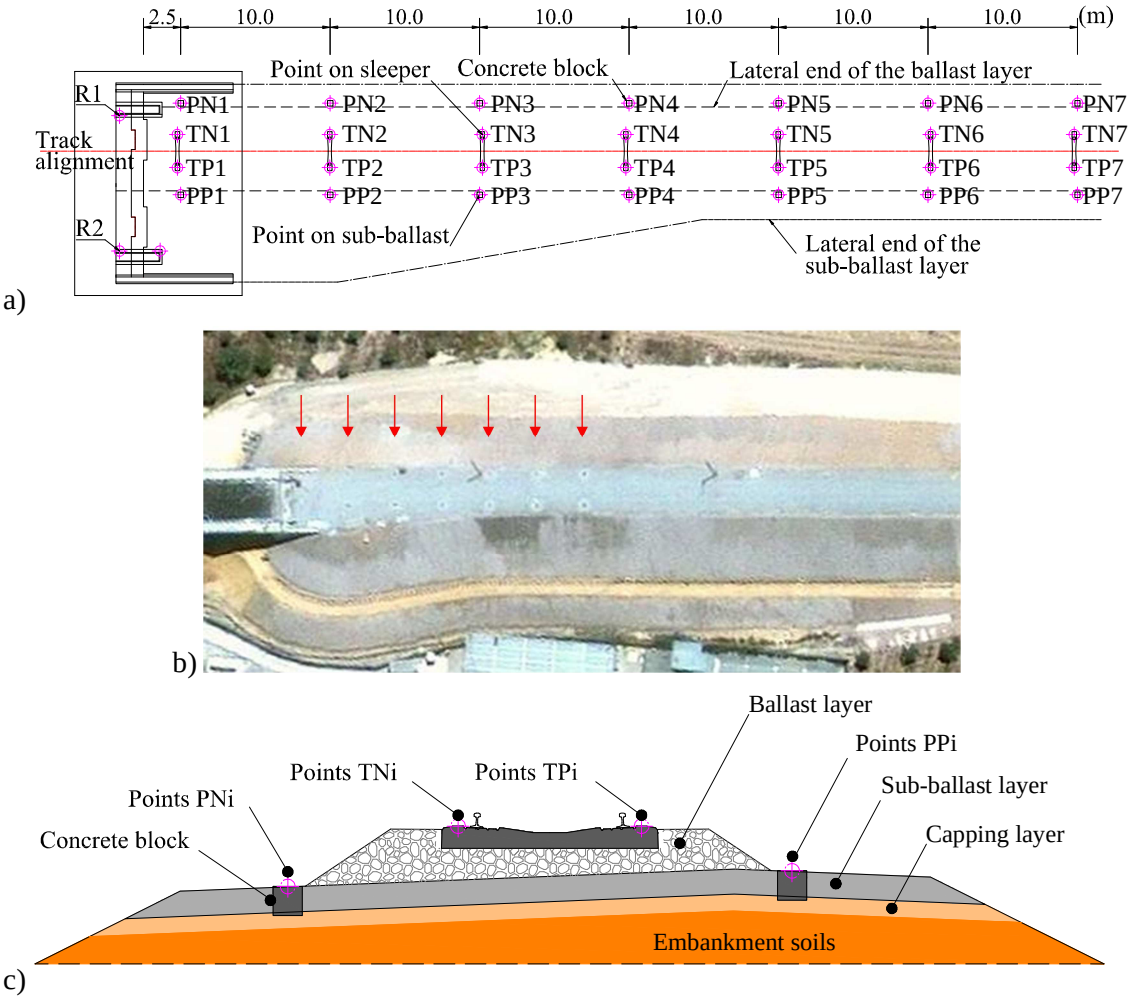

Figure 4-58. Layout of the survey points on the approach to the bridge: a) plan view; b) aerial view during contruction; c) track cross section.

The geodetic survey point placed by REFER in the structure of the abutment (Figure 4-60) was used as a reference. During the period of observation, this mark was considered to have a fixed position, with respect to the backfill.

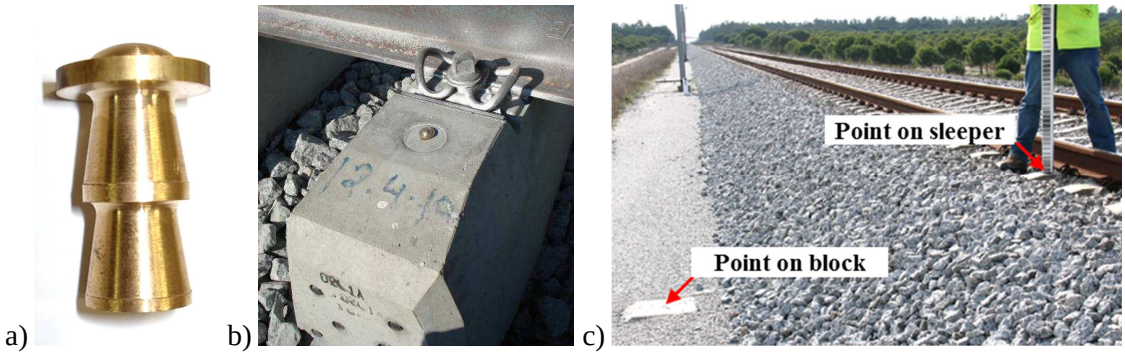

Figure 4-59. Survey points: a) detaild view; b) installation on the sleeper's end; c) levellig survey.

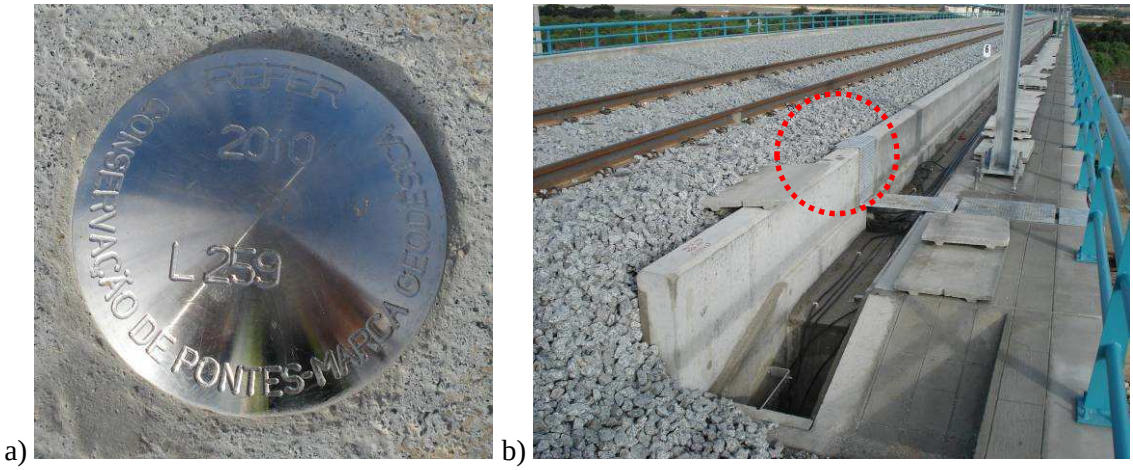

Figure 4-60. Aspects of the geodetic reference mark R1: a) detailed view; b) location.

After the first survey, the point TP1 was found damaged and the point PP1 had been covered by a large amount of ballast, thus the two survey points were not considered in the study.

The backfill was completed at the beginning of May 2010, but the survey points on the sub-ballast were only installed in July 2010. The survey of 8th October 2010, held few days before the first trains used the line, was considered as the reference profile (Figure 4-61). The measurements were performed with an electronic digital level (TOPCON DL101-C) with the precision of 0.4 mm.

According to the design, at this transition zone, the railway line has a gradient of 6 ‰. For the analysis of longitudinal profiles obtained from the levelling surveys, it was possible to verify the same values of inclination.

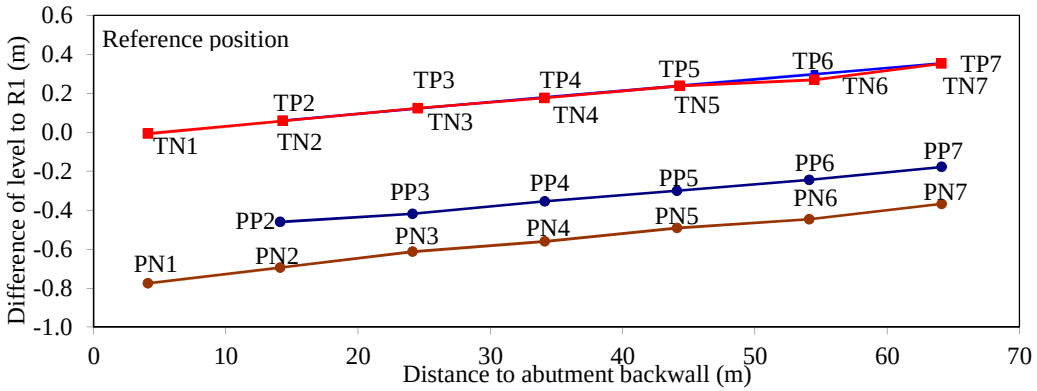

Figure 4-61. Reference profile of the survey points on the sleepers and sub-ballast at the transition zone.

The figures below show the evolution of the profiles of the alignments on the sub-ballast layer (PNi and PPi in Figure 4-62) and on the sleepers (TNi and TPi in Figure 4-63) obtained in subsequent levelling surveys. The average levelling error of closure of the survey points in the sub-ballast was about 0.5 mm and of the survey points in the sleepers was about 0.9 mm.

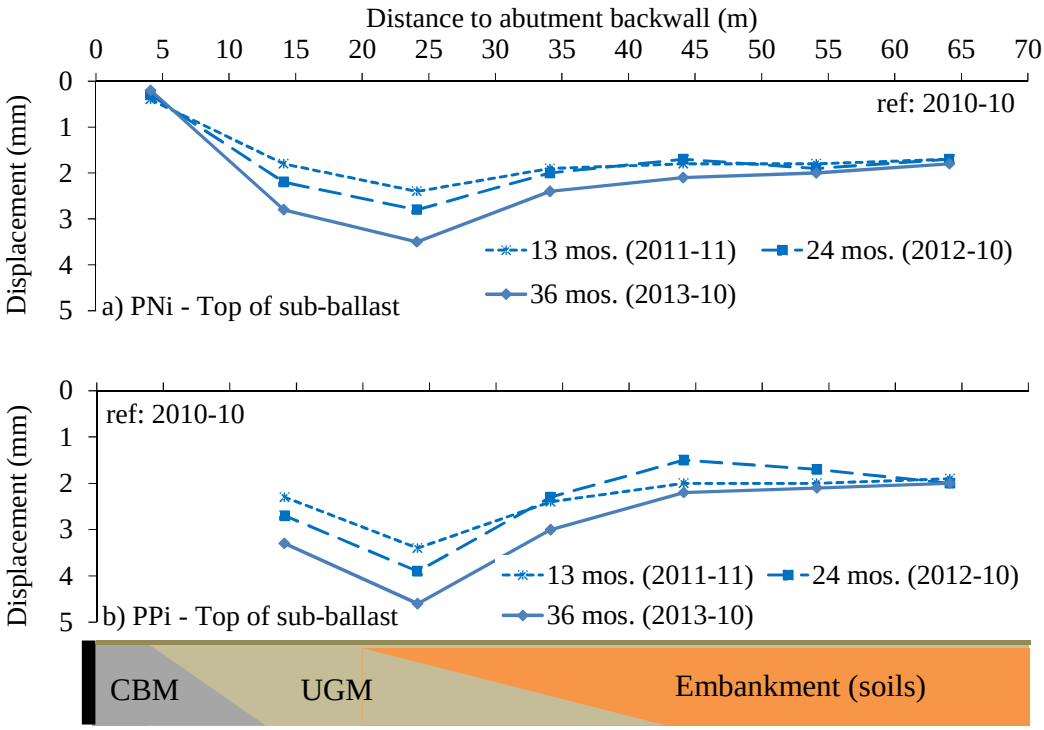

Figure 4-62. Displacements of the survey points on the sub-ballast layer: a) points PN1 to PN7; b) points PP1 to PP7.

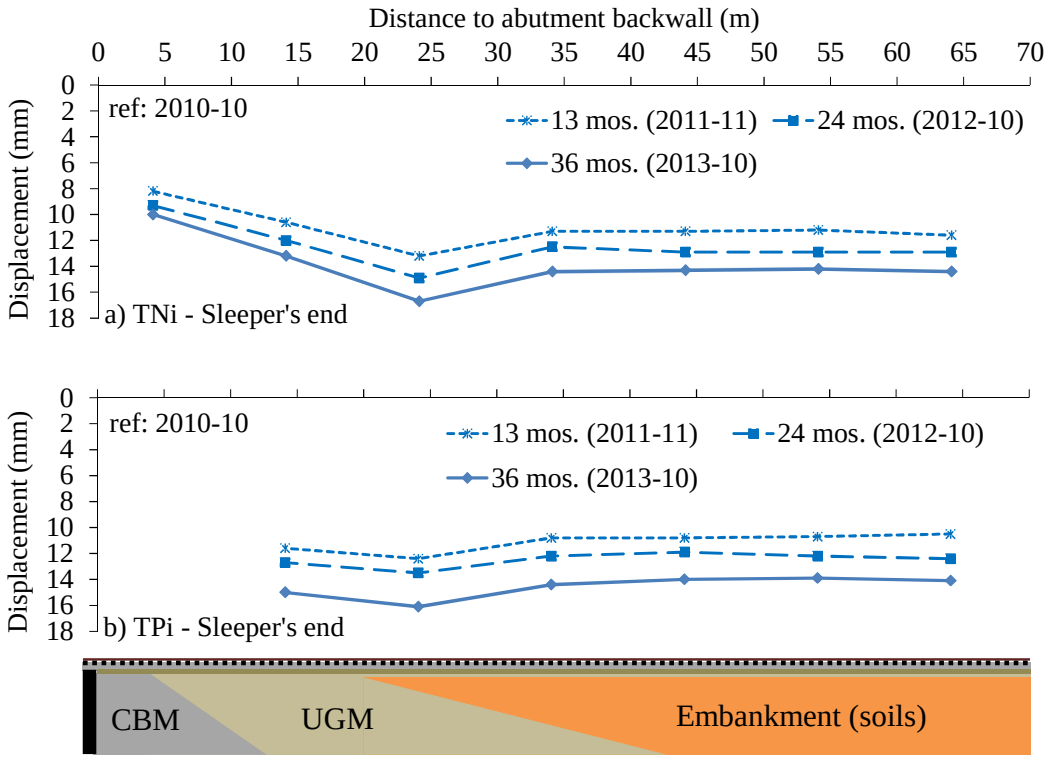

Figure 4-63. Displacements of the survey points on the sleepers' ends: a) points TN1 to TN7; b) points TP1 to TP7.

The analysis of the results shows that the transition zone had higher deformation rates between the reference survey (Oct. 2010) and the survey of November 2011 - the first year after opening the line to traffic - which is in agreement with the findings obtained with the inclinometers.

In general, the survey points farthest from the abutment (more than 30 m away) show similar settlements values, which denotes a rather homogeneity in the behaviour of the embankment constructed using soils.

In the sub-ballast layer, after about one year, the maximum observed settlement was about 3.4 mm, in survey point PP3 (about 25 m from the abutment wall) and after about 3 years, the maximum settlement had only increased to about 4.6 mm, in the same survey point. This corresponds to a settlement rate almost 6 times slower between the 2nd and the 3rd years. The shape of the longitudinal settlement profile seems to be the same in all surveys, apparently, forming a settlement basin at the transition between the UGM wedge and the embankment with soils, which was also observed with the inclinometers (Figure 4-56), as discussed earlier. The average settlement value at alignments PNi and PPi after 3 years was approximately 2.7 mm,

excluding the survey point PN1 that was closest to the abutment and seems to have retained the same position.

It is interesting to note that the survey points on the embankment with soils, more than 40 m away from the abutment, were smaller than those between 10 m and 40 m, which supports that larger displacements are taking place between the UGM and the embankment with soils. As mentioned earlier, this finding suggests that the interface of materials in the wedge-shaped backfill might have caused some constrains to an adequate compaction of the layers, thus resulting in more deformations in the backfill.

It is noted that the survey of October 2012 indicates an upward movement of the points PP5 to PP8 that is not in agreement with the evolution of the remaining survey points. This was probably the result of some reading errors because the error of closure of that survey was 1.78 mm – the highest levelling error of closure, considering all surveys.

As regards the survey points at the sleepers' ends, after the first year, the maximum settlement value was about 13.2 mm, also at about 25 m from the backwall (survey point TN3). After 3 years, the maximum settlement had only increased to about 16.7 mm, also in that survey point, corresponding to a settlement rate of about 7.5 times slower between the 2nd and the 3rd years. In this case, the average settlement value at alignments TNi and TPi, after 3 years, was approximately 14.6 mm, excluding the survey point TN1 that was also closest to the abutment and only had minor settlements since the survey of November 2011.

The shape of the longitudinal settlement profile of the sleepers seems to agree with that of the sub-ballast. However, the survey points on the sleepers showed higher settlement amplitude than those on the sub-ballast; in average, after three years, the settlements on the sleepers were about 5.5 times larger than on the sub-ballast. This difference is probably because of two main reasons:

i) the survey points on the sub-ballast were placed on the sides of the track, therefore their displacements do not reflect de deformation resulting from the cyclic loading of the trains, but the overall long-term deformation of the embankment mainly due to weather conditions and gravity;
ii) the fresh ballast normally undergoes a well-known behaviour of initial densification under the first cyclic loads of the trains (Profillidis, 1995; Esveld, 2001).

Comparing the results of inclinometer 2 in the survey of 2012-10 (Figure 4-56) with those of the levelling in the sub-ballast in the same date (Figure 4-62), it is visible that the inclinometers indicate higher settlement amplitude (a maximum settlement of about 11 m at about 25 m from the abutment, against 4.6 mm in survey point PP3). This difference of more than 5 mm is probably related to the fact that the reference survey of the inclinometers was carried out about 5 months earlier than the reference survey of the levelling. This is in agreement with what was mentioned earlier in that higher deformation rates are expected at earlier ages of the construction of earth structures.

Given that the ballast lies between the sub-ballast and the bottom of the sleepers, it can be considered that the difference between those two levels may be due, in large part, to the normal behaviour of the ballast layer. It is known that, after tamping the ballast layer and during the passage of the first thousands of axles, it undergoes a rapid evolution of permanent deformation. This is a normal behaviour of the track and it is perfectly compatible with the regular operation of the infrastructure. Considering the measurements of the survey points, estimates of the vertical deformation of the ballast were calculated as the difference between the positions of the survey points on the sub-ballast and on the sleepers. Figure 4-64 shows the obtained deformation profile suggesting a uniform vertical deformation of the ballast layer of about 11 mm. Considering the estimated accumulated traffic since inauguration, these results are in agreement with reports from other studies (Selig & Waters, 1994), regarding the contribution of the initial behaviour of the ballast layer to the overall settlements of the track. The results also suggest a slight tendency of increasing deformation with the distance to the abutment.

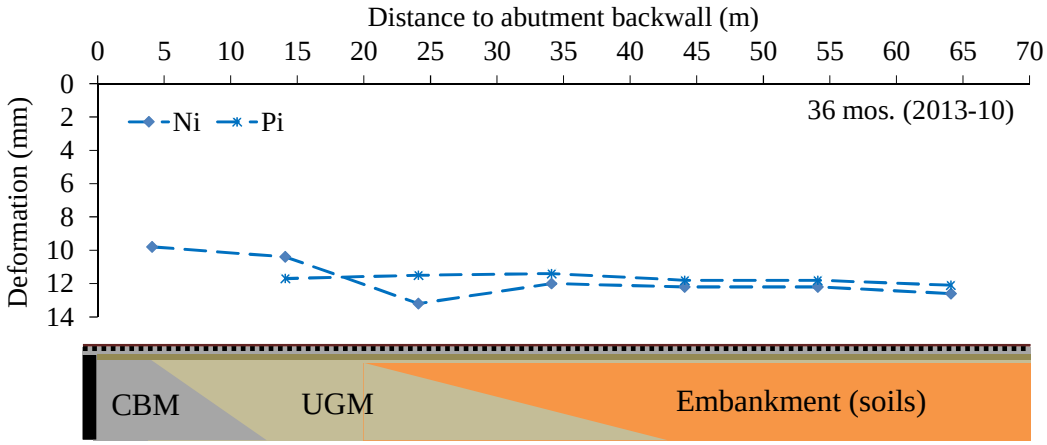

Figure 4-64. Estimate of the vertical deformation of the ballast (Ni = TNi - PNi; Pi = TPi - PPi).

4.7.5 Evolution in track geometry

Three years after opening the line to traffic, no significant settlements were reported at the transition zone and no specific maintenance operations were needed. In Figure 4-65, track geometry recordings obtained with the inspection vehicle are presented, regarding left and right rail longitudinal level measured when the line was opened and after 29 months. Analysing Figure 4-65 it seems that the track geometric quality is still far from reaching the Alert Limit values (±12 mm regarding wavelength range D1, between 3 and 25 m, and ±20 mm regarding wavelength range D2, between 25 and 70 m, see Table 4-5) established by REFER (2009). Moreover, standard deviations of shorter wavelength measurements for the presented 200 m stretch (Figure 4-65a) are also below the established Alert Limit values of 1.9 mm, thus indicating good track quality in terms of longitudinal level. Nevertheless, some changes seem to start occurring at positions 0 m (abutment wall alignment) and 25 m (near the start of the transition) in Figure 4-65a, yet with minor amplitudes.

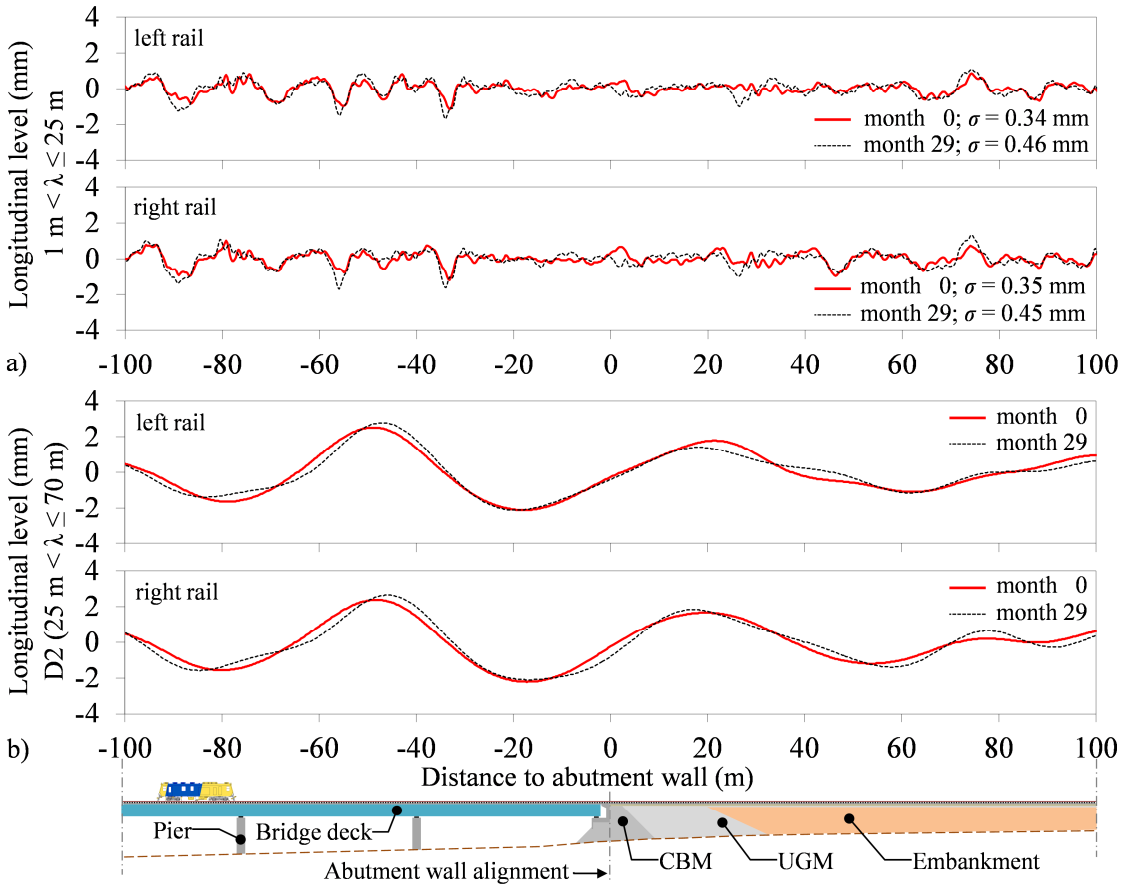

Figure 4-65. Longitudinal level measurements at the transition zone (σ denotes standard deviation).

4.8 Concluding remarks

In this Chapter, a general overview was presented regarding the characteristics of the Alcácer bypass, its transition zones and other track singularities.

From the analysis of the data of the construction quality control, it was possible to conclude that the requirements of the design were met, particularly in what regards the characteristics of the geomaterials and the construction of the layers of the track platform.

Since the bypass was open to traffic it was possible to follow up the results of the REFER's inspection vehicle in what regards the geometric quality of the track. The results showed that after about 17 MGT, the track still had very good track quality and all the geometric parameters were below the limits established in the applicable norms. The analysis of the evolution of the standard deviation of the longitudinal level showed that, in general, transition zones have poorer track quality. The track evidenced normal degradation rates but at some sections, the rates were 5 to 7 times higher. Some of these sections were associated with the presence of transition zones.

The construction of the south approach to the bridge over Sado river was used as a case study. This transition zone comprised a wedge-shaped backfill with well-graded crushed aggregates (UGM) (unbound) and bound aggregate with 5% cement by weight (CBM) in order to provide higher stiffness to the track substructure, to mitigate long-term settlement and to take into account the difficulty to compact the layers close to the walls.

Considering the results of conventional laboratorial and cyclic load triaxial tests performed on the aggregates, the selected geomaterials were considered suitable for those functions. In addition, the resilient modulus determined in the cyclic load triaxial tests provided relevant information for the calibration of the numerical models, as will be addressed in Chapter 5. The analysis of the results of the construction quality control demonstrated a good compaction of the layers.

In situ measurements of deformation modulus of the layers indicate relatively high stiffness values of the transition substructure, suitable for the purposes in question. As expected, gradually increasing E_{V2} values were obtained from the embankment to the UGM wedge, and to the CBM wedge. The stiffness variation was higher at the intermediate layers of the backfill, rather than on top of the sub-ballast.

Measurements performed with sub-horizontal inclinometers installed inside the backfill showed that higher deformation rates took place right after the construction, before opening the line to traffic, as is expected in similar earth structures. The CBM wedge showed negligible settlements during the observation period, but at the transition between the UGM wedge and the embankment with soils larger settlements were observed. This finding may be related to the fact that, considering the geometry of the wedges, it was more difficult to compact the layers at the interface between the different materials.

From the analysis of the vertical displacements of the survey points installed in the sub-ballast and on the sleepers it is concluded that the wedge-shape backfill at the transition case study is showing an adequate behaviour. About three years after opening the line to traffic, the maximum settlement of the track platform was less than 5 mm.

To minimise even further the post-construction settlements, the results evidence that in transition zones with similar wedge-shaped backfills as that of the case study, the track and its substructure should be left to rest at least one year (if possible two years) before establishing the final geometry of the track.

Taking into account what was presented, it is expected a good overall long-term behaviour of the transition zone. Three years after opening the line to traffic, no significant defects on the track longitudinal level were reported at the transition zone and no specific maintenance operations were required.

Chapter 5

Numerical modelling and experimental validation of transition zones*

5.1 Introduction

Structural numerical modelling can be a very useful tool to provide valuable insight into the behaviour of railway tracks. To obtain reliable conclusions, the models need to be properly calibrated and validated. Numerous numerical studies can be found in the literature addressing transition zones, as discussed in Chapter 3, but only a few comprise adequate calibration and validation with *in situ* track measurements. This Chapter aims at giving a contribution to fill the gap between numerical and field studies. The focus will lie on transition zones to two types of railway structures found in the *Alcácer* bypass that are used as two case studies, in particular, transition zones to underpasses and to bridges.

The first case study comprises two transition zones to similar underpasses. During construction, Under Sleeper Pads (USP) were added to the sleepers in one of the transitions aiming at improving the performance of the track. Results of track characterisation using non-destructive tests and measurements of the track response as passenger trains passed by are analysed and discussed. Numerical models were then developed to reproduce those measurements and used to understand the dynamic behaviour of transition zones in more detail, particularly when

---

* This chapter combines the contribution of the following journal articles:

- **Paixão, A.; Alves Ribeiro, C.; Pinto, N.M.P.; Fortunato, E. & Calçada, R.** (2014a) *On the use of under sleeper pads on transition zones at railway underpasses: experimental field testing*; Structure and Infrastructure Engineering; 1744-8980;
- **Alves Ribeiro, C.; Paixão, A.; Fortunato, E. & Calçada, R.** Ibid.*Under sleeper pads in transition zones at railway underpasses: numerical modelling and experimental validation (accepted for publication)*;
- **Paixão, A.; Fortunato, E. & Calçada, R.** (2014b) *Transition zones to railway bridges: track measurements and numerical modelling (accepted for publication)*; Engineering Structures;

influenced by USP. To that aim, the calibration and validation procedure developed by Alves Ribeiro (2012) was applied in this study to determine the mechanical properties of the materials and track components using a 2D FEM modelling approach. The relevance of this approach lays on the fact that:

- It considers all relevant track components and substructure layers;
- It takes into account the train-track interaction;
- It considers experimental data and 3D reduced models in an innovative calibration procedure;
- It requires less computational resources and calculation time than full 3D modelling approaches and still provides accurate results.

The second case study is the southern transition zone to the new railway bridge over Sado River. Track measurements were also performed as trains crossed the transition, using similar instrumentation system of the first case study. Those measurements were then used to validate another numerical model that was developed using the same numerical technique.

5.2 Case study 1 - dynamic train-track interaction at transitions to underpasses

5.2.1 Description of the transition zones to the underpasses

The transition zones to the similar underpasses located at km 62.940 and km 81.187 of the *Alcácer* bypass were selected as the first case study. The two underpasses - UP1 and UP2 (Figure 5-1) - are reinforced concrete closed frame box culverts. At UP1, 44 sleepers with USP were installed, while UP2 comprises standard track. The design established the construction of transition zones in accordance with demanding design requirements similar to those implemented in new European high-speed railway lines, which were introduced in Chapter 3. Relevant aspects of the transition zones at UP1 and UP2 are presented in Figure 5-2. As discussed earlier, the geometry and materials of the wedge-shaped backfills are intended to control long-term deformations that usually occur near these structures, as well as to achieve a smooth transition of the vertical stiffness of the track.

a) b)

Figure 5-1. View of the underpasses UP1 (a) and UP2 (b).

The layers of the backfills, constructed with cement bound mixture (CBM) and unbound granular material (UGM), were compacted with average degree of compaction of about 100% and 99%, respectively, regarding the Modified Proctor compaction reference test (OPM).

The natural foundation of both transition zones generally comprised monogranular fine grained sands providing good foundation conditions. About 35 to 60 blows of the Standard Penetration Test (EN ISO 22476-3, CEN, 2005) were obtained. However, due to the presence of a superficial layer of sandy silty clays at UP1, it was necessary to replace those soils with well-graded crushed unbound granular material down to a depth of about 3.5 m (Figure 5-2).

It should be recalled that the line allows for speeds up to 220 km/h for passenger tilting trains (*Alfa Pendular*) and consists of a wide gauge (1.668 m) ballasted railway track, comprising continuously welded UIC60E1 rails resting on 2.6 m long concrete monoblock sleepers, spaced 0.6 m apart and prepared for both wide and standard gauges (1.453 m). The adopted fastening system was Vossloh W14 using elastomer rail pads Zw700/148/165 with secant static stiffness of 50-70 kN/mm, measured between 18 and 68 kN, as provided by the manufacturer.

To illustrate the different track support conditions along the transition zones, Figure 5-3 shows schematic track cross-sections at key locations identified from S1 to S4 in Figure 5-2. On the box culverts, only the layer of ballast was kept, with the same minimum thickness of 30 cm under the sleepers. The requirements for E_{V2} deformation modulus on top of the layers and degrees of compaction, regarding the Modified Proctor compaction reference test (OPM) were introduced in Chapter 4. Figure 5-4 shows the grading envelopes of the materials applied in the trackbed.

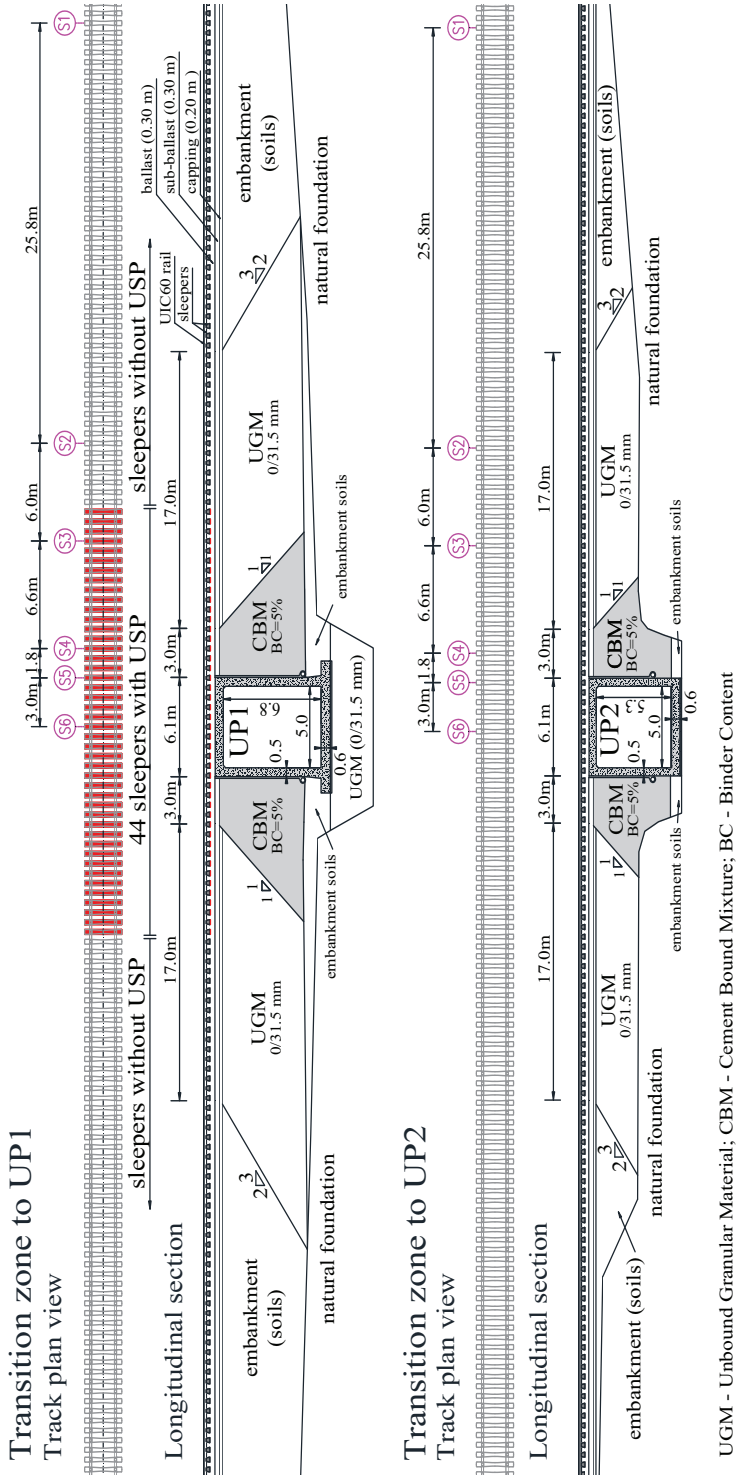

Figure 5-2. Track plan view and longitudinal profile of transition zones at UP1 and UP2.

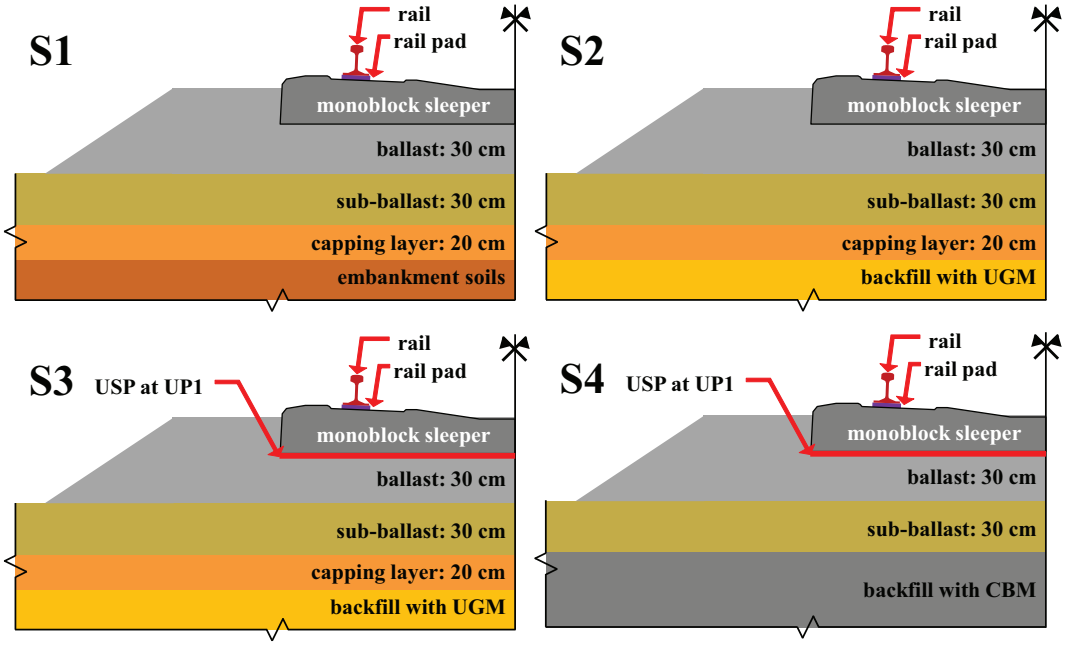

Figure 5-3. Schematic track cross-sections from S1 to S4 (see location in Figure 5-2).

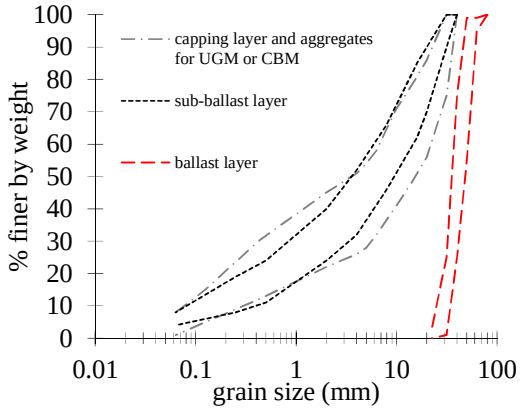

Figure 5-4. Grading envelopes of granular materials.

Table 5-1 presents some characteristics of the resin-bonded rubber USP that were glued to the underside of the sleepers at UP1 (Figure 5-5).

Table 5-1. Characteristics of the under sleeper pads, provided by the manufacturer, CDM.

Parameter	Value
Thickness	10 mm
Length	2.6 m
Maximum width	0.3 m
Static bedding modulus, C_{stat} (CEN/TC 256, 2012)	0.155 N/mm^3
Dynamic bedding modulus, C_{dyn} (CEN/TC 256, 2012)	0.200 N/mm^3

Figure 5-5. Some aspects of the USP preparation.

5.2.2 Characterisation of the substructure and superstructure of the track

5.2.2.1 Measurements of deformation modulus on the substructure performed during construction

During the construction of the transition zones, *in situ* tests were performed. To meet the design requirements regarding the degree of compaction of the layers and respective water contents, sand replacement method and nuclear density gauge tests were performed as the layers were built. Plate load tests (AFNOR, 2000) and surveys with the *portancemètre* equipment (Quibel, 1999) were also performed to evaluate the deformation modulus (E_{V2}) on the platform. Figure 5-6 shows the 3.0 m moving average results of *portancemètre* surveys carried out after construction of the subgrade and on the sub-ballast layer. The analysis of the results of the *portancemètre* indicates that the deformation modulus on the subgrade and on the sub-ballast is quite homogeneous on both sides of the underpasses. Average E_{V2} values of 120 and 90 MPa were obtained on the subgrade for UP1 and UP2, respectively. On the sub-ballast, average E_{V2} values of 185 and 220 MPa were obtained. The slightly higher amplitude and scattering of E_{V2}

values on the sub-ballast near UP2, when compared with the values obtained near UP1, is representative of the well-known mechanical behaviour of unbound granular materials, such as that used in the sub-ballast layer. Among other aspects, these materials are influenced by stress conditions, degree of compaction and, particularly, by water content. The differences found may be due to the different water contents of the sub-ballast material when the *portancemètre* surveys were carried out.

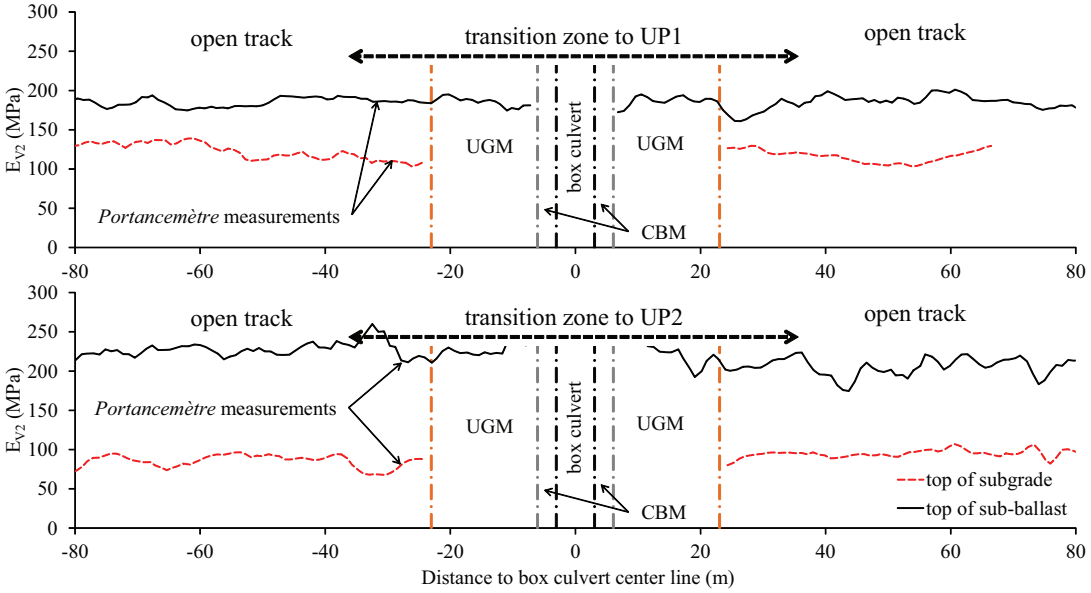

Figure 5-6. Deformation modulus obtained with the *portancemètre* at the transitions to UP1 (above) and UP2 (below).

5.2.2.2 Light Falling Weight Deflectometer tests

The falling weight deflectometer (FWD) is a non-destructive test technique that is traditionally used to perform stiffness assessment of road pavements. More recently, FWD has also been adapted to railway tracks (Brough *et al.*, 2003; Burrow *et al.*, 2007).

In the present case study, the light falling weight deflectometer (LFWD), a portable version of the FWD, was used on the sleepers to assess the support conditions. A load impulse of 15 kN was applied on a 0.10 m diameter plate at the centre of each sleeper (Figure 5-7). A good agreement of results was observed between tests performed on sleepers with similar support conditions. Figure 5-7 shows median deflection values (δ_s) measured at the centre of the sleepers, along the transition zones to UP1 and UP2. It is observed that the deflection of the sleepers without USP is about 100 to 150 μm. At UP1, the use of USP has increased sleeper deflections up to about 450 μm (Figure 5-7). At the transition between sleepers with and without USP, a variation in deflections is observed, denoting the transition in stiffness.

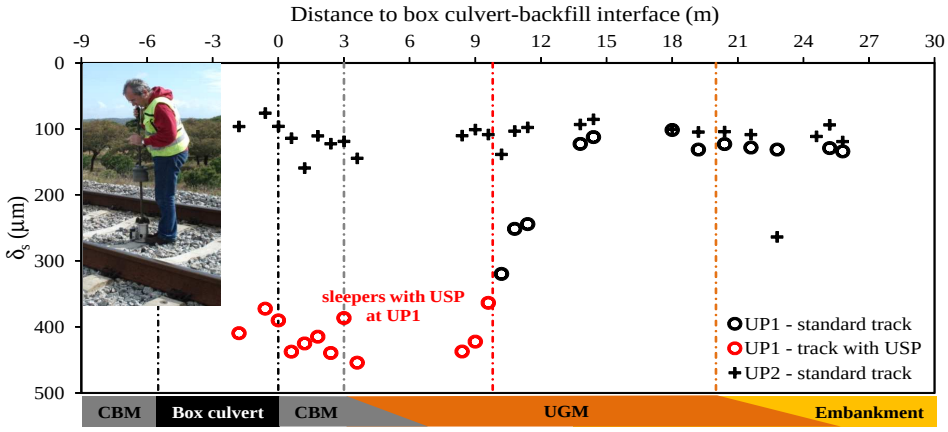

Figure 5-7. Light falling weight deflectometer tests.

5.2.2.3 Receptance tests on the track

Receptance tests are a very practical way to access the dynamic behaviour of the track (De Man, 2002). The receptance tests (Figure 5-8a) consisted in the excitation of the rail using an instrumented impact hammer (range: ±22.24 kN; sensitivity: 0.23 mV/N; see Figure 5-8c), with input frequencies up to 400 Hz, and the evaluation of the track response using accelerometers (range: ±50 g; sensitivity: 100 mV/g; see Figure 5-8b) installed on the rail web and sleepers. In Figure 5-9, an example of a sampled time recording of the measured load impulse is presented, along with its frequency content and respective rail response.

a)

b)

c)

Figure 5-8. View of the track receptance test.

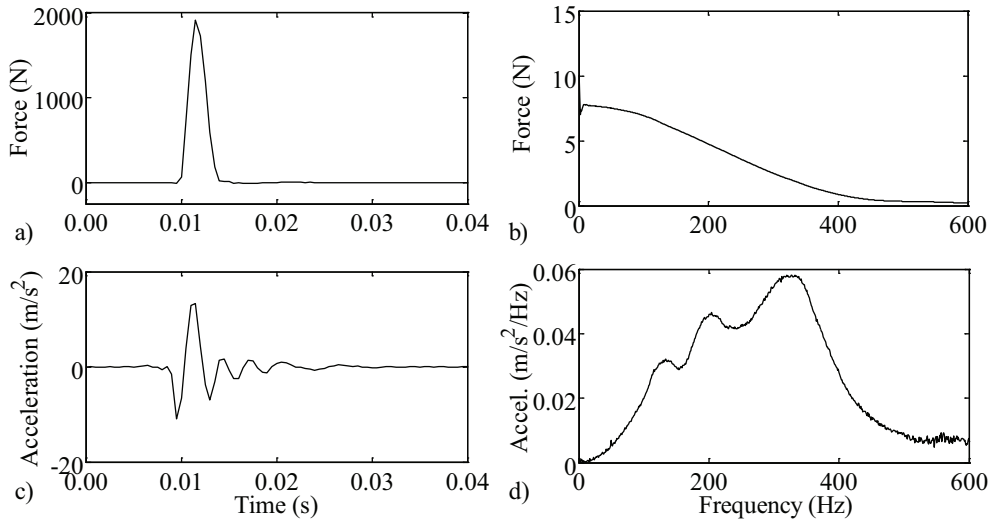

Figure 5-9. Impulse time history (a) and frequency content (b); respective acceleration response in time and frequency domains (c and d).

In order to characterise the dynamic behaviour of the track along both transition zones, receptance tests were performed at specific sections identified in Figure 5-2: S1 on open track; S2 and S3 on the UGM; S4 on the CBM; S5 in the vertical alignment of the box culvert walls; S6 at mid-span of the box culvert.

Figure 5-10 shows average receptance functions obtained in each section for frequencies between 25 and 450 Hz, corresponding to the range of impulse-acceleration signal coherence above 0.95.

In general, apart from the results obtained in sections with USP, no significant differences are observed between the different receptance function curves along the transition zones.

Regarding all the sections, it is possible to identify a resonant frequency between 300 and 375 Hz that corresponds to the vibration of the rail on the rail pads. The variability in the resonant frequency of the rail may be due to uneven preload of the fastening system along the track which generally influences the stiffness of these elements (Wu & Thompson, 1999). This aspect will be discussed and accounted for in section 5.2.5.

It is observed that the presence of USP at UP1 leads to a shift in the resonant frequency peak: the frequency of about 325 Hz in S1 and S2 (sections without USP) is reduced to about 308 Hz in S3 to S6 (sections with USP). This reduction is followed by a slight increase in the amplitude of the receptance function peak.

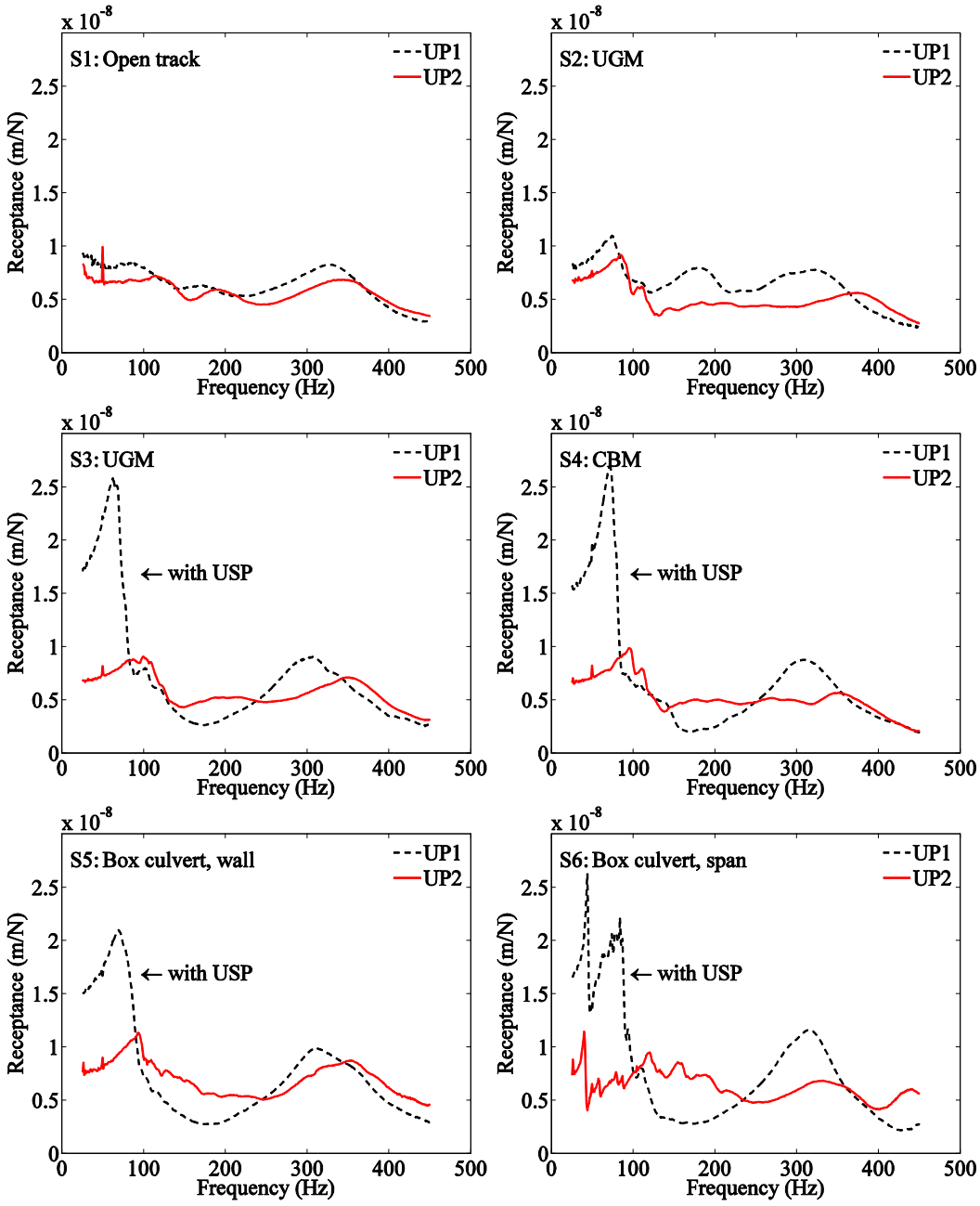

Figure 5-10. Receptance functions obtained in each section.

The full track resonant frequency peaks are also visible at frequencies around 70 Hz for the track with USP (S3 to S6 in UP1) and about 90 to 110 Hz without USP (the remaining sections). As expected, higher amplitudes of the full track resonant frequency peaks are identified in sections with USP, indicating the increase of the dynamic flexibility of the track provided by these resilient elements. It is worth noting the increased amplitude of the receptance function for lower frequencies (f < 55 Hz) in the presence of USP, which denotes an increment of about 90% on the vertical flexibility of the track.

The receptance curves obtained in sections S3 (on the UGM) and S4 (on the CBM) are quite similar, within each transition zone.

In section S6, additional peaks were identified at 44 Hz and 40 Hz, corresponding to the resonant-frequencies of UP1 and UP2 box culverts, respectively.

5.2.3 Monitoring track behaviour during train passage

The monitoring procedure included measurements of the following aspects: i) shear deformations of the rail to assess wheel loads; ii) vertical displacements of the rail; iii) rail-sleeper relative displacements (which are related to the deformation of the rail pad); and iv) vertical accelerations of the sleepers. Identical monitoring setups were considered in both transition zones (Figure 5-11). An additional rail displacement transducer was also placed 40 m away from each box culvert, in open track, which falls outside the stretch shown in the figure.

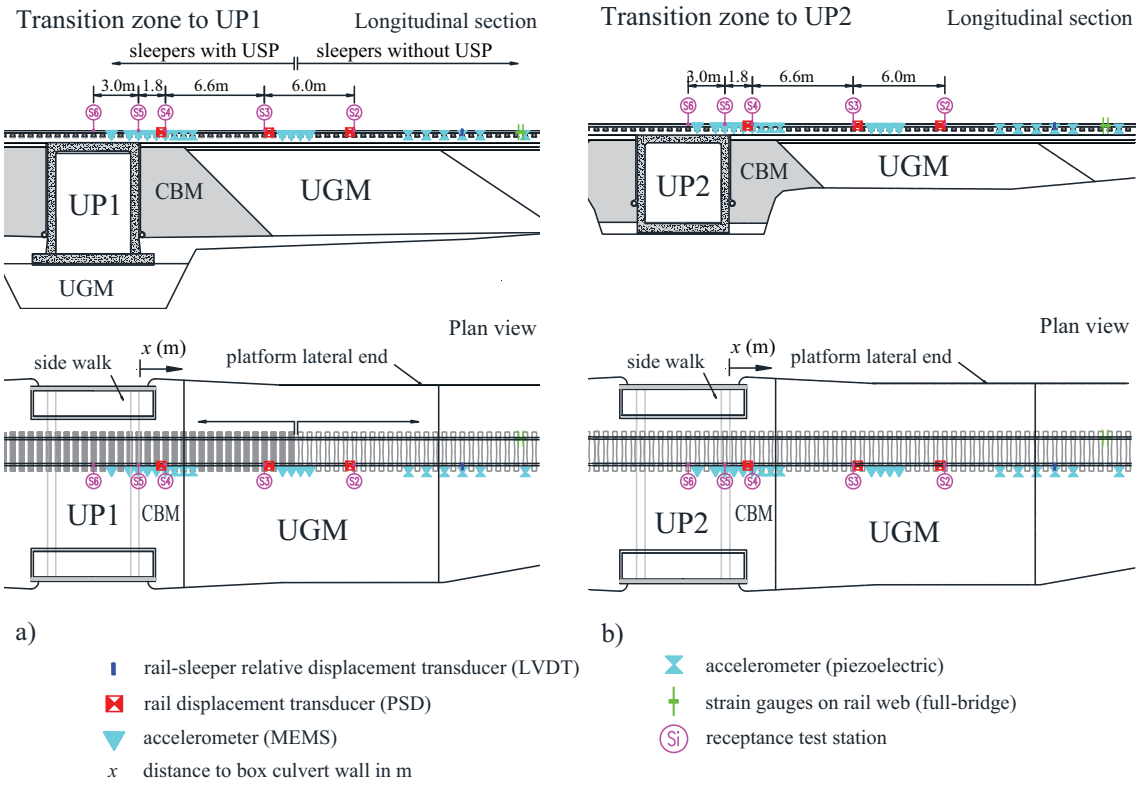

Figure 5-11. Location of the transducers at UP1 (a) and UP2 (b).

To estimate wheel loads, shear deformations of the rail were measured at two sections between two sleepers (Figure 5-11 and Figure 5-13a). To compensate any transversal eccentricity in the load applied by the train, at each measurement section of the rail, a pair of strain gauges (resistance: 350 Ω; gauge factor: 2.0; Figure 5-11a) was welded to each side of the web and connected in a full Wheatstone bridge (Figure 5-11b). Each pair of strain gauges consisted of a shear rosette installed at the level of the neutral axis of the rail and with the respective sensitive patterns oriented +45º and -45º with respect to the rail longitudinal axis. At the longitudinal surface passing through the neutral axis of the rail, a pure shear state is established and the above orientations correspond to principal directions. Thus, deformations along these directions are equal in magnitude and opposite in sign ($\varepsilon_1 = -\varepsilon_2 = \varepsilon$) and shear strain is $\gamma = 2\varepsilon$.

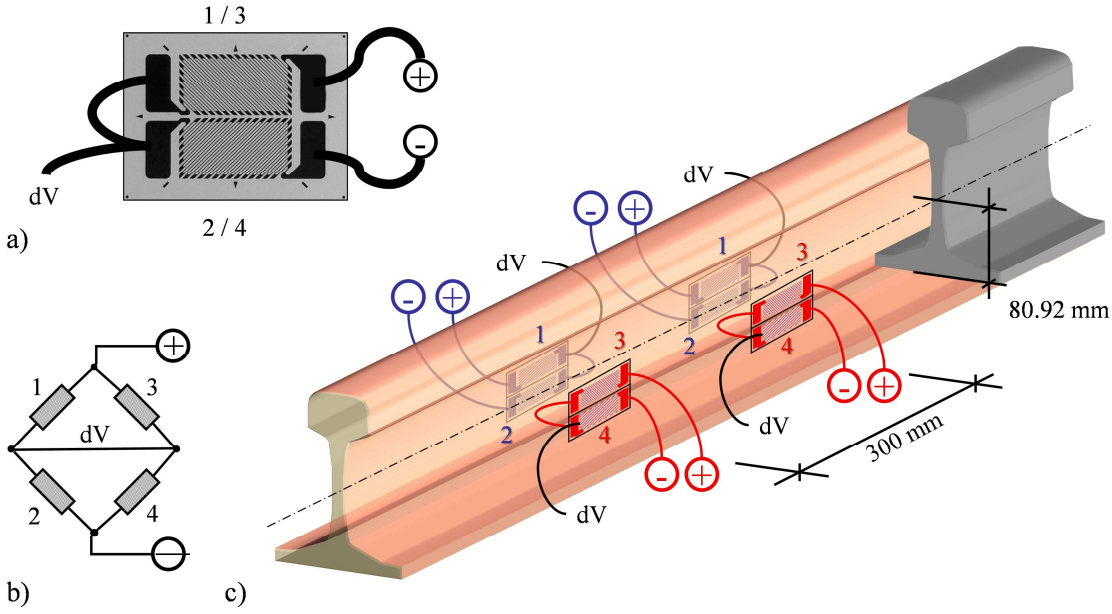

Figure 5-12. Schematic representation of the rail extensometry: a) shear rosette; b) full Wheatstone bridge; c) installed setup.

Absolute rail vertical displacements were measured using optical systems that were developed to assess track deflection at four different sections of the transition zones. Each system (Pinto *et al.*, 2013) is based on a diode LASER module (wavelength: 635 nm; power: 6 mW), mounted away from the track (Figure 5-13b), and a Position Sensitive Detector (PSD) module (range: ±6 mm) attached to a support fixed to the rail web (Figure 5-13c). Using the PSD transducer it was possible to calculate rail displacements during train passages, by measuring variations of the position of the LASER beam spot in the PSD.

Figure 5-13. Track instrumentation: a) strain gauges on the rail web; b) displacement transducers along the transition zone; c) detail of the PSD on the rail; d) rail-sleeper relative displacement transducer; e) general view of the transducers.

The vertical deformation of the rail pad was assessed using a LVDT transducer (range: ±2.5 mm; sensitivity: 2 V/mm) placed between the rail and the sleeper (Figure 5-13d). Vertical accelerations were measured using 9 piezoelectric accelerometers (range: ±50 g; sensitivity: 100 mV/g) and 10 Micro Electro-Mechanical System accelerometers (MEMS) (range: ±18 g; sensitivity: 100 mV/g) placed at the sleeper ends. Figure 5-13e depicts a general view of the positioning of the transducers along the transition zone.

The acquisition system comprised a laptop computer, a National Instruments (NI) acquisition unit (compact DAQ 9178 with seven specific modules) and three support units for PSD, MEMS and LVDT transducers (Figure 5-14).

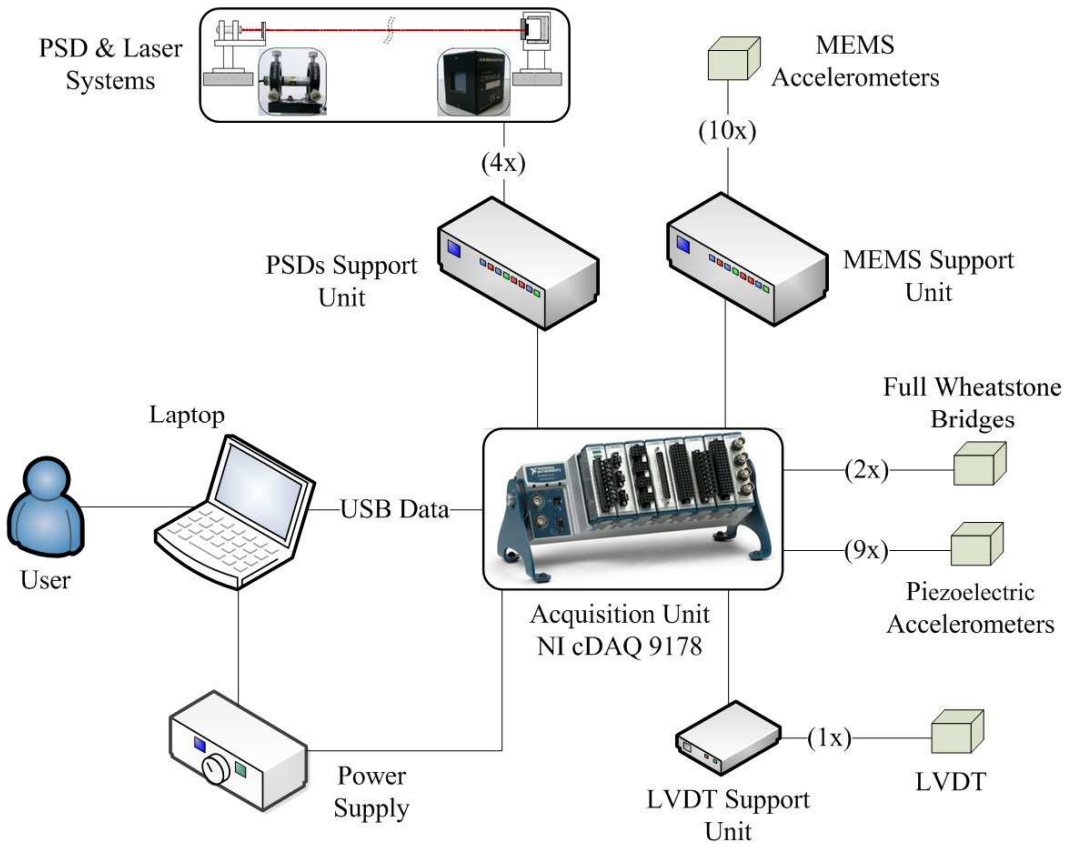

Figure 5-14. Schematic representation of the data acquisition system.

To control, display and collect the data from all transducers, an application was developed in LabVIEW environment. All the measuring systems were previously calibrated and validated in laboratory. For this case study, an acquisition frequency rate of 2000 Hz was considered.

Measurements were performed as the Portuguese A*lfa Pendular* passenger tilting trains crossed the transition zones at speeds of about 220 km/h. Each train comprised six passenger coaches, with average axle loads of 132 kN, with the configuration depicted in Figure 5-15.

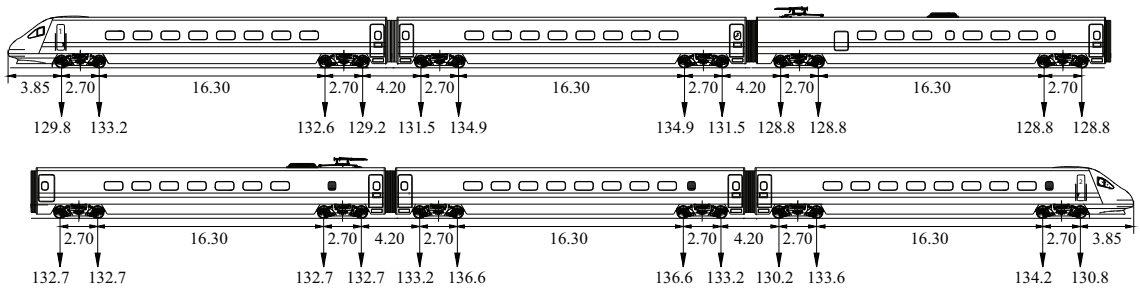

Figure 5-15. Passenger tilting train configuration (in m) and approximate axle loads (in kN).

Recordings were made during the passage of eight trains (four in each direction) at both transitions (UP1 and UP2).

As mentioned earlier, train wheel loads were estimated using the shear strain measurements of the rail ($\gamma = 2\varepsilon$). Knowing the shear modulus (G), moment of inertia (I), web thickness (b) and static moment of area (S) of the rail, it was possible to estimate the load of a passing wheel (Q), by assessing the difference of rail shear forces (V) at two sections (m and n) within a given span between two consecutive sleepers, using the following equation:

$$Q = V_m - V_n = \frac{2(\varepsilon_m - \varepsilon_n)GIb}{S} \tag{5-1}$$

Equation (5-1) can be simplified to $Q = \alpha\,(\varepsilon_m - \varepsilon_n)$, where factor α is about 0.358×10^6, considering Q in kN, $G = 80.8\ GPa$, $I = 3040.4\ cm^4$, $b = 16.5\ mm$ and $S = 226179.5\ mm^3$

Although the above approach yielded fair estimates of the static wheel loads, in practice, given the possible misalignments of the strain gauges, the limitations of the beam theory in this case and the effective rail parameters, it was found necessary to previously calibrate the measuring system *in situ* using trains with known axle loads. As a result, for the calculation of the dynamic wheel loads, the value of $\alpha = 0.415 \times 10^6$ was considered.

An example of time history measurements of dynamic wheel loads (Q) applied by the train to the rail at the beginning of the transition zone (about 25 m from the box culvert walls, see Figure 5-11) is presented in Figure 5-16a. A histogram of measured dynamic wheel loads at UP1 is presented in Figure 5-16b. It should be noted that these measurements were not filtered in order to preserve dynamic wheel load peaks.

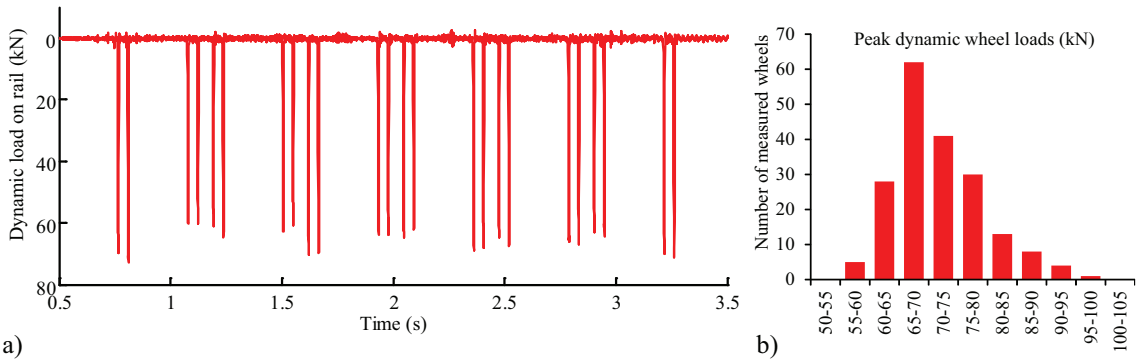

Figure 5-16. Dynamic wheel loads: a) example of a time history; b) distribution of peak loads.

Analysing the frequency content of the shear strains of the rail, some excitation frequencies were found to be consistent for all passing trains, particularly below 50 Hz. These frequencies are related to the train characteristics. Following the method of the Decomposition of Excitation at Resonance suggested by the ERRI D-214 committee (1999), it is possible to calculate the dynamic signature, $S_0(\lambda)$, of these passenger tilting trains, for a given wavelength excitation, λ. The quantification of $S_0(\lambda)$ is independent of the infrastructure and train speed. It depends only on the train characteristics (axle loads and axle spacing) and can be estimated using equation (5-2):

$$S_0(\lambda) \cong \max_{i=1\ to\ M} \left\{ \left[\sum_{k=1}^{i} P_k \cos\left(\frac{2\pi x_k}{\lambda}\right) \right]^2 + \left[\sum_{k=1}^{i} P_k \sin\left(\frac{2\pi x_k}{\lambda}\right) \right]^2 \right\}^{0.5} \quad (5\text{-}2)$$

Where i is the number of axles in the train or sub-train (taken from 1 to the maximum number of axles, *M*); P_k is the load of the k^{th} axle and x_k is the distance from the k^{th} axle to the first axle (ERRI-D214 Committee, 1999).

This procedure was developed for the structural design of railway bridges for a range of wavelengths above 4.0 m. Extending the same procedure for λ as low as 1.0 m, the signature presented in Figure 5-17 was obtained for the Portuguese tilting train.

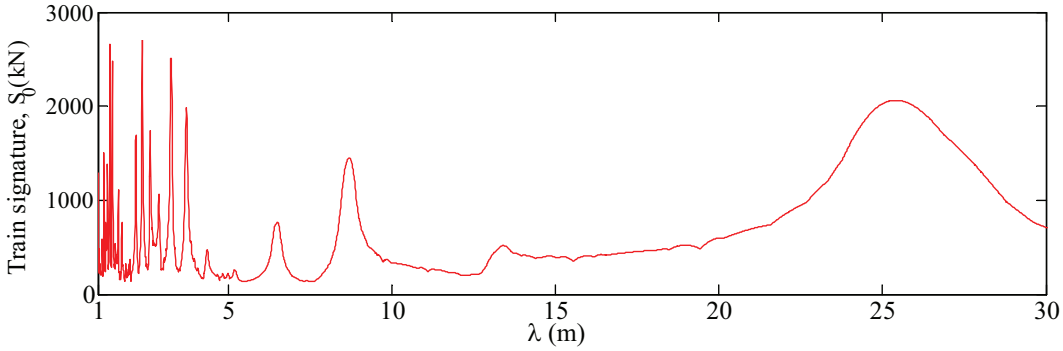

Figure 5-17. Signature $S_0(\lambda)$ of the *Alfa Pendular*.

The obtained λ peaks above 4 m are particularly relevant for railway bridge design, but quite a few other excitation peaks were found below 4 m. When the Portuguese tilting trains travel at a speed (v) of about 220 km/h, the excitation λ between 1.2 and 30 m correspond to excitation frequencies ($f = v/\lambda$) between about 50 and 2 Hz. It was found that the excitation frequencies between 0 and 50 Hz of measured rail shear strains were similar to the excitation frequencies of the calculated train signature, as evidenced in Figure 5-18.

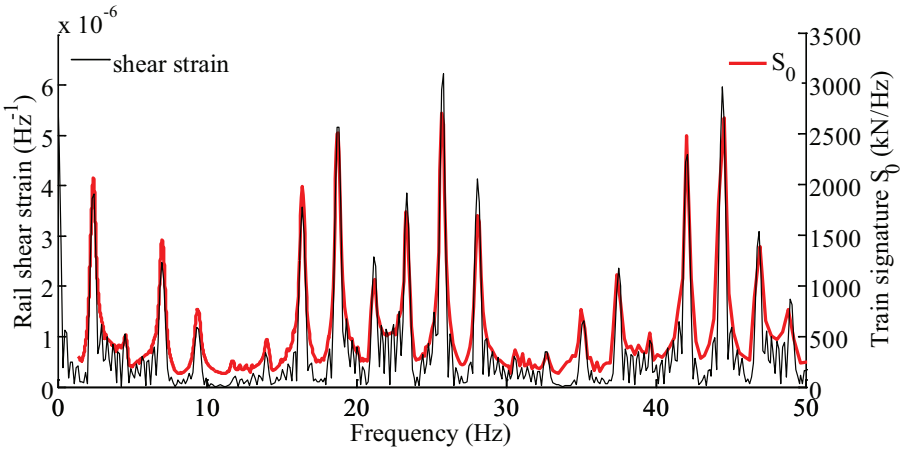

Figure 5-18. Comparison between frequency content of the rail shear strain and the train signature (S_0).

Absolute vertical displacements of the rail were measured between sleeper supports in sections S1 to S4 and some examples are presented in Figure 5-19. A type II Chebyshev filter with cut-off frequency of 80 Hz was applied to time history records. The determination of the cut-off frequency took into account the relevant excitation frequencies of the trains travelling at about 220 km/h and that the dynamic response for high frequencies due to the short-wave irregularities of the rails and wheels (which are outside the scope of this study) are of random nature. The application of this filter also made easier the interpretation of results.

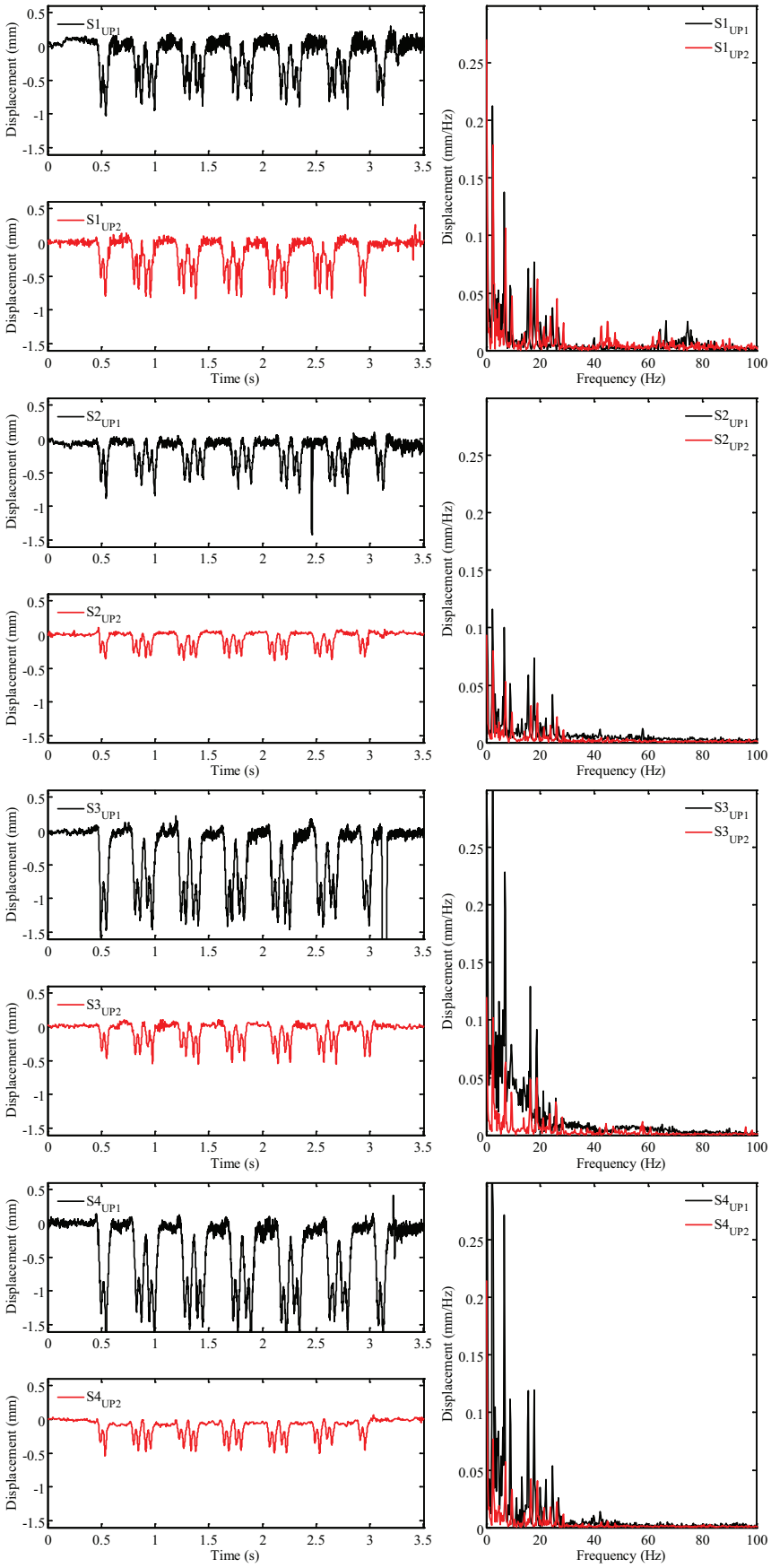

Figure 5-19. Time histories (f<80Hz) and frequency contents of rail displacements measured in sections S1 to S4.

Figure 5-20 shows average peak absolute rail displacements, d_r, calculated for each section (PSD transducer location) and for each train passing at transitions to UP1 and UP2. Average d_r values ($\bar{d}_r$) and respective coefficients of variation (CV) are presented in Table 5-2. Considering the available and validated data and comparing results between UP1 and UP2, it is observed that the displacements measured outside the transition zones (S1) and at the beginning of the UGM wedge (S2) were somewhat similar. In general, rail vertical displacements in sections S2 to S4 of UP2 were lower than those measured in S1. These findings highlight the increase in vertical stiffness provided by the presence of the backfill constructed with high-performance bound and unbound granular materials.

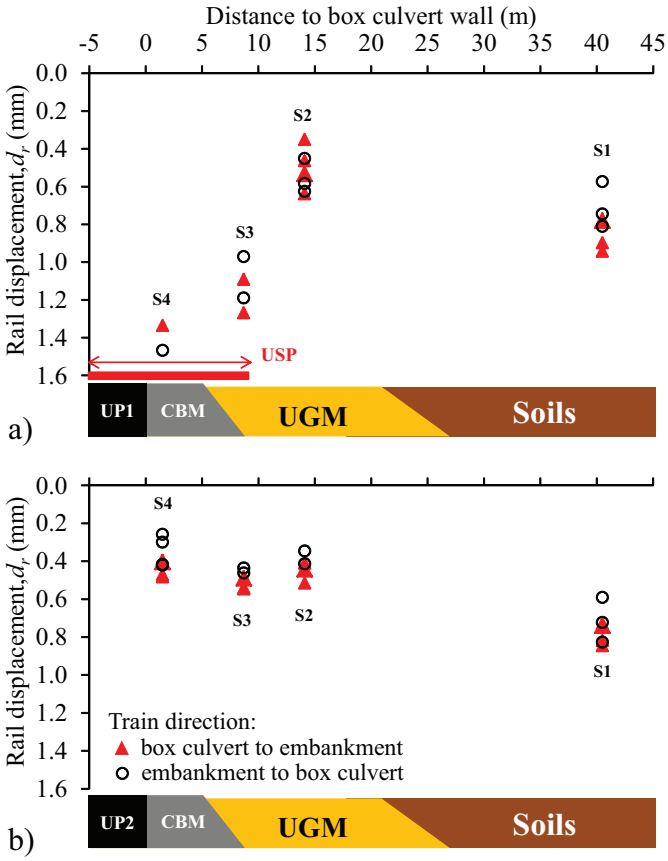

Figure 5-20. Average peak vertical displacements of the rail for each train crossing UP1 (a) and UP2 (b).

Table 5-2. Average peak absolute rail displacements and vertical track stiffness estimates.

Section	Distance to box culvert	UP1				UP2				$\bar{d}_{r,\mathrm{UP1}}$-$\bar{d}_{r,\mathrm{UP2}}$
		$\bar{d}_r$	CV	K_{PSD}	K_R	$\bar{d}_r$	CV	K_{PSD}	K_R	
(-)	(m)	(mm)	(-)	(kN/mm)	(kN/mm)	(mm)	(-)	(kN/mm)	(kN/mm)	(mm)
S1	40.5	0.79	0.19	83.6	107.3	0.75	0.16	87.6	121.1	0.0
S2	14.1	0.52	0.23	126.7	120.8	0.43	0.19	155.2	147.5	+0.1
S3	8.7	1.14	0.13	58.1	58.5	0.50	0.17	133.2	145.9	+0.6
S4	1.5	1.40	0.10	47.1	63.7	0.39	0.23	167.3	150.7	+1.0

The presence of USP at UP1 significantly increases the track flexibility, as denoted by the higher rail displacements observed in sections S3 to S4. When compared with the measurements at UP2, the introduction of USP at the sleepers closer to the UP1 box culvert was accountable for a significant increase in vertical rail displacements: average increments of 129% and 255% were observed in S3 and S4, respectively.

Considering the measurements at UP2, the rail displacements were, in general, slightly higher when trains travelled from the box culvert to the embankment than in the opposite direction. This behaviour was less evidenced in UP1.

Recent numerical studies by other authors (Insa *et al.*, 2013) and some field measurements on transition zones (Lozano del Moral & Cuéllar, 2009) suggest that USP have minor influence on rail displacements, which do not match the field measurements. However, other field studies on USP, yet not necessarily at transition zones, evidence that USP increase rail displacements and sleeper accelerations (Hruzíková *et al.*, 2009; Schneider *et al.*, 2011).

With regard to absolute rail displacements obtained with the PSD transducers, it was possible to calculate an estimate of the track stiffness, K_{PSD} (ratio between wheel load and maximum rail deflection). For this simple calculation, a constant wheel load, Q, of 66 kN (half the average static axle load) was considered. In addition to this procedure, another estimate calculation of the track stiffness, K_R, was carried out inverting the track receptance obtained at the lowest frequency that was possible to analyse (f = 25 Hz).

Table 5-2 and Figure 5-21 show a comparison of estimates using the two methods, denoting a relatively good agreement between the two.

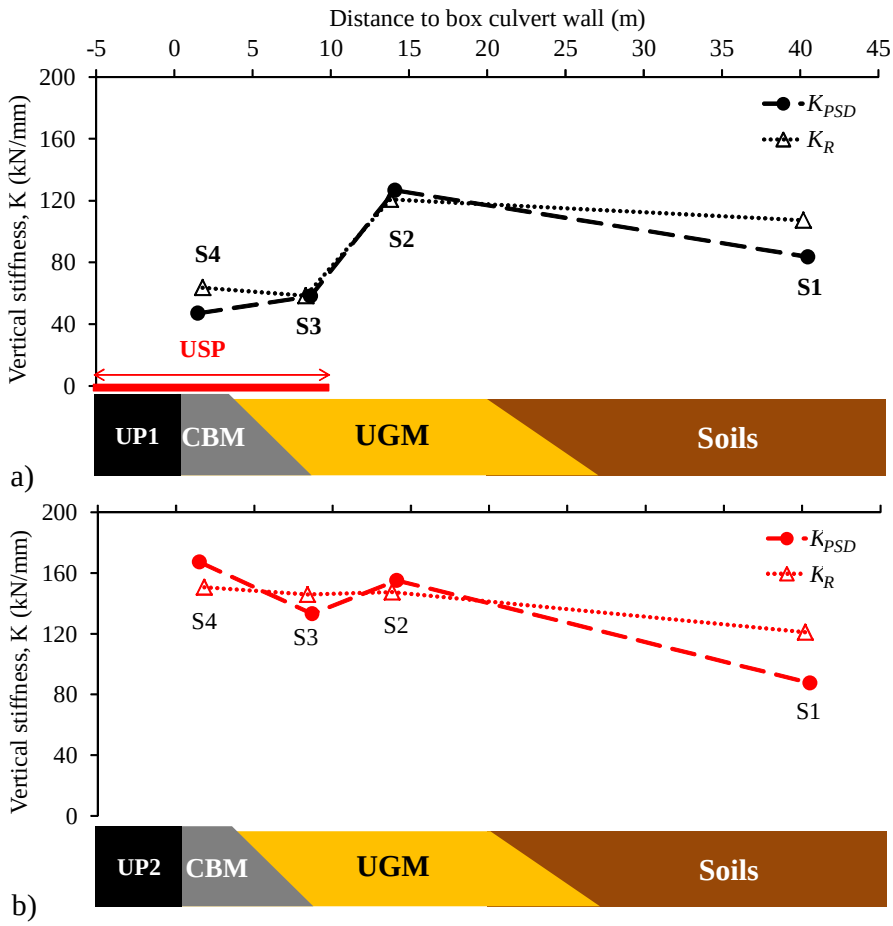

Figure 5-21. Estimated values of vertical track stiffness along transitions: a) to UP1; b) to UP2.

It should be noted that the adopted simplifications might have influenced the results, namely: i) a constant wheel load of 66 kN was assumed; ii) the non-linear behaviour of the track with respect to the load applied to the rail was neglected (the impulse hammer applies a significantly lower load to the rail than the train wheel); iii) the influence of the adjacent wheelset of the same bogie was not considered in the calculation of K_R.

From the analysis of track stiffness estimates, an increasing trend in stiffness is observed at UP2, when approaching the underpass (from S1 to S4). A similar behaviour is observed regarding UP1, but only between S1 and S2, since the presence of USP drastically reduces the track stiffness in sections S3 to S4.

Earlier studies have reported estimates of vertical track stiffness at transition zones ranging between 20 and 120 kN/mm (Cuéllar *et al.*, 2009) and between 100 and 200 kN/mm (Lozano del Moral & Cuéllar, 2009) which are somewhat in agreement with the results presented here. In

the later study, an increase in track stiffness of about 40% was reported when trains travel from track with USP to standard track, but no significant variation was observed in the opposite direction. It is worth noting that those measurements were performed in a double track railway line, which suggests that the two tracks, operated in opposite travelling directions, may have different support conditions.

Examples of time history and frequency contents of rail-sleeper relative displacement measurements are presented in Figure 5-22. Average rail pad deformations of 0.23 mm were observed at both transition zones, denoting flexible rail pads. It is noted that the frequencies of the peaks in the range between 0-50 Hz match the peaks found in the frequency content of the previous rail displacement measurements (see Figure 5-19). As mentioned earlier, in Figure 5-18, these peaks closely relate to the specific train signature.

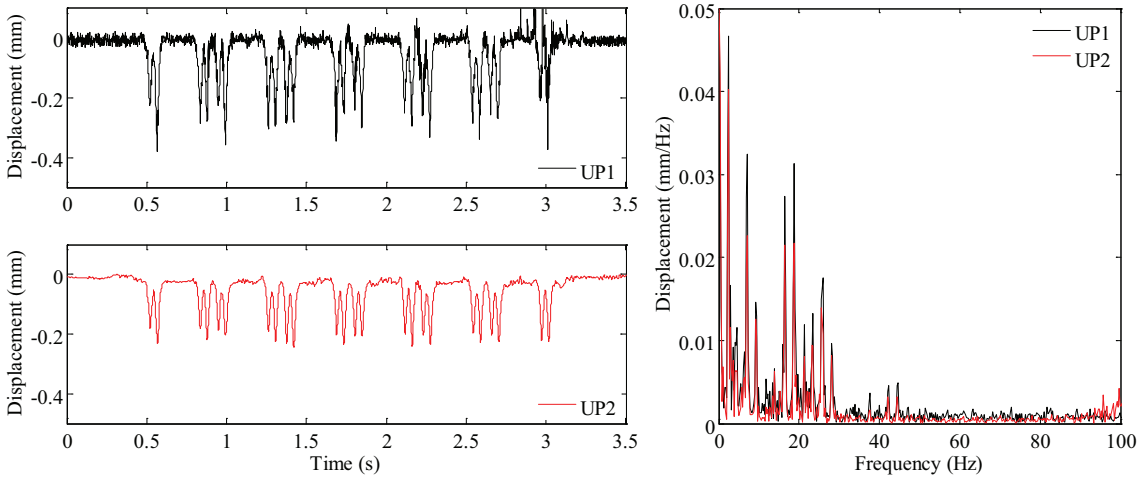

Figure 5-22. Time history and frequency contents of rail pad deformation.

Figure 5-23 shows examples of time histories and frequency contents of vertical accelerations measured at the sleeper's ends. Type II Chebyshev 80 Hz low-cut filters were also applied to the time history records. The minor offsets found in the time history records and frequency peaks are related to slightly different travelling speeds of the trains.

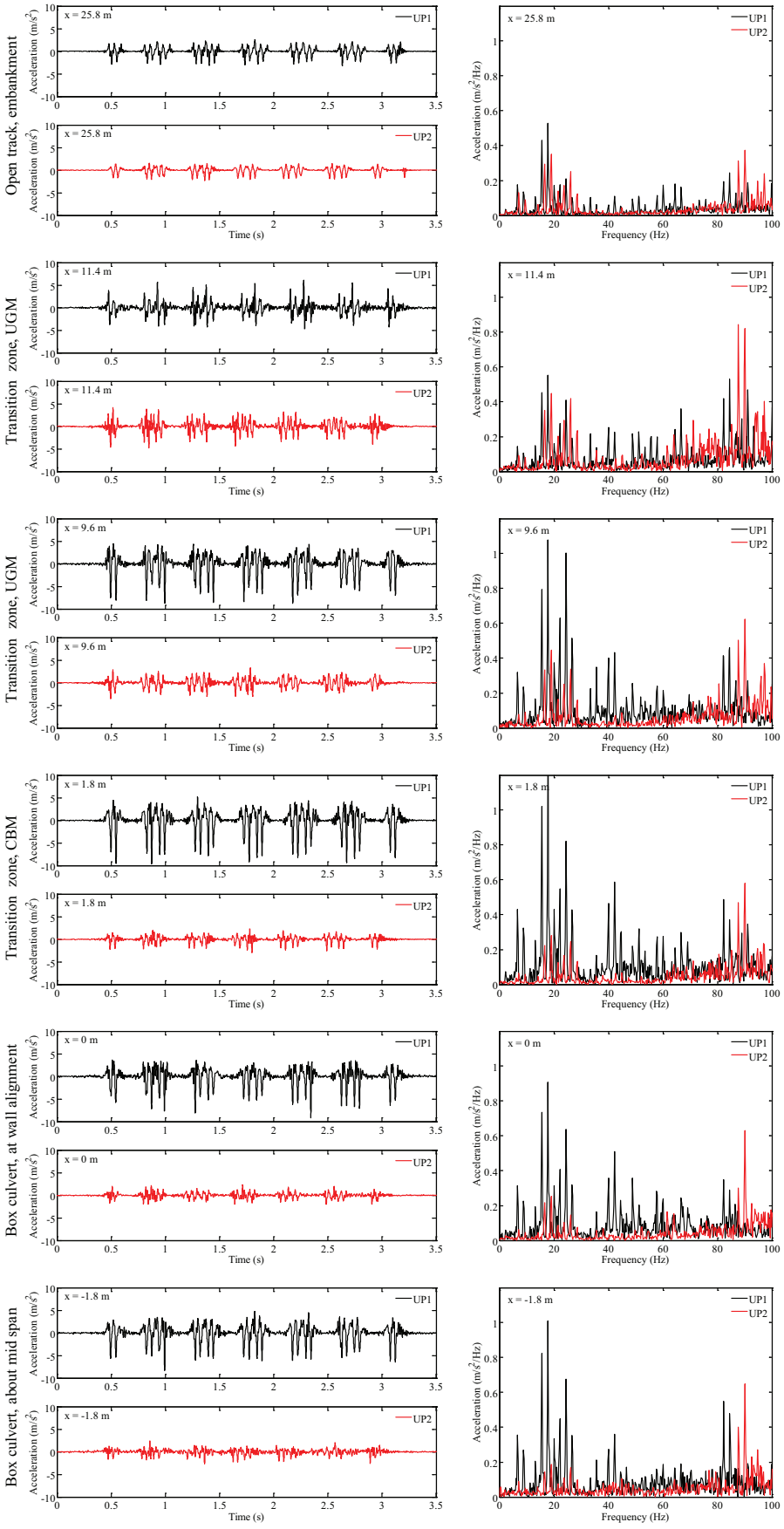

Figure 5-23. Time history and frequency contents of accelerations measured on sleepers at different distances from the box culvert wall (see Figure 5-11).

The results presented in Figure 5-24 and Table 5-3 refer to the average of the maximum ($\bar{a}_{s,max}$) and average of the minimum ($\bar{a}_{s,min}$) peak acceleration values measured on sleepers for all passing bogies, at each position along the transition, considering the 80 Hz low-cut filtered signals. In general, accelerations measured at the transition to UP1 showed higher amplitudes than those measured at UP2. Measurements on the sleepers located at the soil embankment and on the UGM up to 18 m away from the box culvert were relatively close in the two transitions, as was expected, considering the similar track substructures. The use of USP at UP1 was responsible for an increment of absolute acceleration values (about +5 ms^{-2}). The dispersion of the results was also higher for sleepers with USP, as denoted by the respective higher coefficients of variation.

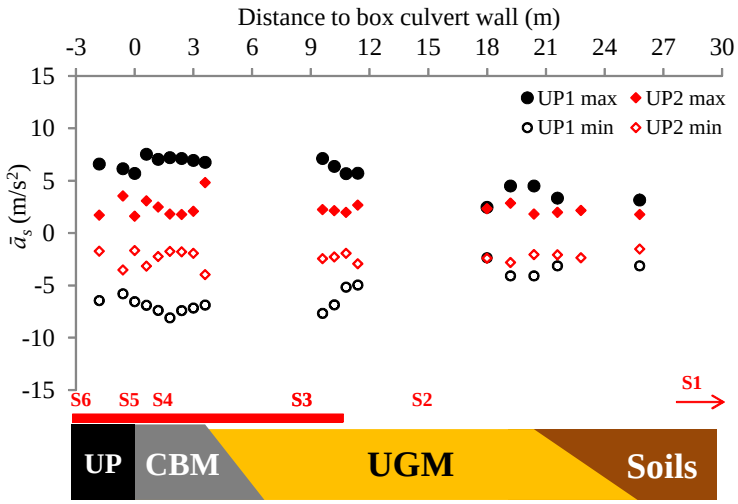

Figure 5-24. Average bogie peak acceleration values at UP1 and UP2.

Table 5-3. Average peak acceleration values for bogie passages (f<80Hz).

Distance to box culvert, x	**UP1**				**UP2**			
	$\bar{a}_{s,max}$	**CV**	$\bar{a}_{s,min}$	**CV**	$\bar{a}_{s,max}$	**CV**	$\bar{a}_{s,min}$	**CV**
(m)	(ms^{-2})	(-)	(ms^{-2})	(-)	(ms^{-2})	(-)	(ms^{-2})	(-)
25.8	3.14	0.45	-3.15	0.42	1.75	0.31	-1.53	0.25
11.4	5.71	0.42	-4.97	0.45	2.66	0.27	-2.95	0.34
9.6	7.11	0.39	-7.68	0.35	2.23	0.32	-2.46	0.26
1.8	7.19	0.37	-8.11	0.39	1.80	0.29	-1.76	0.28
0	5.69	0.50	-6.56	0.38	1.60	0.31	-1.68	0.24
-1.8	6.57	0.44	-6.45	0.27	1.69	0.34	-1.74	0.32

Although there were no USP at positions x = 10.8 m and x = 11.4 m in transitions to UP1 and to UP2, accelerations measured at UP1 were generally higher than those measured at UP2. This difference is possibly due to an increase of flexibility provided by nearby sleepers with USP (at x < 10.5 m).

It is noted that no strong correlation was found between the train direction and peak acceleration values of the sleeper at the studied positions of the track.

It was observed that the dominant frequency content of accelerations measured on sleepers with USP showed significantly higher amplitudes and spreading at higher frequencies, than those on sleepers without USP.

Considering all acceleration measurements on sleepers, good correlations were verified between resonant frequency values up to 50 Hz, regardless of the track structure, in particular, the presence of USP or the different substructure characteristics along the transition zone. Average frequency contents of measured accelerations are presented in Figure 5-25, regarding sleepers with or without USP. As addressed earlier, at this frequency range, the track behaviour is dominated by the excitation frequencies of the trains (see Figure 5-18).

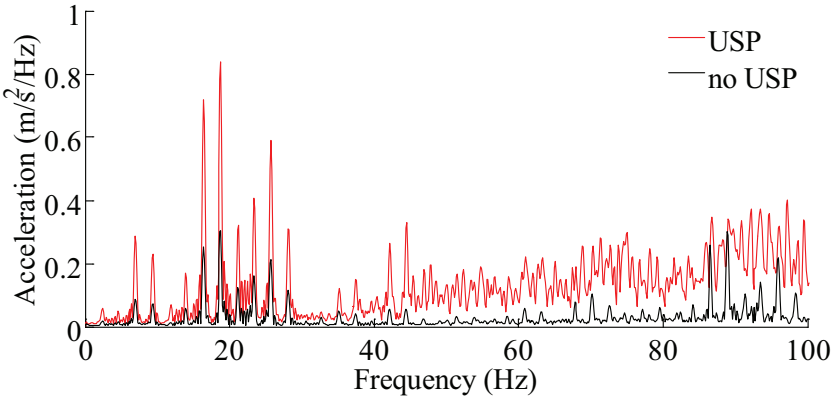

Figure 5-25. Comparison of frequency contents up to 50 Hz.

5.2.4 Description of the models

To reproduce the dynamic behaviour of the train-track system on the transition zones, 2D FEM models were developed with ANSYS® software. The calibration and validation of the models will be discussed in sections 5.2.5 and 5.2.6 and consider the characterisation results and the track measurements performed *in situ*. The relatively complex geometries of the transition zones

were taken into account, as depicted in Figure 5-26, and the train-track interaction was considered using a non-linear contact algorithm. The main advantage of these 2D models is that they provide accurate results even though they require less computational resources than the 3D models used in other studies on transition zones, such as those developed by Alves Ribeiro, Dahlberg, Calçada & Delgado (2009), Banimahd & Woodward (2007), Shan, Albers & Savidis (2013), and Varandas (2013).

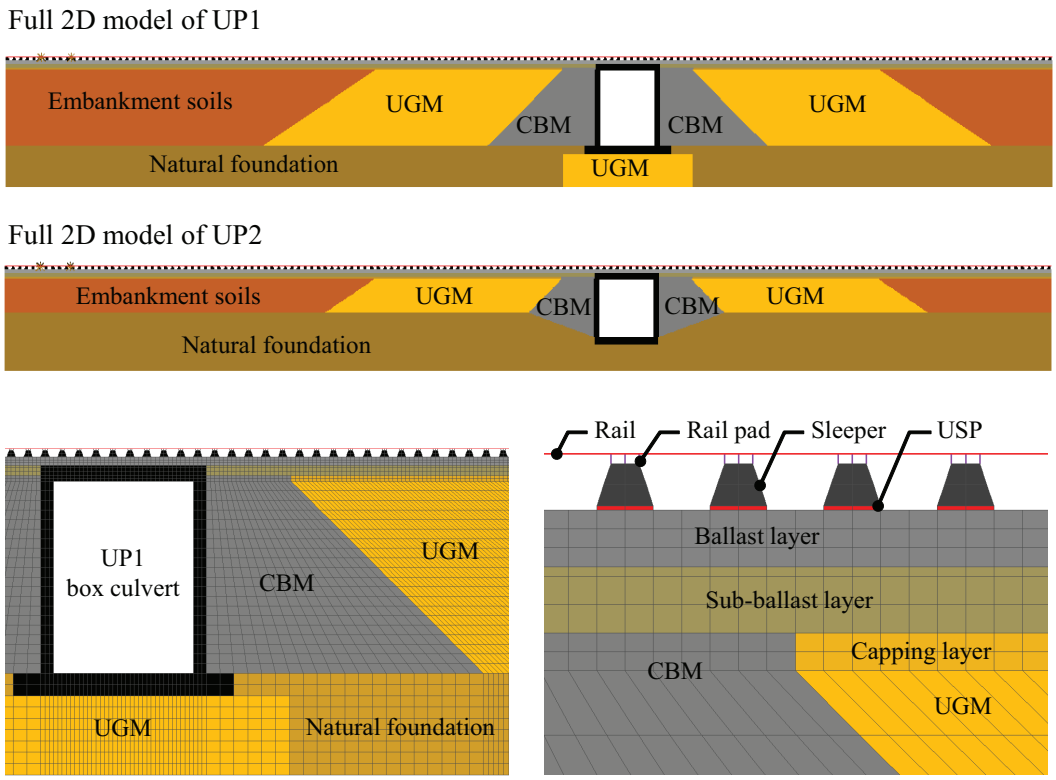

Figure 5-26. Models of the transition zones and details of the finite element mesh.

The transition models of UP1 and UP2 have a total length of 94.5 m (corresponding to approximately 157 sleepers) and a constant depth of 11.5 m and 10.4 m below the rail, respectively. The UP1 model consists of 26,271 nodes and 26,864 elements and the UP2 model, comprises a total of 27,882 elements and 27,131 nodes. They aim at representing the full track cross-section, thus, both rails of the track were modelled as one continuous beam consisting of 7.5 cm long elements (BEAM3), with section properties equivalent to two UIC60 rails: a cross-section area of $2\times7.7\times10^{-3}$ m^2 and a bending inertia of $2\times30.55\times10^{-6}$ m^4. Rails were assumed to have a Young modulus of 210 GPa, a Poisson's ratio of 0.3 and a density of 7850 kg/m^3. The two rail pads on each sleeper were modelled as three vertical spring-damper elements (COMBIN14) positioned alongside in order to simulate the width of the rail support on each sleeper. Considering that the rail pads' resonance frequency is mostly dependent on their

stiffness and damping, their properties were estimated separately for each transition model based on early *in situ* receptance tests. As a result, vertical stiffness, k_{rp}, of 130 and 165 kN/mm and a damping value, c_{rp}, of 15 and 17 kN.s/m were determined for the rail pads at UP1 and UP2, respectively. The sleepers, the USP, the track bed layers, the subgrade layers and the box culverts were modelled using 4-node plane-stress elements (PLANE42). A relevant aspect of the modelling technique is that it necessary to assign different values for the element's width in the perpendicular direction of the model. The width of the 2D elements was calibrated using reduced 3D static models, as addressed in section 3.2.

The calibrated properties of the track materials adopted in this study are presented in Table 5-4. The Rayleigh damping coefficient α was considered the same for all materials, which was determined to be $\alpha = 8.52$ s^{-1} after the calibration.

Table 5-4. Properties of the track materials after calibration.

Component or material	**Young modulus, E_i**	**Poisson's ratio, ν_i**	**Rayleigh damping, β_i**	**Density, ρ_i**
	(MPa)	**(-)**	**(s ×10^{-3})**	**(kg/m^3)**
Sleepers	30×10^3	0.25	-	6360*
USP	1.3	0.00	0.5	800
Ballast	130	0.20	0.4	1530
Sub-ballast	200	0.30	0.4	1935
Capping layer	2820	0.30	2.6	1935
UGM	1030	0.30	2.6	1935
CBM	10×10^3	0.30	0.4	2200
Embankment soils	80	0.30	2.9	2040
Natural Foundation	300	0.30	2.9	2040
Reinf. Concrete structure	30×10^3	0.25	-	2500

* The value corresponds to an equivalent density value was calculated to obtain a total weight of 315 kg for each sleeper.

To minimise the effect of wave reflections, viscous boundary conditions were considered, in accordance with the works by White *et al.* (1977), using the following damping matrix:

$$C = \frac{8\sqrt{G_i \rho_i}}{15\pi}\begin{bmatrix} 18s_i + 2 - 20s_i^3 & 0 \\ 0 & 2s_i + 3 \end{bmatrix} \tag{5-3}$$

where G_i is the shear modulus, ρ_i is the material's density and s_i is:

$$s_i = \sqrt{\frac{1-2\nu_i}{2(1-\nu_i)}} \tag{5-4}$$

To introduce these boundary conditions in the models, normal and tangent damper elements (COMBIN14) were placed at the boundary nodes, with damping parameters set in accordance with (5-3) and considering the size and width of the plane-stress elements.

When modelling the effect of sudden changes in the track support conditions, as in transition zones, train-track interaction needs to be taken into account to avoid underestimating the resulting dynamic effects (Hunt, 1997; Varandas *et al.*, 2014). In this study, the wheel-rail interaction was modelled as a node-to-beam contact – using CONTA175 and TARGE169 elements for the wheel nodes and rail beams, respectively – which allowed sliding and loss of contact. The Penalty algorithm was considered and the full Newton-Raphson method was used to solve the non-linear equations of the problem. This train-track interaction modelling approach was thoroughly tested and validated in earlier works by Alves Ribeiro (2012). To solve the well-known transient dynamic equilibrium equations, the Newmark implicit time integration method was used and time steps of 0.001 seconds were considered.

The *Alfa Pendular* train was modelled crossing the transition zones at 220 km/h. The previous Figure 5-15 shows its axle configurations and approximate loads. Given that this study focuses on the influence of the track stiffness in the dynamic behaviour of the train-track system without uneven rail profiles, it is only necessary to model the train's bogies, rather than the full train with the car bodies, as demonstrated in earlier tests by Alves Ribeiro (2012). Figure 5-27 shows one of the 12 bogies that were considered in the models in order to simulate the effect of the entire passage of the train. The parameters of the train model are provided in Table 5-5. The bogie frame was considered as a rigid body.

In these studies, it was assumed a circular contact surface with a wheel radius of $r_w = 0.445$ m and a rail curvature of $r_r = 0.30$ m, which yield an equivalent curvature radius of $r_{eq} = (r_w r_r)^{1/2} = 0.365$ m. Given a wheel load Q and considering that the wheel and rail are made of same steel material, with Young Modulus of 210 GPa and Poisson's ratio of 0.3, the wheel-rail contact stiffness (K_h) can be estimated using the Hertzian theory as:

$$K_h = \sqrt[3]{\frac{3 r_{eq} Q E^2}{2(1-\nu^2)^2}} \tag{5-5}$$

The above expression was linearised considering an average wheel load of $Q = 132/2 =$ 66 kN, which results in $K_h = 1.24 \times 10^6$ kN/m.

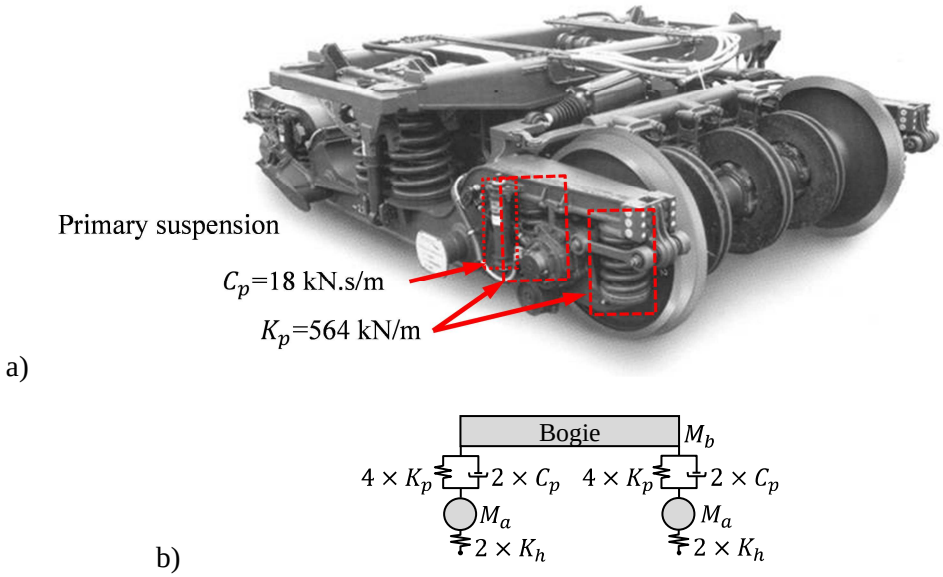

Figure 5-27. Aspects of the vehicle model: a) view of the components of the primary suspension; b) model of one of the 12 bogies of the train (see parameters in Table 5-5).

Table 5-5. Characteristics of the bogie model (see Figure 5-27) (adapted from Alves Ribeiro, 2012; Ribeiro *et al.*, 2013).

Parameter	Value
Bogie mass (without axles), M_b	4932 kg
Primary suspension stiffness, K_p	564 kN/m
Primary suspension damping, C_p	18 kN.s/m
Axle mass, M_a	1800 kg
Hertzian wheel-rail contact spring stiffness, K_h	1.24×10^6 kN/m

Considering that the train has a length of about 158.9 m, and in order to reduce the calculation times and the size of the model, the passage of the train was simulated using the following method (Alves Ribeiro, 2012): i) initially, all bogies were stationary, weightless and located at the same position, near one end of the model; ii) in the subsequent time steps, axle loads and motion attributes were assigned to each bogie, one by one, according to the train speed and axle configuration (Figure 5-15); iii) as each bogie reached the other end of the model, they were stopped, one by one, and the respective axle loads were removed.

The studied railway line was opened to traffic by the end of 2010 and inspection records of track geometry indicate that, in these transition zones, the line still presented a very good quality by 2014 and none of the alert limits by REFER had been reached. For that reason, a perfectly horizontal rail profile was considered on both transition zones.

5.2.5 Model calibration

The calibration of the 2D models used a recent procedure (Alves Ribeiro, 2012), which is based on 3D and 2D reduced models and in experimental data. Figure 5-28 shows a simplified diagram of the calibration procedure that takes into account: 1) the static calibration of the reduced 2D models based on the results obtained with 3D models; 2) the dynamic calibration of the 2D models using receptance test curves obtained in the field. These non-destructive tests were described in section 5.2.2 and allowed the characterisation of the track's dynamic behaviour in the frequency range between about 20 and 450 Hz.

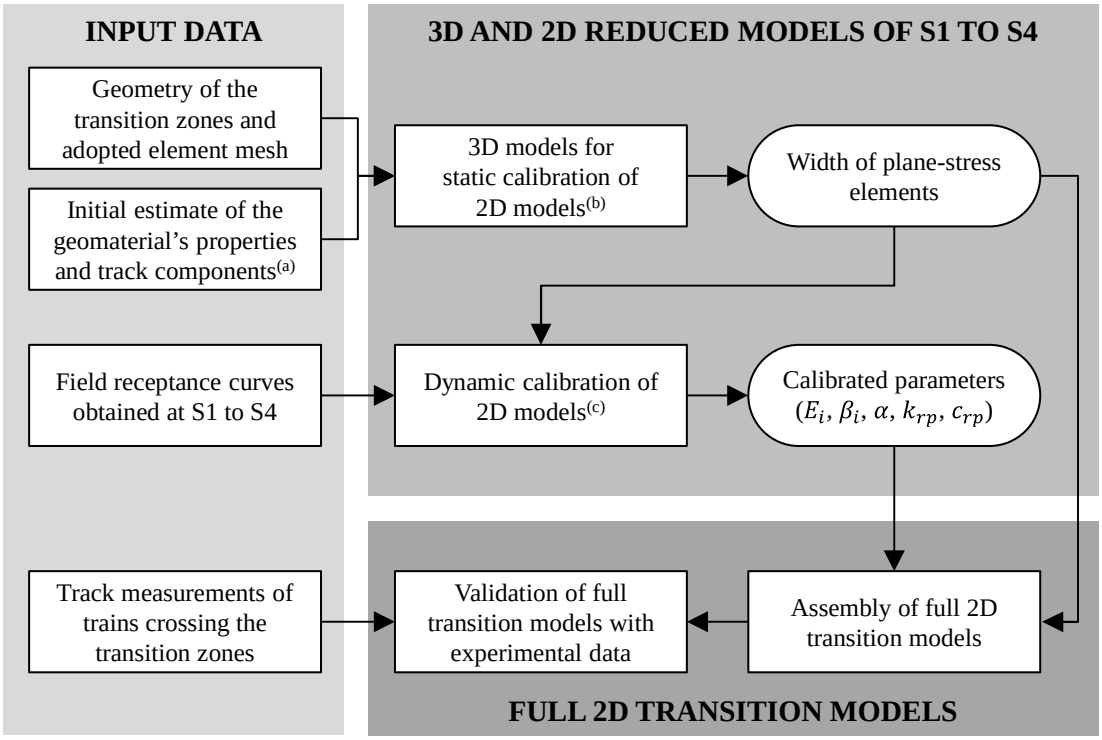

(a) Initial estimates based on the laboratorial characterization and the field measurements.
(b) MATLAB iterative procedure, running ANSYS in batch mode, to determine the width of the plane-stress elements in order to match relative displacements between static 2D and 3D models.
(c) MATLAB optimization algorithm *lsqcurvefit*, interaction with ANSYS in batch mode, to determine material parameters that best fit the experimental receptance curves, in the least-squares sense.

Figure 5-28. Schematic diagram of the procedure adopted for the calibration and validation of the numerical models.

The main steps of the calibration were performed as follows (Figure 5-28):

1) Before the development of the full transition models, four pairs of 3D and 2D reduced FEM models (see Figure 5-29) were prepared for each transition zone, taking into consideration its geometry and aiming at representing the different track support conditions found along the transition zone (S1 to S4), as depicted in Figure 5-3. The reduced models consist of track segments of 30 sleepers with depths of 11.5 m and 10.4 m, regarding UP1 and UP2, respectively, and considering a constant track layout. The mesh pattern of the 2D models is very much similar to that of the full transition models and the mesh of the 3D models is somewhat analogous, as depicted in Figure 5-29a. The initial estimates of the properties of the geomaterials and track components were based on laboratorial characterisation and filed measurements described in Chapter 4 and in (Fortunato *et al.*, 2012), or in accordance with other publications (UIC, 2008);

2) Static calibration: vertical loads of 132 kN were applied on the rail at the centre of the reduced 3D models and the vertical profile of vertical displacements under the rail was calculated. The same loads were applied on the reduced 2D models and the width of the 4-node plane-stress finite elements were adjusted - using an iterative procedure developed in MATLAB, interacting with ANSYS in batch mode (Alves Ribeiro, 2012) - so that the reduced 2D models returned almost identical vertical displacements profiles. The application of this procedure resulted in a rather linear increasing variation of the element's width as depth increased, with a maximum value of 16 m and 14 m at the base, respectively for UP1 and UP2. Figure 5-29b shows an example of the good agreement between the displacement contours of the reduced 3D and 2D static models.

3) Dynamic calibration: considering the elements' width calculated in step 2 and using the reduced 2D models, a MATLAB optimisation algorithm was developed (Alves Ribeiro, 2012) - using the *lsqcurvefit* function from the Optimisation Toolbox of MATLAB, interacting with ANSYS in batch mode - to determine the material parameters (Young modulus and damping ratios of the geomaterials, as well as stiffness and damping values of the rail pads) that best fit the experimental receptance curves, in a least-squares approach. Each iteration of the algorithm included a short dynamic analysis of an impulse load (see Figure 5-9) applied on the rail in the reduced 2D models.

It is important to point out that, because the construction process and the materials used in the construction of both UP1 and UP2 were very similar, the same material properties were assumed for both structures. An exception was made regarding the rail pads, as stated before.

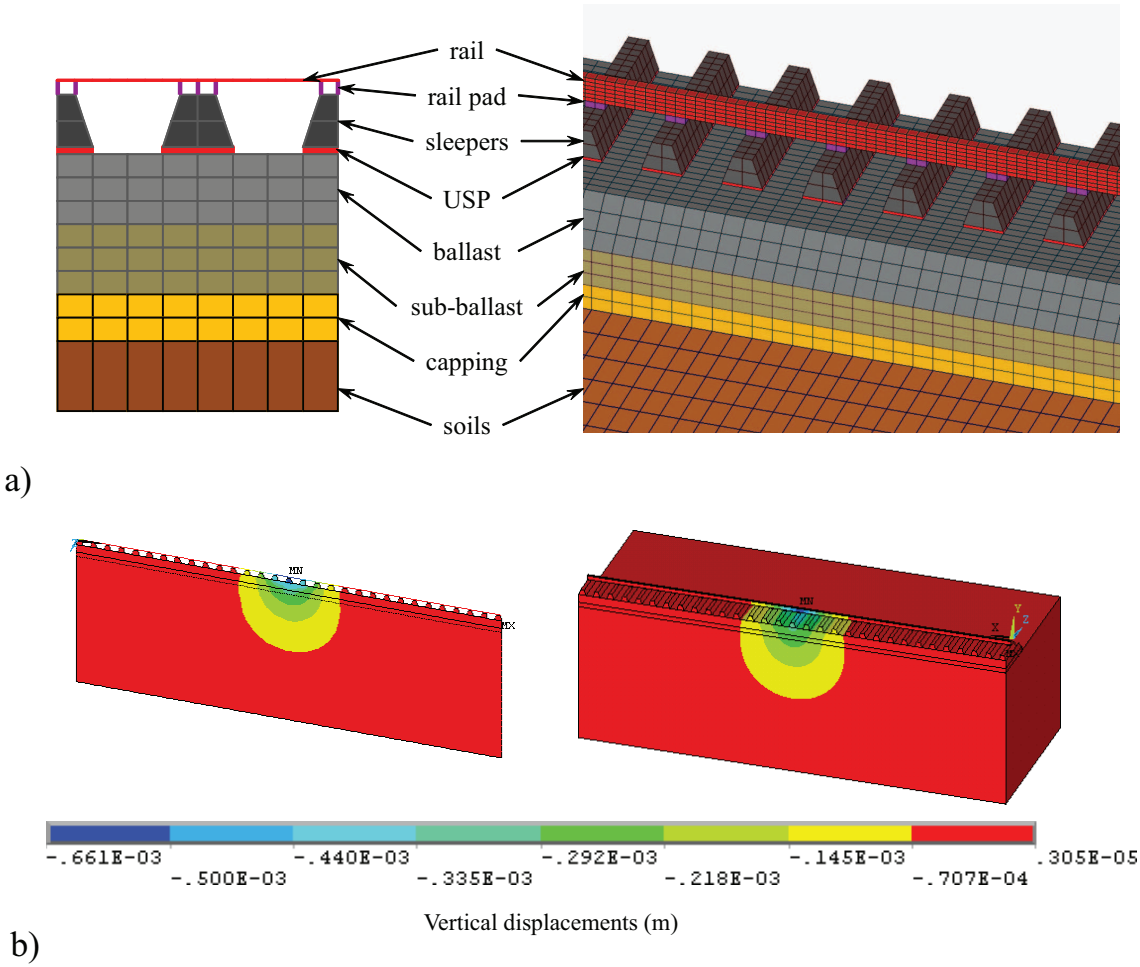

Figure 5-29. Reduced models used in the calibration: a) detailed views of the meshes; b) example of the vertical displacement contours after static calibration (Alves Ribeiro *et al.*, 2014).

Parameters of sections S1 to S4 of UP1 and UP2 were calibrated in the order presented in Table 5-6, starting with S4 of UP2 because it required the calibration of fewer parameters. To maintain coherance, the material parameters calibrated in a given section were considered to have the same value in the subsequent sections. The initial lower and upper limits used in the calibration of the material parameters, also presented in Table 5-6, were established taking into account earlier laboratorial and *in situ* characterisation studies on the geomaterials used in the construction of the backfills, discussed in Chapter 4 and in Fortunato *et al.* (2012), or in other studies (UIC, 2008). Figure 5-30 shows the final fitted numerical receptance curves for sections S1 to S4 at both transition zones.

Table 5-6. Calibration of material properties.

Order	2D reduced models	Parameter	Description	Lower/upper calibration limit	Unit
1	S4 UP2	E_b	Ballast Young modulus	50/500	MPa
		E_{sb}	Sub-ballast Young modulus	100/1000	MPa
		E_{CBM}	CBM Young modulus	10/30	GPa
		α	Damping α for all materials	1/10	s^{-1}
		β_1	Damping β of the three above materials	0.1/4	$s \times 10^{-3}$
		k_{rp}^{UP2}	UP2 rail pad stiffness	50/500	kN/m
		c_{rp}^{UP2}	UP2 rail pad damping	10/30	kN.s/m
2	S3 UP2	E_c	Capping Young modulus	100/4000	MPa
		E_{UGM}	UGM Young modulus	100/4000	MPa
		β_2	Damping β of the two above materials	0.1/4	$s \times 10^{-3}$
-	S2 UP2	-	(calibrated in S3-UP2)	-	-
3	S1 UP2	E_{emb}	Embankment soil young modulus	50/500	MPa
		β_3	Damping β of embankment soil	0.1/4	$s \times 10^{-3}$
4	S4 UP1	E_{USP}	USP Young modulus	0.2/20	MPa
		k_{rp}^{UP1}	UP1 rail pad stiffness	50/500	kN/m
		c_{rp}^{UP1}	UP1 rail pad damping	10/30	kN.s/m
-	S3 UP1	-	(calibrated in S3-UP2 and S1-UP1)	-	-
-	S2 UP1	-	(calibrated in S3-UP2 and S1-UP1)	-	-
-	S1 UP1	-	(calibrated in S1-UP2 and S1-UP1)	-	-

In the receptance tests, the full track vertical resonant frequency, f_t (which corresponds to the vertical vibration of the rail and sleepers on the track layers), lies usually between 40 and 140 Hz (De Man, 2000). This resonant frequency can be observed in Figure 5-30, in both field and numerical receptance curves, as a peak between 60 and 120 Hz. This peak is particularly noticeable in sections with USP, which denote the flexibility increase provided by the USP. It is also possible to identify the resonant frequency of the vibration of the rail on the rail pads, f_{rp}, between 300 and 350 Hz. At sections with no USP, another peak is visible around 190 Hz in the

field receptance curves. Considering studies by Grassie (1995) and some simulations that were performed using 3D dynamic analyses of the track, there is some evidence that the peaks may correspond to a vibration mode of the sleepers. Since the 2D models are unable to simulate the bending behaviour of the sleepers, those peaks are not visible in the numerical curves in Figure 5-30.

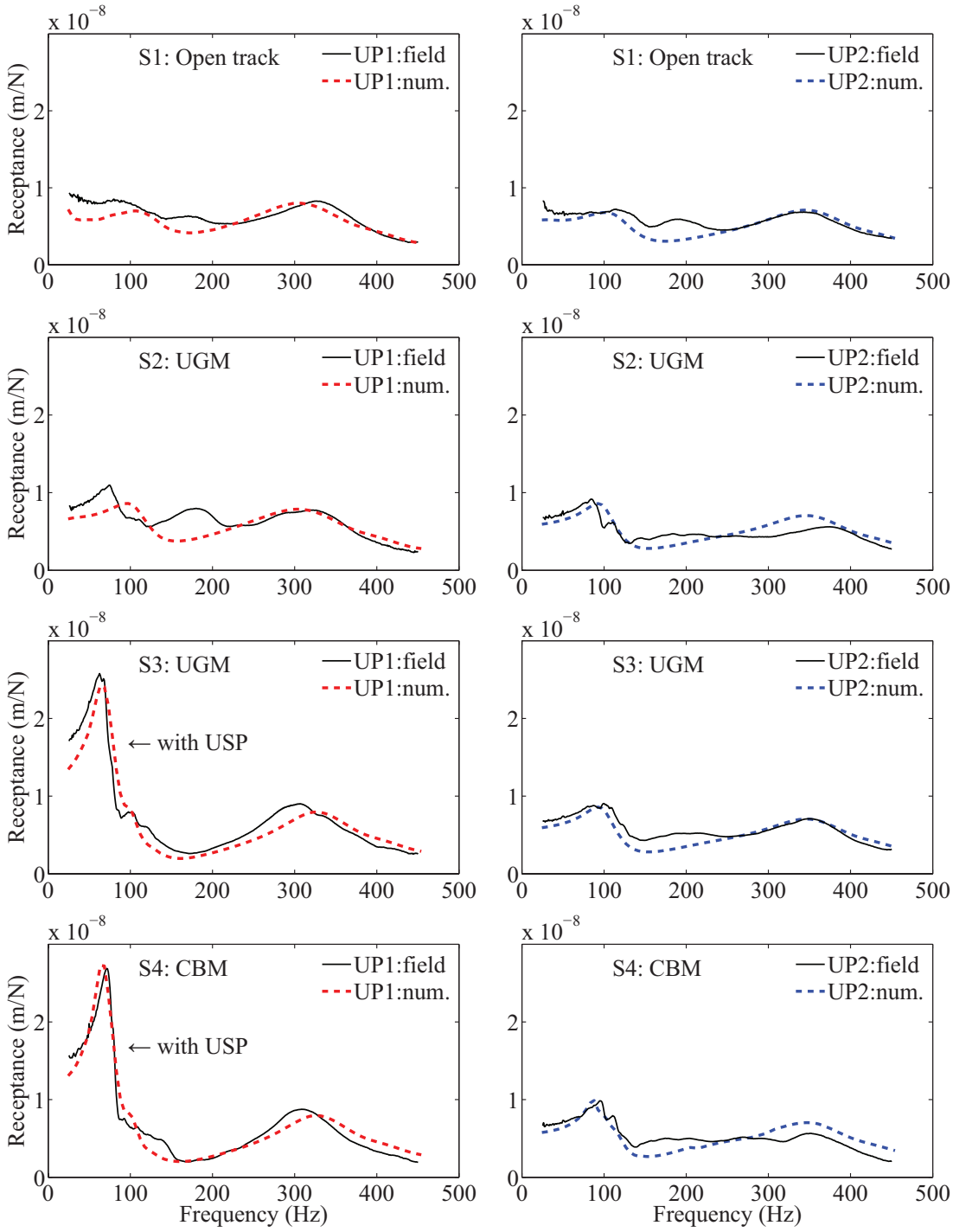

Figure 5-30. Experimental and numerical receptance curves for sections S1 to S4 after dynamic calibration.

Table 5-7 shows a comparison between resonant frequencies f_t and f_{rp} of the curves in Figure 5-30. In general, results show a very good agreement between field and numerical receptance curves. Nevertheless, some experimental curves were better fitted than others. This outcome was somewhat expected given the known variability of the mechanical properties of the geomaterials and of the track components (Oscarsson, 2002). For instance, at UP1, field f_{rp} ranged between 304 and 327 Hz, but showed higher values at UP2: between 344 and 373 Hz (see Table 5-7). As discussed earlier, these differences in the frequencies indicate variations in the stiffness of the rail pads along each transition zone. Moreover, the higher range of frequencies at UP2 also suggests that the rail pads at that underpass may have been installed with higher preloads than the rail pads at UP1. The influence of fastening preloads on the stiffness of rail pads is well documented by Wu & Thompson (1999). To account for this aspect, different values were established for the calibration of rail pad parameters in each transition zone, as mentioned earlier in section 5.2.4.

Table 5-7. Comparison of field and numerical track resonant frequencies f_t and f_{rp} (in Hz).

Track sections	f_t^{UP1} **field / num.**	f_t^{UP2} **field / num.**	f_{rp}^{UP1} **field / num.**	f_{rp}^{UP2} **field / num.**
S1	84 / 107	114 / 103	327 / 303	344 / 347
S2	74 / 93	85 / 93	317 / 308	373 / 347
S3	63 / 64	99 / 92	304 / 327	350 / 346
S4	71 / 64	95 / 88	309 / 327	350 / 346

5.2.6 Validation of the model with experimental data

To validate the numerical models, the numerical results were compared against the field measurements performed on the track, at sections S1 to S4 (see location in Figure 5-2).

After calibration, there was a very good agreement between the field measurements and the dynamic results of the UP2 model. However, at first, it was not possible to validate the UP1 model because the numerical results seemed to underestimate the field measurements in sections

with USP. In fact, some drawbacks were expected, considering that the adopted models are not able to fully account for the complex and non-linear contact established between the USP's underside and the ballast grains. While it may be reasonable to consider USP with the full area of the sleeper's underside for the dynamic calibration of the models (small load impulse on the rail), when trains load the track (significantly higher loads) the effective contact area of the USP becomes smaller and concentrated under the rails. Using the numerical model, it was determined that with an effective contact area of approximately 0.3 m^2 (about 45% of the actual area of the sleeper's underside) it was possible to obtain a good agreement with the field measurements at UP1.

Figures 5-31 to 5-34 show a comparison between numerical and experimental rail vertical displacements in sections S1 to S4, in both transitions. Negative values of displacements denote downward direction. Given the random nature of the dynamic response for high frequencies due to the short-wave irregularities of the rails and wheels (which are outside the scope of this study), and for an easier interpretation of the results, a type II Chebyshev filter with cut-off frequency of 80 Hz was applied to time history records.

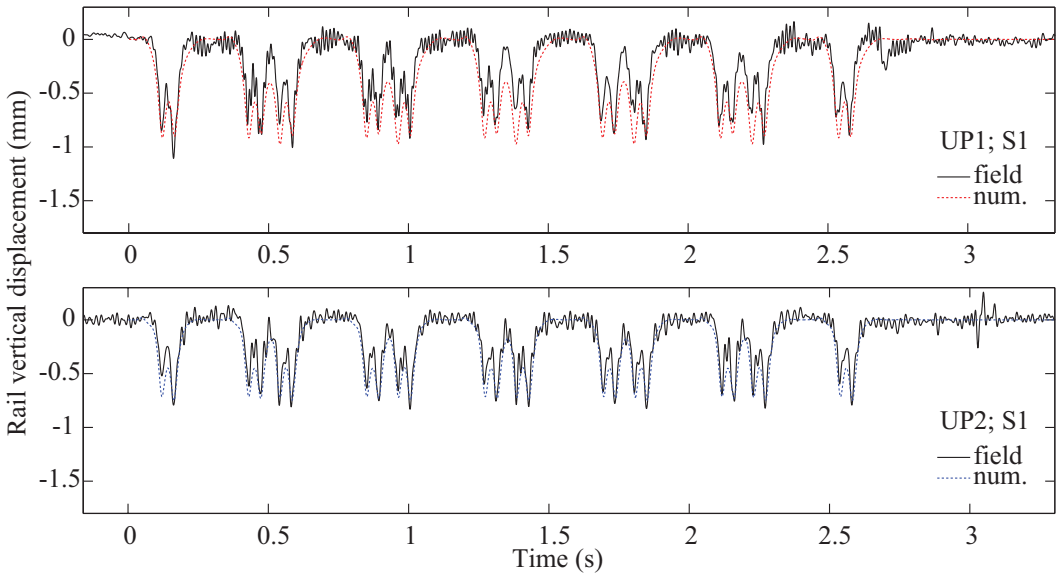

Figure 5-31. Comparison of rail displacements at S1: numerical results against field measurements.

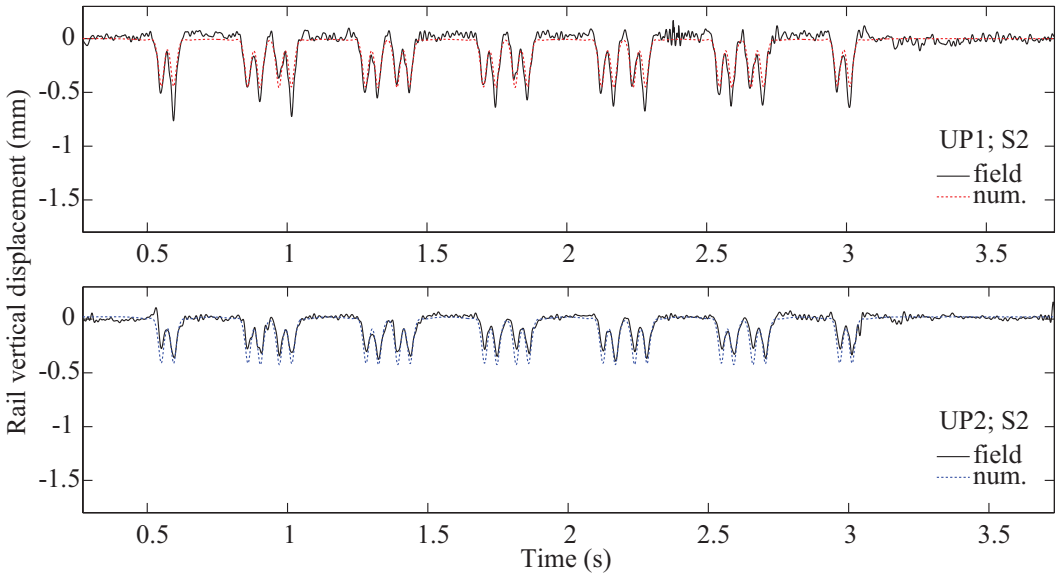

Figure 5-32. Comparison of rail displacements at S2: numerical results against field measurements.

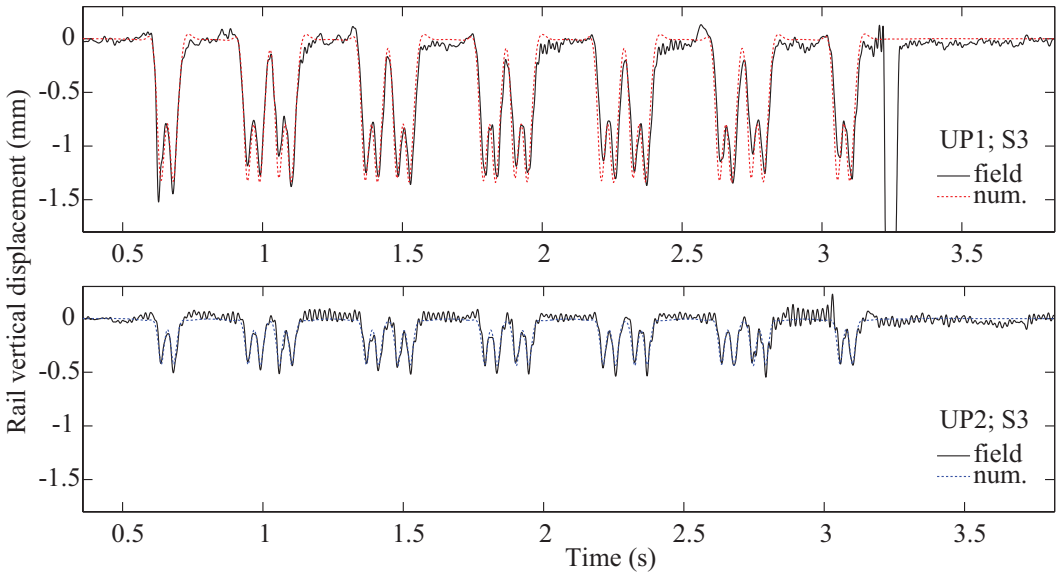

Figure 5-33. Comparison of rail displacements at S3: numerical results against field measurements.

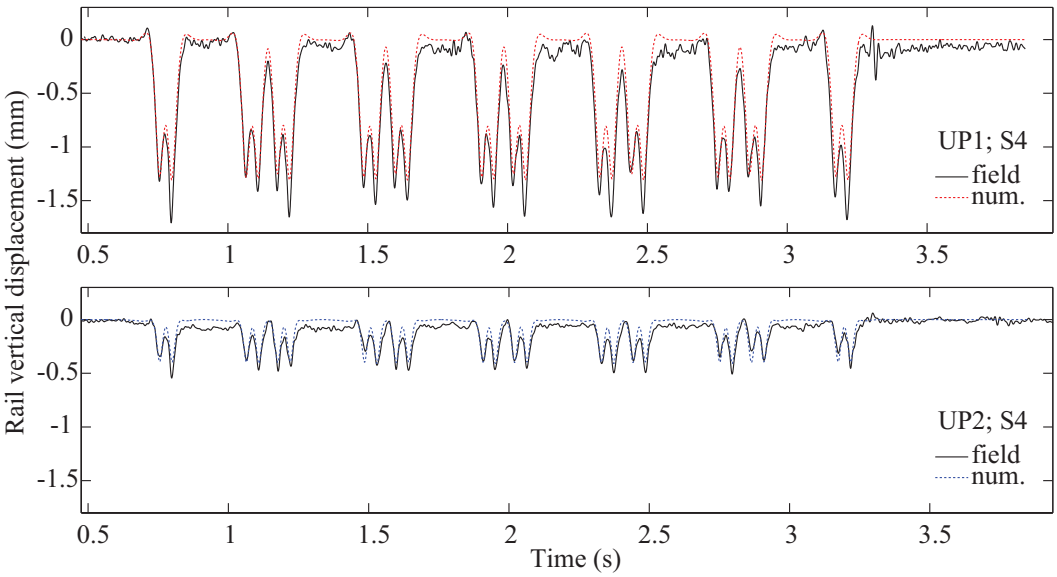

Figure 5-34. Comparison of rail displacements at S4: numerical results against field measurements.

As mentioned earlier, different stiffness and damping values were considered for the rail pads at UP1 and UP2. The analyses of various field measurements confirmed that the amplitudes of the rail-sleeper relative vertical displacements (an estimate of the rail pad deformation) were different in the two transitions (see the example Figure 5-35). These results supported the decision to consider different values for the rail pad parameters at each transition. With this consideration, it was possible to achieve a good agreement between the numerical and the experimental results, as depicted in Figure 5-35.

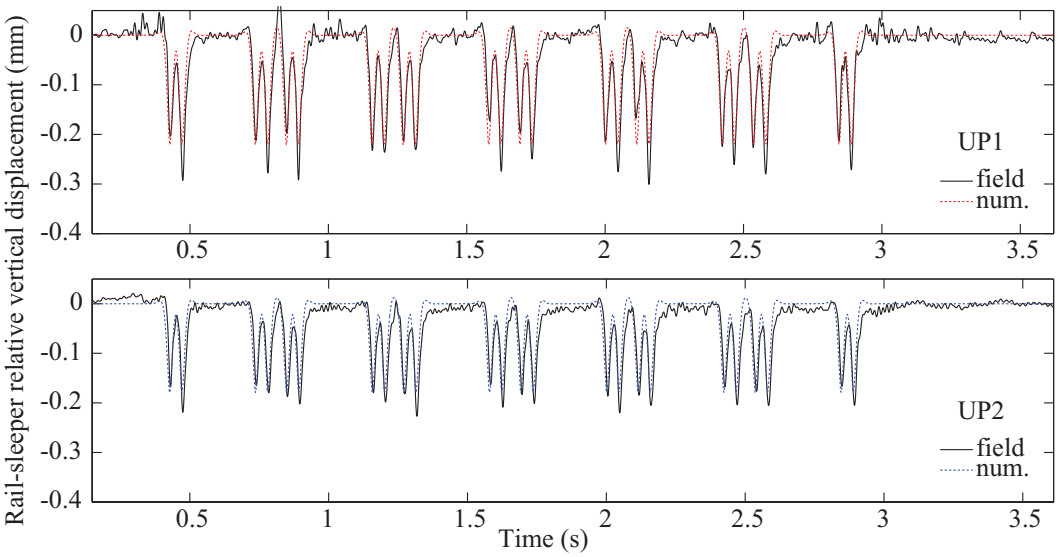

Figure 5-35. Comparison of rail-sleeper relative displacements: numerical results against field measurements.

The vertical accelerations calculated at the sleepers were also validated. Figures 5-36 to 5-39 compare numerical and experimental vertical accelerations of the sleepers near sections S1 to S4, at both transitions (after applying a type II Chebyshev 80Hz low-cut filter).

In general, a very good agreement was obtained. The numerical accelerations of the sleepers near S3 at UP1 (Figure 5-38) somewhat overestimate the experimental acceleration peaks. At S2 of UP1 (Figure 5-37), the numerical results were also slightly different from the track measurements – the later have relatively higher negative peaks. These observations at S3 and S2 of UP1 are probably related to the disturbances in the train-track interaction caused by the transition between sleepers with USP and without USP, as will be addressed later. It is also possible that the track near sections S2 and S3 at UP1 has undergone some degradation, thus affecting the dynamic response of the track, which the model could not reproduce. In addition, it should be noted that the accelerations were measured on the end of the sleepers, near one of the rails. Because the model is bi-dimensional, it cannot simulate the tri-dimensional response of the track that might be causing those differences, such as slight rotations of the sleepers around the track longitudinal axis caused by eventual uneven support conditions.

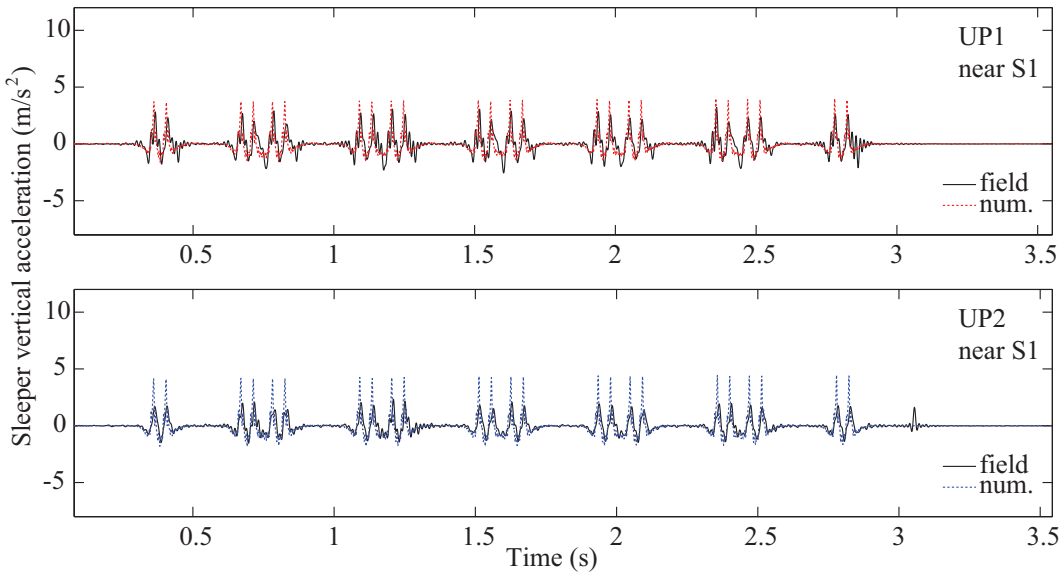

Figure 5-36. Numerical results and field measurements of the vertical accelerations of the sleeper near S1.

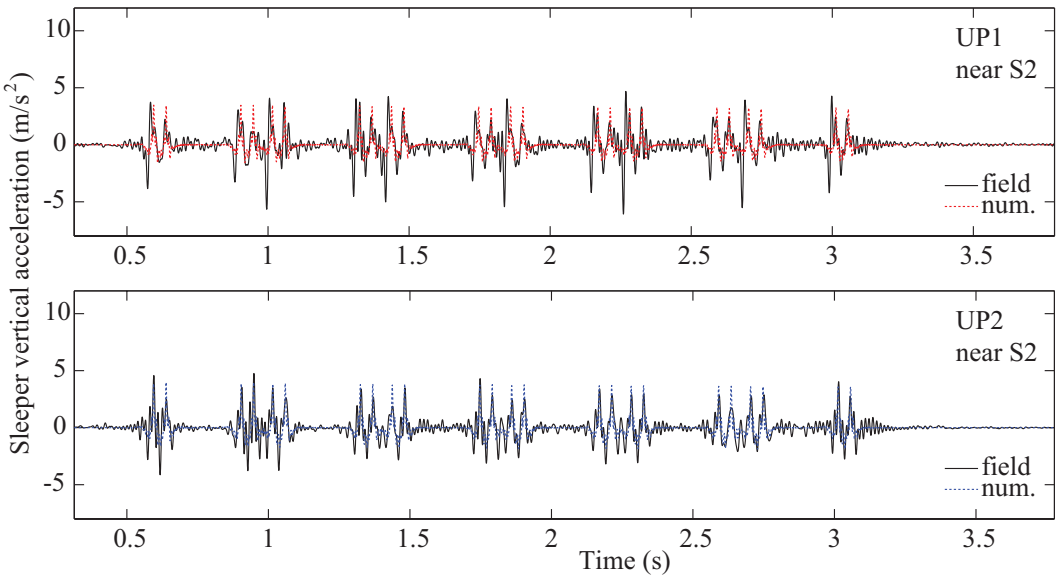

Figure 5-37. Numerical results and field measurements of the vertical accelerations of the sleeper near S2.

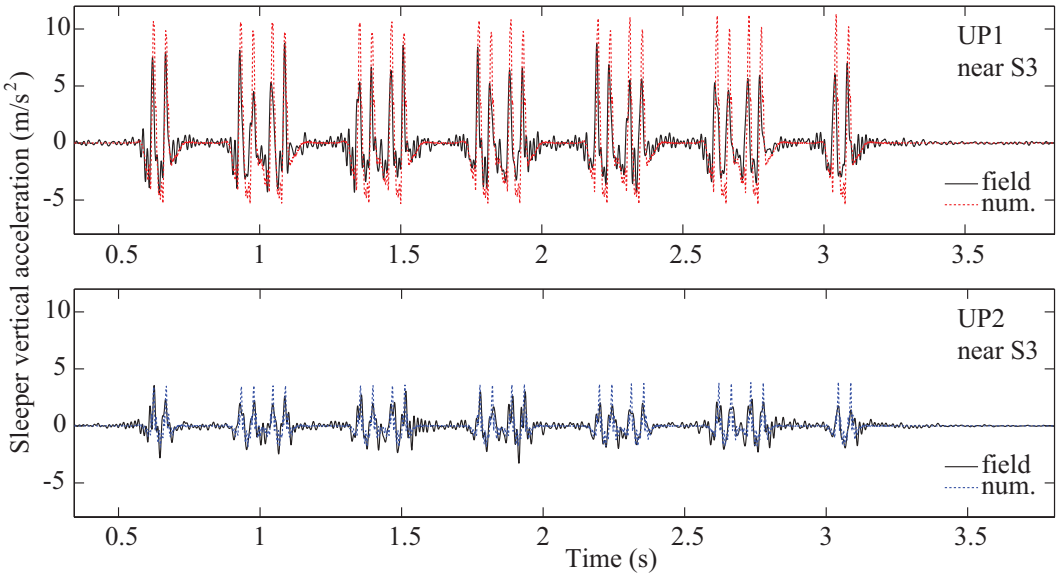

Figure 5-38. Numerical results and field measurements of the vertical accelerations of the sleeper near S3.

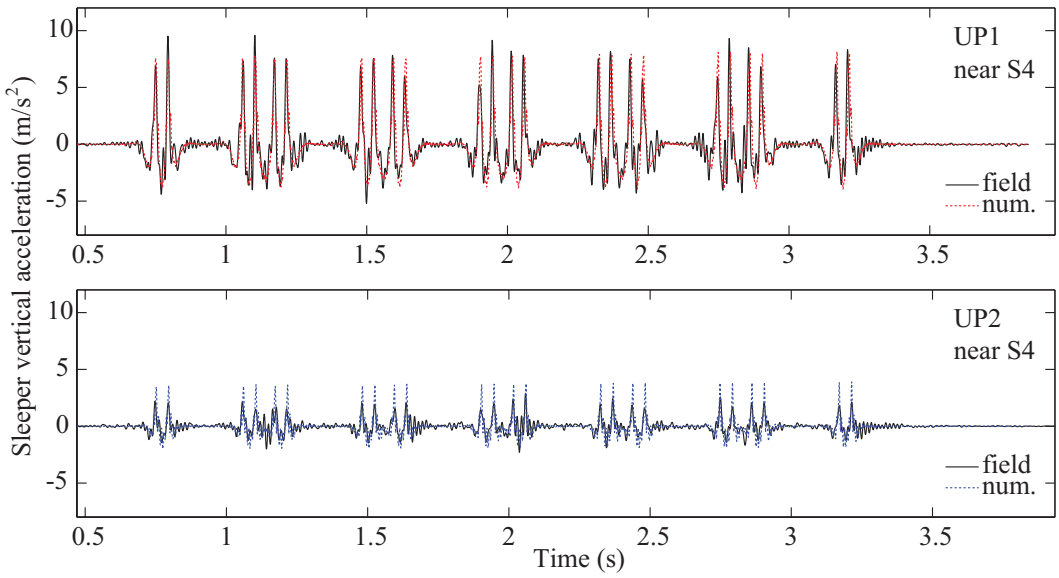

Figure 5-39. Numerical results and field measurements of the vertical accelerations of the sleeper near S4.

Figure 5-40 compares frequency contents of numerical results and field measurements near sections S1 to S4 at UP1 and UP2. The presence of USP is evidenced by the increase in the amplitude of the frequency peaks in the two bottom left plots (S3 and S4 of UP1), as reported earlier. In general, the results show a relatively good agreement, although the numerical results near S3 at UP1 seem to be somewhat overestimated. The prominent peaks in the plots are related to the train's signature, as was analysed in section 5.2.3.

5.2.7 Analysis of the train-track interaction

For this analysis, the two validated models were used. Figure 5-41 presents the vertical displacements of the 1st axle of the train. On both transitions, a smooth variation of rail vertical displacements is visible between the embankment with soils and the wedge-shaped backfills (at about 30 to 23 m from the box culvert). At UP2, a relatively smooth ride is also observed over the backfills (on UGM and CBM) and onto the box culvert, with minor stiffness increases over its walls. This indicates that the backfill of UP2, by itself, can provide a gradual variation of the track vertical stiffness as the train approaches the structure.

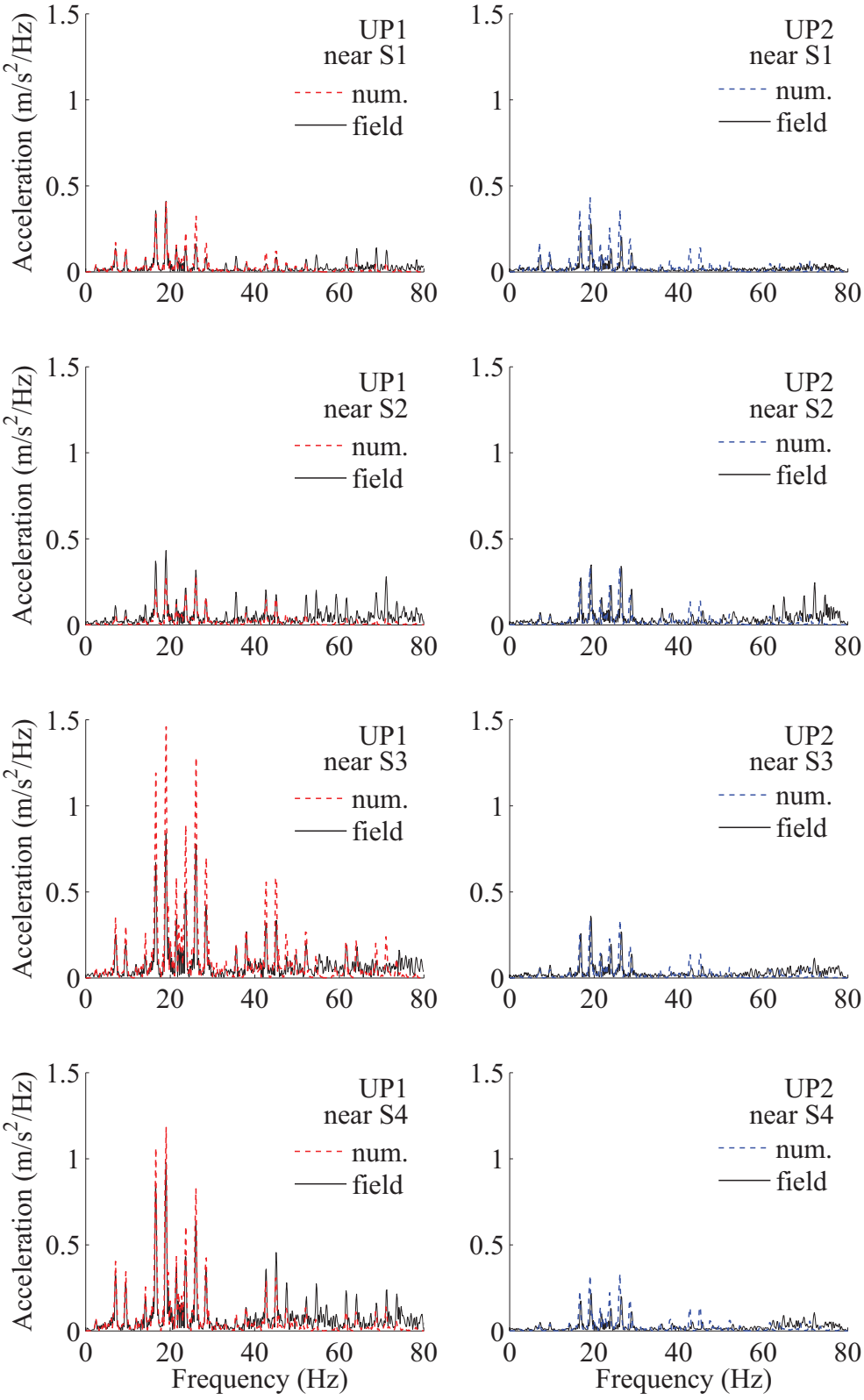

Figure 5-40. Frequency content of numerical results and field measurements of the vertical accelerations of the sleepers.

Comparing the two displacement profiles presented in Figure 5-41, it can be observed that at UP1 there is an increase in the vertical displacement of the axle by 3 to 3.4 times where USP were installed. This evidences the influence of USP on the reduction of the track vertical stiffness. The axle displacement changes abruptly (in a 3 sleeper-span) when entering or exiting the track section with USP (at about 13 m from the box culvert), which indicates a sharp stiffness transition. The relatively higher axle vertical displacements obtained on the embankment with soils at UP1, when compared with the results at UP2, seem to be a result of the higher depth of the embankment soils at UP1 (see Figures 5-1 and 5-2).

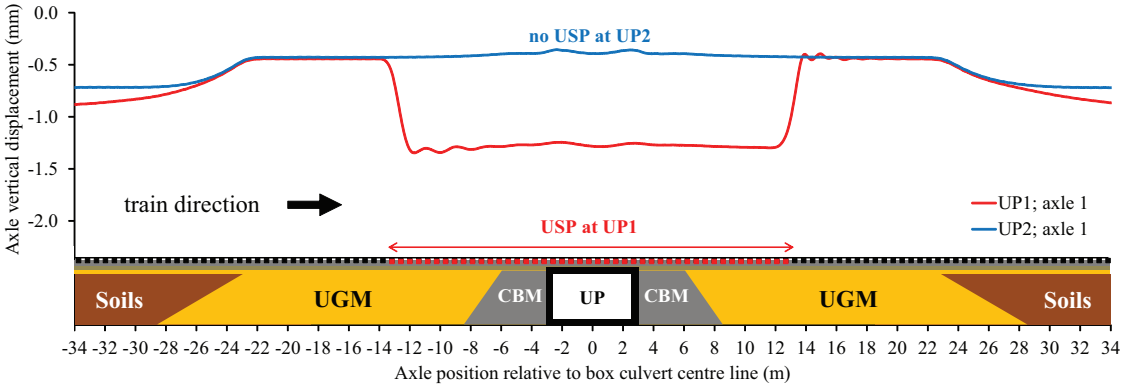

Figure 5-41. Vertical displacement of the 1st axle of the train crossing transition zones UP1 and UP2.

With the consideration of the train-track interaction, additional observations were drawn:

1) Although results at UP2 are not influenced by the direction of the train, it slightly influences the results at UP1, namely when entering or exiting the track section with USP, causing small oscillations in the vertical displacement of the axle (Figure 5-41);
2) The vertical displacement profile of the 2nd axle of each bogie is similar to that of the first axle, though marginally higher in magnitude (1-4% more) on the track section with USP.

Figure 5-42 evidences oscillations on the train-track interaction forces calculated in the wheel-rail contact elements. Although no significant variation of the dynamic train-track interaction forces is observed when the train crosses UP2, higher oscillations were visible at UP1 when it entered or exited the track section with USP. Contact force amplitudes obtained in the direction from track with USP (soft support conditions) to track without USP (stiff support conditions) were higher than those obtained in the opposite direction, and oscillated between -12% to +7%

of the average static axle load of 132 kN. Interaction forces were almost identical for all axles of the train.

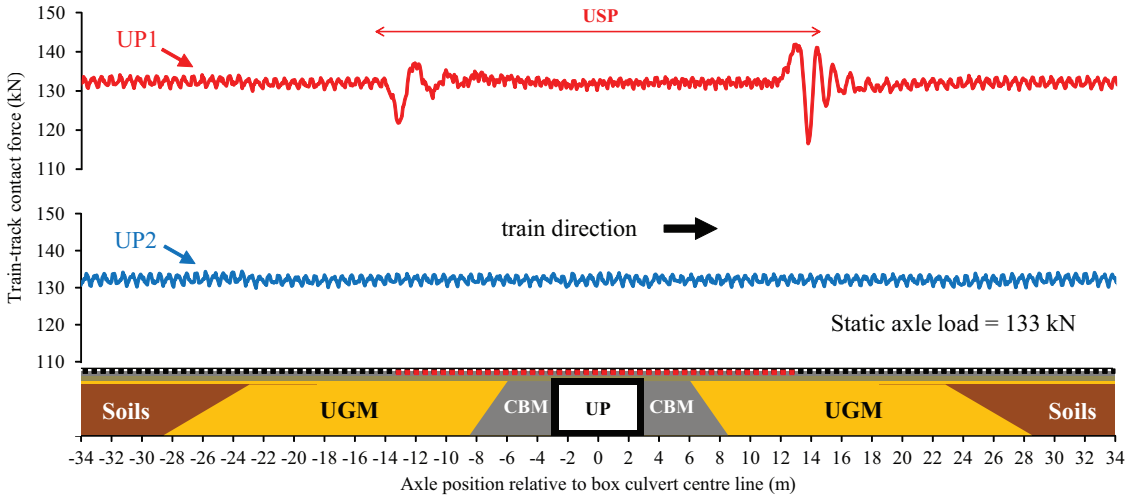

Figure 5-42. Interaction forces between the 1st axle of the train and the rails.

Figure 5-43 shows a comparison of the peak rail seat loads. It can be observed that the USP in UP1 result in higher rail seat loads on the sleepers immediately before the track section with USP, with a maximum increment of about 42%. However, at the central part of the track section with USP, it is possible to identify the eventual benefit of the USP regarding the long-term behaviour of the track. In fact, the use of USP was responsible for the reduction of about 33% of the maximum rail seat loads. In practice, this results in lower contact forces between the sleepers' underside and the angularities of the ballast particles (reducing ballast crushing and abrasion) and may contribute to reduce track degradation rates in that section.

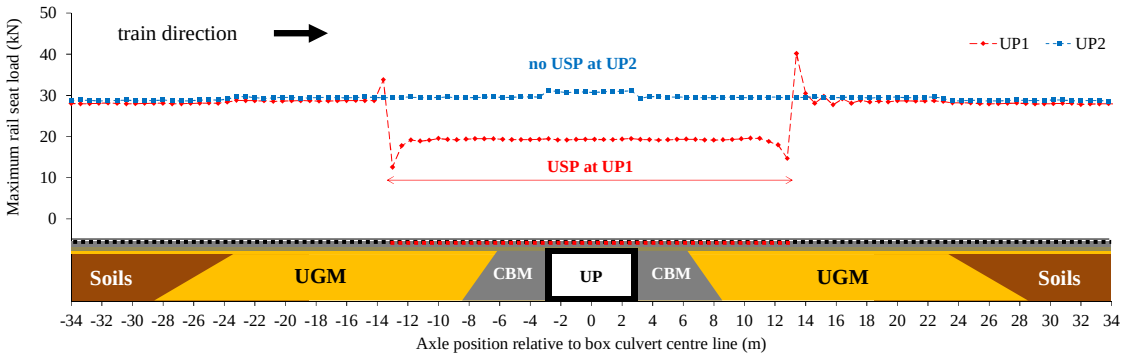

Figure 5-43. Maximum rail seat loads on the transition zones to UP1 and UP2.

Because the numerical model only considers the transient dynamic response of the train-track system and not the long-term behaviour, no further conclusions can be drawn regarding the benefit of USP to reduce track degradation rates at transition zones.

Considering the complexity involved in the contact between the sleepers and the particles of ballast, other numerical techniques, such as the Discrete Element Method (DEM), seem to be a more adequate approach to assess in greater depth the benefit of USP to reduce ballast degradation. However, the application of DEM to study large segments of the track, with the consideration of train models and the train-track interaction, is yet impractical due to the considerable computation effort that is required. A recent application of the DEM to study transition zones was presented by Chen & McDowell (2014), using a small track model with dimensions 2.1 m × 0.3 m × 0.4 m. In the simulations, it was found that an abrupt stiffness change caused more ballast settlement on the softer track section due to the sliding of the particles; while a gradual variation of the subgrade stiffness resulted in a more stable particle interlocking. This micromechanical approach provided relevant insight on the factors that can influence the track degradation rates. It also demonstrated that the DEM has a significant potential to study partial sections of transitions in more detail, thus contributing to the understanding of the track degradation process and appropriate mitigation. The approach seems to be very useful to study, not only conventional track designs, but also innovative solutions such as USP, in that it allows assessing the amplitude of the contact forces of the ballast particles and their force chains under the sleepers.

As mentioned earlier, previous numerical studies also suggest that USP influence the track's behaviour (Lundqvist *et al.*, 2006; Witt, 2008). However, some field measurements (Lozano del Moral & Cuéllar, 2009) and a numerical study by Insa *et al.* (2013) suggest that USP have minor influence in the track's behaviour at transition zones. The track measurements reported earlier and the numerical results presented here clearly demonstrate that USP can have a significant influence on the track dynamic behaviour. The contrasting results may be related to the fact that different studies focused on USP with very distinct stiffness properties. This suggests that caution is necessary when drawing conclusions regarding the use of USP at transition zones and indicates that further studies are required. Johansson *et al.* (2008) highlight that the stiffness properties of the USP should be carefully determined for plain track; the same certainly applies to transition zones.

5.2.8 Optimisation of the design of the transition zone with USP

In this study, the results indicate that the adopted USP at UP1 are too soft and introduce sharp stiffness transitions, which result in dynamic amplifications in the train-track interaction when the trains enter or exit the sections with USP. However, in the central part of the section with USP, rail seat loads and stresses on the ballast layer were reduced, as mentioned above. Thus, to provide a smoother ride, other alternative arrangements of USP along the transition zones with different elastic properties might be more effective than the case under study. Recent studies report the need to use sets of rail pads and under sleeper pads with different elastic properties at transition zones between different track structures in order to minimise the negative effects found of new high-speed lines (Costa D'Aguiar *et al.*, 2013).

With the aim to improve the design of the transition zone with USP, a parametric study was carried out using the numerical model of UP1.

Although the dynamic analyses of the passage of the entire train through the transition zones are relatively fast to compute considering a total of 3850 time steps of 0.001 s (about 7 hours using a desktop computer with a quad-core processor and 16 GB of RAM), it was found that it was possible to reduce hard disk usage and calculation times even further. In this case study, it was observed that all the bogies produced the same dynamic response. Thus, instead of modelling all 12 bogies of the train, the same result could be obtained by calculating only one bogie and then superimposing its effect 12 times, spaced in time, according to the train speed and axle configuration. With this simplification, the number of required time steps and calculation time was reduced in about 67%. This conclusion may be particularly relevant for simulation-based optimisation, where a large number of runs are normally required. Figure 5-44 shows a comparison of rail vertical displacements and sleeper vertical accelerations caused by the 11^{th} bogie of the train, either considering all the bogies or using the above simplified method. Since the differences appear to be insignificant, this simplification was adopted in the parametric study in order to reduce calculation times and computational effort. It is suggested that preliminary tests should be carried out before adopting this simplification to other case studies.

The parametric study aimed at determining a more adequate design so that the axle vertical displacement of the train, across the transition zone, remained close to the value observed in plain track (about 0.9 mm) – an uniform track vertical stiffness. It was found that using at least 3 sets of USP, with different stiffness in specific track sections, produced significant better results. The best design of the parametric study comprised the following three different track sections (identified in Figure 5-45):

a) Section A (up to about 23 m from both sides of the box culvert centre line) - 78 sleepers with USP with a stiffness 2.2 times greater than the USP in the case study;

b) Section B (at about 23 m to 28 m from both sides of the box culvert centre line) - 8 sleepers with USP with a stiffness 5 times greater than the USP in the case study;

c) Section C (at about 28 m to 33 m from both sides of the box culvert centre line) - 8 sleepers with USP with a stiffness 15 times greater than the USP in the case study;

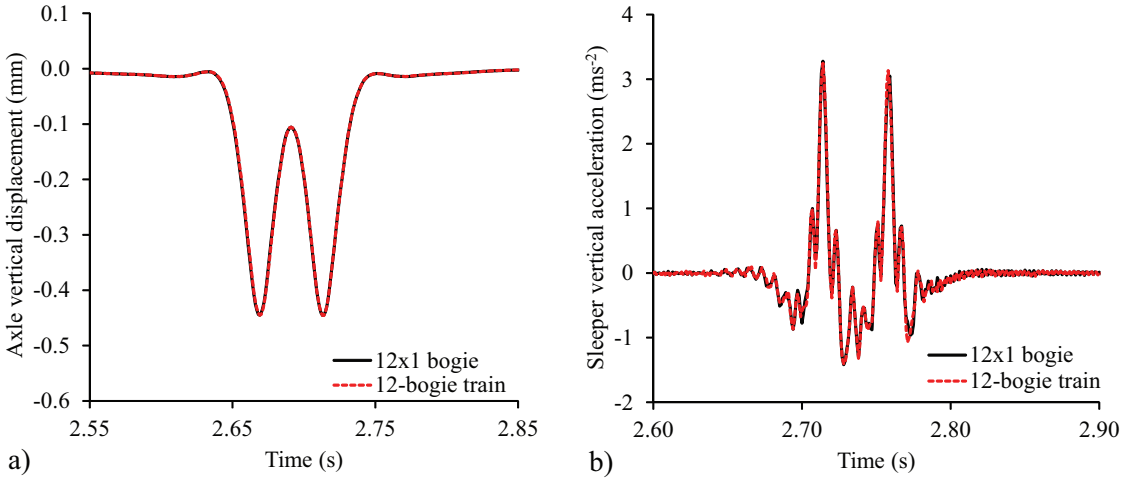

Figure 5-44. Axle's vertical displacements (a) and sleeper's vertical acceleration (b) considering the effect of a 12-bogie train model or the superimposition of the effect of 12 times one bogie spaced in time.

With the improved design it was possible to: i) even the track vertical stiffness along the transition zone and consequently limit the variations of the axle displacement (Figure 5-45); ii) limit the oscillations of the train-track interaction forces down to about +/-3% of the static axle load (Figure 5-46); iii) reduce rail seat loads throughout the transition zone by at least 26%, in comparison to the results in UP2 (Figure 5-47).

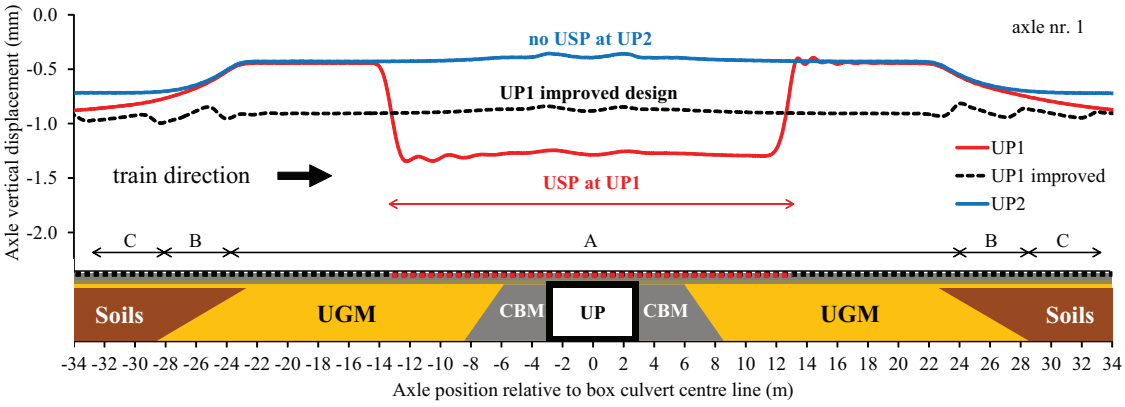

Figure 5-45. Vertical displacement of the 1st axle of the train crossing transition zones UP1 and UP2, including the improved design of UP1.

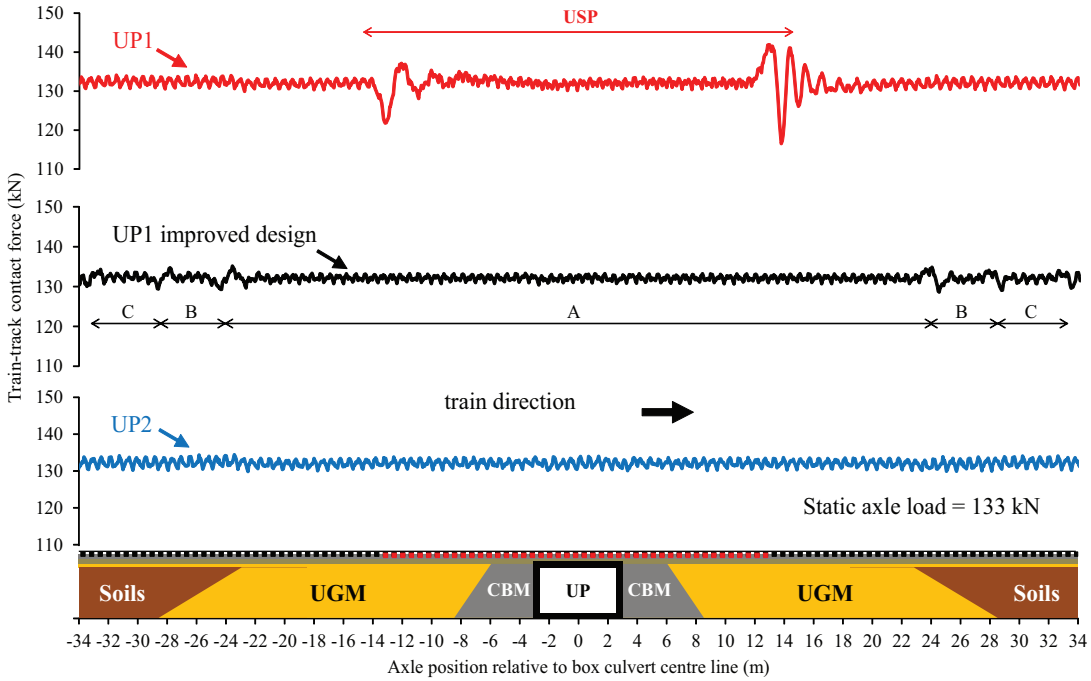

Figure 5-46. Interaction forces between the 1st axle of the train and the rails, including the improved design of UP1.

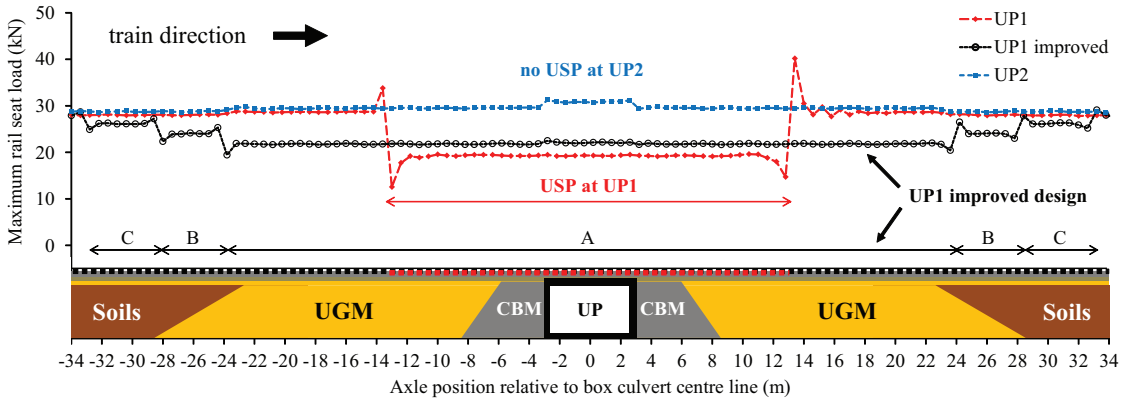

Figure 5-47. Maximum rail seat loads on the transition zones to UP1 and UP2, including the improved design of UP1.

Given that the track was only opened to traffic in recent years, it was not possible to draw further conclusions regarding the long-term behaviour of the transition zones with USP, including the optimised design. Moreover, considering that the numerical models were developed for transient dynamic analyses and to reproduce the *in situ* measurements, they cannot predict the track degradation or the plastic deformation of the track elements.

5.3 Case study 2 - dynamic train-track interaction at the transition zone to a bridge

5.3.1 Description of the transition zone case study

The second case study is the transition zone at the southern approach of the new railway bridge over *Sado* river in the *Alcácer* bypass (Figure 5-48). The track has the same characteristics of the previous case study, described in 5.2.1. This is the same transition zone that was used as a case study in Chapter 4.

Figure 5-48. General views of transition zone during the construction of the backfill and in operation.

The southern part of the bridge deck is a composite structure with a concrete slab supported by a steel plate girder with multiple spans of 37.5 m. The last span rests on a counterfort abutment in reinforced concrete, founded on ten 21 m-deep piles, with a large opening at the front. The natural foundation of the transition zone consists mostly of monogranular fine-grained sands that provide good foundation conditions to the embankment of track – see Chapter 4. The transition zone includes a backfill, about 9 m high, depicted in Figure 5-49, that was constructed using similar materials and the same requirements as the previous case study. The average degree of compaction (Dc) of the CBM obtained *in situ* was Dc=100%, regarding the Optimum Modified Proctor reference value (OPM). The UGM, located between the CBM and the embankment with soils, also comprises a well graded crushed limestone aggregate with min./max. particle sizes of 0/31.5 mm, placed with average Dc=99% OPM. Figure 5-49 also depicts aspects of the track instrumentation that will be addressed in section 5.3.3.

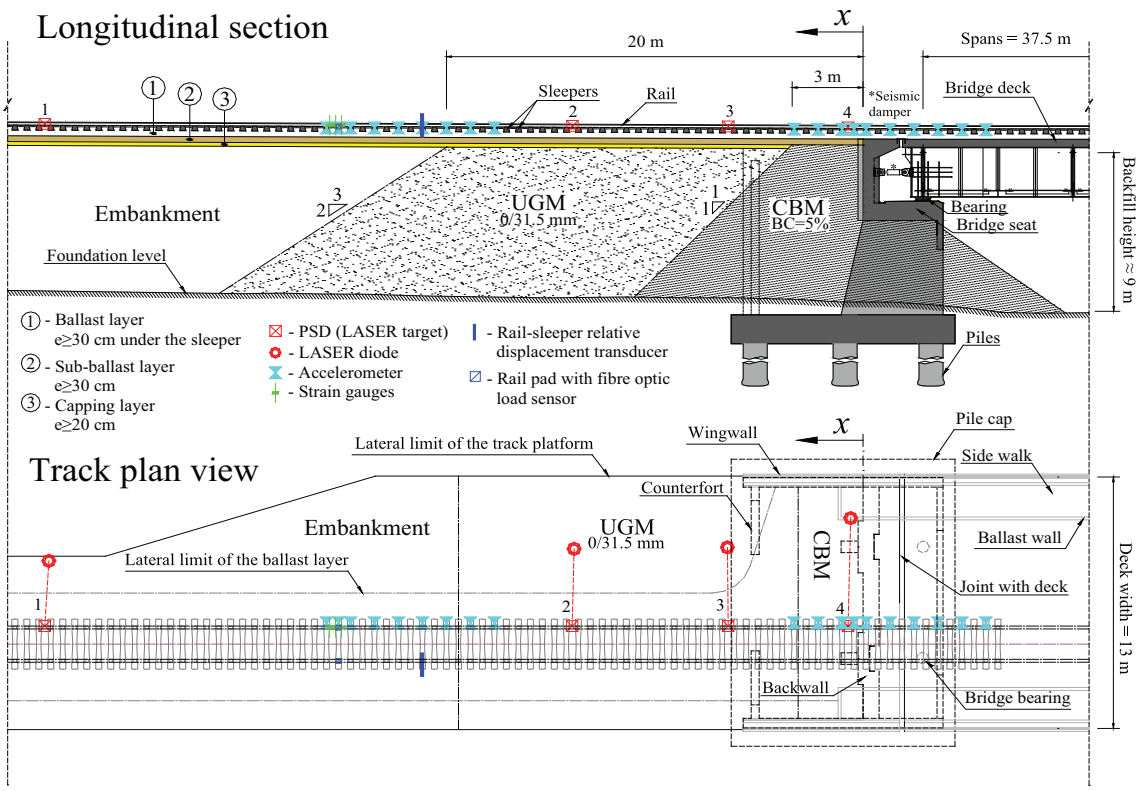

Figure 5-49. Schematic longitudinal profile and plan view of the transition zone.

A minimum ballast thickness (e) of 0.30 m under the sleepers was also established both for the track on embankment and on the bridge. Figure 5-50 shows cross-sections of the track and requirements for the upper layers of the track platform, namely: minimum thickness; Dc (%OPM); and deformation modulus calculated in the 2nd cycle of the plate load test (E_{V2}).

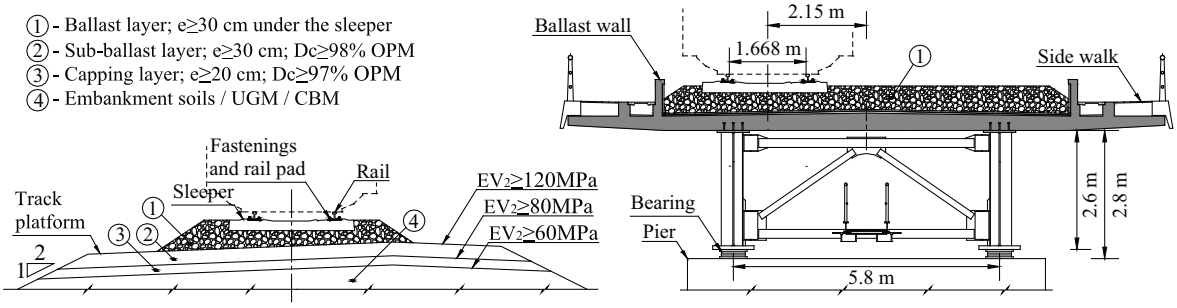

Figure 5-50. Track cross sections on earthworks and on the bridge (REFER, 2006).

5.3.2 Characterisation of the track

According to what was mentioned in Chapter 4, the laboratorial characterisation using cyclic load triaxial tests were specifically intended to assess the resilient and long-term deformation behaviour of the geomaterials applied in the backfill of this transition. It focused on the materials applied in the layers of sub-ballast, capping, UGM and CBM. The results revealed that the geomaterials were adequate for the track substructure, in terms of their physical and mechanical characteristics and followed the design requirements (REFER, 2009). Data from the inspection vehicle indicates that the track geometric quality is very good at the transition zone and no maintenance operations had been required up to this date. During construction, *portancemètre* surveys were carried out at different levels of the substructure, as described in Chapter 4.

In order to assess the support conditions of the sleepers and its variability during the year, light falling weight deflectometer (LFWD) tests were performed on two separate occasions: firstly during Spring, after a rainy season, and then in the following Autumn. The test procedure that was presented in 5.2.2.2 was also used here. It consisted in the application of a load impulse of 15 kN on a 0.10 m diameter plate at the centre of each sleeper. The results of the two surveys are presented in Figure 5-51 regarding average deflection values (δ_s) measured at the centre of the sleepers. In the second survey, it was not possible to assess the same number of sleepers. In general, it is observed only minor differences between the deflections measured in the two surveys, which denotes a relative stability of the sleepers' support condition in that period. The median values of the deflections of the first survey were about 129 μm, which was similar to the results of the previous case study. The deflection values on the Embankment, on the UGM and on the deck were relatively stable, which suggest uniform support conditions of the sleepers in those sections of the track. On the other hand, a few sleepers showed deflection significantly higher than the median value, mainly those located between about x = -2 m and x = 3 m. This may be related to the constantly changing characteristics of the track substructure that takes place in a length of less than 5 m (bridge, joint with the deck, abutment, CBM). In particular, it was noticed that the sleeper at the joint with the deck showed the highest value, 567 μm, that was about 4.4 times higher than the median value.

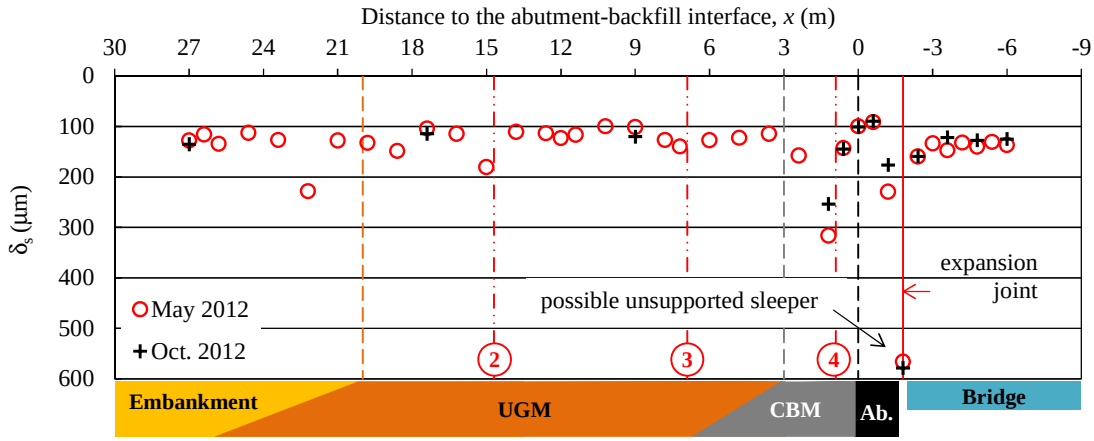

Figure 5-51. Light falling weight deflectometer tests.

5.3.3 Track monitoring during train passages

To analyse the response of the track along the transition zone when the *Alfa Pendular* trains (see Figure 5-15) passed by, field measurements were carried out in two separate occasions. In the first measurements it was possible to record 4 trains and in the second 8 trains, travelling at speeds of about 220 km/h.

The monitoring comprised various types of transducers (Figure 5-52) connected to a single acquisition system that were described in the previous section. The following measurements were performed (at the positions depicted in Figure 5-49): i) shear deformations of the rail web, using strain gauges to calculate the dynamic wheel loads and the reaction force at the rail seat portion of the sleeper (Figure 5-52b); ii) rail seat loads on the rail pads, using fibre optic sensors (Sensor Line, model FORPS - Figure 5-52c); iii) rail vertical displacements at positions 1-4, using four contactless systems that comprise a LASER and a Position Sensitive Detector (PSD) (Figure 5-52d); iv) rail-sleeper vertical relative displacement, using a LVDT (Figure 5-52e); v) vertical accelerations of the sleepers, using micro electro-mechanical system (MEMS) (Figure 5-52f) and piezoelectric accelerometers (Figure 5-52g). The different measuring systems were previously calibrated in laboratory or in field tests.

Figure 5-52. Track instrumentation: a) general aspect of the site; b) strain gauges; c) fibre optic rail pad sensor (installation during construction and final aspect); d) LASER-PSD system; e) LVDT transducer; f) MEMS accelerometer; g) piezoelectric accelerometer.

At this transition zone, rail shear forces, V_i, were calculated at three different sections (1 to 3), following the procedure described in 5.2.3 (see Figure 5-12), using three full Wheatstone bridges in this case. Figure 5-53 shows the calculated differences in shear forces obtained between two consecutive sections. For example, the difference between V_2 and V_3 yields an estimate of the dynamic axle loads of the train. The difference between V_1 and V_2 is as estimate of the rail seat load when the axle load is acting outside the segment of the rail between sections 1 and 2. As estimate of the rail seat load (R_{strain}) can be obtained by adding the two above results, after applying an offset corresponding to the time the axle takes to travel between two consecutive sections: $R_{strain} = (V_2-V_3)+(V_1-V_2)$. This calculation procedure assumes that the dynamic axle load has the same amplitude from sections 1 to 3.

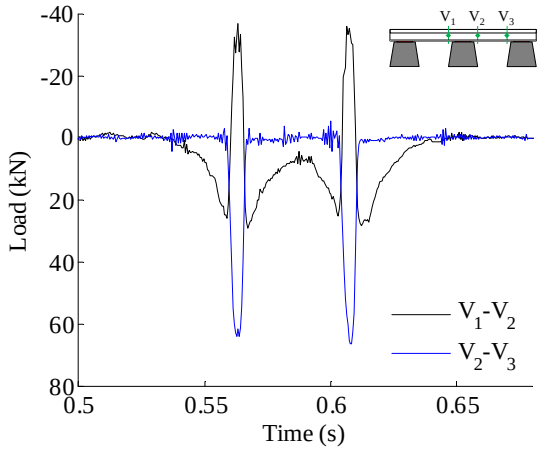

Figure 5-53. Differences in shear forces between sections 1 and 2.

Figure 5-54 shows an example of the dynamic wheel loads of the passenger train, measured at the end of the transition zone, at about *x*=26.4 m from the abutment backwall (Figure 5-49). In Figure 5-54, it is visible that the peak loads are in agreement with the vehicle's static axle loads.

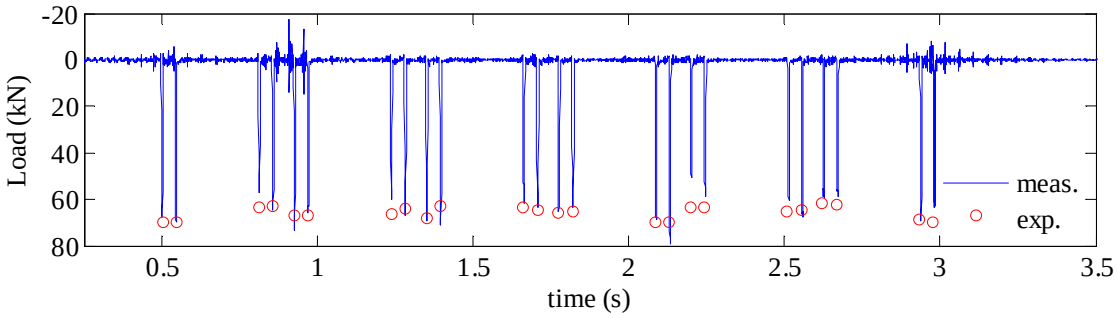

Figure 5-54. Measured dynamic wheel loads of the *Alfa Pendular* and expected values.

In modern railway tracks with adequate bearing conditions and considering the track characteristics (particularly the rail cross section, sleeper spacing and the stiffness of the components), it is expected a maximum rail seat load of about 40% of the axle load (Selig & Waters, 1994; Lundqvist & Dahlberg, 2005; Alves Ribeiro, 2012). In the example presented in Figure 5-55, the maximum load transferred to each rail pad - calculated using both the data obtained with the strain gauges and the rail pad fibre optic sensors - was about 50% of the 1st wheel load (139/2=69.5 kN). This result is higher than what was expected, which may suggest a stiff track structure.

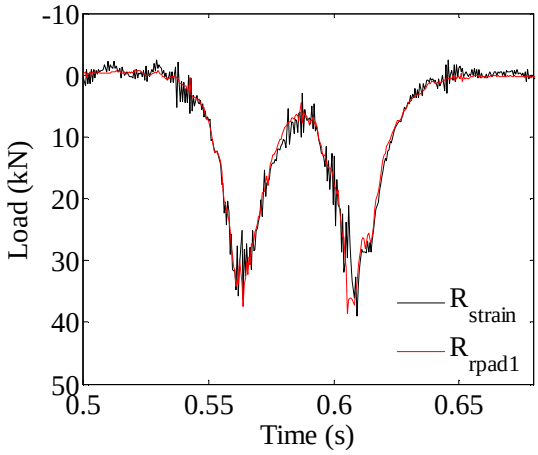

Figure 5-55. Vertical loads transferred to the rail pad, calculated using the strain gauges (R_{strain}) and the rail pad load sensor (R_{rpad1}).

Table 5-8 summarises the measured peak vertical displacements of the rail under each axle, obtained with the LASER-PSD system, in terms of average values, 25th and 75th percentiles (Q1 and Q3). The results regard the validated data from 8 trains with 24 axles each.

Table 5-8. Summary of peak vertical displacements of the rail (mm).

Position / x (m)	Q1	Average	Q3
1 - Emb. / 41.1	0.69	0.77	0.84
2 - UGM / 14.7	0.68	0.76	0.82
3 - UGM / 6.9	0.66	0.72	0.78
4 - CBM / 0.9	0.58	0.64	0.71

The results suggest that the track stiffness increases as approaching the bridge. For example, the average value of the vertical displacements on the embankment was 20% higher than on the CBM. This stiffness variation is less evident when comparing the average values obtained on the embankment with those on the UGM. However, the values of Q1 and Q2 do evidence a trend of stiffness increase from the embankment to the UGM and to the CBM. The increase of the track stiffness at the approach to structures has also been reported in other field studies (Cuéllar *et al.*, 2009; Tijera *et al.*, 2012; Pinto *et al.*, 2013) and at the approach to the underpass UP2 discussed in section 5.2.3 (the transition without USP). However, in that case, the amplitude of the displacements was somewhat lower, particularly on the CBM. At the approach to the bridge the displacements ranged between about 0.77 on the embankment to about 0.64 mm on the CBM, while at UP2, the average values decreased from 0.75 mm to about 0.36 mm,

thus denoting a steeper transition in vertical stiffness. The construction of both transition zones followed the same specifications. The main difference is that the transition to the bridge comprised a backfill that was almost three times higher as that of UP2. However, this aspect does not seem to justify the differences because the average displacements on the embankment were quite similar on both transitions (0.77 mm and 0.75 mm). Analysing Figure 5-51, it seems that the sleeper adjacent to section 4 (where rail displacements were measured, see also Figure 5-49) is experiencing higher deflections under the LFWD, suggesting that the sleepers may have poorer support conditions and the track has higher vertical flexibility in that area. This is a plausible explanation for the higher displacements measured on the CBM in that transition compared with the measurement at underpass UP2.

The variability of the measurements at each position resulted from different factors: i) each axle has different static loads (up to ±8 kN of the average axle load; see Figure 5-15); ii) each train had different passenger occupancy (the trains have a maximum of 62 seats per coach, which can add up to 10 kN to each axle); iii) the random nature of the dynamic response of the system for high frequencies induces additional train-track interaction forces due to the irregularities of the track and the wheel.

The results obtained with the 19 accelerometers on the sleepers (Figure 5-49) did not evidence any abnormal track response and were in the same range of measurements obtained in the transition to UP1 (section 5.2.3). Figure 5-56 shows the median values of the maximum and minimum peak vertical accelerations, for each of the passing axles. These values were calculated after applying a type II Chebyshev filter with cut-off frequency of 80Hz to the time history records. The filter aimed at minimizing the influence of the random nature of the dynamic response of the track for high frequencies that results from the irregularities of the track and wheels. It also makes it easier to analyse time history records.

It is interesting to note that the higher variations in peak values between consecutive sensors occur near the interface backfill-abutment (x = 0 m) and the joint with the deck (x = -2.4 m). The beliefs are that this behaviour is related to the sudden changes in track support conditions in those sections.

The median value of the peak vertical rail-sleeper relative displacements - an estimate of the vertical rail pad deformation - was about 0.15 mm, after applying the cut-off filter. Figure 5-57 shows a comparison between filtered and non-filtered vertical rail-sleeper relative displacements.

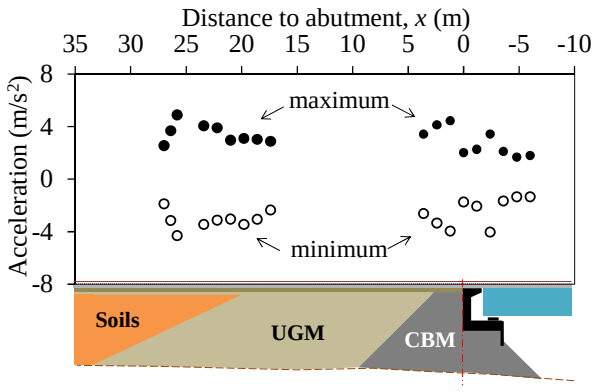

Figure 5-56. Median values of the peak vertical accelerations of the sleepers (f<80Hz).

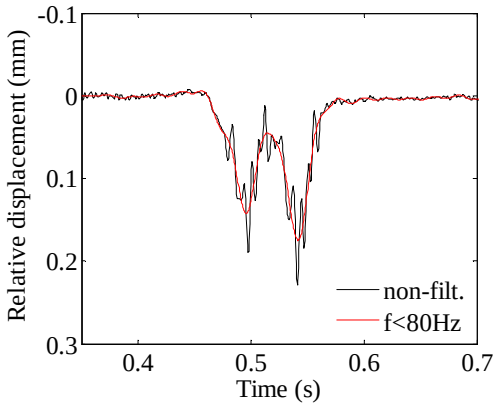

Figure 5-57. Vertical rail-sleeper relative displacements.

In general, the track measurements were in agreement with those obtained in the previous case study of underpass without USP.

5.3.4 Description of the model

To investigate the dynamic behaviour of the train-track system at the transition zone to the bridge, the numerical technique of section 5.2.4 was also applied in this case study. Again, the model was developed with ANSYS® software using an element mesh as close as was deemed necessary to adequately reproduce the behaviour and geometry of this problem (Figure 5-58). This model is based on the earlier underpass models and was modified to comprise 57 m of the track on earthworks (which includes the wedge-shaped backfill), the abutment and six 37.5 m-long spans of the southern part of the bridge. It is made of a total of 31,566 nodes and 37,605 elements. The representation of the track superstructure is rather identical to the model of UP2

of section 5.2.4 (see Figure 5-58b). Rail pads were considered to have vertical stiffness of k_{rp} =160 kN/mm and damping value of c_{rp} =17 kN.s/m. The sleepers, ballast, track substructure layers and the abutment were also modelled using 4-node plane-stress elements. The width of these elements was calibrated initially considering the new geometry of the transition using reduced 3D static models, following the same optimisation algorithm mentioned in section 5.2.4.

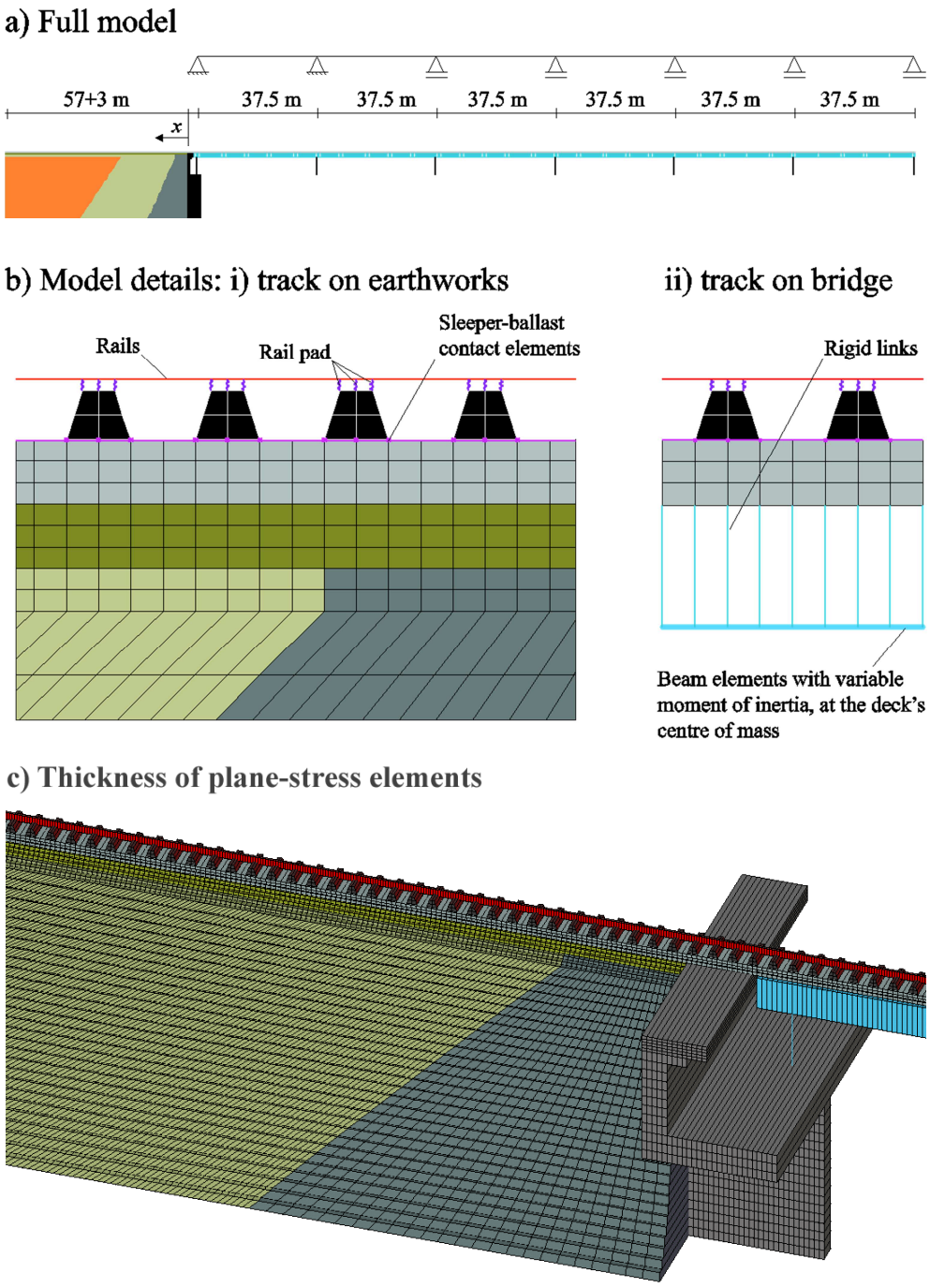

Figure 5-58. Model of the transition zone: a) complete view; b) details of the mesh; c) schematic representation considering the thickness values assigned to the plane-stress elements.

The bridge deck was modelled using a continuous beam made of 15 cm long elements, placed at the deck's centre of mass (Figure 5-58b). Different values of area and moment of inertia were assigned to these elements in order to reproduce the effect of bending and torsion of the deck on the track longitudinal alignment (the deck and the track alignments distance 2.15 m apart, see Figure 5-50). Vertical rigid links were established between the bottom nodes of the ballast layer and the nodes of the deck beam (Figure 5-58b), and between the deck beams and the bridge bearings. Viscous boundary conditions were considered to minimise the effect of wave reflections, following the works by White *et al.* (1977).

Considering the length of the spans (37.5 m), it was necessary to investigate the possible vertical excitation of the carbodies as the train passed over the successive spans of the bridge. The respective excitation frequency (f) can be estimated using the simple expression $= v/\lambda$, where v is the vehicle speed of 220 km/h (61.1 m/s), and λ the wavelength of the excitation – the span of 37.5 m – thus yielding about f=1.63 Hz. The frequency of the vertical rigid body vibration mode of the car body can be estimated as the undamped natural frequency of a 1DOF (degree-of-freedom) mass-spring system, using:

$$f = \frac{1}{2\pi}\sqrt{\frac{2\times 4\times K_s}{M_c}} = 1.19 \text{ Hz} \tag{5-6}$$

Where K_s is the stiffness of each spring of the vehicle's secondary suspension in N/m (4 spring in each bogie – see Figure 5-59), of about 256.4 kN/m, and M_c is the car body mass, of about 36 901 kg. This frequency estimate is somewhat in agreement with the findings of the experimental calibrations of a three-dimensional numerical model of the *Alfa Pendular* carried out by Ribeiro (2012). The author showed that the first frequencies of the rigid body vibration modes of the car body ranged between 1.01 Hz and 1.59 Hz. In particular, the frequencies of the vertical and pitching vibration modes were 1.33 Hz and 1.59 Hz, respectively, which are the most relevant vibration frequencies for the study presented here. It can be verified that these frequencies are very close to the value of the excitation frequency when the train runs at about 220 km/h on the bridge (1.63 Hz). Thus, to account for the possible influence of the bending of the deck on the vehicle's motion and to assess the accelerations inside the coach cars, it was decided to model the passenger train as a set of 6 coaches, as depicted in Figure 5-59. The car bodies and bogie frames were considered as rigid bodies.

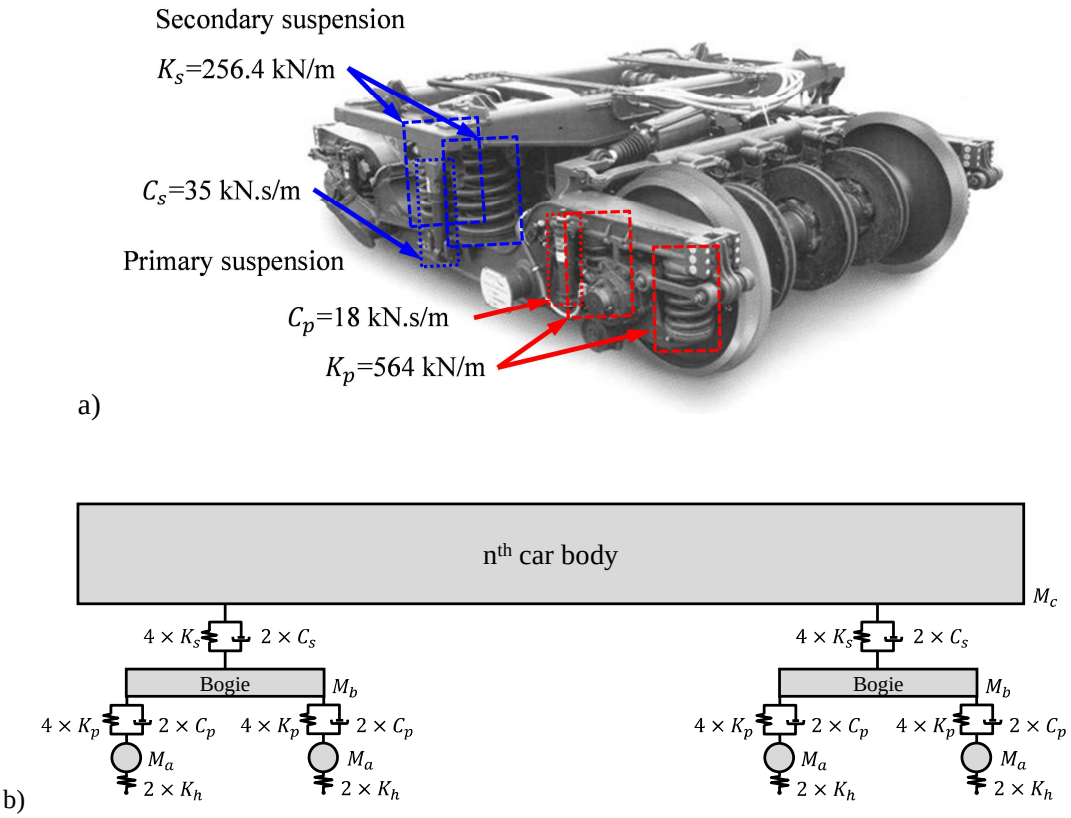

Figure 5-59. Aspects of the vehicle model: a) identification of the components of the primary and secondary suspensions; b) model of one of the 6 coaches (see parameters in Table 5-9).

Table 5-9. Characteristics of the coach model (see Figure 5-59) (adapted from Alves Ribeiro, 2012; Ribeiro *et al.*, 2013).

Parameter	**Value**
Car body mass, M_c	36901 kg
Secondary suspension stiffness, K_s	256.4 kN/m
Secondary suspension damping, C_s	35 kN.s/m
Bogie mass (without axles), M_b	4932 kg
Primary suspension stiffness, K_p	564 kN/m
Primary suspension damping, C_p	18 kN.s/m
Axle mass, M_a	1800 kg
Hertzian wheel-rail contact spring stiffness, K_h	1.24×10^6 kN/m

The wheel-rail interaction was also modelled as a node-to-beam contact allowing for sliding and loss of contact, using the Penalty algorithm. Contact elements were considered in the sleeper-ballast interface to account for the possible separation of these track elements. This is one of the

main differences from the models used in the previous section. The full Newton-Raphson method was also used to solve the non-linear equations of the problem. The Newmark implicit time integration method was used, with time steps of 0.001 sec, to solve the transient dynamic equilibrium equations.

Given the very good quality of the track geometry, a perfectly horizontal profile was considered in the model.

5.3.5 Model calibration

In the previous section, it was possible to calibrate some properties of the track elements and of the backfill layers. Because the construction process and the materials used in this transition zone are essentially the same, those calibrated parameters were also used in this case (see Table 5-4).

Regarding the moments of inertia of the various beam elements that comprise the different spans of the bridge, initial estimates of these parameters were calculated considering the drawings of the bridge design (REFER, 2006) and the results of load testing prior to opening (Santos *et al.*, 2010). As mentioned earlier, because the deck and the track were not aligned vertically (Figure 5-50), the 2D beam model of the bridge could not account for the deck torsion. Thus, the moments of inertia were then calibrated in order to minimise differences between the numerical model and the field measurements. The vertical stiffness of the bearings of the bridge on the abutment was also calibrated with *in situ* measurements. Figure 5-60 compares the numerical displacements of the rail with those obtained with the LASER-PSD system, aimed at position x = -4.5 m (track on the bridge). Despite the limitations of the bridge model, it is visible that the agreement between the results is very good.

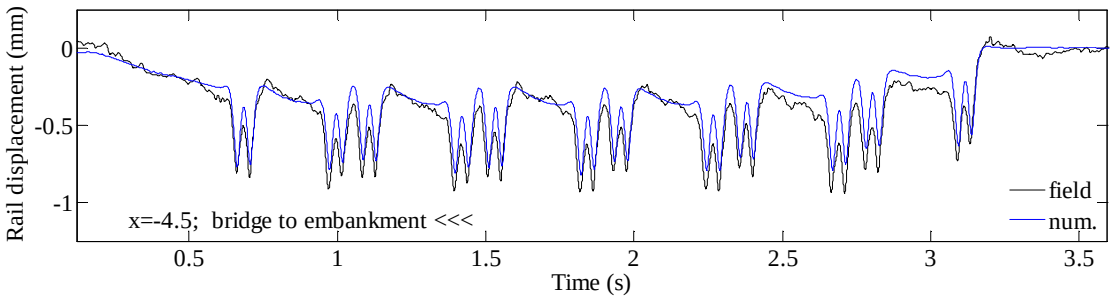

Figure 5-60. Rail displacements at position 5 (x = -4.5 m), on the bridge.

5.3.6 Validation with experimental measurements

To validate the model, some numerical results were compared with field measurements. The results demonstrate a very good overall agreement. As explained earlier, a type II Chebyshev filter with cut-off frequency of 80Hz was applied to field and numerical time history records presented in this section. Figures 5-61 to 5-63 compare the obtained numerical vertical rail displacements with *in situ* measurements at positions 1, 2 and 4 (Figure 5-49), for both train directions. Results at position 3 were similar to those of position 2, therefore not presented here. In general, it was possible to verify a good agreement between the results. The analysis of the numerical results showed a gradual stiffness increment as approaching the bridge.

The numerical results of the rail-sleeper relative displacements and the load transferred to the rail pad also showed an overall good agreement with the field measurements, as exemplified in Figure 5-64 and Figure 5-65, respectively.

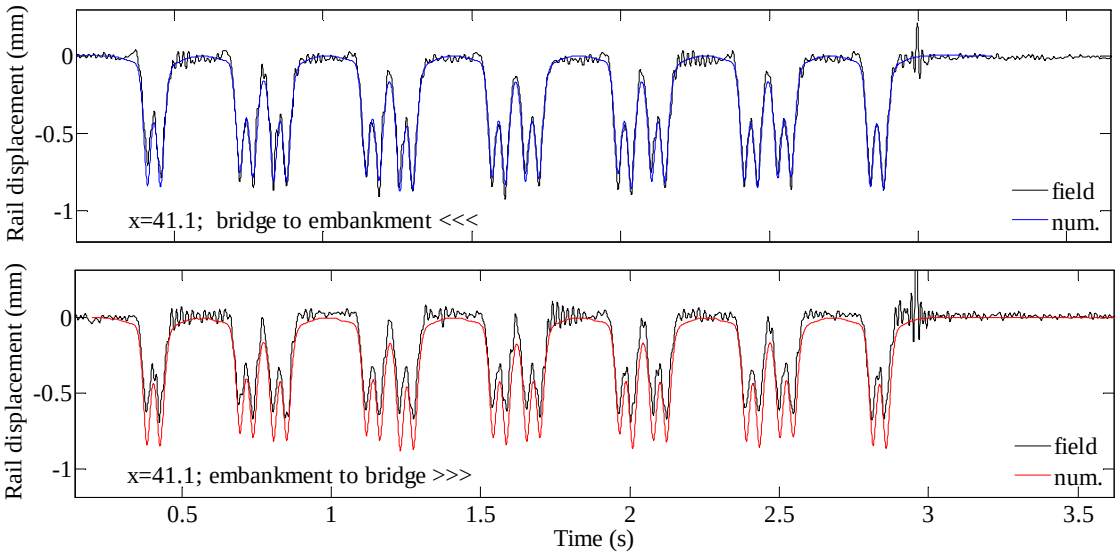

Figure 5-61. Rail displacements at position 1 (x = 41.1 m), in plain track.

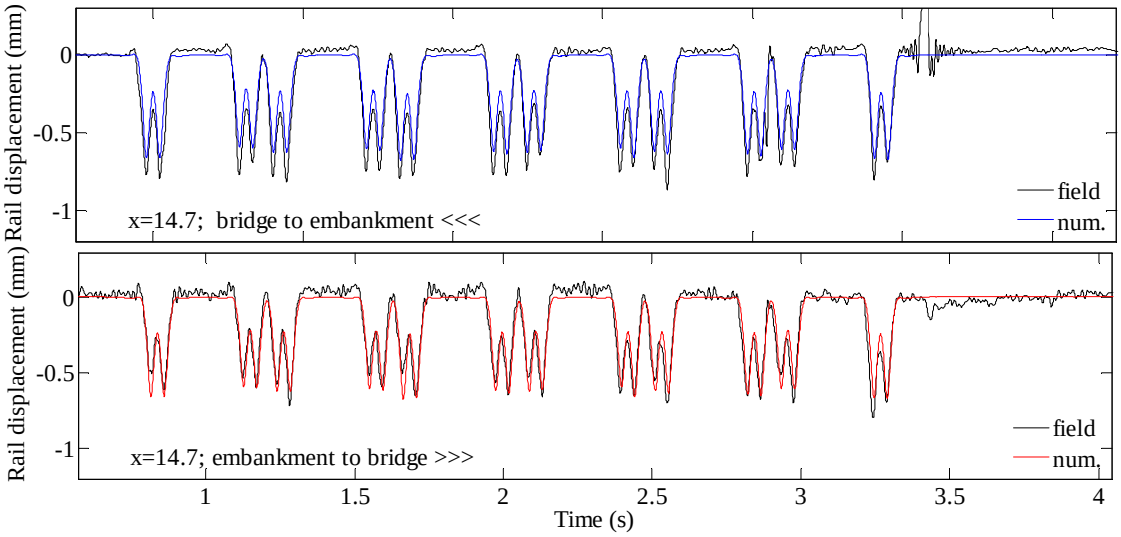

Figure 5-62. Rail displacements at position 2 (x = 14.7 m), on the UGM.

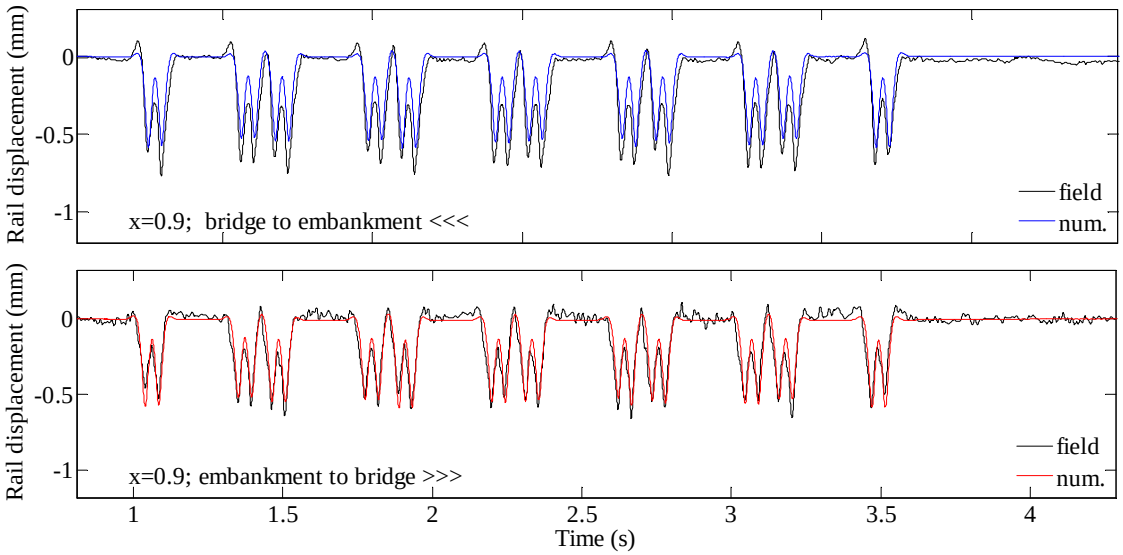

Figure 5-63. Rail displacements at position 4 (x = 0.9 m), on the CBM.

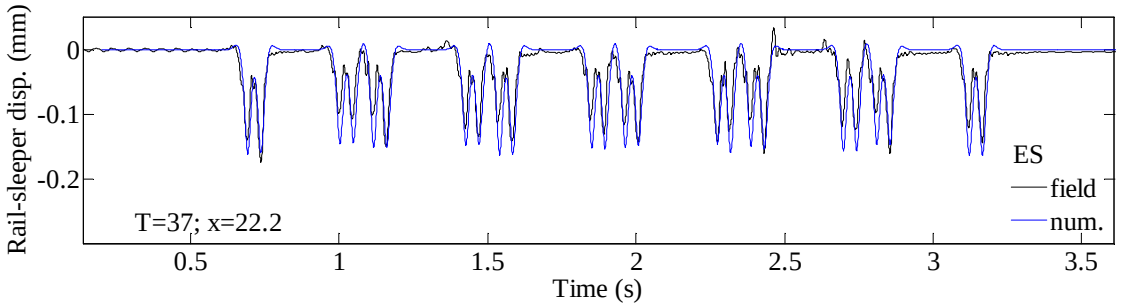

Figure 5-64. Rail-sleeper relative displacements at x = 22.2 m.

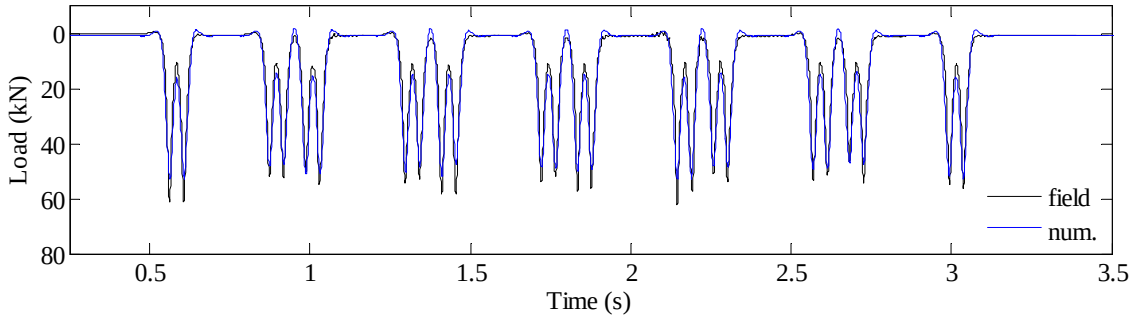

Figure 5-65. Vertical loads transferred to the rail pads at x = 26.4 m.

Regarding the vertical acceleration of the sleepers, a good agreement was also observed, as depicted in Figure 5-66. However, the positive peak accelerations of the numerical model were somewhat overestimated. For example, in average, maximum peak accelerations at x=18.6 m were 59% higher, while at x=26.4 m were only 18% higher. This aspect may be related to the introduction of the sleeper-ballast contact interface and to fact that in the numerical model there was no ballast between the sleepers, thus reducing the stability of the sleepers due to fewer constraints to motion.

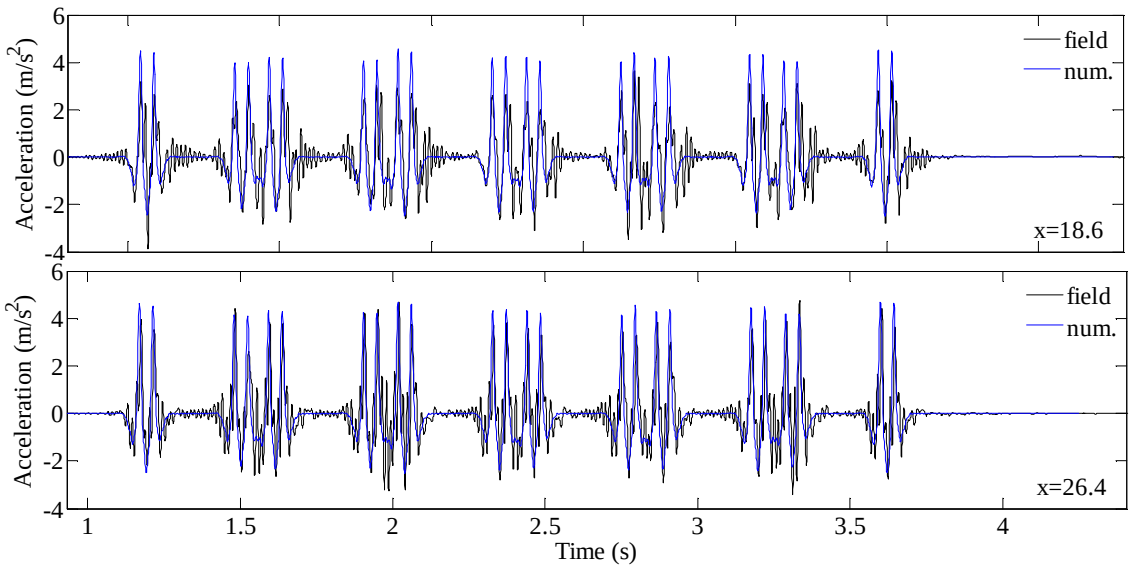

Figure 5-66. Vertical sleeper accelerations at x =18.6 m and x =26.4 m.

5.3.7 Simulation analysis of train-track interaction

After validating the model, it was possible to analyse relevant aspects of the transition zone behaviour, such as the train-track interaction forces and the vertical displacements of the wheelsets along the transition zone, as depicted in Figure 5-67. The results regard the first axle, for both train directions. The results of the remaining axles were analogous.

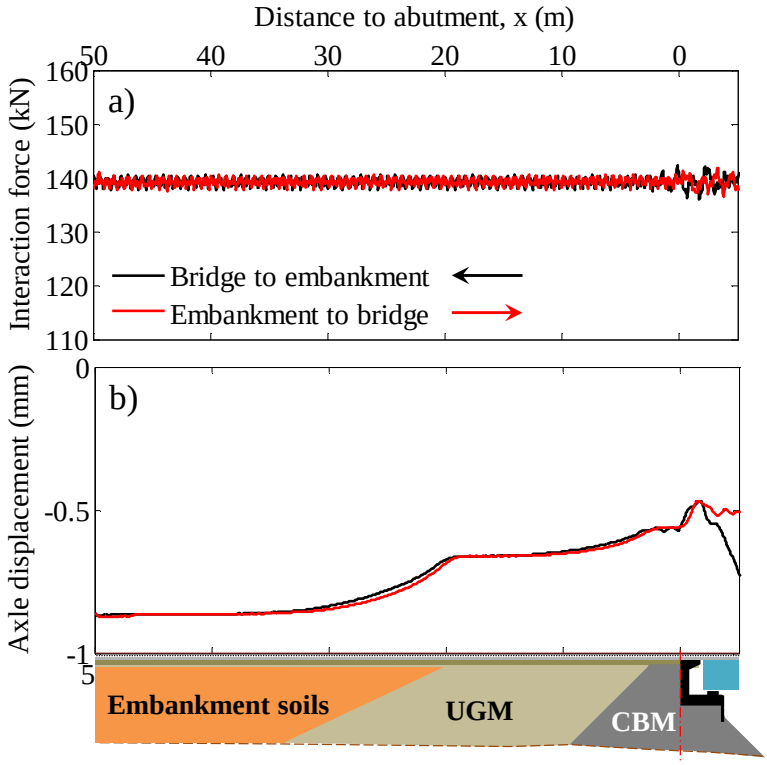

Figure 5-67. Numerical train-track interaction forces (a) and vertical axle displacements (b).

As regards the vertical displacements, some variations can be observed that are caused by the changes in the track vertical stiffness, similarly to what was observed in the underpass case without USP. It is the wedge-shaped backfill that increases the track stiffness at the approach, which is particularly visible at the transition from the embankment to the UGM ($45 > x > 20$ m) and from the UGM to the CBM ($10 > x > 3$ m). A more rapid stiffness variation is visible from the backfill to the abutment (x = 0 m). Regarding the train-track interaction forces (Figure 5-67a), they oscillate with a small amplitude (about ±3 kN), and remain very close to the train's static load of the 1st axle of 139.2 kN. This shows that, given this train speed and the very good geometric quality of the track, the train undergoes a smooth ride along the transition zone.

However, slight disturbances can be observed on the abutment and on the bridge that are related to the sudden changes in the track support conditions in that stretch.

Later tests considering the *Alfa Pendular* train model with the bogies only (without car body and secondary suspension, similarly to what was performed in section 5.2) showed that it yields almost identical results as considering the vehicle model with the carbodies. This result is probably a consequence of the high bending stiffness of the deck in that it produces minimal vertical excitation of the carbodies as the vehicles pass over successive spans of the bridge. Therefore, it seems acceptable to consider only one bogie, travelling in one direction only, to study transition zones to bridges that do not evidence excessive track deterioration. This conclusion is in agreement with those of sections 5.2. However, the same does not seem to apply for scenarios with uneven rail profiles, as will be discussed in Chapter 6.

5.4 Concluding remarks

This Chapter aimed at using numerical models to provide insight into the dynamic behaviour of the train-track system at transition zones to two railway underpasses and a bridge that comprise backfills made of bound and unbound granular geomaterials. Considering that the track evidenced very good geometric quality, longitudinal level defect were not taken into account. Therefore, the focus of this chapter laid mainly on the influence of the variations in the vertical stiffness of the track. Extensive track measurements were performed, which were then used to calibrate and validate the numerical models. In addition, it was investigated the influence of under sleeper pads (USP) at transition zones.

Two case studies were analysed. Firstly, two similar railway underpasses, with good and comparable track foundation conditions, were studied. One of the underpasses comprised 44 sleepers with USP. The second case study addressed the transition zone to a bridge.

Initially, to characterise the track substructure and superstructure, non-destructive tests were performed during construction and after the track opened to traffic. An unconventional procedure using the light falling weight deflectometer (LFWD) test at the centre of the sleeper was found to be a very simple, straightforward and effective procedure to swiftly assess track support conditions, such USP or poorly supported sleepers at the joint with the deck. Results indicate that an experienced operator can obtain good testing repeatability for a number of drops at the same sleeper. The receptance tests on the rail, performed at different positions along the

transition zones, allowed assessing the dynamic flexibility of the track for different support conditions, including the influence of USP. The results of these tests were very valuable for the calibration of some dynamic parameters of the materials in the numerical models.

For the experimental works, specific measuring systems were developed to assess the track dynamic response as the *Alfa Pendular* trains crossed the transition zones at speeds of about 220 km/h. The rail vertical displacements measured at different positions along the transition zones confirmed the existence of a smooth increase of track stiffness at the approach to underpasses and bridges, which is one of the objectives of the construction of backfills with high-performance bound and unbound granular materials.

The models accounted for all relevant track components and geomaterials of the supporting layers. Their mechanical parameters were calibrated using a fast procedure that included 3D and 2D reduced models and track receptance curves obtained in the field works. In general, a very good agreement was obtained between the numerical results and the field measurements at different sections along the transition zones under study.

The installation of sleepers with USP was planned to achieve a smooth stiffness transition, providing similar track flexibility at different sections of the transition zone. However, USP added excessive flexibility to the track, thus increasing stiffness unevenness and affecting its dynamic response. These findings highlight the need to carefully design USP for transition zones, not only with regard to its resilient properties but also to its geometry and arrangement along transition zones.

In the studied scenarios, it was found that the influence of the train's direction is not significant when variations of track support conditions are relatively smooth, either at the approach to a underpass or to a bridge. However, a small influence was observed when the train entered or exited track sections with USP at the transition to an underpass. A parametric study was carried out (in terms of the stiffness of USP and the number of sleepers with USP) in order to improve the design of that transition zone. The best solution that was found comprised sleepers with gradually increasing stiffer USP at different track sections of the transition zone.

Considering the characteristics of the *Alfa Pendular* passenger train and for speeds of about 220 km/h, it can be concluded that the design of the wedge-shaped backfill is adequate to minimise the negative effects resulting from the abrupt stiffness variations that are normally present at bridge approaches. Given the characteristics of the backfill materials, it can be expected an adequate performance of the transition zone in the long-term. These conclusions only apply if

the dynamic component of the train-track interaction force does not increase significantly over the following years. This problem could be triggered by the development of differential settlements at the backfill, thus causing defects in track longitudinal profile. Due to the high degree of complexity of the train-track system at transition zones, more studies are required to properly assess the long-term behaviour of the studied transition zone.

Chapter 6

Numerical simulations of transition zones with uneven rail profiles*

6.1 Introduction

In this Chapter it is investigated the effect of the differential settlements on the dynamic response of the train-track system at the approach to structures. These problems cause uneven longitudinal level of the rails that induce amplifications of the dynamic response of the system and contribute to increase degradation rates of the track. This type of track defect is commonly designated as "bump" or "dip" profiles at the approach to bridges, viaducts, tunnels and other structures (Nicks, 2009). Earlier studies report that more research is required on the effect of differential settlements at transition zones because this issue seems to be more critical than the influence of stiffness variation (Schooleman, 1996; ERRI, 1999). Moreover, recent studies show that a smooth stiffness variation can be achieved using resilient elements of the track superstructure with optimised elastic properties (Costa D'Aguiar *et al.*, 2013) – and also discussed in Chapter 5 – and/or with an adequate design of the backfill (see Chapter 4). On the other hand, solutions to overcome the problems encountered with differential settlements at transition zones do not seem to be efficient, they are extremely expensive and disrupt the normal operation of the tracks.

---

* Part of this chapter is based on the following manuscripts:
- **Paixão, A.; Fortunato, E. & Calçada, R.** (2014) *Numerical study on the influence of backfill settlements in the train-track interaction at transition zones to railway bridges (in review)*;
- **Paixão, A.; Fortunato, E. & Calçada, R.** (2014) *The effect of differential settlements on the dynamic response of the train-track system: a numerical study (in review).*

Although there have been many numerical studies addressing the influence of the vertical stiffness at transition zones, only a few authors have focused on the influence of the settlement profile of the backfill, and some of them used very simple numerical models, as discussed in Chapter 3. In order to address this gap, a numerical study is presented here using a model that is similar to that presented in section 5.3. It also takes into account: i) all the relevant components of the track, bridge and backfill; ii) the train model with primary and secondary suspensions; iii) the train-track interaction using contact algorithms at the wheel-rail interface; iv) a previous calibration and validation procedure that used extensive field measurements.

Different settlement profiles were introduced in the numerical model to assess the influence of the shape and amplitude of the profiles, aiming at providing greater insight in the dynamic behaviour of the train-track system at transition zones with different settlement scenarios.

After a brief description of the model, two parametric studies are presented here firstly focusing on the influence of the shape of bump profiles, and then on dip profiles. The first study considers hypothetical settlement profiles at the backfill, while the second was derived from a pronounced settlement profile found at the approach to a viaduct in the *Alcácer* bypass. In this case, vertical accelerations measured inside the coach cars are compared with the numerical results. Finally, considering the impact of differential settlements in the amplification of the train-track response at transition zones, a more comprehensive parametric study is presented to establish performance indicators that can be useful for Railway Infrastructure Managers.

6.2 Description of the numerical model

This numerical model was also developed in ANSYS and it is mainly identical to that of section 5.3. It comprises a track stretch of about 57 m on the embankment (on the backfill of the bridge's abutment) and a stretch of approximately 115.5 m on the bridge (on the abutment and on the deck), as illustrated in Figure 6-1a. The main differences between this model and that of Chapter 5 are that uneven rail profiles were introduced and that the number of spans of the bridge was reduced to only three. The reduction of the number of spans was justified because this analysis focused mainly on the trains running from the embankment to the bridge. Moreover, in the previous Chapter, it was found that the passage of the train over the successive spans of the bridge only had a slight influence on the vertical excitation of the carbodies.

Apart from that, the model considered the same geometry, materials, mechanical properties and boundary conditions as those described in section 5.3 and in Table 5-6. It also included train-

track interaction using contact elements and sleeper-ballast contact interfaces to allow for the development of hanging sleepers. The train model includes primary and secondary suspensions; the bogie frames and carbodies are considered as rigid bodies, with the characteristics described earlier in Figure 5-57 and in Table 5-9.

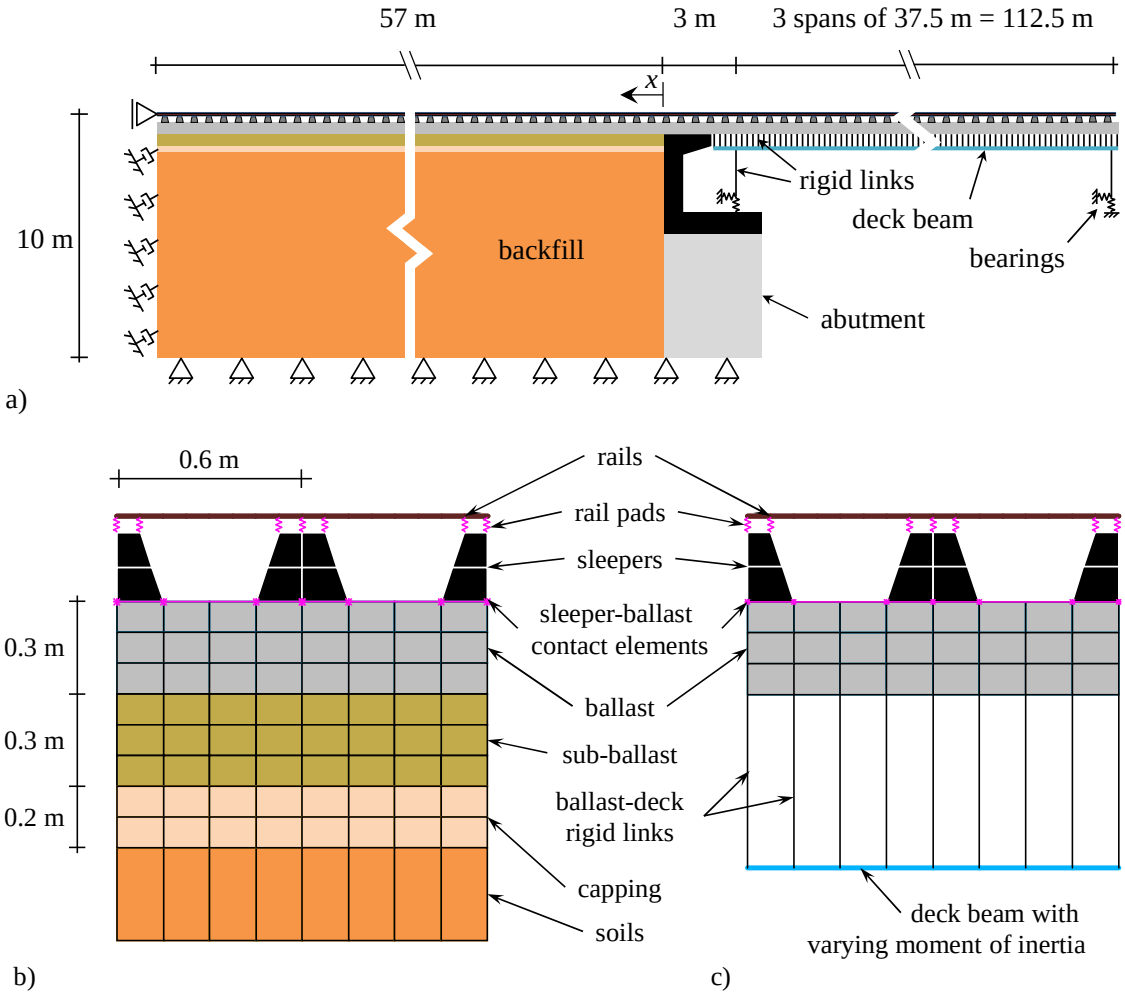

Figure 6-1. Schematic representation of the numerical model (a), and detailed aspects of the track on the backfill (b) and on the bridge (c).

6.3 Influence of the bump settlement profiles on the train-track interaction

6.3.1 Preliminary simulations with uniform settlement of the backfill

In an attempt to simulate scenarios in which settlements occurred in the backfill, at the substructure level, the mesh of the model was modified to reproduce those conditions. Four hypothetical scenarios of uniform settlement of the backfill were studied, considering maximum settlement values of δ_{max} = 1, 5, 10 and 15 mm in each case (Figure 6-2). To that aim, the top nodes of the ballast layer, on the backfill section, were moved downwards, according to those values, as depicted in Figure 6-2b. In the initial time steps of the calculation, the rails, sleepers and rail pads on the backfill settled on top of the ballast surface due to the gravity force applied to those track components. Shortly after, a new equilibrium was established, resulting in an uneven longitudinal rail profile.

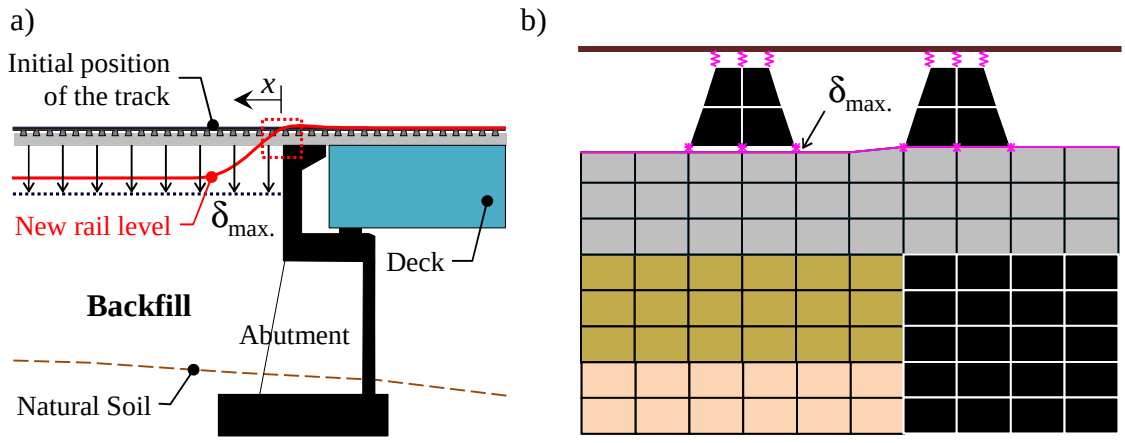

Figure 6-2. Backfill settlements: a) schematic representation; b) detail of the top nodes of the ballast layer moved downwards by δ_{max}.

As expected, due to the bending stiffness of the rails and the uneven surface of the ballast that was created, some of the sleepers on the backfill (those closer to the abutment) were hanging from the rails. This aspect represents a track malfunction that is frequently reported by railway infrastructure managers at transition zones and is considered to induce severe track degradation (Zhang *et al.*, 2008; Zhu *et al.*, 2011; Luomala & Nurmikolu, 2012; Shi *et al.*, 2013).

Figure 6-3 shows the comparison between the vertical displacements of the first axle along the transition zone, obtained for different settlement values, δ_{max}: 0, 1, 5, 10 and 15 mm. The results regard trains running from the embankment to the bridge only.

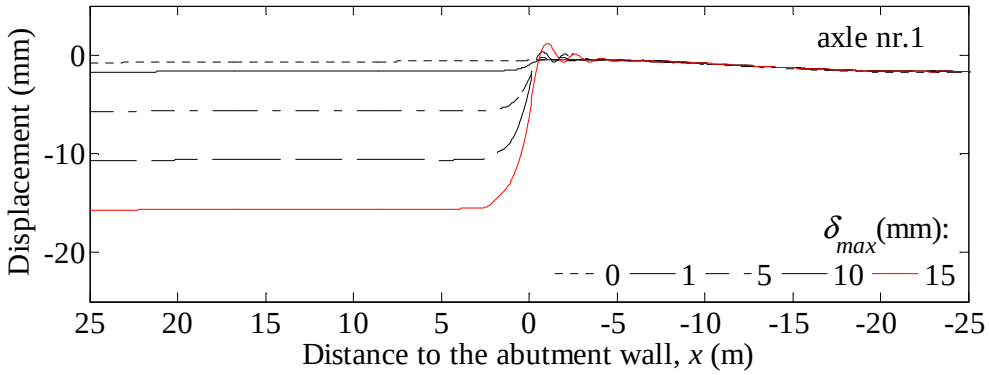

Figure 6-3. Vertical displacements of the first axle along the transition zone due to diffferent settlement values.

Although the settlements were introduced in the track section on the backfill, up to the abutment's backwall (at x = 0 m), it can be observed that the train's axle starts an upward movement a few meters prior to that position. This aspect is related to the existence of hanging sleepers in that location. Some of the hanging sleepers applied short impulse loads on the ballast when the axles passed over them, while others were never in contact with the ballast.

Figure 6-4, presents examples of the rail displacements at x = 0.9 m, which correspond to a position between two hanging sleepers on the backfill. The results show that the amplitude of the displacements increases with δ_{max}, indicating a growing track instability.

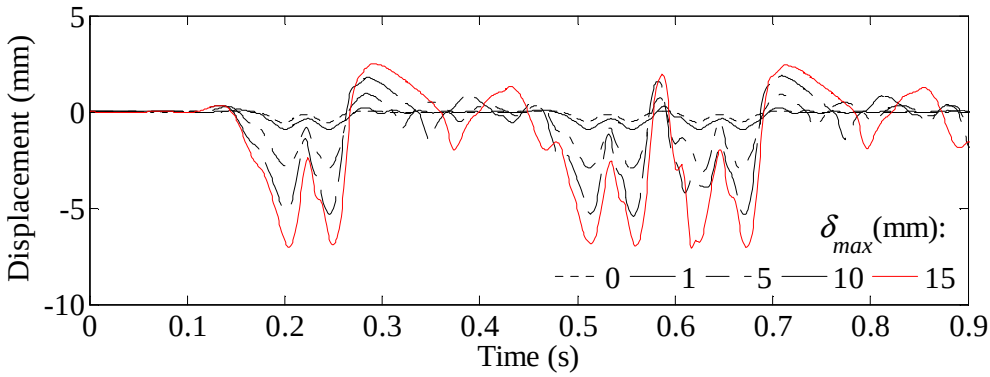

Figure 6-4. Vertical displacements of the rail at x = 0.9 m, due to the first six axles of the train.

Figure 6-5 evidences the severity caused by the uneven rail profiles, in terms of the train-track interaction forces obtained with the contact elements of the first axle, in the normal direction,

with respect to the rail alignment. While no significant variation of this parameter was expected in very good track conditions, the dynamic component of the train-track interaction reached very high values as settlements increased: up to about 1.6 times the static axle load value, with δ_{max} = 15 mm.

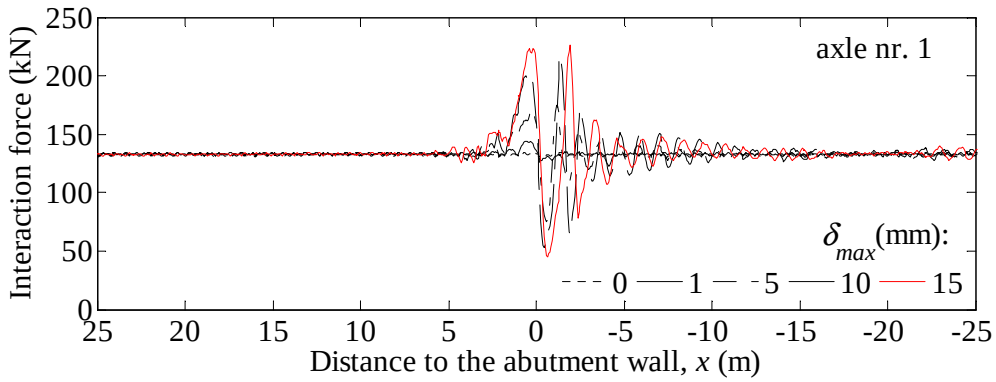

Figure 6-5. Influence of the settlement of the backfill on the train-track interaction force.

In numerical studies, Zhang et al. (2008) performed a parametric study on the effect of unsupported sleepers, considering different train speeds, the number of consecutive hanging sleepers and their gap sizes (distances between the bottom of the sleeper and the ballast layer). Considering gap sizes of 1 and 5 mm, they reported interaction force increments of about 10% and 52%, respectively, for a train speed of 220 km/h with an axle load of about 150 kN. Comparatively, in this study, the increments of the interaction force were about 8% and 31% for δ_{max} = 1 and 5 mm, respectively. The lower increments obtained here may be a consequence of the lower axle load of 132 kN. Moreover, while the study by Zhang et al. (2008) considered 6 consecutive hanging sleepers with the same gap size, the total number of hanging sleepers in this study was not constant (3 and 6 sleepers for δ_{max} = 1 and 5 mm, respectively) and the gap size decreased with the distance to the abutment, from slightly less than δ_{max} to almost 0 mm. Other numerical studies also reported the negative effect of hanging sleepers in the train-track interaction, showing results similar to those presented here (Lundqvist & Dahlberg, 2005; Zhu *et al.*, 2011).

With regards to the influence of the train's direction, Figure 6-6 shows axle displacements and train-track interaction forces along the transition zone for δ_{max} = 15 mm. In Figure 6-6a, some differences are perceived around 3 > *x* > -3 m. In terms of train-track normal interaction forces (Figure 6-6b), some differences were also observed, but the amplitudes of the dynamic component were of the same order. When the train exits the bridge, the peak values of the 1st axle occur on the backfill (at about *x* = 1.5 to 2 m from the abutment wall), with peak load

variations of +69% and -49%, regarding the static axle load of 132 kN. In the opposite direction, the axle induces two important peaks: one on the backfill section, immediately behind the abutment wall, and another one on the bridge, with load increments of +68% and +70%, respectively. The lowest peak value was also obtained when the train entered the bridge, denoted by a load reduction of -66%. Considering the conditions of the simulations, this direction seems to be the worst-case scenario in terms of both track degradation and loss of contact between the wheels and the rails. In the previous Chapter, it was found that with very good track conditions and without sharp variations of support conditions, the train's direction only had a minor influence over the results. That conclusion does not seem to apply in cases that present an uneven rail profile, as demonstrated here.

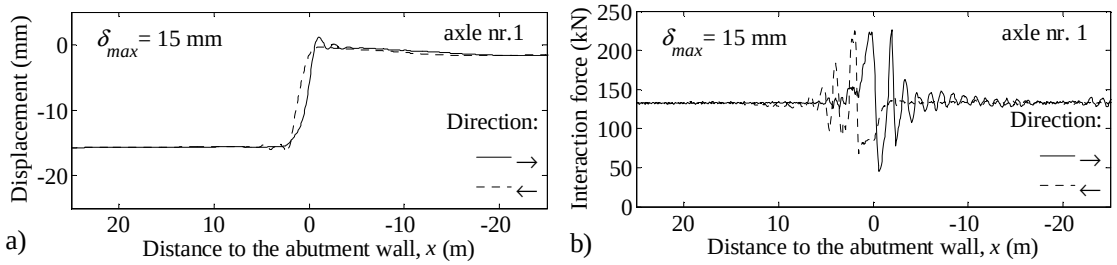

Figure 6-6. Influence of the train's direction in the: a) vertical axle displacements; b) train-track normal interaction force.

In the simulations presented in the subsequent sections, and taking into account the obtained results, the focus will be on the train's direction from the embankment to the bridge. The tested scenarios also seem to cause problems related to rail fatigue, but this aspect was thought to be outside the scope of this study.

To evidence the relevance of modelling the car bodies and secondary suspensions, vertical accelerations inside the car bodies were also analysed. Figure 6-7 presents vertical accelerations of the car body and normal forces transferred to the bogie, considering both train directions and for the case of δ_{max} = 15 mm. The peak vertical acceleration of the car body was about 0.86 m/s^2 and the maximum variation of the interaction force between the car body and each bogie was roughly 18 kN. The scenario of no settlements at the backfill produced negligible accelerations inside the car body. The results confirm that, when studying transition zones with uneven rail profiles, the consideration of the car body can induce relevant load variations on the bogies and, consequently, on the wheelsets and track. Thus, in these conditions, it seems inadequate to simplify the train model as independent bogies (without car bodies).

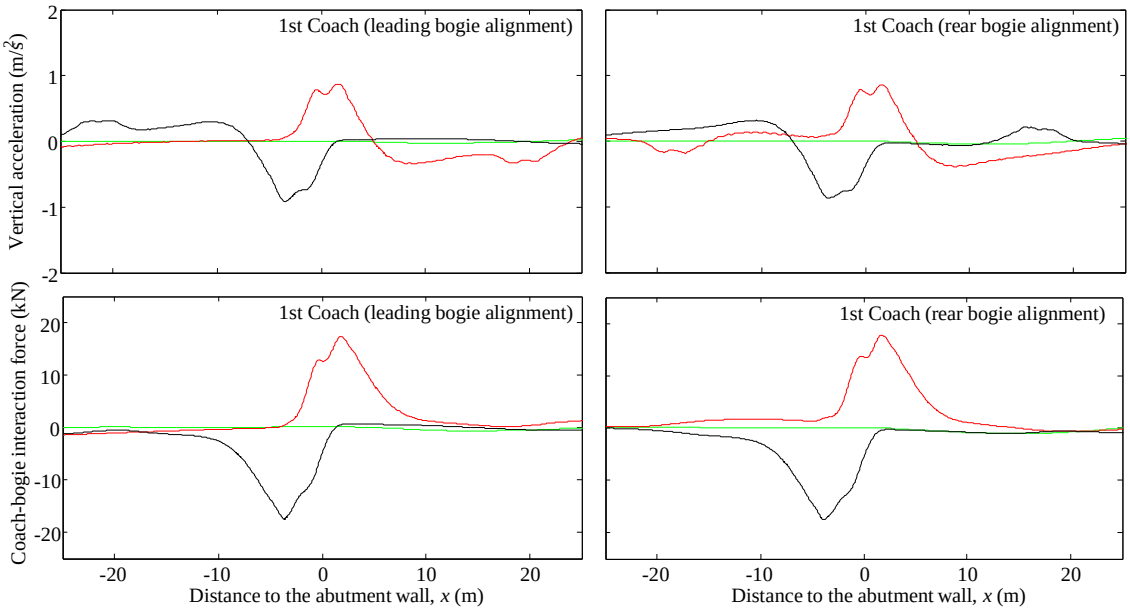

Figure 6-7. Vertical accelerations of the coach, a) and b), and vertical coach-bogie interaction forces, c) and d), obtained at the leading and rear bogies of the 1st coach, considering: no differential settlements (in green) and 15 mm settlement from trains running from the the abutment to the bridge (in red) or from the bridge to the abutment (in black).

The "Eurocode 0" (CEN, 2005) recommends threshold values for the vertical accelerations inside the car body, corresponding to different levels of passenger comfort, as described in Table 6-1, during travel on the approach to, passage over and departure from the bridge.

Table 6-1. Recommended levels of comfort (CEN, 2005).

Level of comfort	Acceleration limit inside the coach (m/s^2)
Very good	± 1
Good	± 1.3
Acceptable	± 2

The peak vertical accelerations obtained in the simulations were slightly below the limit denoting very good comfort. Nevertheless, the scenarios of uneven rail profiles induced important variations in the normal forces between the car body and bogies, and severe load variations at the wheel-rail interface, as mentioned above (Figure 6-6b). This emphasises that passenger trains are effective in assuring very good comfort level for this type of short-wave track defects, despite the severe impacts at the rail and track levels.

6.3.2 Simplification of the train model

Considering *in situ* measurements in Chapter 5 and the results presented here, it was evident that segments of time history records seem to be repeated at every pair of enclosed bogies. The effect of the enclosed second and third bogies is almost identical to the subsequent enclosed bogies. This is due to the very similar configuration and axle loads of the coach cars and to the considered mechanical properties of the railway track. Moreover, the train speed is not excessively high and well below the critical velocities.

It was found that, for the scenarios under study and considering that the axles have the same load value of approximately 132 kN (the average axle load of the train), it was sufficient to model a minimum number of 2 cars. To demonstrate this aspect, the previous scenario of a uniform settlement of 15 mm at the backfill is used as an example. Figure 6-8 shows that the vertical displacements and train-track interaction forces are practically the same for the 5th and 21st axles (the first axle of the 3rd and 11th bogies, respectively) obtained with the full train (6-car) and the 2-car models.

As a result, a replication procedure was used in the following simulations to reproduce the effect of the full train using a 2-car model, which allowed the reduction in the calculation times and computational effort. Figure 6-9 shows the replication procedure applied to the rail displacements obtained at a track section with hanging sleepers, close to the backwall (at x = 0.9 m). The same behaviour of the train-track system repeats itself for every pair of enclosed bogies (segments inside the dotted box in Figure 6-9). The simulated results (after replication) of a full train are practically the same as those obtained with the actual full train (6 cars).

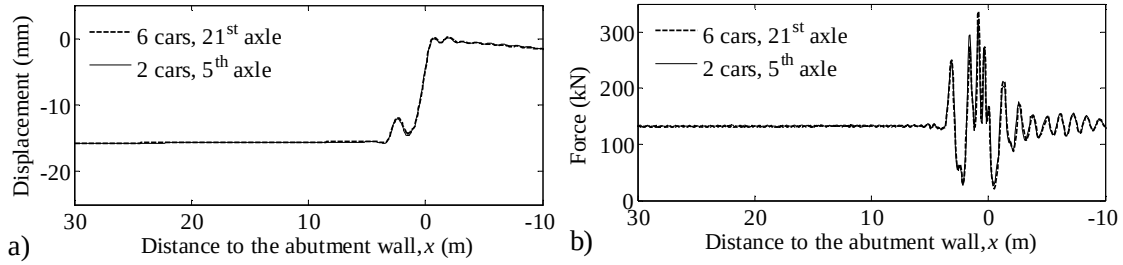

Figure 6-8. Vertical axle displacements (a) and train-track interaction forces (b) of the 5th and 21st axles of 6-car and 2-car models.

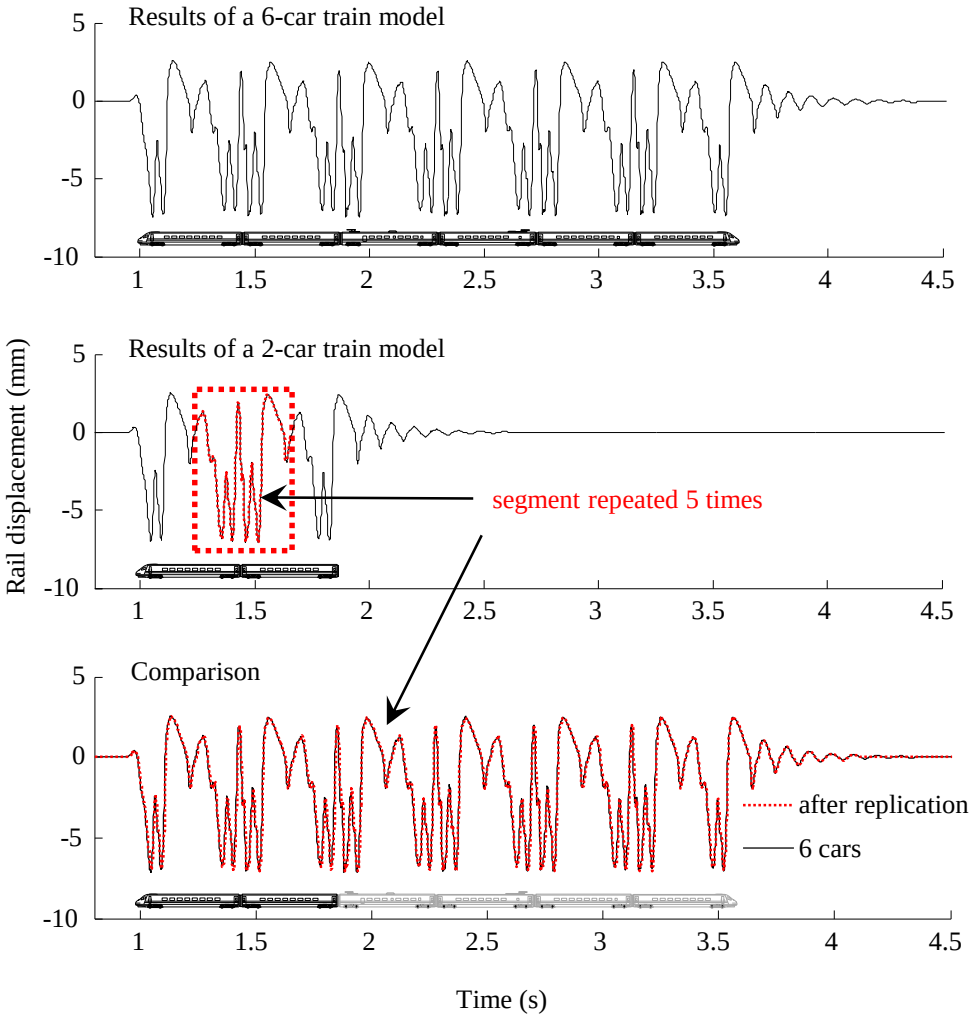

Figure 6-9. Replication of the results of a 2-car train model in order to simulate the effect of a full train.

6.3.3 Influence of different bump profiles at the backfill

Aiming at assessing the influence of different bump profiles on the levelling of the track and on the dynamic response of the train-track system, four shapes of hypothetical bump profiles were studied, as depicted in Figure 6-10:

a) U – uniform settlement of the track substructure along the approach;
b) W – settlement profile resulting from a wedge-shaped backfill using materials with improved mechanical properties (as discussed in Chapter 4): unbound granular material (UGM) and cement-bound mixture (CBM);
c) S – sharp settlement variation at the bridge approach;
d) G – gradual settlement variation at the bridge approach.

For each shape (U, W, S and G), four bump profiles were analysed corresponding to different maximum amplitudes of settlement, δ_{max}: 1, 5, 10 and 15 mm. The first profile shape, U, regards the scenarios presented earlier in section 6.3.1. The bump profiles were also applied to the top nodes of the ballast layer in the model (Figure 6-2).

The four profile shapes under study were determined in resemblance with profiles reported by railways infrastructures managers (ERRI, 1999; Nicks, 2009) and based on previous reports (Schooleman, 1996; England *et al.*, 2000; Kempfert & Stadel, 2000; Luomala & Nurmikolu, 2012; Abu-Farsakh & Chen, 2014).

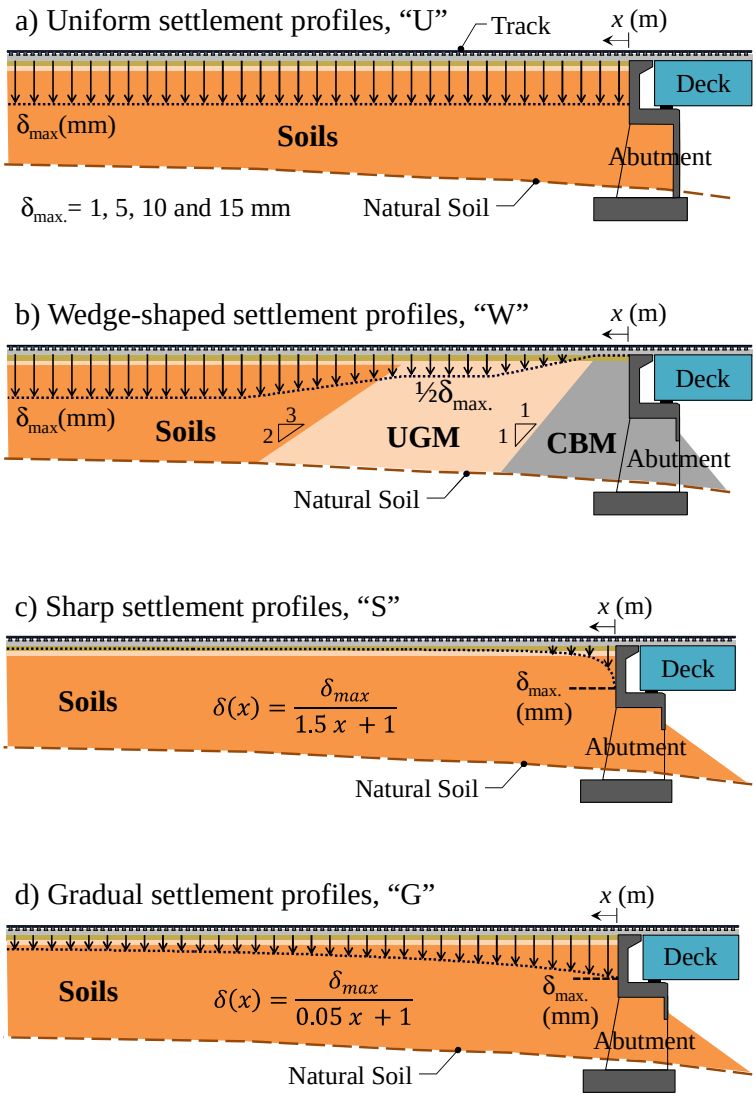

Figure 6-10. Schematic representation of the bump profile shapes U, W, S and G.

Figure 6-11 shows the bump profiles and the positions of the sleepers that resulted from the adjustment of the track to the respective bump profile in unloaded conditions (only gravity acting in the track frame). In the legend of the subsequent figures, the capital letters represent the profile shape (Figure 6-10), followed by the value of δ_{max}, in mm. As mentioned earlier, due to the bending stiffness of the rails, some sleepers were hanging from the rails with gaps under them. For each profile shape, the number of hanging sleepers increased with the value of δ_{max}. The position of the hanging sleepers is identified in Figure 6-12 with the respective size of the gap.

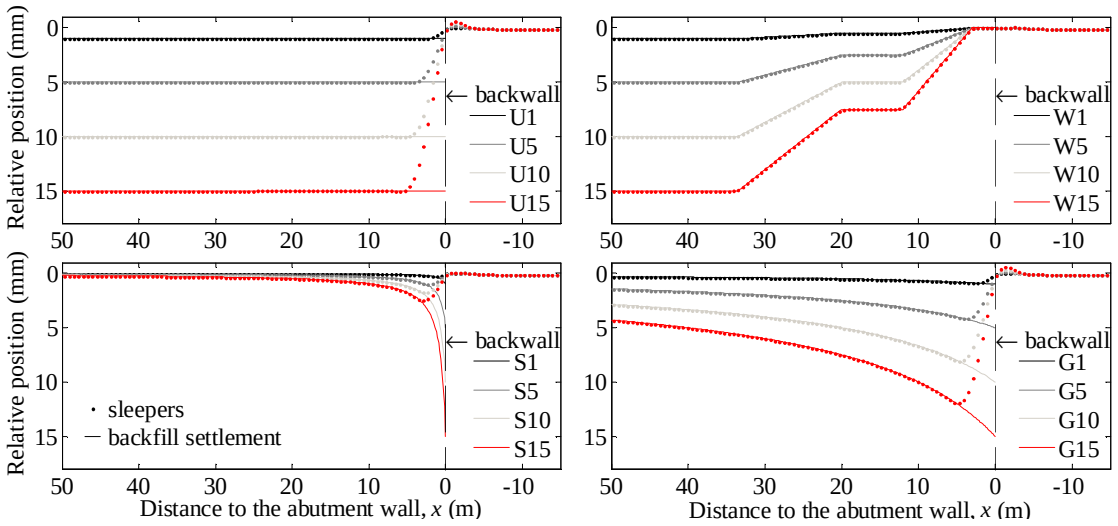

Figure 6-11. Backfill bump profiles and consequent positions of the sleeper.

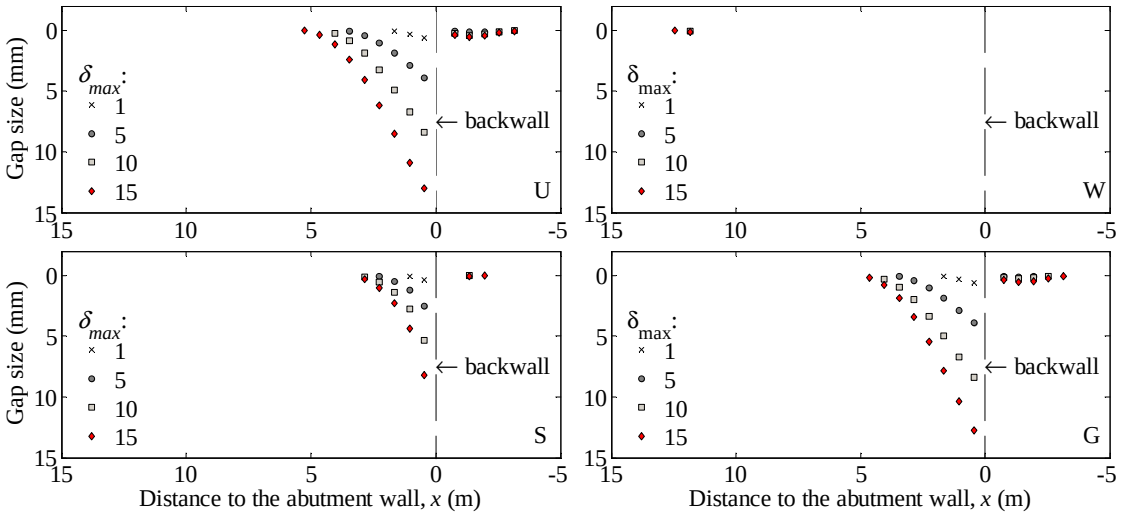

Figure 6-12. Location of hanging sleepers and respective gap sizes in unloaded conditions.

As expected, profile shapes U and G yielded the highest number of hanging sleepers and the largest gaps for each value of δ_{max}, for example: in shapes U and G, with δ_{max} = 15 mm, the results revealed 9 and 8 consecutive hanging sleepers, respectively, and maximum gap sizes of about 13 mm. It is visible that some of the profiles with shape W yielded very few hanging sleepers at about x = 12 m with almost insignificant gap sizes.

Figure 6-13 shows a comparison between the various rail profiles, in their unloaded position, and the vertical displacements of the 5th axle. In general, the 5th axle yielded the highest vertical displacements. In some cases, it underwent important oscillations near the abutment, indicating track instability due to the presence of hanging sleepers. Except for profile shape W, some of the hanging sleepers closer to the backfill did not establish contact with the ballast elements, when directly loaded by the axles. In some cases, an important uplift was visible on the track over the abutment, also yielding hanging sleepers. Profiles with shape S seemed to be less severe than profiles with shape G, because they create a track defect with shorter amplitude and length. Luomala & Nurmikolu (2012) measured comparable vertical displacement amplitudes on the sleepers at faulty transition zones, with similar train speeds and axle loads.

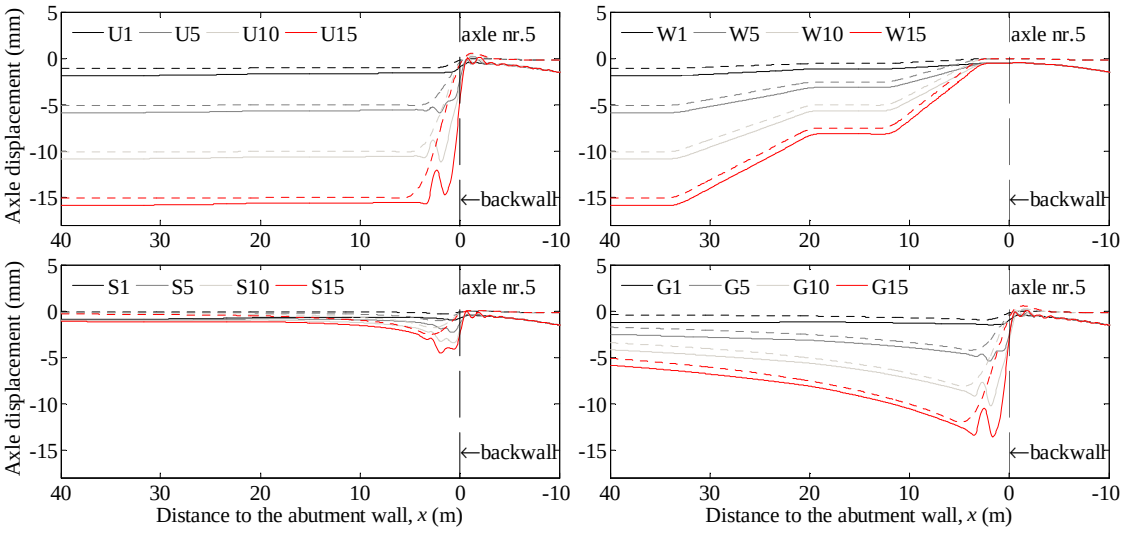

Figure 6-13. Unloaded rail position (dashed lines) and vertical axle displacements of the 5th axle (solid lines).

The accelerations measured in the axles of the trains are related to the quality of the track. For example, in high-speed railway lines in Spain, the track sections that yield vertical accelerations

above 30 m/s^2, measured on the axle, need to be followed up with intense monitoring; accelerations above 50 and 70 m/s^2 require, respectively, planned maintenance and immediate intervention (López Pita *et al.*, 2006; ADIF, 2012). Considering these limits, the results of the peak values of the vertical accelerations (Figure 6-14) show that profiles with shape W are characterised by a very good ride quality. Peak values obtained with profile shapes U and G were quite similar and exceeded all the above limits in several axles when $\delta_{max} \geq 5$ mm. Profiles with shape S exceeded the 30 m/s^2 limit when $\delta_{max} \geq 10$ mm and the 50 m/s^2 limit when δ_{max} = 15 mm, but the 70 m/s^2 limit was never surpassed. For δ_{max} = 1 mm, all the profiles showed peak accelerations below 10 m/s^2. Despite the high axle accelerations obtained in most profiles, the maximum vertical acceleration in the car body still remained below the limit of 1 m/s^2 established in EN1990 (CEN, 2005), in all studied scenarios. This denotes a very good comfort level for the passengers, as addressed earlier. It should be mentioned that the numerical model does not account for the random nature of the dynamic response of the track in high frequencies - that result from the short-wave irregularities of the track and wheels - nor considers lateral movements, yawing or rolling of the car's bodies and bogies. Consequently, higher amplitudes of the axle acceleration can be expected if measurements are performed in real situations with similar conditions of bump profiles.

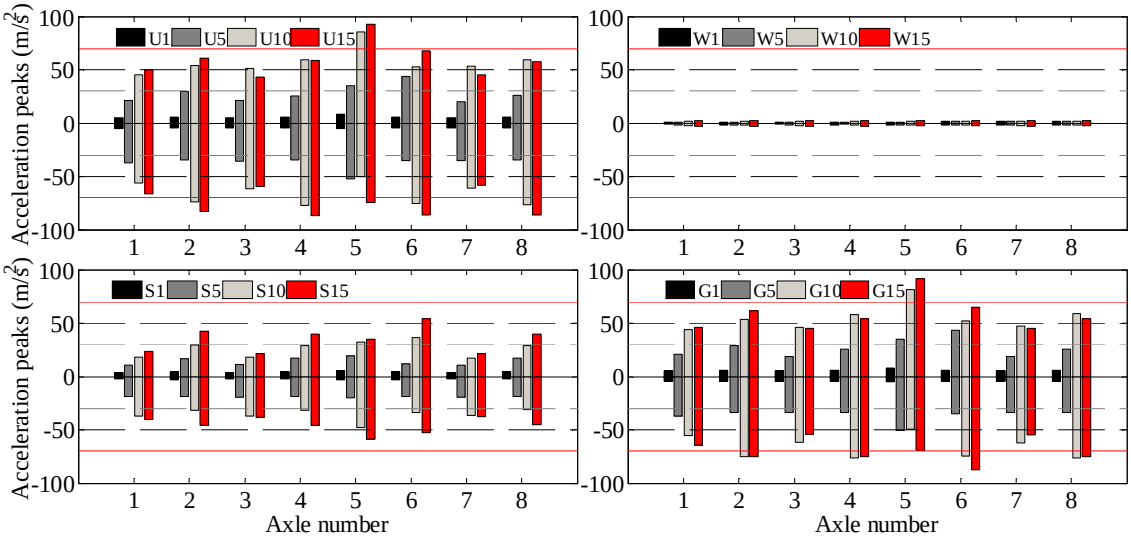

Figure 6-14. Positive and negative peaks of the vertical acceleration of the first 8 axles.

Figure 6-15 shows peak variations of the normal train-track interaction force (in percentage) for the first eight axles of the train, calculated as $\Delta P_p = (P_p - P_s)/P_s$, where P_s is the static axle load of 132 kN and P_p is the peak axle load. The results confirm that very low variations of the train-track interaction can be expected for profiles with shape W, suggesting reduced track degradation. On the other hand, the amplitude of the interaction force in the remaining profile shapes seems to increase significantly with the settlement, due to the sharp variations of the rail's position at the approach to the abutment. Some variability is observed, depending on the profile's shape and value of δ_{max}, and there are a few cases where the load increased by 100 to 150% in profiles with shapes U and G.

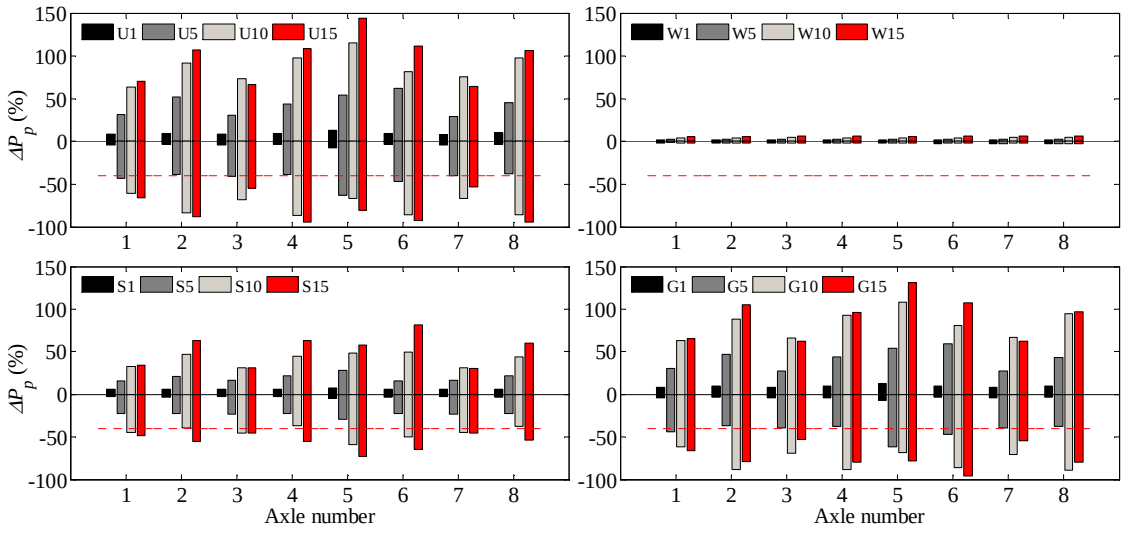

Figure 6-15. Peak variations of the dynamic train-track interaction force.

The lower horizontal lines in Figure 6-15 represent the recommended axle offload limit (-40%) for the train-track interaction forces, considered in other studies (Xia *et al.*, 2006). It is clear that only profiles with shape W or with δ_{max} < 5 mm seem to comply with this limit. This aspect highlights the risk involved in transition zones without adequate maintenance, although the vertical accelerations obtained inside the car bodies denote very good passenger comfort.

Regarding the frequency content, the effect of the tested uneven rail profiles is mostly visible below 100 Hz for this train speed, as depicted in Figure 6-16, which regards the train-track interaction force of the 5th axle in the frequency domain.

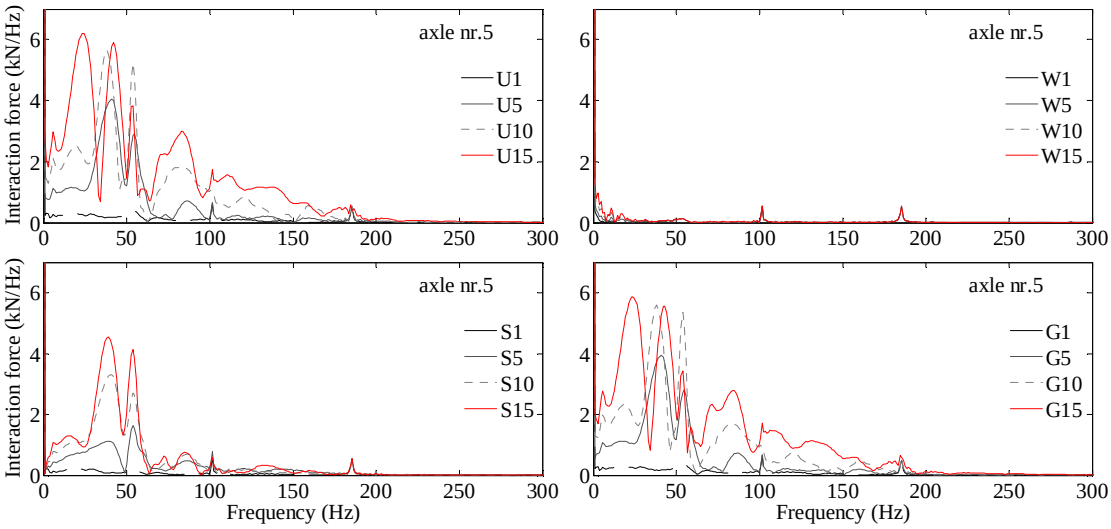

Figure 6-16. Frequency content of the interaction force of the 5th axle.

To illustrate the severity caused by the hanging sleepers, Figure 6-17 shows peak values of the total contact force obtained between the underside of each sleeper and the ballast layer, depending on the value of δ_{max} and the distance from the sleeper to the abutment wall, *x*. Profile shapes U and G produced comparable results and seem to yield very severe situations, amplifying the load on the ballast by about 1.7, 3.6, 5.0 and 5.8 times, under the sleeper aligned with the abutment wall, when δ_{max} = 1, 5, 10 and 15 mm, respectively. This aspect suggests a significant increase in the degradation of the ballast layer with increasing δ_{max}. On the other hand, profiles with shape W did not evidence significant amplifications of the contact forces – the peak values were kept between 55-65 kN for all the sleepers in the different cases. Numerical studies by Lundqvist and Dahlberg (2005) using 3D models reported that the case of one unsupported sleeper with a gap of 1 mm can increase loads onto the ballast from approximately 50 kN to 70 kN - about 1.4 times - considering a static axle load of 107.5 kN travelling at 216 km/h. A similar result was obtained in a profile with shape S with δ_{max} = 1 mm, which had two hanging sleepers with smaller gap sizes of 0.4 and 0.1 mm, but considered a higher axle load of 132 kN, travelling at about 220 km/h, and resulted in a force increment from 55 kN to 79 kN - also by about 1.4.

It was observed that, in each tested case, the highest peak loads occurred at the sleepers that were not hanging, but were adjacent to the hanging sleepers that had the largest gaps (in these

cases, the first sleeper behind the abutment wall, at about *x*=-0.15m). This can be explained by the fact that the static weight of the rail and of the hanging sleepers, plus part of the axle load, was directly transferred to those sleepers that were not hanging. Similar observations were reported in other numerical studies (Lundqvist & Dahlberg, 2005; Alves Ribeiro, 2012; Varandas *et al.*, 2014).

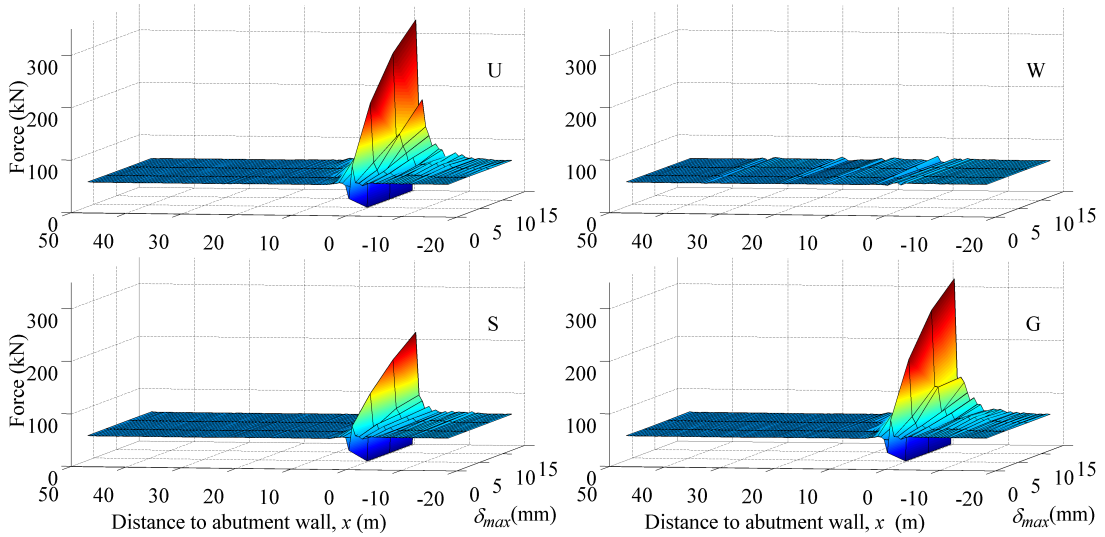

Figure 6-17. Peak contact forces between sleepers and ballast layer.

Figure 6-18 shows peak vertical accelerations of the sleepers along the transition. Again, profile shapes U and G seem to produce similar results with increasing acceleration values of δ_{max}, not only near abutment wall, but also in a zone stretching by about 10 m on the backfill and on the bridge.

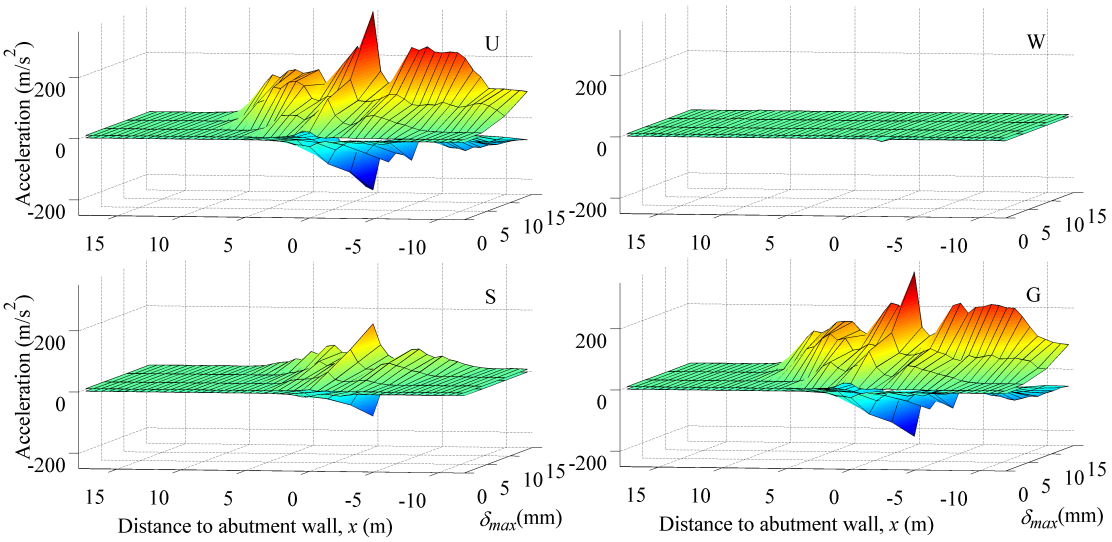

Figure 6-18. Peak vertical accelerations of the sleepers, along the transition zone.

6.4 Influence of the dip settlement profiles on the train-track interaction

6.4.1 The viaduct over the EN120

The analysis of the evolution of the track geometric measurements performed with REFER's inspection vehicle showed that the northern and southern approaches to the viaduct over the EN120 are experiencing relative fast degradation rates nearby km 26.325 and km 26.475.

The viaduct is a 52 m long prestressed concrete structure (with a 12.9 m wide deck), with three spans of 15+22+15 m. The structure has an important skew angle of about 51.5º with the roadway. The abutments are open and founded on piles (Figure 6-19).

The geometry and materials applied in the transition zones followed the same requirements as those presented in the case studies in Chapters 4 and 5.

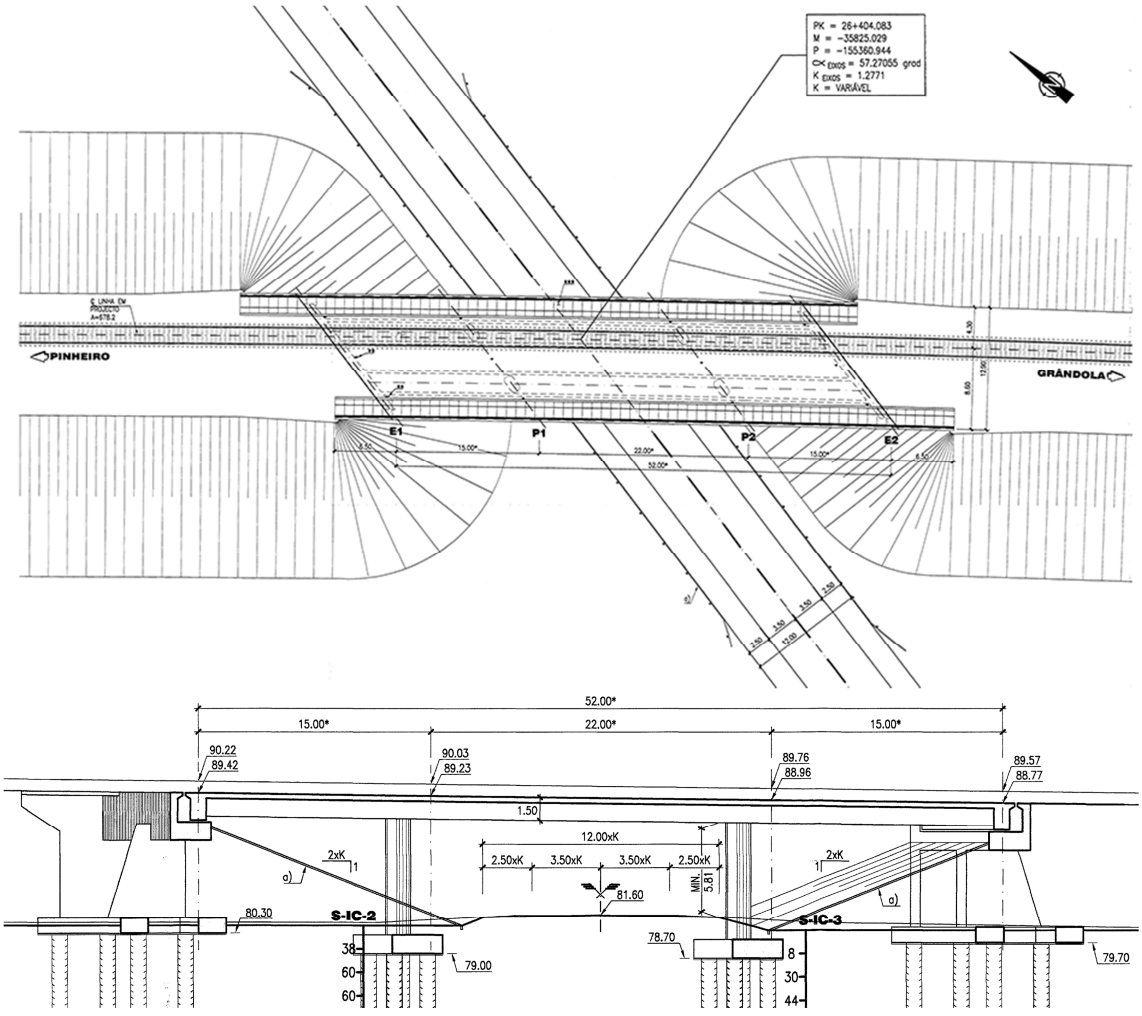

Figure 6-19. Plan and longitudinal views of the design of the viaduct over EN 120 (REFER, 2006).

At the time of the construction of the viaduct, the northern and southern embankments with soils were already partially concluded. Figure 6-20 shows aerial views of the site after the conclusion of the nearby soil embankments; after the construction of the viaduct; and its final aspect. The backfill of the abutments are technical blocks type 1 with adjusted geometry to accommodate the skew of the viaduct. The earthworks between the viaduct and the existing embankments with soils were concluded lastly, which comprised the construction of the technical blocks.

Figure 6-20. Aspects of the construction of the viaduct over road N120 (REFER, 2010): a) before the construction of the viaduct and respective technical blocks; b) before laying the track; c) after its conclusion (imagery: © 2012 Nokia, © 2012 Microsoft).

The adopted procedure for the construction of the earthworks in two separate stages (probably caused by constrains related to the construction of the viaduct) is believed to have contributed to the rapid track degradation at the north and south approaches. It should be noted that the case study of the south approach to the bridge over Sado river did not evidence this problem (see sections 4.7). That case study comprised a higher backfill which was constructed at the same pace as the adjacent embankment with soils. As regards the approaches to the viaduct over the road N120, the following factors may have also contributed to this outcome:

- The remaining earthworks included placing different materials (soils, UGM and CBM) and in a section with a complex geometry with excessive skew that comprised the wedge shape of the technical blocks and the existing high embankment with soils;

- The resulting geometry and the short length of the remaining earthworks made placing and compacting the layers more difficult;
- The sections of the previously concluded embankment and the more recent backfill had different age, which is an aspect that can induce differential settlements, considering the typical deformation behaviour of embankments.

6.4.2 Measurements of accelerations inside the car body

Due to the increasing sensing capabilities and cost reduction of smartphones, in recent years there has been significant development and increase in the application of micro electro mechanical systems (MEMS) to assessing the performance of transport systems. Numerous applications can be found in the literature regarding its use to characterise the transport infrastructure and the vehicle's motion (Heirich *et al.*, 2011; Mednis *et al.*, 2011; Heirich *et al.*, 2013; Higuera de Frutos & Castro, 2014). Other applications evidence the potential of large-scale surveys to assess the performance of transport networks, in that they can be used to study mobility patterns (Nitsche *et al.*, 2014) and to assess the ride quality of public transport systems (Lin *et al.*, 2011).

To evaluate the accelerations inside the car body of the *Alfa Pendular* at the approach to the viaduct over EN120, built-in MEMS accelerometers (triaxial) found in modern and conventional smartphones were used. To have more confidence on the results, the measurements were performed simultaneously with two Android™ smartphones, with slightly different characteristics, as described in Table 6-2. After initial tests, it was decided to use the application "Sensor Log" (v1.04), available in Google Play Store (more details at: https://github.com/hfalan/sensor-log-android), because it provided accelerometer and GPS readings at faster sampling frequencies than other similar applications that were also available at the time.

Table 6-2. Description of the MEMS 3-axis accelerometers of the smartphones.

ID	A	B
Smartphone	Samsung Galaxy® SIII, GT-I9300	Samsung Galaxy® SIV mini, GT-I9195
Sensor	LSM330DLC (STMicroelectronics®)	MPU-6000 (Invensense®)
Power	0.23 mA	0.2 mA
Range	±19.6133 m/s^2 (±2g)	±39.24 m/s^2 (±4g)
Resolution	0.009576807 m/s^2	0.15328126 m/s^2
Average sampling frequency	98 Hz	76 Hz

The measurements were performed inside the fifth coach car of the *Alfa Pendular* (ID: BBN 994 060), near the vertical alignment with the rear bogie, under seat nr. 17, at the location identified in Figure 6-21. The two smartphones were joined firmly using strong rubber bands and aligned with the car so that the orientation of the sensors' axes (x, y, z – see Figure 6-21c) matched the transverse, longitudinal and vertical alignments of the coach car, respectively.

Both smartphones were used to record the accelerations in the three directions (*x*, *y* and *z*) over a few seconds, as the train passed by the track section under study. At each measurement, the acceleration values in the three directions were recorded and a timestamp was assigned. Because the sampling frequencies of the two smartphones were different (see Table 6-2) and inconstant, the measurements were downsampled to 70 Hz.

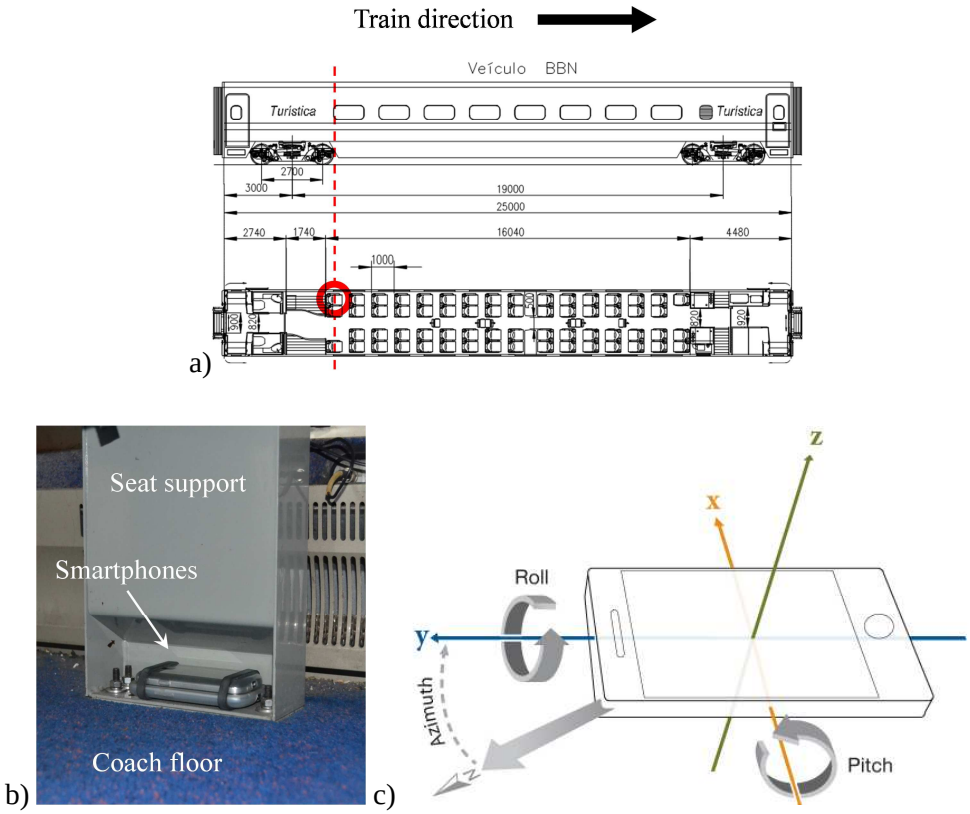

Figure 6-21. Location of the accelerometers inside the coach car (a and b) and schematic representation of the orientation of the accelerometers' axes *x*, *y* and *z* (image: www.mathworks.com).

Figure 6-22 shows a comparison between the measured vertical accelerations inside the car body in June 2014 and the earlier measurements of the longitudinal level of the track, *LL*, with the inspection vehicle (sum of the D1 and D2 components of the left and right rail, $LL_{\mathrm{D1+D2}}$; the components D1 and D2 correspond to the wavelength ranges between 3 to 25 m and between 25 to 70 m, respectively, as described in Chapter 4). It should be mentioned that between the two measurements of the longitudinal level, a small maintenance intervention was carried out at the location of the two dips (near kms 26.325 and 26.475), namely, new ballast was added and compacted manually. This intervention justifies the differences found between the two measurements, in particular, the fact that the peak settlement at km 26.325 was reduced by about 20%.

As mentioned earlier, the "Eurocode 0" (CEN, 2005) recommends threshold values for the vertical accelerations inside the car body (see Table 6-1). From the analysis of Figure 6-22 the peak accelerations measured inside de coach were slightly higher than the threshold value denoting good level of comfort, thus corresponding to an acceptable level of comfort. This is

probably the reason why the track recently had a maintenance intervention in an attempt to restore the level of comfort.

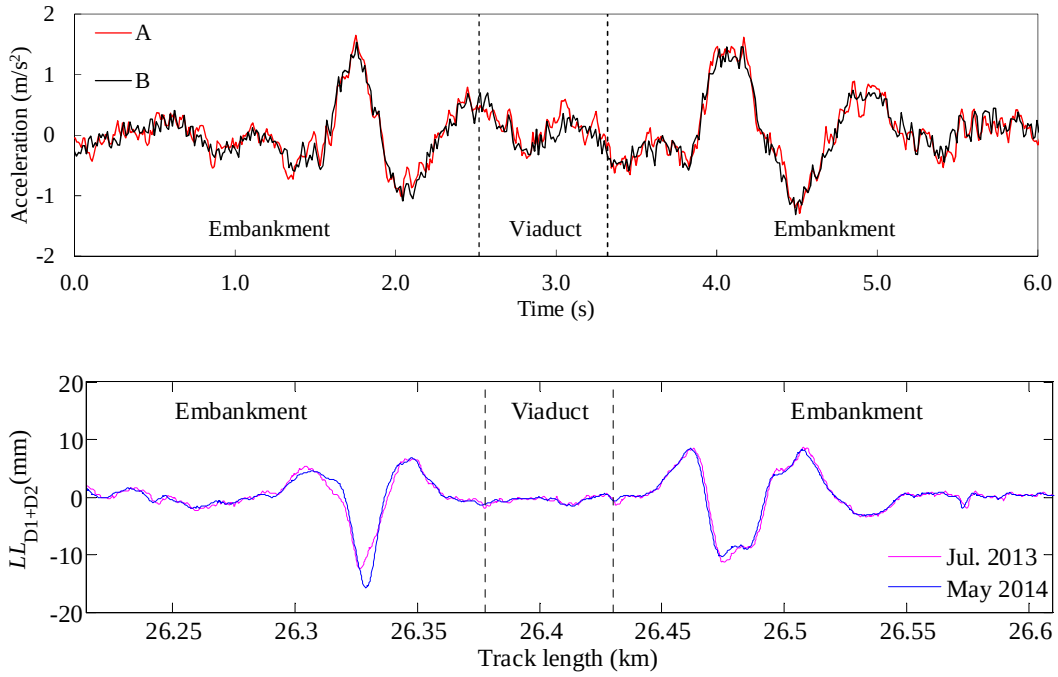

Figure 6-22. Summary of the parametric results.

6.4.1 Validation of the numerical accelerations inside the car model

This section aims at reproducing the accelerations measured inside the coach, using the same numerical model described in section 6.2.

To that aim, the settlement profile presented in Figure 6-23a was applied to a section of the backfill in the numerical model. This profile is equivalent to the segment of the longitudinal level found at the north approach to the viaduct, as indicated Figure 6-23b, and corresponds to the sum of the D1 and D2 components ($LL_{\mathrm{D1+D2}}$). The profile in Figure 6-23a resulted from an offset of about 7.5 mm, subtracted from the profile in Figure 6-23b, thus obtaining the same peak-to-peak amplitude of about 23 mm.

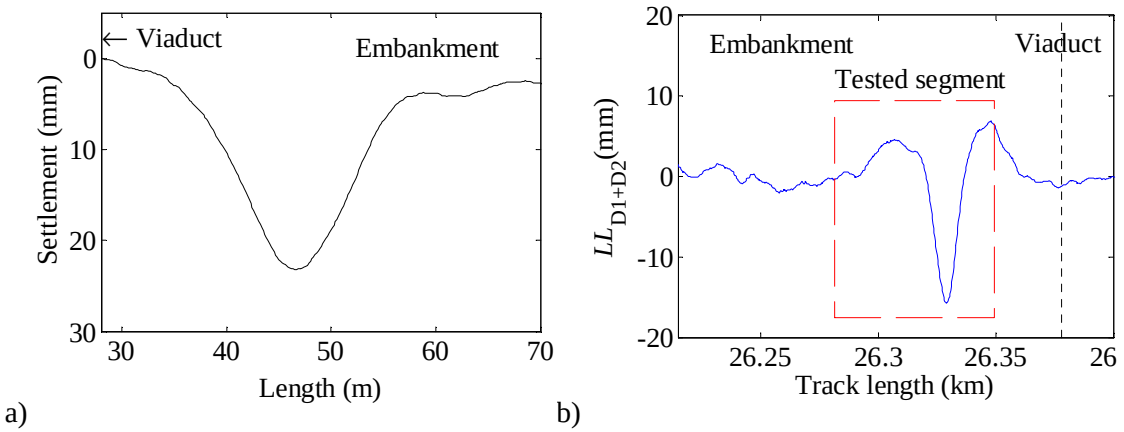

Figure 6-23. Settlement profile applied in the numerical model (a) and longitudinal level of the rail at the approach to the viaduct (b).

Figure 6-24 shows the comparison between the experimental and the numerical results of the vertical accelerations obtained inside the coach. The numerical results were obtained at the alignment with the rear bogie of the second coach car. Figure 6-25 shows the respective frequency content of the results, which highlights the fact that the frequency content of the numerical accelerations falls up to a great extent in the range of 0-5 Hz. For this reason, a low pass filter with cut off frequency of 5 Hz was applied to the experimental accelerations and the results were included in Figure 6-24 for comparison.

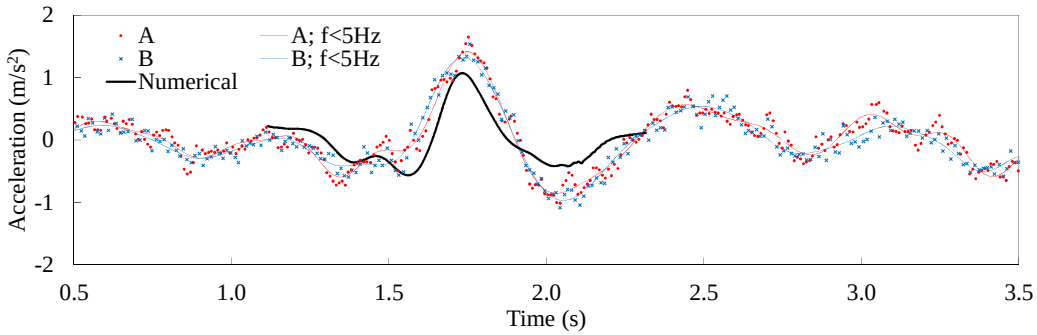

Figure 6-24. Comparison of experimental and numerical vertical accelerations, obtained inside the coach car.

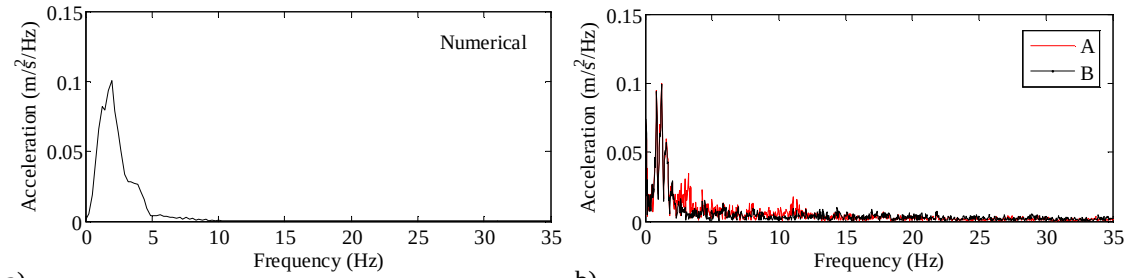

Figure 6-25. Frequency content of the numerical (a) and experimental (b) vertical accelerations, obtained inside the coach car.

Analysing the results in Figure 6-24, it can be concluded that the numerical model underestimated the peak acceleration by about 20%: the peak numerical acceleration was 1.1 m/s^2 and the peak experimental values, after applying the low pass filter, were about 1.4 m/s^2 and 1.3 m/s^2, respectively, for sensors A and B. Although the numerical results were different from the measured data, the results are very satisfactory in that the model is bi-dimensional and considers a very simple representation of the vehicle. Thus, part of the differences can be justified due to the following reasons:

- The train model cannot account for rolling and other movements of the coach (see Figure 6-26). Because de accelerometers were placed a few meters from the longitudinal central alignment of the coach car, the acceleration measurements may have been amplified by rolling oscillations. Considering that the rolling vibration has a frequency of 1.01 Hz (Ribeiro, 2012) (which is very close to the frequencies of the pitching and vertical vibration modes – see Chapter 5) it was not possible to eliminate/mitigate its influence.
- The settlement profile applied in the model only represented the range of wavelengths between 1 m and 70 m. At 220 km/h, track defects with longer wavelengths would correspond of excitation frequencies lower than $f = v/\lambda = 0.87$ Hz. In fact, analysing Figure 6-24 and Figure 6-25 it seems that some lower frequency content is missing from the numerical results, when comparing with the experimental data.

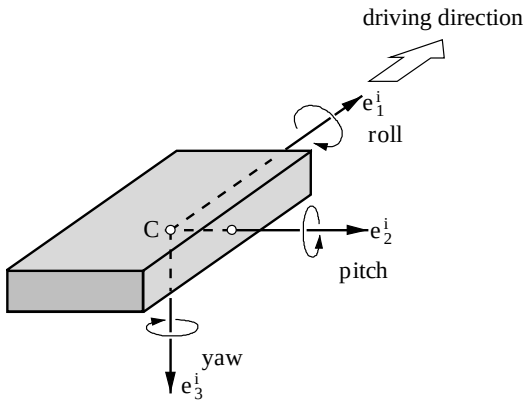

Figure 6-26. Notation of rotary vehicle motions (Popp & Schiehlen, 2010).

6.4.2 Simulations of the train-track dynamic interaction

To further investigate the effect of dip profiles on the train-track interaction at transition zones, a hypotetical settlement profile was created with similar settlement amplitude and length of the dip found at the north approach to the viaduct over EN 120 (Figure 6-23). Figure 6-27 shows a comparison between the hypothetical profile (in red) and the longitudinal level (after applying the same offset of about 7.5 mm).

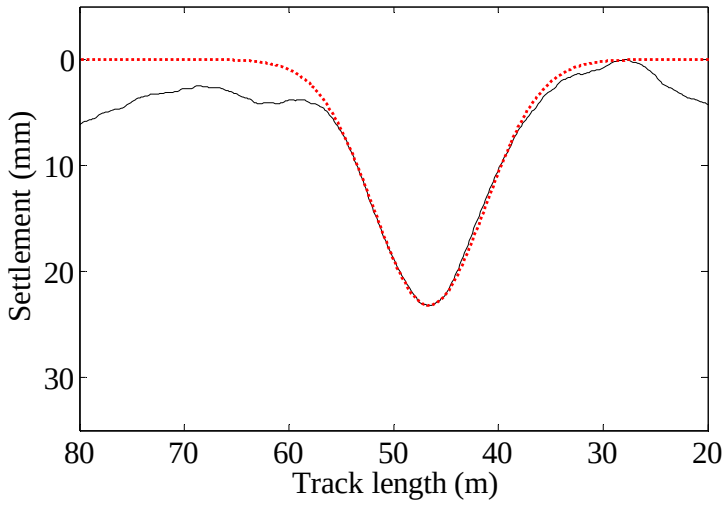

Figure 6-27. Hypothetical dip settlement profiles.

The hypothetical profile was obtained using the following Dirac delta-type function (as the limit of Gaussian functions):

$$s(x) = \frac{k_A \times 308}{7.5\sqrt{\pi}} e^{-(x-x_{dip})^2/(k_L \times 7.5)^2} \quad (6\text{-}1)$$

Where s is the track settlement in mm, x is the distance to the abutment in m, x_{dip} is the distance between the abutment and the centre of the dip, with a value of 40 m. In Figure 6-27, both parameters k_A and k_L take the value of 1.0.

To assess the effect of the shape of the dip in the train-track system, two sets of models were studied with different dip configurations (Table 6-3). In the first set, the amplitude of the dip was changed by the ratio k_A, which ranged between 0.25 and 1.50, in steps of 0.25; k_L was kept equal to 1.0. In the second set, the length of the dip was changed by the ratio k_L, also ranging between 0.25 and 1.50. In the second, k_A was set equal to 1.0. The dip profiles of the two sets are depicted in Figure 6-28.

Table 6-3. Designation of the profiles and values of the parameters k_A and k_L.

Sets of models	Designation	Amplitude ratio, k_A	Length ratio, k_L	Amplitude of the dip (mm)	Length of the dip (m)
Change in Amplitude	A150	1.50	1.00	35	35
	A125	1.25	1.00	29	35
	A100	1.00	1.00	23	35
	A75	0.75	1.00	17	35
	A50	0.50	1.00	12	35
	A25	0.25	1.00	6	35
Change in Length	L150	1.00	1.50	23	53
	L125	1.00	1.25	23	44
	L100	1.00	1.00	23	35
	L75	1.00	0.75	23	26
	L50	1.00	0.50	23	18
	L25	1.00	0.25	23	9

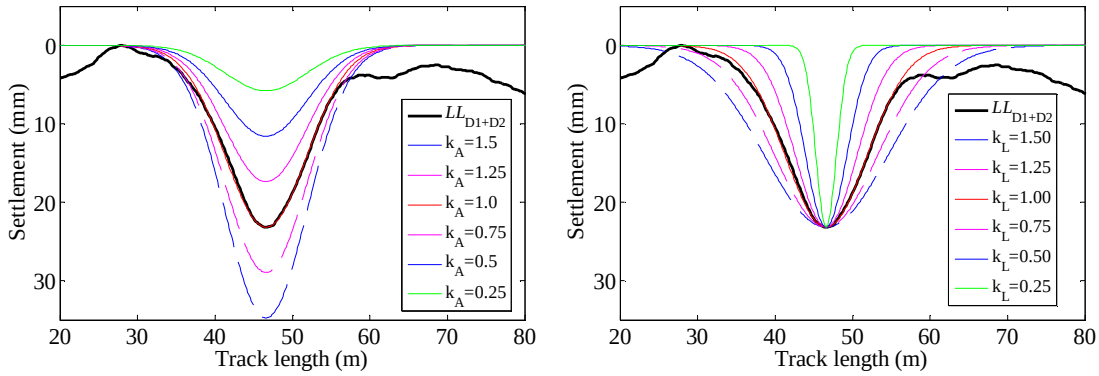

Figure 6-28. Dip settlement profiles and actual rail revel (LL_{D1+D2}): change in dip amplitude (left); change in dip length (right).

Figure 6-29 shows the settlement profiles and the positions of the sleepers that resulted from the adjustment of the track to the respective settlement profile in unloaded conditions. As mentioned earlier, due to the bending stiffness of the rails and to the sharp differential settlement, in models L25 and L50, some sleepers were hanging from the rails and developed gaps under them.

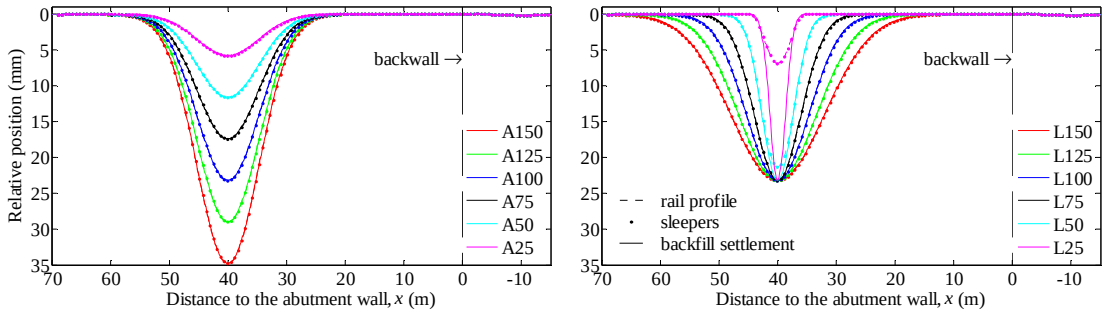

Figure 6-29. Backfill settlement profiles and consequent positions of the sleeper (in unloaded conditions).

The position of the hanging sleepers is identified in Figure 6-30 with the respective size of the gap. Although models L25 and L50 had approximately the same number of hanging sleepers in unloaded conditions (9 sleepers), the size of the gaps in model L25 were significantly higher than in model L50, which is a consequence of the narrower dip profile.

Figure 6-31 and Figure 6-32 show a comparison between the various rail profiles, in their unloaded position, and the vertical displacements of the 1st and 5th axles.

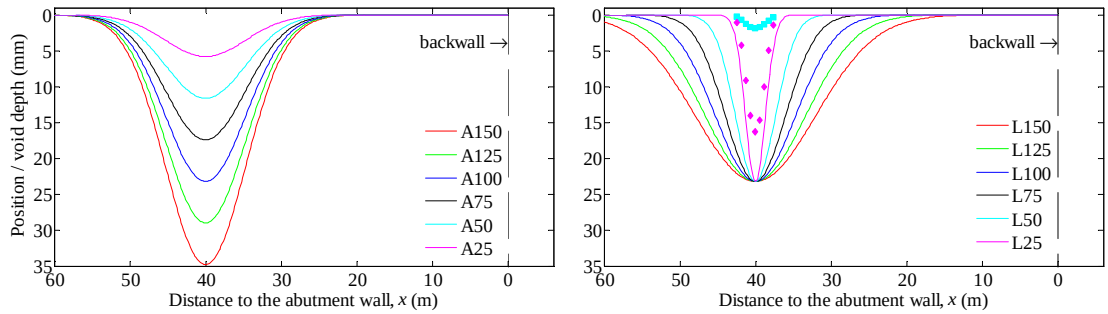

Figure 6-30. Location of hanging sleepers (markers) and respective gap sizes in unloaded conditions.

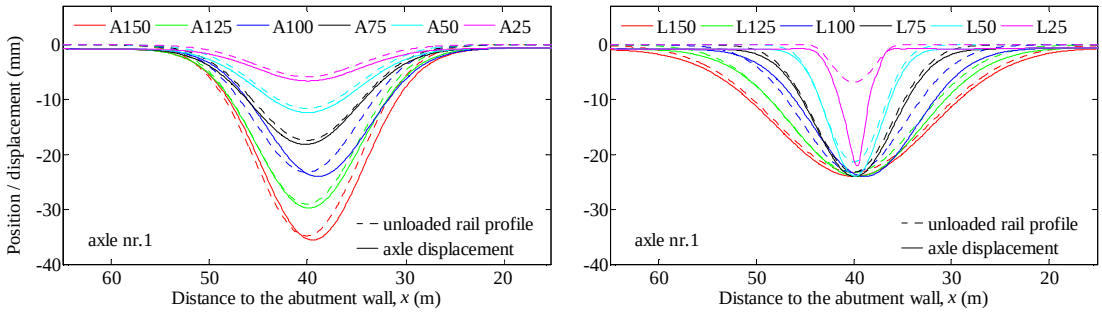

Figure 6-31. Unloaded rail position (dashed lines) and vertical displacements of the 1st axle (solid lines).

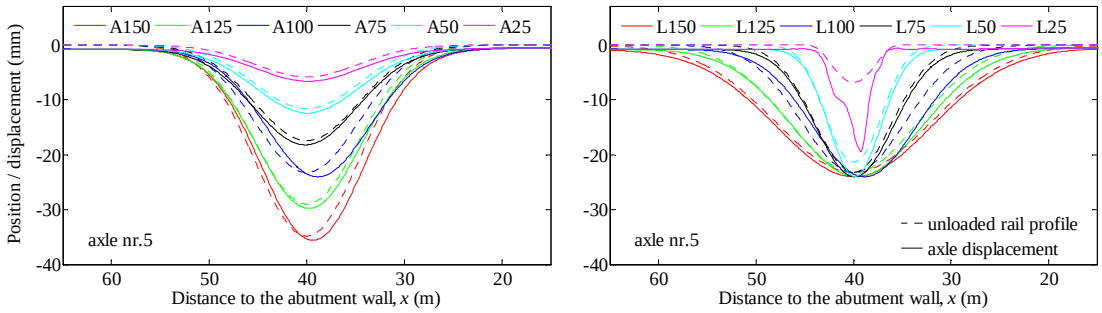

Figure 6-32. Unloaded rail position (dashed lines) and vertical displacements of the 5th axle (solid lines).

The results evidence that while, in most cases, the different axles undergo almost identical vertical displacements, in cases with hanging sleepers, such as model L25, the axles may experience some oscillations at the sections with larger gaps under the sleepers. Figure 6-33 shows peak vertical displacements of the first eight axles. In the second set, “L”, it is visible that the vehicle’s axles in model L25: i) undergo different peak displacements; ii) experience a lower

displacement amplitude as that of the remaining models of the same set, although the amplitude of the settlement is the same for all of them. This behaviour is due to the bending stiffness of the rails in that the hanging sleepers resulting from the settlement (a shortwave defect) did not establish contact with the ballast elements, when directly loaded by the axles. The fluctuation of the displacement peaks is related to the vertical vibration of rails and sleepers after the passage of the axles, which adds to the effect caused by the axle load itself.

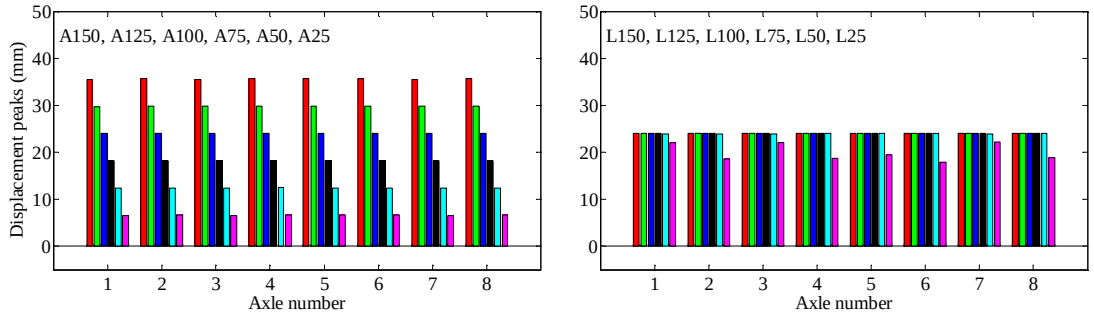

Figure 6-33. Peak vertical displacements of the first eigth axles.

This behaviour is particularly evident when analysing the vertical accelerations of the vehicle's axes. Figure 6-34 and Figure 6-35 show the vertical accelerations of the axles, denoting high acceleration values and amplitudes as the length of the dip profile is reduced.

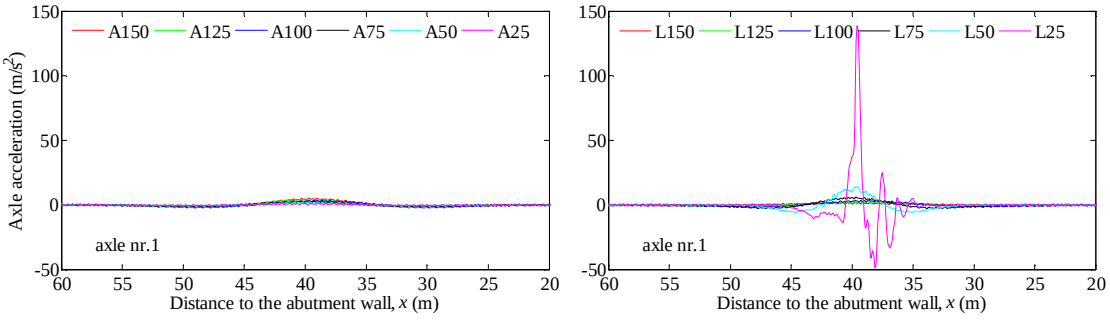

Figure 6-34. Vertical acceleration of the 1st axle.

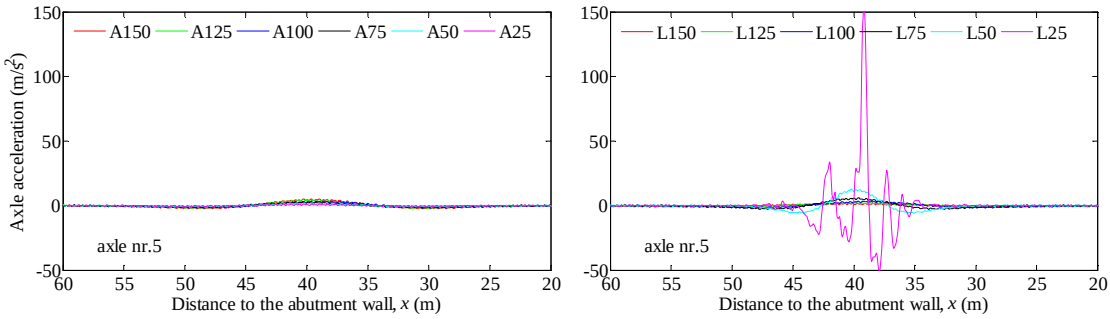

Figure 6-35. Vertical acceleration of the 5th axle.

Considering the limits of axle accelerations established by ADIF (2012), the results of the peak values in Figure 6-36 show that, with the exception of profile L25, most of the tested dip profiles are still characterised by a very good ride quality. Although profile L50 already shows 9 hanging sleepers, the vertical acceleration of the axles is still below the minimum limit. This is probably because the gaps under the sleepers are smaller (less than 2 mm) and when the sleeper is directly loaded by the axle, it eventualy presses against the ballast layer.

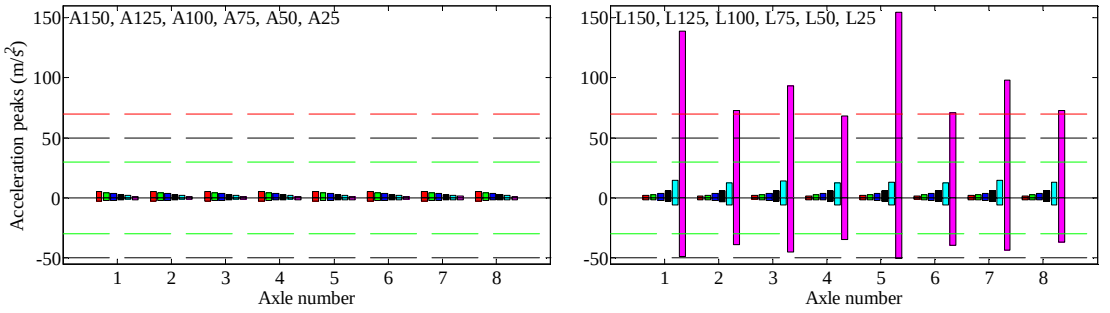

Figure 6-36. Positive and negative peaks of the vertical acceleration of the first 8 axles.

The dynamic amplification resulting from the presence of the dip can also be assessed in terms of interaction forces. Figure 6-37 and Figure 6-38 show the normal train-track interaction force between the rails and the 1st and 5th axles, respectively. Again, the case of L25 yield higher dynamic amplification with very high values and oscillations of the interaction force. Figure 6-39 presents a summary with the peak values of the dynamic train-track interaction force for the different scenarios, considering the first 8 axles. The lower horizontal lines in Figure 6-39 represent the recommended axle offload limit (-40%) for the train-track interaction forces,

considered in other studies (Xia *et al.*, 2006). It is clear that only profile with shape L25 does not seem to comply with this limit.

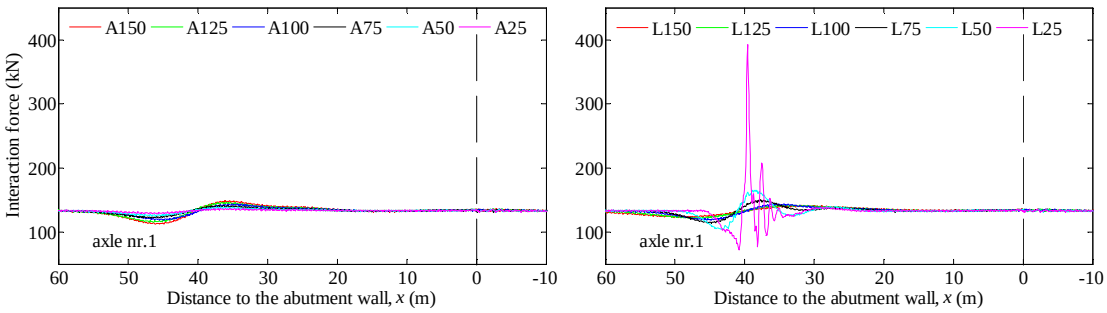

Figure 6-37. Normal train-track interaction force 1st axle.

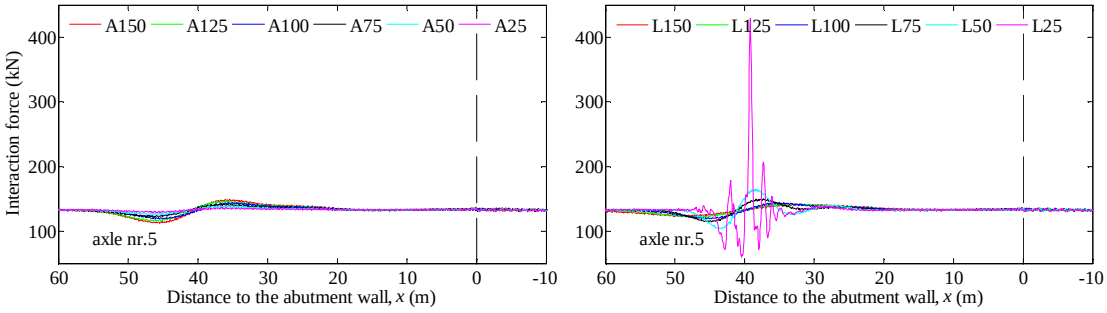

Figure 6-38. Normal train-track interaction force 5th axle.

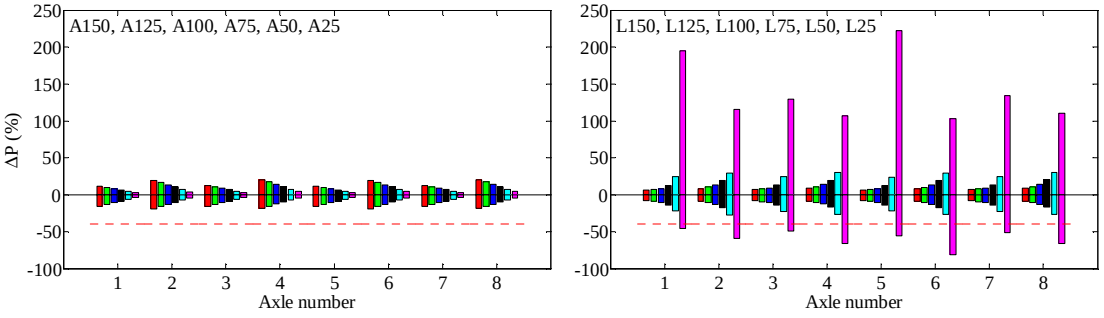

Figure 6-39. Peak variations of the dynamic train-track interaction force.

Figure 6-40 shows the vertical acceleration obtained inside the 2nd car of the *Alfa Pendular*, at the alignment with the respective leading and rear bogies. Time histories of the accelerations

inside the first car body were very similar to those of the second car body. The horizontal lines denote the Eurocode's (CEN, 2005) threshold levels of comfort (see Table 6-1). Figure 6-41 shows positive and negative peaks of the vertical acceleration inside the body.

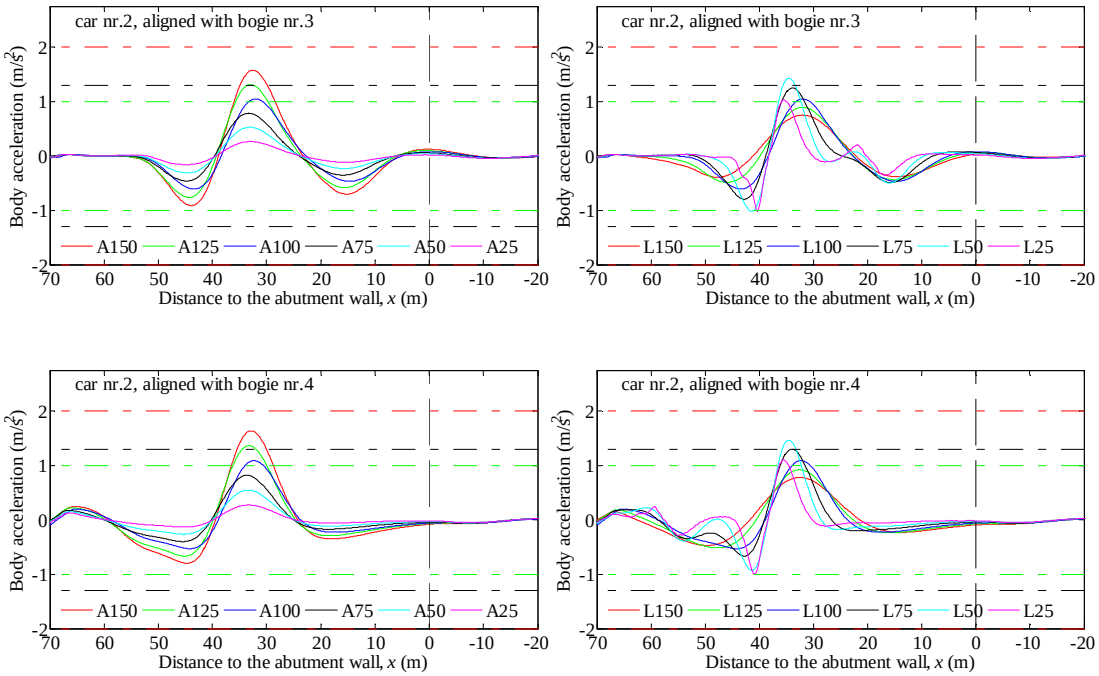

Figure 6-40. Vertical acceleration inside the 2nd coach car at the alignments with the leading and rear bogies.

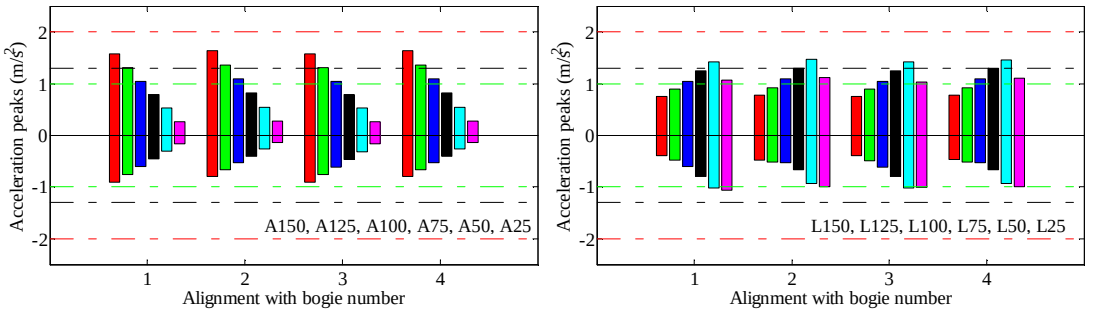

Figure 6-41. Positive and negative peaks of the vertical acceleration inside the first two coach cars, at the alignments with the respective leading (1 and 3) and rear bogies (2 and 4).

The peak vertical accelerations in the car body in some scenarios was higher than the limit of the very good comfort level (1 m/s^2). In some of these cases, it was even higher that the good

comfort limit of 1.3 m/s^2. An interesting aspect is that the cases with higher car body accelerations in each set were A150 and L50, respectively, 1.6 m/s^2 and 1.5 m/s^2. The L25 – which had a few hanging sleeper with large gaps and yielded very high acceleration and interaction force peaks – showed a lower peak value of 1.1 m/s^2. Once again, this emphasises that passenger trains are very effective in assuring good comfort level for short-wave track defects, despite the severe impacts that take place at the wheel-rail interface. As was expected, the passenger comfort is mostly influenced by track defects with greater wavelengths. However, as highlighted by Ribeiro (2012), the range of wavelengths between 3 to 25 m also seems to be important for peak accelerations inside the car bodies. This can be explained because the first structural vibration modes of the car body and rigid body modes of the bogies have frequency values higher than 7 Hz (car body: longitudinal torsion, f = 8.34 Hz; longitudinal bending, f = 12.26 Hz; bogie 7-14 Hz), that can be excited by track defects with wavelengths shorter than 25 m. At the normal maximum speed of the *Alfa Pendular* - 220 km/h – those excitation frequencies (>7 Hz) correspond to defects with wavelengths shorter than about 8.7 m ($f = v/\lambda = 61.1/8.7 = 7$ Hz).

To illustrate the severity caused by the hanging sleepers, Figure 6-42 shows peak values of the total normal contact force obtained between the underside of each sleeper and the ballast layer, depending on the value of δ_{max} and the distance from the sleeper to the abutment wall, *x*. Each marker represents the peak value at each sleeper. It can be observed that the typical peak force under each sleeper is about 56 kN on the backfill and about 60 kN on the bridge, which is about 42% and 45% of the static axle load (132 kN), respectively. With the exception of cases L50 and L25, at the section of the track with the dip, the maximum peak values of the contact force ranged between 57 and 66 kN (corresponding to a variation of about +2% to +18%), depending on the dip profile. The maximum peak values seem to be located at the second half of the dip: in this case, with the vehicles approaching the bridge, the sleepers with maximum peaks were located at $x = [30, 40]$ m. Apparently, lower peak values were obtained at the first half of the dip, representing a reduction of the contact force by about the same percentage as the respective maximum peak values, in each scenario. These results seem to be related to the train direction and the train-track interaction, in that lower contact forces are developed when the train starts the descending movement into the dip, while the higher forces occur in the ascending movement, when exiting the dip. Cases L50 and L25 showed a significant increment in the maximum peak contact forces near the track section with the dip, up to 77 kN (+38%) and 206 kN (+268%), respectively. It is interesting to note that in profile L25, only one sleeper (at

$x = 40$ m) never established contact with the ballast layer, despite the fact that in the unloaded track configuration, nine sleepers were hanging from the rails.

Figure 6-43 shows peak vertical accelerations of the various sleepers located along the transition. It is visible that, in normal conditions, the peak sleeper accelerations (positive and negative) fall in the range of $\pm 7\ \mathrm{m/s^2}$, which is somewhat in agreement with the experimental results presented earlier (see Chapter 5). Again, it seems that only cases L50 and L25 yield important amplifications of the track response, in this case, the vertical accelerations. While the remaining dip profiles do not induce amplifications in the peak accelerations of the sleepers, in L50 and L25, the peak vertical accelerations reach up to +207/-156 $\mathrm{m/s^2}$ and +101/-28 $\mathrm{m/s^2}$, respectively. Another aspect worthnotting is that altough case L25 refers to a dip with a length of 9 m, it appears to amplify the response of the sleepers that are more than 10 m away from the dip centre. On the other hand, case L50 – a 18 m-long dip – only seems to affect the accelerations of 13 sleepers, which corresponds to a length of less than 8 m. This behaviour may be related to the fact that the sleepers in L25 have significantly larger gaps than those in L50, thus contributing to the instability of the track in that section.

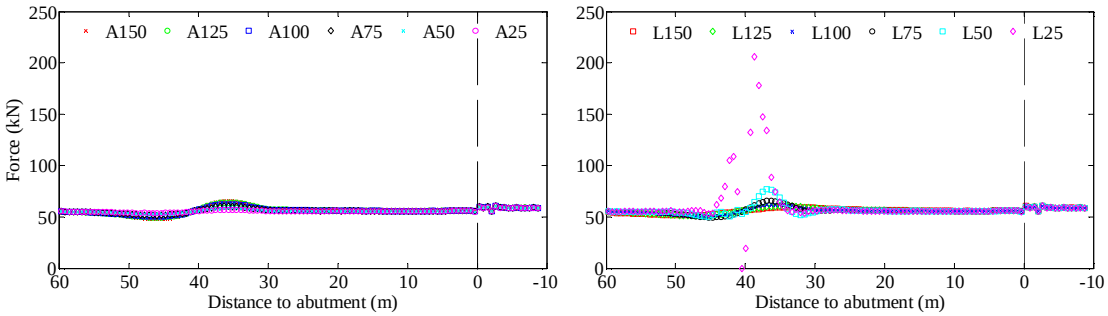

Figure 6-42. Peak contact forces between each sleeper and the ballast layer.

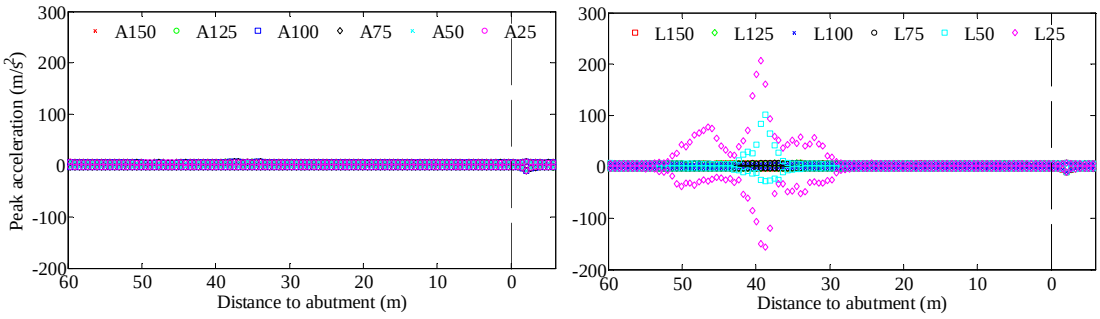

Figure 6-43. Peak vertical accelerations of the sleepers, along the transition zone.

6.5 Comprehensive parametric study on the influence of the shape of dip profiles in the train-track interaction

6.5.1 Initial considerations

In the previous section, it was demonstrated that both the length and the amplitude of the dip settlement profiles influenced the dynamic train-track interaction. However, that approach was somewhat limited in assessing the effect of other shapes of settlement profiles.

This section aims at investigating in more detail the influence of a wider range of different possible combinations of amplitude and length of dip profiles on the dynamic response of the train-track system. To that aim, a parametric study was carried out to study different settlement profiles, using the same numerical method. The settlement profiles were determined using the previous expression (6-1). The values of the parameters k_A and k_L were selected from the interval]0, 1[, to form multiple combinations in the space (k_L, k_A) – see Figure 6-44a. Considering the significant computation effort and time to run each simulation, it was decided to divide both axes of this domain into ten equally-spaced intervals, thus resulting in 10^2 settlement profiles to be tested. This resulted in a range of combinations of amplitude from 1.16 mm to 22.0 mm, and lengths from 1.75 m to 33.3 m, which are identified in Figure 6-44b. Figure 6-45 shows an overlay with all the tested profiles.

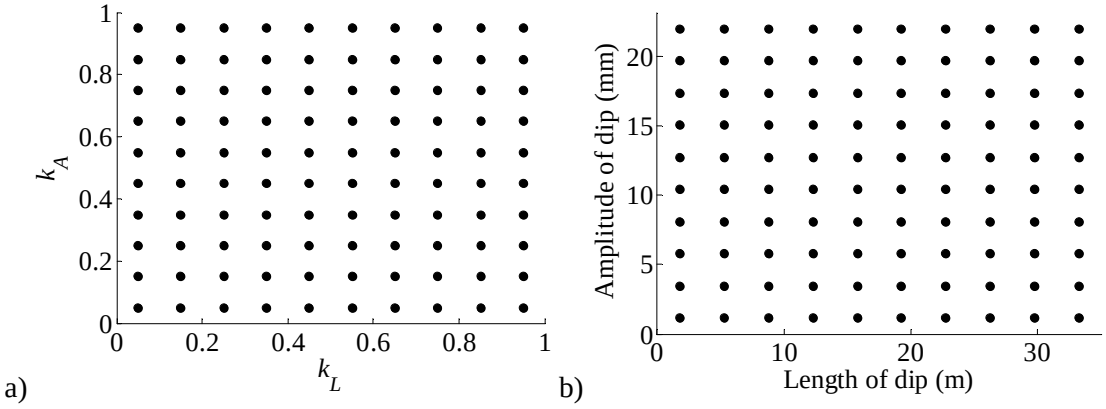

Figure 6-44. Combinations of k_A and k_L (a) and respective amplitudes and lengths of the dip (b).

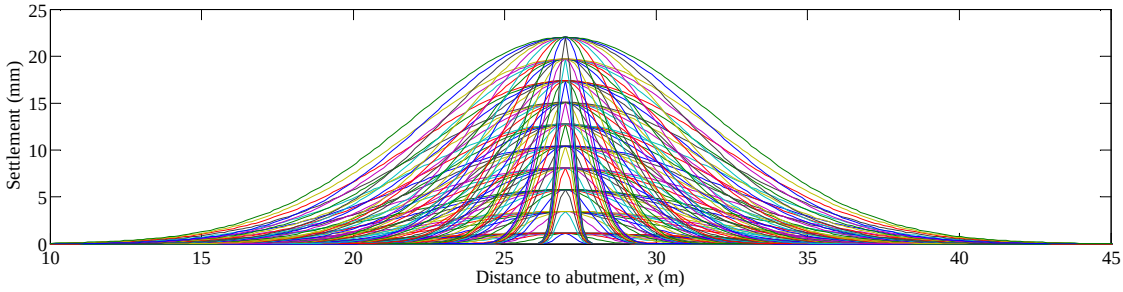

Figure 6-45. Overlay with the 100 profiles considered in the parametric study.

6.5.2 Results and discussion

In an attempt to summarise the output of the numerical models, in the following figures of this section the results are presented using tri-dimensional plots or two-dimensional contour graphs. In general, the plots regard the peak values (positive and/or negative) of a given variable, with respect to the maximum settlement in mm (the dip amplitude) and the length of the defect in m (the length of the dip).

Figure 6-46 shows the increasing peak vertical displacements of the *Alfa Pendular*'s axles with the increasing amplitude of the dip, regarding the 1st axle (a) or all the axles (b). The results regarding the 1st axle are comparable to those that regard all the axles of the vehicle. The results highlight an aspect that was discussed earlier, related to the fact that for dip defects with lengths shorter than about 9 m, the vehicle and the track frame experience vertical displacements smaller than the actual settlement amplitude at the level of the ballast layer. This behaviour is clearly identified in Figure 6-46 by the inflection in the tri-dimensional surface, for dip lengths shorter than 9 m.

Figure 6-47 and Figure 6-48 present 3D plots of the positive and negative accelerations of the vehicle's axles, regarding the 1st axle or all the axles, respectively. The results regarding the 1st axle denote slight lower amplitudes, but yet comparable to the results that consider all the axles of the vehicle. Figure 6-49, presents a contour graph based on the results of Figure 6-48, with the representation of the contour lines denoting the threshold values used by the Spanish infrastructure manager (ADIF, 2012), as mentioned earlier. In general, for each tested profile, the negative peak accelerations were lower, in absolute value, than the positive peak values. It is worth noting that the higher amplitudes of the vertical acceleration of the axles ($\geq |30|\ \mathrm{m/s^2}$) extend to values of dip lengths larger than 9 m, from about 1.75 m up to about 10 to 15 m, depending on the amplitude of the settlement. In Figure 6-46, the lengths shorter than 9 m were

associated with unwanted scenarios where the sleepers did not establish contact with the ballast layer under the axle loads.

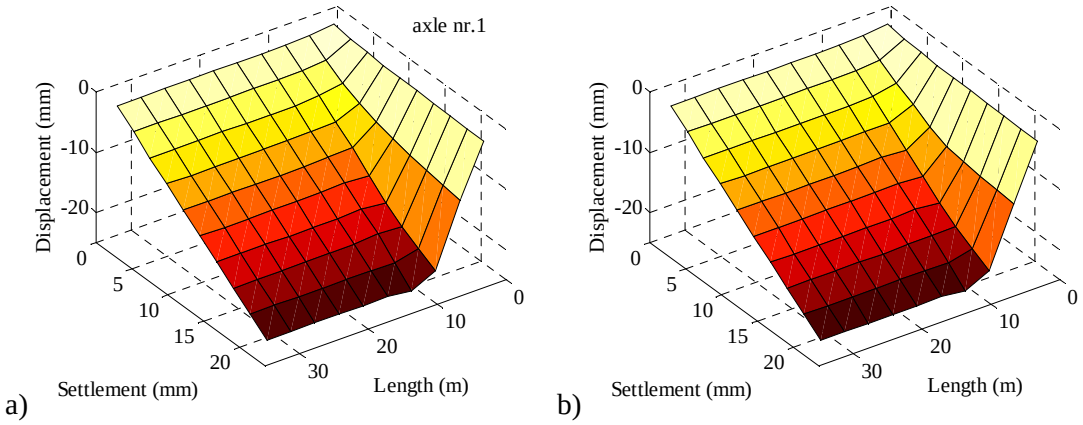

Figure 6-46. Peak axle displacements: a) obtained with axle nr. 1; b) considering all axles.

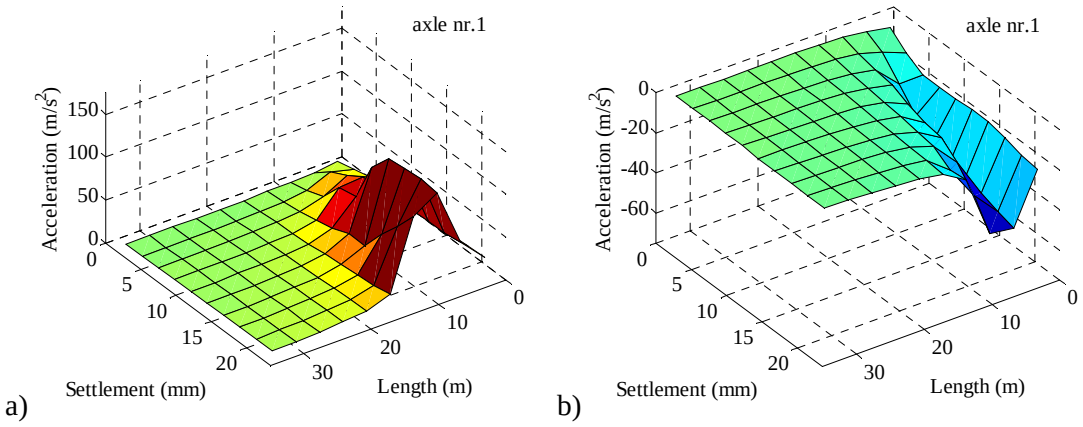

Figure 6-47. Peak accelerations on the 1st axle: a) positive values; b) negative values.

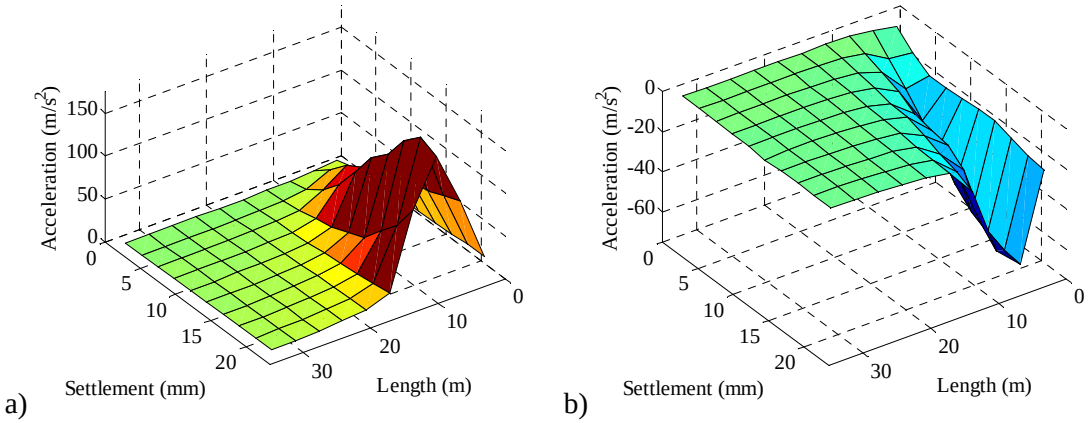

Figure 6-48. Peak axle accelerations, considering all axles: a) positive values; b) negative values.

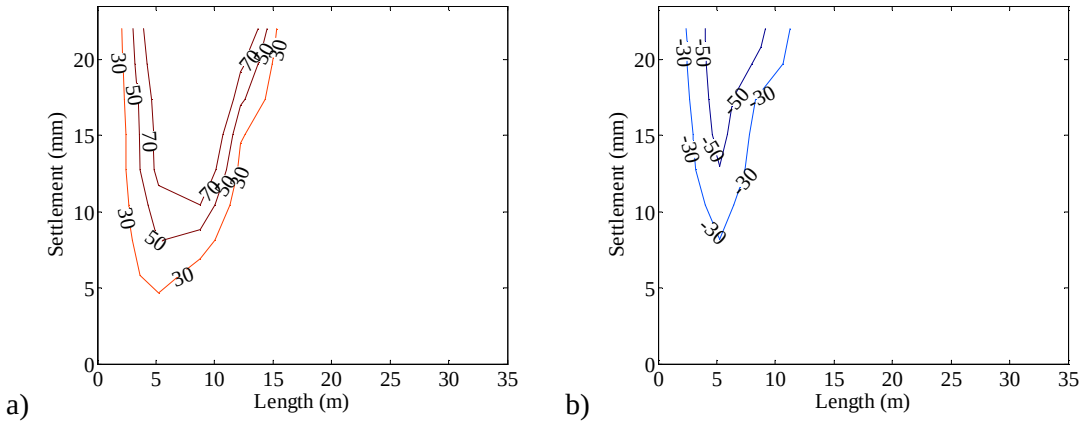

Figure 6-49. Peak axle accelerations (m/s^2), considering all axles: a) positive values; b) negative values.

Considering the results in Figure 6-49, the acceleration of the axles may be a more sensible parameter to identify the same problem because: i) there is a very rapid increase in the peak acceleration values in the region that is associated with the hanging sleepers; ii) the increase in the peak values starts even before the problem seems the be detected in Figure 6-46.

The observations regarding the positive and negative peak interaction forces between the wheelsets and the rails are somewhat analogous to that of the accelerations of the axles, as depicted in Figure 6-50 and Figure 6-51, considering the 1st axle or all the axles, respectively. The contour lines in Figure 6-52 regard the peak dynamic coefficients, calculated as the ratio between the peak interaction force (Q_{dyn}), positive or negative values, and the respective static axle load (Q_{sta}). The results indicate that the development of dip profiles with lengths shorted than 15 m and amplitudes higher than 5 mm, may imply severe dynamic amplifications of the axle loads to the track and increase the risk of derailment. As mentioned earlier, some studies consider the value of 0.6 to be the acceptable offload limit (Xia *et al.*, 2006).

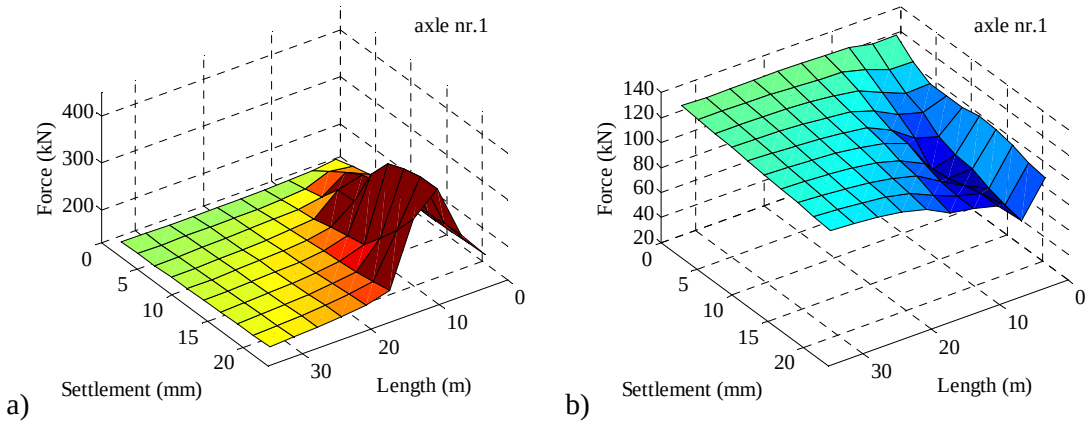

Figure 6-50. Peak interaction force on the 1st axle: a) positive values; b) negative values.

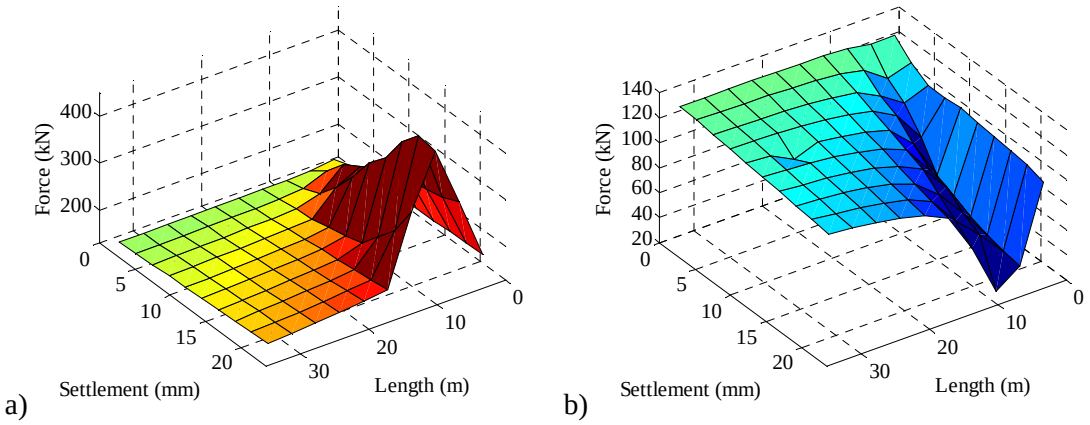

Figure 6-51. Peak interaction force, considering all axles: a) positive values; b) negative values.

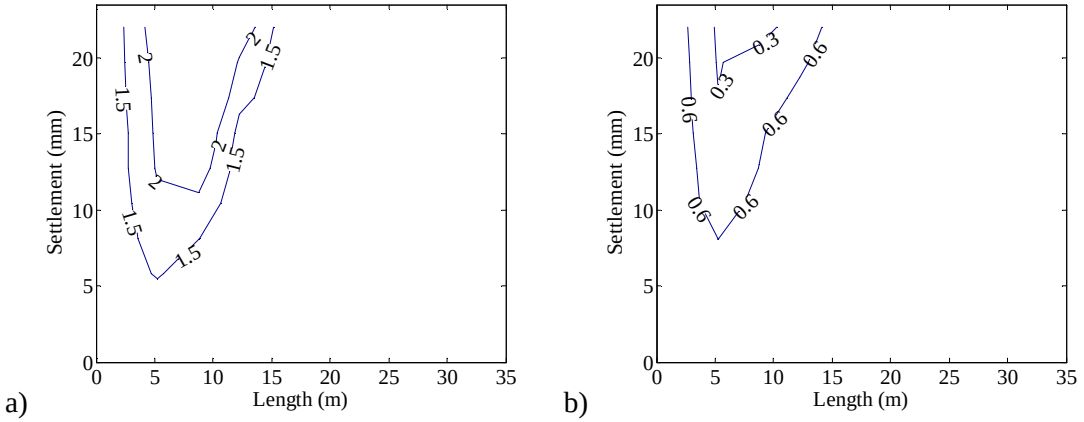

Figure 6-52. Peak dynamic coefficients (Q_{dyn} / Q_{sta}), considering all axles: a) maximum values; b) minimum values.

As regards the passenger comfort, Figure 6-53 shows the peak (positive and negative) vertical accelerations obtained inside the coach, at the alignment with the bogies. In general, the acceleration peaks increase with the settlement amplitude. However, the results indicate that the critical scenarios are not the same as those identified in the analysis of earlier parameters. Here, dip profiles with shorter lengths (up to about 5 m) and amplitudes (up to about 5 mm) seem to have negligible effect in the passenger comfort. This also confirms the effectiveness of the suspension of the vehicles in reducing the effect of shortwave defects in the passenger comfort and is in agreement with results presented earlier. The critical scenarios regarding the passenger comfort seem to be dip profiles with lengths greater than about 9 m, in particular, between about

11 and 24 m. Based on these results, Figure 6-54 shows the contour lines denoting different levels of passenger comfort, established in (CEN, 2005).

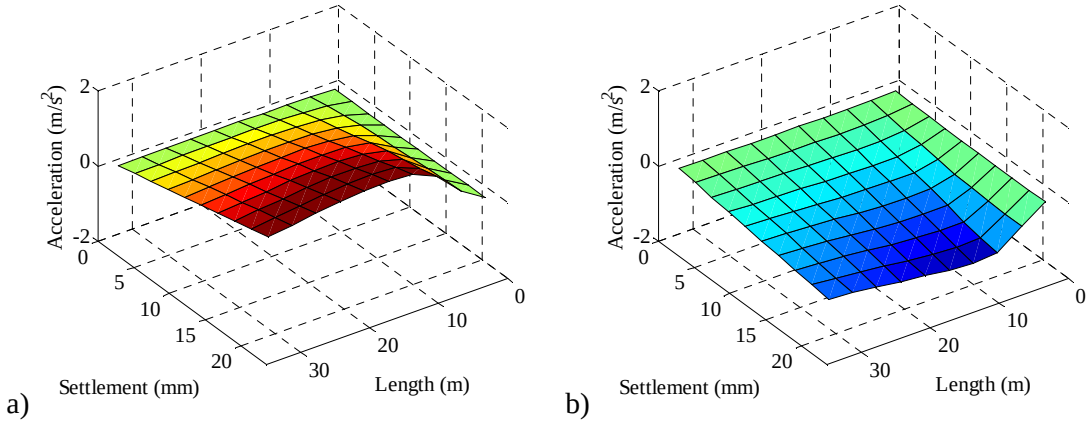

Figure 6-53. Peak car body accelerations at the alignment with the bogies: a) positive values; b) negative values.

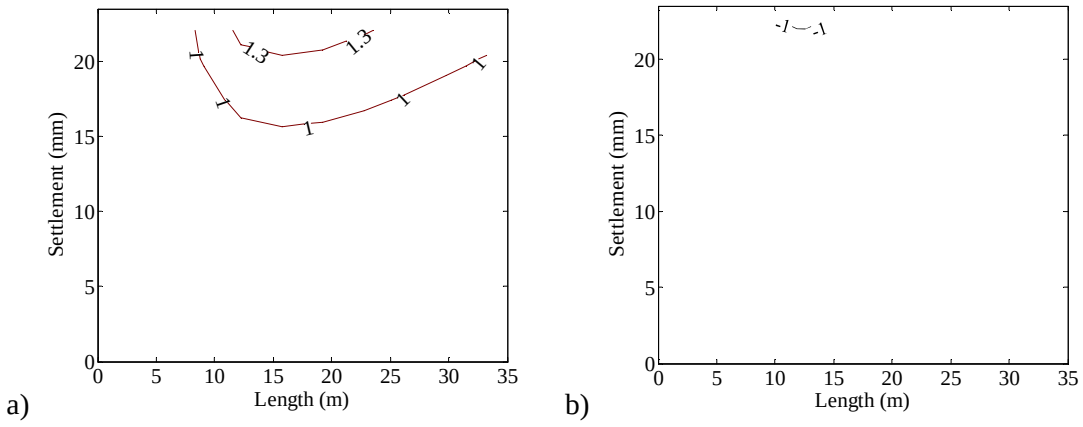

Figure 6-54. Peak car body accelerations (m/s^2) at the alignment with the bogies: a) positive values; b) negative values.

It is visible that the highest amplitudes correspond to positive vertical accelerations which were higher than 1.0 m/s^2 (the threshold for very good comfort), for settlement amplitudes greater than 15 mm and dip lengths longer than about 9 m. The acceleration threshold denoting good comfort level (1.3 m/s^2) was exceeded when the settlement amplitude was greater than about 20 mm and for dip lengths between about 11 and 24 m.

In order to analyse the influence of the different dip profiles on the severity caused by the train onto the track, the resulting peak sleeper-ballast contact forces were compared. Firstly, the

results of three representative cases are discussed, namely, cases nr. 10, 21 and 93, which correspond to the profiles presented in Figure 6-55.

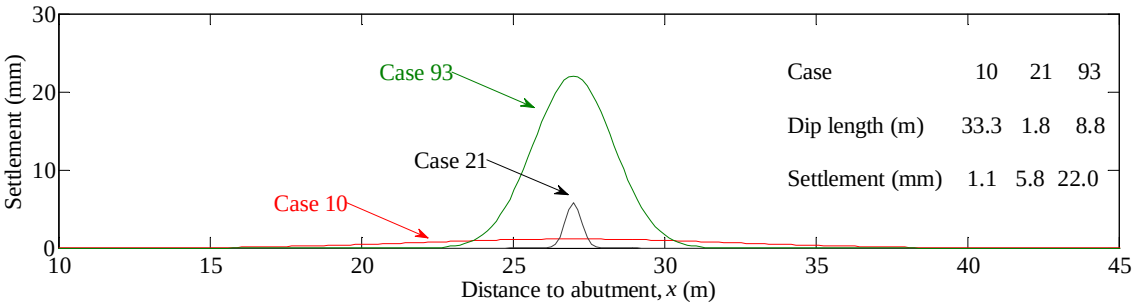

Figure 6-55. Settlement profiles of cases 10, 21 and 93.

Figure 6-56 (a to c) shows the time histories of the sleeper-ballast contact forces, calculated for 24 sleepers that were closest to the centre line of the dip, and obtained during the passage of the 1st bogie of the *Alfa Pendular*. Case 10 (Figure 6-56a) represents a situation where the dip profile had minimal influence on the sleeper-ballast contact forces, with all sleepers applying very similar loading to the ballast layer: the same peak load of about 55 kN and a normal load of 3.8 kN due to the own weight of the track frame. For easier interpretation, Figure 6-56d shows only the results of the sleepers *n*-1, *n* and *n*+1, where *n* is the sleeper located at about the centre line of the dip. In Case 10, the minor influence the response on the track is due to the small amplitude (1.1 mm) and long profile of the dip (33.3 m). In Case 21 (Figure 6-56b), despite the small amplitude of the settlement (5.8 mm), the negative effect is evidenced with some sleepers showing higher peak loads, corresponding to load increments up to about +89%, compared with normal track conditions. In Figure 6-56e, it is visible that sleeper *n* remains hanging during the passage of the bogie, while sleeper *n*-1 (which is initially hanging), eventually presses against the ballast layer when directly loaded by each axle. As regards Case 93 (Figure 6-56c), it was found to be one of the worst-case scenarios in terms of sleeper-ballast contact forces. The results indicate that there is an important disturbance in the track that induces significant variations in the sleeper-ballast contact and results in peak loads higher than 100 kN under a few sleepers. Figure 6-56f shows that some of the sleepers that were initially hanging eventually apply severe impulse loads onto the ballast layer. This type of sudden impulse load may aggravate crushing and abrasion of ballast particles, thus promoting settlements, as discussed in studies by other authors (Baessler & Ruecker, 2003; Kono & Matsushima, 2012). It is reported that the impact exerted by hanging sleepers yields higher volumetric deformation and prevents the formation of

a stable and compact layer of ballast. This can be explained because the particles undergo a cyclic process under each axle: they are initially loosened, then suffer the impact (which induces breakage and rearrangement of the particles), and loosened again.

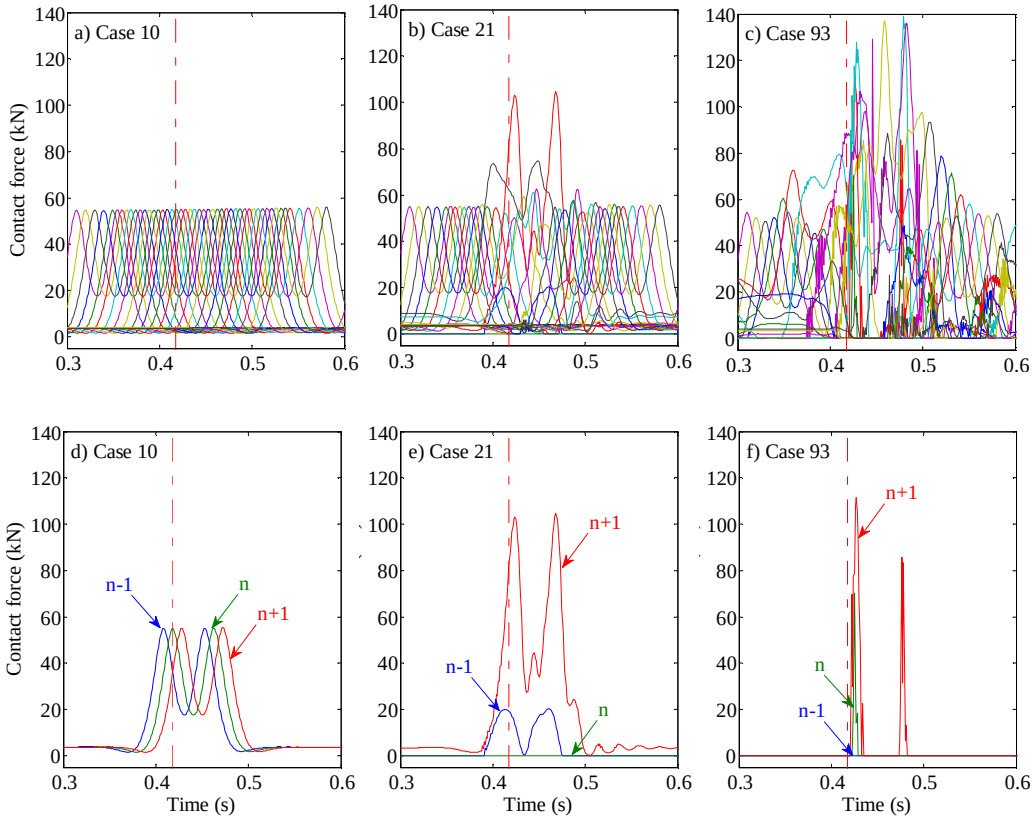

Figure 6-56. Time histories of the sleeper-ballast contact forces near the dip ceter line in cases 10, 21 and 93: a) to c) sleepers *n*-11 to *n*+12; d) to f) sleepers *n*+1, n and *n*+1.

Figure 6-57 shows a summary of the contact forces between the sleepers *n*-4 to *n*+4 and the ballast layer (peak values and contact forces in unloaded track conditions), during the passage of the first bogie of the *Alfa Pendular*, regarding cases 10, 21 and 93. The figure evidences that although the track may have a few hanging sleepers in unloaded conditions, most of them eventually exert loads onto the ballast layer. It is also visible that the sleepers located after the dip centre line, seem to apply higher loads, which is probably a consequence of the train's motion and interaction with the track, as discussed earlier. Considering Case 21, it seems that the sleepers with higher contact forces (*n*-2 and *n*+1) are those adjacent to the sleepers that were initially hanging (*n*-1 and *n*).

Similarly to what was reported in section 6.4, the numerical results suggest that the sleepers that undergo higher loads are not those that are hanging, but generally those located at the end of the dip and that do not show gaps on the underside. Those sleepers bear most of the weight of the adjacent hanging track frame, in addition to the vertical loads of the axles on the hanging section of the track. Figure 6-58 shows a schematic representation of this load redistribution.

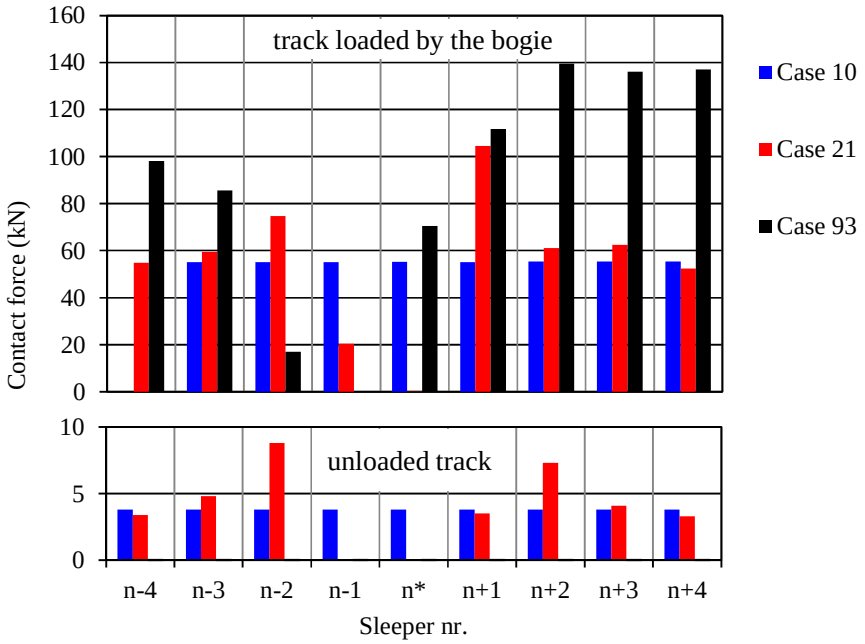

Figure 6-57. Summary of the sleeper-ballast contact forces under the 1st bogie of the vehicle, for three example cases (10, 21 and 93).

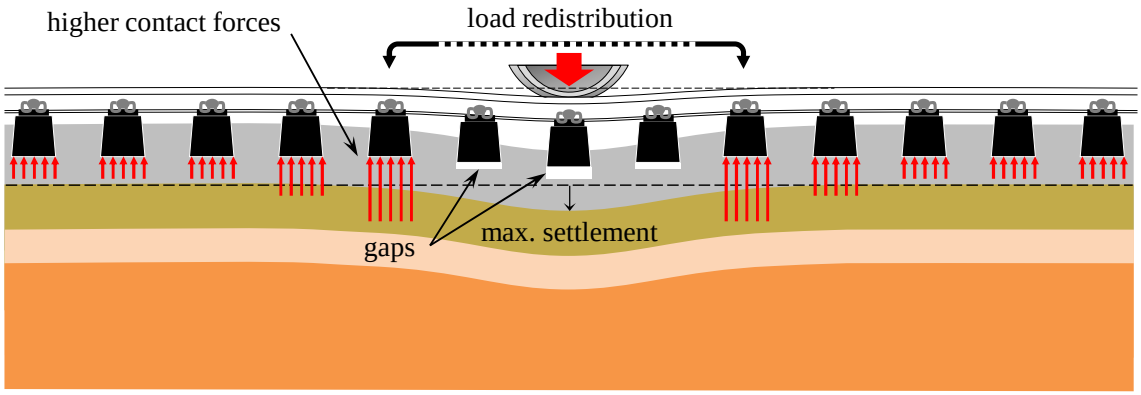

Figure 6-58. Schematic representation of load redistribution on a track section with hanging sleepers.

Considering all the tested cases, it is interesting to compare the number of sleepers that are initially hanging (Figure 6-59a) with those that undergo very low peak contact forces (for example, less than 5 kN - Figure 6-59b). It is visible that the majority of sleepers that are hanging in unloaded track conditions eventually establish contact with the ballast layer, exerting a load greater than 100 kN. Although it is not presented here, the number and distribution of sleepers that remain hanging is almost identical to that in Figure 6-59b.

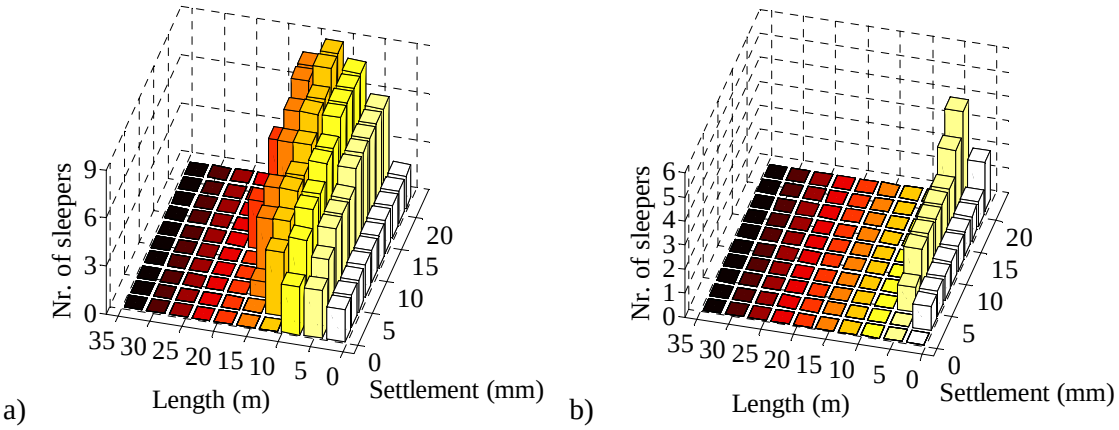

Figure 6-59. Number of sleepers that are initially hanging (a) and have peak loads lower than 5 kN (b).

To identify the range of dip profiles that may cause more damage to the ballast layer, Figure 6-60 shows the number of sleepers with peak values greater than 100 kN - a load increment of about +82% compared with good track conditions. The results indicate that these extreme loading conditions only appear for settlements greater than 5 mm and for lengths shorter than 15 m, depending on the settlement amplitude.

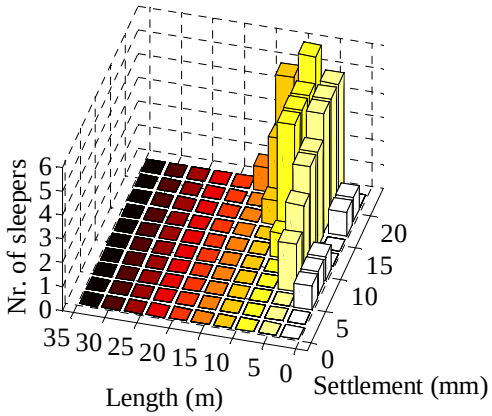

Figure 6-60. Number of sleepers with peak loads higher than 100 kN.

That observation is in agreement with Figure 6-61 which shows that higher peak values were obtained for shorter dip lengths (< 15 m) and that they increase with the settlement amplitude in that range of dip lengths. In addition, it is noticed that the shape of the resulting surface is similar to that of the maximum axle accelerations (Figure 6-48) and of the maximum train-track interaction forces (Figure 6-51). This suggests that the peak sleeper-ballast contact forces are strongly related to those two variables.

From the analysis of all the tested cases, it was confirmed that higher sleeper-ballast contact force normally occurred when the train exited the dip, while the lowest values were found near the centre of the dip. As mentioned earlier, this finding seems to be a consequence of the hanging sleepers, in addition to the influence of the downward and upward motion of the vehicle across the dip.

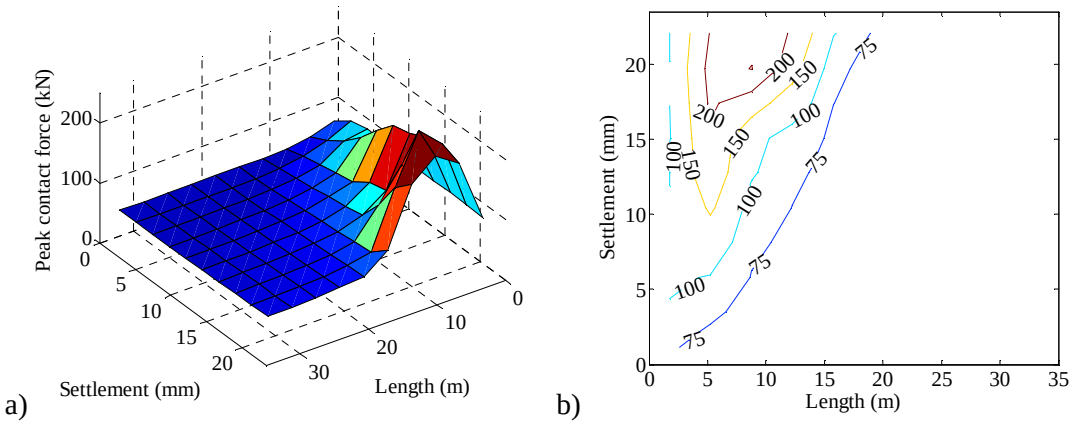

Figure 6-61. Maximum sleeper-ballast contact force: a) 3D surface; b) contour lines (kN).

Considering the vertical accelerations obtained in the sleepers, Figure 6-62 shows the 3D surface of the positive and negative values of the tested scenarios and Figure 6-63 depicts the respective contour lines. Because the hanging sleepers are less restrained than those that are adequately supported, the region with higher number of hanging sleepers (Figure 6-59b) and with higher sleeper loads (Figure 6-51) seems to yield higher acceleration amplitudes.

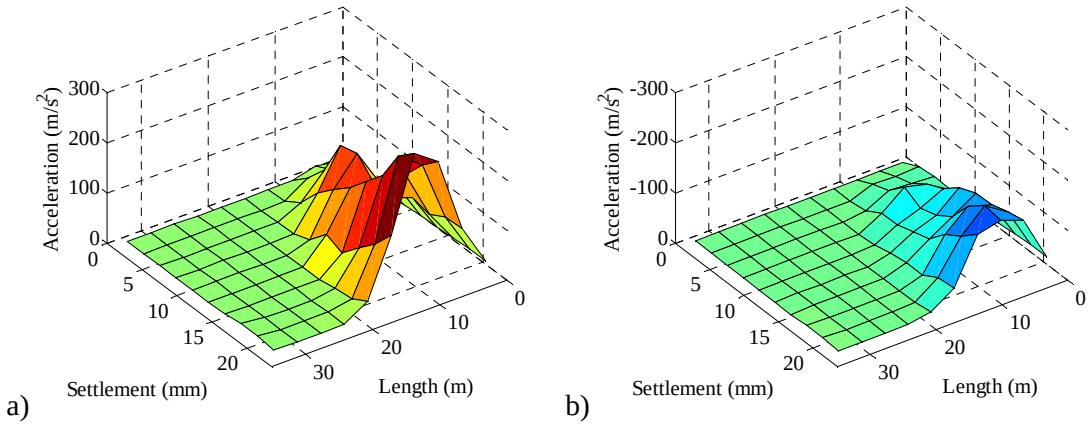

Figure 6-62. Peak sleeper accelerations: a) positive values; b) negative values.

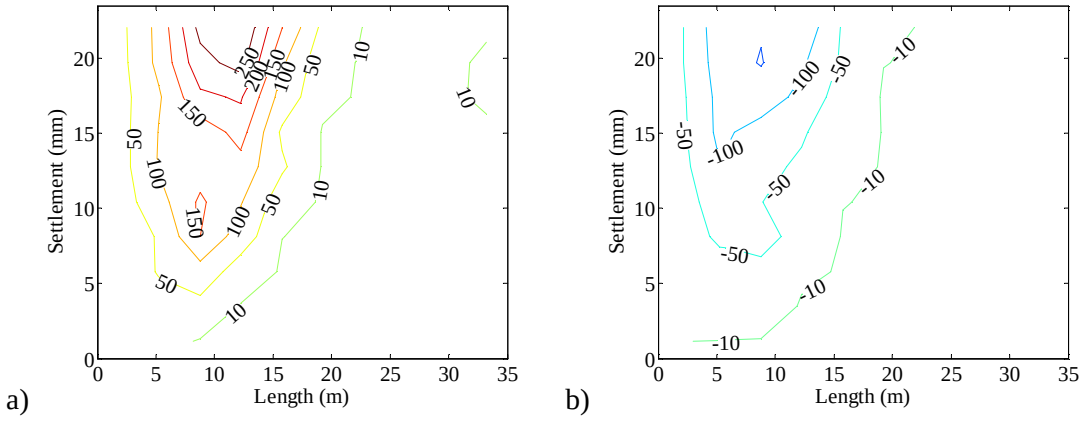

Figure 6-63. Peak sleeper accelerations in m/s^2: a) positive values; b) negative values.

The vertical accelerations measured in the field at transition zones with conventional ballasted track, presented in chapter 5, evidenced a normal track response, denoting peak vertical accelerations falling in the range of ± 5 m/s^2. A low-pass type II Chebyshev filter, with cut-off frequency of 80 Hz, was applied to those results. Thus, for an adequate comparison with the numerical results, the same low-pass filter was applied to the numerical data. Figure 6-64 and Figure 6-65 present the 3D surfaces and contour lines of the filtered results, respectively. Considering the results presented earlier in this section and from the analysis of the two figures, it is possible to verify that the range of the vertical accelerations of the sleepers that were measured *in situ* (± 5 m/s^2) correspond to good track conditions, as was expected given the early age of the railway line, the results of the track measurements and the reports of the inspection vehicle.

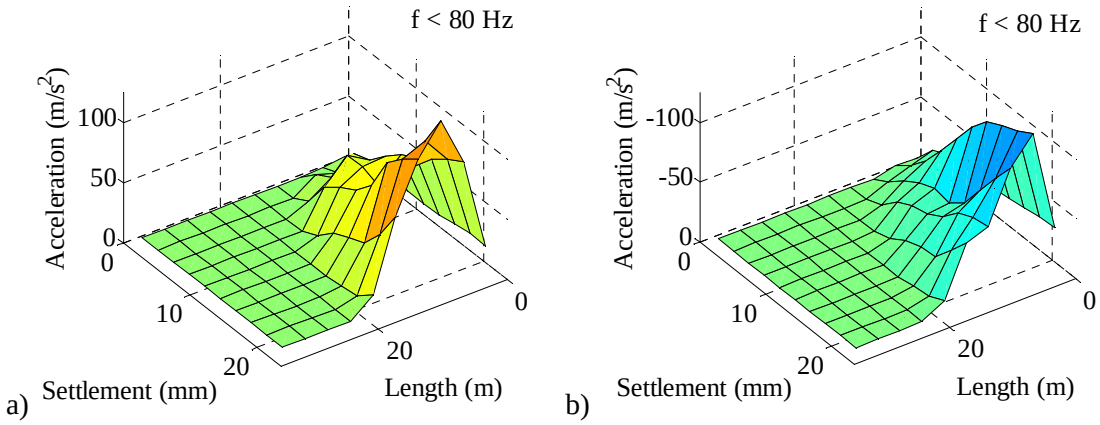

Figure 6-64. Peak sleeper accelerations (f < 80 Hz): a) positive values; b) negative values.

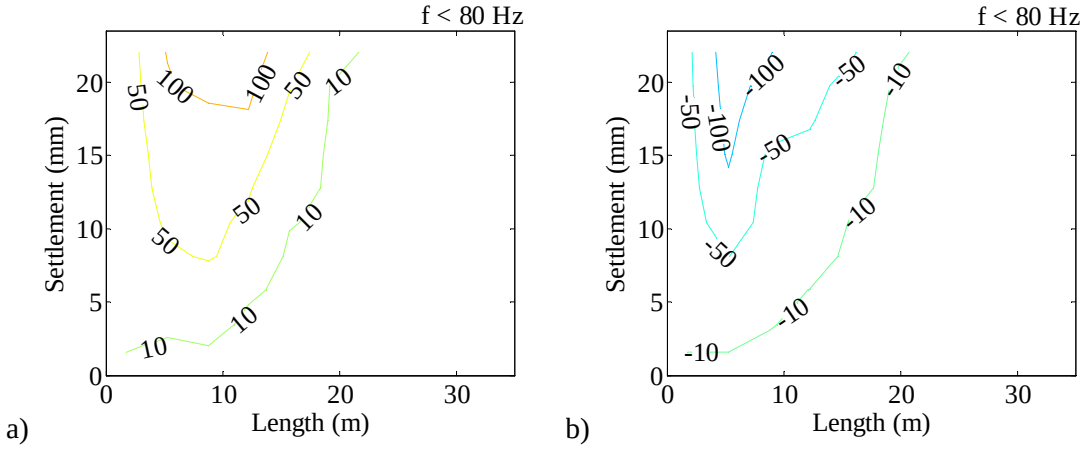

Figure 6-65. Peak sleeper accelerations in m/s^2 (f < 80 Hz): a) positive values; b) negative values.

The direct measurement of vertical accelerations of the sleepers seems to be promising procedure to assess the track dynamic response and prematurely identify abnormal track behaviour.

In general, regarding the simulations of dip profiles, it was evidenced that track defects with length shorten than about 20 m should be carefully followed up to avoid rapid degradation rates, even if their amplitude is still under the sum of the alert limits of LL_{D1} and LL_{D2}: 12 + 20 = 32 mm.

This raises another issue that is worth discussing. The track geometry obtained with the inspection vehicle, in particular the longitudinal level, only represents the position of the rails when they are loaded by the vehicle's axles, but not the actual settlement of the layers. As

explained earlier, this is due to the high bending stiffness of the rails, which prevents the frame of the track to adjust completely to situations of uneven ballast surface (as in dip profiles), specifically if they exhibit defects with shorter wavelengths. In fact, as illustrated in some scenarios, the vertical displacements of the axles may not represent the actual settlement profile of the tracklayers. This means that the current methods for track inspection may underestimate problems related to differential settlements. The track longitudinal level only represents the position of the rail, but at the same time, a larger settlement problem may be developing without notice and a severe problem related to hanging sleepers may be pass unnoticed.

6.5.3 Establishing performance indicators

In an attempt to integrate the analysis of all the numerical results presented above and to establish performance indicators, it was prepared an overlay (Figure 6-66) with the information of relevant contour plots presented earlier. The figure integrates information regarding the following aspects:

- Vertical accelerations inside the coach car: the region in Figure 6-54 denoting accelerations higher than the threshold of 1 m/s^2 was associated with decreasing passenger comfort (CEN, 2005);
- Dynamic coefficients of the train-track interaction force (Q_{dyn} / Q_{sta}): the region in Figure 6-52 with values lower than 0.6 – the offload threshold (Xia *et al.*, 2006) - was associated with increasing risk of train derailment;
- Vertical axle accelerations, train-track interaction forces, sleeper-ballast contact forces and vertical sleeper accelerations: the regions in Figure 6-49, Figure 6-51b, Figure 6-61 and Figure 6-63 that showed higher values were associated with situations that induced rapid track degradation.

Considering the above results and the regions identified in Figure 6-66, some remarks can be drawn:

- Increasingly higher track degradation rates can be expected with the amplitude of the defect, particularly amplitudes greater than 10 mm and for longitudinal defects with lengths shorter than 15 m.
- Critical oscillations in the train-track interaction start to occur when the longitudinal defects show lengths between about 2.5 m and 15 m, mainly for amplitudes greater than about 8 mm. These scenarios seem to increase the risk of derailment and correspond to the extreme situations of track loading that were analysed.

- Passenger comfort decreases with the amplitude of the defect, namely for amplitudes higher than 15 mm and for defects with lengths greater than about 8 m.

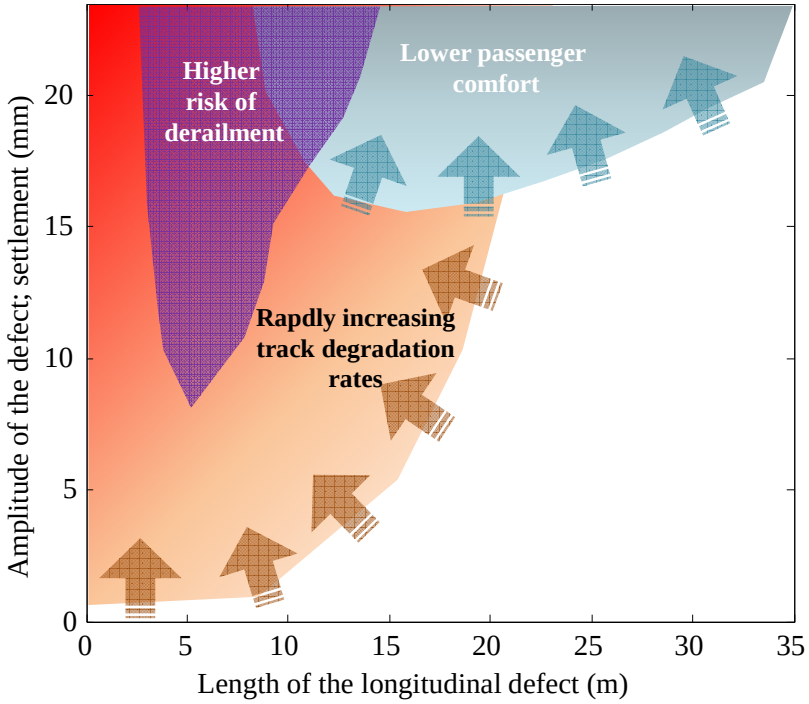

Figure 6-66. Summary of the parametric results.

The results also evidence that lower comfort levels resulting from the amplification in vertical accelerations inside the car body may not be associated with higher track degradation scenarios. For example, longitudinal defects of the track with lengths greater than 20 m, denoted lower passenger comfort for settlement amplitudes slightly greater than 15 mm, but there were no evidences that might suggest amplifications in the track response or in the train's loads.

The findings of this parametric study may be particularly relevant for the Portuguese Railway Infrastructure Manager in managing priorities for maintenance operations. For example, in different scenarios of track longitudinal level with similar defect amplitudes, the infrastructure manager could decide which sections to act with greater priority in order to address either aspects related to the track or to the passenger's comfort.

However, it should be noted that the obtained information was derived for the case of the passenger train *Alfa Pendular*, running at about 220 km/h in the railway track of the *Alcácer*

bypass. It is expected that analogous parametric studies, considering trains with different configurations or running at different speeds, would produce different results and identify different critical regions as those in Figure 6-66.

On the other hand, the findings from this parametric study seem to be applicable not only to the transition zones of the *Alcácer* bypass but also to other sections of the track on embankments. The dip profile was introduced in the model at the end of the wedge-shaped backfill, thus the influence of the transition zone structure is believed to be minimal. Consequently, similar results are expected if the numerical model only comprises track on embankments.

6.6 Concluding Remarks

A numerical study was presented on the influence of the settlement profiles of backfills in the dynamic train-track interaction at the approach to bridges - the transition zone. To that aim, a numerical model was used to simulate the effect caused by different shapes of settlement profiles.

It was observed that the number of hanging sleepers and the gap between the sleepers' underside and the ballast layer depended not only on the maximum settlement amplitude, but also on the shape of the settlement profile. The results also indicate that the development of differential settlements on the backfill can lead to critical situations in terms of track degradation (due to excessive load on the track), safety requirements (offload limits and loss of axle-rail contact) and passenger comfort (due to amplifications in the accelerations obtained inside the coach cars). In general, peak axle loads and accelerations increased with the amplitude of the settlement, but it also depends on the shape of the settlement profile. Generally, the greater the number of hanging sleepers and gap sizes, the higher the vertical accelerations of the sleepers and the larger the vertical contact forces between the sleepers and the ballast layer.

The simulations of hypothetical bump settlement profiles of a wedge-shaped backfill indicate an adequate behaviour of the train-track system because none of the limits related to track degradation, safety or passenger comfort were exceeded. This finding supports the conclusion that wedge-shaped backfills seem adequate to address the problems related to abrupt variations of the track's stiffness and differential settlements normally found at transition zones.

Regarding simulations of dip profiles at transition zones, performance indicators were established based on the results of a parametric study on the shape of the settlement profiles.

These indicators are related to the different combinations of settlement amplitude and length of the track defects, in that they may induce, in different ways, critical situations of track degradation, train safety and passenger comfort.

The results highlighted the risks involved in transition zones without adequate maintenance, although the vertical accelerations obtained inside the car bodies may denote very good passenger comfort.

The findings were derived for the *Alfa Pendular* running at about 220 km/h in the track of the *Alcácer* bypass, but the methodology seems to be applicable to other situations of train operation and track configurations.

Chapter 7

Integrated analysis of field data and numerical results

7.1 Scope

This chapter aims at integrating the information that was obtained in the previous sections with the main objective of contributing to the understanding of the track behaviour at transition zones or other track singularities, thus providing practical outputs that may be considered in maintenance and asset management activities by railway infrastructure managers. To achieve these objectives, some tools were developed and presented to analyse in more detail the track geometry data obtained with REFER's inspection vehicle on the *Alcácer* bypass and to assess the influence of the characteristics of the track longitudinal level in the dynamic train-track interaction.

As discussed in previous chapters, the European Standard series 13848 and the Portuguese regulation (REFER, 2009) establish that the Alert Limits (AL), the Intervention Limits (IL) and the Immediate Action Limits (IAL), regarding the longitudinal level, are analysed in terms of average to peak values rather than peak-to-peak values (in the case of AL, the data is also analysed in terms of standard deviations). This means that, for a given wavelength range, there might be situations of uneven longitudinal rail profiles that comply with those track quality levels but may induce higher dynamic amplifications of the train-track interaction than other longitudinal profiles than actually do not comply with those limits. Figure 7-1a exemplifies this point of view, showing segments of two defective hypothetical longitudinal profiles derived from simple sine functions, in the wavelength range of 3 to 25 m (D1). It is observed that, near x = 6 m, the profile in green evidences defects larger than the IAL limit. However, considering defects of wavelengths of about 5 m (Figure 7-1a), the green profile shows peak-to-peak amplitudes that are lower than the profile in black (which complies with the IAL limit). Higher

peak-to-peak amplitudes are normally associated with higher dynamic amplifications of the train-track interaction. Thus, in the wavelength range around 5 m, the green profile that exceeds the IAL limit may not be as severe for the track and vehicles as the black profile. On the other hand, analysing larger wavelengths (Figure 7-1b), it is observed that the green profile yields the highest peak-to-peak values, therefore suggesting that it is the worst scenario associated with effects caused by larger wavelengths.

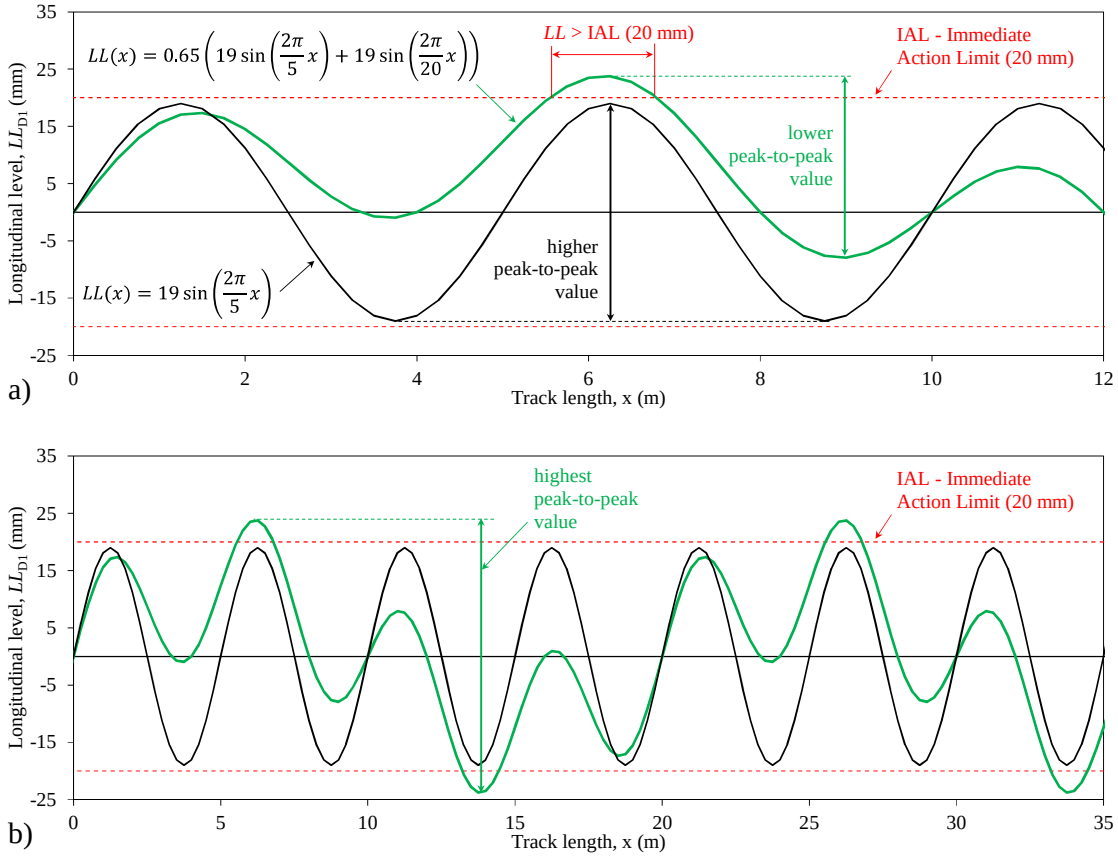

Figure 7-1. Hypothetical longitudinal track profiles derived from simple sine functions, in the wavelength range between 3 m and 25 m: a) shorter track segment of 12 m; b) longer track segment of 35 m using the same sine functions as in (a).

This example evidences another relevant aspect regarding the classification of the track quality levels. Following what was mentioned in chapters 2 and 4, different limits of the track quality levels are established for two wavelength ranges: D1 ($3 < \lambda < 25$ m) and D2 ($25 < \lambda < 70$ m). This classification establishes that, within each of these two wavelength ranges, track defects with different wavelengths have the same threshold value, thus are classified with the same quality level. However, they may correspond to different levels of risk of derailment or track

degradation. For example, track defects mainly associated with $\lambda = 3$ m and denoting amplitudes near AL's limit correspond to the same track quality level as defects with the same amplitude, but with λ = 25 m. Nevertheless, because the range D1 influences the resonance phenomena in sprung and semi-sprung masses of the vehicles and significantly contributes to the track degradation, different wavelengths affect different aspects of the train-track interaction - obviously depending on the train speed. This was clearly demonstrated in the numerical parametric study presented earlier in section 6.5.3.

In theory, it could be argued that the track quality limits should be established as a function of the wavelength (or spatial frequency) of the track defects, instead of separating the information into a couple of wavelength ranges and considering the data corresponding to each wavelength to have equal importance and limited by the same amplitude threshold. In practice, considering that the speed of the trains significantly influence the train-track excitation frequencies and that there is a large variability in the characteristics of different tracks and vehicles, it would be a challenge to implement an approach that took into account all these factors in the determination of the track quality limits as a function of the wavelength of the defect.

In any case, the successive track geometry surveys carried out on the tracks can provide crucial information for railway infrastructure managers if more advanced tools are used to analyse the data.

7.2 Advanced characterisation of the longitudinal level

7.2.1 Average longitudinal level considering wavelength ranges D1 and D2

In this section, the data of the longitudinal level of the track (*LL*) of the *Alcácer* bypass was analysed in more detail, in particular the measurements of REFER's inspection vehicle carried out in the survey of July 2013 (introduced in Chapter 4). Because this thesis focuses only on the vertical component of the train-track interaction, other geometric parameters were not considered and the differences between the longitudinal levels of both rails were discarded. Therefore, the data corresponds to the average longitudinal level of the left and right rails ($\overline{LL}$) after adding up the respective D1 and D2 components ($\overline{LL}_{\mathrm{D1+D2}}$), following the same approach used in Chapter 6 (see case study in section 6.4). Figure 7-2 shows the longitudinal level $\overline{LL}_{\mathrm{D1+D2}}$, along the track in the wavelength range between 3 m and 70 m.

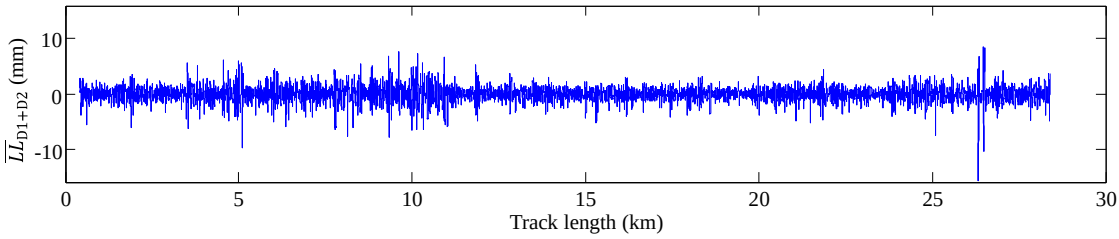

Figure 7-2. Longitudinal level (average of left and right rails) considering wavelength ranges D1 and D2 (3 m to 70 m).

7.2.2 Analysis of the longitudinal level by means of spectrograms

As mentioned earlier, there are complex tools available to analyse the track geometry data obtained with the inspection vehicles, other than just analysing the respective means, peak values and standard deviations. For example, the spectrograms of track records can provide a visualisation of the spectrum of the spatial frequency content of the defects along the length of the track. The main purpose of this technique is to characterise the type of defects and to highlight persistent spatial frequencies of the defects in a stretch of the track.

In the present case, using MATLAB "`spectrogram`" function (MATLAB, 2012), it was calculated the one-sided modified periodogram estimate of the power spectral density (PSD) of each windowed segment of the signal. Each segment was delimited by a Hamming moving window and had a length of 128 points (corresponding to about 32 m of track length), overlapping by 64 points. For each segment, 256 spatial frequency samples were calculated in the process. The spatial sampling rate was considered to be 4 samples/m (the inspection vehicle provides a data point at every 25 cm). Figure 7-3a shows the obtained spectrogram of the longitudinal level of the track, where the warmer colours denote the spatial frequencies, $\xi = 1/\lambda$, with higher content (in terms of Power/ ξ). In this figure, it is visible a larger content for lower spatial frequencies because the track measurements correspond to the wavelength ranges D1 and D2, thus, corresponding to the spatial frequency range between about 0.33 m^{-1} and 0.014 m^{-1}. The Figure 7-3b is a zoom of the upper spectrogram, considering this range of spatial frequencies and using a different colour scaling to evidence the peaks in the lower spatial frequency content. In general, the noticeable track defects fall in the range of 0.014 m^{-1} to 0.1 m^{-1} and correspond to longer wavelength defects between 70 m and 10 m that are associated with the normal ballasted track degradation (Esveld, 2001). However, there are also a few locations denoting track defects with higher spatial frequency content, mostly up to about 0.15 m^{-1}, that is, wavelengths down to about 6 m. Some of the locations evidencing larger track

defects appear to be related to track singularities, as will be discussed later in this chapter. In Figure 7-3a, it is visible two predominant spatial frequency ranges centred at about 0.8 m^{-1} and 0.4 m^{-1} that appear to be multiples of the sleeper spacing frequency (1/0.6 m = 1.6(6) m^{-1}). This result suggests that the signals provided by the inspection vehicle in the D1 wavelength range might extend to wavelength ranges below 3 m.

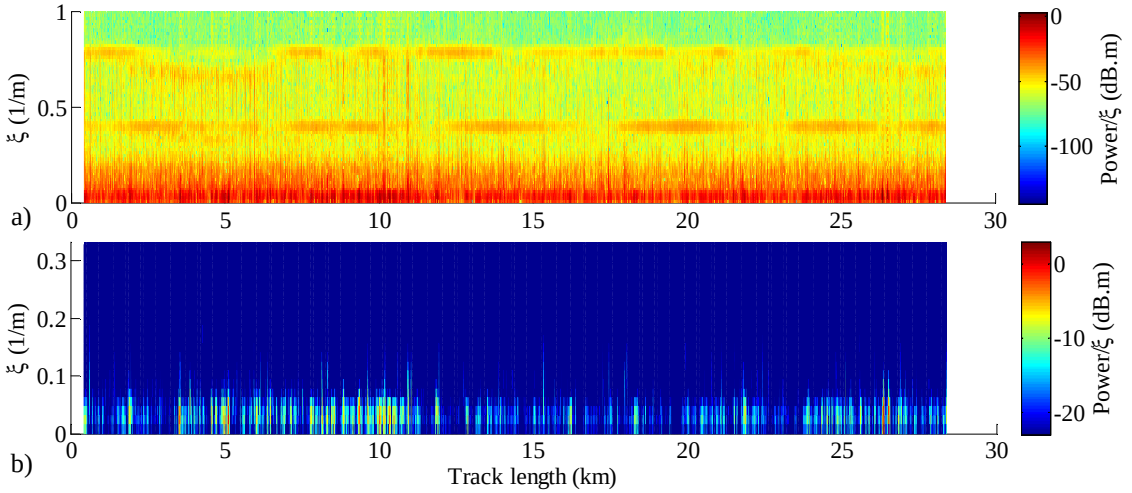

Figure 7-3. Spectrograms of the longitudinal level of the track: a) representation of spatial frequencies, ξ, up to 1 m^{-1}; b) content for spatial frequencies between 0.33 m^{-1} and 0.014 m^{-1}.

For easier interpretation, the results were divided into stretches of 5 km and the respective spatial frequencies were converted to the respective wavelength, λ. The results were then plotted in Figure 7-4, in a graphical representation of length vs λ. The figure also provides a comparison with some information presented earlier in Chapter 4, namely, relevant aspects of the substructure (height of the embankment, depth of the cutting, relevant substructure reinforcements, values of the E_{V2} obtained with the *portancemètre* on the sub-ballast in March 2010) and the locations of track singularities.

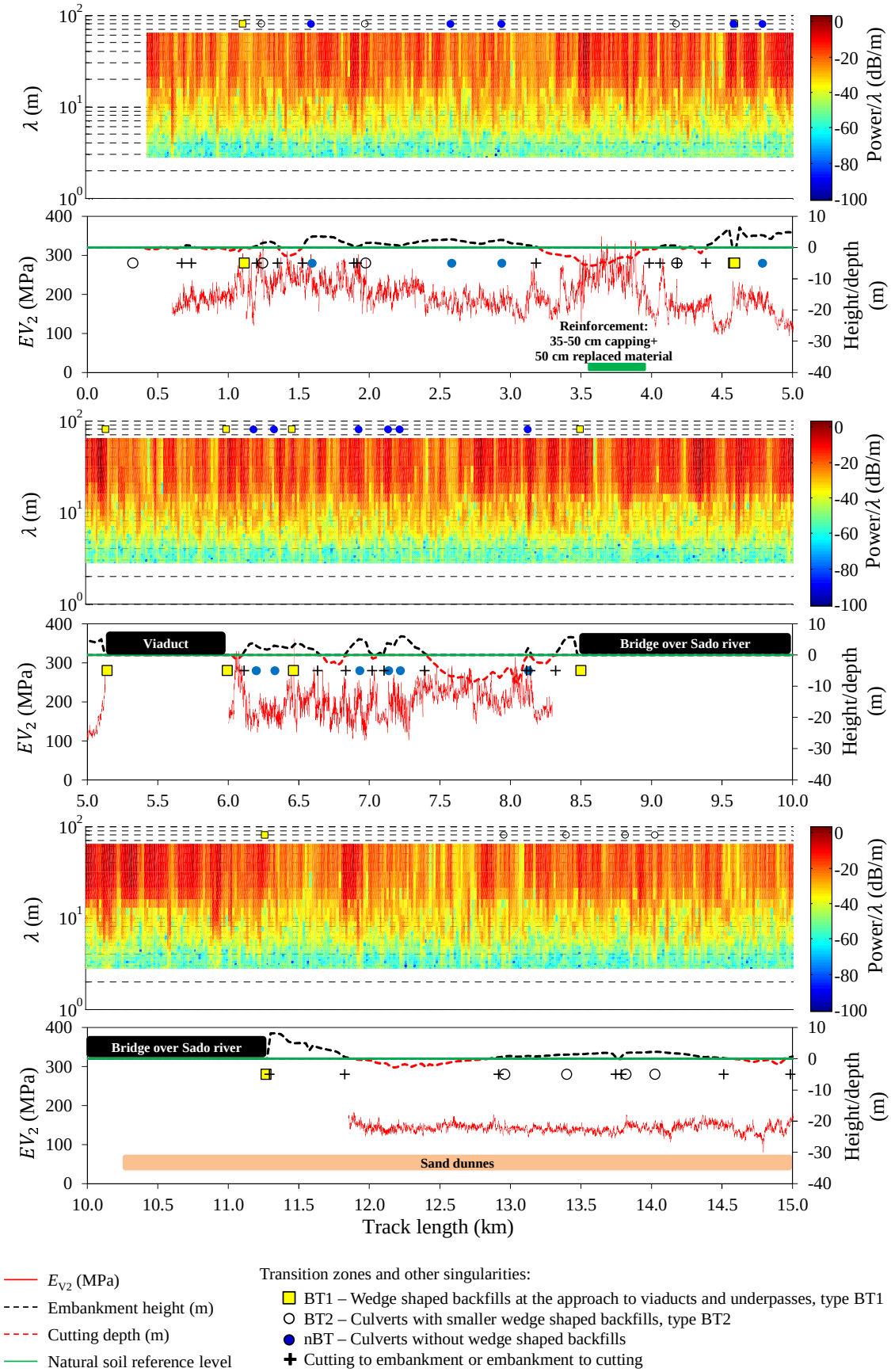

Figure 7-4. Comparison of the wavelength content of the longitudinal level and relevant aspects of the track substructure (continues).

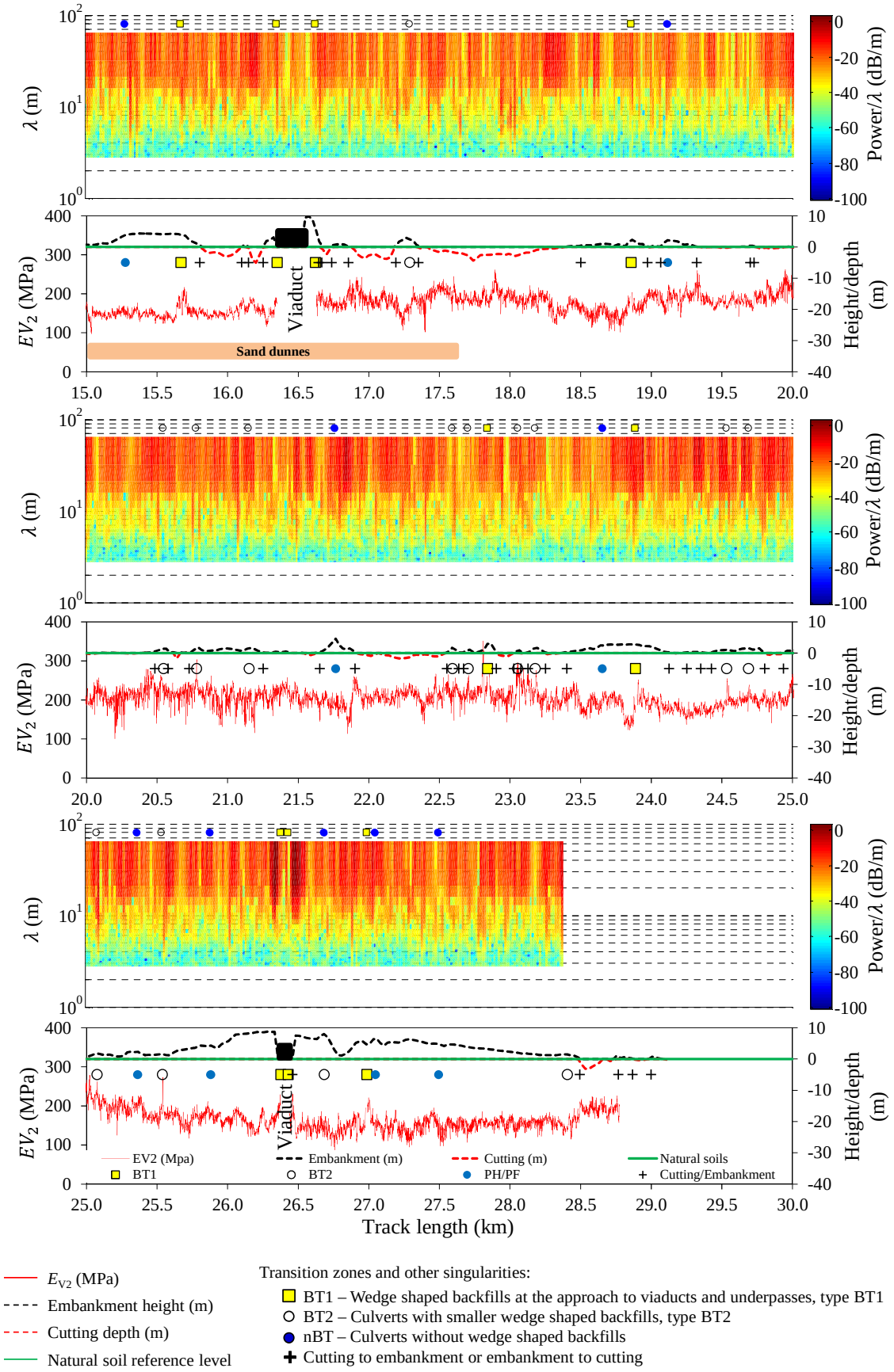

E_{V2} (MPa)
Embankment height (m)
Cutting depth (m)
Natural soil reference level

Transition zones and other singularities:
- BT1 – Wedge shaped backfills at the approach to viaducts and underpasses, type BT1
- BT2 – Culverts with smaller wedge shaped backfills, type BT2
- nBT – Culverts without wedge shaped backfills
- Cutting to embankment or embankment to cutting

Figure 7-4 (continued): Comparison of the wavelength content of the longitudinal level and relevant aspects of the track substructure.

Although it is not completely clear from the analysis of Figure 7-4, it appears that near some track singularities there are sudden increases in the content of wavelengths greater than about 10 m. These locations include the approaches to the viaducts over *S. Martinho* stream and over EN120 near 26.5 km mark, as well as the rail expansion joints on the bridge over Sado river between 8.5 km and 11 km marks. In addition, more than twenty other track singularities seem to be correlated with higher contents of the wavelengths smaller than about 6 m. Nevertheless, the complexity and amount of information provided by the spectrograms makes it difficult to obtain further meaningful results and correlate it with other aspects of the track and its substructure. For this reason, and aiming at incorporating the results of the numerical study, a simple yet efficient approach is presented in the next section to analyse the defects of the longitudinal level.

7.2.3 Analysis of the longitudinal level based on a range of chords and the respective amplitudes at mid-chord

With the final objective to integrate the results of the track geometry of the *Alcácer* bypass with the numerical results presented in the parametric study of section 6.5.3, this section aims to characterise the defects of the longitudinal level considering a range of chords and determining the respective defect amplitudes at mid-chord. The method consisted of calculating, at each position i of the track (in intervals of 0.25 m), successive j defect amplitudes of the longitudinal level (A_{ij}) based on overlapping chord lengths (L_j) between 3 and 35 m, in increments of 0.25 m. The method is schematically represented in Figure 7-5 considering the generic i position in the track. Each calculated pair of chord length and respective amplitude at mid-chord is denoted in the text as one “occurrence”.

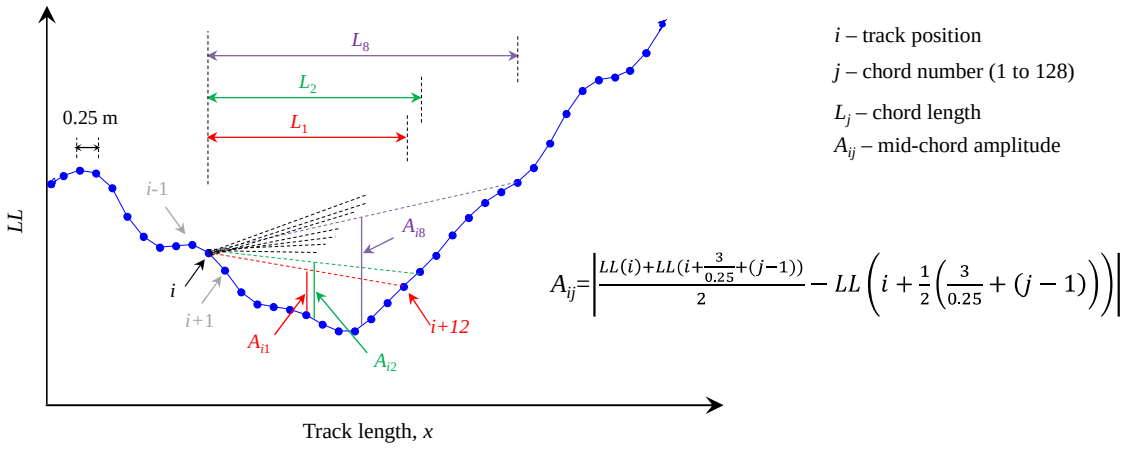

Figure 7-5. Schematic representation of the calculation procedure to determine the amplitude at mid point of the chords.

This approach implied performing 128 calculations per 0.25 m of track ((35 - 3)/0.25 = 128), yielding a data set of slightly more than 14 million values. For this reason, it was necessary to develop an algorithm in MATLAB environment to analyse this large set of data.

After the determination of all occurrences, it was possible to plot the results in graphs of chord length vs respective amplitude at mid-chord. Figure 7-6 shows an example of the application of this method to a portion of the track. In this example, the starting point of the chords was fixed at about 26.32 km mark, while the other end was located 3 m to 35 m away, thus forming chords lengths between 3 m (L_1) and 35 m (L_{128}) as illustrated in Figure 7-6a. The respective amplitudes at mid-chord were determined for that portion of track, resulting in the curve presented in Figure 7-6b that correlate the chord length with the respective amplitude at mid-chord. From the analysis of Figure 7-6, it was possible to confirm that, considering chords fixed at about 26.32 km mark, the maximum amplitude at mid-chord is A = 20 mm and occurs when the chord length is approximately 26.7 m (chord number L_{95}).

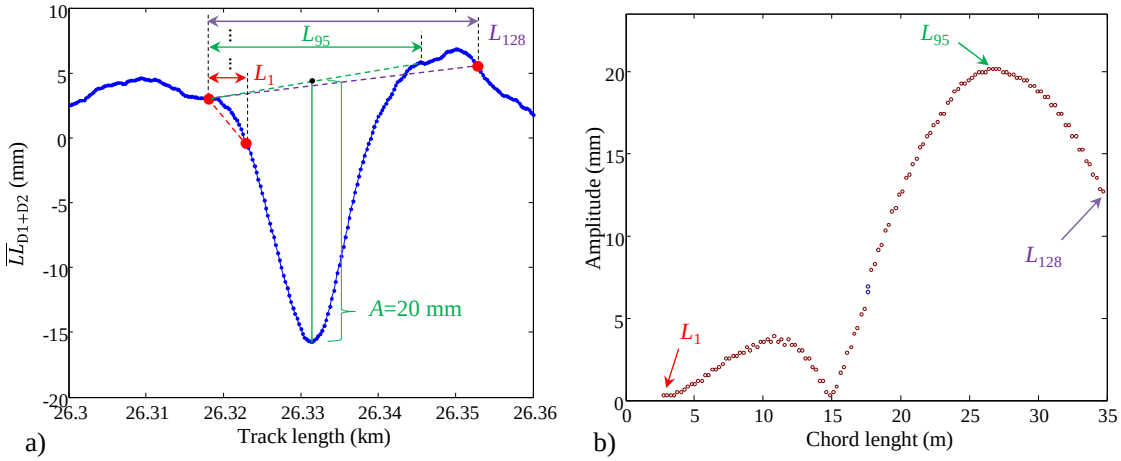

Figure 7-6. Example of the application of the method to a portion of the track at 26.32 km mark: a) measuring mid-chord amplitudes of the longitudinal level; b) chord lengh vs mid-chord amplitude representation.

Figure 7-7 presents the distribution of the occurrences (in terms of the number of occurrences) in the space chord length vs amplitude. The calculation of the amplitude at mid-chord instead of the calculation of the maximum amplitude, for a given chord length, guarantees that every location in the track is taken into account with equitable representation, denoted by the same number of occurrences. Otherwise, the analysis of the overall distribution of the occurrences

would be distorted, increasing the emphasis given to defects with larger amplitudes, which would not be representative of the real measurements.

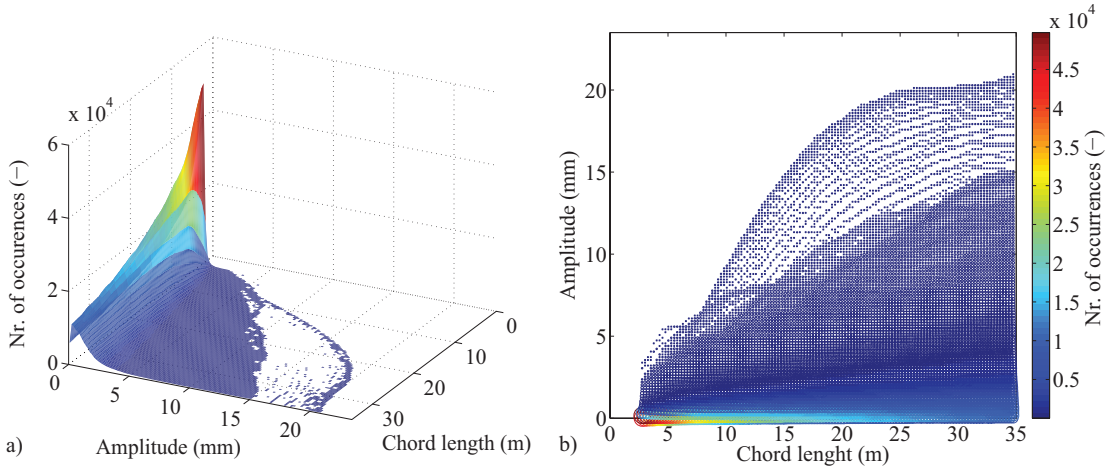

Figure 7-7. Two representations of the density of occurences: a) 3D surface; b) scatter plot (the size of the dots is proportional to the root square of the number of occurences).

It is important to note that, in Figure 7-7b, even a small segment of track is represented by a large number of occurrences (dots). For example, a 10 m-long segment of track (actually, spanning up to 10 m + 35 m to cover the chord length range) yields (10/0.25)128 = 5120 occurrences.

Considering the very good track quality level, it was expected that a significant part of the occurrences would fall in the region denoting small amplitude defects. In fact, for chord lengths of about 3 m to 10 m, the large majority of the occurrences had less than 1 mm of amplitude. As the chord length increases, the amplitude of the defect evidences more variability, reaching up to about slightly more than 20 mm.

Figure 7-8 shows the same data as the previous figure but separated into six segments of track, of about 5 km each. This figure evidences that, for each chord length, there is not a uniform distribution of the respective amplitudes along the track. In general, the track section between 10 km and 25 km marks (Figure 7-8c, d and e) shows mid-chord amplitudes lower than about 7.5 mm for the studied range of chord lengths. Whereas other portions of the line show amplitudes higher than 15 mm for chord lengths larger than about 25 m (Figure 7-8f), or higher than 5 mm for chord lengths smaller than 5 m (Figure 7-8a). These differences seem to be

related to some characteristics of the track superstructure and substructure, which is discussed later in this chapter.

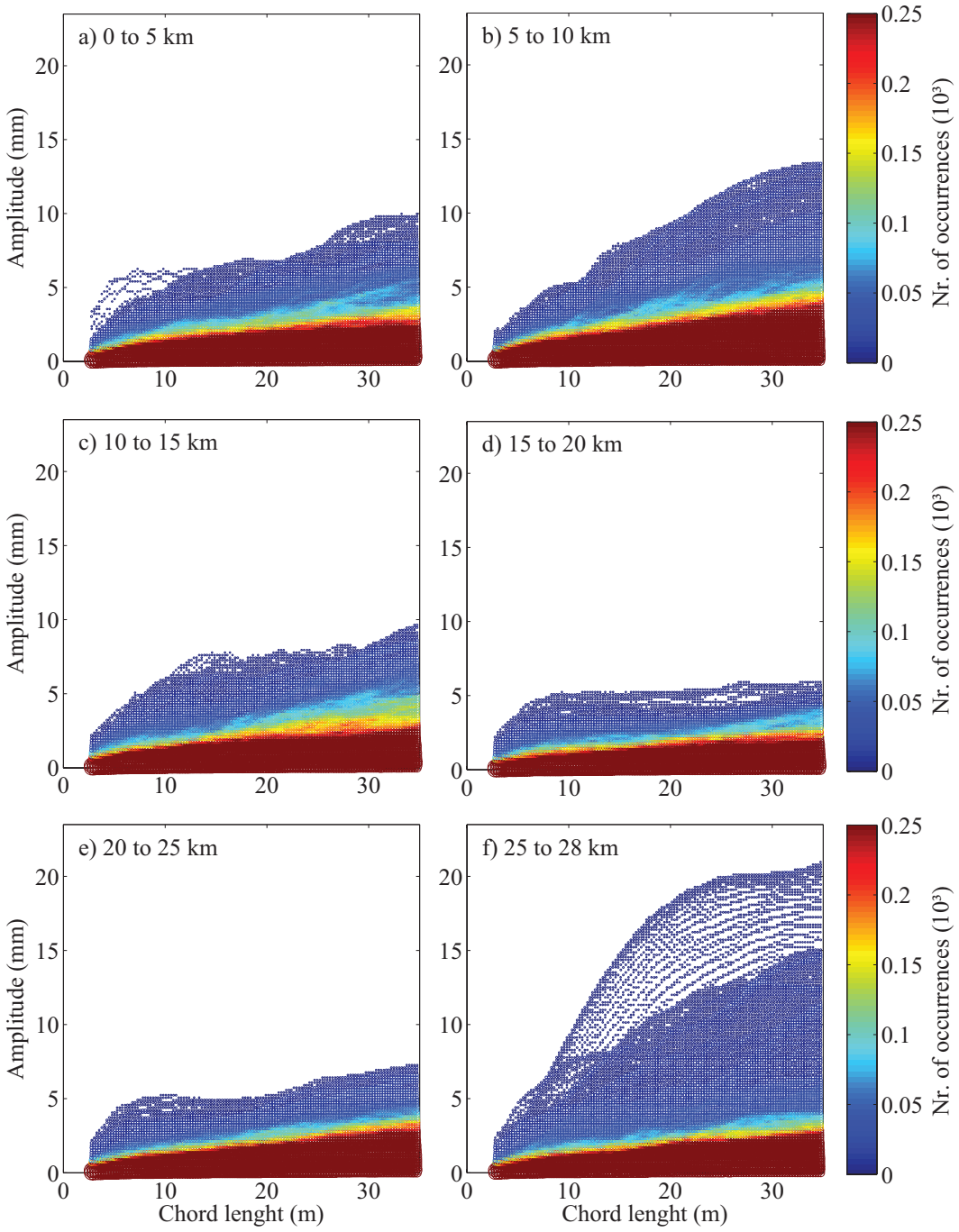

Figure 7-8. Occurrences corresponding to track segments of about 5 km.

7.3 Comparison of the longitudinal level defects with the numerical results from Chapter 6

7.3.1 Overlay plots of chord length vs amplitude at mid-chord

In this section, the information regarding the characterisation of the longitudinal level is integrated with the information obtained earlier in the parametric study of section 6.5.3 that concern the results of the train-track interaction obtained with the numerical model. The information from that numerical study resulted from different scenarios of uneven longitudinal rail profiles ("dip" rail profiles) that were tested in the model, considering the passenger train *Alfa Pendular* travelling at 220 km/h. The scenarios covered a range of defect amplitudes up to 23.5 mm and lengths of the defects up to 35 m that were imposed in the top nodes of the ballast layer.

The aim of this section is to analyse if the occurrences in the longitudinal level (in terms of chord length and respective amplitude at mid-chord) matched some scenarios that were identified in the numerical study to be associated with higher risk of derailment, rapidly increasing track degradation and lower passenger comfort. These aspects are known to affect the performance of transition zones.

In the following figures, it is presented an overlay of the density of the occurrences calculated in the previous section (Figure 7-7) with the contour lines of the numerical results that regard different aspects of the dynamic train-track interaction (figures 6-61 to 6-65).

The overlay in Figure 7-9 shows that the regions that were associated with higher amplitudes of the axle accelerations barely intersect the region of occurrences that was calculated. This result suggests that, in general, the defects in the longitudinal level of the *Alcácer* bypass are not causing high accelerations (amplitudes greater than 30 m/s^2) on the *Alfa Pendular*'s wheelsets. This result is also reflected in Figure 7-10, which suggests that the dynamic amplification of the axle loads of the *Alfa Pendular* remains low (occasionally reaching values of about 1.5 times the static load) and that the region denoting offload values lower than 0.6 was not reached – offload values above that limit are associated with higher risk of derailment (Xia *et al.*, 2006).

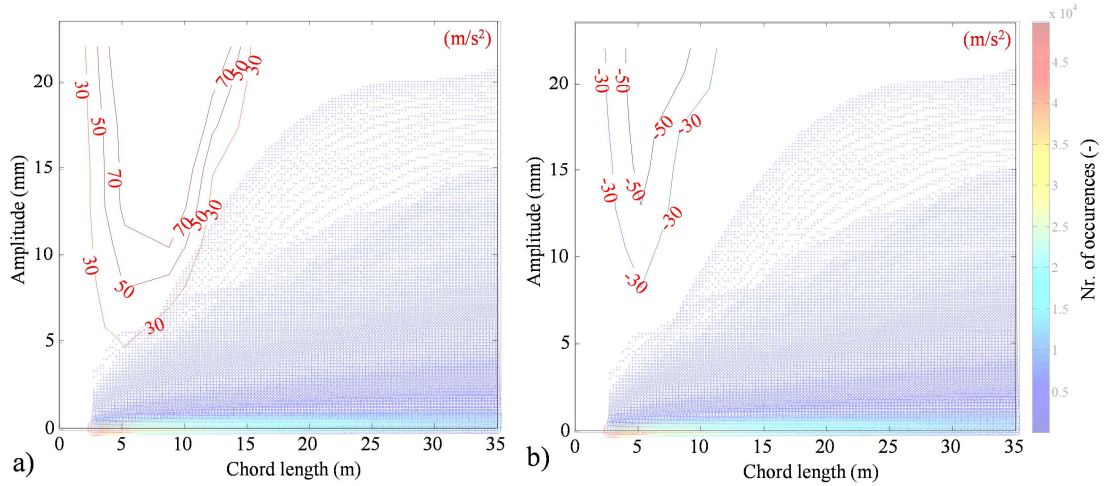

Figure 7-9. Overlay of the contour lines of the positive peak (a) and negative peka (b) axle accelerations (m/s^2) obtained in section 6.5.3 and the measured track defects.

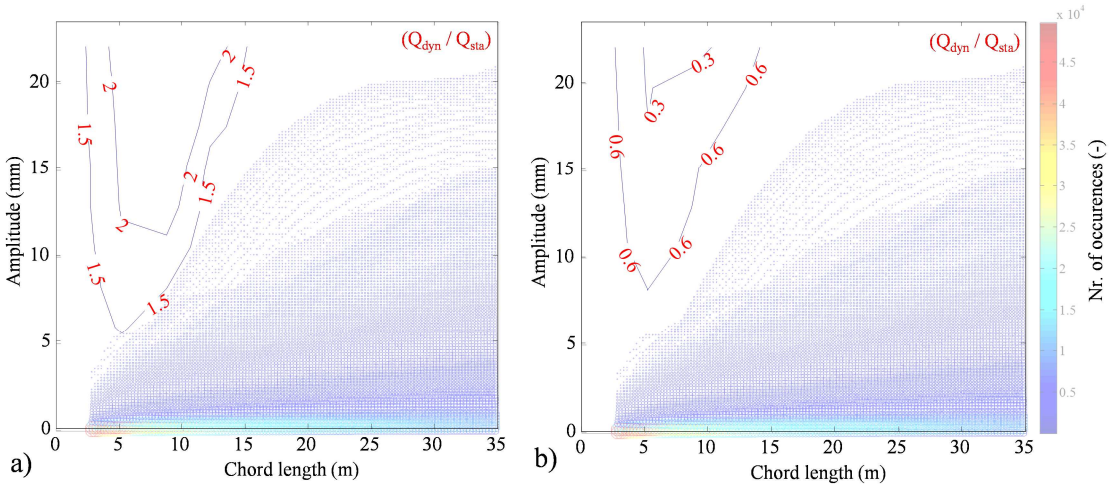

Figure 7-10. Overlay of the contour lines of the numerical maximum (a) and minimum (b) dynamic coefficients (Q_{dyn} / Q_{sta}) obtained in section 6.5.3 and the measured track defects.

As regards vertical accelerations inside the cars of the *Alfa Pendular*, some occurrences were associated with accelerations higher than 1 m/s^2 which correspond to the threshold value denoting very good passenger comfort, as established in the Eurocode EN 1990 (CEN, 2005). These occurrences regard chord lengths greater than about 15 m and amplitudes slightly higher than 15 mm. In particular, they correspond to the case study of the *Alcácer* bypass presented in section 6.4 (the approaches to the viaduct over the EN120).

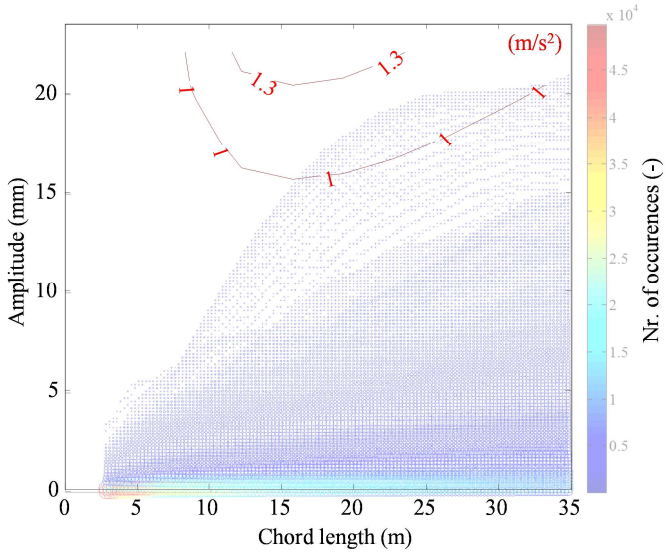

Figure 7-11. Overlay of the contour lines of the numerical maximum vertical accelerations inside the *Alfa Pendular* car body (m/s^2) obtained in section 6.5.3 and the measured track defects.

In Figure 7-12, the density of occurrences is overlaid with regions associated with important amplifications of the sleeper-ballast contact forces. The results suggest that, in some locations corresponding to occurrences with chord lengths lower than 15 m and amplitudes up to about 15 mm, may be developing sleeper-ballast contact forces greater than 75, yet lower than 100 kN.

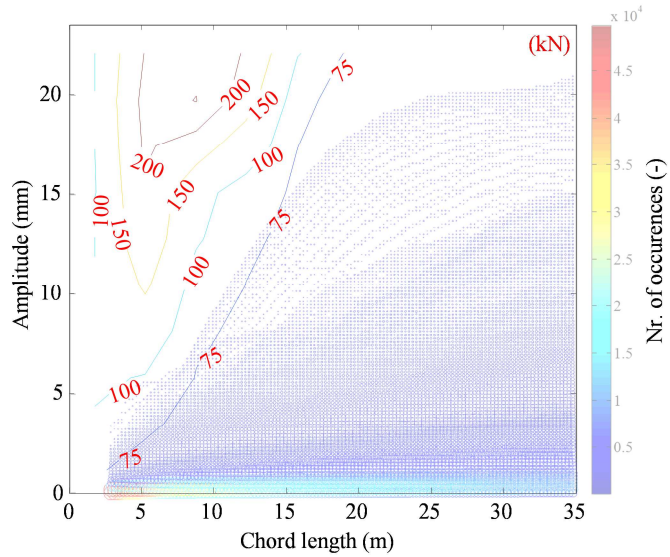

Figure 7-12. Overlay of the contour lines of the numerical maximum sleeper-ballast contact force (kN) obtained in section 6.5.3 and the measured track defects.

As regards the vertical accelerations of the sleepers, the density of occurrences was overlaid in Figure 7-13 with the regions relative to important amplifications of accelerations (regarding the numerical results after applying a low-pass filter with cut-off frequency of 80 Hz). In the graphs, it is possible to verify that the contour lines of +/-10 m/s^2 extend over some occurrences with chord lengths lower than 20 m and amplitudes up to about 17.5 m. After a detailed analysis, it was found that among these occurrences, the ones with amplitudes greater than about 7.5 mm were related to the case study in section 6.4 that was already mentioned.

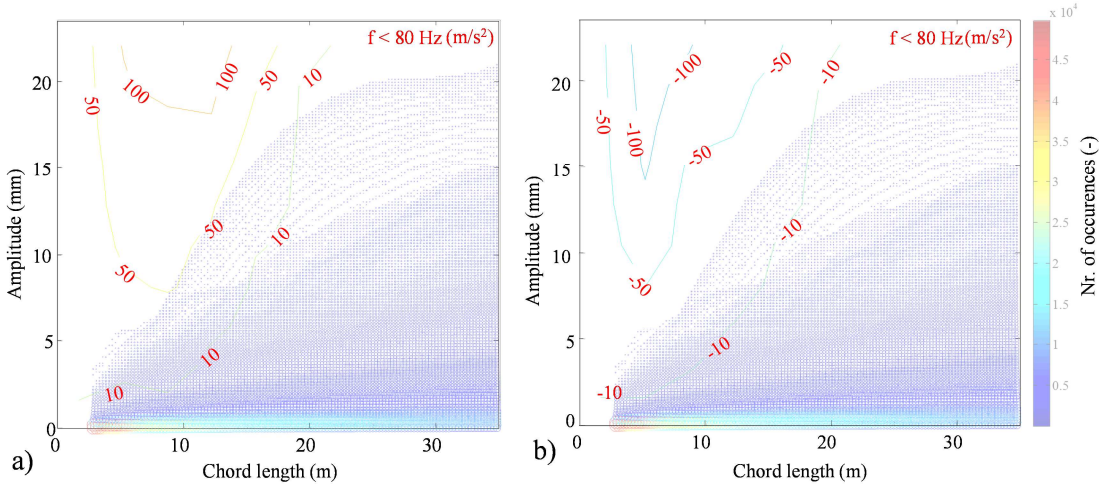

Figure 7-13. Overlay of the contour lines of the numerical positive peak (a) and negative peak (b) sleeper accelerations (m/s^2) after applying a low-pass filter with cut-off frequency of 80 Hz (see section 6.5.3) and the measured track defects.

The presence of hanging sleepers was not analysed here using the same method because of two main reasons: i) according to the results in section 6.5.3, the worse cases of hanging sleepers occurred for defects with lower lengths, up to about 5 m, which are not completely covered by the D1 wavelength range; ii) the presented method of analysis of the longitudinal level is not adequate to identify hanging sleepers because the high bending stiffness of the track frame prevents the track from deforming for shorter spans, thus not evidencing situations of hanging sleepers.

Figure 7-14 summarises the above information and follows the approach presented in section 6.5.3, grouping the aspects that affect the dynamic train-track interaction into three main regions, whether they are related to: i) higher risk of derailment; ii) rapidly increasing track

degradation rates; iii) lower passenger comfort. The figure shows than the large majority of occurrences falls outside those three regions. There are some occurrences suggesting rapidly increasing track degradation rates or lower passenger comfort, and even others, which may be associated with both track degradation and low passenger comfort.

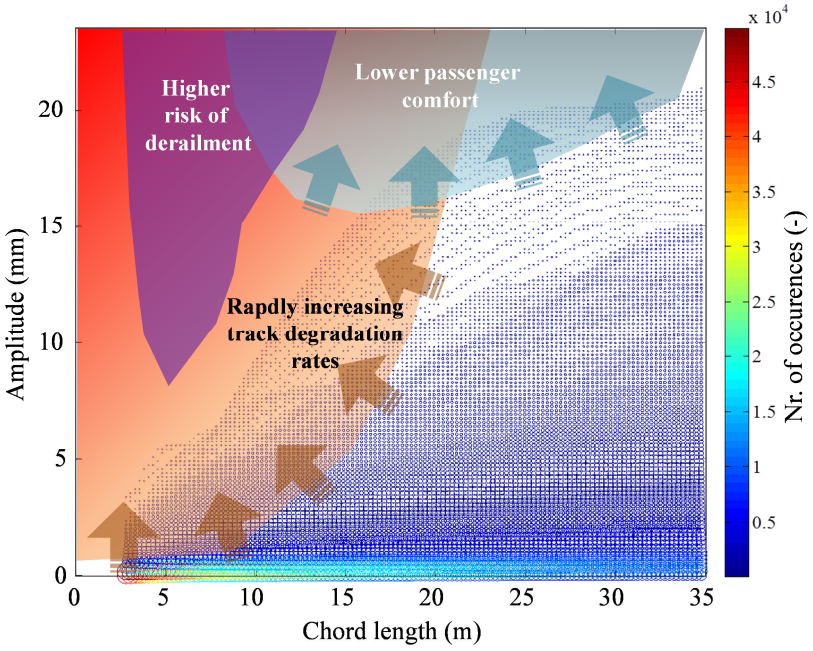

Figure 7-14. Overlay of the results in Figure 7-7 with the summary of the numerical results obtained in section 6.5.3.

It should be highlighted that the approach presented here has some limitations and drawbacks. Firstly, the study concerns the dynamic train-track interaction of the Portuguese *Alfa Pendular* train only, particularly travelling at 220 km/h, and considering the specific characteristics of the track of the *Alcácer* bypass. Therefore, it does not represent other types of vehicles or different train speeds.

In addition, the uneven rail profiles tested in the previous numerical study were representations of possible longitudinal level defects that initially were derived to match an important track defect found in the *Alcácer* bypass (see section 6.5.3). They do not represent all possible shapes of longitudinal level defects found in that railway line. Each rail profile tested in the numerical model was characterised by the approximate length of the dip and its maximum amplitude, whereas, the actual longitudinal level of the track was characterised by the chord length and the

respective amplitude at mid-chord. This means that the rail profiles tested in the numerical study should only be regarded as simplifications or approximations to the segments of the longitudinal level calculated for each chord length. Take the example of an uneven rail profile tested in the numerical model with a dip length of about 15 m and maximum amplitude of 10 mm: if it was considered a chord length of 15 m, the amplitude at mid-chord of that theoretical profile would also correspond to 10 mm. However, infinite possible segments of the longitudinal level with different shapes would also fit that criterion, as exemplified in Figure 7-15.

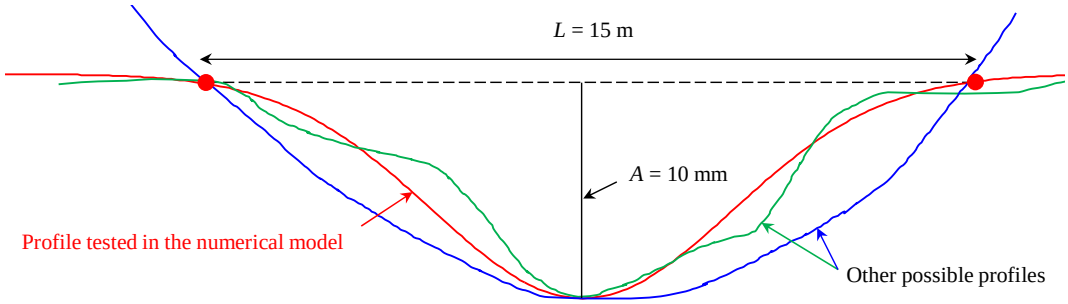

Figure 7-15. Examples of rail profiles with the same amplitude (at mid-chord) for a given chord length.

Consequently, the results and correlations presented here only provide a suggestion to the possible effects on the train-track interaction caused by different shapes of track defects. It would be necessary to perform additional parametric studies similar to the numerical study in section 6.5.3, covering different shapes of track dips for the same range of defect lengths and amplitudes, and considering other types of trains (with different axle loads and axle arrangement) and running at different speeds.

Nevertheless, the results may be regarded as guidelines for the analysis of the evolution of the track longitudinal level, particularly in the assessment of the performance of transition zones of the *Alcácer* bypass or other sections of the track with comparable longitudinal defects.

7.3.2 Analysis of the locations that suggest scenarios of lower performance of the track

This sections aims at identifying which locations in the track corresponded to the specific occurrences that were found to be associated with lower track performance, that is, locations

suggesting higher risk of derailment, increasing degradation rates or lower passenger comfort identified by the three regions in Figure 7-14. To that aim, the contour of those regions was determined (Figure 7-16) and then intersected with the list of occurrences.

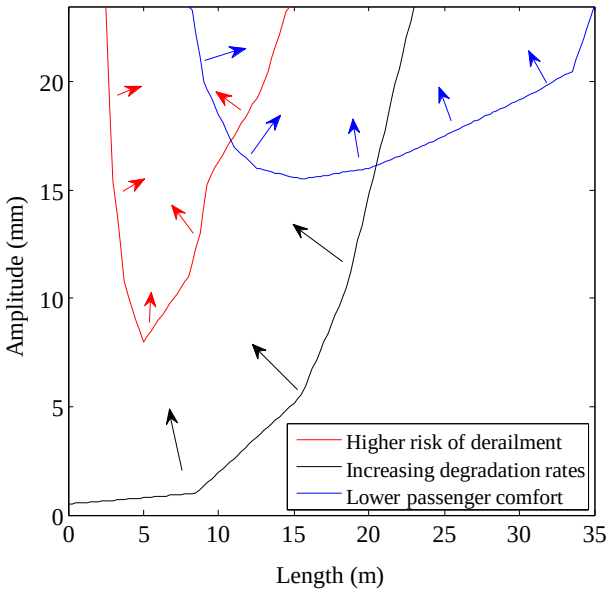

Figure 7-16. Longitudinal level measurements at the transition zone.

Because each occurrence also had the information of its location on the track, it was then possible to represent the occurrences with respect to their position in the *Alcácer* bypass. Figure 7-17 shows the locations of the track singularities (identified in Chapter 4) and the only location (at about 26.3 km mark) that was found to have a high number of the occurrences denoting lower passenger comfort. At that location, the results suggest vertical accelerations inside the coach car of the *Alfa Pendular* above the threshold value of 1 m/s^2. As could be expected, this result is in agreement with the actual measurements that were performed inside the coach car, as the train approached the viaduct over EN120, as discussed earlier in the case study presented in section 6.4. The results suggest that the defects of the longitudinal level at the other transition zones to structures of the *Alcácer* bypass correspond to situations that remain under the threshold value of 1 m/s^2.

As was mentioned in section 7.2.3, none of the occurrences was found to be associated with higher risk of derailment of the *Alfa Pendular* on the *Alcácer* bypass; therefore, the corresponding figure will be omitted from this section.

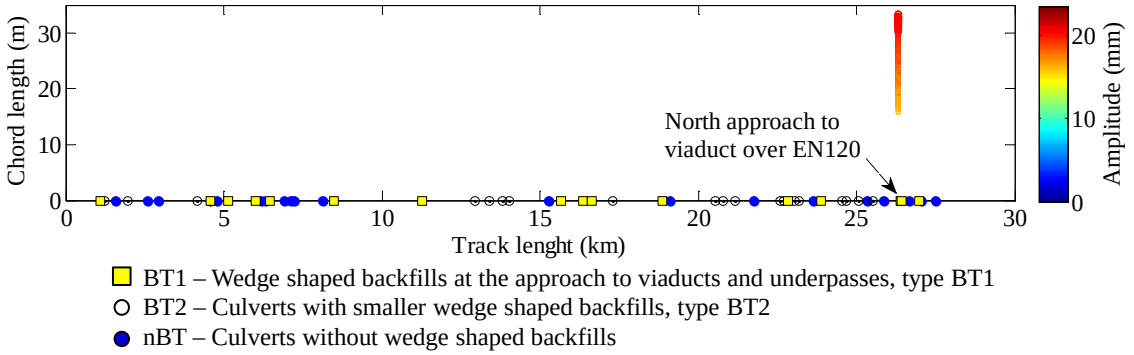

Figure 7-17. Locations that may be causing lower passenger comfort.

Figure 7-18 presents the location of the occurrences that fall inside the region associated with increasing degradation rates, in track segments of about 5 km. The figure also provides a comparison with the values of E_{V2} obtained with the *portancemètre* on the sub-ballast in March 2010, the height of the embankment or the depth of the cutting, relevant substructure reinforcements and the locations of track singularities.

In Figure 7-18, it is noticeable that the first 10 km evidence a higher density of occurrances, compared with the rest of the line. In part, this appears to be related to the characteristics of the substructure, in particular with the existance of higher embankments and deeper cuttings in that stretch, and possibly with the higher variability of the deformation modulus E_{V2} measured on the sub-ballast layer. On the other hand, the lower and more uniform values of the E_{V2} found between km 20 and 30 might have contributed to this outcome, considering the important contribution of the track stiffness – in this case the stiffness of the substructure that contributes to the overall stiffness of the track – to the amplification of the dynamic loads of the trains and to the track degradation (Prud' Homme, 1970; Fröhling, 1997), as discussed in Chapter 3.

Some concentrations of occurrences may be related to the presence of transition zones to structures or other singularities, while many others seem to be related to additional factors for which no obvious justification was found.

The locations evidencing higher concentration of occurrences (identified in Figure 7-18 using red arrows and the respective capital letters) are listed and described in Table 7-1. Plausible explanations are provided in an attempt to justify the higher density of occurrences at these locations.

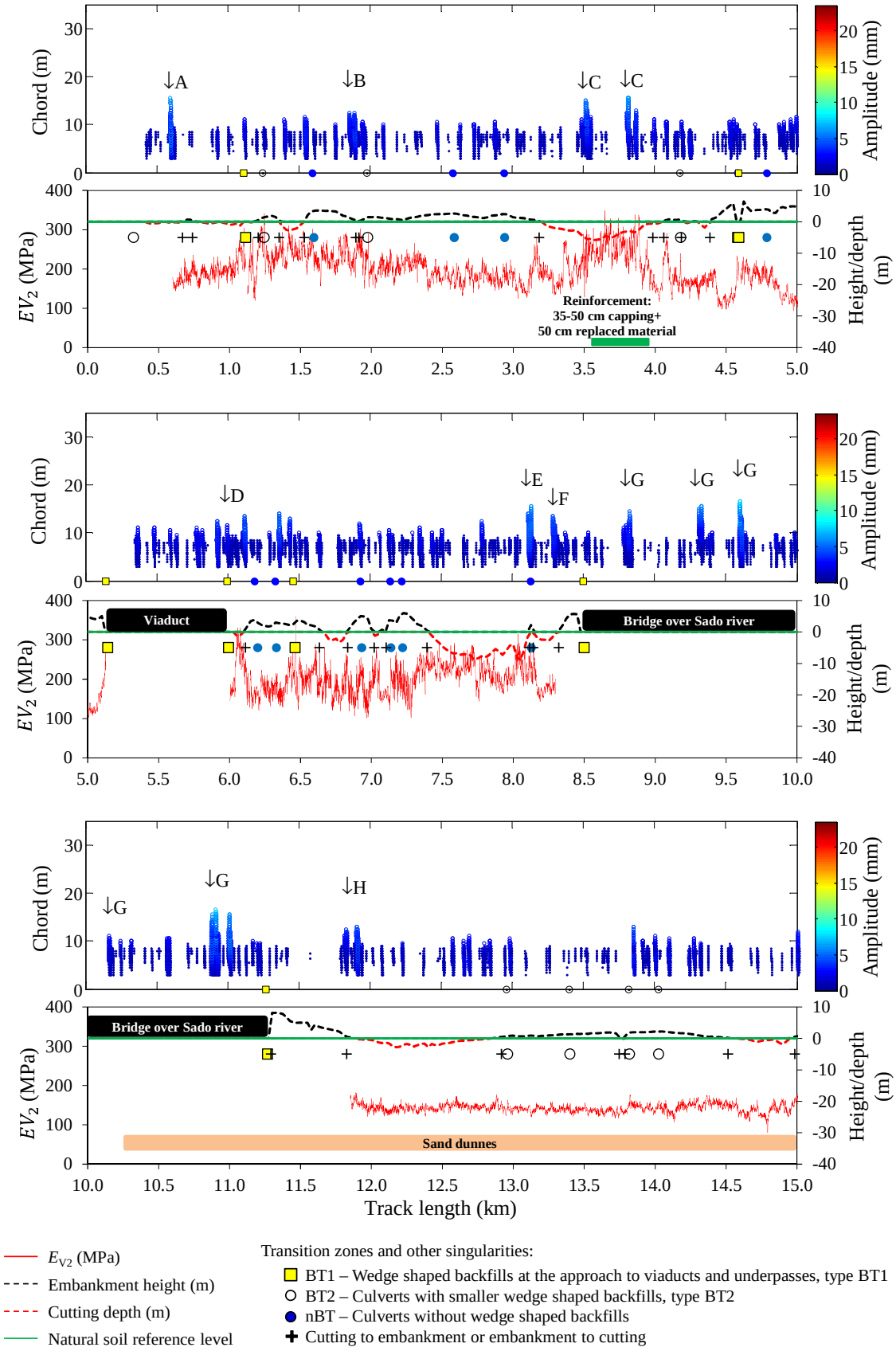

Figure 7-18. Locations that may be causing the increase of track degradation rates (continues).

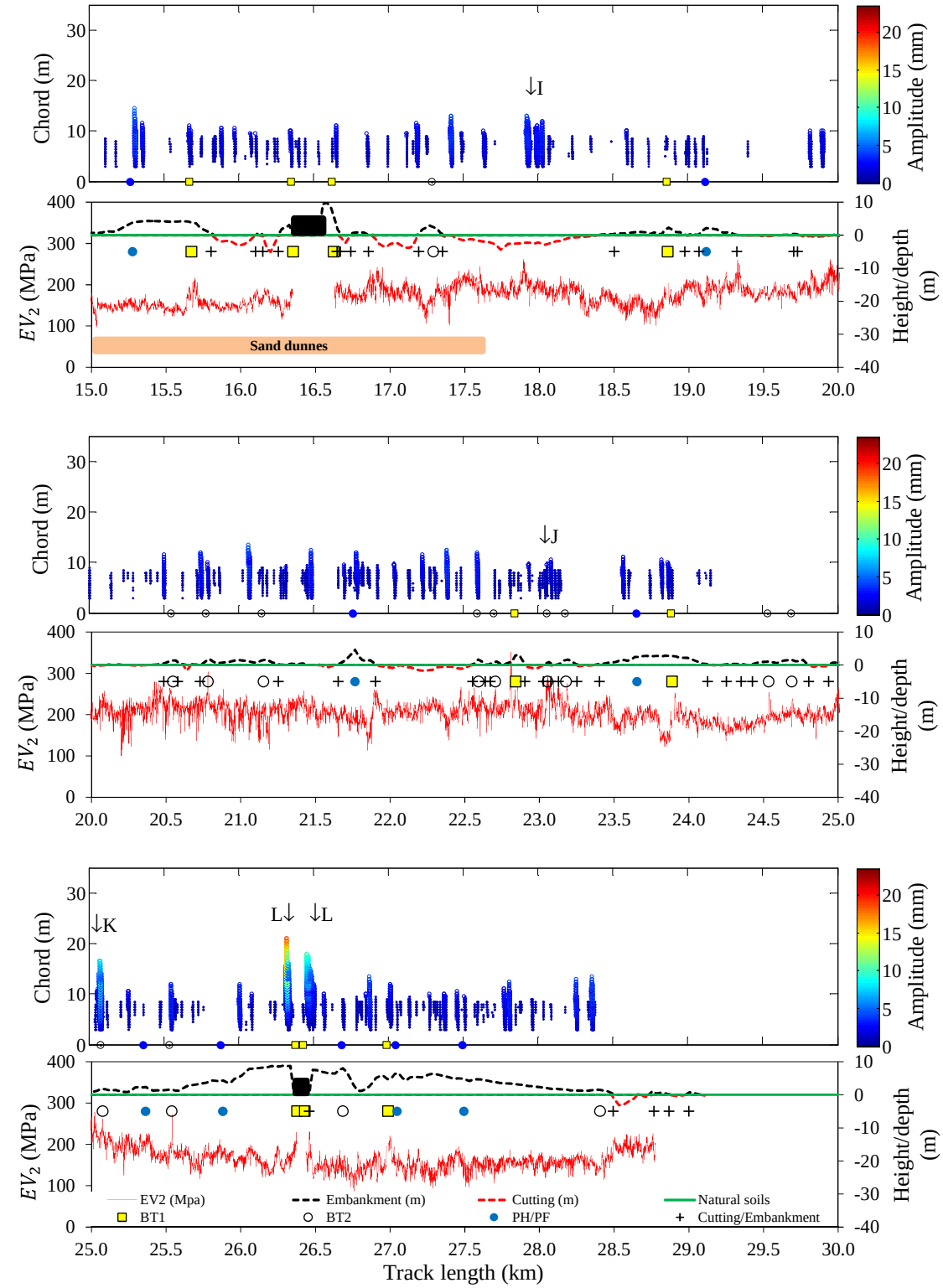

Figure 7-18 (continued). Locations that may be causing the increase of track degradation rates.

Table 7-1. Locations of higher concentration of track defects and with higher amplitudes that suggest higher degradation – see Figure 7-18 (continues).

ID in Figure 7-18	Aprox. location (km)	Singularity	Description / plausible justification
A	0.6	Transition between the 1st and 2nd stages	This is the location where the 1st and 2nd construction stages meet, which might have made it more difficult to compact the layers of the substructure. In addition, the fact that the earthworks from each construction stage were concluded in different periods might have contributed to the development of differential settlements in this area, considering the typical long-term deformation behaviour of embankments.
B	1.9	Embankment-cutting-embankment transition, followed by a culvert (BT2)	The transition embankment-cutting-embankment in a short length (about 75 m), followed by a transition to a culvert might induce abrupt variations of the track stiffness. This is supported by the abrupt changes in the values of the E_{V2}, starting at about 200 MPa, raising to 290 MPa, and then decreasing to about 150 MPa. Moreover, the presence of sucessive track singularities in a short distance might have influenced the quality of the construction works, in particular laying and compaction of the layers.
C	3.5 and 3.8	Extremities of a reinforced section of the substructure	The two locations correspond to the endings of a 300 m-long stretch of the line in cutting that was reinforced during construction due to poor bearing conditions. At the ends, there is a transition between different substructures: i) the normal track configuration and ii) a reinforced substructure with the thickness of the capping layer increased from 20 cm to 50 cm, resting on top of an additional 50 cm-thick layer of crushed aggregate. The reinforced stretch resulted in a stiffer substructure, which might have caused an abrupt stiffness transition between the two track configurations. Another possible cause is that outside of the reinforced segment, the track exhibits poor bearing conditions that might have contributed to the development of differential track settlements.
D	6.0	Approach to a viaduct and short reinforcement of the substructure	This location evidences a very sharp variation of E_{V2} values (increasing from about 150 MPa to 310 MPa and, followed by a rapid decrease to 120 MPa) at the south approach to a viaduct in cutting. This is possibly related to the local reinforcement of the capping layer from 20 cm to 35 cm in a stretch of about 75 m, thus providing a track stiffness transition.
E	8.1	Deep culvert in a cutting-embankment-cutting transition	The culvert was constructed in a short embankment, about 25 m long and 2 m high, located between two cutting sections, about 9 m and 3 m deep, respectively. The changes in the substructure in a short length and the possible disturbance it caused in the construction of the layers might have induced variations in the track stiffness and contributed to the development of track defects in this location.
F	8.3	Transition between the 1st and 2nd stages, and cutting-embankment transition	This is another location where the 1st and 2nd construction stages meet, which might have made it more difficult to compact the layers of the substructure and caused differential settlements. In addition, it corresponds to a cutting-embankment transition at the north approach to the bridge over Sado river.
G	8.8, 9.3, 9.6, 10.1, 10.9	Rail expansion joints on the bridge	These track singularities are known to cause rapid track degradation due to the variations in the track configuration (see Figure 4-21) and the impact it causes in the wheel-rail contact, increasing the train's dynamic loads acting on the track.

Table 7-1 (continued). Locations of higher concentration of track defects and with higher amplitudes that suggest higher track degradation rates - see Figure 7-18.

ID in Figure 7-18	Aprox. location (km)	Singularity	Description / plausible justification
H	11.8	Transition between the 1st and 2nd stages, and embankment-cutting transition	This is also another location where the 1st and 2nd construction stages meet. It also corresponds to an embankment-cutting transition at the south approach to the bridge over Sado river.
I	17.9	Reinforced section of the substructure	This location corresponds to one end of a stretch were the substructure was submitted to reinforcement during construction (constructions of a 50 cm layer of crushed aggregate under the capping layer). This might have caused the development of track defects due to changes in the substructure (stiffness transition and differential settlements). However, the concentration of occurrences extends beyond 18 km mark, which does not include the mentioned reinforcement.
J	23.1	Two culverts (BT2), an overpass and successive embankment-cutting transitions	The location refers to a road overpass, located between two culverts with wedge-shaped backfills BT2, where the line changes four times from embankment to cutting at about every 50 m. The construction of the overpass implied the widening of the track platform in this location. The combination of these aspects might have influenced the construction quality of the earthworks, causing difficulties in placing and compacting of the layers, thus contributing to the track degradation in the long-term
K	25.1	A culvert (BT2) next to an overpass	This scenario appears to be similar to the previous one, but with one culvert only and regarding a stretch on embankment. Again, the change in the substructure due to the overpass and the presence of the underpass seem to be contributing to the track degradation.
L	26.3 and 26.5	North and south approach to a viaduct	This case has been addressed in detail in Chapter 6 and corresponds to the largest longitudinal defect found in the *Alcácer* bypass. The amplitude of the defects seem to be contributing significantly to the track degradation in this stretch of the line.

Apart from the case of the north approach to the EN 120, it is apparent that no concentration of occurrences takes place at transition zones with wedge-shaped backfills of type BT1, which could adds to the conclusion that the design of these transition zones in the *Alcácer* bypass achieves its purpose in assuring the adequate performance of these earth structures. However, a further analysis of the data, as the one presented in section 7.4, shows that transition zones of type BT1 are experiencing higher degradations rates, compared to the rest of the line.

7.4 Assessment of the track degradation at singularities of the track

This section aims at presenting innovative modifications to the conventional methods normally used to characterise the geometric quality of the track, with the objective to evaluate the performance of transition zones, based on the analysis of the longitudinal level.

In general, the track degradation is normally assessed by analysing the variation of the standard deviation of a given geometric parameter during a time interval or with the accumulated traffic. Traditionally, the wavelength range D1 of the longitudinal level ($SD_{LL,\mathrm{D1}}$) is considered in the analysis using 200 m-long segments of track or moving windows of the same size. This approach was presented earlier in Chapter 4 and applied to the longitudinal level of the *Alcácer* bypass. However, the degradation that occurs at track singularities, such as at the approach to transition zones or at rail expansion joints, normally only extends up to a few meters or tens of meters. Consequently, the length of 200 m commonly used to analyse the evolution of the standard deviation of the longitudinal level does not seem a proper tool to highlight possible high degradation rates at these critical locations.

The results of the longitudinal level obtained in different inspections that were presented in Chapter 4 were analysed once more, this time using a different approach. The approach consisted in calculating the average standard deviation of the longitudinal level of both rails in the wavelength range D1, $\overline{SD}_{LL,\mathrm{D1}}$, but using shorter window sizes, particularly 10 m and 75 m. The reduction of the size of the window from the normal 200 m to 10 m or 75 m implied that the successive inspections needed to were carefully aligned with each other (that task was carried out earlier in Chapter 4). The shorter window length of 10 m aimed to analyse local defects on the track related to short longitudinal level defects, such as dips at the approach to structures or due to rail expansion joints. It was derived to cover slightly more than twice the smallest wavelength of the range D1, centred on a specific location of the track. The window length of 75 m was selected to analyse larger portions of the track that would include the total length of the two wedge-shaped backfills type BT1 that are adjacent to the underpasses.

The following three figures show $\overline{SD}_{LL,\mathrm{D1}}$ values using moving windows of 10 m and 75 m along the *Alcácer* bypass, in segments of 10 km, regarding the eith track measurements performed between May 2011 and July 2013. The figures also present graphs with the variation of the $\overline{SD}_{LL,\mathrm{D1}}$ during that period, denoted as $\Delta\overline{SD}_{LL,\mathrm{D1}}$. The location of track singularities are indicated by vertical dash-dot lines, namely, transition zones with backfills of type BT1 and BT2, culverts without wedge shaped backfills (no BT) and rail expansion joints (EJ).

As was expected, the standard deviation using the shorter moving window (10 m) results in higher amplitudes and variability of $\overline{SD}_{LL,\mathrm{D1}}$. It is visible that the values of $\overline{SD}_{LL,\mathrm{D1}}$ for both window sizes are generally located below 0.5 mm. However, there are some locations in the track where the values of $\overline{SD}_{LL,\mathrm{D1}}$ are higher than 1.0 mm: about 70 locations using a moving window of 10 m and 11 locations with the larger window of 75 m. Considering the results with

the shorter window of 10 m, 25 out of the 70 location match the same location of the track singularities that were identified, while many others lay in a range of less than 50 m from the closest track singularity. As regards the results with the window of 75 m, 8 cases out of eleven location are also related to track singularities (4 cases due to the expansion joints, 2 due to backfills type BT1, one of type BT2 and one box culvert).

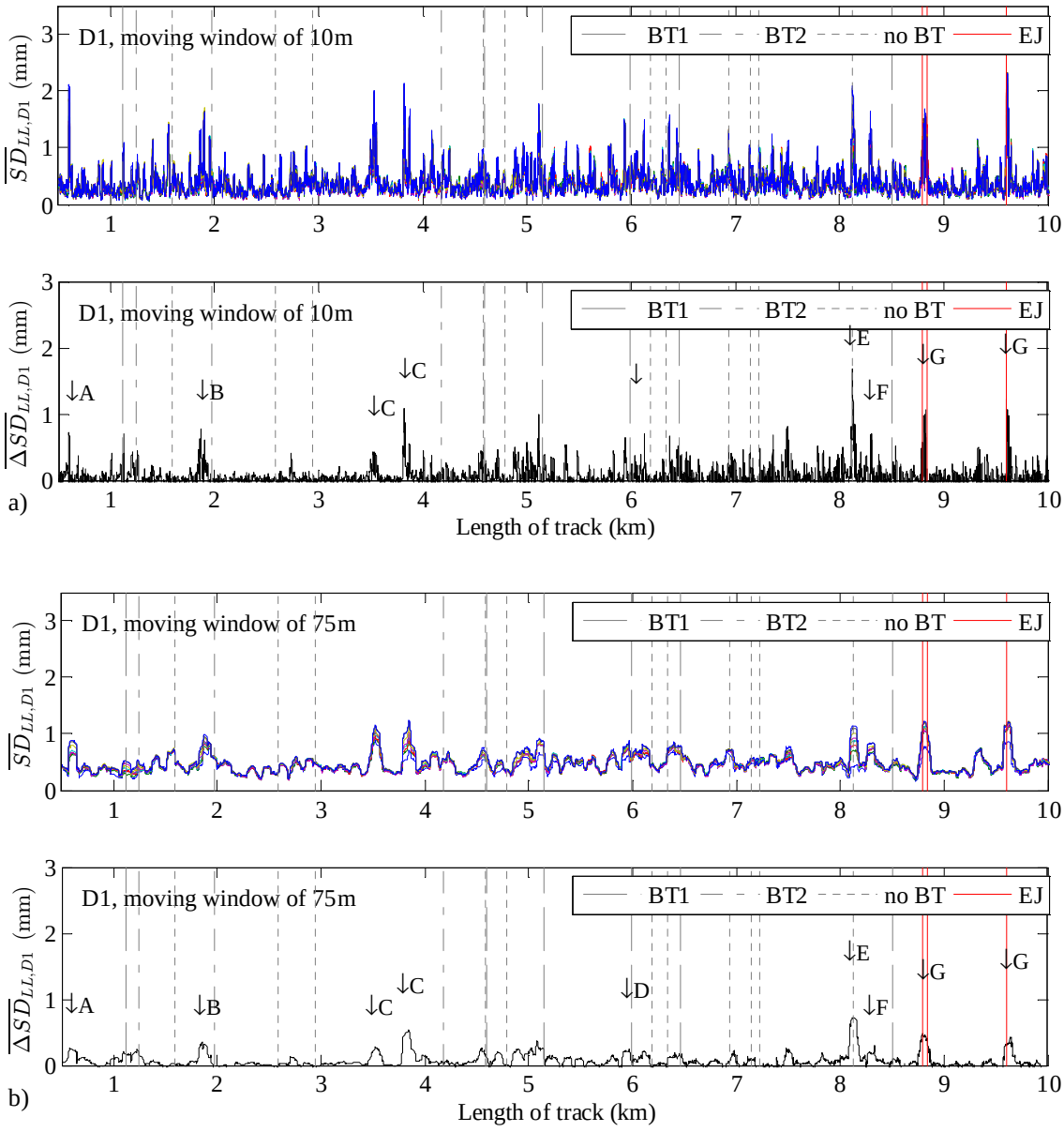

Figure 7-19. Average standard deviation of the longitudinal level (D1), $\overline{SD}_{LL,\mathrm{D1}}$, between 0.5 and 10 km, calculated with moving window of 10 m (a) and 75 m (b), regarding the surveys carried out between May 2011 and July 2013 and evolution between the first and last surveys, $\Delta\overline{SD}_{LL,\mathrm{D1}}$.

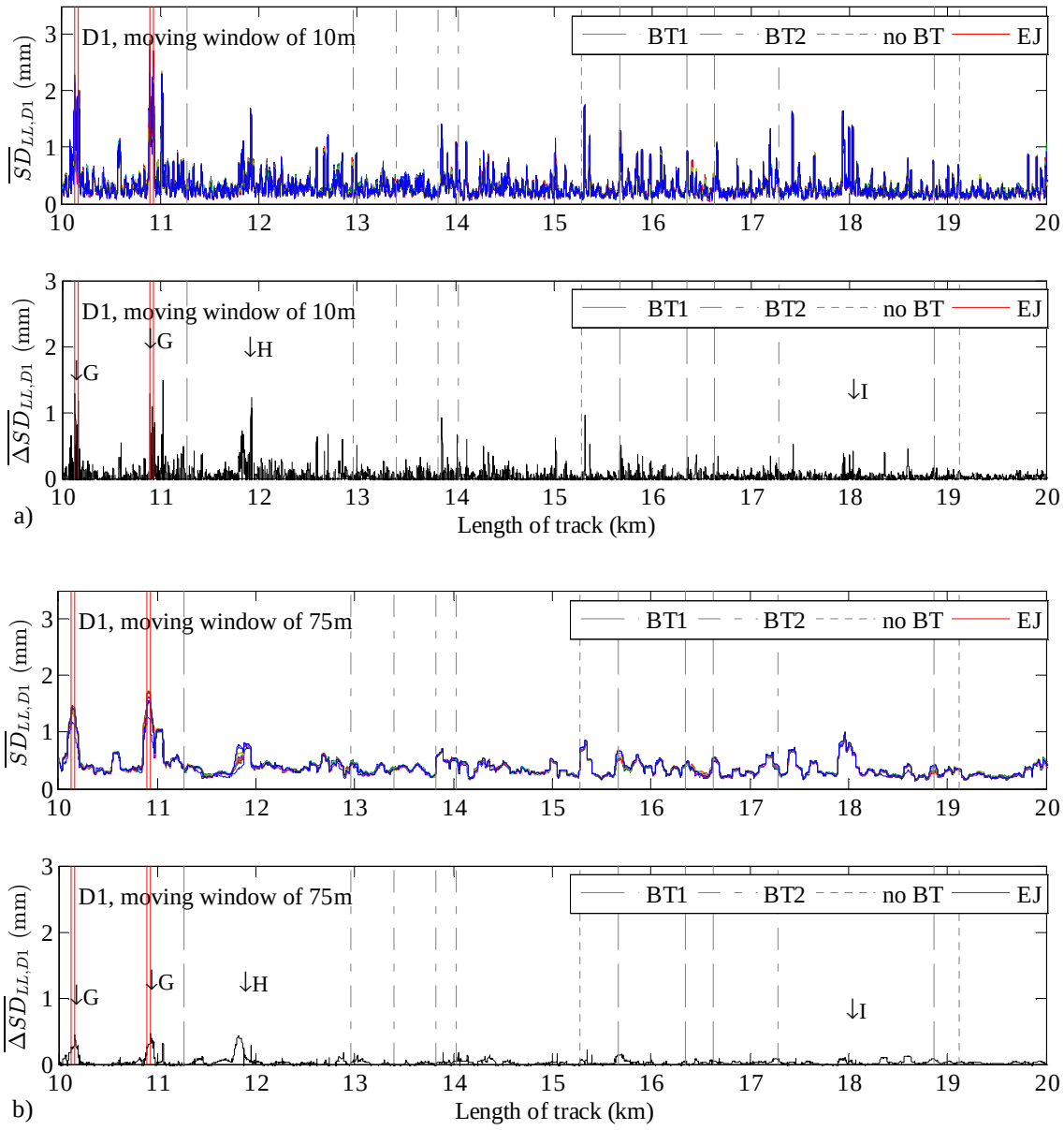

Figure 7-20. Average standard deviation of the longitudinal level (D1), $\overline{SD}_{LL,\mathrm{D1}}$, between 10 and 20 km, calculated with moving window of 10 m (a) and 75 m (b), regarding the surveys carried out between May 2011 and July 2013 and evolution between the first and last surveys, $\Delta\overline{SD}_{LL,\mathrm{D1}}$.

In what regards the variation of the standard deviation, $\Delta\overline{SD}_{LL,\mathrm{D1}}$, and considering both sizes of moving windows, it was verified that most locations denoting relatively larger values of $\overline{SD}_{LL,\mathrm{D1}}$ also evidenced high values of $\Delta\overline{SD}_{LL,\mathrm{D1}}$. These correspond to the locations where the longitudinal level of the track is showing higher degradation rates. The locations with relatively high values of $\overline{SD}_{LL,\mathrm{D1}}$, but denoting low values of $\Delta\overline{SD}_{LL,\mathrm{D1}}$ (approx. 0 mm), seem to be

segments of the track that developed early longitudinal level defects (before May 2011) that did not cause further track degradation. The four vertical peaks of $\overline{SD}_{LL,\mathrm{D1}}$ larger than 1 mm found between 20.0 km and 21.5 km marks (Figure 7-21) are some examples of this track behaviour.

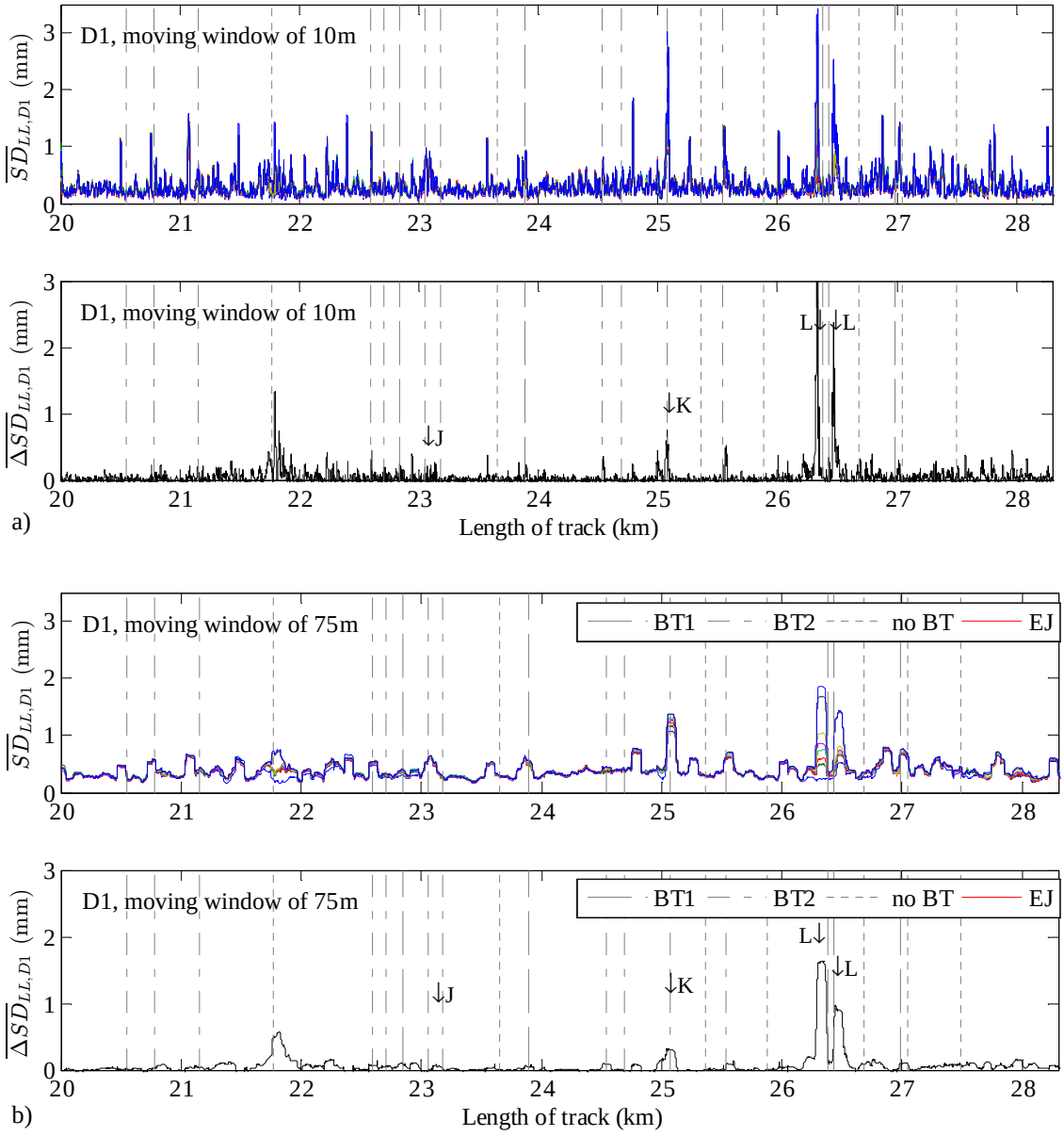

Figure 7-21. Average standard deviation of the longitudinal level (D1), $\overline{SD}_{LL,\mathrm{D1}}$, between 20 and 28.4 km, calculated with moving window of 10 m (a) and 75 m (b), regarding the surveys carried out between May 2011 and July 2013 and evolution between the first and last surveys, $\Delta\overline{SD}_{LL,\mathrm{D1}}$.

It is also interesting to note that almost all the locations identified earlier in Table 7-1, that were associated with possible situations denoting higher degradation rates (also identified in Figure 7-19 to Figure 7-21 using red arrows and the respective capital letters), show relatively large values of $\Delta\overline{SD}_{LL,\mathrm{D1}}$. This observation is particularly more evident considering the results with the window size of 75 m. Cases D, I and J appear to be the exception: the first two cases correspond to reinforcements in the substructure and seem to be locations where the track showed some initial track defects but that did not increase much further ($\overline{SD}_{LL,\mathrm{D1}}$ >1 mm and $\Delta\overline{SD}_{LL,\mathrm{D1}}$ <0.5 mm); while case J is a concentration of track singularities, in a short length of track, that were highlighted in Table 7-1 simply because there was a higher concentration of small track defects (see Figure 7-18). On the other hand, the track at 21.76 km mark (see Figure 7-21) seems to be experiencing higher degradation rates but this location was not identified earlier in Table 7-1. This track behaviour appears to be related to the presence of a box culvert without wedge-shaped backfill (no BT) in that location.

Looking in more detail at the case studies of transition zones analysed in chapters 5 and 6, it was possible to identify different behaviours of the track, regarding the degradation of the longitudinal level.

Figure 7-22 shows the values of $\overline{SD}_{LL,\mathrm{D1}}$ (using a moving window of 10 m) obtained near the underpasses presented in section 5.2, in the different surveys between May 2011 and July 2013, as well as the difference between the first and the last measurement, $\Delta\overline{SD}_{LL,\mathrm{D1}}$. The results regard the underpass at 4.590 km mark, denoted as UP1 (Figure 7-22a), and the underpass at 22.842 km mark, denoted as UP2 (Figure 7-22b). It should be recalled that the respective transition zones to these two structures comprise wedge-shaped backfills of type BT1. At UP1, 44 sleepers with under sleeper pads (USP) were installed during construction in a length of about 26 m, as identified in Figure 7-22a.

Both transition zones evidence low values of $\Delta\overline{SD}_{LL,\mathrm{D1}}$, generally lower than 0.5 mm. A careful analysis of Figure 7-22a shows that the track near UP1, between about 4.523 km and 4.610 km marks (on the wedge-shaped backfills and up to about 60 m to the north of the underpass), is evidencing higher values of $\Delta\overline{SD}_{LL,\mathrm{D1}}$, sometimes around 0.5 mm. On the other hand, the track near the UP1 shows values of $\Delta\overline{SD}_{LL,\mathrm{D1}}$ lower than 0.25 mm. These results indicate that the track near the two underpasses may be going through different degradation behaviour.

As regards the section of the track with USP at UP1, lower track degradation rates were expected in that location because it was demonstrated in Chapter 5 the possible contribution of

USP to reduce sleeper-ballast contact forces, thus lower abrasion and fragmentation of the ballast particles. However, no clear evidences of this contribution were observed yet, probably due to the limited period of observation. It is also noted that relatively larger variations of $\overline{SD}_{LL,\mathrm{D1}}$ occurred at the ends of the track segment with USP (at about 4.578 km and 4.602 km marks). This is in agreement with the results obtained with the numerical modelling, which indicated amplification of the train-track interaction forces, thus causing more damage to the track in those particular locations. Considering that the track continues to exhibit good geometric quality near both underpasses, it seems that more observations need to be carried out in the future to adequately assess the effect of the USP in the long-term degradation of the track at transition zones.

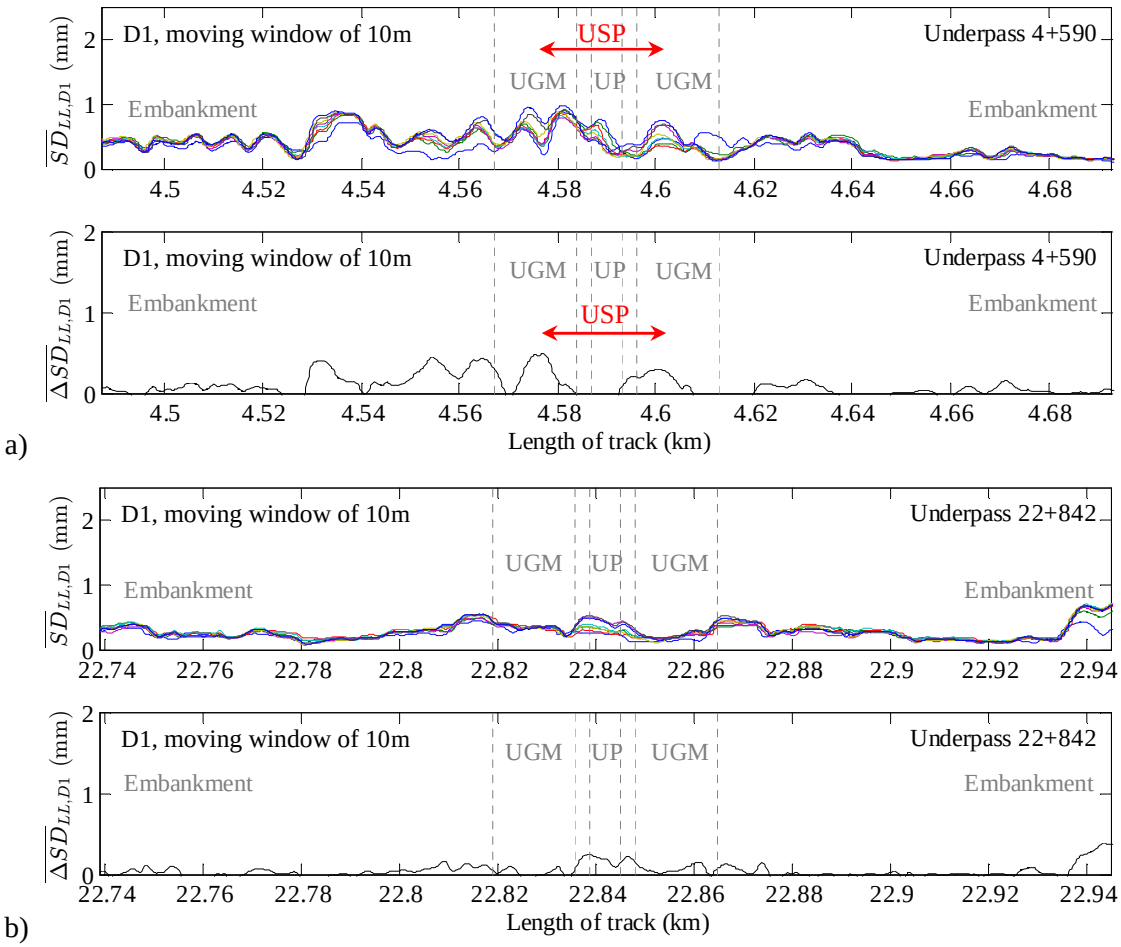

Figure 7-22. Values of the $\overline{SD}_{LL,\mathrm{D1}}$ and $\Delta\overline{SD}_{LL,\mathrm{D1}}$ obtained at the underpasses at: a) 4.590 km mark (UP1) and b) 22.842 km mark (UP2).

Figure 7-23 shows the results of $\overline{SD}_{LL,\mathrm{D1}}$ and $\Delta\overline{SD}_{LL,\mathrm{D1}}$ (also using a moving window of 10 m) obtained on the south approach to the bridge over Sado river (the case study presented in section 5.2). The results show that the track at the transition zone evidenced very small variations in the longitudinal level. It is noted that, locally, at the approach to the bridge (between the bridge end and the 11.28 km mark) small variations were observed between different surveys. Despite this fact, there was almost no difference between the first and the last survey in that section ($\Delta\overline{SD}_{LL,\mathrm{D1}} \cong 0\ mm$). The differences between the surveys are very small to draw conclusive explanations to this behaviour.

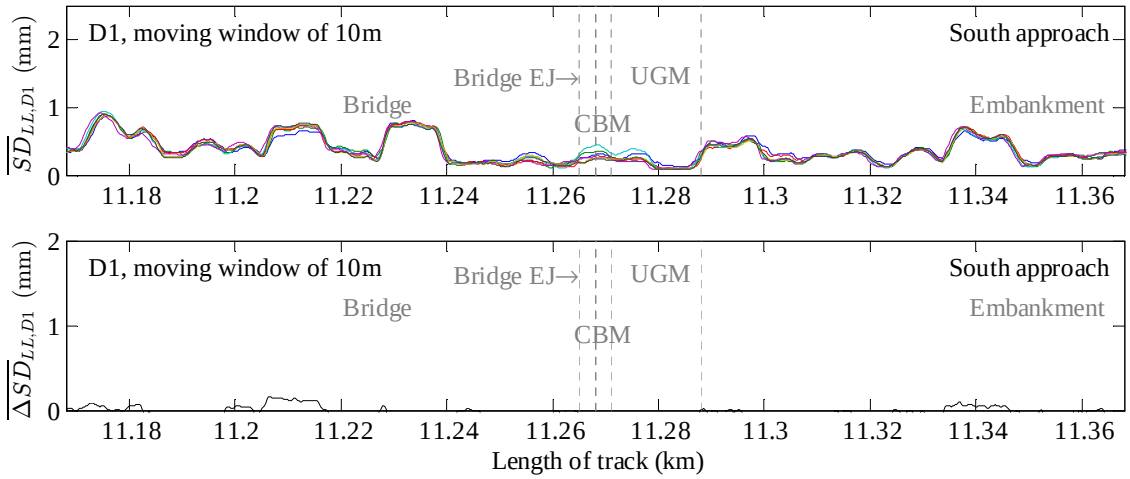

Figure 7-23. Average standard deviation of the longitudinal level D1, $\overline{SD}_{LL,\mathrm{D1}}$, at the South approach to the Sado bridge, calculated with moving window of 10 m and 75 m, regarding the surveys carried out between May 2011 and July 2013 and evolution between the first and last surveys, $\Delta\overline{SD}_{LL,\mathrm{D1}}$.

Lastly, Figure 7-24 shows, in detail, the results of $\overline{SD}_{LL,\mathrm{D1}}$ and $\Delta\overline{SD}_{LL,\mathrm{D1}}$ (considering moving windows of 10 m) obtained at the north and south approaches to the viaduct over EN120 (see case study in section 6.5.3). As mentioned earlier, this location is evidencing the largest longitudinal level defects in the *Alcácer* bypass. It is visible that the track was installed with a very good track quality, denoting $\overline{SD}_{LL,\mathrm{D1}}$ values under 0.5 mm. However, it increased rapidly (particularly in the last two surveys) up to about 3.5 mm at the north approach and about 2.8 mm at the south approach. On both sides of the viaduct, the larger defects are located on the embankment with soils, at the end of the wedge-shaped backfills. This suggests that the problem at the approach to this structure is related to settlements on the embankments as discussed earlier.

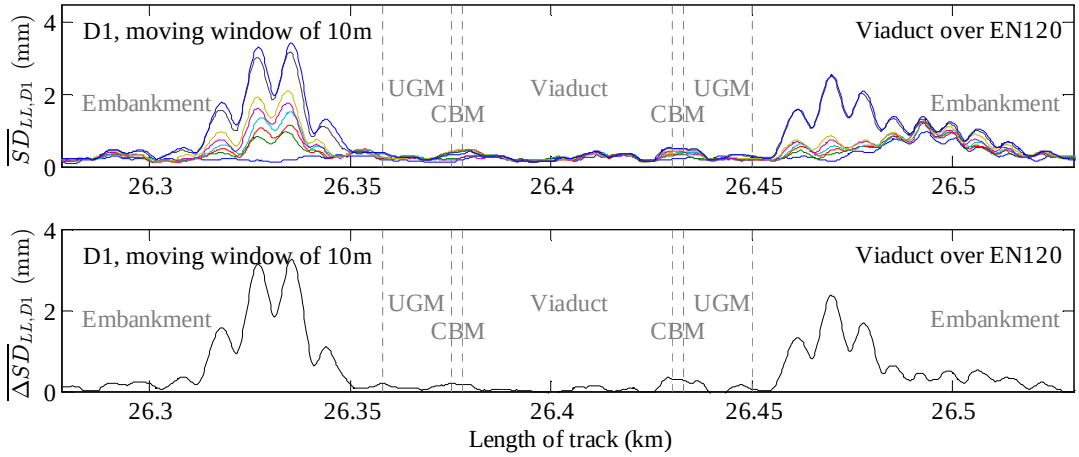

Figure 7-24. Average standard deviation of the longitudinal level D1, $\overline{SD}_{LL,\mathrm{D1}}$, at the Viaduct over EN120, calculated with moving window of 10 m and 75 m, regarding the surveys between May 2011 and July 2013 and evolution between the first and last surveys, $\overline{\Delta SD}_{LL,\mathrm{D1}}$.

Following the approach presented in Chapter 4 to analyse the evolution of the cumulative distribution curves of the $\overline{SD}_{LL,\mathrm{D1}}$, the same approach was applied here, now considering the shorter moving windows of 10 m and 75 m. The cumulative distribution curves refer to the two surveys carried out in May 2011 and July 2013. Figure 7-25 shows the cumulative distribution curves, for both window sizes, and includes the identification of the track sections that correspond to the following track singularities: i) transition zones to structures with wedge-shaped backfills of type BT1 (Figure 7-25a); ii) transition zones to structures with BT2 (Figure 7-25b); iii) culverts without technical blocks, located deeper in the embankments (Figure 7-25c); and iv) rail expansion joints on the bridge (Figure 7-25d). The positions of the singularities in the cumulative curves were determined as the maximum value of $\overline{SD}_{LL,\mathrm{D1}}$ found near the location of the singularity in the track, in a range that was half the size of the window length that was being considered, that is, 5 m and 37.5 m, respectively for window sizes of 10 m and 75 m. For easier interpretation of the results, the representation of the curves was limited to $\overline{SD}_{LL,\mathrm{D1}}$ = 1.5 mm and 2.0 mm, regarding the window sizes of 10 m and 75 m, correspondingly.

From the analysis of the figures, it is visible that, the majority of the track singularities that were analysed fall in the upper half of the cumulative distribution curves. This finding shows that the track at these locations evidences higher values of $\overline{SD}_{LL,\mathrm{D1}}$, with respect to the average values found along the line. With time (due to the accumulated traffic), a track section identified in the

curves may move upwards or downwards in the cumulative distribution. It was verified that this movement also depends on the window size considered in the analysis.

Analysing Figure 7-25a, it is noticed that for window sizes of 10 m (plot on the left), the values of $\overline{SD}_{LL,\mathrm{D1}}$ corresponding to BT1 transition zones (identified by red and white squares) did not evidence relevant variations between the two surveys. This suggests that the short section of the track in a range of 5 m, centred on the exact location of the abutments or underpasses, showed minor degradation. Moreover, the black squares seem to have moved downwards, relative to the position of the red squares, which means that the track in those locations did not degrade as fast as the average degradation rate of the *Alcácer* bypass. However, considering a window size of 75 m (plot on the right), the sections of the track in a range of 37.5 m centred on the exact location of the abutments or underpasses showed some degradation because the squares have moved to the right. Moreover, the vertical positions of a few black squares in the curve have moved upwards, with respect to the position of the red squares – all black squares are on the upper half of the curve. This means that using a window length of 75 m it was possible to detect portions of the track near BT1 transition zones that evidenced higher degradation rates than the average values calculated along the line. In the plot on the right in Figure 7-25a (75 m window), the highest black squares in the curve correspond to the north and south approaches to the viaduct over EN120, but those locations are not visible in the plot on the left because the $\overline{SD}_{LL,\mathrm{D1}}$ axis was truncated at 1.5 mm ($\overline{SD}_{LL,\mathrm{D1}}$ values reach up to 3.5 mm for windows of 10 m in that location, as showed in Figure 7-24).

As regards the track near BT2 transition zones (culverts with smaller wedge-shaped backfills), Figure 7-25b shows the respective positions (red and black circles) in the accumulated distribution curves of $\overline{SD}_{LL,\mathrm{D1}}$. In general, the majority of the corresponding points were also located in the upper half of the curves of both surveys and for both window sizes. Again, this suggests that the track at these singularities shows lower geometric quality, compared with the average quality of the line. Considering window lengths of 10 m (plot on the left of Figure 7-25b), it is also visible that the 10 m-long segments of the track centred with the structures did not show relevant degradation between the two surveys. Because the black circles moved downwards, comparing with the respective red circles, those segments of the track degraded slower than the average degradation of the line. These observations seem to be in agreement with was commented regarding the BT1 transition zones and using window sizes of 10 m.

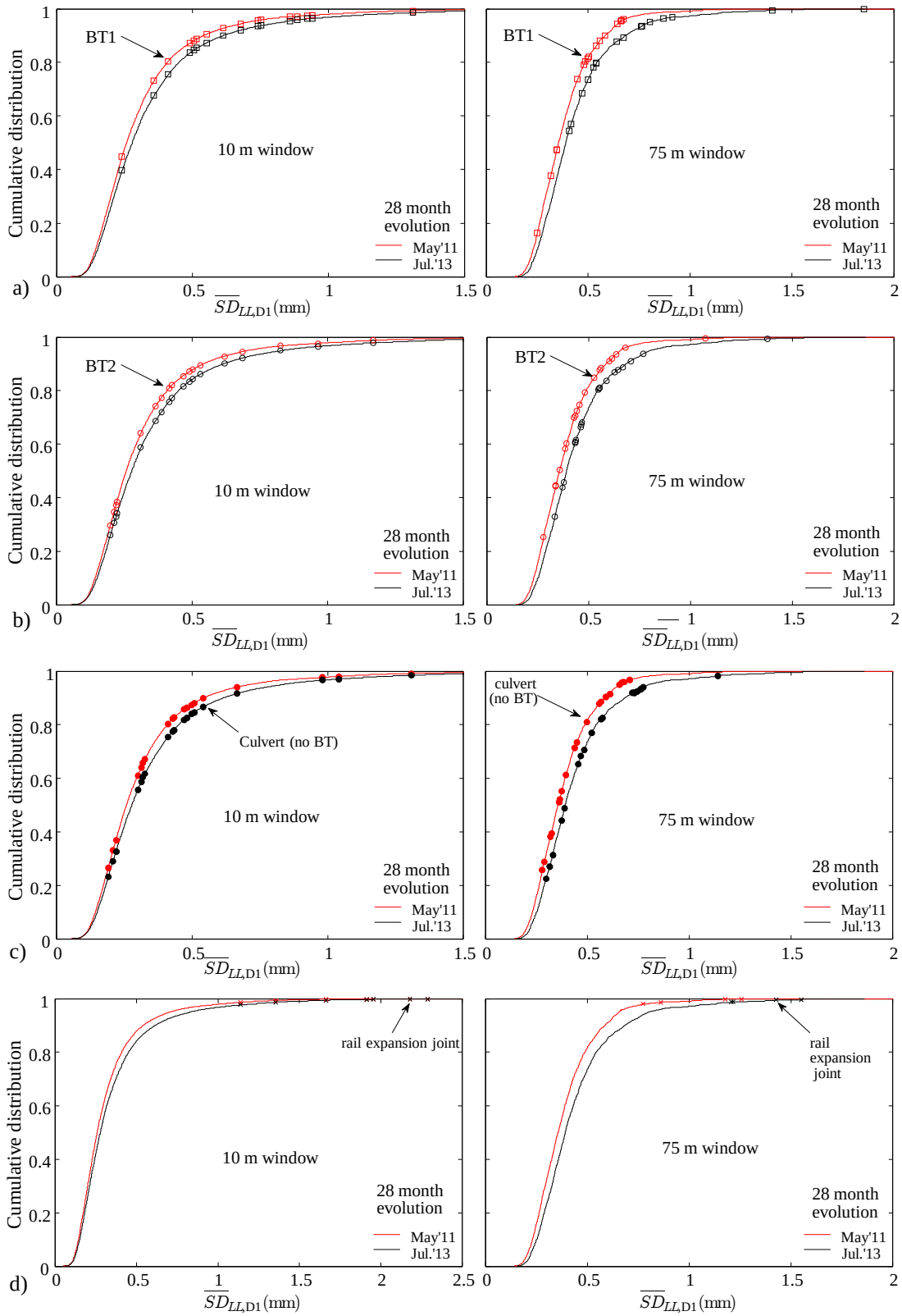

Figure 7-25. Cumulative distribution functions of $\overline{SD}_{LL,D1}$ (May 2011 and July 2013 surveys), calculated with moving windows of 10 m and 75 m, and representative points corresponding to different types of track singularities: a) Technical Blocks type 1 (BT1); b) Technical Blocks type 2 (BT2); c) culverts without technical blocks (no BT); d) rail expansion joints.

Considering windows of 75 m, it appears that the track at different BT2 transition zones evidences different evolutions because some black circles seemed to have moved upwards while others downwards with respect to the respective initial position denoted by the red circles. This suggests that the track sections of 75 m degraded faster near some singularities but slower in others, with respect to the average on the line. In any case, the black circles have moved to the right, meaning that the track has actually degraded in those sections. The same observations seem to apply to the values of $\overline{SD}_{LL,\mathrm{D1}}$ calculated at buried culverts placed without wedge-shaped backfills, as showed in Figure 7-25c.

Figure 7-25d regards the same cumulative distribution curves, but with the points (red and black crosses) related to the rail expansion joints on the bridge over *Sado* river. To be able to represent the points in the curves relative to window sizes of 10 m (plot on the left), it was necessary to extend the $\overline{SD}_{LL,\mathrm{D1}}$ axis up to 2.5 mm. Considering the higher position of the points in the distribution curves, it is visible that the track near the rail expansion joints shows significantly higher values of $\overline{SD}_{LL,\mathrm{D1}}$ in both window sizes, compared with the general values obtained in the line. Regarding windows of 10 m, the values of $\overline{SD}_{LL,\mathrm{D1}}$ did not seem to have increased much near the expansion joints. In particular, the three top black crosses on the curves are practically in the same position as the red crosses, thus the last are not visible in the figure.

Considering the curves obtained with the larger moving window (plot on the right side of Figure 7-25d), some crosses appear overlaid with each other because there are three pairs of expansion joints that the distance between joints in each pair is about 45 m (less than 75 m). Consequently, those crosses correspond to the same maximum value of $\overline{SD}_{LL,\mathrm{D1}}$ in the respective track segment of 75 m. Therefore, considering this short distance between some rail expansion joints, the use of window sizes of about 75 m seems to be too wide to analyse in detail the evolution at each location. Nevertheless, it still may be used to assess the evolution of track segments that have groups of expansion joints. In this way, it is visible that the track segments of 75 m in the area around groups of expansion joints are probably experiencing some of the higher degradation rates in the *Alcácer* bypass – the same appears to be happening at the approaches to the Viaduct over EN120.

Having in mind the results presented here, the use of window sizes smaller than 200 m to analyse the standard deviation of the longitudinal level seems to be a very useful tool to follow up not only the track quality at track singularities but also the track degradation compared with other sections of the same line. It was also demonstrated that the length of the moving window may lead to different interpretations, therefore it needs to be determined according to the type of

track singularity, particularly with regard to the length of track segments to be analysed or that is expected to evidence higher degradation.

7.5 Proposed methods to monitor the performance of transition zones and promoting early detection of critical situations

Considering the experience and the information gathered during the works presented in the previous sections and chapters, it is possible to draw some recommendations aiming at continuously monitoring the performance of transition zones and promoting the early detection of situations that may lead to critical event in the long term.

Low-cost methods or tools can be implemented to address different aspects that affect the performance of transition zones or other track singularities. In agreement with what was presented in this thesis, the aspects that affect the performance of transition zones can be grouped into three categories, depending on whether they contribute: i) the increasing risk of derailment of the trains; ii) the rapid increase of track degradation rates at some locations of the track; iii) the reduction of the passenger comfort when the trains cross sections of the track with important geometric defects. For each of these categories, different interventions or actions are suggested. These comprise simple methods or low-cost tools than can contribute to a better assessment of the evolution of the behaviour of transition zones or other track singularities, and thus detect the early development of critical situations.

As regards the risk of derailment, offload factors relative to the dynamic train-track interaction forces can be assessed by measuring axle box accelerations. The vehicles can be instrumented using accelerometers to detect amplifications and to monitor accelerations of the wheels, followed by appropriate post-processing of the data (Bocciolone *et al.*, 2007; Tanaka & Furukawa, 2008, 2009; Jun Seok *et al.*, 2012). This approach seems to be current practice by some railway infrastructure managers in high-speed lines that have implemented maintenance contracts establishing different levels of acceleration limits of the axle boxes, bogies and car bodies in modern inspection vehicles (ADIF, 2012).

The instrumentation of the vehicles and the respective monitoring and post-processing of the data may also be relevant to detect locations on the track suggesting rapid degradation rates denoted by amplifications of the train-track interaction forces. Other approaches to assess the rapid degradation at track singularities include:

a) Advanced analysis methods to correlate the geometric data obtained with the inspection vehicle and the results from numerical simulations considering the train-track interaction, as presented in chapters 6 and 7;
b) Unconventional *in situ* testing approaches on the track, such as the light falling weigh deflectometer, to assess the support conditions of the sleepers at transition zones and detect track sections with hanging sleepers (see chapter 5);
c) Track instrumentation and continuous monitoring, deploying low-cost MEMS accelerometers at transition zones or other critical locations to collect the data of vertical accelerations under passing wheels with the aim to alert for situations denoting higher sleeper accelerations that are associated with higher track degradation rates and hanging sleepers.

As to the impact of the performance of transition zones on the passenger comfort, the analysis of the geometric surveys and the correlation with the numerical results, as mentioned above, can also contribute to anticipate some problems at these critical locations of the track. Moreover, the instrumentation of the vehicles can also be extended to the interior of the carbodies to assess the accelerations perceived by the passengers. In this thesis, it was demonstrated in Chapter 6 that a simple approach using MEMS accelerometers inside coach cars can provide a cost-efficient tool to assess passenger comfort. Integrating such low cost systems inside passenger cars to perform regular measurements and data analysis in a daily basis can provide relevant information for the maintenance management of the railway system.

Table 7-2 summarises the information in terms of the category of the aspects that affect the performance of the transition zone and the respective proposed actions (methods or tools) to monitor and early detect those critical situations.

Table 7-2. Summary of the main aspects that affect the performance of transition zones and possible actions to monitor and detect the early development of critical situations.

Reference of the numerical study	Increasing risk of derailment	Rapidly increasing degradation rates	Lower passenger comfort
Advanced analysis of track geometric data	●	●	●
Vehicle instrumentation and monitoring	●	●	●
In situ testing at transition zones		●	
Track instrumentation and monitoring		●	

7.6 Concluding remarks

In this chapter, novel and unconventional approaches were introduced to analyse the geometry of the track, with the aim to assess the performance of the transition zones at the *Alcácer* bypass, as well as other track singularities found along that line.

The information obtained using the spectrograms of the longitudinal level did not seem to be very helpful for the above objective. Therefore, aiming to integrate the track geometry data and numerical results of the parametric study in section 6.5.3, another method was developed and presented in this chapter. The method consisted in analysing the track longitudinal level in terms of a range of chords and respective amplitudes at mid-chord, and correlating the results with different numerical scenarios simulated in an earlier parametric study. Consequently, based on criteria that were established in chapter 6, it was possible to associate different defects of the longitudinal level of the *Alcácer* bypass with scenarios that suggested higher risk of derailment, increasing degradation rates and lower passenger comfort. The results showed that the approach to the viaduct over EN120 was experiencing important degradation rates and inducing lower passenger comfort, in agreement with the results presented in Chapter 6. Moreover, many other locations in the track appeared to be associated with early stages of increasing degradation rates when compared with the general behaviour of the track in that line. The locations where this behaviour was more noticeable were also found to be related to track singularities, most of them related to changes in the track substructure. The findings suggest that track singularities and

changes in the substructure seem to trigger rapid track degradation, when compared with other locations in the track.

A subsequent analysis of the standard deviation of the longitudinal level using an unconventional approach highlighted that the locations that were associated with higher track degradation were, in fact, the locations that were evidencing higher degradation rates. This analysis of the standard deviation of the longitudinal level using shorter moving windows of 10 m and 75 m showed to be a promising approach to assess and monitor the degradation rates at track singularities.

Lastly, aiming at promoting a continuous monitoring of the performance of transition zones or other track singularities and to prevent the development of critical situations, some actions and tools were suggested to railway infrastructure managers.

Chapter 8

Conclusions and Future Work

This chapter aims at summarising the main conclusions of this research and at evidencing the major contributions to this field of research. Considering the work that was carried out, directions for future research are also provided.

The research presented in this Thesis aimed at obtaining a more comprehensive understanding of the structural behaviour of transition zones, considering a case study of a recent railway track in Portugal, the *Alcácer* bypass, using an integrated approach comprising: i) laboratorial characterisation of the materials used in the track; ii) *in situ* characterisation of the structures; iii) analysis of the evolution of the geometric quality of the track; iv) instrumentation and monitoring of structures; v) numerical modelling of transition zones considering the dynamic train-track interaction.

8.1 Final considerations and achievements

The railway track degrades faster at locations denoting abrupt variations in the track support conditions – the transition zones – as in approaches to bridges, viaducts, underpasses, tunnels and other civil engineering structures, or between different track configurations. From the analysis of the track geometry data obtained with the inspection vehicle in the *Alcácer* bypass, similar conclusions were drawn in this research. Because the track is relatively recent, the track evidenced very good track quality and normal degradation rates (in terms of the standard deviation of the longitudinal level with moving widows of 200 m). However, at some locations, those degradation rates were 5 to 7 times higher than normal. The results suggested that changes in the substructure were responsible for those high degradation rates.

During the construction of the *Alcácer* bypass, the south approach to the bridge over Sado river was used as a case study to obtain more insight into the behaviour of transition zones. The

transition zones to large engineering structures (bridges, viaducts and road underpasses) in that line comprised a wedge-shaped backfill with well-graded crushed aggregates (UGM) and bound aggregate with 5% cement by weight (CBM). It was demonstrated with *portancemètre* surveys that this backfill design provides a gradual stiffness increase measured on the substructure. Gradually increasing E_{V2} values were obtained from the embankment to the UGM wedge, and to the CBM wedge. The stiffness variation was higher at the intermediate layers of the backfill, rather than on top of the sub-ballast. The initial results also suggested additional contributions of this design: i) mitigate long-term settlement; ii) account for the difficulty to compact the layers close to the walls of the structures.

The results of conventional laboratorial and cyclic load triaxial tests performed on the aggregates used in the transition zones indicated that the selected geomaterials evidenced high resilient deformation modulus and high resistance to plastic deformation, corresponding to very high performance class of aggregates. Therefore, they were suitable for the specific functions in the track substructure.

In general, measurements performed at the same transition zone case study with sub-horizontal inclinometers installed inside the backfill and with the topographic surveys showed negligible settlements after opening the line to traffic. However, at the transition between the UGM wedge and the embankment with soils, larger settlements were observed in that case study. This finding was related to the difficulty to compact the layers at the interface between the different materials. To minimise even further the post-construction settlements, the results evidence that in transition zones with similar wedge-shaped backfills, the track and its substructure should be left to rest at least one year (if possible two years) before establishing the final geometry of the track.

In what regards the dynamic response of the transition zones of the *Alcácer* bypass, extensive track measurements were performed at the approach to different structures comprising underpasses and bridges. Track measurements evidenced the existence of a smooth increase of track stiffness at the approach to these structures, which is one of the objectives of the construction of the wedge-shaped backfills. It was also demonstrated the direct correlation between the measurements performed on the rail, when the trains crossed the transition, and the respective dynamic signatures using the Decomposition of Excitation at Resonance method, but considering wavelengths shorter than 4 m. This finding makes possible the determination of the relevant excitation frequencies caused by vehicles on the track, solely based on the axle arrangement and velocity of any given train, comprising a practical contribution to other studies.

In addition, it was found that under sleeper pads (USP) at transition zones can strongly amplify the vertical flexibility of the track, as demonstrated with receptance tests and with an innovative approach using the light falling weight deflectometer on the sleepers. Later simulations evidenced the potential contribution of USP to reduce degradation rates in the long-term due to lower contact forces developed at the sleeper-ballast interface.

The application of a calibration procedure based on receptance curves and on optimisation algorithms, showed to be very effective in the determination of some parameters of the numerical models, considering the initial range of values derived from laboratorial and field characterisation. In the validation of the models, very good agreement was obtained between the numerical results and the field measurements at different sections along the various transition zones under study.

Considering the characteristics of the *Alfa Pendular* passenger train and for speeds of about 220 km/h, it can be concluded that the design of the wedge-shaped backfill was adequate to minimise the negative effects resulting from the abrupt stiffness variations that are normally present at bridge approaches. Given the characteristics of the backfill materials, it can be expected an adequate performance of the transition zone in the long-term. These conclusions only apply if the dynamic component of the train-track interaction force does not increase significantly over the following years. This problem could be triggered by the development of differential settlements at the backfill, thus causing defects in track longitudinal profile.

Further numerical simulations evidenced the negative impact of settlements of the backfill in the dynamic train-track interaction. Depending on the shape and amplitude of the track longitudinal level resulting from differential settlements, various scenarios can be initiated, either affecting more significantly: i) track degradation due to excessive loads on the track; ii) running safety if offload limits are reached or if there is loss of axle-rail contact; iii) passenger comfort due to amplifications in the accelerations inside the coach cars. The simulations of hypothetical bump settlement profiles of a wedge-shaped backfill indicated an adequate behaviour of the train-track system because none of the limits related to track degradation, safety or passenger comfort were exceeded. Again, the findings support the conclusion that wedge-shaped backfills seem adequate to address the problems related to abrupt variations of the track's stiffness and differential settlements normally found at transition zones. Nevertheless, the transition zones at one of the viaducts in the *Alcácer* bypass evidenced important track degradation rates a few meters away from the end of both wedge-shaped backfills. In this case, the problem was

associated with differential settlements in the substructure and was affecting passenger comfort at those locations. The problem has recently been addressed with maintenance operations.

Taking into account the various parametric studies that were carried out, it was concluded that the accelerations on the axles of the vehicles, the contact forces between wheel and rail, as well as the acceleration levels inside the vehicle body could be used as performance indicators of the dynamic behaviour of transition zones.

Considering the results of the parametric studies, a novel approach was developed and applied aiming to integrate the numerical results with the track geometry data. The method consisted in analysing the track longitudinal level in terms of a range of chords and respective amplitudes at mid-chord, and correlating the results with different numerical scenarios. It was possible to associate various locations in the track of the *Alcácer* bypass with scenarios that suggested increasing degradation rates and lower passenger comfort. Most of these locations were found to be associated with track singularities, particularly denoting changes in the track substructure. The findings suggest that track singularities and changes in the substructure seem to trigger rapid track degradation, when compared with other locations in the track. An unconventional approach to analyse the evolution of the standard deviation of the longitudinal level using moving windows of 10 and 75 m was presented and applied. The method allowed identifying most of the locations that were thought to be associated with higher degradation rates based on the numerical simulations, thus comprising a promising method to analyse track degradation rates and the impact on the operation of the lines.

Lastly, aiming at promoting a continuous monitoring of the performance of transition zones or other track singularities and to prevent the development of critical situations, some actions and tools were suggested to railway infrastructure managers, which included: i) continuous monitoring of the vehicle's motion; ii) and monitoring of track response at transition zones; iii) innovative *in situ* testing; iv) advanced analysis of track geometry data.

8.2 Perspectives for Future Work

The long-term behaviour of the track substructure is paramount for the overall performance of the railway system. Therefore, in addition to dealing with the almost inevitable degradation at the superstructure, particularly the ballast layer, efforts should also be put into preventing and mitigating problems associated with the poor performance of the substructure. This aspect is particularly relevant in areas of abrupt change of support conditions of the track, as in transition

zones. In this sense, during the construction or renewal of railway tracks, there should be extra caution in these locations so that the characteristics of the platform are as homogeneous as possible and to ensure that any changes in the substructure are implemented with gradual transitions. This approach would not only provide a smoother change in vertical stiffness of the track (with benefits in reducing the oscillation of the dynamic component of the vehicle-track interaction), but mostly contribute to minimise the development of differential settlements that were found to be critical to the infrastructure. For this purpose, the abrupt changes in the support conditions identified during the conception of the line should comprise a careful design to ensure the above aspects. During construction, the placement and compaction of materials in layers should be followed up more closely to attain very good construction quality and achieve the maximum possible homogeneity of the substructure.

As regards the use of under sleeper pads (USP) at transition zones and considering the complex behaviour of the railway track, more studies are required to provide more insight into the mechanisms that control the dynamic and long-term behaviour of these types of applications. More studies should be carried out on the transition zones with USP of the Alcácer bypass to the follow up the long-term behaviour of the track in those locations over the coming years and to conclude on its actual benefit to mitigate degradation at transition zones.

Considering the promising results obtained with the application of the light falling weight deflectometer (LFWD) to assess the support conditions for the sleepers in the track, the method and the measuring system should be improved to provide more insight into the track behaviour. The dynamic characterisation of the track using the receptance tests is extremely valuable to assess the track flexibility in the frequency domain. However, that type of non-destructive testing is normally time consuming and implies the application of small impulse loads, compared with the LFWD load and even more with the actions imposed by the trains. Because the track evidences a non-linear behaviour, different load amplitudes can produce significantly different results. Consequently, effort should be put into improving the LFWD equipment to allow for the application of the receptance test principles, possibly providing real time results in the frequency domain, including the receptance curves obtained in each test.

Due to the high degree of complexity of the train-track system at transition zones, more numerical studies are required to contribute to the understanding of the long-term behaviour of transition zones. These should comprise not only the train-track dynamic interaction, but also the non-linear resilient behaviour of the geomaterials and their plastic deformation under loading cycles. Due to the limitations of the continuous element models and taking into account

increasing computational capacity and numerical tools available, the discrete element modelling approaches seem to have a significant potential in the near future to study the railway track in more detail.

The findings presented in the last chapters, linking the results of the numerical studies with the actual track geometry, were derived only for the *Alfa Pendular* running at about 220 km/h in the track of the *Alcácer* bypass. A more comprehensive analysis should be carried out using the same approach to account for possible effects caused by other type of trains, travelling at other speeds, and also considering other geometric parameters. This could contribute to establish a continuous monitoring framework of transition zones or other locations in the track, by analysing different performance indicators in real time, using feasible solutions and tools such as: instrumentation of the axles, bogies and car bodies of passenger cars; deployment of low-cost measuring systems at critical locations in the track; use of more advanced analysis of the track geometry data. These actions could provide valuable information to the management decision processes of Railway Infrastructure Managers, thus contributing to a more efficient and sustainable railway transport system.

References

Abu-Farsakh, M.Y. & Chen, Q. (2014) *Field Demonstration of New Bridge Approach Slab Designs and Performance*; Baton Rouge, LA: Louisiana Transportation Research Center; FHWA/LA. 13/520;

Adegoke, C.W.; Chang, C.S. & Selig, E.T. (1979) *Study of analytical models for track support systems*; Transportation Research Record; n.º 733; p. 12-19;

ADIF (2012) *Pliego de condiciones tecnicas para el premantenimiento de infraestructura, vía y desvios de alta velocidad del tramo Albacete-Alicante*; Madrid: Administrador de Infraestructuras Ferroviarias;

AFNOR (2000) *NF P 94-117-1: Plate test static deformation module (EV2)*; Paris: Association Française de Normalisation;

Al-Shaer, A.; Duhamel, D.; Sab, K.; Foret, G. & Schmitt, L. (2008) *Experimental settlement and dynamic behavior of a portion of ballasted railway track under high speed trains*; Journal of Sound and Vibration; Vol. 316; p. 211-233;

Allaart, A. (1992) *Design principles for flexible pavements, a computational model for granular bases*; Ph.D. Thesis; Delft: Technische Universiteit Delft;

Alves Costa, P. (2011) *Vibrações do sistema via maciço induzidas por trafego ferroviário - Modelação numérica e validação experimental*; Ph.D. Thesis; Departamento de Engenharia Civil; Porto: Faculdade de Engenharia da Universidade do Porto;

Alves, R. & Vieira, J.G.M. (2014) *Track maintenance - rectification of geometrical deficiencies*; European Railway Review; Vol. 20; n.º 3; p. 40-43;

Alves Ribeiro, C. (2012) *Transições aterro-estrutura em linhas ferroviárias de alta velocidade: análise experimental e numérica*; Ph.D. Thesis Thesis; Department of Civil Engineering; Porto: Faculty of Engineering, University of Porto (FEUP);

Alves Ribeiro, C.; Calçada, R. & Delgado, R. (2008) *Efeitos dinâmicos em zonas de transição em vias férreas de alta velocidade*; XI Congresso Nacional de Geotecnia, IV Congresso Luso-Brasileiro de Geotecnia; Coimbra; 07-11 Abr. 2008; pp. 289-296;

Alves Ribeiro, C.; Calçada, R. & Delgado, R. (2010) *Monitorização de vibrações induzidas por tráfego ferroviário numa transição aterro-passagem hidráulica*; XII Congresso Nacional de Geotecnia; Guimarães; 26-29 Abr. 2010; pp. 1607-1616;

Alves Ribeiro, C.; Dahlberg, T.; Calçada, R. & Delgado, R. (2009) *Dynamic analysis of transition zones on high speed railway lines by explicit analysis methods*; COMPDYN 2009 2nd International Conference on Computational Methods in Structural Dynamics and Earthquake Engineering; Rhodes, Greece; 22-24 Jun. 2009;

Alves Ribeiro, C.; Paixão, A.; Fortunato, E. & Calçada, R. (2014) *Under sleeper pads in transition zones at railway underpasses: numerical modelling and experimental validation (accepted for publication)*; Structure and Infrastructure Engineering; 1744-8980;

Andersen, L. & Nielsen, S.R.K. (2003) *Vibrations of a track caused by variation of the foundation stiffness*; Probabilistic Engineering Mechanics; Vol. 18; n.º 2; p. 171-184; 0266-8920;

Andersson, C. & Dahlberg, T. (1998) *Wheel/rail impacts at a railway turnout crossing*; Proceedings of the Institution of Mechanical Engineers, Part F: Journal of Rail and Rapid Transit; Vol. 212; n.º 2; p. 123-134;

ATSB (2014) *Insert document title Derailment of train 7SP5 between Caragabal and Wirrinya NSW*; Canberra: Australian Transport Safety Bureau; RO-2011-017;

Azéma, E. (2007) *Etude numérique de matériaux granulaires à grains polyédriques: rhéologie quasi-statique, dynamique vibratoire et application au procédé de bourrage du ballast*; Ph.D Thesis; Montpellier: Université Montpellier II - Sciences et Techniques du Languedoc;

Baessler, M. (2008) *Lageveränderungen des Schottergleises durch zyklische und dynamische Beanspruchungen*; Ph.D. Thesis; Berlin: Technischen Universität Berlin;

Baessler, M. & Ruecker, W. (2003) *System dynamics and long-term behaviour of railway vehicles, track and subgrade*; New York: Springer; Track settlement due to cyclic loading with minimum pressurre and vibrations; 3 540 43892 0;

Balay, J.; Gomes Correia, A.; Jouve, P.; Hornych, P. & Paute, J.L. (1998) *Ètude expérimentale et modélisation du comportement mécanique des graves non traitées et des sols supports de chaussées. Dernières avancées*; Bulletin des Laboratoires des Ponts et Chaussées; n.º 216; p. 3-18;

Banimahd, M. & Woodward, P.K. (2007a) *3-dimensional finite element modelling of railway transitions*; 9th International Conference on Railway Engineering; London; Jun. 2007;

Banimahd, M. & Woodward, P.K. (2007b) *Numerical study of train speed effect on railway track response*; 9th International Conference on Railway Engineering; London; Jun. 2007;

Banimahd, M.; Woodward, P.K.; Kennedy, J. & Medero, G. (2012) *Behaviour of train-track interaction in stiffness transitions*; Proceedings of the Institution of Civil Engineers: Transport; Vol. 165; n.º TR3; p. 205-214;

Berawi, B. (2013) *Improving railway track maintenance using power spectral density PSD*; Ph.D. Thesis; Department of Civil Engineering; Porto: Faculty of Engineering, University of Porto (FEUP);

Berggren, E. (2005) *Dynamic Track Stiffness Measurement - A new tool for condition monitoring of track substructure*; Licentiate Thesis; Stockholm, Sweden: KTH;

Berggren, E. (2009) *Railway Track Stiffness - Dynamic Measurements and Evaluation for Efficient Maintenance*; Ph.D Thesis; Stockholm, Sweden: KTH;

Berggren, E. (2010) *Track stiffness measurements – motives, techniques and examples*; IV Jornadas Internacionales: "Ingeniería para Alta Velocidad"; Córdoba; 16-18 Jun. 2010;

Bezin, Y.; Iwnicki, S.; Cavalletti, M.; de Vries, E.; Shahzad, F. & Evans, G. (2009) *An investigation of sleeper voids using a flexible track model integrated with railway multi-body dynamics*; Proceedings of the Institution of Mechanical Engineers, Part F: Journal of Rail and Rapid Transit; Vol. 223; n.º 6; p. 597-607;

Bobet, A.; Fakhimi, A.; Johnson, S.; Morris, J.; Tonon, F. & Yeung, M.R. (2009) *Numerical Models in Discontinuous Media: Review of Advances for Rock Mechanics Applications*; Journal of Geotechnical and Geoenvironmental Engineering; Vol. 135; n.º 11; p. 1547-1561;

Bocciolone, M.; Caprioli, A.; Cigada, A. & Collina, A. (2007) *A measurement system for quick rail inspection and effective track maintenance strategy*; Mechanical Systems and Signal Processing; Vol. 21; n.º 3; p. 1242-1254; 0888-3270;

Boyce, J.R. (1980) *A non-linear model for the elastic behaviour of granular materials under repeated loading*; International Symposium on Soil Under Cyclic and Transient Loading; Swansea; 7-11 Jan. 1980; pp. 285-294;

Brecciaroli, F. & Kolisoja, P. (2006) *Deformation behaviour of railway embankment materials under repeated loading: Literature review*; Helsinki: Finnish Rail Administration A 5/2006;

Briaud, J.L.; James, R.W. & Hoffman, S.B. (1997) *NCHRP synthesis 234: Settlement of Bridge Approaches (the bump at the end of the bridge)*; Washington, D.C.: Transportation Research Board;

Brough, M.; Stirling, A.; Ghataora, G. & Madelin, K. (2003) *Evaluation of railway trackbed and formation: a case study*; NDT & E International; Vol. 36; n.º 3; p. 145-156; 0963-8695;

Burrow, M.; Bowness, D. & Ghataora, G. (2007a) *A comparison of railway track foundation design methods*; Proceedings of the Institution of Mechanical Engineers, Part F: Journal of Rail and Rapid Transit; Vol. 221; n.º 1; p. 1-12;

Burrow, M.P.N.; Chan, A.H.C. & Shein, A. (2007b) *Deflectometer-based analysis of ballasted railway tracks*; Proceedings of the Institution of Civil Engineers: Geotechnical engineering; Vol. 160; n.º 3; p. 169-177; 1353-2618;

Calçada, R. (1995) *Efeitos dinâmicos em pontes resultantes do tráfego ferroviário a alta velocidade*; M.Sc. Thesis; Departamento de Engenharia Civil; Porto: Faculdade de Engenharia da Universidade do Porto;

Carrascal, I.A.; Casado, J.A.; Polanco, J.A. & Gutiérrez-Solana, F. (2007) *Dynamic behaviour of railway fastening setting pads*; Engineering Failure Analysis; Vol. 14; n.º 2; p. 364-373; 1350-6307;

CEN (1999) *European Standard EN 50126-1:1999 Railway applications - The specification and demonstration of Reliability, Availability, Maintainability and Safety (RAMS) - Part 1: Basic requirements and generic process*; Brussels: CEN TC 9X - Comité Européen de Normalisation;

CEN (2003) *European Standard EN 13848-1:2003 Railway applications - Track - Track geometry quality - Part 1: Characterisation of track geometry*; Brussels: CEN/TC 256 - Railway applications, Comité Européen de Normalisation;

CEN (2004) *European Standard EN 13286-7:2004, Unbound and hydraulically bound mixtures - Part 7: Cyclic load triaxial test for unbound mixtures*; Brussels: Comité Européen de Normalisation;

CEN (2005a) *EN ISO 22476-3: Geotechnical investigation and testing - Field testing - Part 3: Standard penetration test*; Brussels: CEN;

CEN (2005b) *European Norm 1990:2005, Eurocode: Basis of Structural design. Annex A2: Application for bridges.*; Brussels: Comité Européen de Normalisation;

CEN (2005c) *European Standard EN 14363:2005 Railway applications - Testing for the acceptance of running characteristics of railway vehicles - Testing of running behaviour and stationary tests*; Brussels: CEN/TC 256 - Railway applications, Comité Européen de Normalisation;

CEN (2008) *European Standard EN 13848-5:2008+A1:2010 Railway applications - Track - Track geometry quality - Part 5: Geometric quality levels - Plain line*; Brussels: CEN/TC 256 - Railway applications, Comité Européen de Normalisation;

CEN (2014) *European Standard EN 13848-6:2014 Railway applications - Track - Track geometry quality - Part 6: Characterisation of track geometry quality*; Brussels: CEN/TC 256 - Railway applications, Comité Européen de Normalisation;

CEN/TC 256 (2012) *TC 256 WI 00256XXX - Railway applications - Track - Concrete sleepers and bearers - Concrete sleepers and bearers with under sleeper pads (Submitted to CEN Enquiry)*;

Chang, C.S.; Selig, E.T. & Adegoke, C.W. (1980) *GEOTRACK Model for Railroad Track Performance*; Journal of the Geotechnical Engineering Division; Vol. 106; n.º 11; p. 1201-1218

Chen, C. (2013) *Discrete element modelling of geogrid-reinforced railway ballast and track transition zones*; Ph.D. Thesis; Nottingham: University of Nottingham;

Chen, C. & McDowell, G.R. (2014) *An investigation of the dynamic behaviour of track transition zones using discrete element modelling*; Proceedings of the Institution of Mechanical Engineers, Part F: Journal of Rail and Rapid Transit;

Clements, R.P. (1984) *Post-Construction Deformation of Rockfill Dams*; Journal of Geotechnical Engineering; Vol. 110; n.º 7; p. 821-840;

Coelho, B. (2011) *Dynamics of railway transition zones in soft soils*; Ph.D. Thesis; Delft: Faculty of Civil Engineering, Delft University of Technology;

Coelho, B.; Hölscher, P.; Priest, J.; Powrie, W. & Barends, F. (2011) *An assessment of transition zone performance*; Proceedings of the Institution of Mechanical Engineers, Part F: Journal of Rail and Rapid Transit; Vol. 225; n.º 2; p. 129-139;

Costa D'Aguiar, S.; Arlaud, E.; Potvin, R.; Laurans, E. & Funfschillling, C. (2013) *Railway transitional zones: the challenges of very high speeds*; WCRR 2013 - World Congress on Railway Research; Sydney, Australia; 25-28 Nov. 2013; p. 8;

Cuéllar, V.; Valerio, J.; Rivas, J.A. & Rodríguez, M. (2009) *Improvement of transition zones for an old embankment*; 17th Int Conf on Soil Mechanics and Geotechnical Engineering; Alexandria, Egypt; 5-9 Oct. 2009; pp. 1901-1908;

Dahlberg, T. (2001) *Some railroad settlement models - a critical review*; Proceedings of the Institution of Mechanical Engineers, Part F: Journal of Rail and Rapid Transit; Vol. 215; n.º 4; p. 289-300;

Dahlberg, T. (2003) *Railway track dynamics - a survey*; Linköping: Linköping University; RAILTRDY.DOC/2003-11-06/TD;

Dahlberg, T. (2004) *Railway track settlements - a literature review*; Report for the EU project SUPERTRACK;

Dahlberg, T. (2010a) *Railway track stiffness variations – causes, consequences and countermeasures*; IV Jornadas Internacionales: "Ingeniería para Alta Velocidad"; Córdoba; 16-18 Jun. 2010;

Dahlberg, T. (2010b) *Railway track stiffness variations – consequences and countermeasures*; International Journal of Civil Engineering; Vol. 8; n.º 1; p. 1-8;

DB AG (1995) *Anforderungskatalog zum Bau der Festen Fahrbahn, Ed. 3, Richtlinie der Deutschen Bahn AG*; Deutsche Bahn AG;

De Man, A.P. (2000) *Pin-pin resonance as a reference in determining ballasted railway track vibration behaviour*; Heron; Vol. 45; n.º 1; p. 35-51; 0046-7316;

De Man, A.P. (2002) *DYNATRACK: a survey of dynamic railway track properties and their quality*; Ph.D. Thesis; Delft: Faculty of Civil Engineering, Delft University of Technology;

DIN (2012) *Baugrund - Versuche and Versuchsgeräte - Plattendruckversuch, DIN 18134:2012-04*; Berlin: Deutsches Institut fur Normung;

EC (2005) *Trans-European Transport Network - TEN-T priority axes and projects 2005*; Brussels: European Commission;

EC (2008) *Commission Decision 2008/217/CE of 20 December 2007 concerning a technical specification for interoperability relating to the 'infrastructure' sub-system of the trans-European high-speed rail system*; Luxemburg: Official Journal of the European Union;

EC (2011a) *Commission Decision of 26 April 2011 concerning a technical specification for interoperability relating to the 'infrastructure' subsystem of the trans-European conventional rail system*; Luxemburg: Official Journal of the European Union;

EC (2011b) *WHITE PAPER - Roadmap to a Single European Transport Area – Towards a competitive and resource efficient transport system* Brussels: European Commission;

EC (2013a) *The Core Network Corridors, Trans-European Transport Network 2013*; Brussels: European Commission;

EC (2013b) *Regulation (EU) no 1316/2013 of the European Parliament and of the council of 11 December 2013 establishing the Connecting Europe Facility, amending Regulation (EU) No 913/2010 and repealing Regulations (EC) No 680/2007 and (EC) No 67/2010* Luxemburg: Official Journal of the European Union;

EC (2014) *EU transport in figures*; Brussels: European Commission;

Eisenman, J. & Leykauf, G. (1977) *Track geometry faults at the transition to engineering structures (in German)*; ETR-Eisenbahntechnische Rundschau; Vol. 26; n.º 10; p. 51-61;

England, G.L.; Tsang, N.C.M. & Bush, D.I. (2000) *Integral bridges: A fundamental approach to the time-temperature loading problem*; Ed. 3; Prague: Thomas Telford; 0-7277-2845-8

ERRAC (2007) *Strategic Rail Research Agenda 2020*; Brussels: European Rail Research Advisory Council;

ERRAC (2011) *Rail route 2050: The Sustainable Backbone of the Single European Transport Area*; Brussels: European Rail Research Advisory Council;

ERRI-D214 Committee (1999) *Ponts rails pour vitesses sur 200km/h. Rapport final (Rail Bridges for Speeds > 200 km/h, Final Report)*; Utrecht: European Rail Research Institute; 9;

ERRI (1975) *D 117/R7: Adaptation optimale de la voie classique au trafic de l'avenir - Etude de l'évolution de la géométrie de la voie en fonction du trafic*; Utrecht: European Rail Research Institute - Office de Recherches et d'Essais de l'Union Internationale des Chemins de Fer;

ERRI (1983) *D 117/R28: Optimum Adaptation of the Conventional Track to Future Traffic - Design charts for the track/foundation system*; Utrecht: European Rail Research Institute - Office de Recherches et d'Essais de l'Union Internationale des Chemins de Fer;

ERRI (1999) *Bridge Ends - Embankment Structure Transition, State of Art Report, D230.1 Committee*; Utrecht: European Rail Research Institute; 3;

Esveld, C. (2001) *Modern Railway Track*; Ed. 2; Zaltbommel: MRT-Productions; 9080032433;

Ferreira, P. (2008) *State of the art on dynamica railway track modelling; REVA Project (PT – 2006 – 046 – 17IAPM) REducción de las VAriaciones de rigidez vertical de la vía. Establecimiento de criterios de diseño, recepción y mantenimiento de las infraestructuras ferroviarias.* ; Lisboa: CESUR, Universidade Técnica de Lisboa, Instituto Superior Técnico;

FGSV Verlag GmbH (2012) *TP BF-StB, Teil B 8.3: Dynamischer Plattendruckversuch mit Leichtem Fallgewichtsgeraet*; Köln: FGSV;

Fortunato, E. (2005) *Renovação de Plataformas Ferroviárias. Estudos Relativos à Capacidade de Carga*; Ph.D. Thesis; Departamento de Engenharia Civil; Porto: Faculdade de Engenharia da Universidade do Porto;

Fortunato, E.; Caspurro, I. & Monteiro, B. (2000) *Caracterização de materiais, instrumentação e observação de aterros rodoviários no lanço Régua/Reconcos do IP3*; VII Congresso Nacional de Geotecnia; Porto; 10-13 Abr. 2000; Vol. 1; pp. 477-488;

Fortunato, E.; Paixão, A. & Calçada, R. (2013) *Railway Track Transition Zones: Design, Construction, Monitoring and Numerical Modelling*; The International Journal of Railway Technology; Vol. 2; n.º 4; p. 33-58; 2049-5358;

Fortunato, E.; Paixão, A. & Fontul, S. (2012a) *Improving the use of unbound granular materials in railway sub-ballast layer*; Advances in Transportation Geotechnics II; Hokkaido University, Japan; 10-12 Sep. 2012; pp. 522-527;

Fortunato, E.; Paixão, A.; Lopes, D.; Fardilha, R. & Correia, J. (2012b) *Estudo laboratorial sobre agregados aplicados em vias-férreas utilizando ensaios de carga triaxial cíclica*; XIII Congresso Nacional de Geotecnia; Lisbon; 17-20 Abr. 2012;

Fortunato, E. & Resende, R. (2006) *Mechanical behaviour of railway track structure and foundation - Three-dimensional numerical modelling*; Railway Foundations (RailFound'06); Birmingham; 11-13 Sep. 2006; pp. 217-227;

Fortunato, E. & Veiga Pinto, A. (1997a) *Assentamentos em aterros rodoviários*; VI Congresso Nacional de Geotecnia - A Geotecnia nas Insfraestruturas de Transporte, Energia e Ambiente; Lisboa; 15-18 Set. 1997; Vol. 2; pp. 1187-1198;

Fortunato, E. & Veiga Pinto, A. (1997b) *Via Longitudinal do Algarve. Análise de assentamentos em aterros rodoviários*; Lisboa: Junta Autónoma de Estradas / Laboratório Nacional de Engenharia Civil;

Fröhling, R.D. (1997) *Deterioration of railway track due to dynamic vehicle loading and spatially varying track stiffness*; Ph.D Thesis; Pretoria, South Africa: University of Pretoria;

Fröhling, R.D. (1998) *Low Frequency Dynamic Vehicle/Track Interaction: Modelling and Simulation*; Vehicle System Dynamics: International Journal of Vehicle Mechanics and Mobility; Vol. 28 (Suppl.); p. 30-46; 0042-3114;

Fröhling, R.D.; Scheffel, H. & Ebersöhn, W. (1996) *The Vertical Dynamic Response of a Rail Vehicle caused by Track Stiffness Variations along the Track*; Vehicle System Dynamics:

International Journal of Vehicle Mechanics and Mobility; Vol. 25; n.º 1 supp 1; p. 175 - 187; 0042-3114;

Frühauf, W.; Jungwirth, J.; Scholz, M. & Stoiberer, H. (2008) *Slab track systems on engineering structures - A holistic design approach*; Railway Technical Review; Vol. Special, The German High Speed Rail System; n.º Mar. 2008; p. 78-88; 9783777103822;

Gallego Giner, I.; López Pita, A.; Vieira Chaves, E. & Rivas Álvarez, A.M. (2011) *Design of embankment–structure transitions for railway infrastructure*; Proceedings of the Institution of Civil Engineers: Transport; Vol. 165; n.º 1; p. 27-37;

Gidel, G.; Hornych, P.; Chauvin, J.-J.; Breysse, D. & Denis, A. (2001) *Nouvelle approche pour l'étude des déformations permanentes des graves non traitées à l'appareil triaxial à chargements répétés*; Bulletin des Laboratoires des Ponts et Chaussées; n.º 233; p. 5-21;

GIF (2004a) *Pliego de prescripciones técnicas tipo para los proyectos de plataforma*; Madrid: Gestor de Infraestructuras Ferroviarias;

GIF (2004b) *Recomendaciones sobre las cuñas de transición; Instrucciones y Recomendaciones para redacción de proyectos y plataformas*; Madrid: Gestor de Infraestructuras Ferroviarias;

Gomes Correia, A. (1985) *Contribution à l'étude mécanique des sols soumis à des chargements cycliques*; Ph.D Thesis; Paris: Ecole Nationale des Ponts et Chaussées;

Gomes Correia, A. (2004) *Evaluation of mechanical properties of unbound granular materials for pavements and rail tracks*; Int. Seminar on Geotechnics in Pavement and Railway Design and Construction; Athens; 16-17 Dec.; pp. 35-60;

Grassie, S. (1995) *Dynamic modelling of concrete railway sleepers*; Journal of Sound and Vibration; Vol. 187; n.º 5; p. 799-813; 0022-460X;

Hao, J.; Gao, L.; Xu, Z. & Xiao, H. (2009) *Research on Transitional Section between Ballasted Track on Subgrade and Ballastless Track on Bridge of High-speed Railway* Proceedings of the 3rd ICMEM - International Conference on Mechanical Engineering and Mechanics Beijing, China Oct. 21−23, 2009; pp. 1855-1860;

Hawari, H.M. (2007) *Minimising track degradation through managing vehicle/track interaction* Ph.D. Thesis; Centre for Railway Engineering; Queensland: Central Queensland University;

Heirich, O.; Lehner, A.; Robertson, P. & Strang, T. (2011) *Measurement and analysis of train motion and railway track characteristics with inertial sensors*; In: Intelligent Transportation Systems (ITSC), 2011 14th International IEEE Conference on; 5-7 Oct. 2011; p. 1995-2000; 2153-0009;

Heirich, O.; Steingass, A.; Lehner, A. & Strang, T. (2013) *Velocity and location information from onboard vibration measurements of rail vehicles*; In: Information Fusion (FUSION), 2013 16th International Conference on; 9-12 July 2013; p. 1835-1840;

Higuera de Frutos, S. & Castro, M. (2014) *Using smartphones as a very low-cost tool for road inventories*; Transportation Research Part C: Emerging Technologies; Vol. 38; n.º 0; p. 136-145; 0968-090X;

Hossain, Z.; Indraratna, B.; Darve, F. & Thakur, P.K. (2007) *DEM analysis of angular ballast breakage under cyclic loading*; Geomechanics and Geoengineering: An International Journal; Vol. 2; n.º 3; p. 175 - 181; 1748-6025;

Hosseingholian, M.; Froumentin, M. & Levacher, D. (2009) *Continuous Method to Measure Track Stiffness A New Tool for Inspection of Rail Infrastructure*; World Applied Sciences Journal; Vol. 6; n.º 5; p. 579-589; 1818-4952;

Hruzíková, M.; Plášek, O.; Smutný, J.; Svoboda, R. & Salajka, V. (2009) *Test Track Section with Under Sleeper Pads in the Czech Republic*; XII International scientific conference, Transport structures; Brno, Czech Republic; 20-22 Apr. 2009; pp. 47-51;

Huang, Y.; Lin, C.; Deng, X. & Rose, J. (1984) *Kentrack: A computer program for hot-mix asphalt and conventional ballast railway trackbeds*; Lexington, KY, USA: RR-84-1;

Hunt, G.A. & Wood, J. (2005) *Review of the Effect of Track Stiffness on Track Performance*; London: Rail Safety & Standards Board;

Hunt, H.E.M. (1997) *Settlement of railway track near bridge abutments*; Proceedings of the Institution of Civil Engineers: Transport; Vol. 123; n.º 1; p. 68-73;

Indraratna, B. & Salim, W. (2005) *Mechanics of ballasted rail tracks. A Geotechnical Perspective* Taylor & Francis; 978-0415383295;

Indraratna, B.; Thakur, P.K. & Vinod, J.S. (2010) *Experimental and Numerical Study of Railway Ballast Behavior under Cyclic Loading*; International Journal of Geomechanics; Vol. 10; n.º 4; p. 136-144;

INNOTRACK (2006) *First phase report on the modelling of poor quality sites*; Project no. TIP5-CT-2006-031415O, co-funded by the European Commission within the Sixth Framework Programme (2002-2006); Report D2.1.3;

INNOTRACK (2008) *Methods of track stiffness measurements*; Project no. TIP5-CT-2006-031415O, co-funded by the European Commission within the Sixth Framework Programme (2002-2006); Report D2.1.11;

Insa, R.; Salvador, P.; Inarejos, J. & Medina, L. (2013) *Analysis of the performance of under-sleeper pads in high-speed line transition zones*; Proceedings of the Institution of Civil Engineers: Transport; Vol. 167; n.º 2; p. 63 –77; 1751-7710;

Insa, R.; Salvador, P.; Inarejos, J. & Roda, A. (2012) *Analysis of the influence of under sleeper pads on the railway vehicle/track dynamic interaction in transition zones*; Proceedings of the Institution of Mechanical Engineers, Part F: Journal of Rail and Rapid Transit; Vol. 226; n.º 4; p. 409-420;

Jardine, R.J. (1992) *Some observations on the kinematic nature of soil stiffness*; Journal of the Japanese Geotechnical Society: Soils and Foundations; Vol. 32; n.º 2; p. 111-124; 03851621;

Jofré Ibáñez, C. & Ruiz Rubio, A. (2009) *Manual de firmes con capas tratadas con cemento*; Ed. 2; Madrid: CEDEX, Centro de Estudios de Carreteras; 978-84-7790-489-2;

Johansson, A.; Nielsen, J.C.O.; Bolmsvik, R.; Karlström, A. & Lundén, R. (2008) *Under sleeper pads-Influence on dynamic train-track interaction*; Wear; Vol. 265; n.º 9-10; p. 1479-1487; 0043-1648;

Jun Seok, L.; Sunghoon, C.; Sang-Soo, K.; Choonsoo, P. & Young Guk, K. (2012) *A Mixed Filtering Approach for Track Condition Monitoring Using Accelerometers on the Axle Box and Bogie*; Instrumentation and Measurement, IEEE Transactions on; Vol. 61; n.º 3; p. 749-758; 0018-9456;

Kang, Y.S.; Yang, S.C.; Lee, H.S.; Kim, Y.B.; Jang, S.Y. & Kim, E. (2008) *A study of track and train dynamic behavior of transition zone between concrete slab track and ballasted track* World Congress on Railway Research 2008; Seoul, South Korea; Mai. 2008;

Karrech, A. (2007) *Comportement des matériaux granulaires sous vibration - Application au cas du ballast*; Ph.D Thesis; Paris: Ecole Nationale des Ponts et Chaussées - ENPC PARIS / MARNE LA VALLEE;

Kaynia, A.M. & Clouteau, D. (2007) *Design and Construction of Pavements and Rail Tracks: Geotechnical Aspects and Processed Materials*; Leiden: Taylor & Francis Group; Cap. 2; Improved Performance of Ballasted Tracks; 0–203–93754–6;

Kaynia, A.M.; Schmitt, L.; Lozano del Moral, A.; Pecker, A.; Cuéllar, V.; Clouteau, D.; Dahlberg, T. & Berggren, E. (2005a) *SUPERTRACK, Sustained Performance of Railway Tracks: Final Report*;

Kaynia, A.M.; Schmitt, L.; Lozano del Moral, A.; Pecker, A.; Cuéllar, V.; Clouteau, D.; Dahlberg, T. & Berggren, E. (2005b) *SUPERTRACK: Final Report - Instrumentation, monitoring and physical modelling of high-speed line*; CEDEX-ADIF Final Report for European Commission under contract G1RD-CT-2202-00777;

Kaynia, A.M.; Schmitt, L.; Lozano del Moral, A.; Pecker, A.; Cuéllar, V.; Clouteau, D.; Dahlberg, T. & Berggren, E. (2005c) *SUPERTRACK: Final Report - Numerical simulation of train-track dynamics*; LU Final Report for European Commission under contract G1RD-CT-2202-00777;

Kempfert, H.-G. & Stadel, M. (2000) *Geotechnische Konstruktionen am Übergang Brücke-Erdbauwerk*; Vorträge der Baugrundtagung 2000; Hannover, Germany; 18-21 Sep. 2000; pp. 295-301;

Kennedy, J.; Woodward, P.K.; Banimahd, M. & Medero, G. (2012) *Railway track performance study using a new testing facility*; Proceedings of the Institution of Civil Engineers: Geotechnical Engineering; Vol. 165; n.º GE5; p. 309-319;

Kerr, A.D. (2000) *On the determination of the rail support modulus k*; International Journal of Solids and Structures; Vol. 37; n.º 32; p. 4335-4351; 0020-7683;

Knothe, K. & Wu, Y. (1998) *Receptance behaviour of railway track and subgrade*; Archive of Applied Mechanics; Vol. 68; n.º 7; p. 457-470; 0939-1533;

Kobbacy, K.A.H. & Murthy, D.N.P. (2008) *Complex System Maintenance Handbook*; London: Springer; 9781848000100;

Kolias, S. & Williams, R.I.T. (1984) *Estimation of the Modulus of Elasticity of Cement Stabilized Materials*; Geotechnical Testing Journal; Vol. 7; n.º 1; p. 26-35;

Kongsukprasert, L. & Tatsuoka, F. (2007) *Small strain stiffness and non-linear stress-strain behaviour of cement-mixed gravelly soil*; Journal of the Japanese Geotechnical Society: Soils and Foundations; Vol. 47; n.º 2; p. 375-394;

Kono, A. & Matsushima, T. (2012) *Deformation characteristics of crushed-stone layer under cyclic impact loading from micro-mechanical view*; Journal of Japan Society of Civil Engineers, Ser. A1 (Structural Engineering & Earthquake Engineering (SE/EE)); Vol. 68; n.º 1; p. 173-190;

Lackenby, J. (2006) *Triaxial behaviour of ballast and the role of confining pressure under cyclic loading*; Ph.D. Thesis; Civil Mining and Environmental Engineering; Wollongong: University of Wollongong;

Lei, X. & Mao, L. (2004) *Dynamic response analyses of vehicle and track coupled system on track transition of conventional high speed railway*; Journal of Sound and Vibration; Vol. 271; n.º 3-5; p. 1133-1146; 0022-460X;

Lei, X. & Zhang, B. (2010) *Influence of Track Stiffness Distribution on Vehicle and Track Interactions in Track Transition*; Proceedings of the Institution of Mechanical Engineers, Part F: Journal of Rail and Rapid Transit; Vol. 224; n.º 6; p. 592-604;

Lekarp, F.; Isacsson, U. & Dawson, A. (2000a) *State of the Art. I: Resilient Response of Unbound Aggregates*; Journal of Transportation Engineering; Vol. 126; n.º 1; p. 66-75;

Lekarp, F.; Isacsson, U. & Dawson, A. (2000b) *State of the Art. II: Permanent Strain Response of Unbound Aggregates*; Journal of Transportation Engineering; Vol. 126; n.º 1; p. 76-83;

Li, D. & Davis, D. (2005) *Transition of Railroad Bridge Approaches*; Journal of Geotechnical and Geoenvironmental Engineering; Vol. 131; n.º 11; p. 1392-1398;

Li, D.; Otter, D. & Carr, G. (2010) *Railway Bridge Approaches under Heavy Axle Load Traffic: Problems, Causes, and Remedies*; Proceedings of the Institution of Mechanical Engineers, Part F: Journal of Rail and Rapid Transit; Vol. 224; n.º 5; p. 383-390;

Li, D. & Selig, E.T. (1995) *Wheel/Track Dynamic Interaction: Track Substructure Perspective*; Vehicle System Dynamics: International Journal of Vehicle Mechanics and Mobility; Vol. 24; n.º 1 supp 1; p. 183 - 196; 0042-3114;

Li, D. & Selig, E.T. (1998) *Method for Railroad Track Foundation Design. I: Development*; Journal of Geotechnical and Geoenvironmental Engineering; Vol. 124; n.º 4; p. 316-322;

Li, Z.G. & Wu, T.X. (2009) *On vehicle/track impact at connection between a floating slab and ballasted track and floating slab track's effectiveness of force isolation*; Vehicle System Dynamics; Vol. 47; n.º 5; p. 513-531; 0042-3114;

Liegner, N. (2004) *Influence of the annual variation of the humidity content of the subgrade on the ballast coefficient of the railway tracks*; Intersections/Intersecţii; Vol. 1; n.º 2; p. 12-22; 1582-3024;

Lin, C.-y.; Chen, L.-j.; Chen, Y.-y. & Lee, W.-c. (2011) *A Comfort Measuring System for Public Transportation Systems Using Participatory Phone Sensing*; In: International Workshop on Sensing for App Phones (PhoneSense'10, in conjunction with ACM SenSys'10); Zurich, Switzerland; Nov. 2, 2010;

Lobo-Guerrero, S. & Vallejo, L. (2006) *Discrete Element Method Analysis of Railtrack Ballast Degradation during Cyclic Loading*; Granular Matter; Vol. 8; n.º 3; p. 195-204;

López Pita, A. (2006) *Infraestructuras ferroviarias*; Barcelona: Universitat Politècnica de Catalunya; 84-8301-853-5;

López Pita, A.; Teixeira, P.F.; Casas-Esplugas, C. & Ubalde, L. (2006) *Deterioration in geometric track quality on high speed lines: the experience of the Madrid-Seville high speed line (1992-2002)*; TRB 85th Annual Meeting; Washington, DC; 22-25 Jan. 2006; p. 14;

López Pita, A.; Teixeira, P.F. & Robusté, F. (2004) *High speed and track deterioration: the role of vertical stiffness of the track*; Proceedings of the Institution of Mechanical Engineers, Part F: Journal of Rail and Rapid Transit; Vol. 218; n.º 1; p. 31-40;

Loy, H. (2008) *Under Sleeper Pads: improving track quality while reducing operational costs*; European Railway Review; n.º 4; p. 46-51;

Lozano del Moral, A. & Cuéllar, V. (2009) *Track stiffness variations observed in transition zones of Spanish railways*; 3as Jornadas Hispano Portuguesas sobre Geotecnia en las Infraestructuras Ferroviarias; Madrid; 25-26 Jun. 2009; pp. 2-13;

Lu, M. & McDowell, G.R. (2007) *The importance of modelling ballast particle shape in the discrete element method*; Granular Matter; Vol. 9; n.º 1; p. 69-80;

Lundqvist, A. (2005) *Hanging sleepers, track stiffness variations and track settlement*; Licentiate Thesis; Division of Solid Mechanics; Linköping: Linköping University;

Lundqvist, A. & Dahlberg, T. (2005) *Load impact on railway track due to unsupported sleepers*; Proceedings of the Institution of Mechanical Engineers, Part F: Journal of Rail and Rapid Transit; Vol. 219; n.º 2; p. 67-77;

Lundqvist, A.; Larsson, R. & Dahlberg, T. (2006) *Influence of Railway Track Stiffness Variations on Wheel/Rail Contact Force*; Track for High-Speed Railways; Porto, Portugal; Oct, 2006;

Luomala, H. & Nurmikolu, A. (2012) *Railway Track Stiffness Measurements at Bridge Transition Zones*; Advances in Transportation Geotechnics II; Hokkaido University, Japan; 10-12 Sep. 2012; pp. 811-816;

Machan, G. & Bennett, V.G. (2008) *Use of Inclinometers for Geotechnical Instrumentation on Transportation Projects: State of the Practice*; Transportation Research E-Circular - Transportation Research Board; n.º E-C129; p. 92; 0097-8515;

MATLAB (2012) *MATLAB release R2012a documentation*; Natick, MA, USA: The MathWorks, Inc.;

Mednis, A.; Strazdins, G.; Zviedris, R.; Kanonirs, G. & Selavo, L. (2011) *Real time pothole detection using Android smartphones with accelerometers*; In: Distributed Computing in Sensor Systems and Workshops (DCOSS), 2011 International Conference on; 27-29 June 2011; p. 1-6;

Melis Maynar, M. (2006) *Terraplenes y balasto en Alta Velocidad Ferroviaria; Primera parte*; Revista de Obras Públicas; Vol. Mai. 2006; n.º 3464; p. 7-36;

Mira, P.; Nasarre y de Goicoechea, J.; Pastor, M.; Rodríguez, J. & Santos, J. (1999) *Recomendaciones para el proyecto de plataformas ferroviarias*; Madrid: Ministerio de Fomento; 978-84-498-0411-3;

Moreno, J.; González, J.; Santos, A. & Cuéllar, V. (2005) *SUPERTRACK: Final Report - Retrofitting of Track Sections*;

Muramoto, K.; Nakamura, T. & Sakurai, T. (2012) *A Study of the Effect of Track Irregularity Prevention Methods for the Transition Zone between Different Track Structures*; Quarterly Report of RTRI; Vol. 53; n.º 4; p. 211-215;

Namura, A. & Suzuki, T. (2007) *Evaluation of Countermeasures against Differential Settlement at Track Transitions*; Quarterly Report of RTRI; Vol. 48; n.º 3; p. 176-182;

Nicks, J.E. (2009) *The Bump at the End of the Railway Bridge*; Ph.D. Thesis Thesis; Texas A&M University;

Nielsen, J.C.O. & Oscarsson, J. (2004) *Simulation of dynamic train-track interaction with state-dependent track properties*; Journal of Sound and Vibration; Vol. 275; n.º 3-5; p. 515-532; 0022-460X;

Nitsche, P.; Widhalm, P.; Breuss, S.; Brändle, N. & Maurer, P. (2014) *Supporting large-scale travel surveys with smartphones – A practical approach*; Transportation Research Part C: Emerging Technologies; Vol. 43, Part 2; n.º 0; p. 212-221; 0968-090X;

Ochoa de Olza Galé, A. (2007) *Nuevas Tendencias en el Diseño de Vía*; Alta Velocidade, Jornadas Técnicas: Ingeniería para Alta Velocidad, Veinte Años de Experiencia en España; Córdoba; 27-29 Jun. 2007; pp. 281-301;

ORE (1970) *D 71/R10: Stresses in the rails, the ballast and in the formation resulting from traffic loads - Deformation properties of ballast (Laboratory and track tests)*; Utrecht: European Rail Research Institute - Office de Recherches et d'Essais de l'Union Internationale des Chemins de Fer;

Oscarsson, J. (2001) *Dynamic Train-Track Interaction: Linear and Non-Linear Track Models with Property Scatter*; Ph.D. Thesis; Dept of Solid Mechanics; Gothenburg: Chalmers University of Technology;

Oscarsson, J. (2002) *Dynamic Train-Track Interaction: Variability Attributable to Scatter in the Track Properties*; Vehicle System Dynamics: International Journal of Vehicle Mechanics and Mobility; Vol. 37; n.º 1; p. 59 - 79; 0042-3114;

Paixão, A.; Alves Ribeiro, C.; Pinto, N.M.P.; Fortunato, E. & Calçada, R. (2014a) *On the use of under sleeper pads on transition zones at railway underpasses: experimental field testing*; Structure and Infrastructure Engineering; 1744-8980;

Paixão, A. & Fortunato, E. (2009a) *Análise estrutural de via-férrea com recurso a um modelo numérico tridimensional*; 3as Jornadas Hispano Portuguesas sobre Geotecnia en las Infraestructuras Ferroviarias; Madrid; 25-26 Jun. 2009; pp. 136-146;

Paixão, A. & Fortunato, E. (2009b) *Novas soluções de superstrutura de via para a Alta Velocidade Ferroviária - Comparação com a via balastrada tradicional*; INCVC 5 - NIF/DT; Lisboa: Laboratório Nacional de Engenharia Civil; 9789724921730;

Paixão, A. & Fortunato, E. (2010) *Variante entre a Estação do Pinheiro e o km 94 da Linha do Sul - Estudos sobre construção das terraplenagens, dos blocos técnicos e da camada de sub balastro da 2ª fase*; Lisboa: Laboratório Nacional de Engenharia Civil; Relatório 455/2010 - NIF/DT (Confidencial);

Paixão, A.; Fortunato, E. & Antunes, M.L. (2009) *Emerging Trends for High-Speed Rail Track Superstructures: Ballastless Track as an alternative to the Ballasted Track*; Eighth International Conference on the Bearing Capacity of Roads, Railways, and Airfields (BCR2A'09); Champaign, USA; 29 Jun. - 02 Jul. 2009; Vol. 2; pp. 1231-1241;

Paixão, A.; Fortunato, E. & Calçada, R. (2011) *Avaliação do comportamento das zonas de transição na via-férrea da Variante de Alcácer - Relatório de caracterização laboratorial das misturas "agregado-cimento"; Relatório 04/2011*; Lisboa: Laboratório Nacional de Engenharia Civil e Faculdade de Engenharia da Universidade do Porto;

Paixão, A.; Fortunato, E. & Calçada, R. (2013) *Design and construction of backfills for railway track transition zones*; Proceedings of the Institution of Mechanical Engineers, Part F: Journal of Rail and Rapid Transit;

Paixão, A.; Fortunato, E. & Calçada, R. (2014b) *Numerical study on the influence of backfill settlements in the train-track interaction at transition zones to railway bridges (in review)*;

Paixão, A.; Fortunato, E. & Calçada, R. (2014c) *Transition zones to railway bridges: track measurements and numerical modelling (accepted for publication)*; Engineering Structures;

Pardo de Santayana, F.; Fortunato, E. & Veiga Pinto, A. (2006) *Comportamento estrutural de barragens portuguesas de enrocamento com cortina a montante*; Geotecnica, Revista da Sociedade Portuguesa de Geotecnia; Vol. 107;

Patra, A.P. (2007) *RAMS and LCC in Rail Track Maintenance*; Licentiate thesis Thesis; Luleå Railway Research Center; Luleå, Sweden: Luleå University of Technology;

Paute, J.L.; Hornych, P. & Benaben, J.-P. (1994) *Comportement mécanique des graves non traitées*; Bulletin des Laboratoires des Ponts et Chaussées; n.º 190; p. 27-38;

Peña Peña, M. (2003) *Tramos de ensayo de vía en placa en la línea del corredor del Mediterráneo para su explotación a alta velocidad; 1. Diseño y construcción*; Revista de Obras Públicas; Vol. Oct. 2003; n.º 3431; p. 57-68;

Percival, M.; Woodward, P.K. & Laghrouche, O. (2013) *GRAFT II - Large scale railway fatigue testing*; 12th International Conference on Railway Engineering; London; 10-11 Jul. 2013;

Pinto, N.; Ribeiro, C.A.; Gabriel, J. & Calçada, R. (2013) *Dynamic monitoring of railway track displacement using an optical system*; Proceedings of the Institution of Mechanical Engineers, Part F: Journal of Rail and Rapid Transit;

Plotkin, D. & Davis, D. (2008) *Bridge Approaches and Track Stiffness* U.S. Department of Transportation, Federal Railroad Administration; RR07-12;

Popp, K.; Knothe, K. & Pöpper, C. (2005) *System dynamics and long-term behaviour of railway vehicles, track and subgrade: report on the DFG Priority Programme in Germany and subsequent research*; Vehicle System Dynamics: International Journal of Vehicle Mechanics and Mobility; Vol. 43; n.º 6; p. 485 - 521; 0042-3114;

Popp, K.; Kruse, H. & Kaiser, I. (1999) *Vehicle-Track Dynamics in the Mid-Frequency Range*; Vehicle System Dynamics: International Journal of Vehicle Mechanics and Mobility; Vol. 31; n.º 5; p. 423 - 464; 0042-3114;

Popp, K. & Schiehlen, W.O. (2010) *Ground Vehicle Dynamics*; Springer; 9783540240389;

Powrie, W. & Le Pen, L. (2008) *Testing the ultimate resistance at the sleeper/ballast interface*; Advances in Transportation Geotechnics - Proceedings of the International Conference; Nottingham, England; 25-27 August 2008; pp. 607-613;

Prause, R.H. & Kennedy, J.C. (1977) *Parametric study of track response*; Dept. of Transportation, Federal Railroad Administration, Office of Research and Development;

Profillidis, V.A. (1995) *Railway Engineering*; Ed. 1; Aldershot: Avebury Technical;

Prud' Homme, M.A. (1970) *La voie*; Revue Générale des Chemins de Fer Vol. 1; p. 52-72;

Prud' Homme, M.A. (1976) *Les problèmes que pose, pour la voie, la circulation des rames à grande vitesse*; Revue Générale des Chemins de Fer; p. 695-704;

Puppala, A.J. (2008) *NCHRP synthesis 382: Estimating Stiffness of Subgrade and Unbound Materials for Pavement Design*; Washington, D.C.: Transportation Research Board;

Quante, F. (2001) *Innovative Track Systems - Technical Construction*; Karlsruhe:

Quibel, A. (1999) *Unbound Granular Materials - Laboratory testing, in-situ testing and modelling*; Rotterdam: A. A. Balkema; New in situ devices to evaluate bearing capacity and compaction of unbound granular materials;

Quibel, A.; Hosseingholian, M. & Guillevic, G. (2010) *The role of stiffness in railway infrastructures and its measurement*; IV Jornadas Internacionales: "Ingeniería para Alta Velocidad"; Córdoba; 16-18 Jun. 2010;

Read, D. & Li, D. (2006) *Design of Track Transitions*; Washington: Transportation Research Board;

REFER (2006) *Projecto de Execução; Variante de Alcácer (1ªFase)*; Rede Ferroviária Nacional, EPE;

REFER (2007) *IT.GEO.006 - Características técnicas do sub-balastro*; Lisboa: Rede Ferroviária Nacional, EPE;

REFER (2009a) *IT.VIA.018 - Tolerâncias dos parâmetros geométricos da via*; Lisboa: Rede Ferroviária Nacional, EPE;

REFER (2009b) *Projecto de Execução; Variante de Alcácer (2ªFase): Via-Férrea e Instalações Fixas de Tracção Eléctrica*; Rede Ferroviária Nacional, EPE;

REFER (2010) *Variante de Alcácer*; Lisboa: Rede Ferroviária Nacional, EPE;

RFI (2005) *Capitolato costruzioni opere civil - Documentazione societaria specifiche tecniche*; Roma: RFI;

Ribeiro, D. (2012) *Efeitos dinâmicos induzidos por tráfego em pontes ferroviárias: modelação numérica, calibração e validação experimental*; Ph.D. Thesis; Department of Civil Engineering; Porto: Faculty of Engineering, University of Porto (FEUP);

Ribeiro, D.; Calçada, R.; Delgado, R.; Brehm, M. & Zabel, V. (2013) *Finite-element model calibration of a railway vehicle based on experimental modal parameters*; Vehicle System Dynamics; Vol. 51; n.º 6; p. 821-856; 0042-3114;

Riessberger, K. (2010) *Remarks on Track Design*; IV Jornadas Internacionales: "Ingeniería para Alta Velocidad"; Córdoba; 16-18 Jun. 2010;

Rodríguez, R.; Romana, M.; Jordá, L. & Lastra de la Rubia, E. (2000) *Deformaciones de los terraplenes de los subtramos IX y X de la nueva línea ferroviaria de alta velocidad Madrid-Barcelona*; Simposio sobre Geotecnia de las Infraestructuras del Transporte; Barcelona; Sep. 2000; pp. 801-811;

RTRI (2007) *Design Standards for Railway Structures and Commentary (Earth Structures)*; Tokyo: RTRI;

Santos, L.O.; Min, X. & Santos, J.P. (2010) *Ensaios de carga da ponte ferroviária sobre o rio Sado na Variante de Alcácer*; Lisboa: Laboratório Nacional de Engenharia Civil; Relatório 401/2010 - NOE/DE (Confidencial);

Sauvage, R. & Larible, G. (1982) *La modélisation par "éléments finis" des couches d'assise de la voie ferrée*; Revue Générale des Chemins de Fer; Vol. Septembre; p. 475-483;

Schilder, R. (2006) *USP - Under Sleeper Pads, Applications and Benefits of Elastic Elements in Ballasted Tracks, UIC Project No. I/05/U/440*; Paris: Union Internationale des Chemins de Fer; Oct. 17;

Schneider, P.; Bolmsvik, R. & Nielsen, J.C.O. (2011) *In situ performance of a ballasted railway track with under sleeper pads*; Proceedings of the Institution of Mechanical Engineers, Part F: Journal of Rail and Rapid Transit; Vol. 225; n.º 3; p. 299-309;

Schooleman, R. (1996) *Overgang kunstwerk-aardebaan voor de hoge-snelheidslijn*; M.Sc Thesis; Delft: Technische Universiteit Delft;

SEITC (2014) *PETI3+, Plano Estratégico dos Transportes e Infraestruturas, Horizonte 2014-2020*; Lisboa: Secretário de Estado das Infraestruturas, Transportes e Comunicações; Ministério da Economia; Governo de Portugal;;

Selig, E.T. & Waters, J.M. (1994) *Track geotechnology and substructure management*; London: Thomas Telford; 0727720139, 9780727720139;

Shan, Y.; Albers, B. & Savidis, S.A. (2013) *Influence of different transition zones on the dynamic response of track–subgrade systems*; Computers and Geotechnics; Vol. 48; n.º -; p. 21-28; 0266-352X;

Shi, J.; Burrow, M.P.N.; Chan, A.H. & Wang, Y.J. (2013a) *Measurements and simulation of the dynamic responses of a bridge-embankment transition zone below a heavy haul railway line*; Proceedings of the Institution of Mechanical Engineers, Part F: Journal of Rail and Rapid Transit; Vol. 227; n.º 3; p. 254-268;

Shi, J.; Chan, A.H. & Burrow, M.P.N. (2013b) *Influence of unsupported sleepers on the dynamic response of a heavy haul railway embankment*; Proceedings of the Institution of Mechanical Engineers, Part F: Journal of Rail and Rapid Transit; Vol. 227; n.º 6; p. 657-667;

Slope Indicator (2006) *Horizontal Digitilt Inclinometer Probe*; Mukilteo, Washington: Slope Indicator;

SNCF (2001) *Application Ferroviaire, Spécification Technique - ST 590 Ind. B: Fournitures de granulats utilises pour la realisation et l'entratien des voies ferrees a usage electrique* Paris: SNCF;

SNCF (2002) *IGLGS*; Livre 1, Tome II; Paris: SNCF; Cap. 8; Remblais contigues aux maconneries;

Soriano, A. & Sanchez, F.J. (1999) *Settlements of railroad high embankments*; Proceedings of the 12th European Conference on Soil Mechanics and Geotechnical Engineering Amsterdam, Netherlands; Jun. 1999; Vol. 3; pp. 1885-1890;

Suiker, A.S.J. (2002) *The Mechanical Behaviour of Ballasted Railway Tracks*; Ph.D Thesis; Civil Engineering and Geosciences; Delft: Delft University of Technology;

Suiker, A.S.J.; Selig, E.T. & Frenkel, R. (2005) *Static and Cyclic Triaxial Testing of Ballast and Subballast*; Journal of Geotechnical and Geoenvironmental Engineering; Vol. 131; n.º 6; p. 771-782;

Sussmann, T.R.; Ebersöhn, W. & Selig, E.T. (2001) *Fundamental Nonlinear Track Load-Deflection Behavior for Condition Evaluation*; Transportation Research Record; n.º 1742; p. 61-67;

Suzuki, T.; Ishida, M.; Abe, K. & Koro, K. (2005) *Measurement on Dynamic Behaviour of Track near Rail Joints and Prediction of Track Settlement*; Quarterly Report of RTRI; Vol. 46; n.º 2; p. 124-129;

Täljsten, B.; Carolin, A. & Pedersen, H. (2007) *Sustainable Bridges, SB-STR: Repair and Strengthening of Railway Bridges - Guideline, Deliverable D6.1*; Project no. TIP3-CT-2003-001653, co-funded by the European Commission within the Sixth Framework Programme (2002-2006); Report D6.1;

Tanaka, H. & Furukawa, A. (2008) *The estimation method of wheel load and lateral force using the axlebox acceleration*; WCRR 2008 - World Congress on Railway Research; Seoul, Korea; 18-22 Jun. 2006; p. 10;

Tanaka, H. & Furukawa, A. (2009) *Management Method for Large Wheel Loads and Lateral Forces Using Axle-box Acceleration and Track Irregularity*; Quarterly Report of RTRI; Vol. 50; n.º 2; p. 116-122;

Tarabji, S.D. & Thompson, M.R. (1976) *Finite Element Analysis of a Railway Track Support System. Ballast and Foundation Materials Research Program. Users manual.*; Illinois Univ. at Urbana-Champaign. Dept. of Civil Engineering.;

Tatsuoka, F.; Tateyama, M.; Aoki, H. & Watanabe, K. (2005) *Ground Improvement, Case Histories*; Ed. 1; Amsterdam: Elsevier; Cap. 29; Bridge Abutment Made of Cement-Mixed Gravel Back-Fill; 0-080-44633-7;

Teixeira, P.F. (2003) *Contribución a la reducción de los costes de mantenimiento de vías de alta velocidad mediante la optimización de su rigidez vertical*; Ph.D Thesis; Infraestructura del Transport I del Territori; Barcelona: Universitat Politècnica de Catalunya;

Thom, N.H. (2006) *Rail trafficking testing*; Jubilee Symposium on Polymer Geogrid Reinforcement; London; 8 Sep. 2009;

Tijera, A.; Ruiz, R.; Cuéllar, V. & Rodríguez, M. (2012) *Variacones de rigidez de vía en zonas de transición*; Ingeneriería Civil; Vol. 165; p. 103-112; 0213-8468;

Ubalde, L. (2004) *La auscultación y los trabajos de vía en la línea del AVE Madrid – Sevilla: análisis de la experiencia y deducción de nuevos criterios de mantenimiento*; Ph.D Thesis Thesis; Infraestructura del Transport I del Territori; Barcelona: Universitat Politècnica de Catalunya;

Ubalde, L.; López Pita, A.; Teixeira, P.F.; Bachiller, A. & Gallego Giner, I. (2007) *Track deterioration in high-speed railways*; European Railway Review; n.º 2;

UIC (2008a) *Best practice guide for optimum track geometry durability*; Paris: Union Internationale des Chemins de Fer; 2-7461-1456-9;

UIC (2008b) *CODE 719 R, Earthworks and track bed for railway lines*; Paris: Union Internationale des Chemins de Fer; 2-7461-0568-3;

UIC (2009a) *CODE 518, Testing and approval of railway vehicles from the point of view of their dynamic behaviour - Safety - Track fatigue - Ride quality* Paris: Union Internationale des Chemins de Fer;

UIC (2009b) *Under Sleeper Pads - Summarising Report*; Vienna: Union Internationale des Chemins de Fer;

Vale, C. (2010) *Influência da qualidade dos sistemas ferroviários no comportamento dinâmico e no planeamento da manutenção preventiva de vias de alta velocidade*; Ph.D. Thesis; Departamento de Engenharia Civil; Porto: Faculdade de Engenharia da Universidade do Porto;

Varandas, J.N. (2013) *Long-term behaviour of railway transitions under dynamic loading*; Ph.D. Thesis Thesis; Lisboa: Faculdade de Ciências e Tecnologia da Universidade Nova de Lisboa;

Varandas, J.N.; Holscher, P. & Silva, M.A.G. (2014a) *Settlement of ballasted track under traffic loading: application to transition zones*; Proceedings of the Institution of Mechanical Engineers, Part F: Journal of Rail and Rapid Transit; Vol. 228; n.º 3; p. 242-259;

Varandas, J.N.; Hölscher, P. & Silva, M.A.G. (2011) *Dynamic behaviour of railway tracks on transitions zones*; Computers & Structures; Vol. 89; n.º 13–14; p. 1468-1479; 0045-7949;

Varandas, J.N.; Paixão, A.; Fortunato, E.; Hölscher, P. & Calçada, R. (2014b) *Non-linear elastic behaviour of unbound aggregates in FEM representing railway transition zones*; Railways 2014, The Second International Conference on Railway Technology: Research, Development and Maintenance; Ajaccio, Corsica, France; 8-11 Apr. 2014; p. 21;

Watanabe, K.; Matsumaru, T. & Tateyama, M. (2011) *Soft ground improvement method for railway embankment using cement-mixed gravel and geosynthetic*; GEORAIL 2011, International Symposium Railway geotechnical engineering; Paris; May 2011; Vol. 1; pp. 389-396;

Werkmeister, S. (2003) *Permanent Deformation Behaviour of Unbound Granular Materials in Pavement Constructions*; Ph.D Thesis; Infrastructure and Planning; Dresden, Germany: Technischen Universität Dresden;

Werkmeister, S.; Dawson, A. & Wellner, F. (2001) *Permanent Deformation Behavior of Granular Materials and the Shakedown Concept*; Transportation Research Record; n.º 1757; p. 75-81;

White, W.; Lee, I.K. & Valliappan, S. (1977) *Unified boundary for finite dynamic models*; Journal of the Engineering Mechanics Division; Vol. 103; n.º 5; p. 949-964;

With, C. & Bodare, A. (2009) *Evaluation of track stiffness with a vibrator for prediction of train-induced displacement on railway embankments*; Soil Dynamics and Earthquake Engineering; Vol. 29; n.º 8; p. 1187-1197; 0267-7261;

Witt, S. (2008) *The Influence of Under Sleeper Pads on Railway Track Dynamics*; Division of Solid Mechanics; Linköping: Linköping University;

Woodward, P.; Kacimi, A.; Laghrouche, O.; Medero, G. & Banimahd, M. (2012) *Application of polyurethane geocomposites to help maintain track geometry for high-speed ballasted railway tracks*; Journal of Zhejiang University SCIENCE A; Vol. 13; n.º 11; p. 836-849; 1673-565X;

Woodward, P.K.; Laghrouche, O.; El-Kacimi, A.; Medero, G.; Banimahd, M.; Kennedy, J.; Connolly, D.; Giannopoulos, A. & Forde, M.C. (2011) *High-speed rail geotechnical issues*; 11th International Conference on Railway Engineering; London; 29-30 Jun.;

Wu, T.X. & Thompson, D.J. (1999) *Effects of local preload on the foundation stiffness and vertical vibration of railway track*; Journal of Sound and Vibration; Vol. 219; n.º 5; p. 881-904; 0022-460X;

Xia, H.; Han, Y.; Zhang, N. & Guo, W. (2006) *Dynamic analysis of train–bridge system subjected to non-uniform seismic excitations*; Earthquake Engineering & Structural Dynamics; Vol. 35; n.º 12; p. 1563-1579; 1096-9845;

Xuan, D.X.; Houben, L.J.M.; Molenaar, A.A.A. & Shui, Z.H. (2012) *Mechanical properties of cement-treated aggregate material – A review*; Materials and Design; Vol. 33; n.º 0; p. 496-502; 0261-3069;

Zhang, S.; Xiao, X.; Wen, Z. & Jin, X. (2008) *Effect of unsupported sleepers on wheel/rail normal load*; Soil Dynamics and Earthquake Engineering; Vol. 28; n.º 8; p. 662-673; 0267-7261;

Zhu, J.J.; Ahmed, A.K.W.; Rakheja, S. & Khajepour, A. (2010) *Development of a vehicle–track model assembly and numerical method for simulation of wheel–rail dynamic interaction due to unsupported sleepers*; Vehicle System Dynamics: International Journal of Vehicle Mechanics and Mobility; Vol. 48; n.º 12; p. 1535 - 1552; 0042-3114;

Zhu, J.Y.; Thompson, D.J. & Jones, C.J.C. (2011) *On the effect of unsupported sleepers on the dynamic behaviour of a railway track*; Vehicle System Dynamics: International Journal of Vehicle Mechanics and Mobility; 0042-3114;

Zoeteman, A. & Esveld, C. (2004) *State of the art in railway maintenance management: planning systems and their application in Europe*; In: Systems, Man and Cybernetics, 2004 IEEE International Conference on; Vol. 5, p. 4165-4170 vol.5; 1062-922X;

Zwanenburg, W.-J. (2009) *Modelling degradation processes of switches & crossings for maintenance & renewal planning on the Swiss railway network*; LITEP; EPFL;

Annex A

Detailed analysis of track singularities in *Alcácer* bypass

PI at km 1.114 (Technical Block Type 1)

Excerpt from Design:

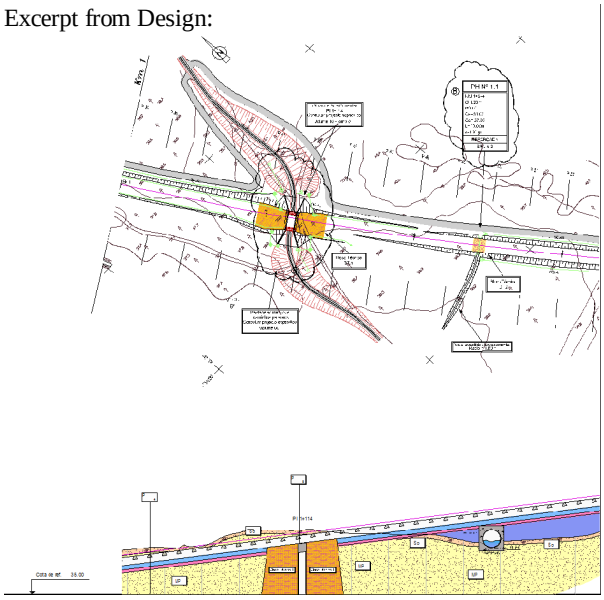

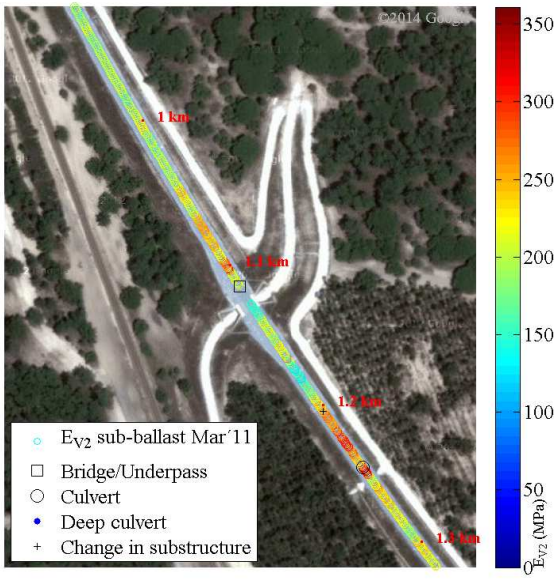

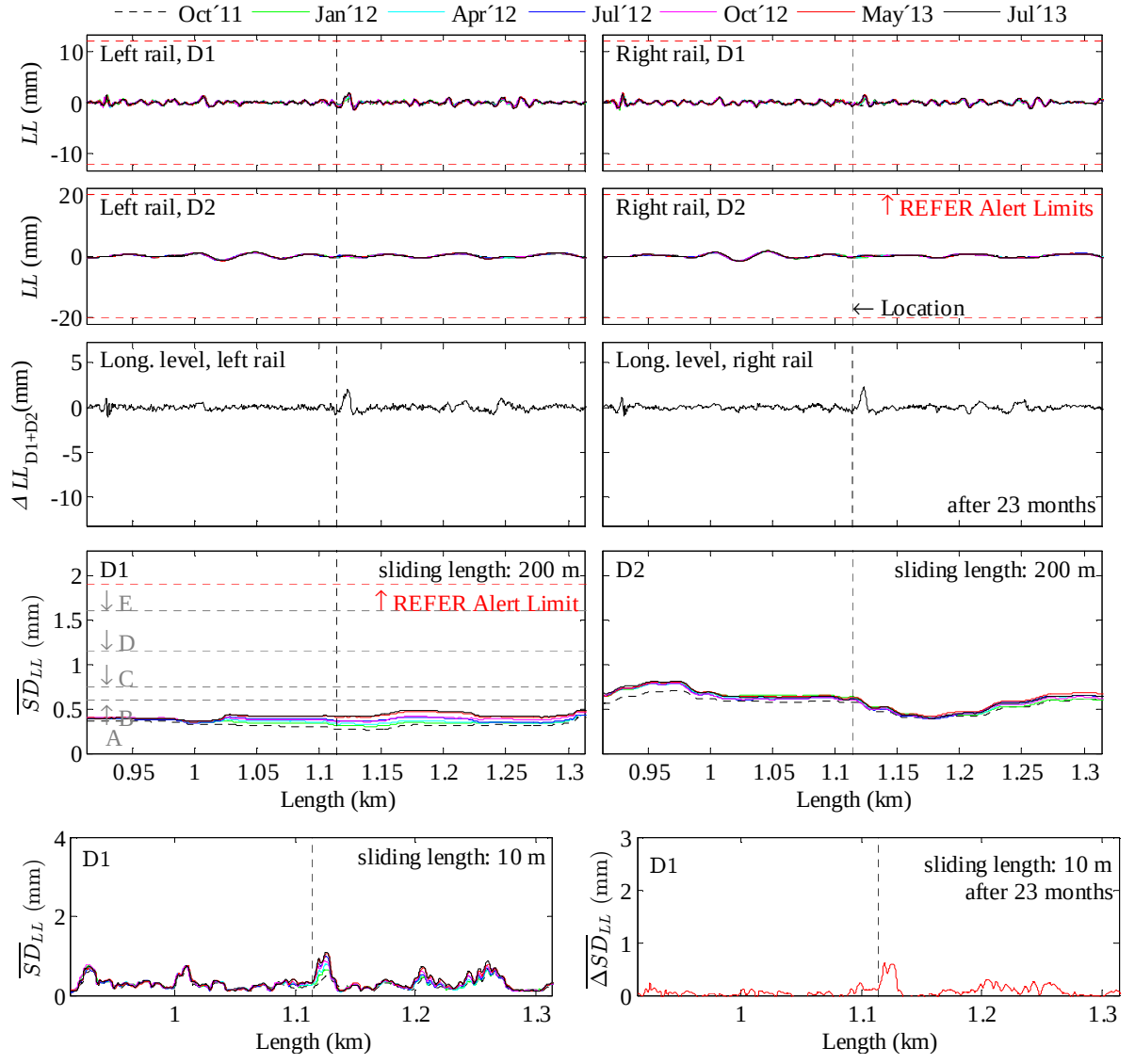

PIA at km 4.59 (Technical Block Type 1)

Excerpt from Design:

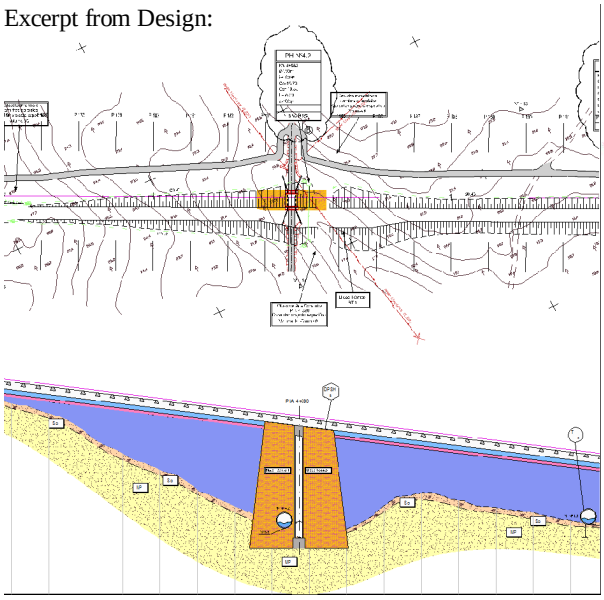

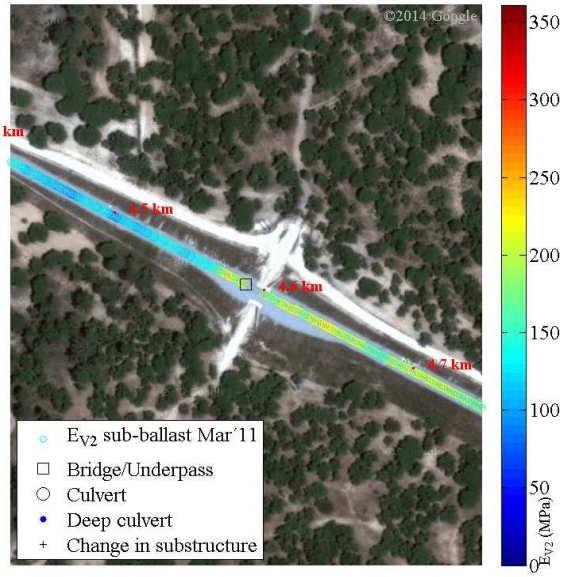

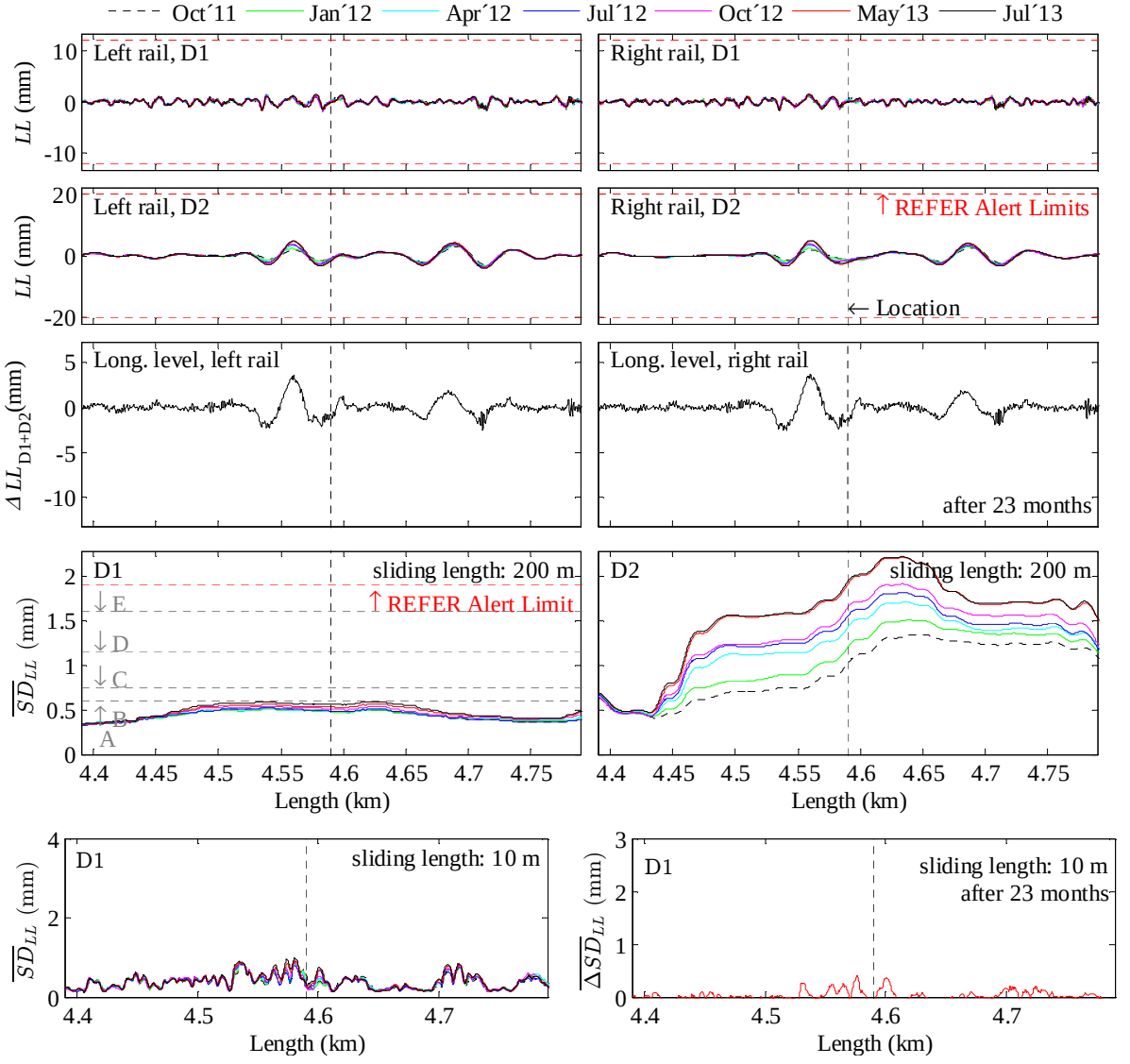

Viaduct of S. Martinho at km 5.142 (Technical Block Type 1)

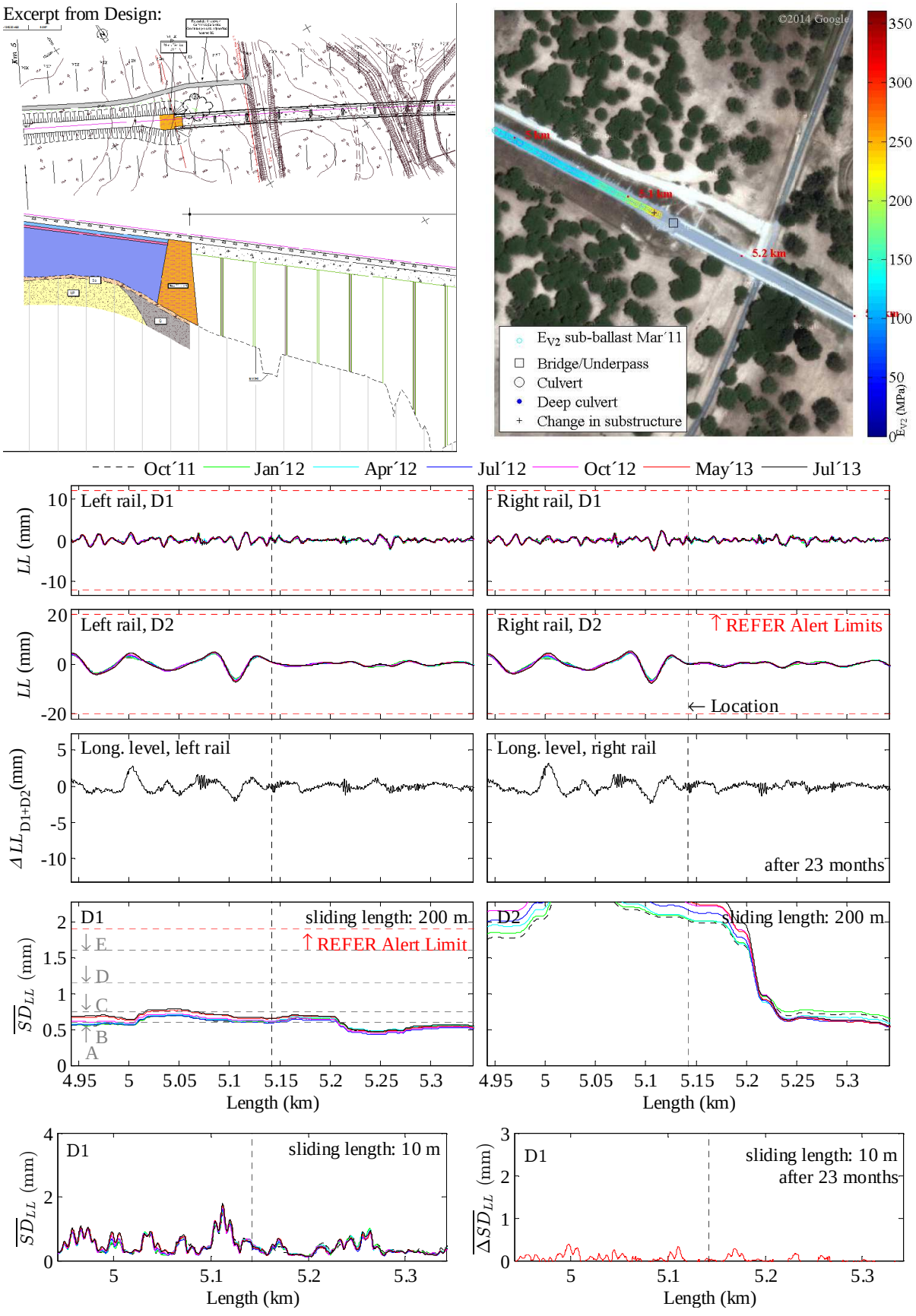

Viaduct of S. Martinho at km 5.994 (Technical Block Type 1)

Excerpt from Design:

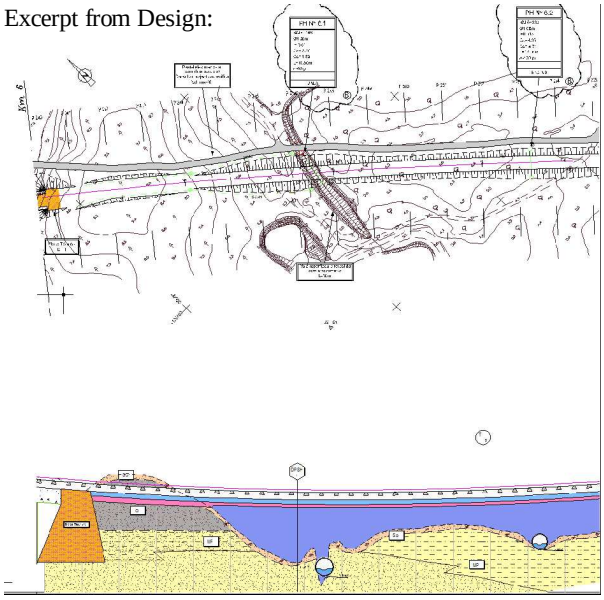

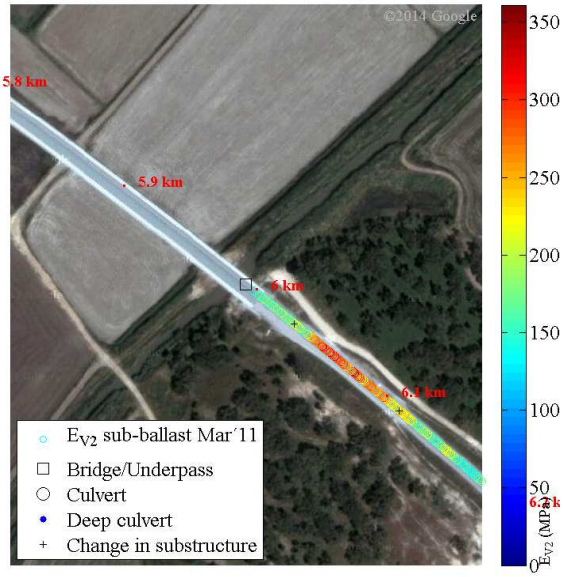

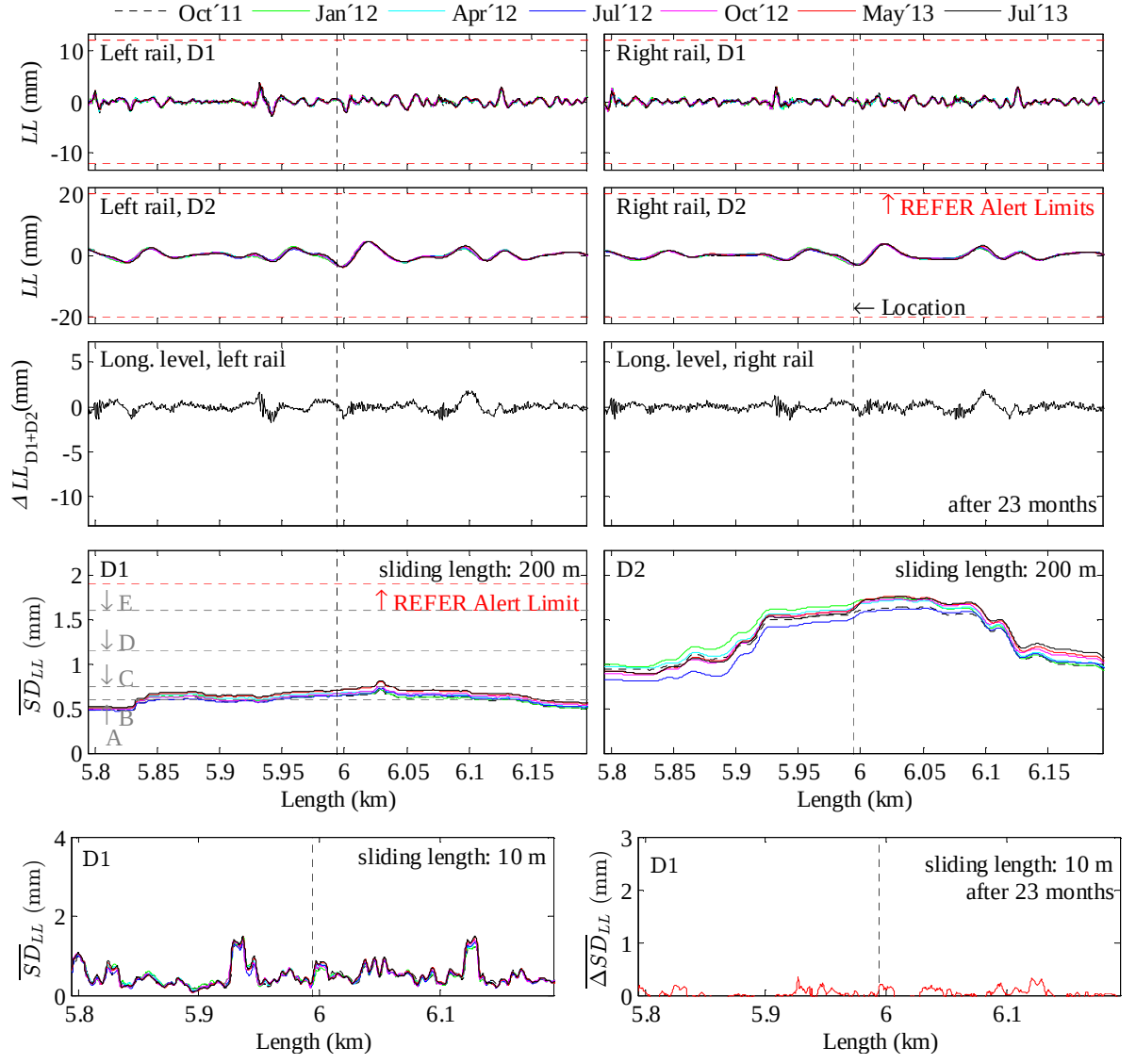

PIA at km 6.463 (Technical Block Type 1)

Excerpt from Design:

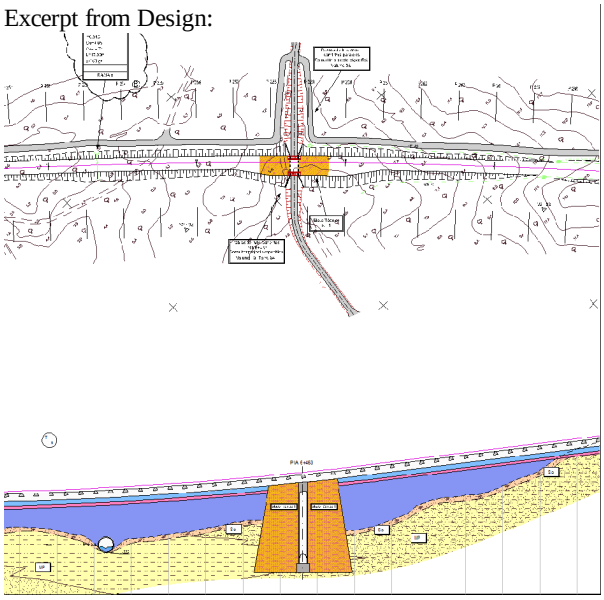

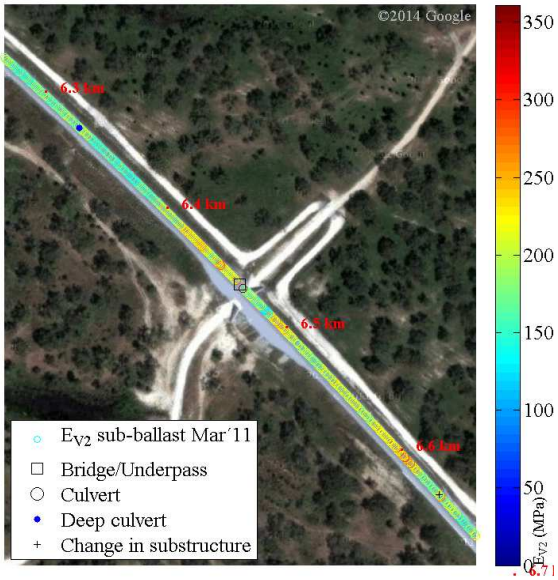

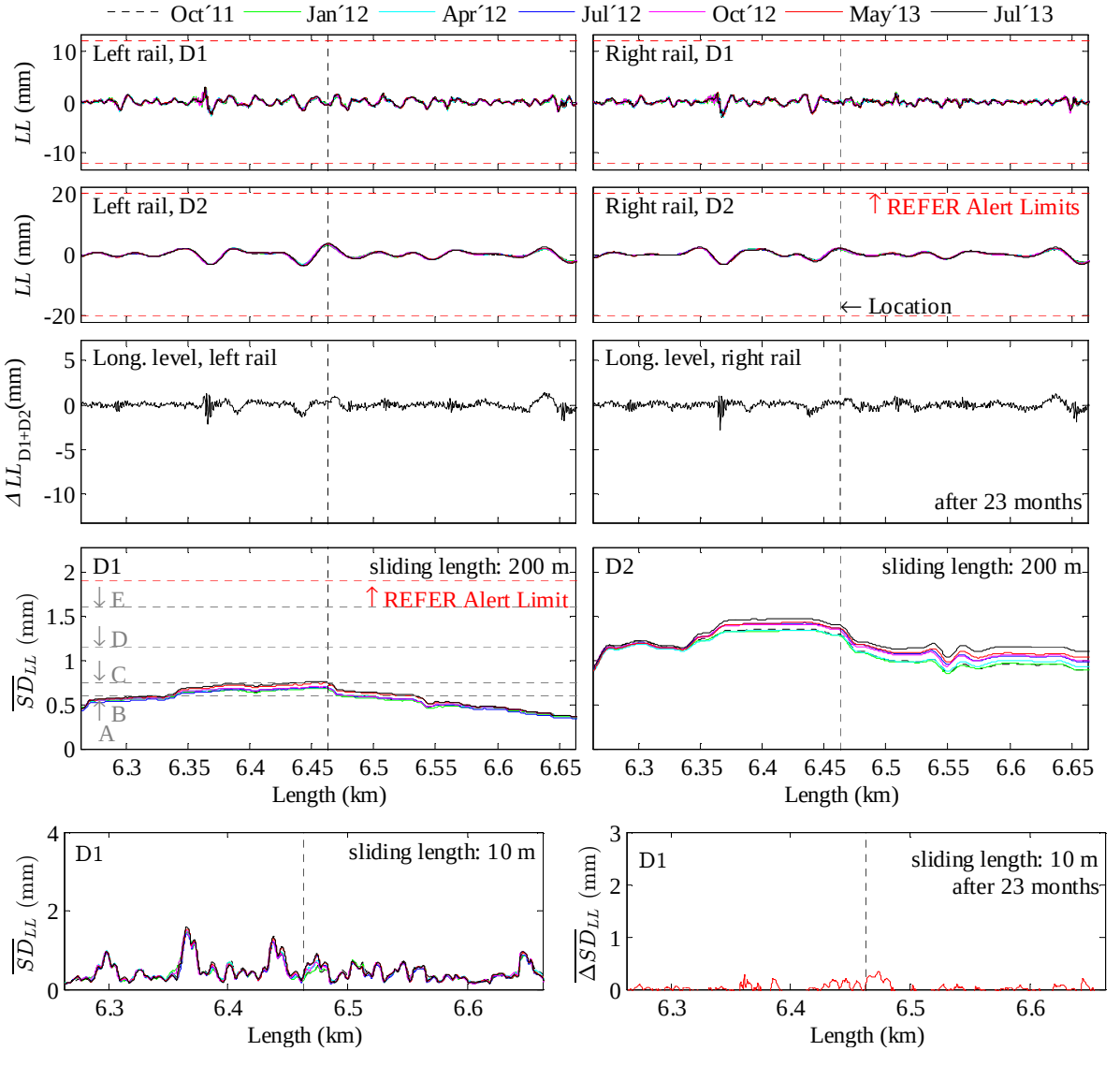

Northen approach to bridge over Sado river at km 8.312 (Technical Block Type 1)

Excerpt from Design:

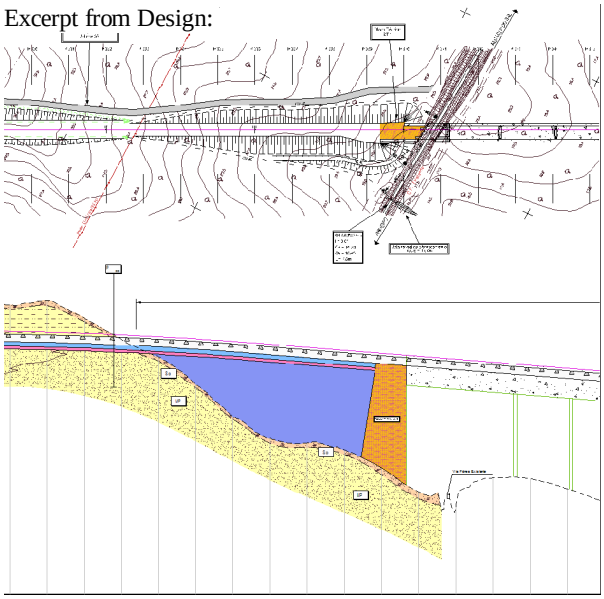

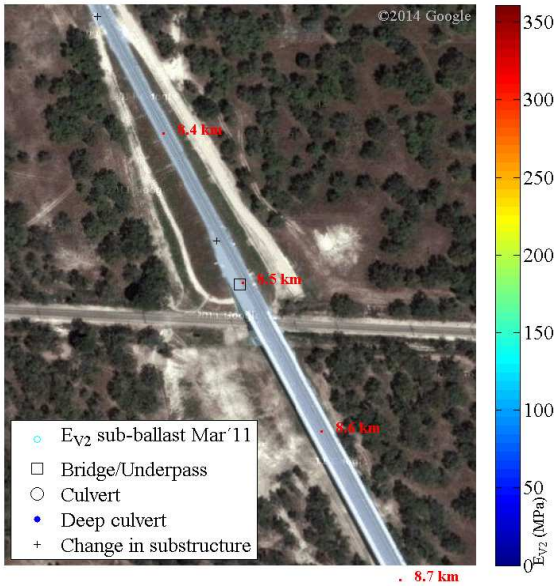

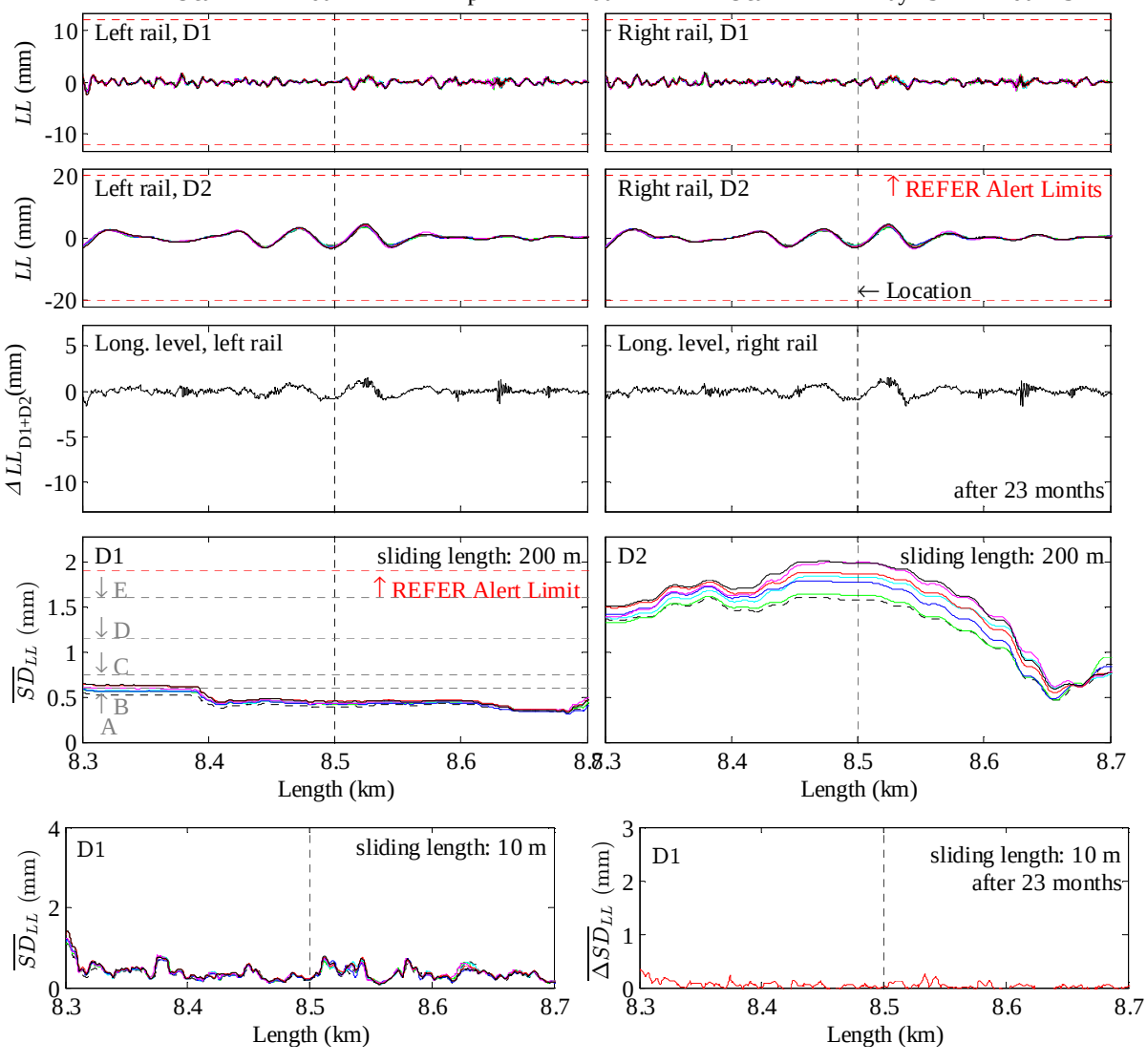

Southern approach to bridge over Sado river at km 11.837 (Technical Block Type 1)

Excerpt from Design:

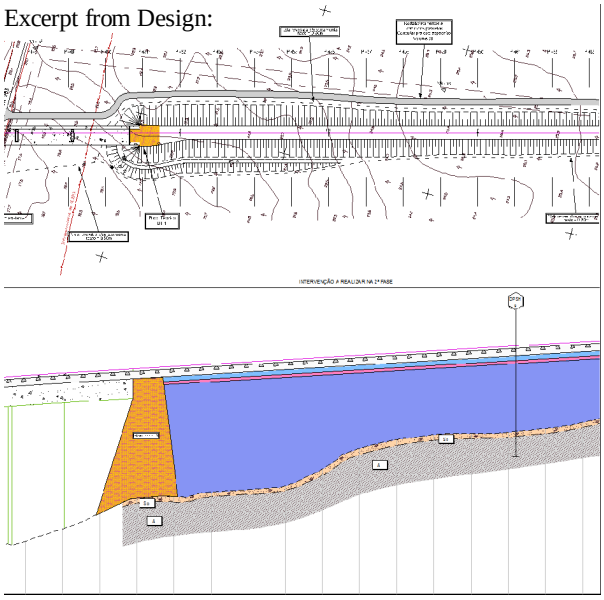

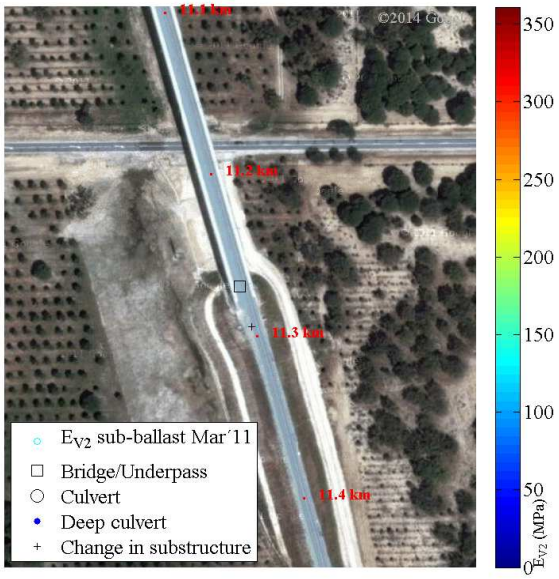

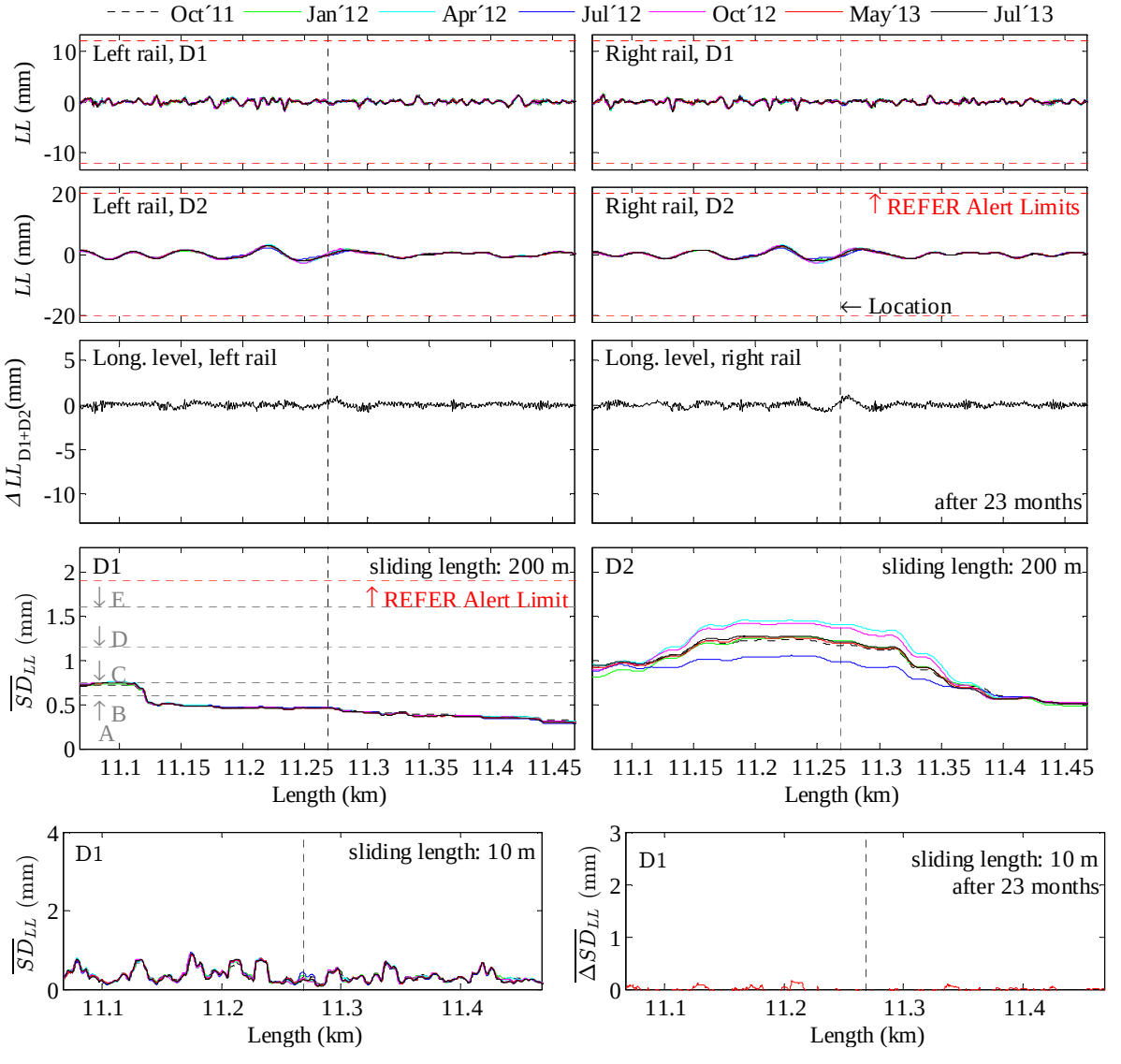

PIA at km 15.671 (Technical Block Type 1)

Excerpt from Design:

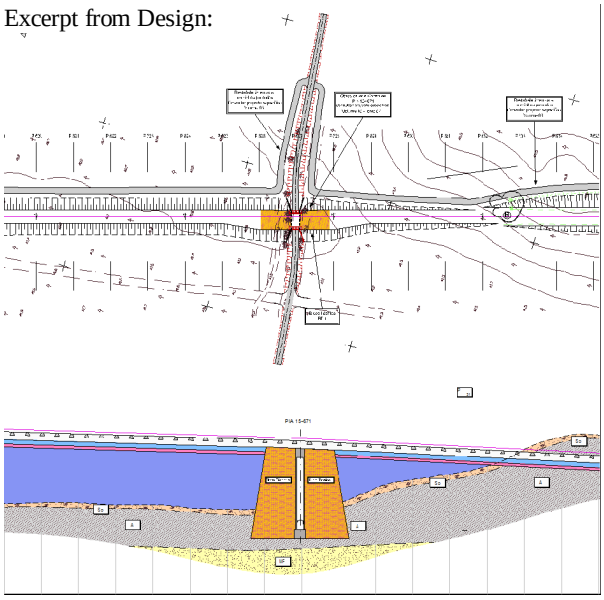

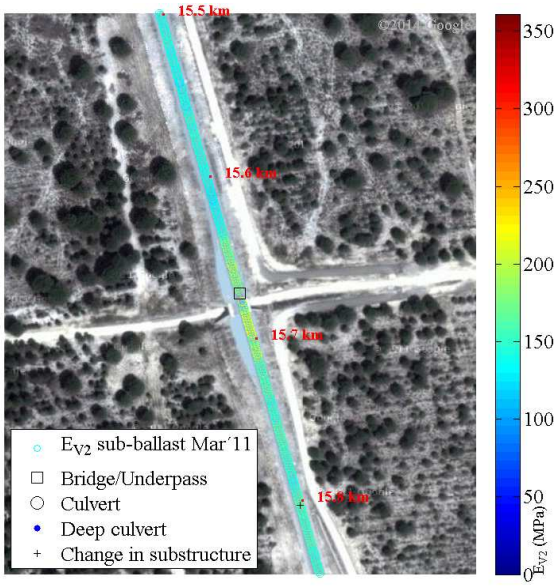

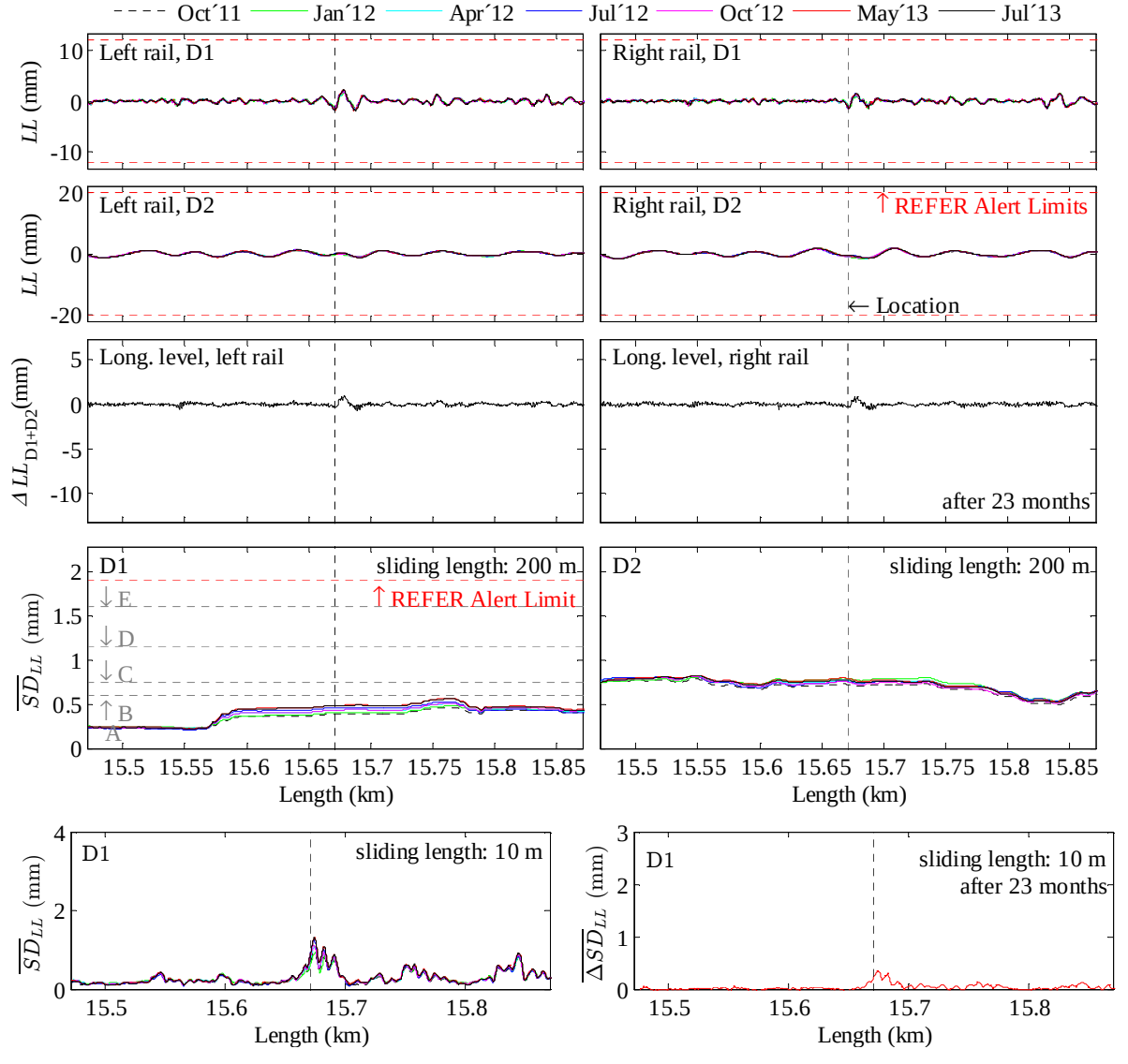

Viaduct of Água Cova at km 16.352 (Technical Block Type 1)

Excerpt from Design:

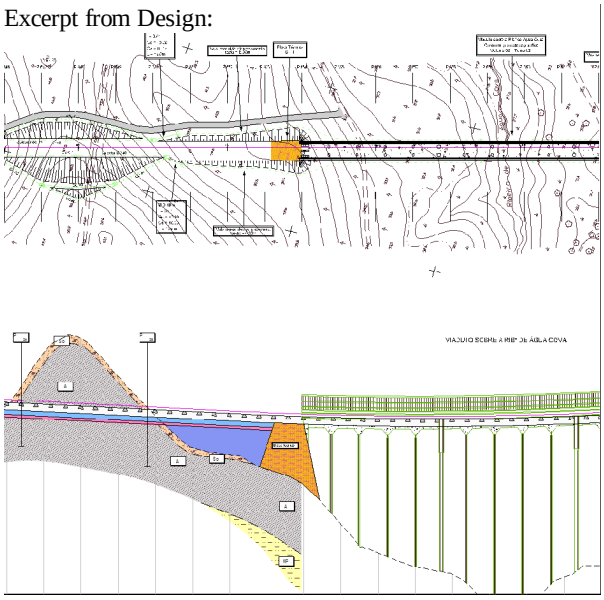

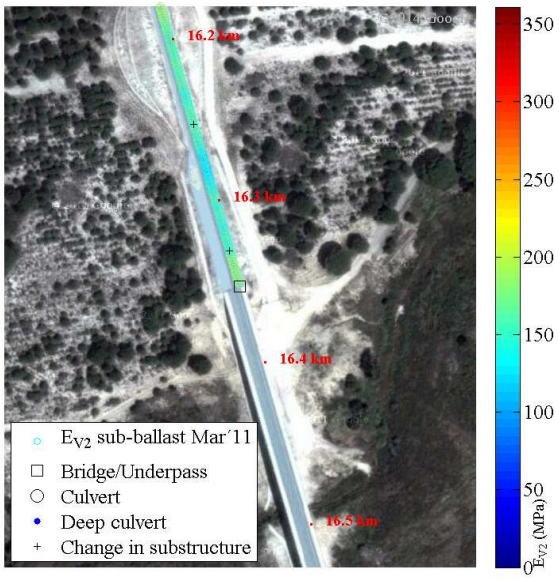

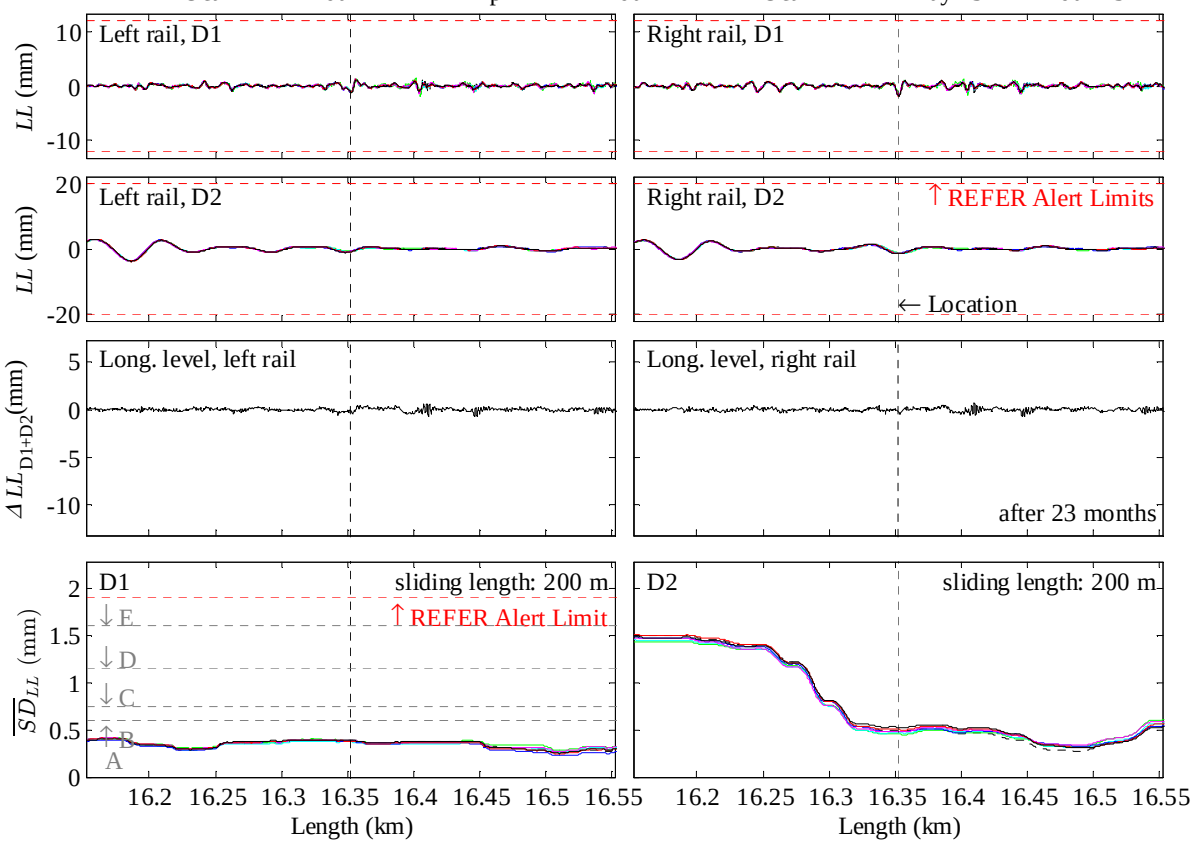

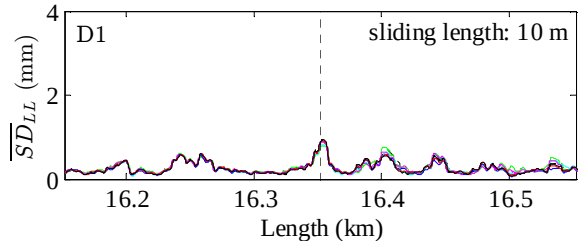

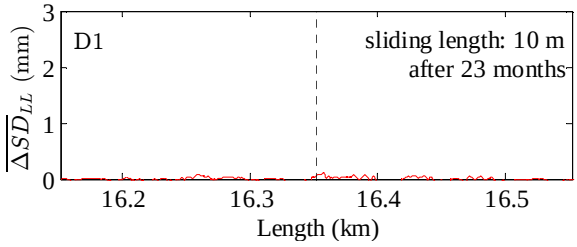

Viaduct of Água Cova at km 16.623 (Technical Block Type 1)

Excerpt from Design:

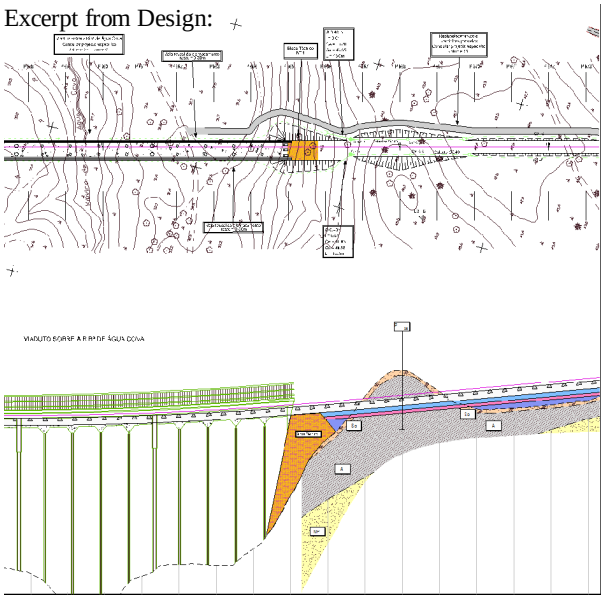

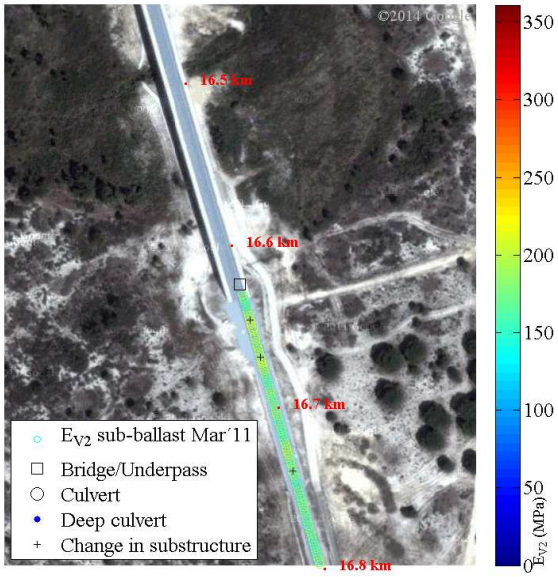

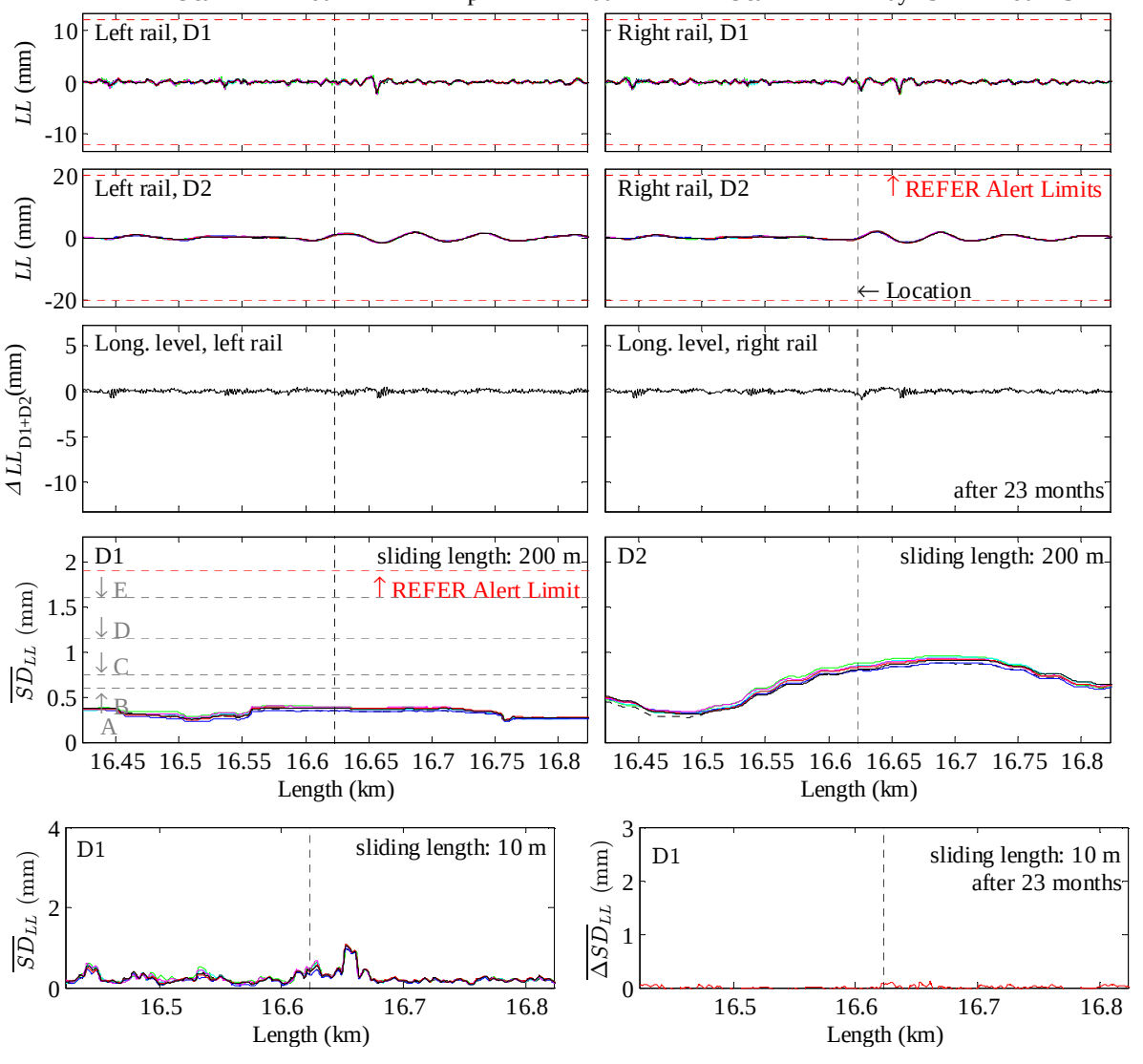

PIA at km 18.859 (Technical Block Type 1)

Excerpt from Design:

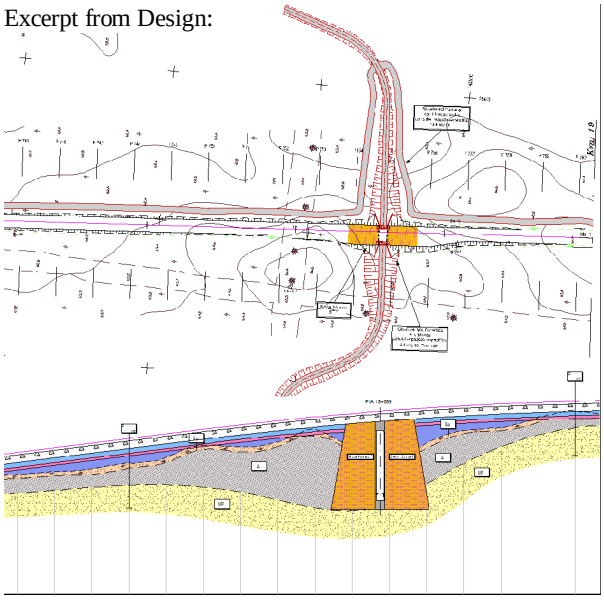

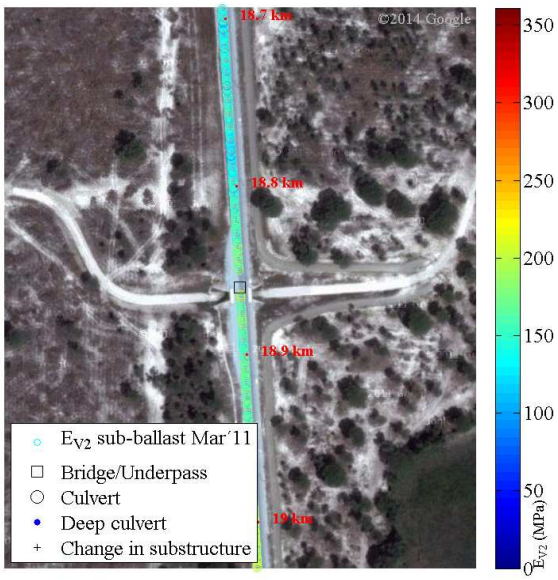

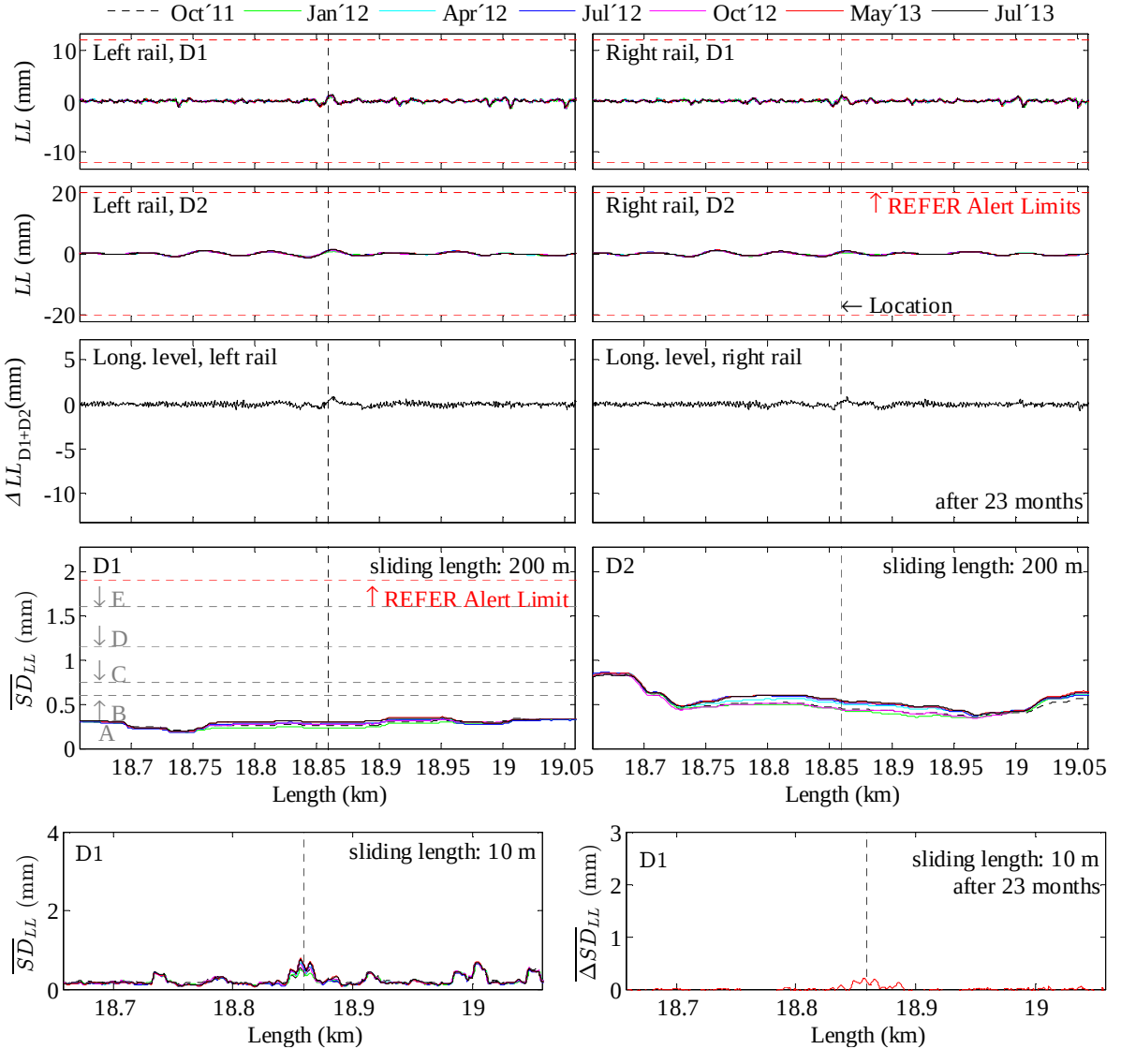

PIA at km 22.842 (Technical Block Type 1)

Excerpt from Design:

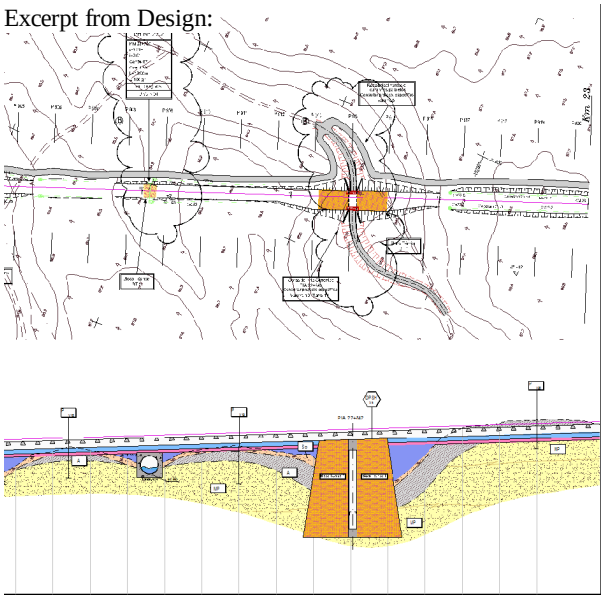

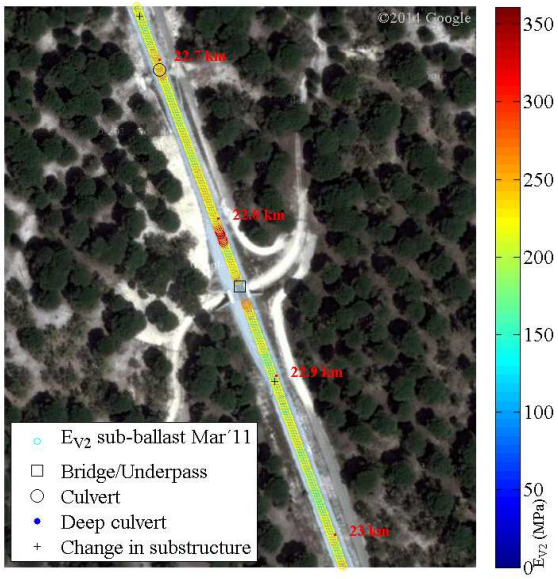

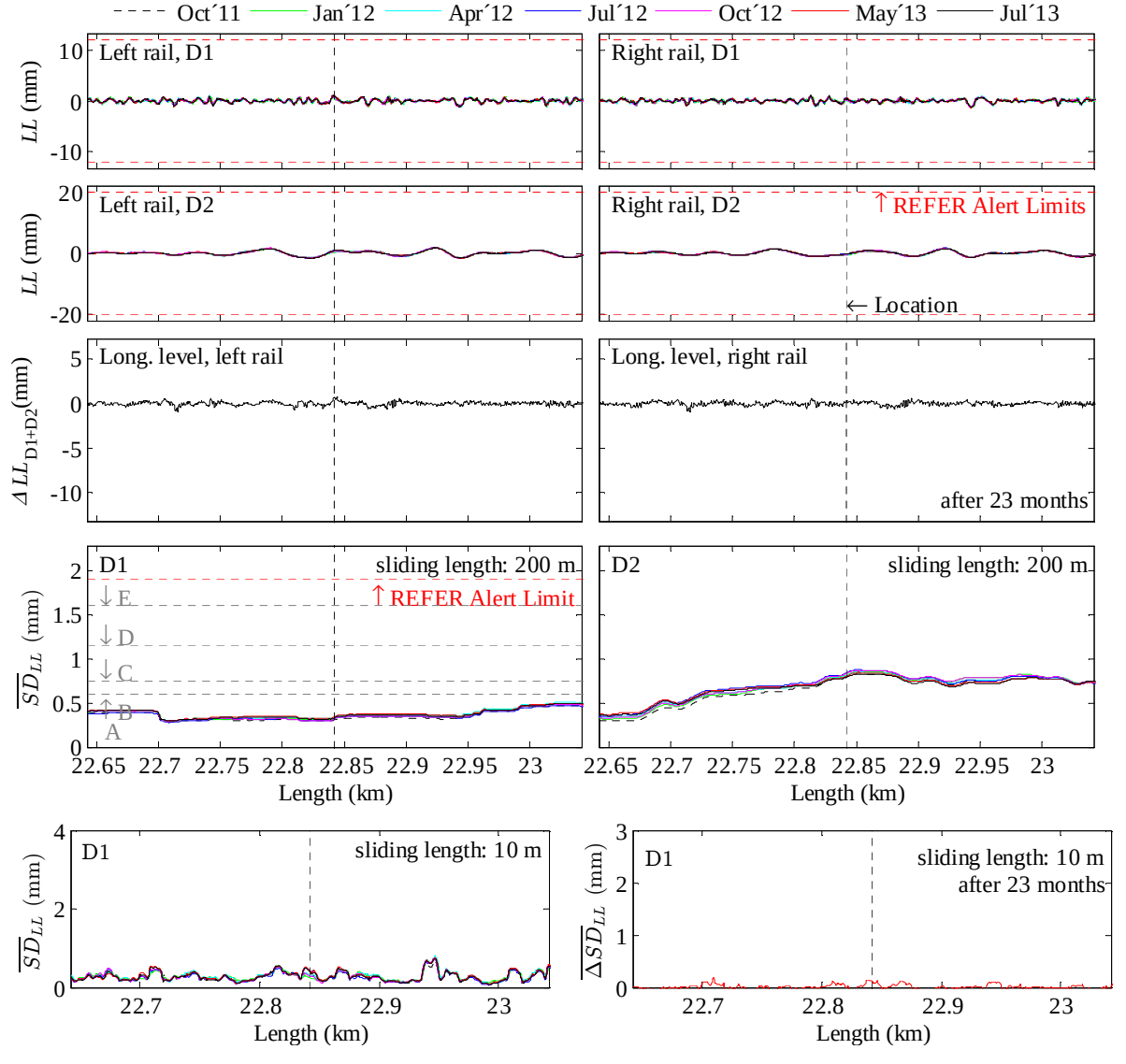

PI at km 23.889 (Technical Block Type 1)

Excerpt from Design:

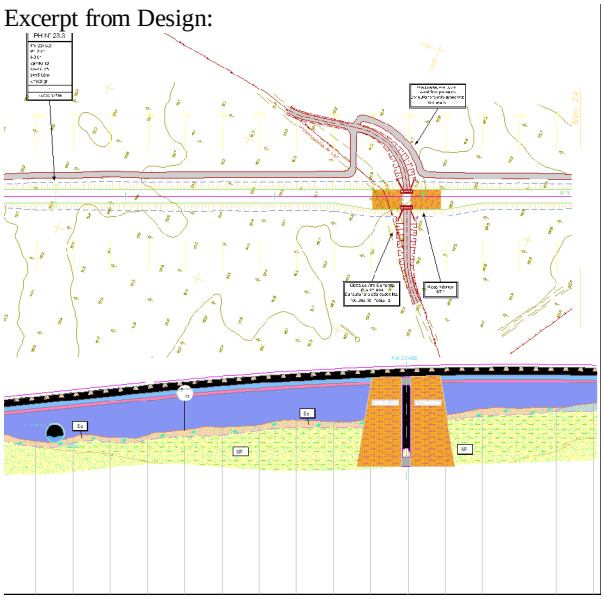

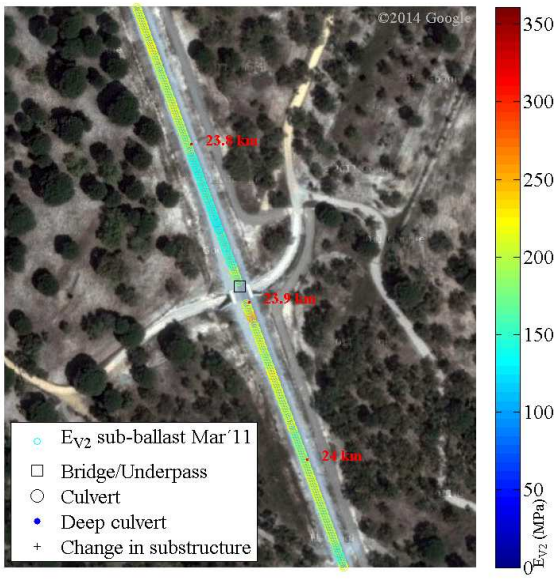

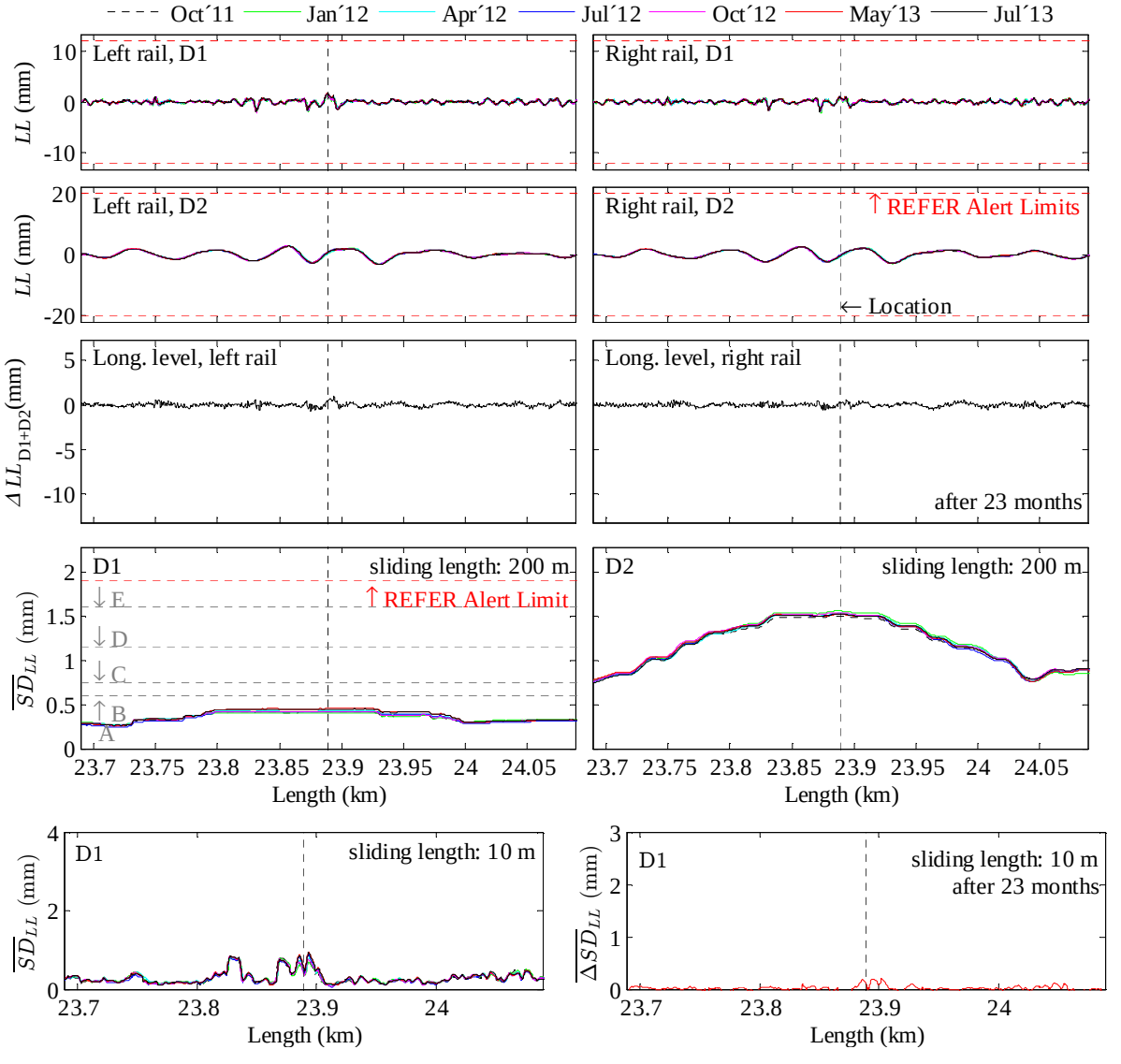

Viaduct over EN120 at km 26.378 (Technical Block Type 1)

Excerpt from Design:

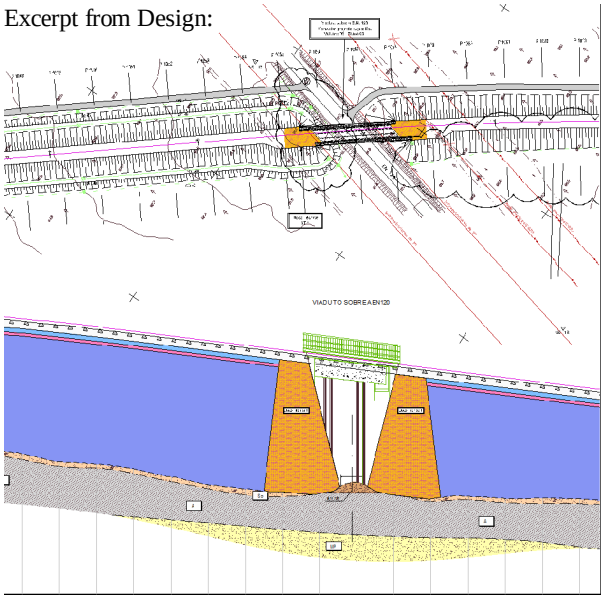

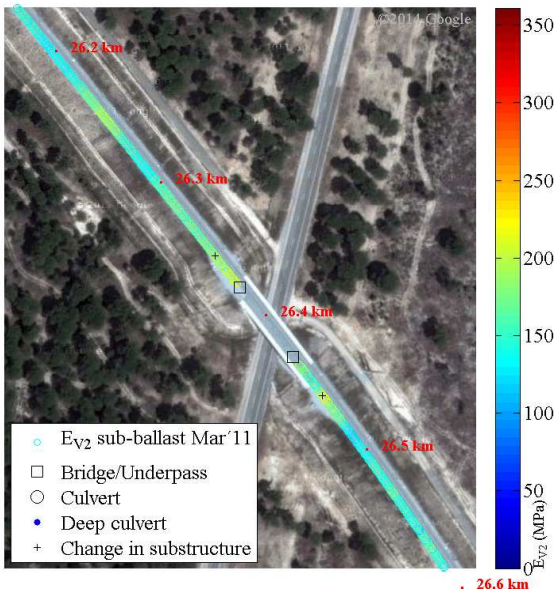

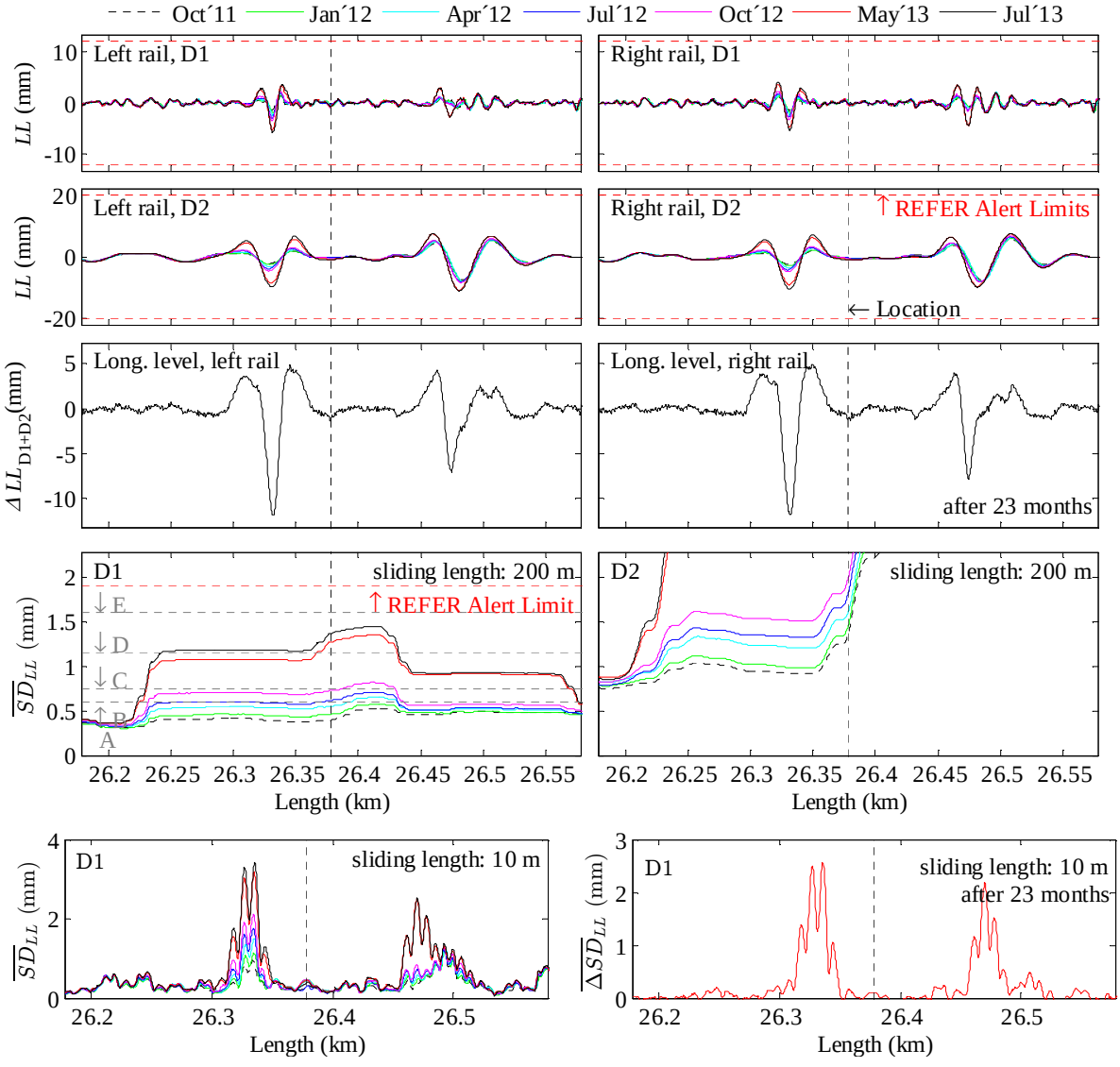

Viaduct over EN120 at km 26.43 (Technical Block Type 1)

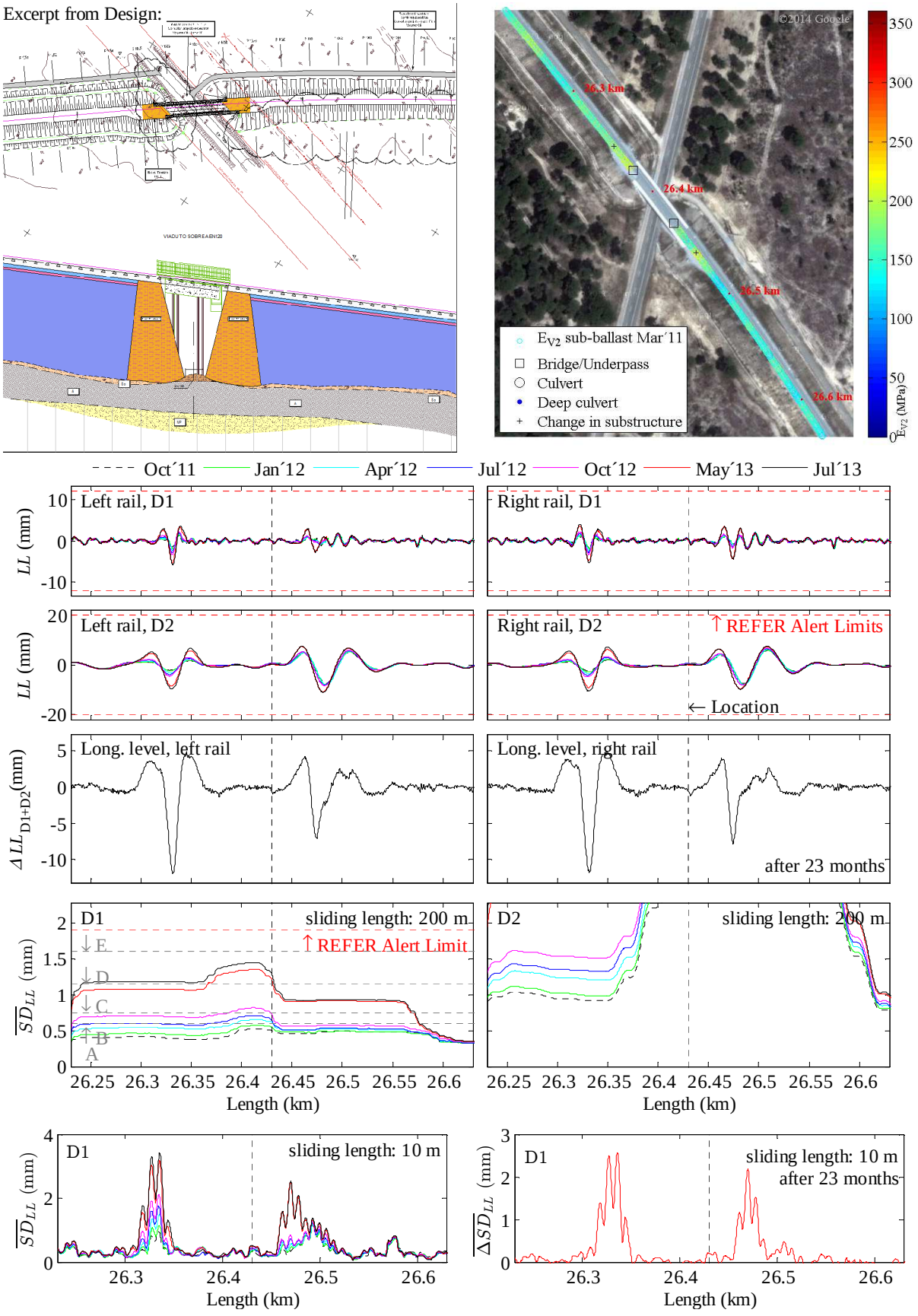

PIA at km 26.987 (Technical Block Type 1)

Excerpt from Design:

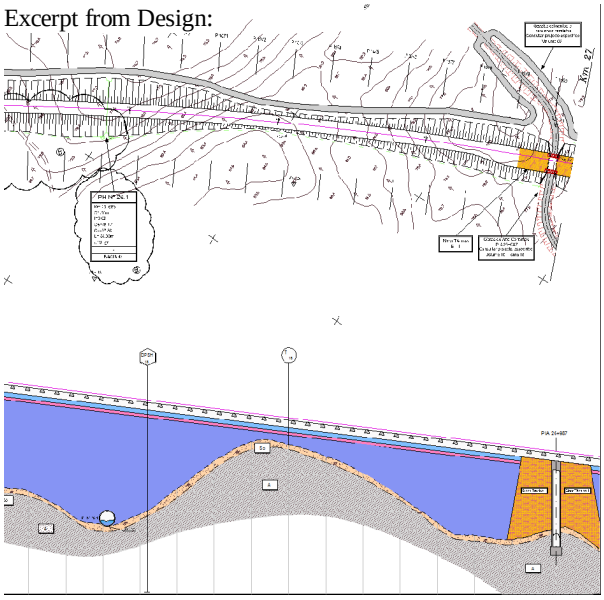

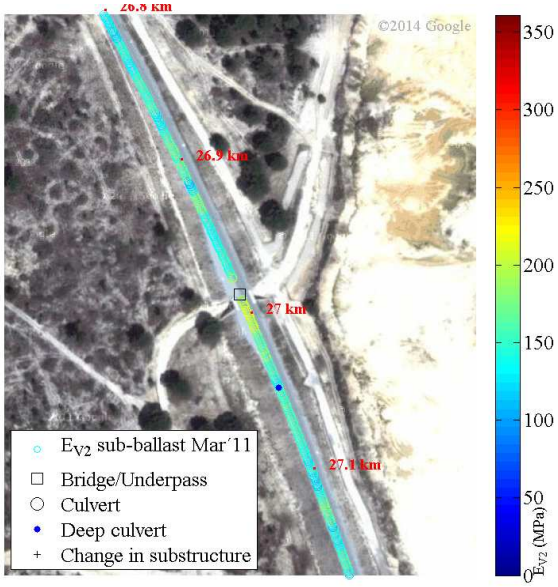

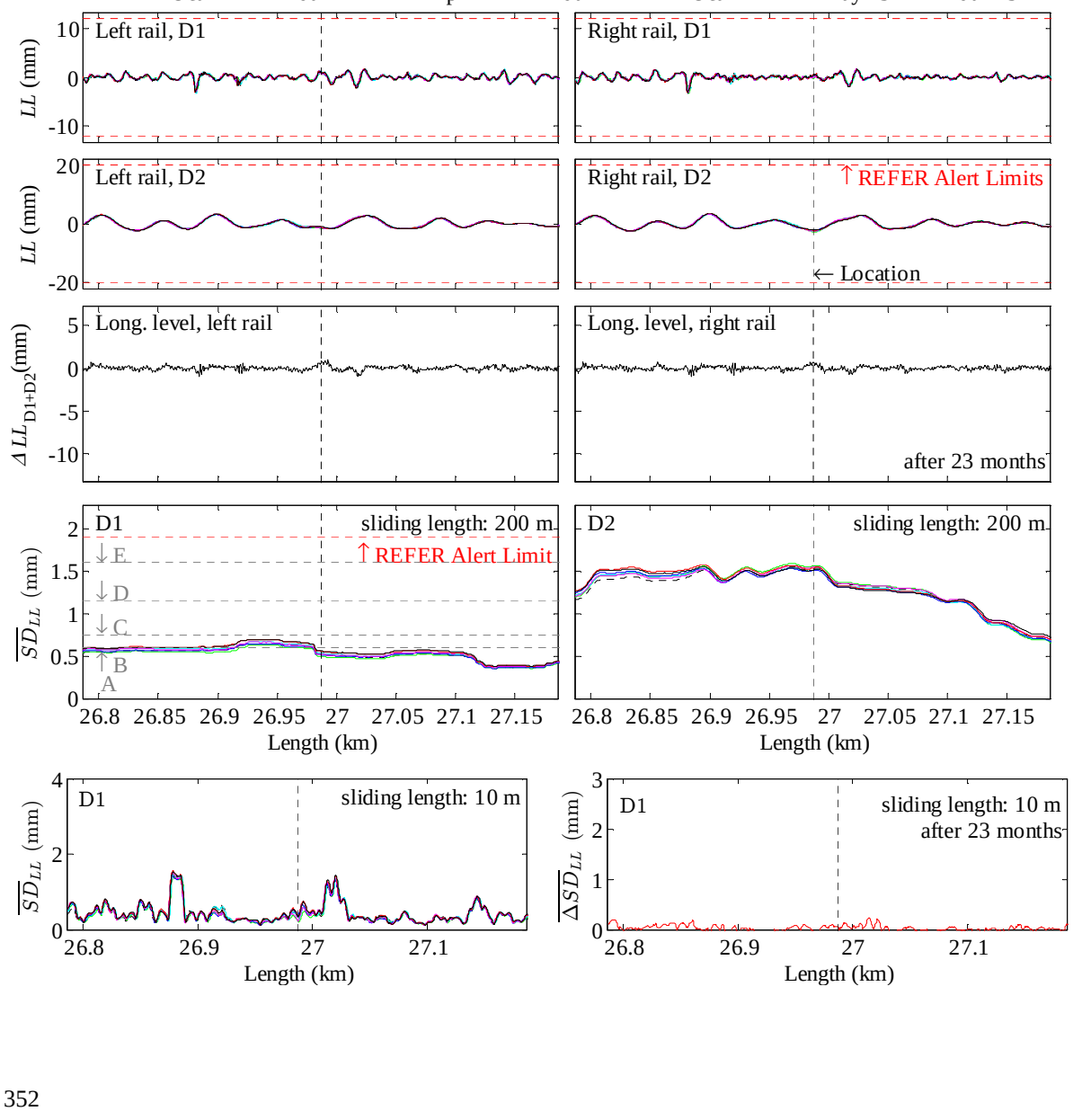

PH 1.1 at km 1.244 (Technical Block Type 2), Ø=1.2m

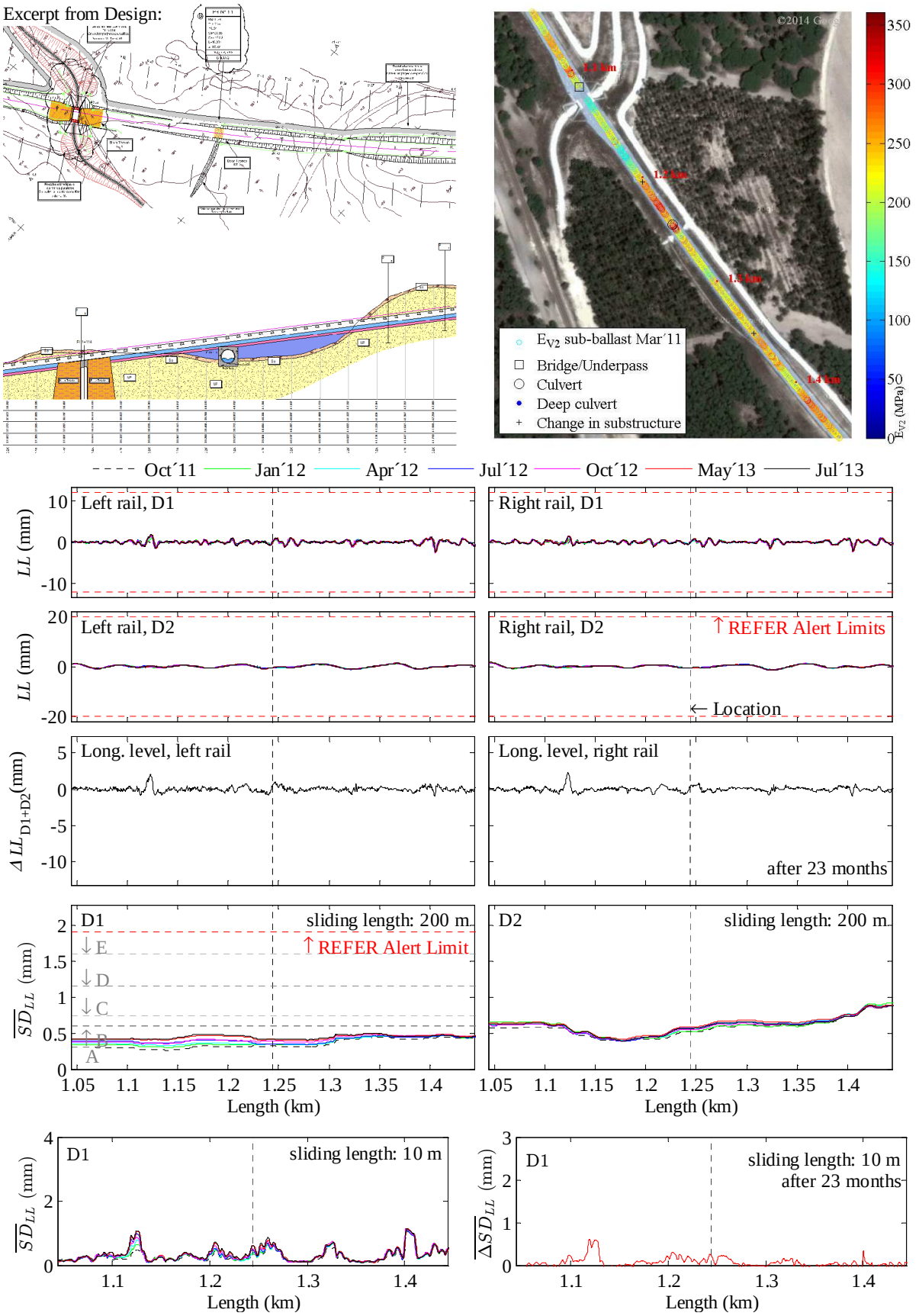

PH 1.3 at km 1.975 (Technical Block Type 2), Ø=1m

Excerpt from Design:

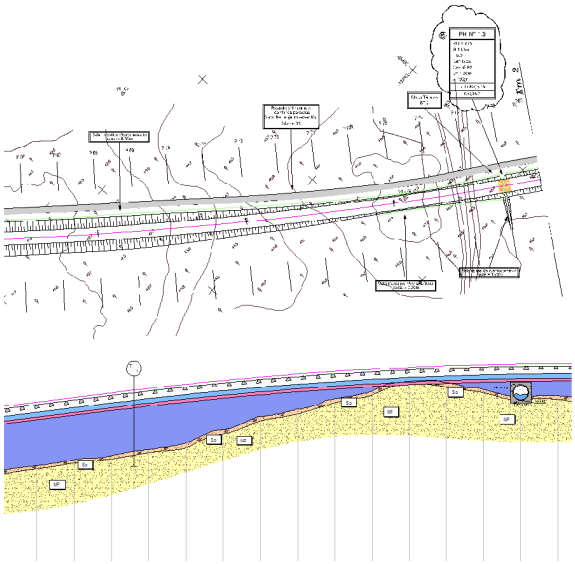

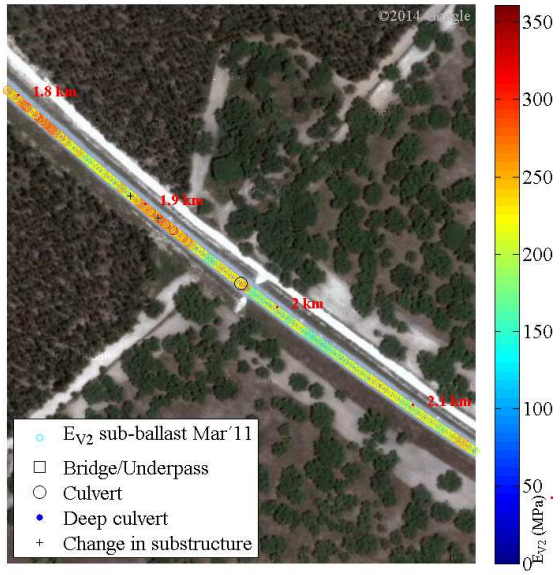

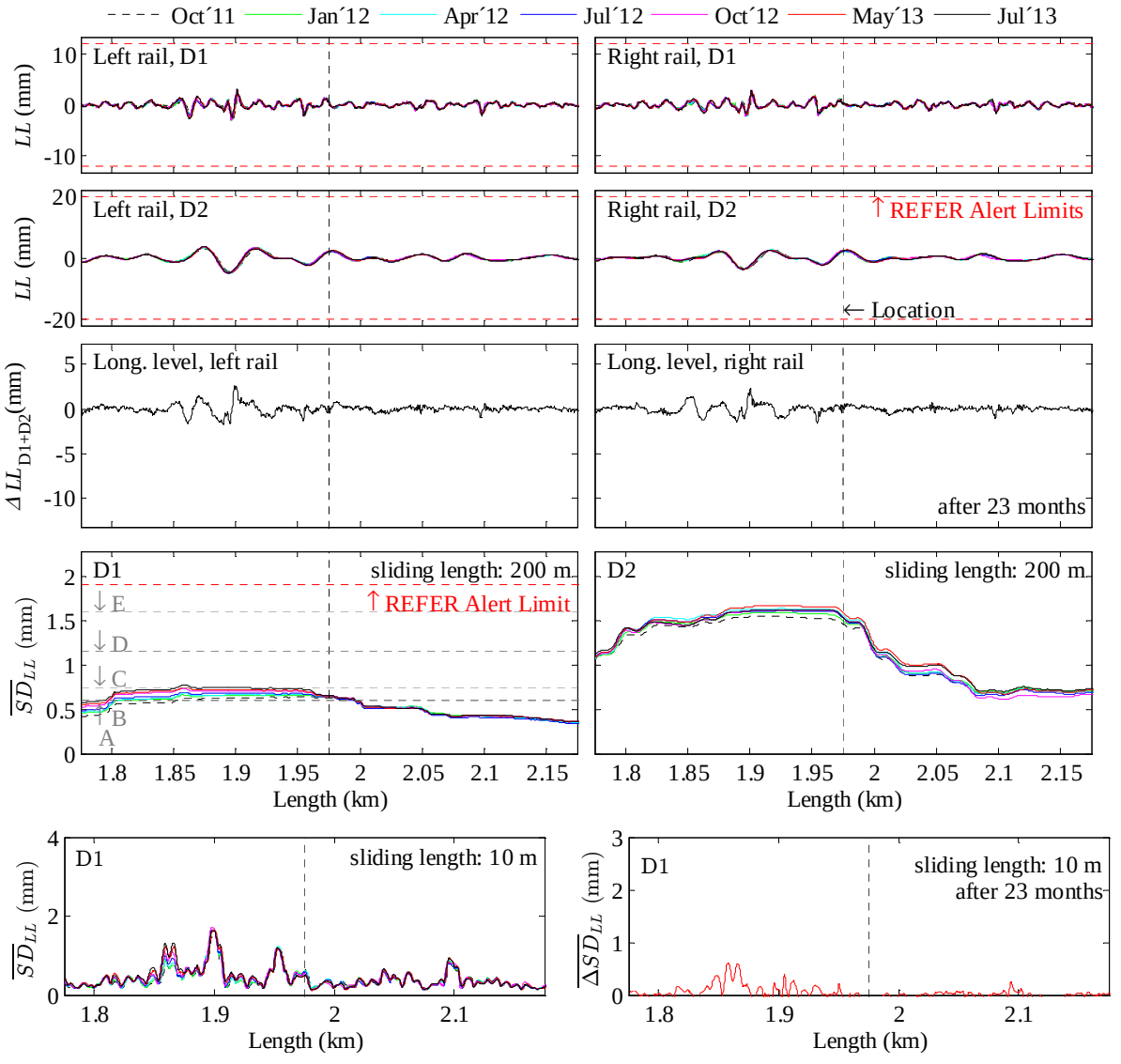

PH 4.1 at km 4.181 (Technical Block Type 2), Ø=1m

Excerpt from Design:

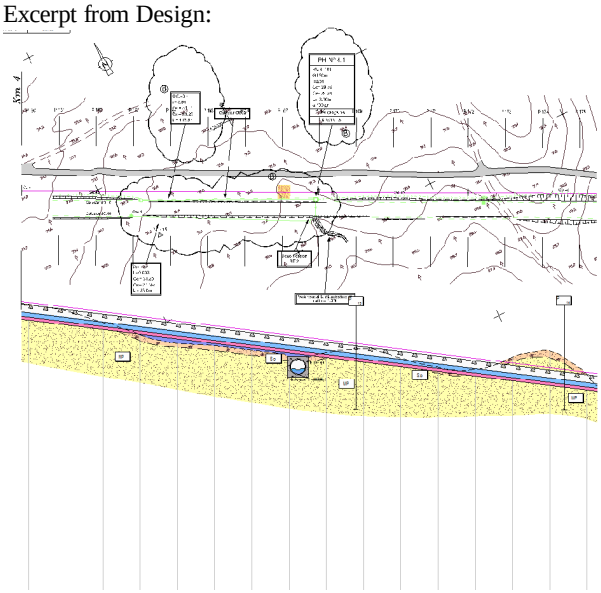

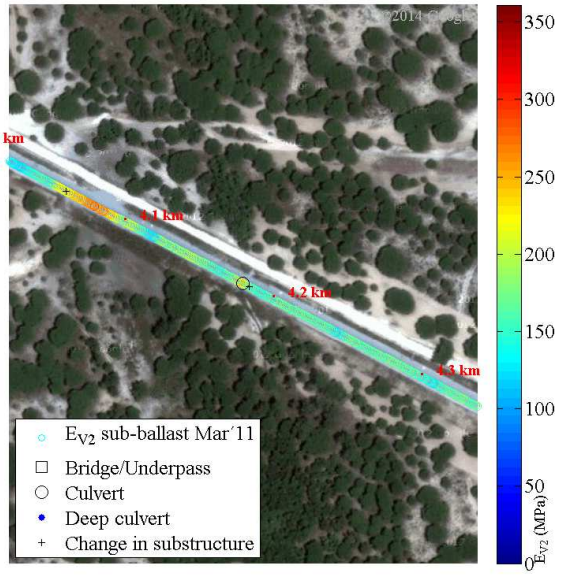

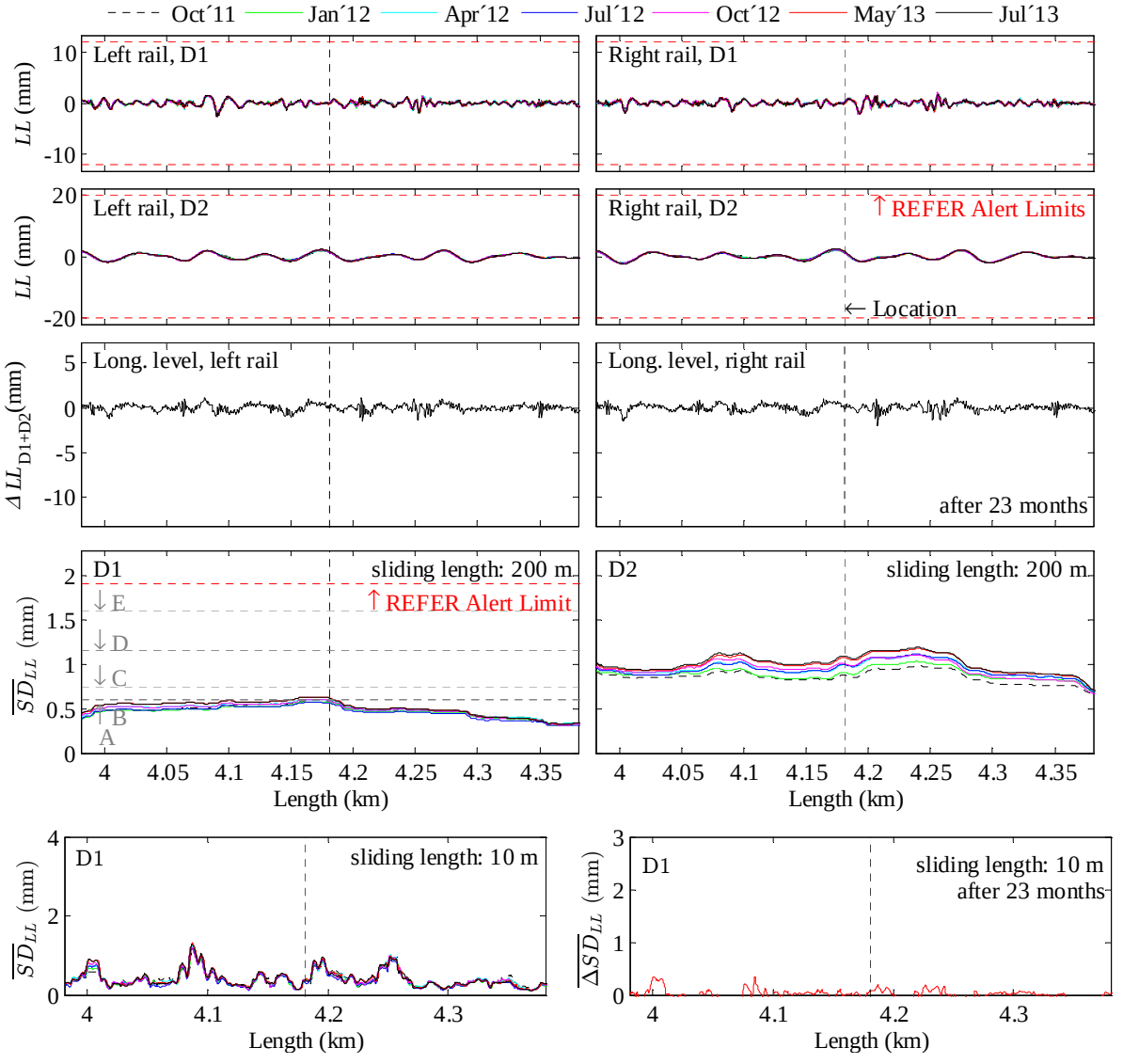

PF 12.1 at km 12.96 (Technical Block Type 2), Ø=1.2m

Excerpt from Design:

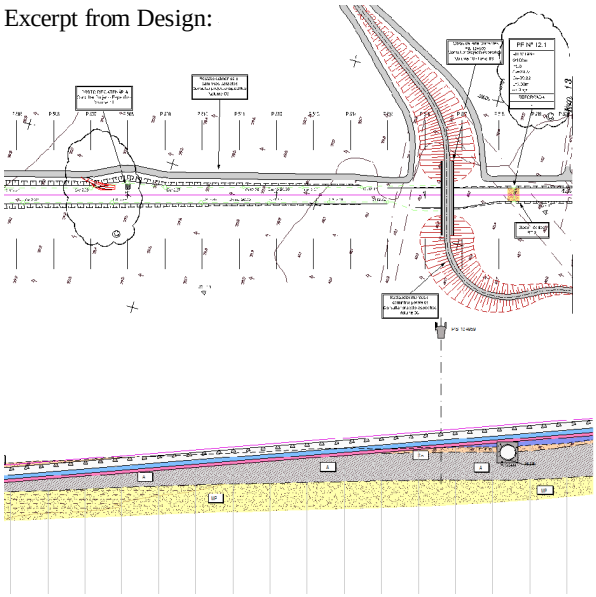

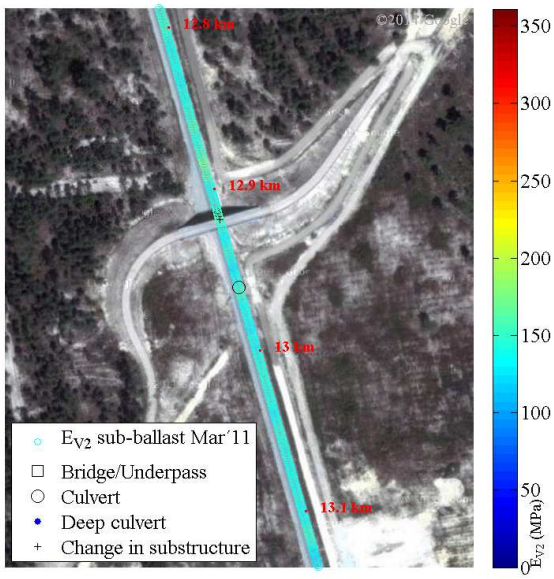

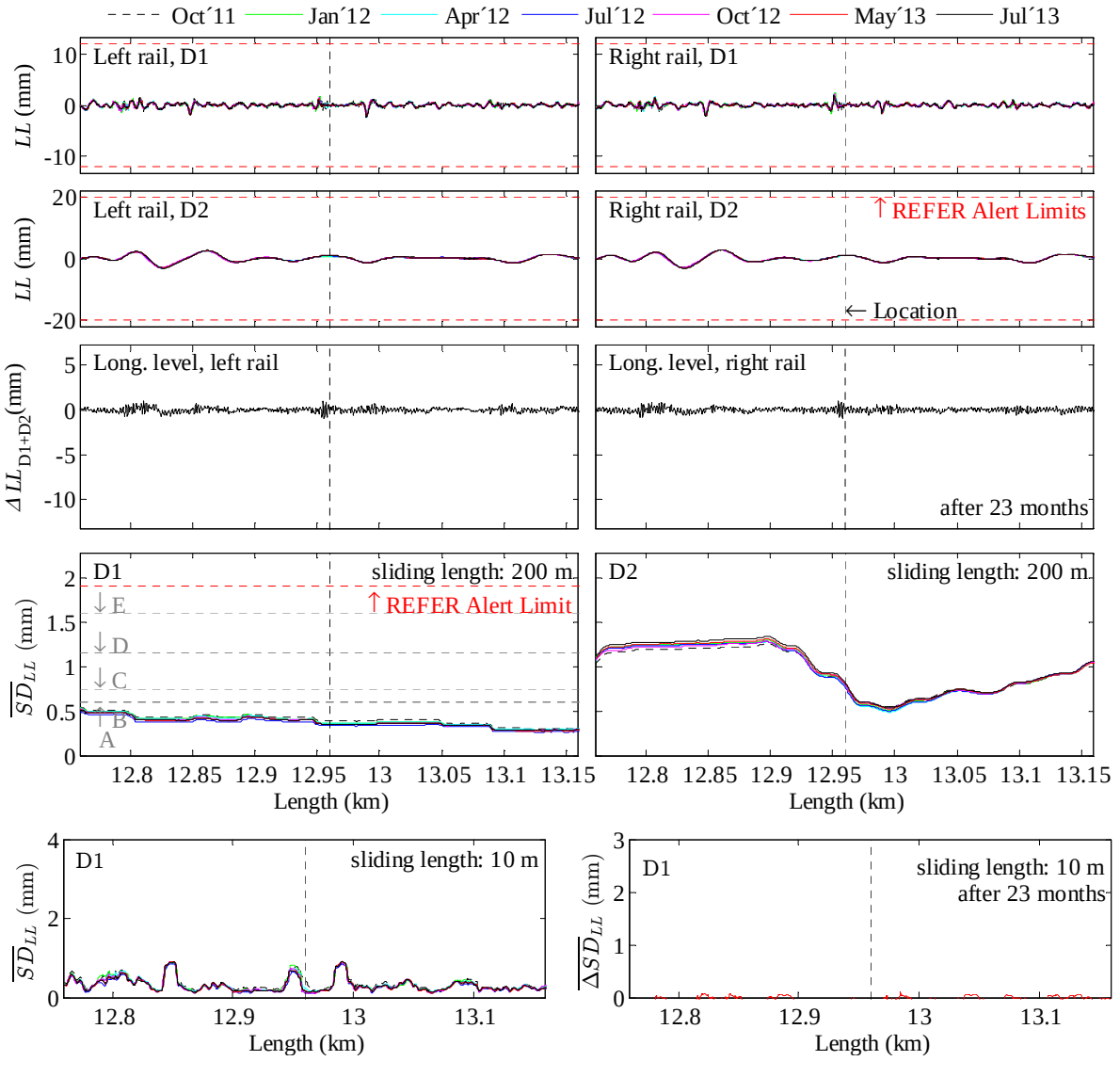

PF 13.1 at km 13.4 (Technical Block Type 2), Ø=1m

Excerpt from Design:

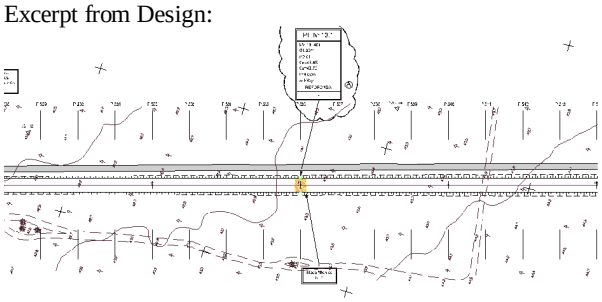

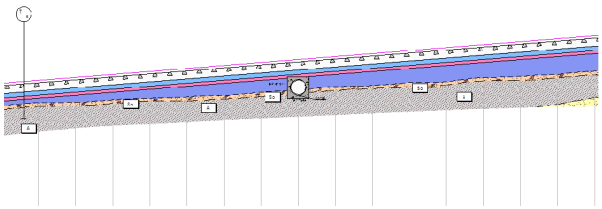

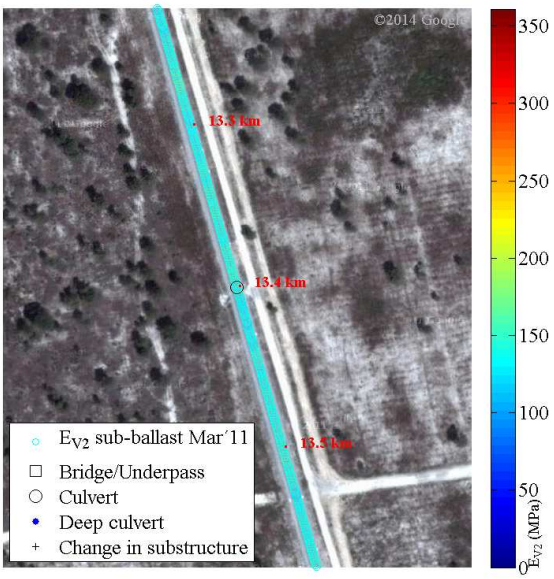

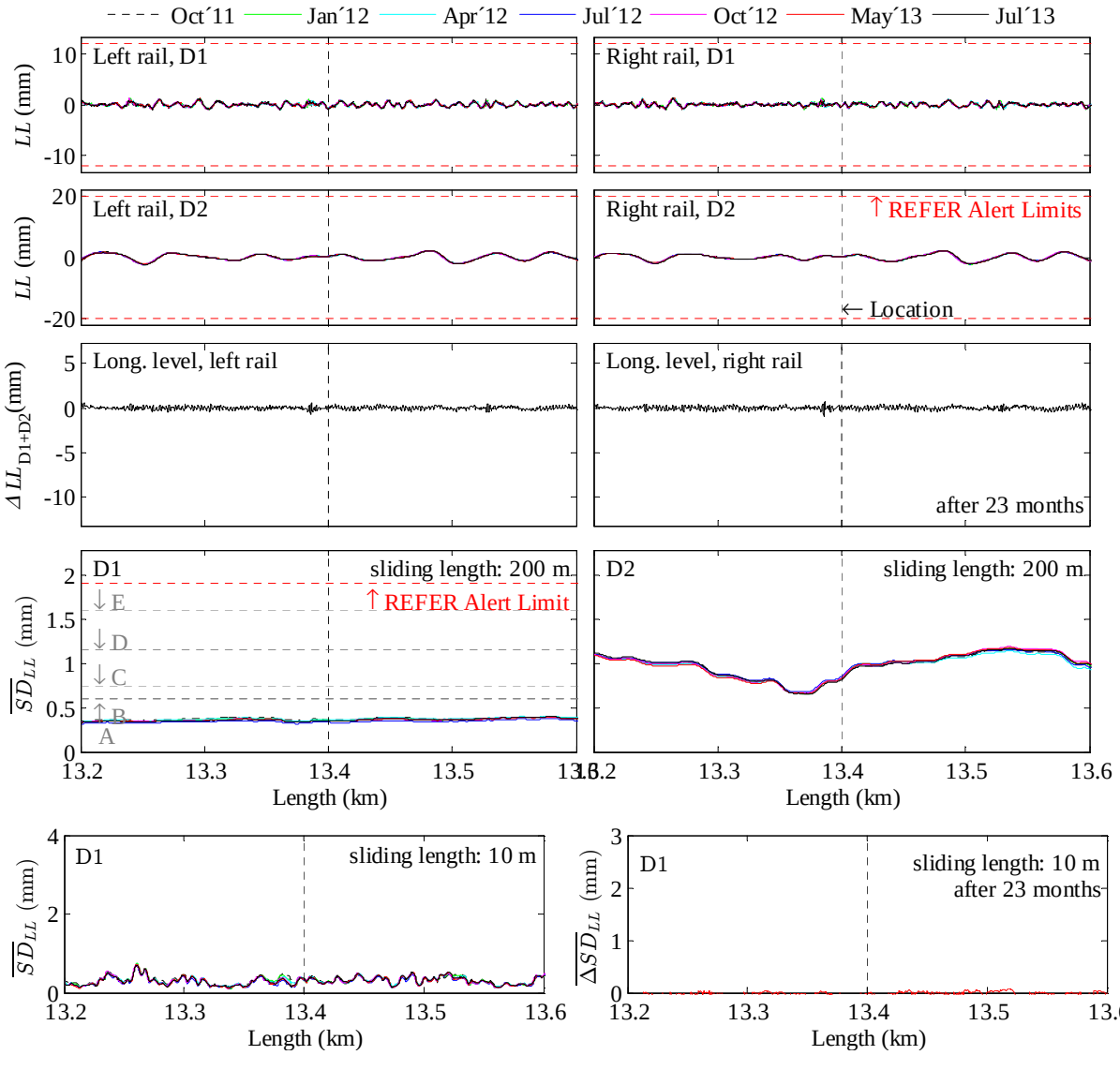

PH 13.2 at km 13.82 (Technical Block Type 2), Ø=1m

Excerpt from Design:

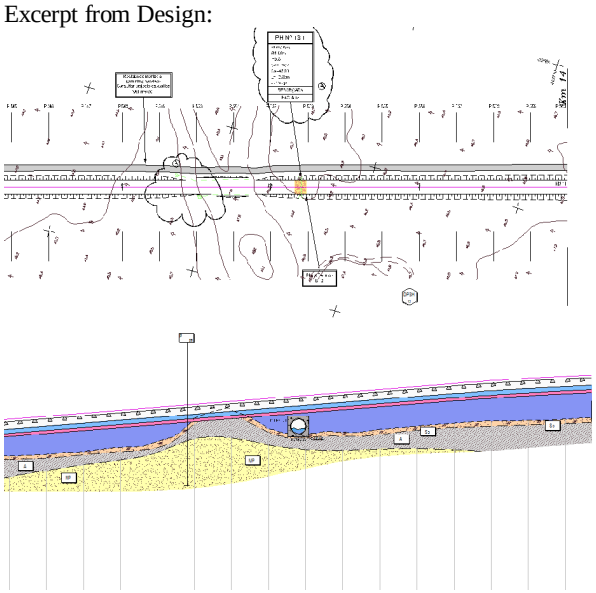

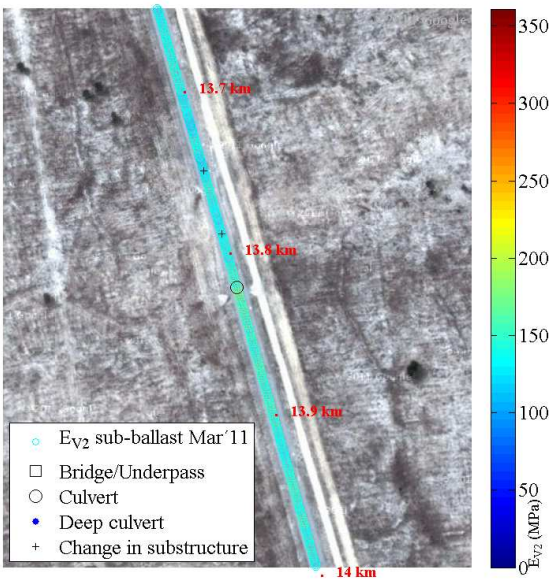

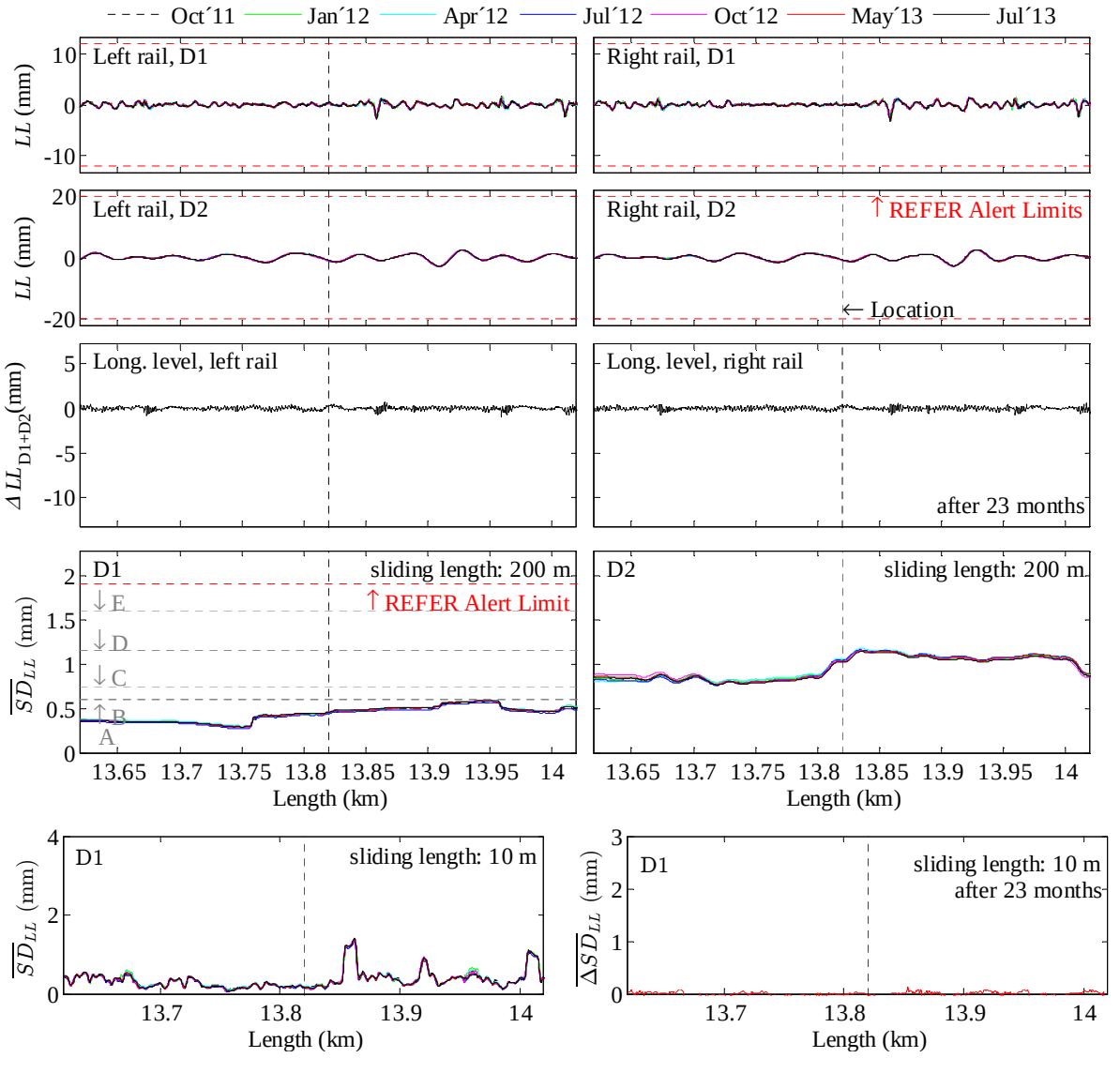

PF 14.1 at km 14.025 (Technical Block Type 2), Ø=1m

Excerpt from Design:

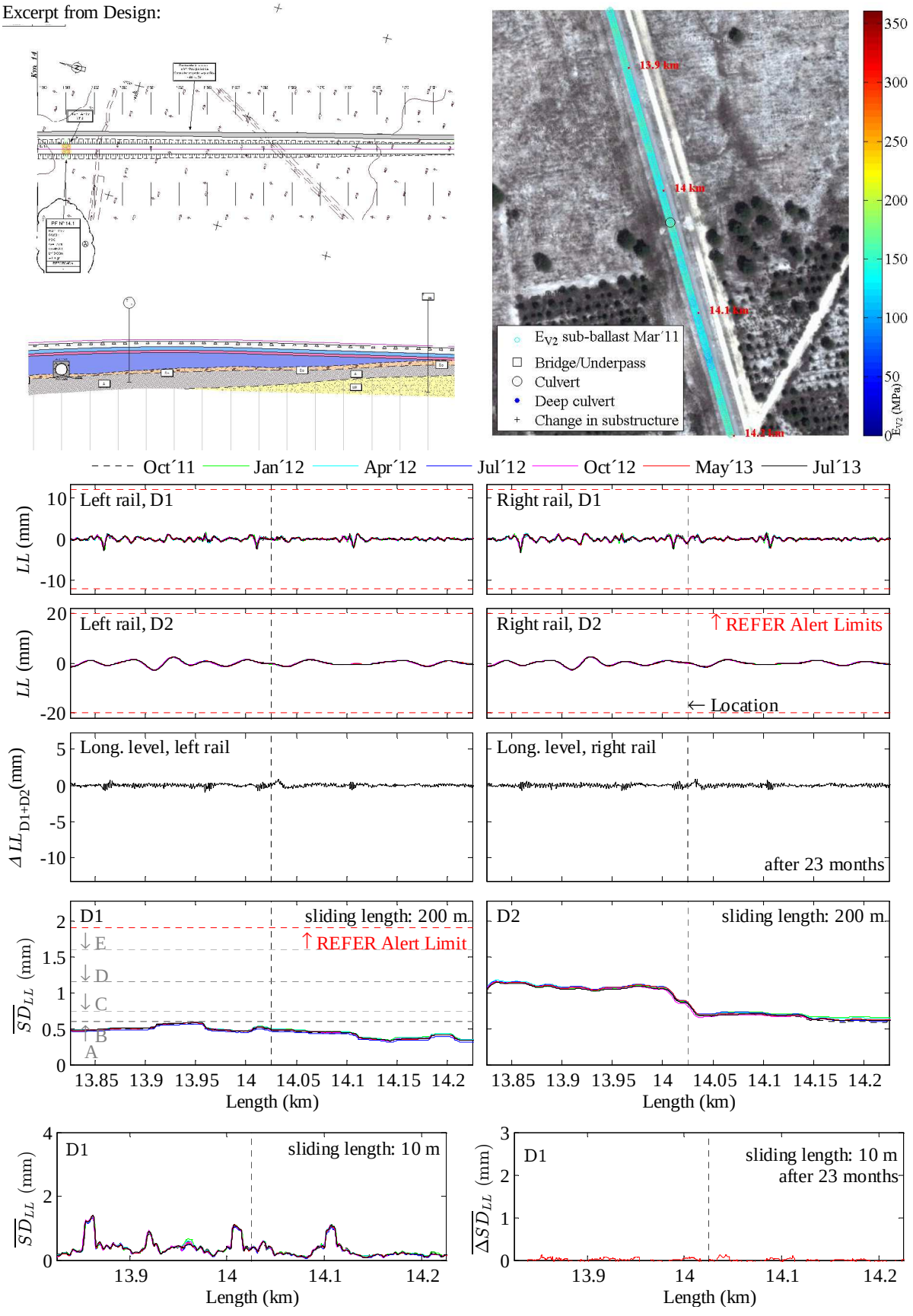

PH 17.1 at km 17.29 (Technical Block Type 2), Box 1.5x1.0m

Excerpt from Design:

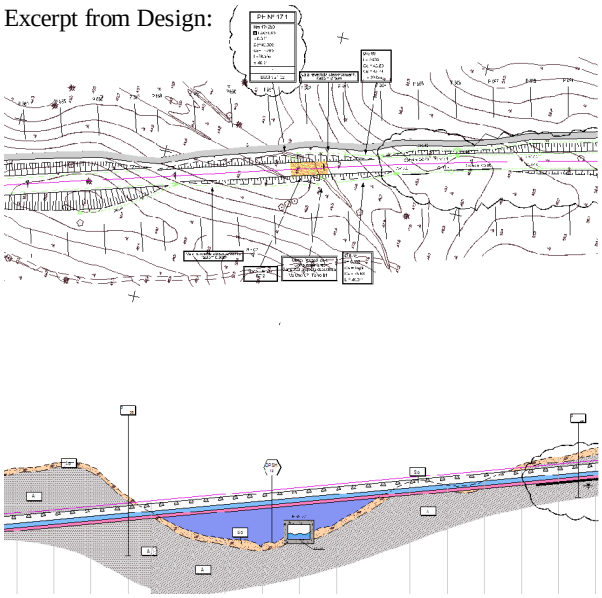

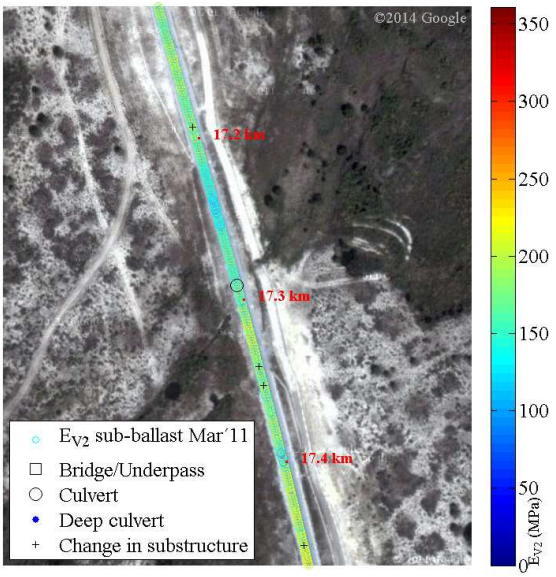

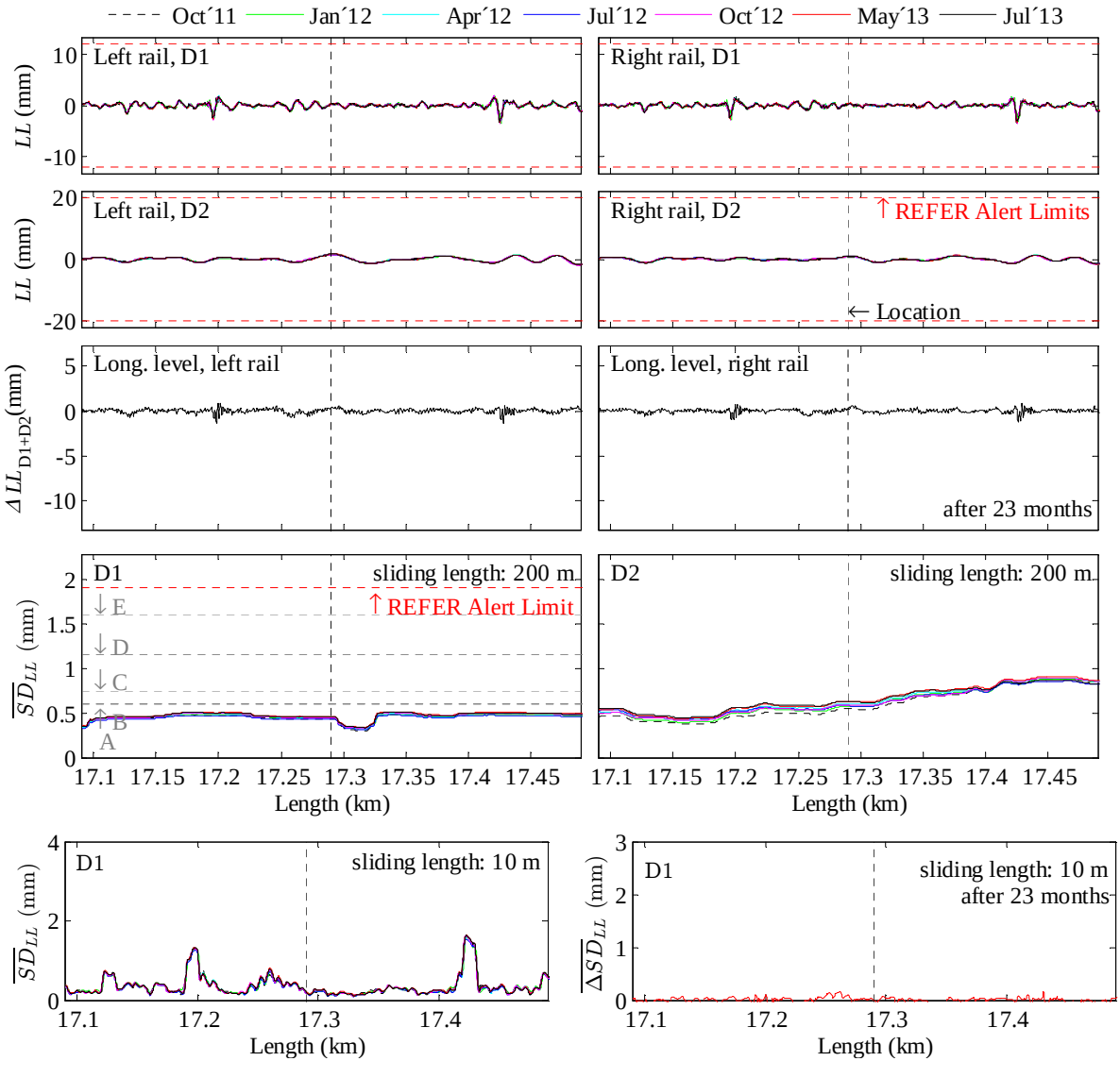

PH 20.1 at km 20.546 (Technical Block Type 2), Ø=1.2m

Excerpt from Design:

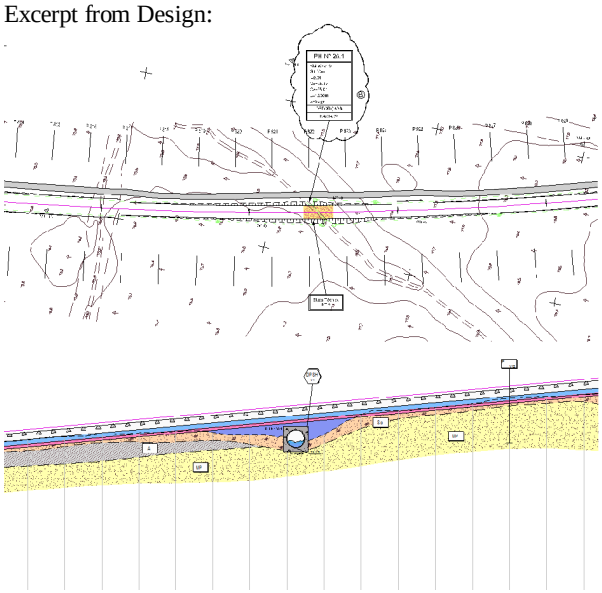

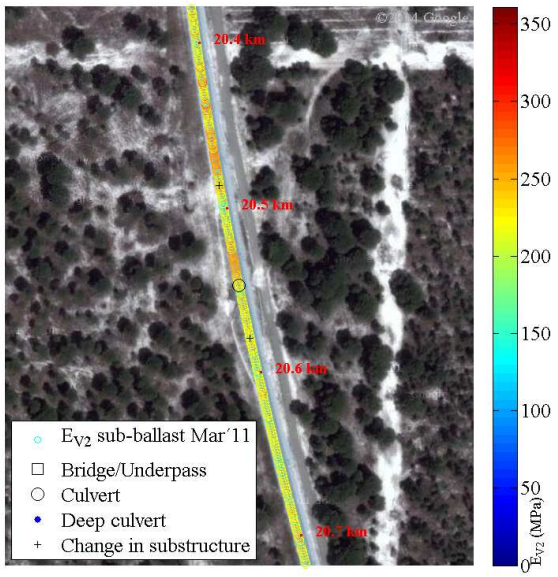

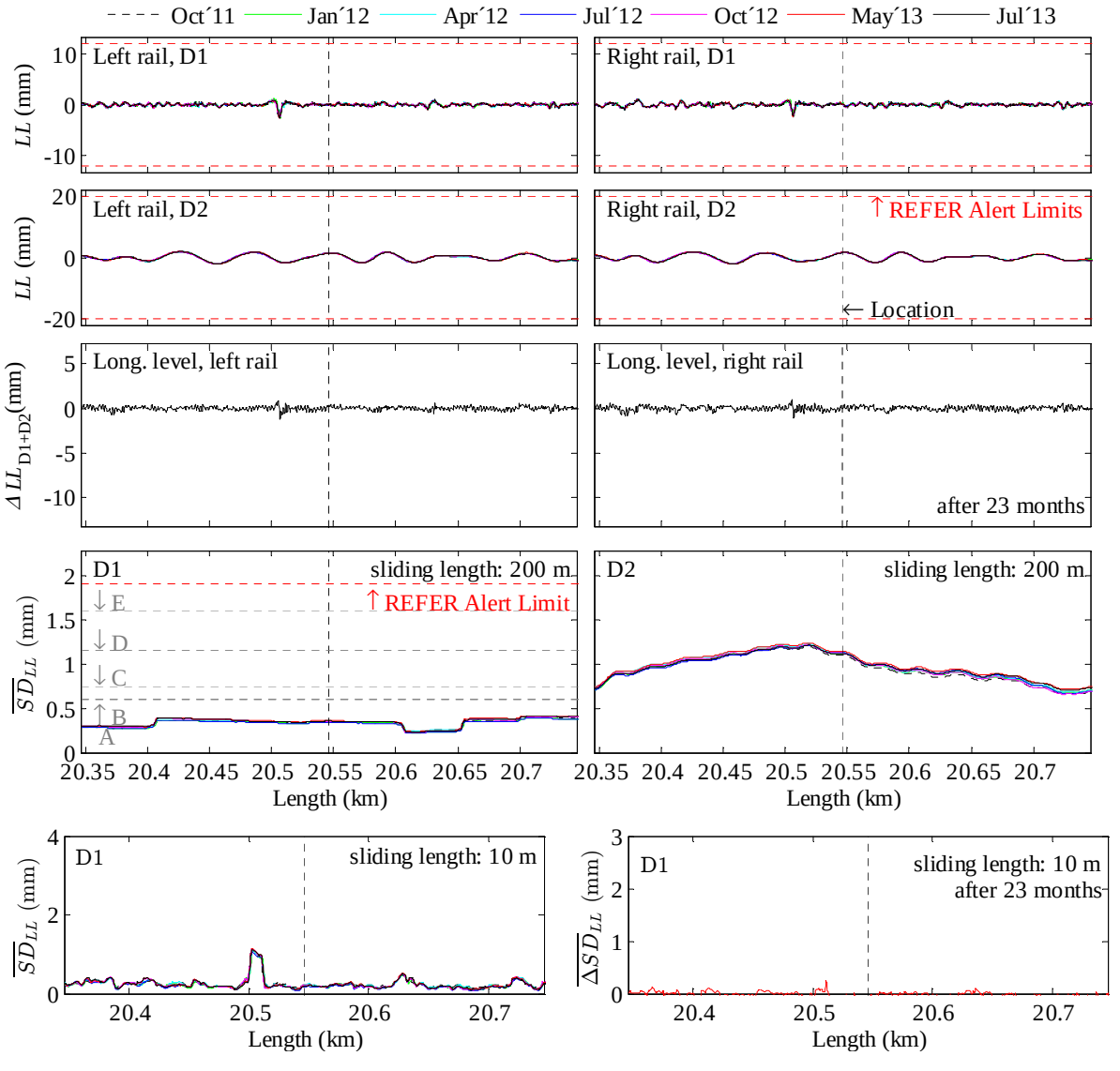

PH 20.2 at km 20.781 (Technical Block Type 2), Ø=1.2m

Excerpt from Design:

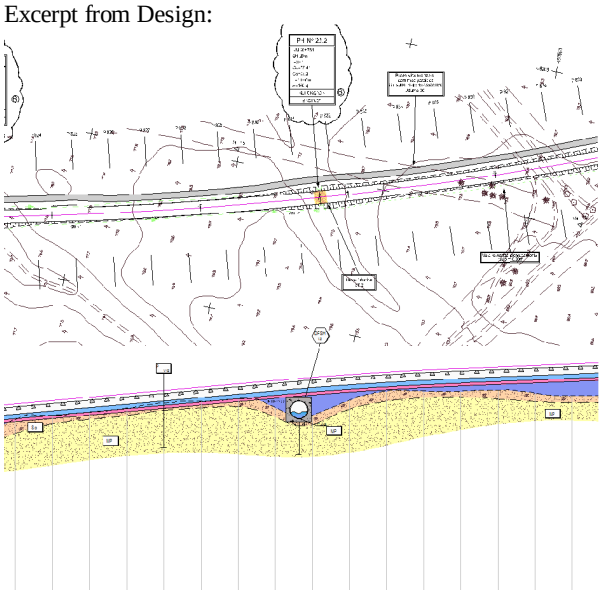

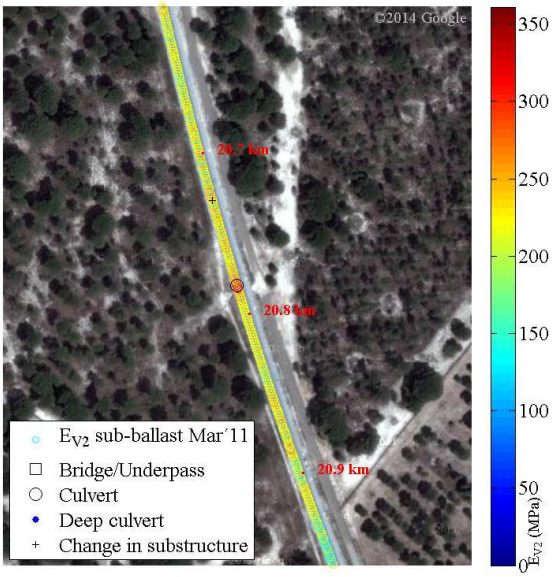

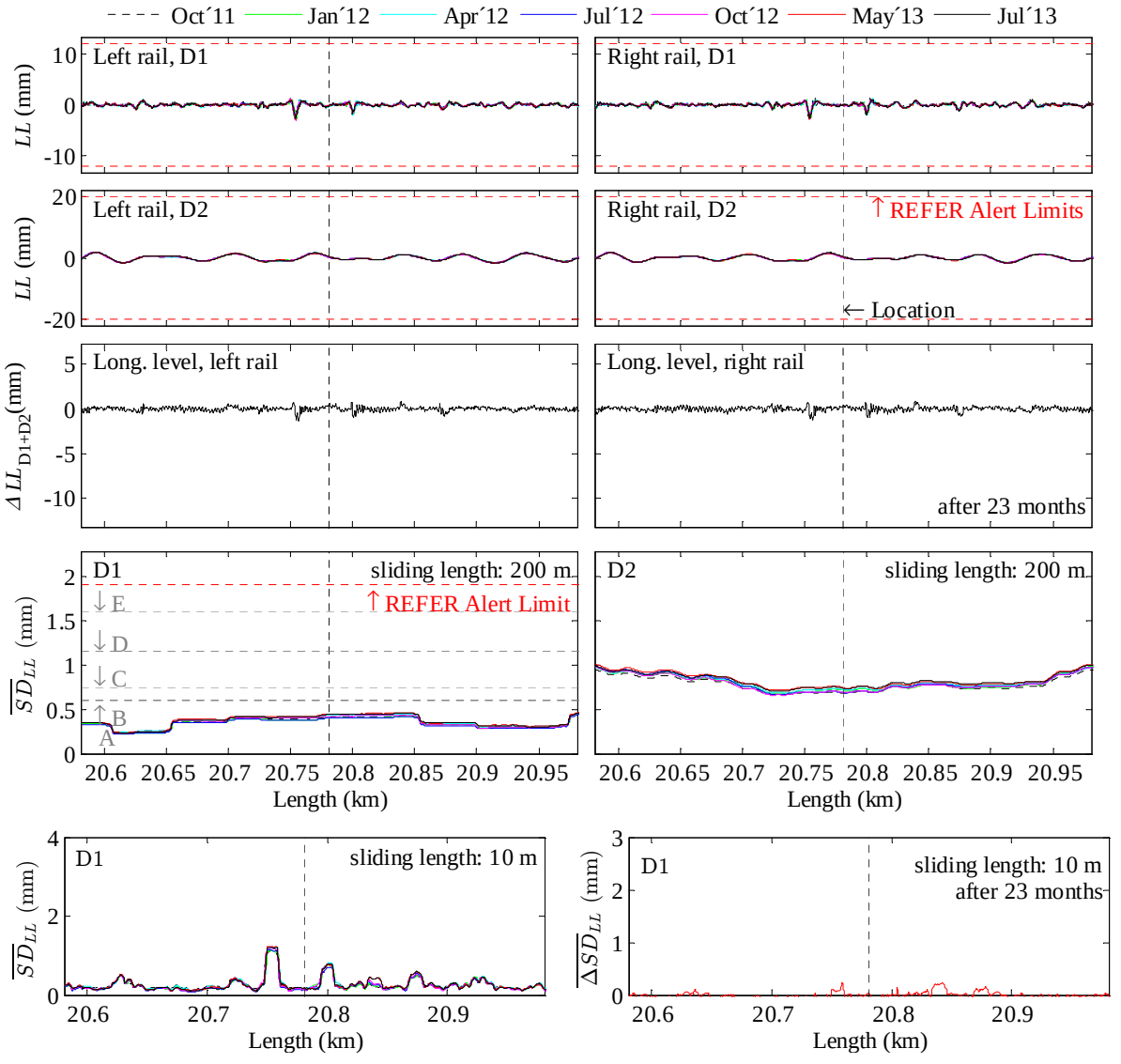

PH 21.1 at km 21.153 (Technical Block Type 2), Ø=1m

Excerpt from Design:

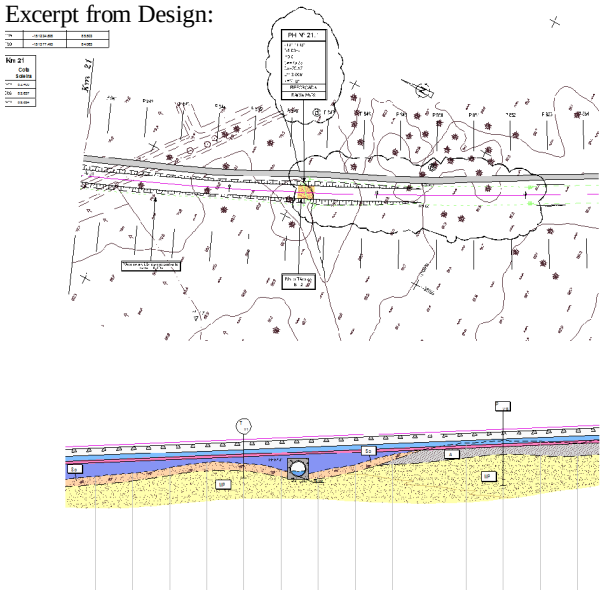

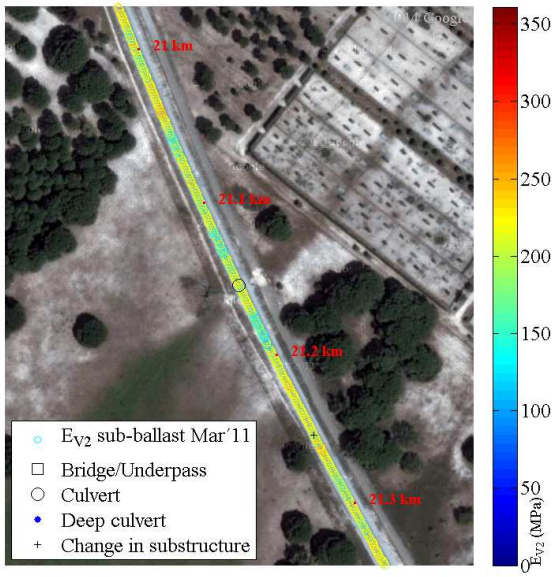

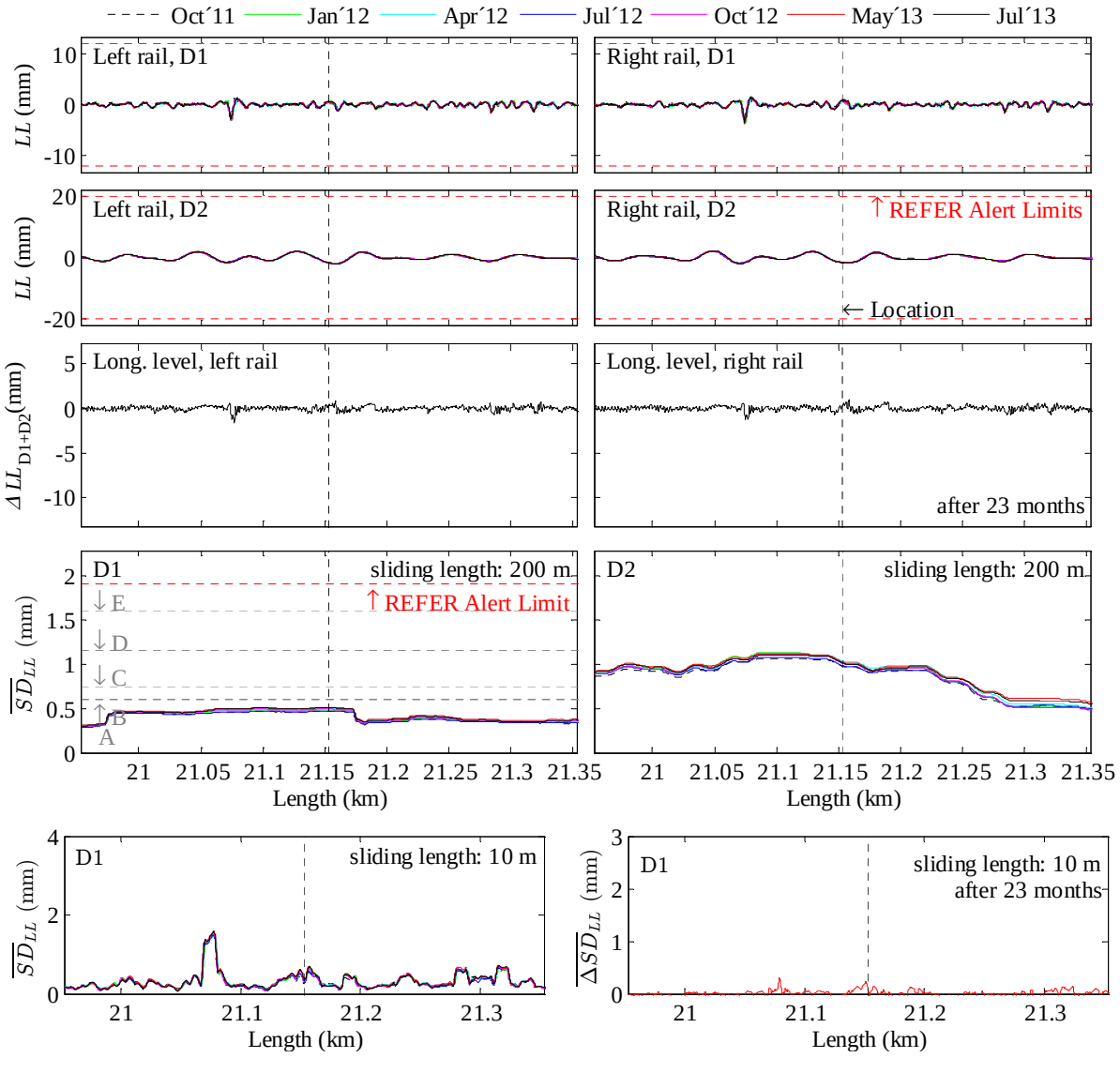

PH 22.1 at km 22.593 (Technical Block Type 2), Ø=1m

Excerpt from Design:

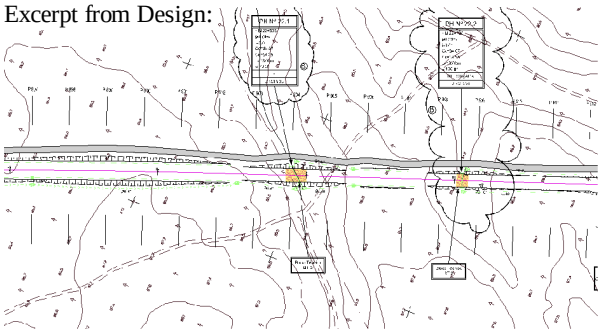

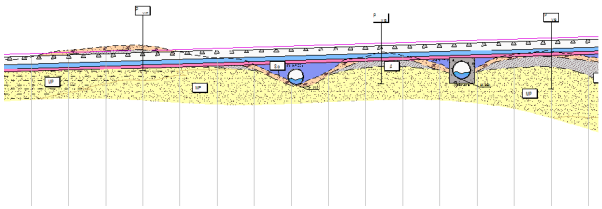

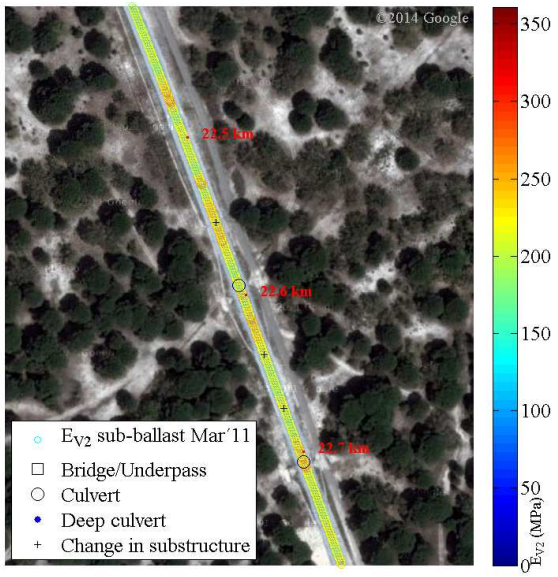

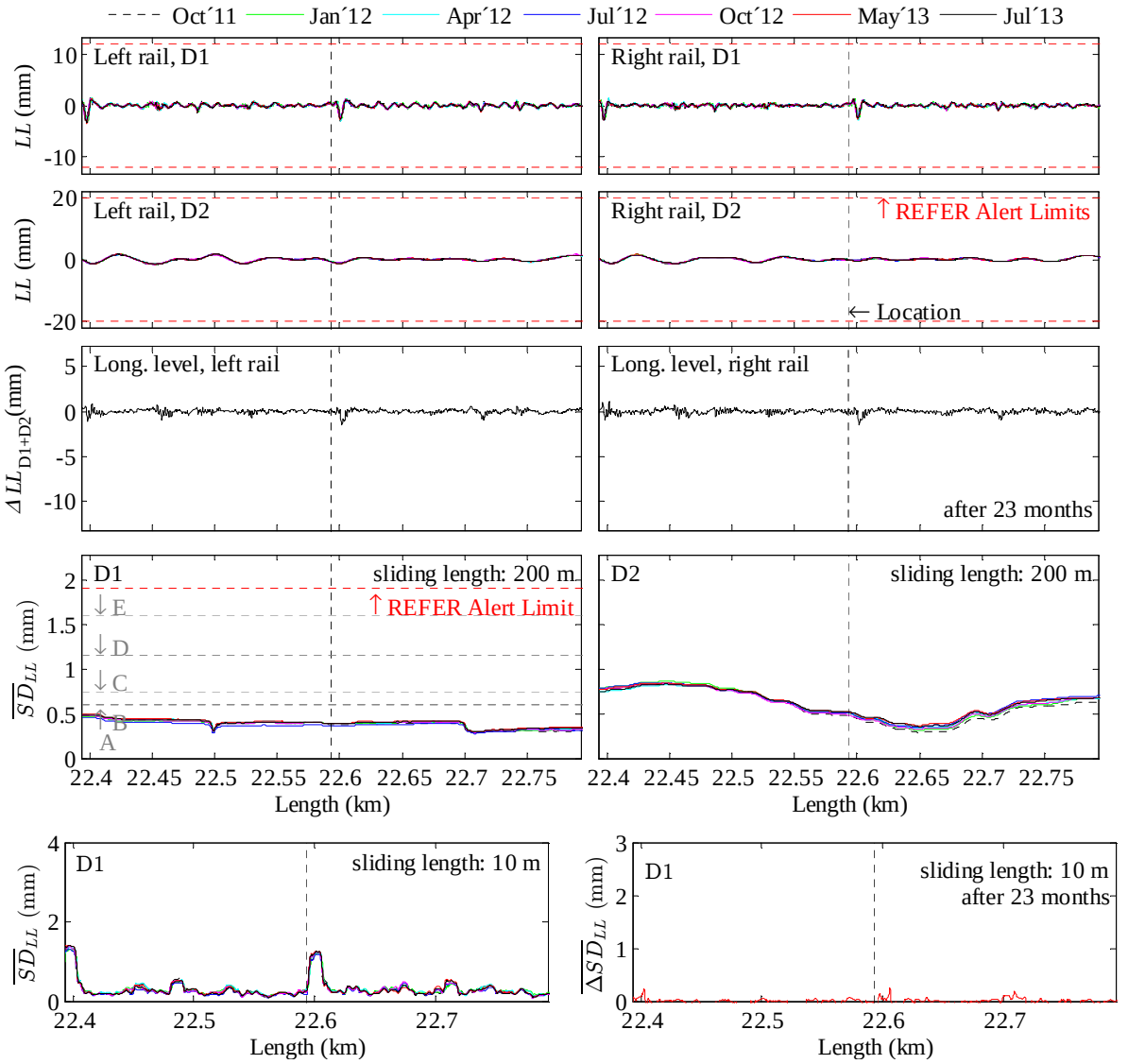

PH 22.2 at km 22.705 (Technical Block Type 2), Ø=1.2m

Excerpt from Design:

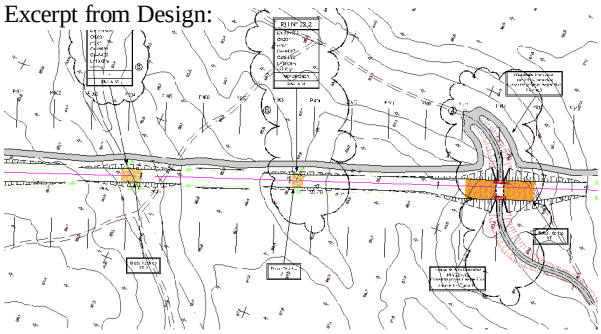

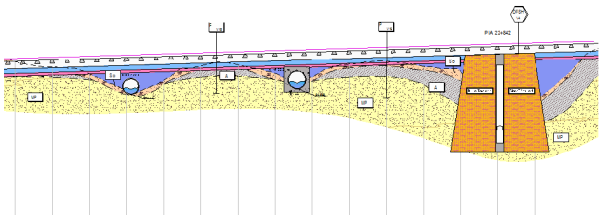

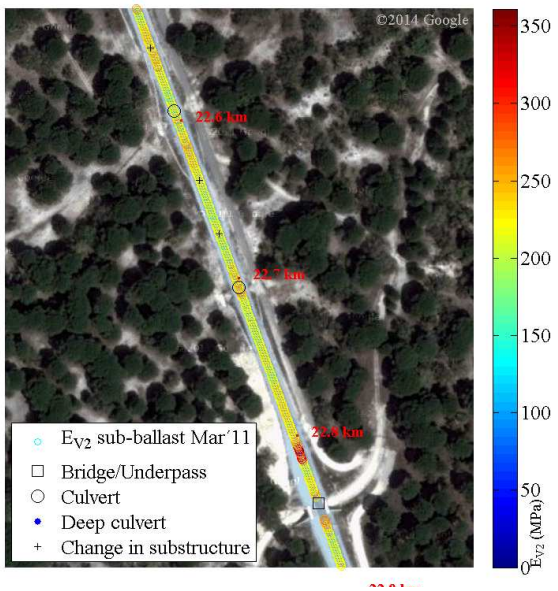

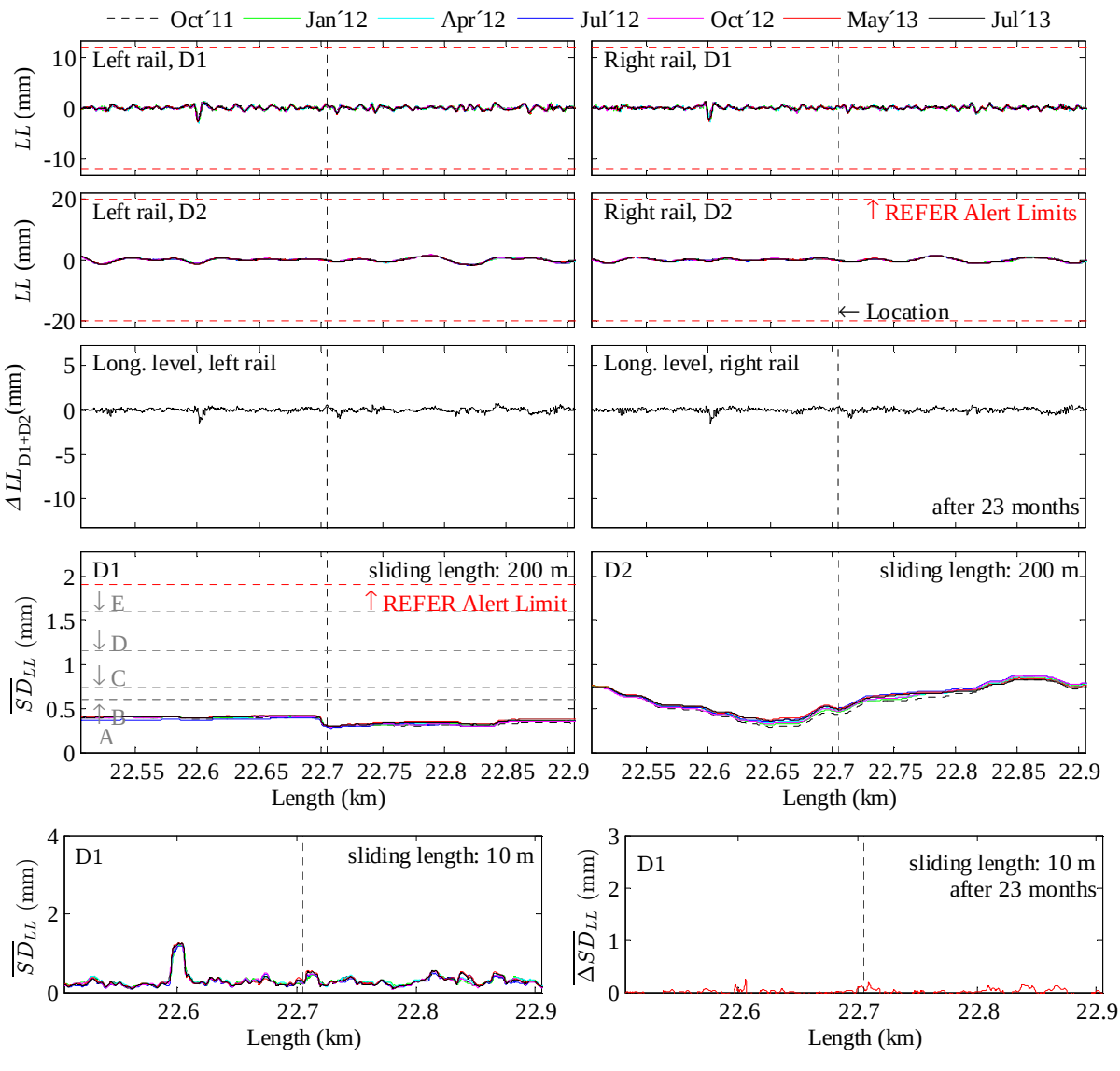

PH 23.1 at km 23.055 (Technical Block Type 2), Ø=1m

Excerpt from Design:

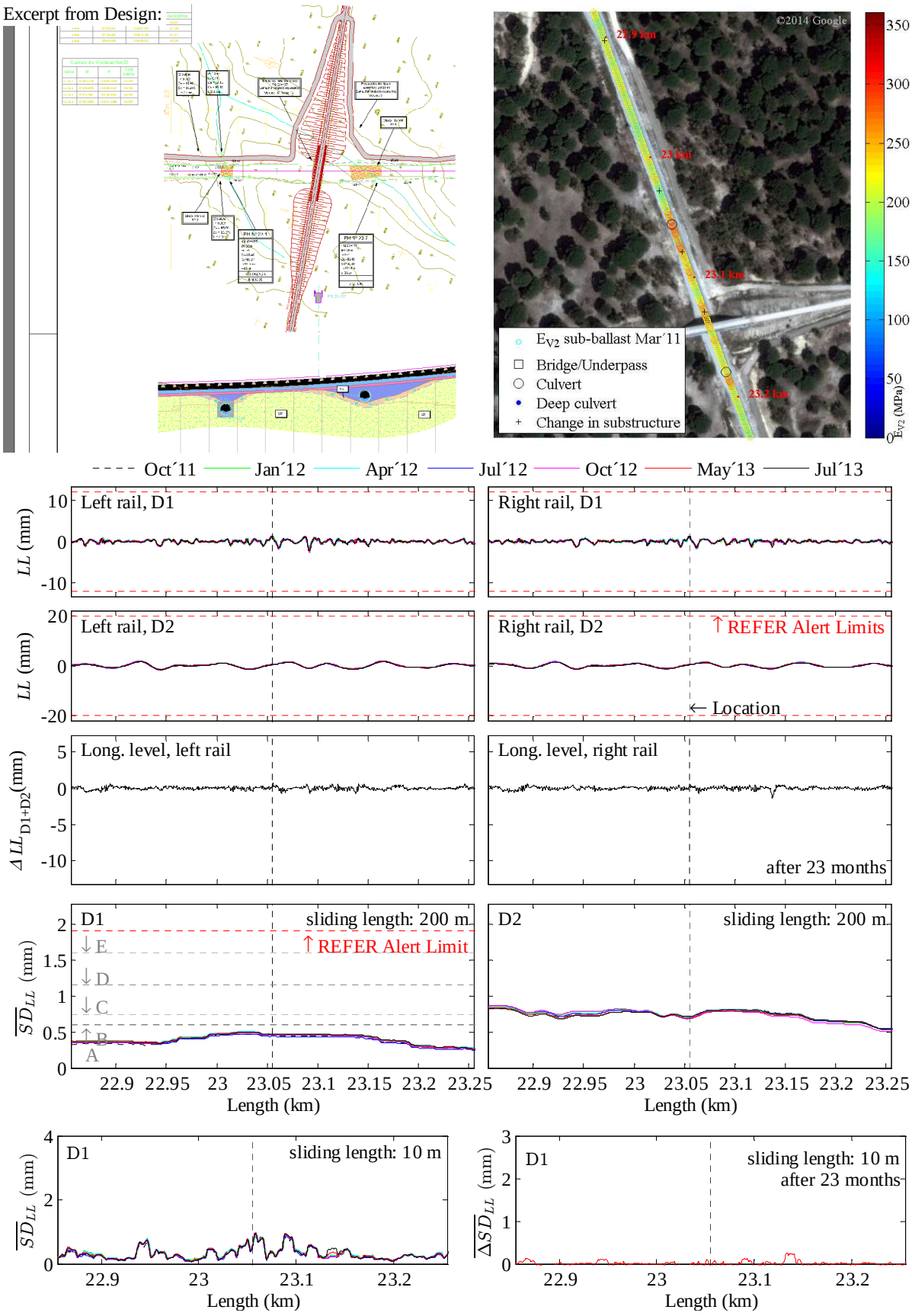

PH 23.2 at km 23.178 (Technical Block Type 2), Ø=1m

Excerpt from Design:

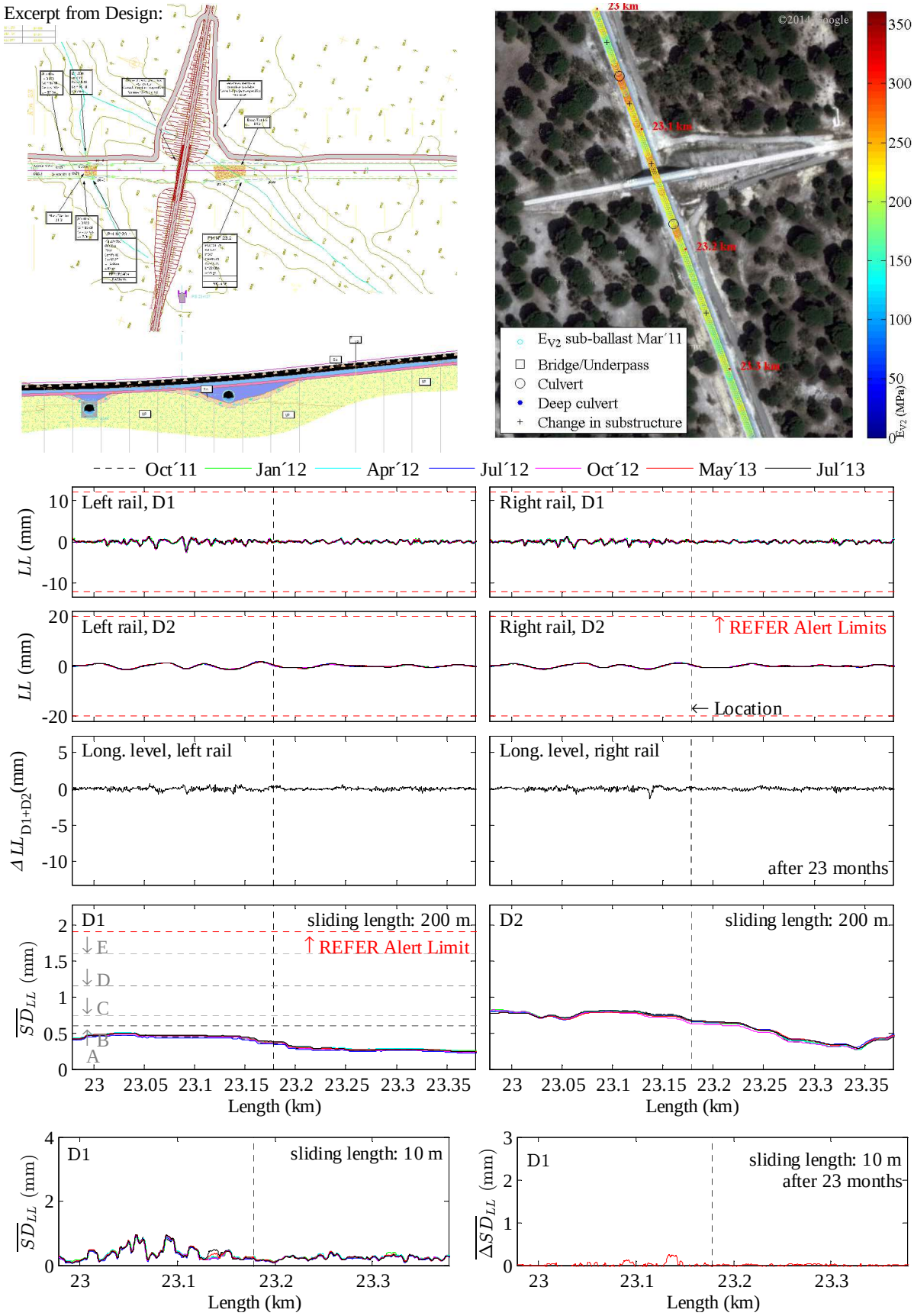

PH 24.1 at km 24.535 (Technical Block Type 2), Ø=1m

Excerpt from Design:

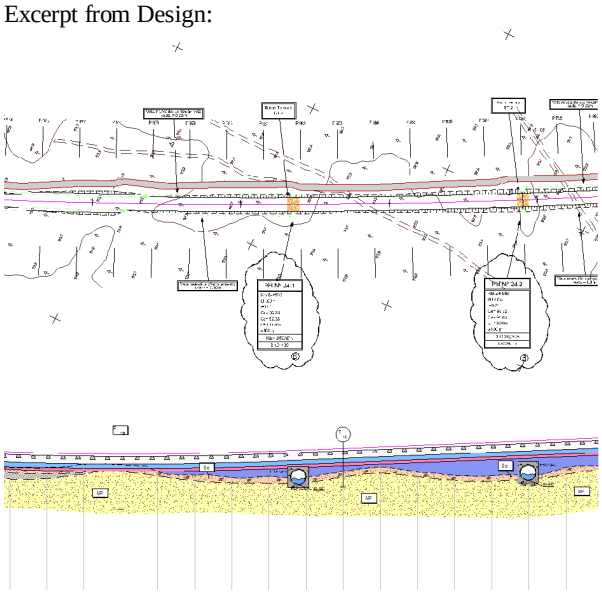

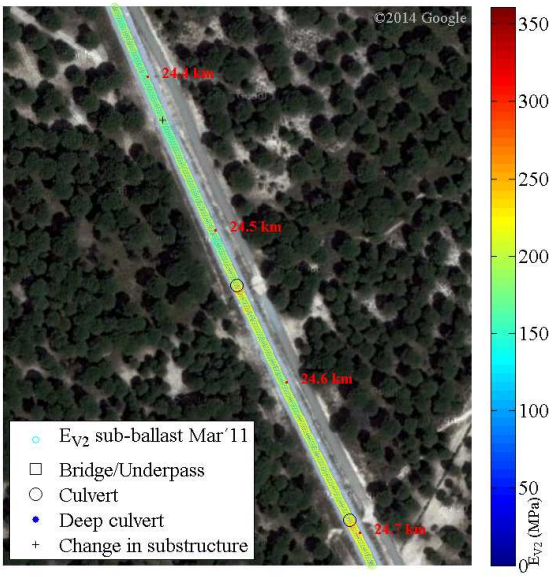

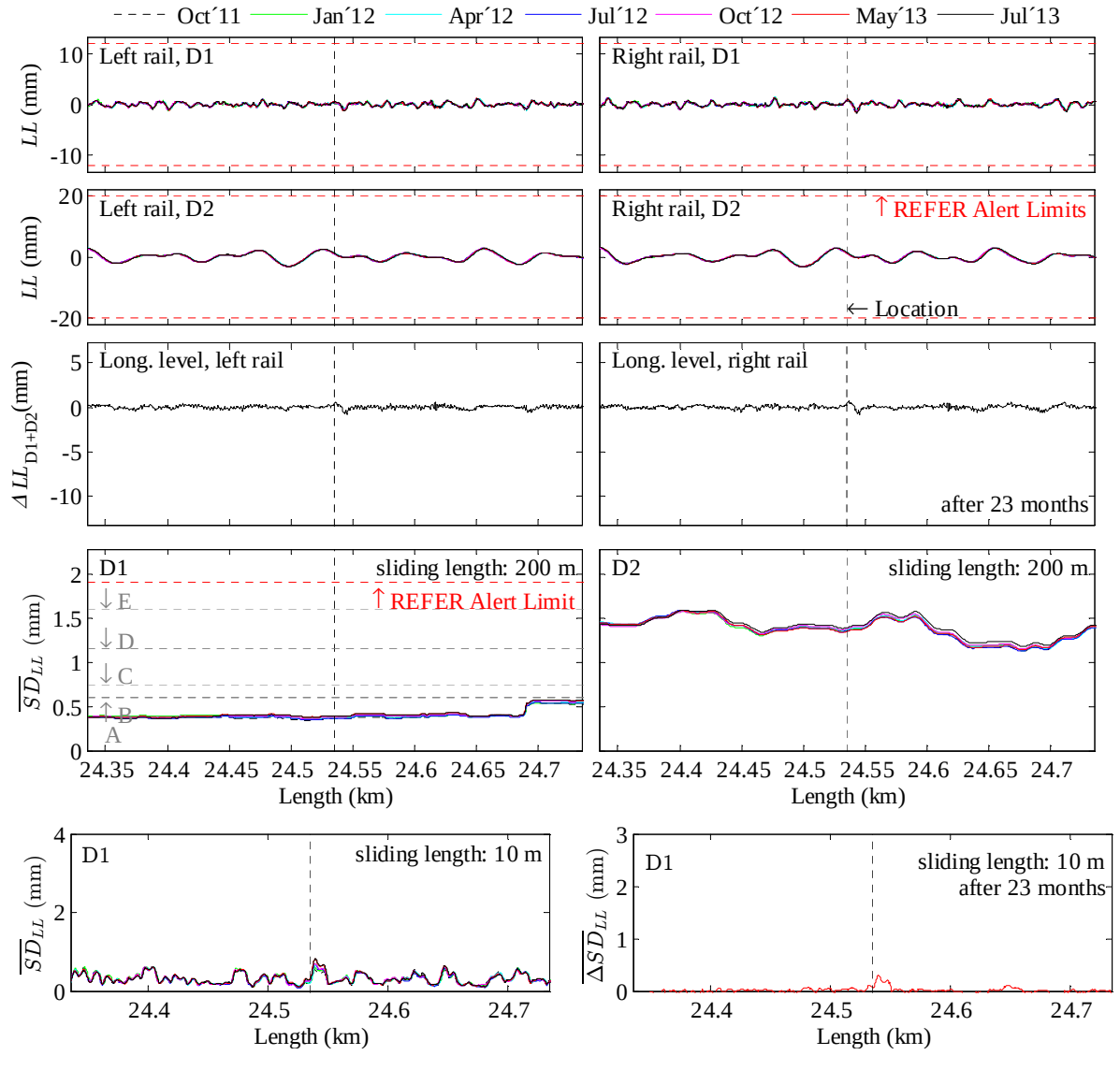

PH 24.2 at km 24.69 (Technical Block Type 2), Ø=1m

Excerpt from Design:

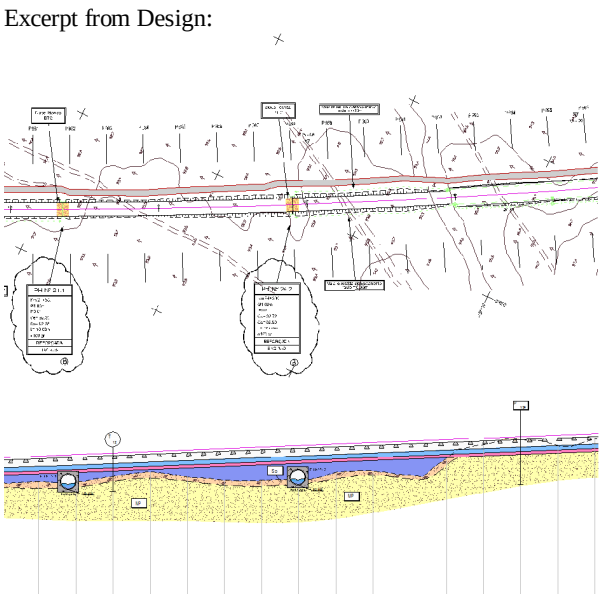

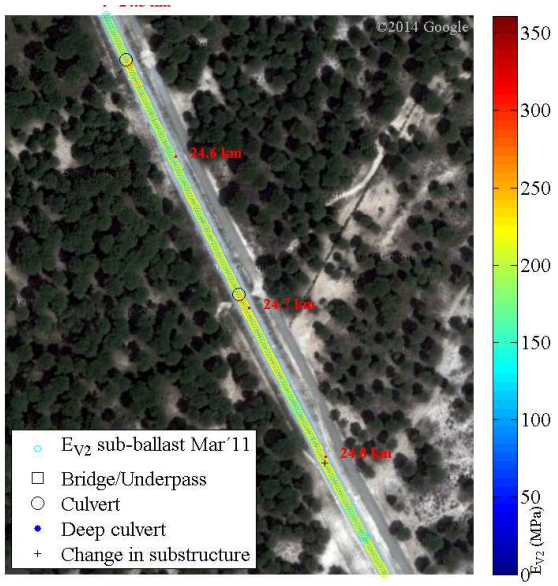

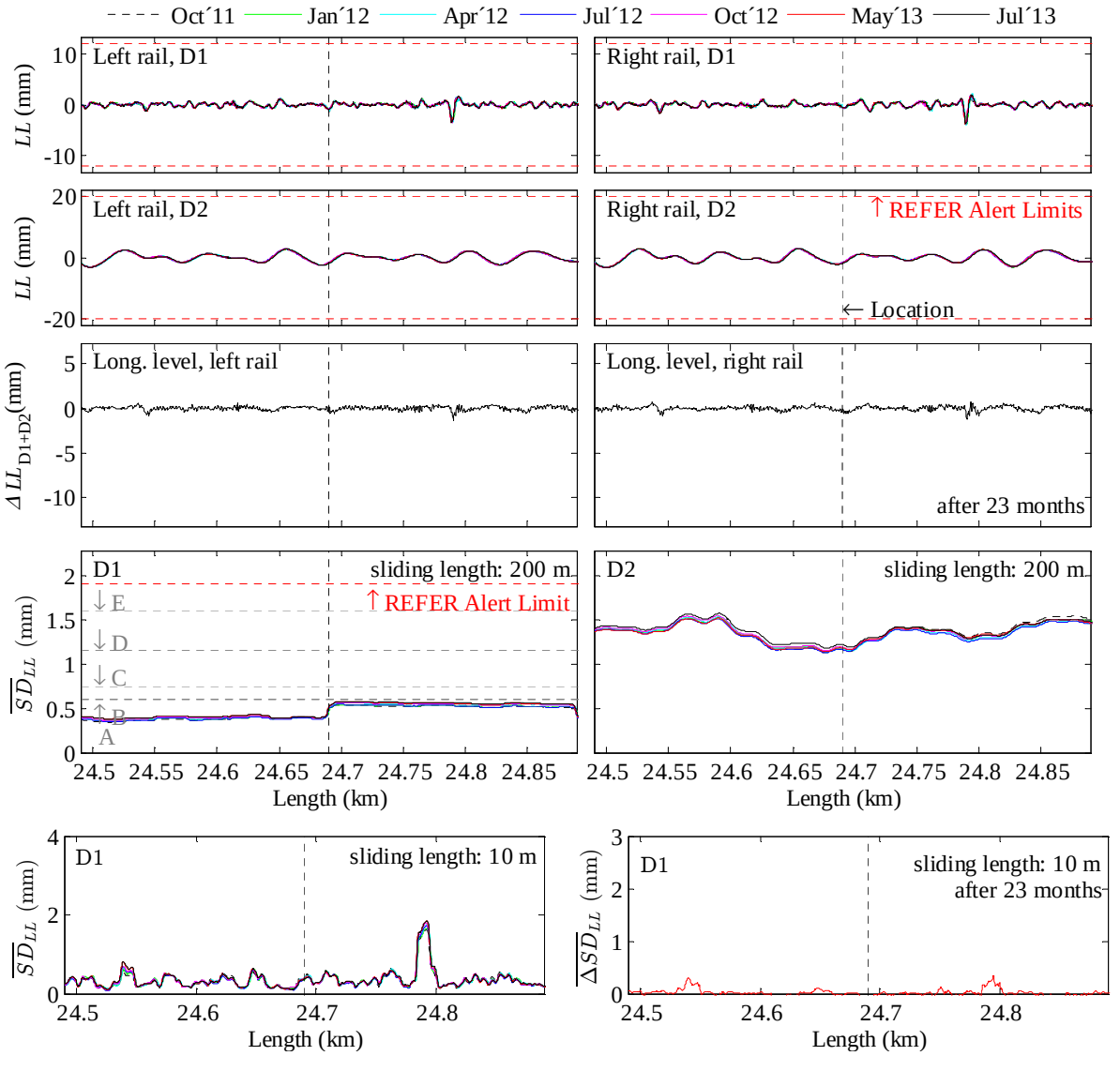

PH 25.1 at km 25.076 (Technical Block Type 2), Ø=1m

Excerpt from Design:

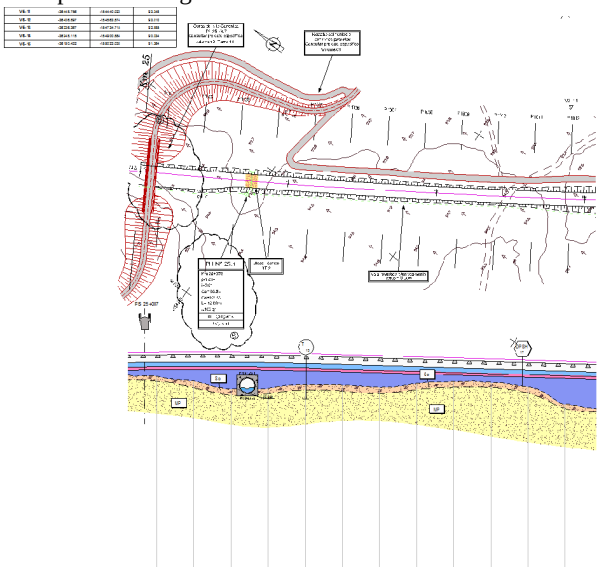

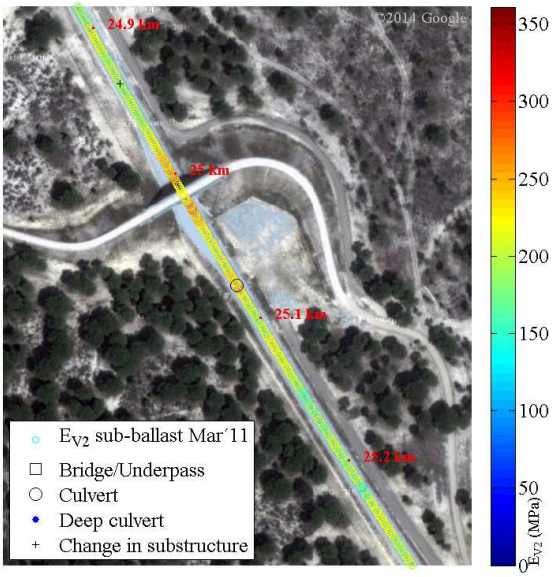

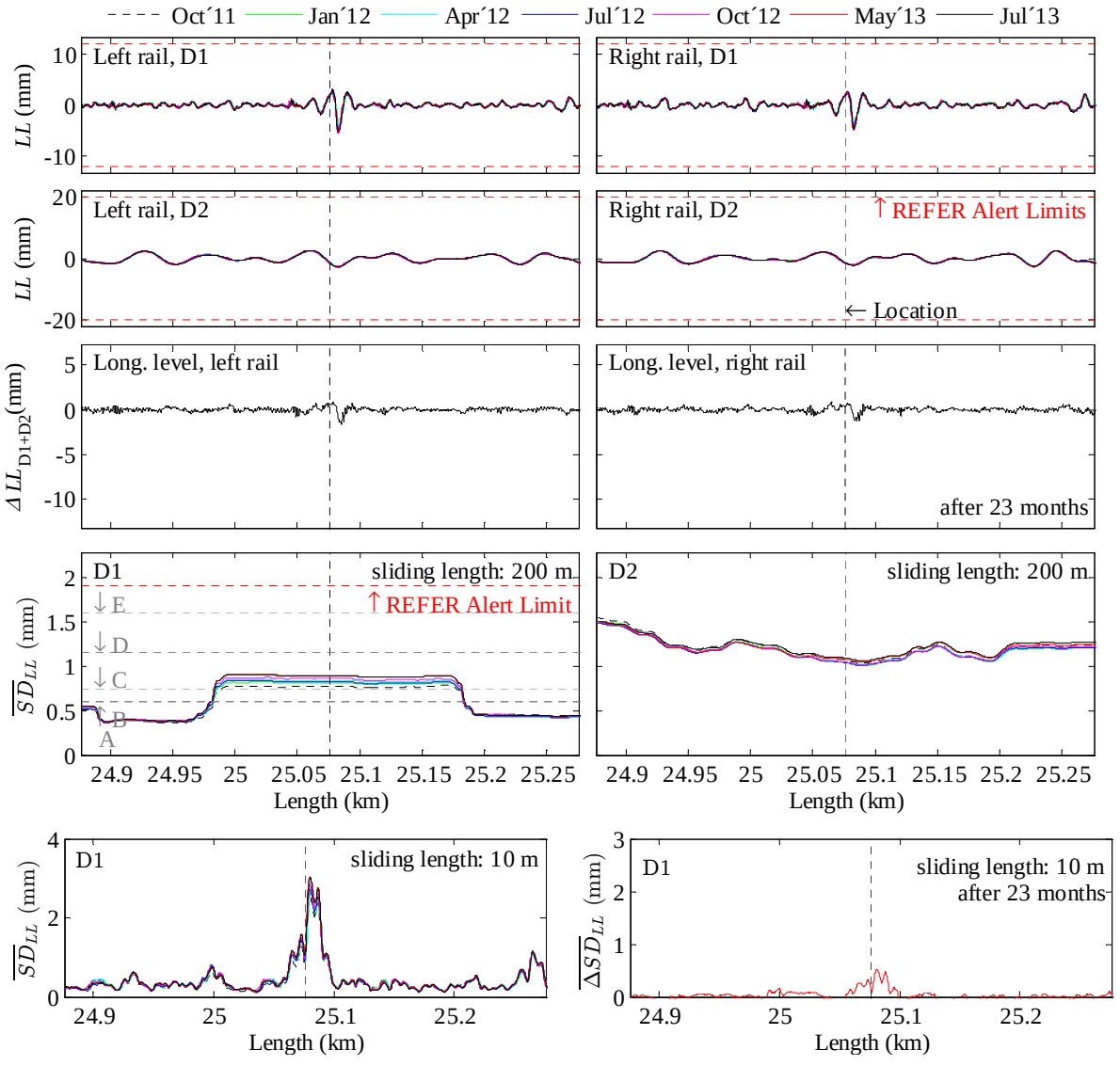

PH 25.3 at km 25.539 (Technical Block Type 2), Ø=1.2m

Excerpt from Design:

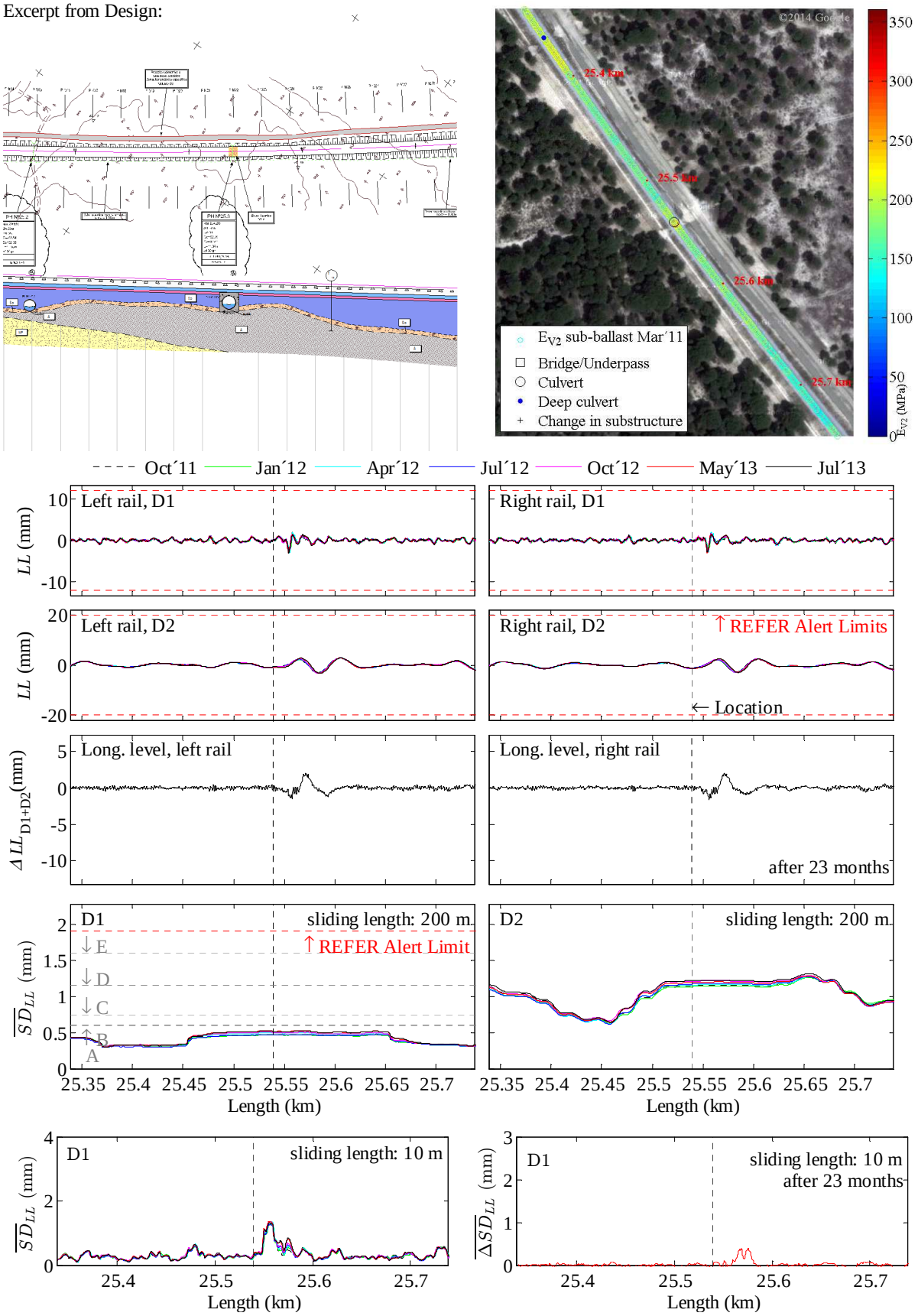

PH 1.2 at km 1.595 (deep culvert, no Technical Block), Ø=1m

Excerpt from Design:

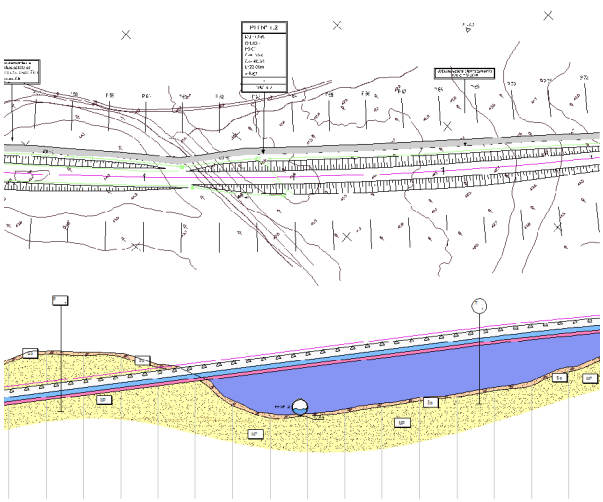

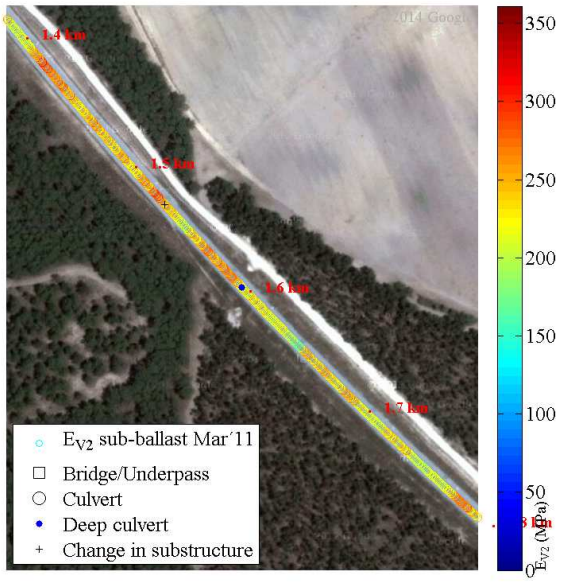

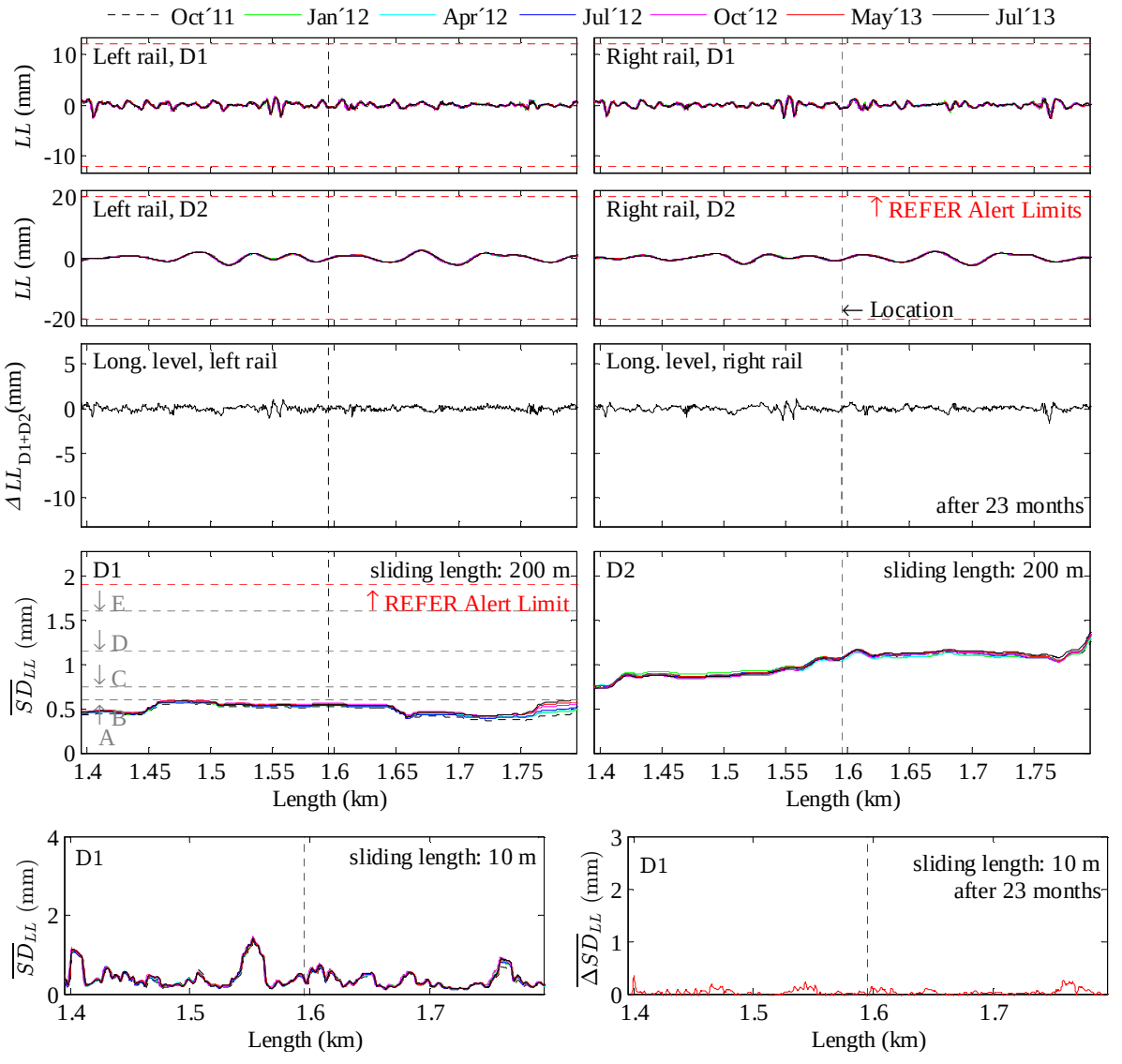

PH 2.1 at km 2.584 (deep culvert, no Technical Block), Ø=1m

Excerpt from Design:

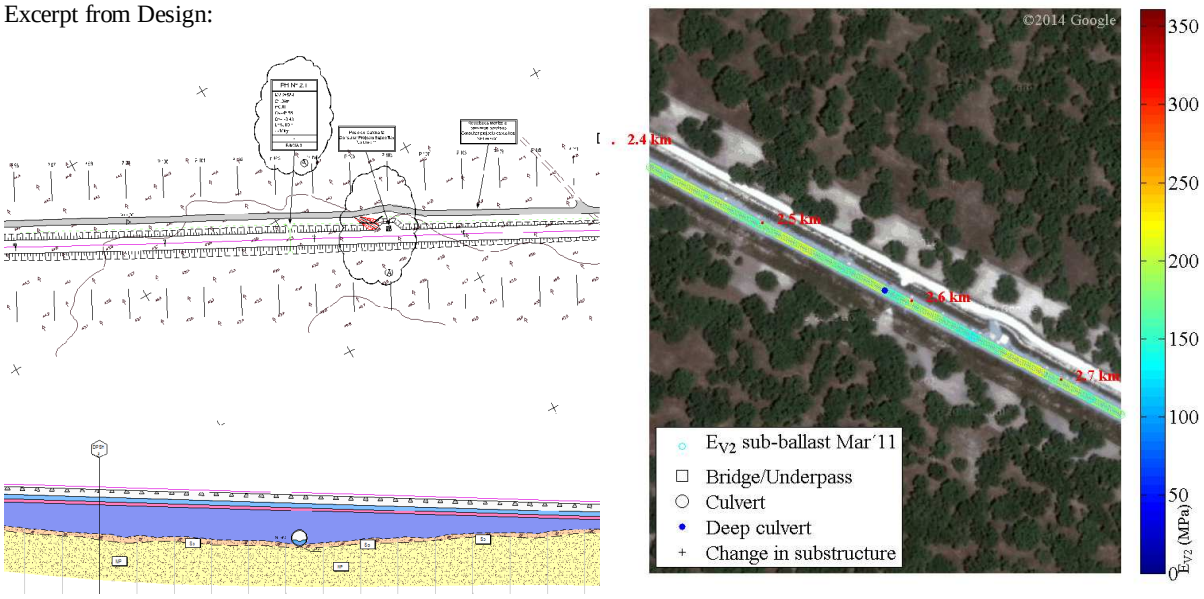

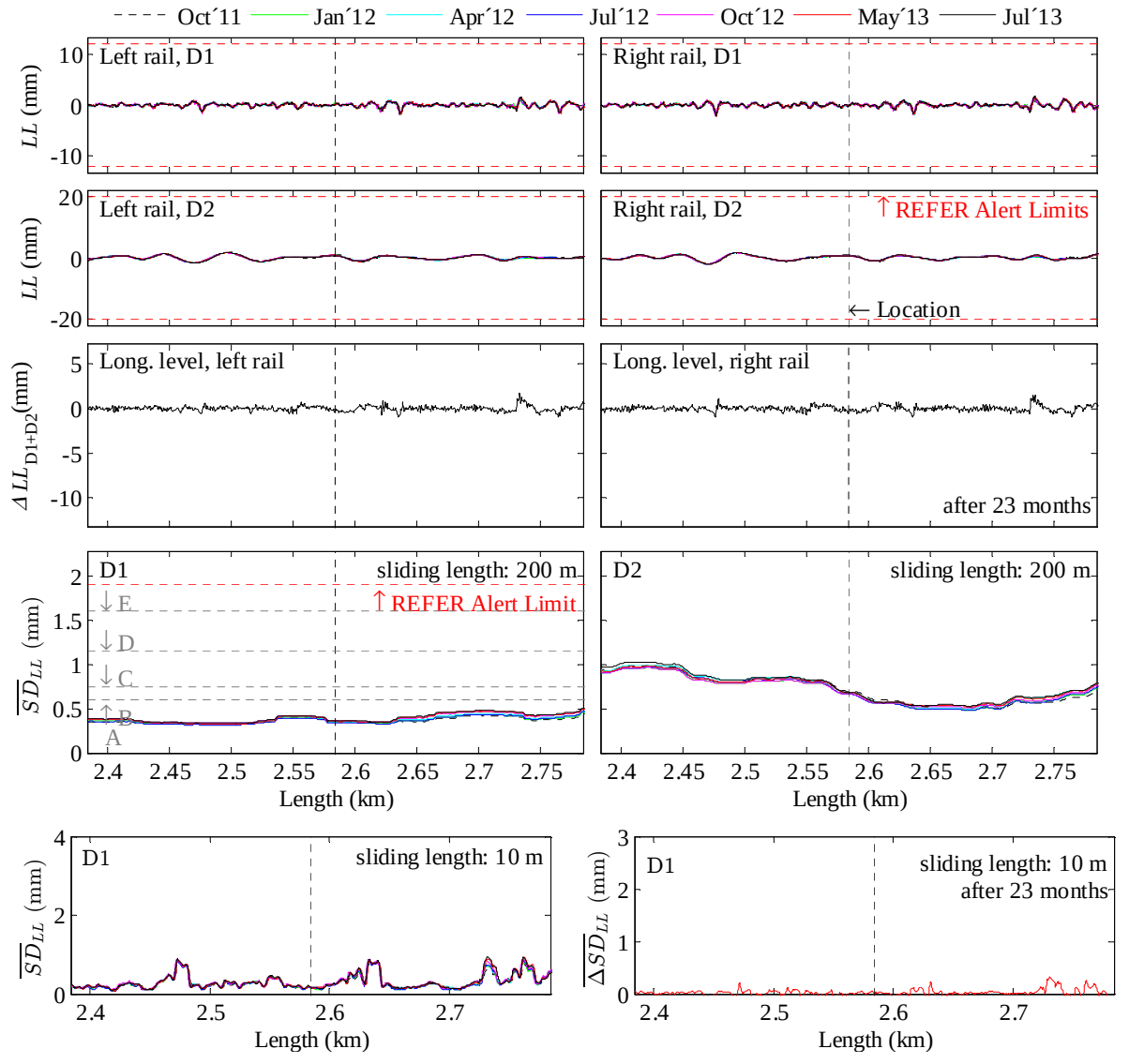

PH 2.2 at km 2.939 (deep culvert, no Technical Block), Ø=1m

Excerpt from Design:

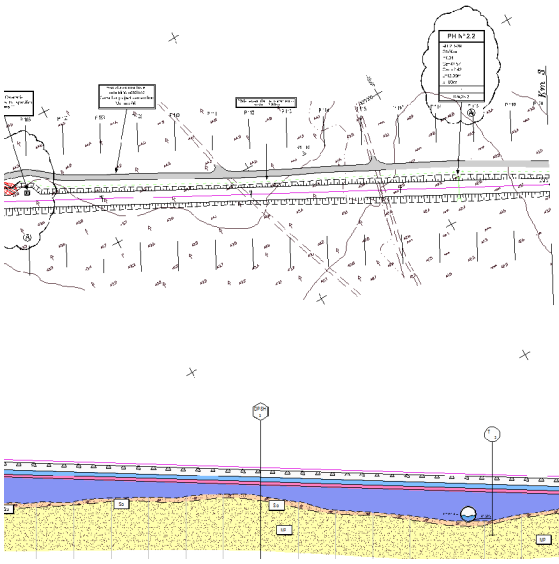

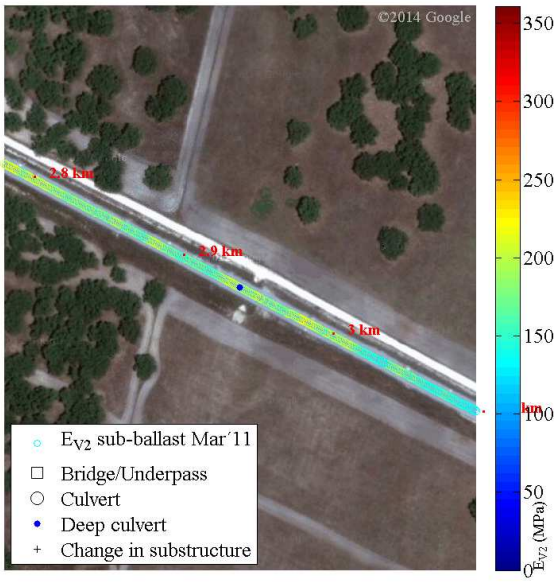

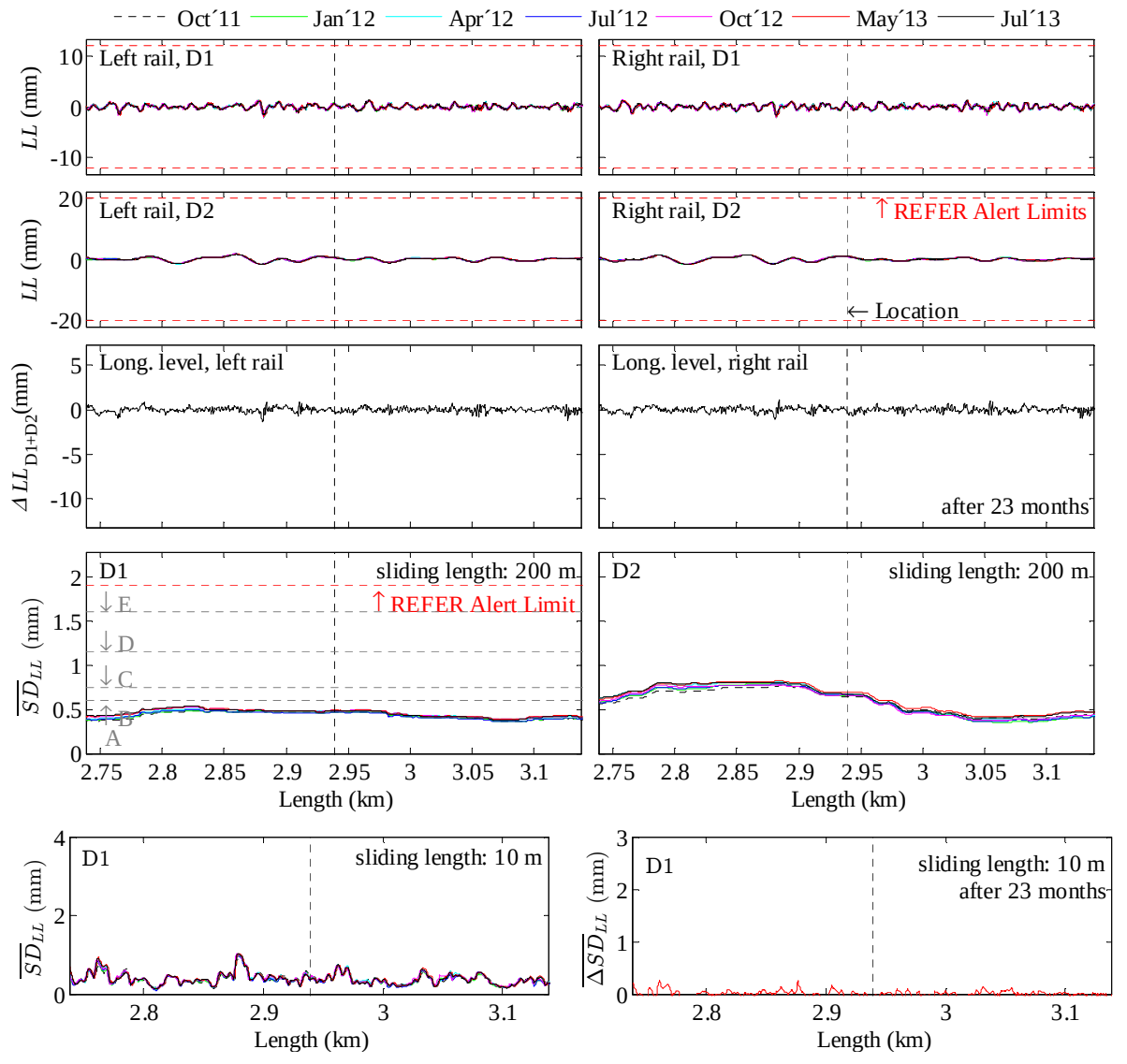

PH 4.2 at km 4.583 (deep culvert, no Technical Block), Ø=1m

Excerpt from Design:

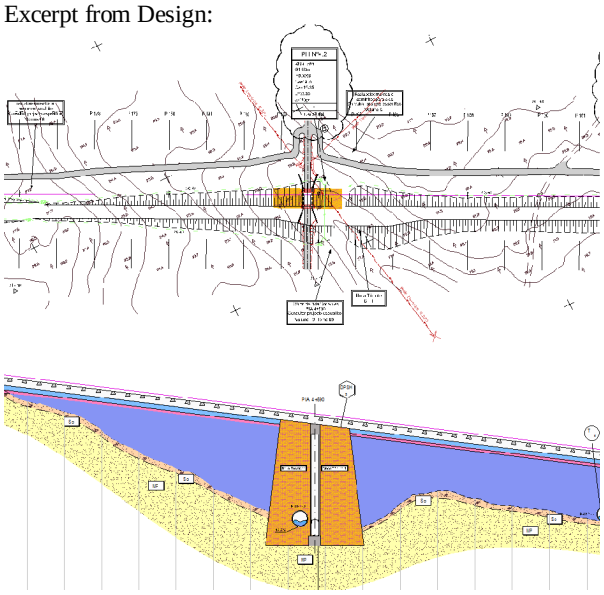

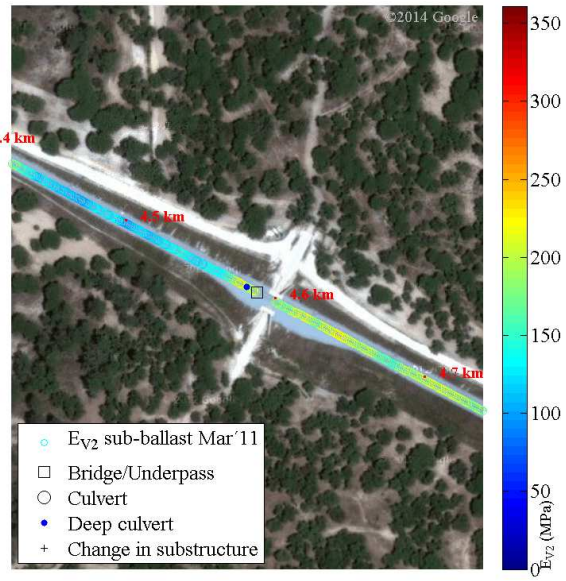

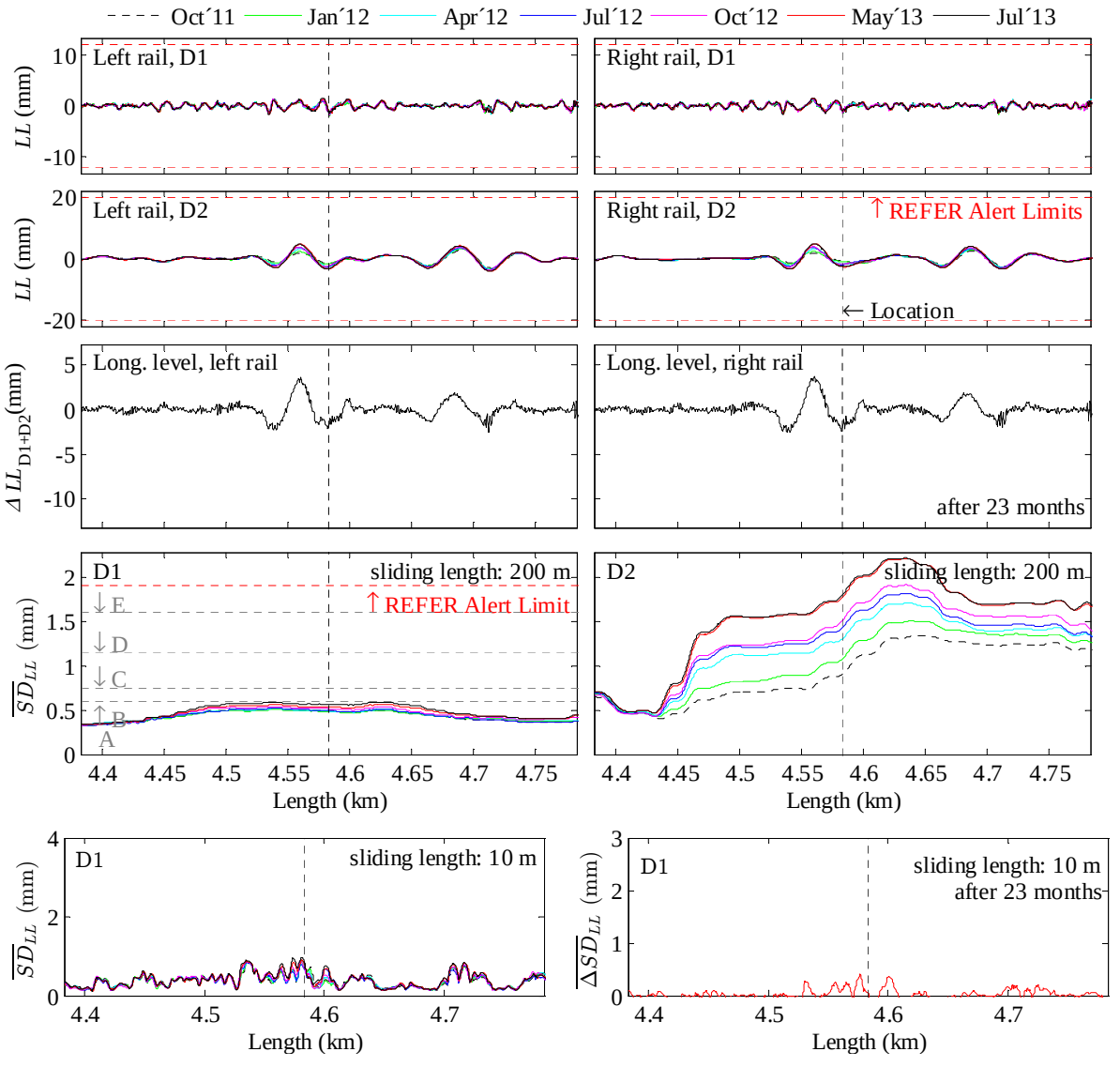

PH 4.3 at km 4.787 (deep culvert, no Technical Block), Ø=1m

Excerpt from Design:

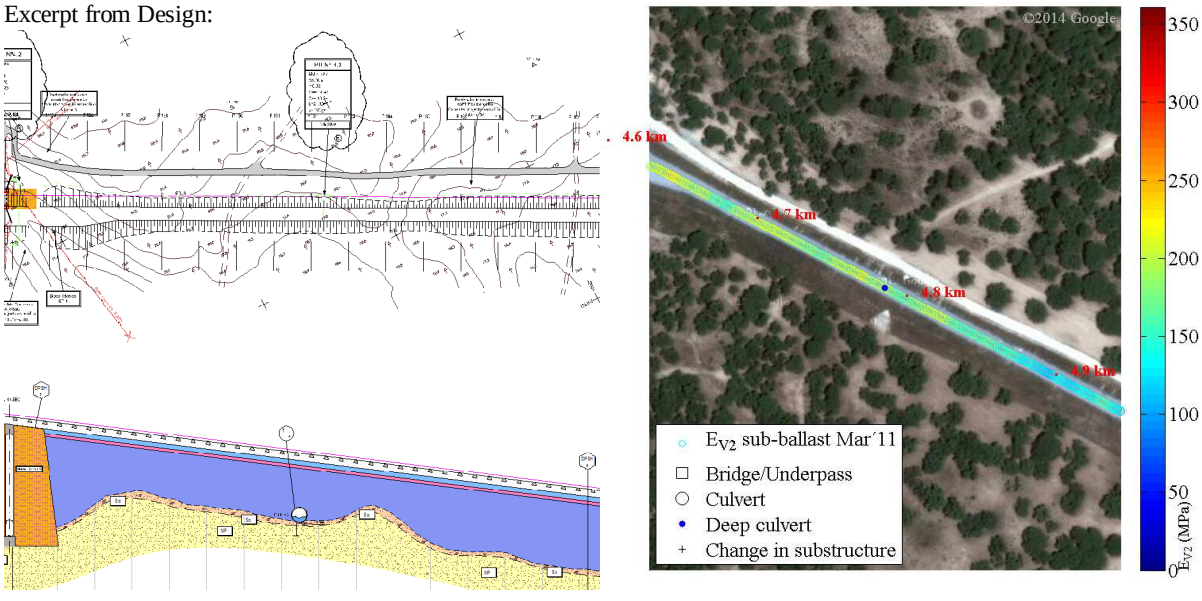

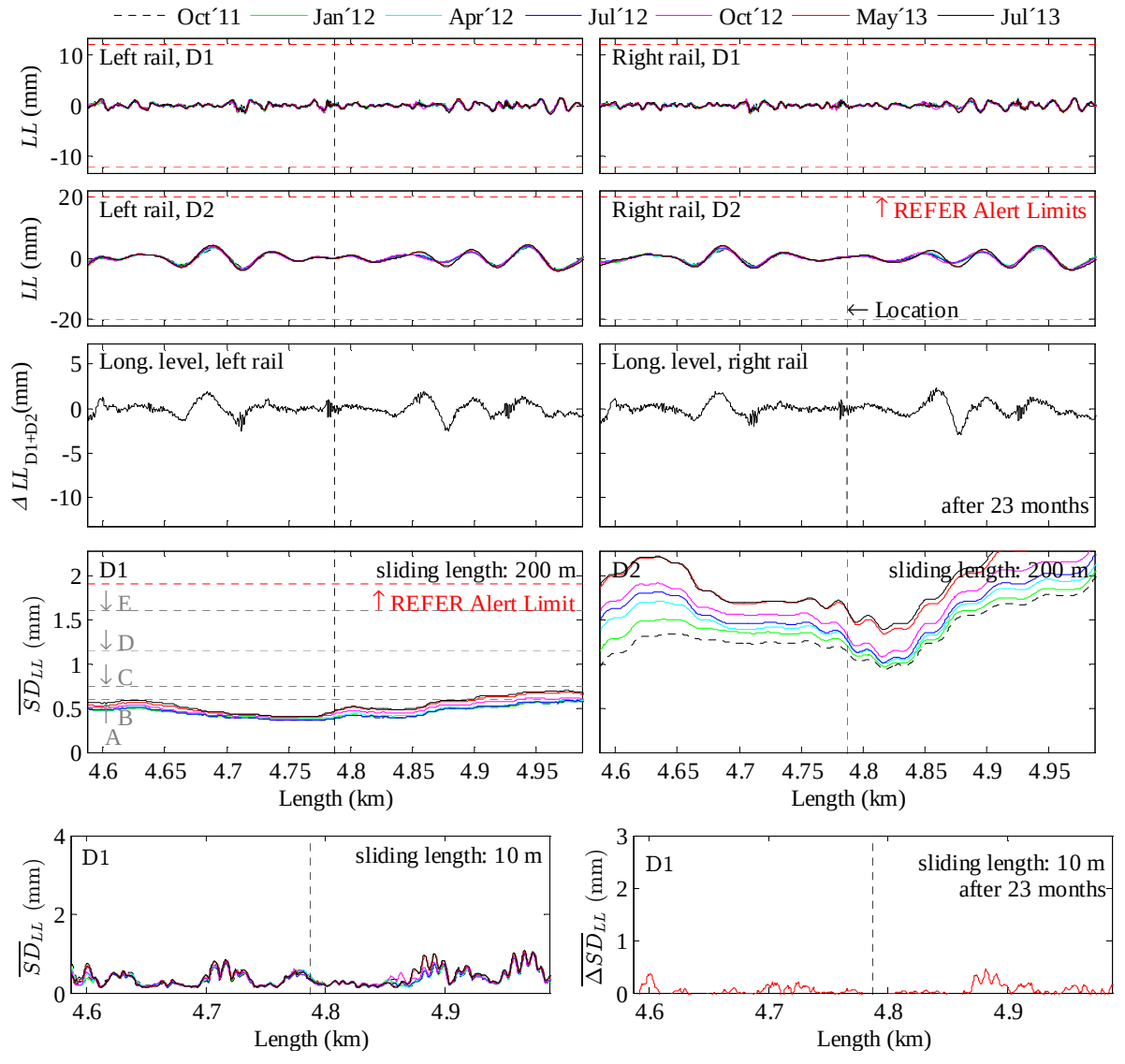

PH 6.1 at km 6.188 (deep culvert, no Technical Block), Ø=1.2m

Excerpt from Design:

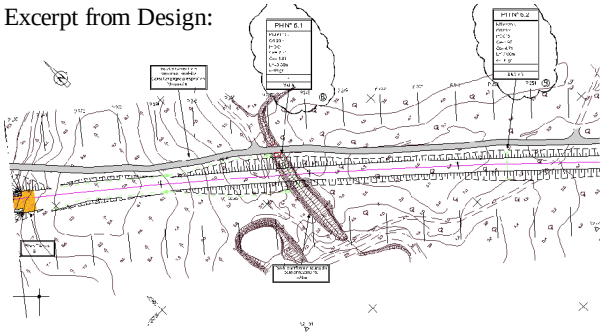

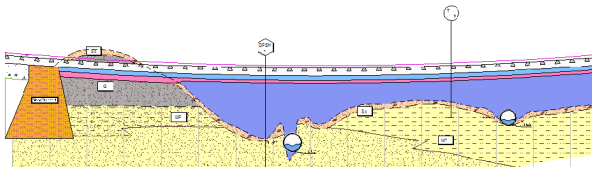

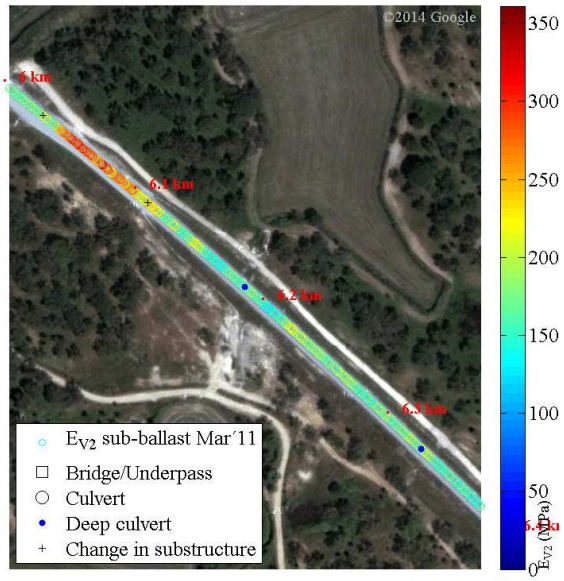

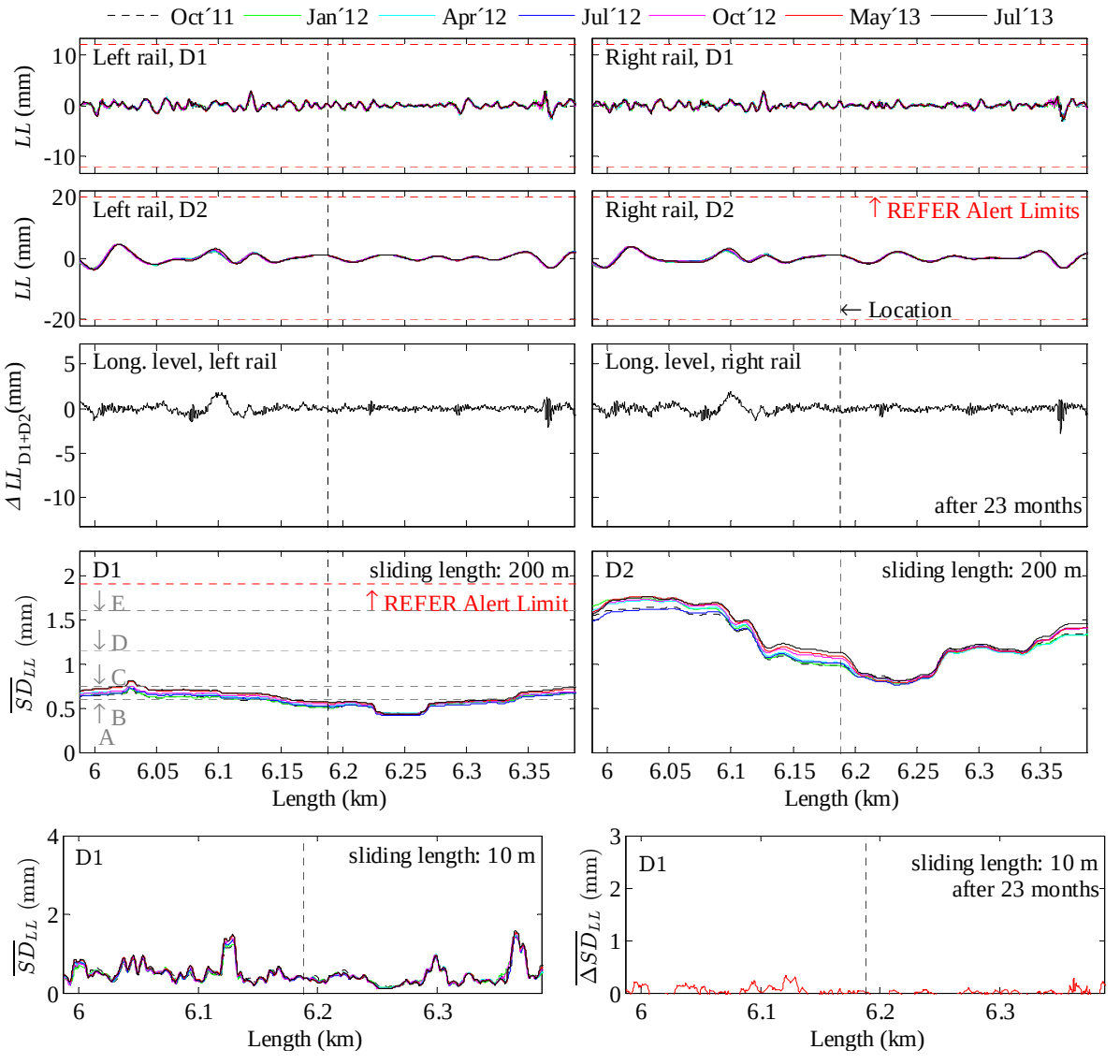

PH 6.2 at km 6.33 (deep culvert, no Technical Block), Ø=1m

Excerpt from Design:

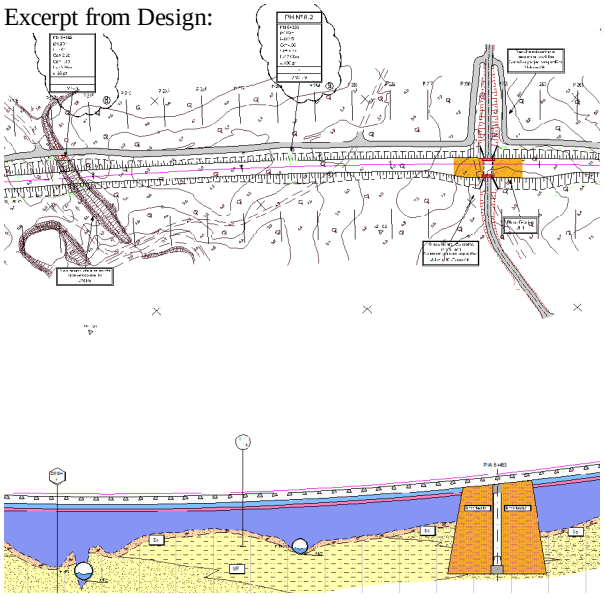

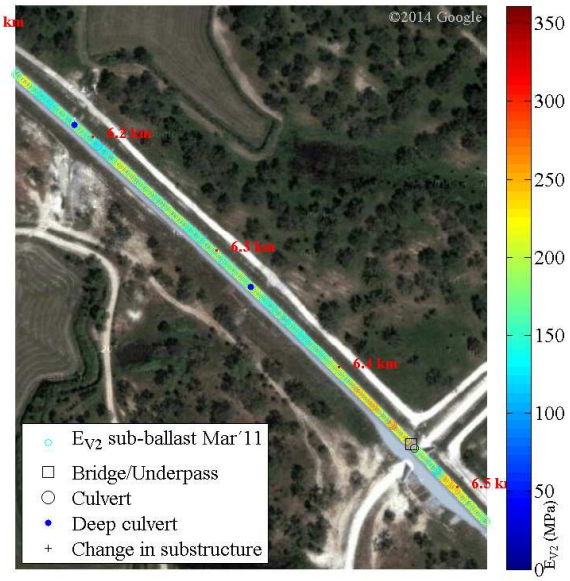

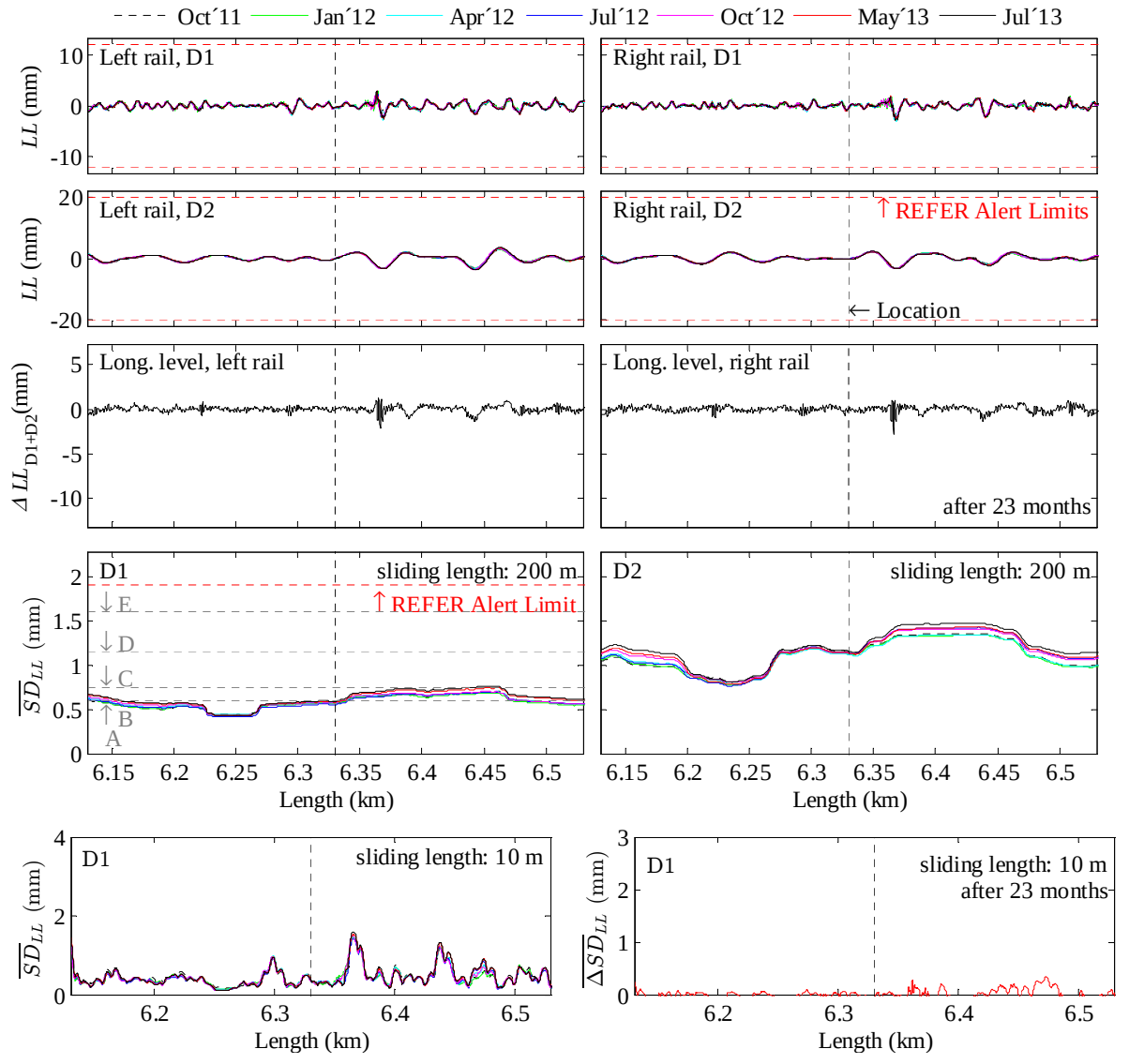

PH 6.3 at km 6.932 (deep culvert, no Technical Block), Ø=1m

Excerpt from Design:

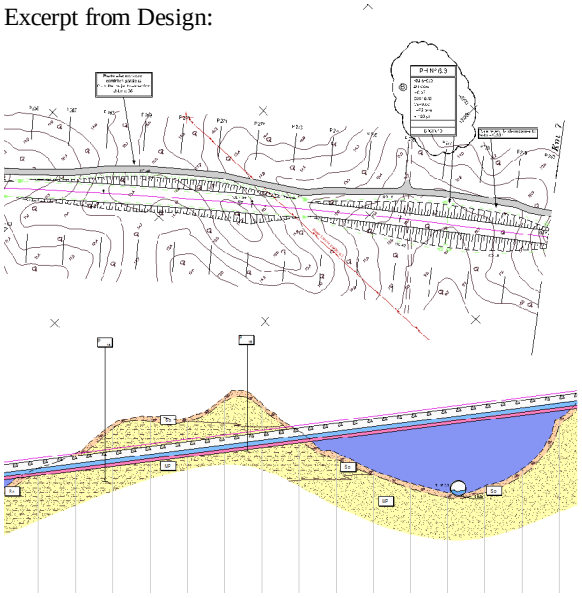

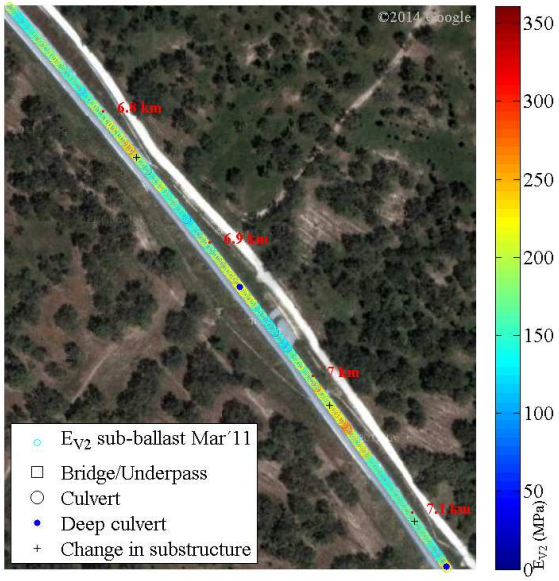

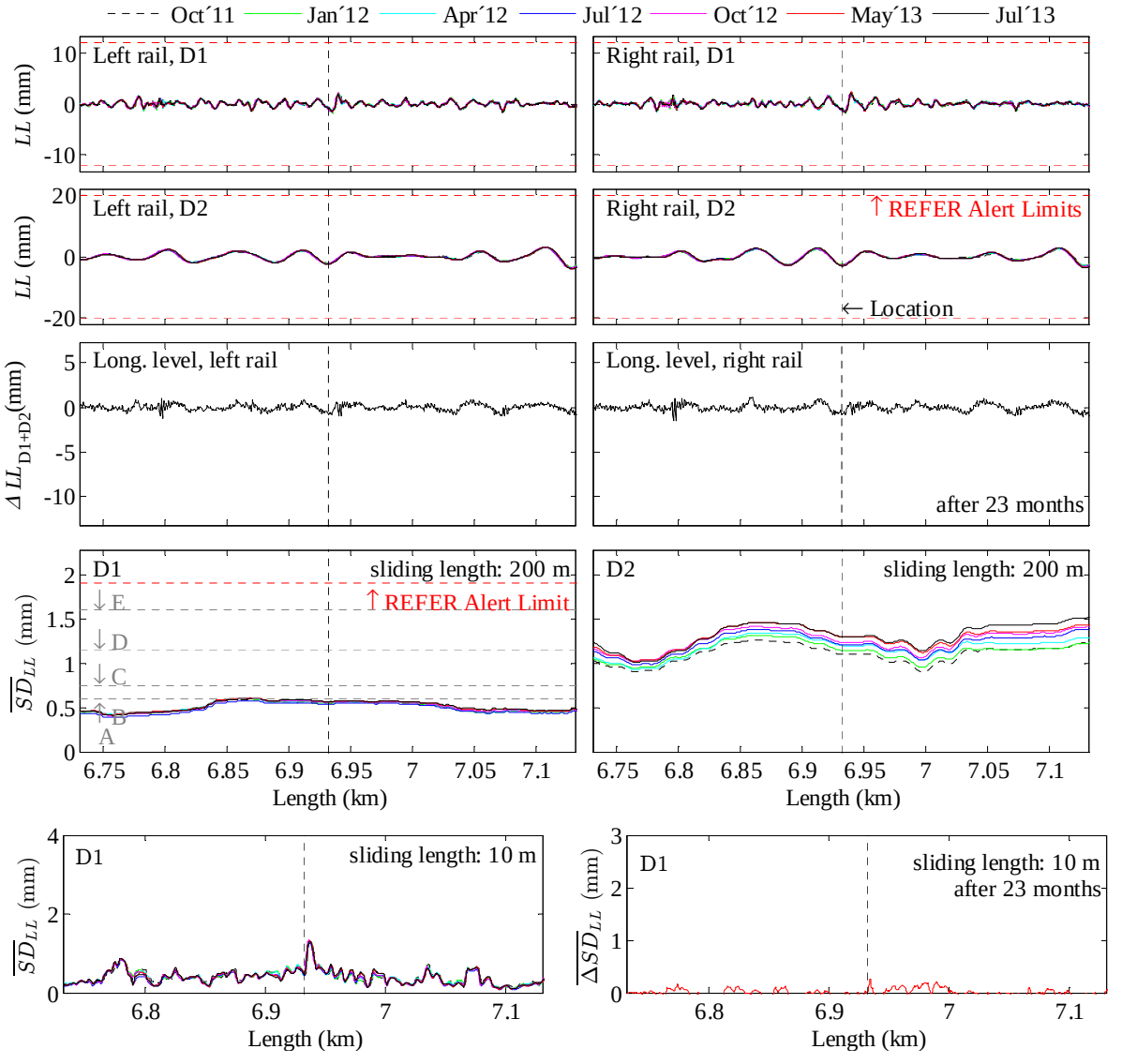

PH 7.1 at km 7.138 (deep culvert, no Technical Block), Ø=1.2m

Excerpt from Design:

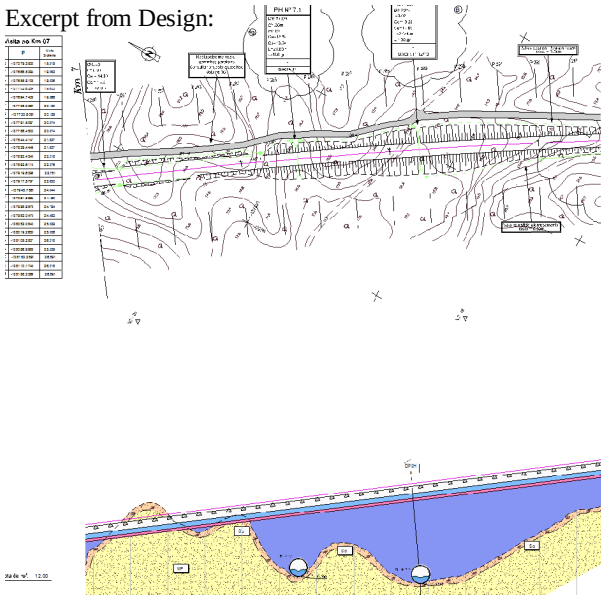

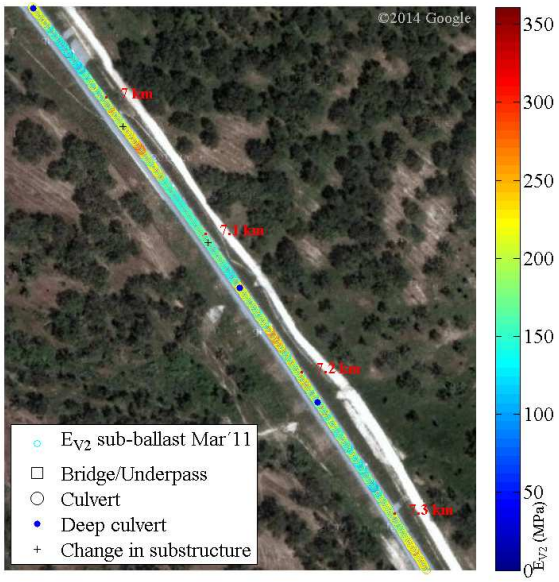

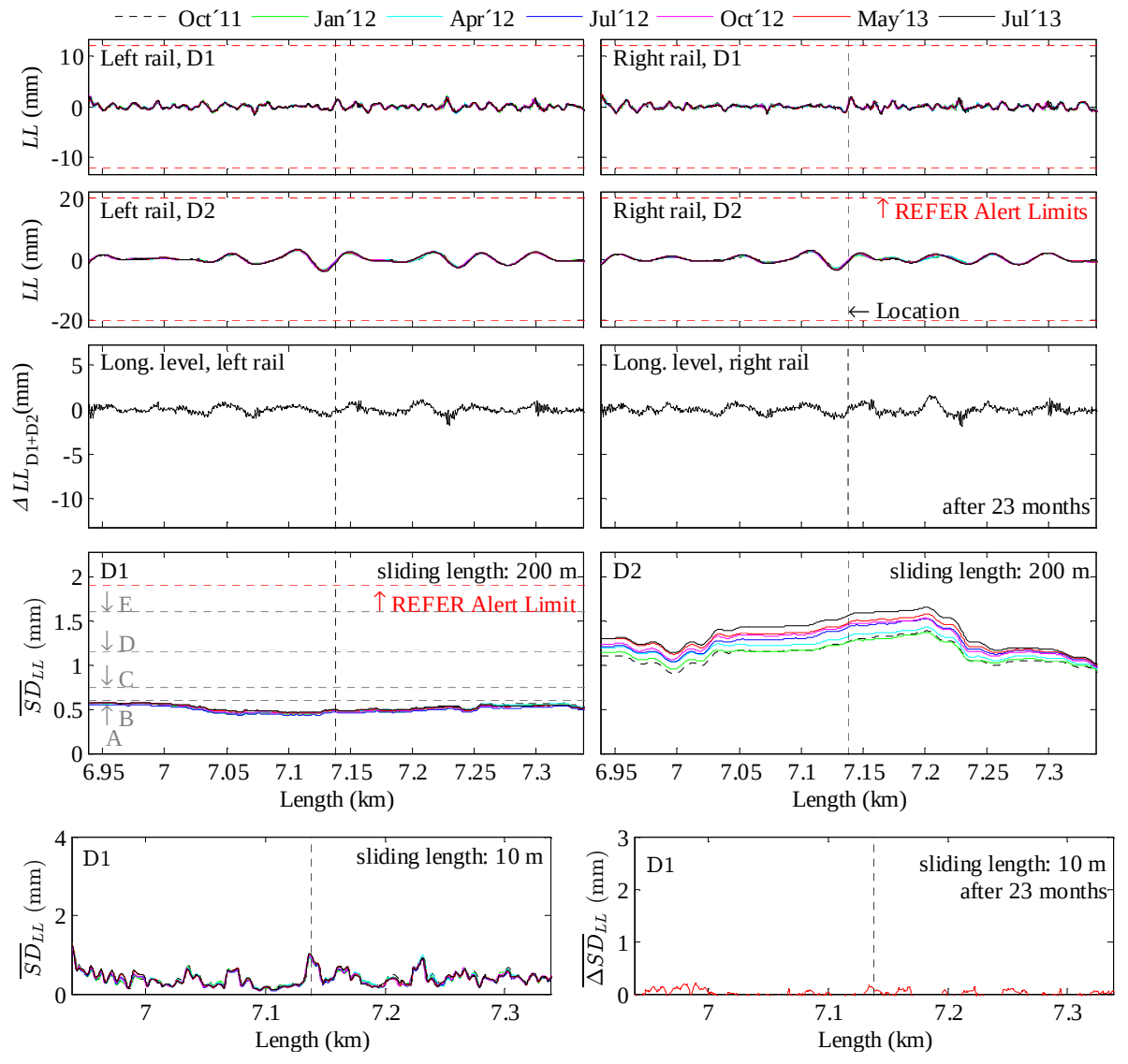

PH 7.2 at km 7.22 (deep culvert, no Technical Block), Ø=1.2m

Excerpt from Design:

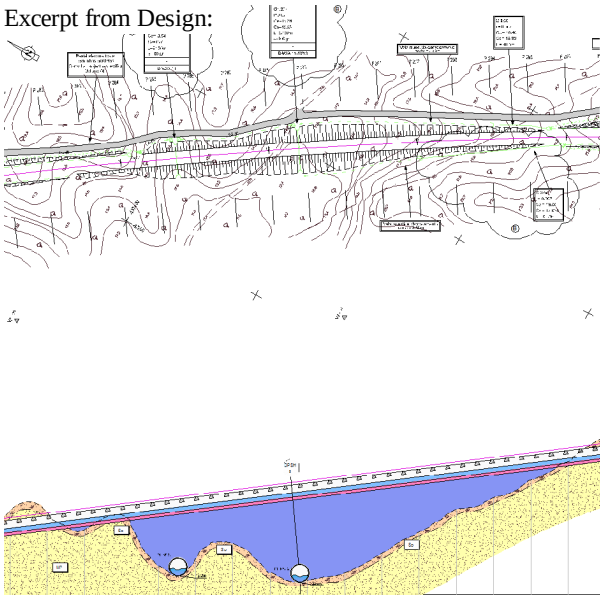

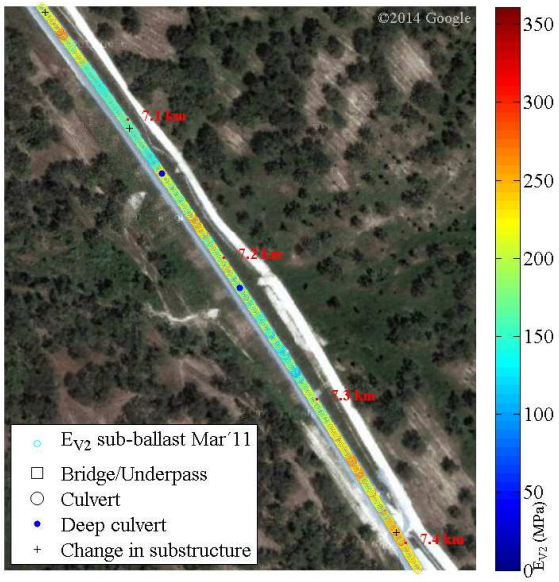

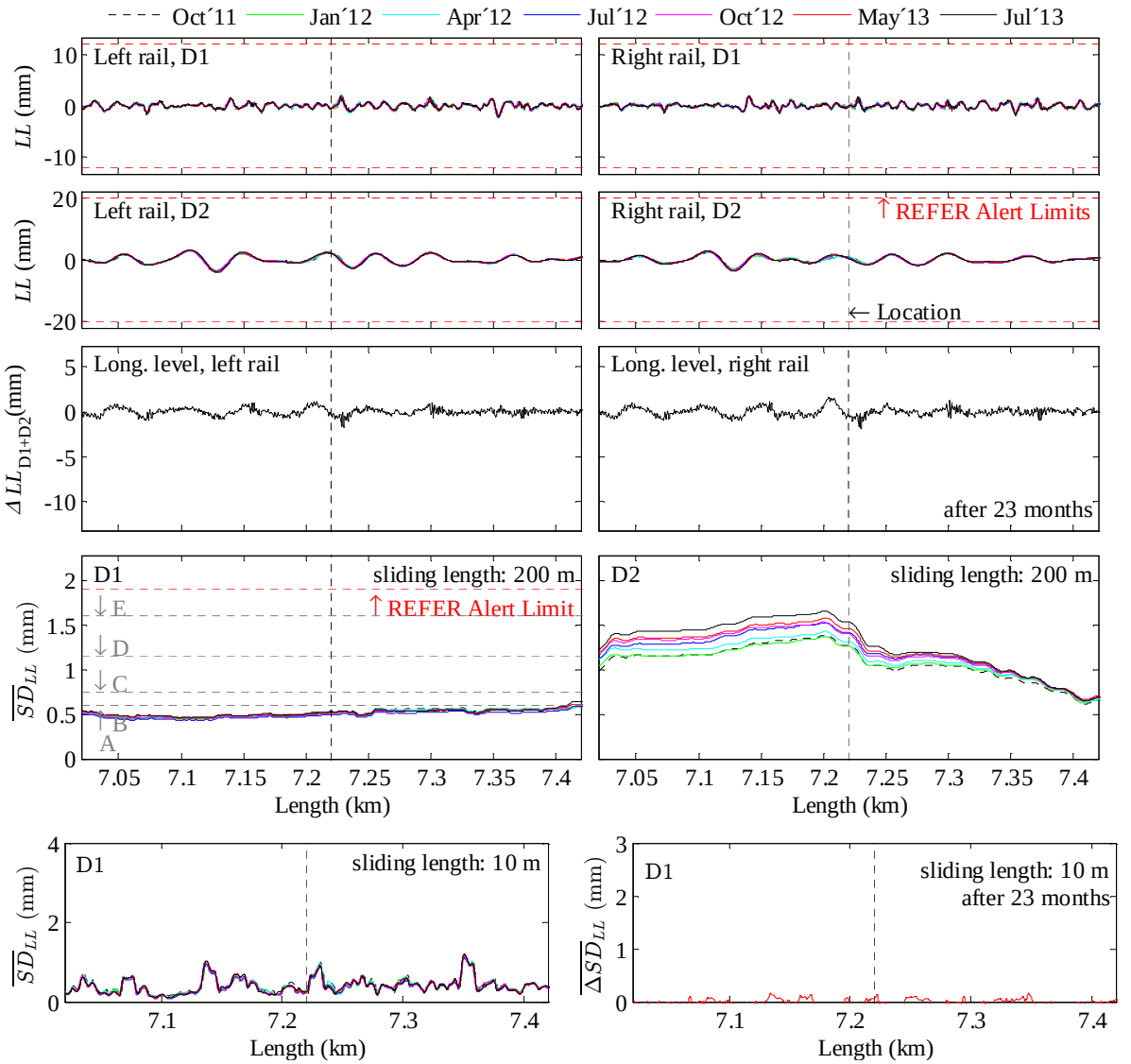

PH 8.1 at km 8.127 (deep culvert, no Technical Block), Ø=1m

Excerpt from Design:

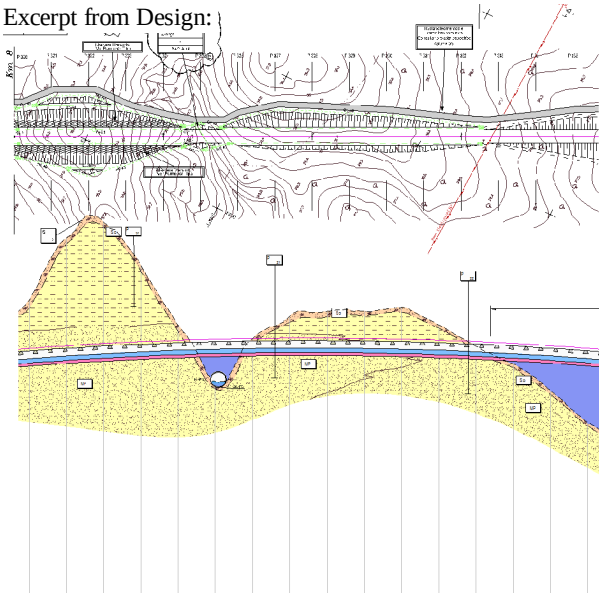

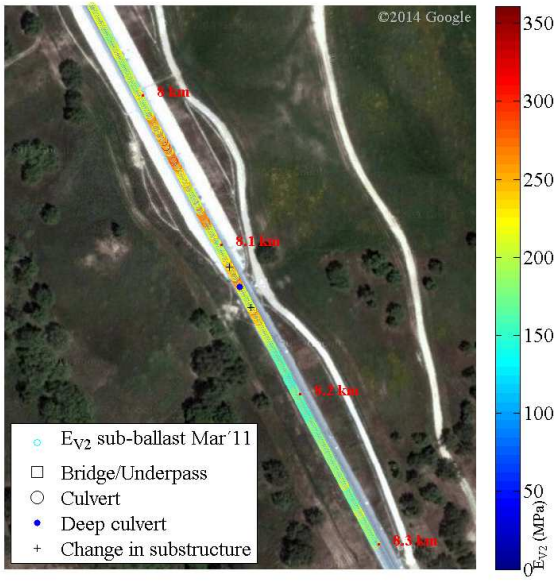

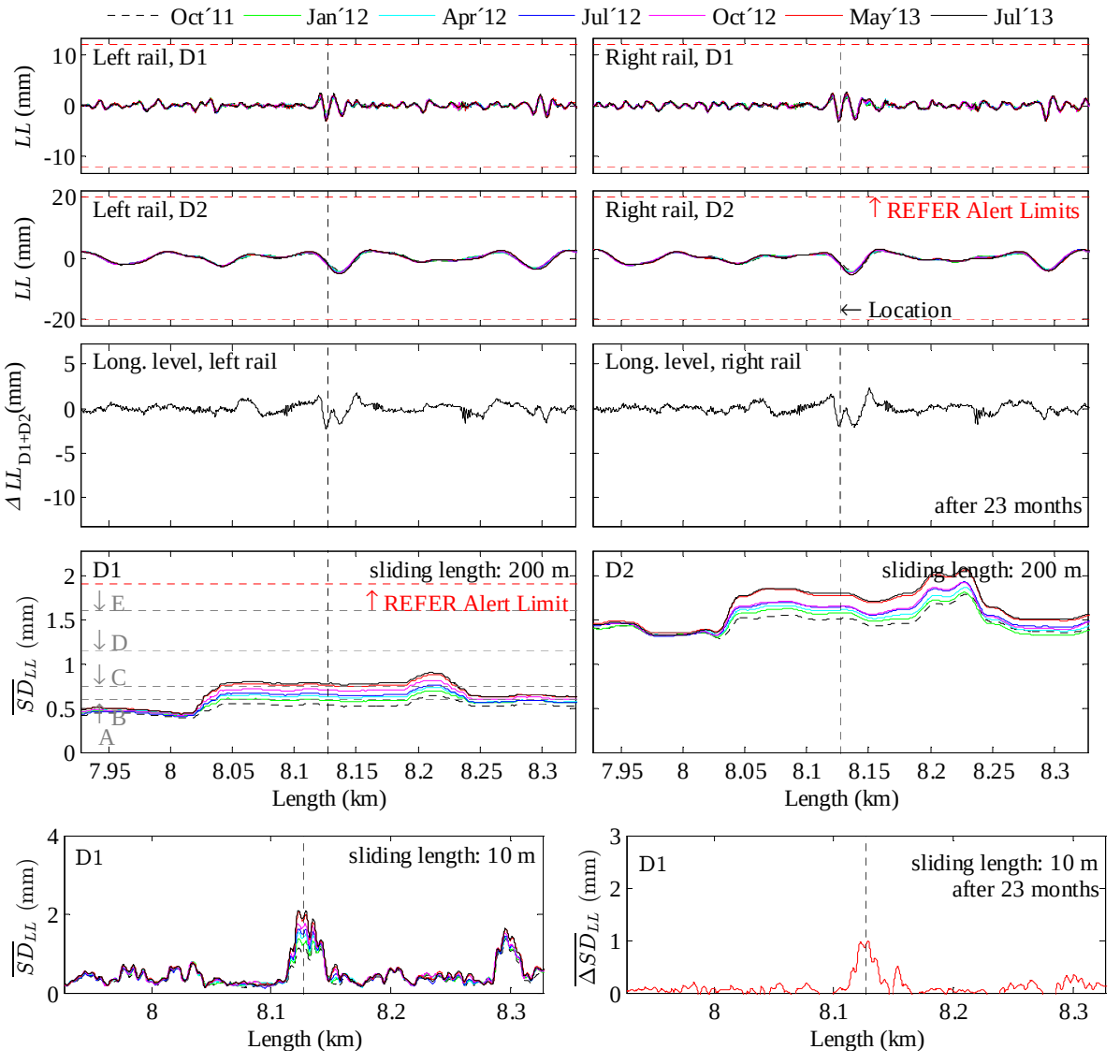

PF 15.1 at km 15.275 (deep culvert, no Technical Block), Ø=1m

Excerpt from Design:

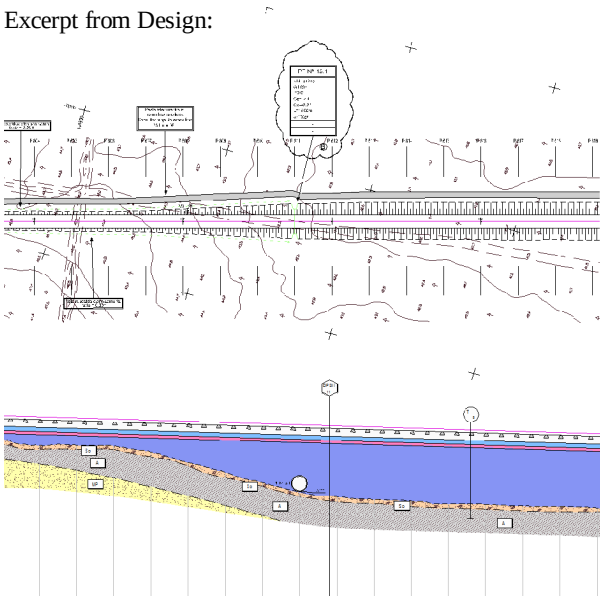

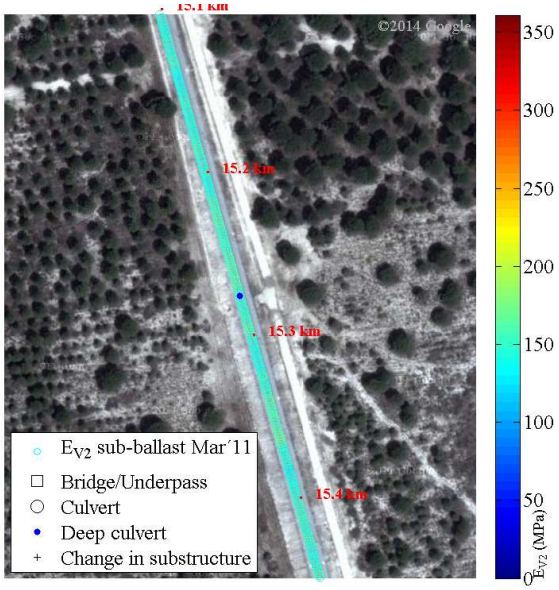

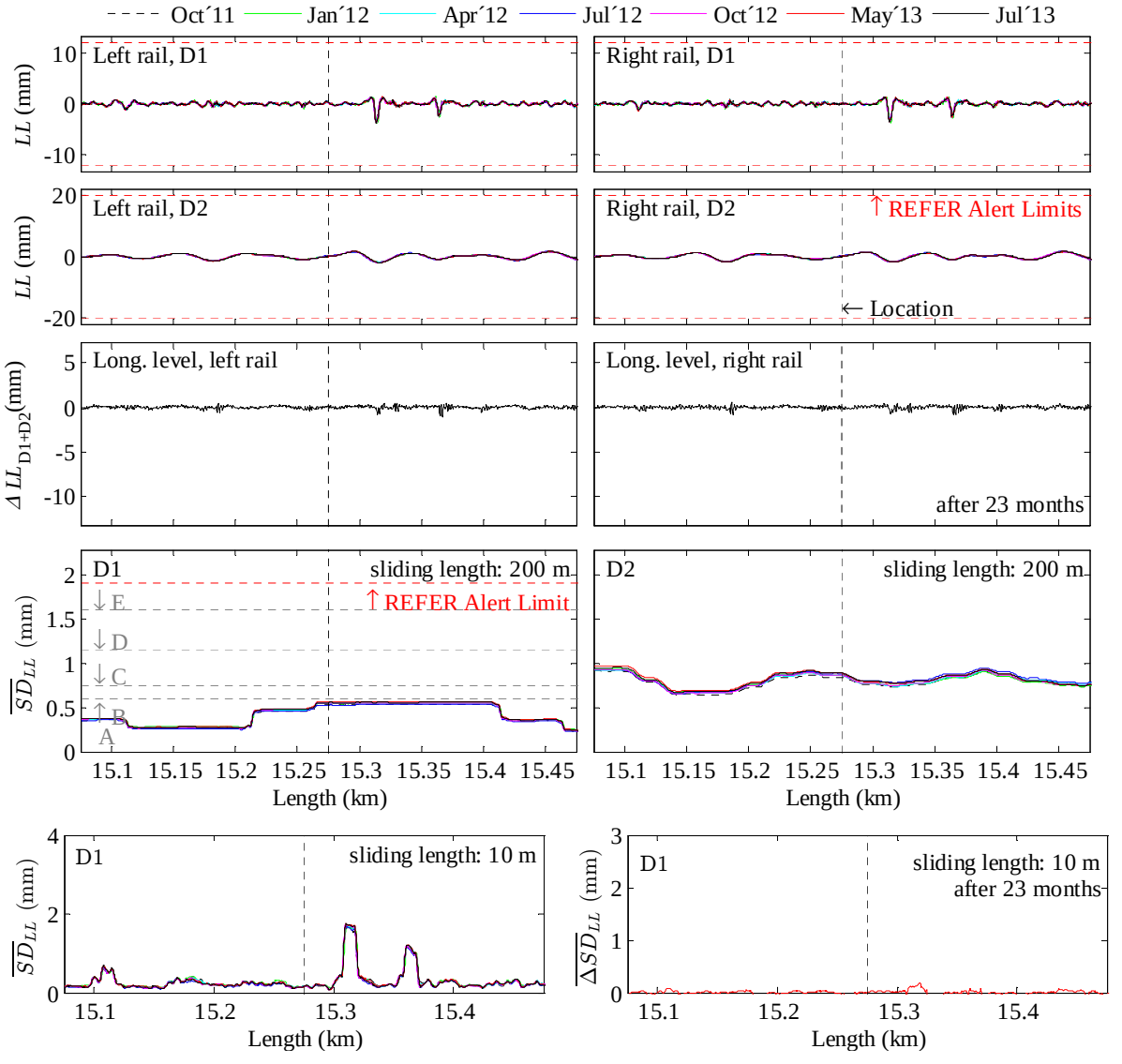

PH 19.1 at km 19.117 (deep culvert, no Technical Block), Ø=1.2m

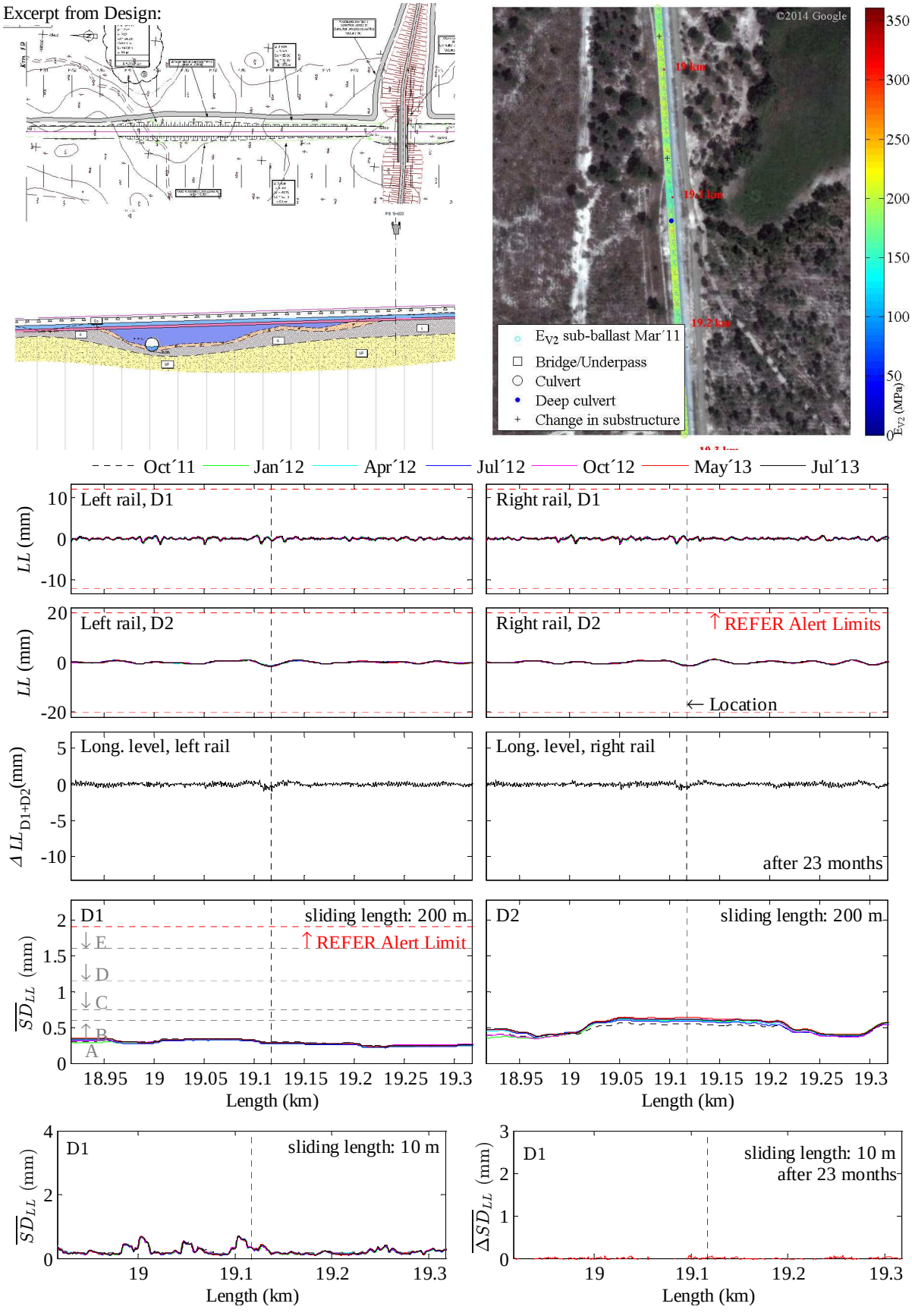

PH 21.2 at km 21.765 (deep culvert, no Technical Block), Box 1.5x1.0m

Excerpt from Design:

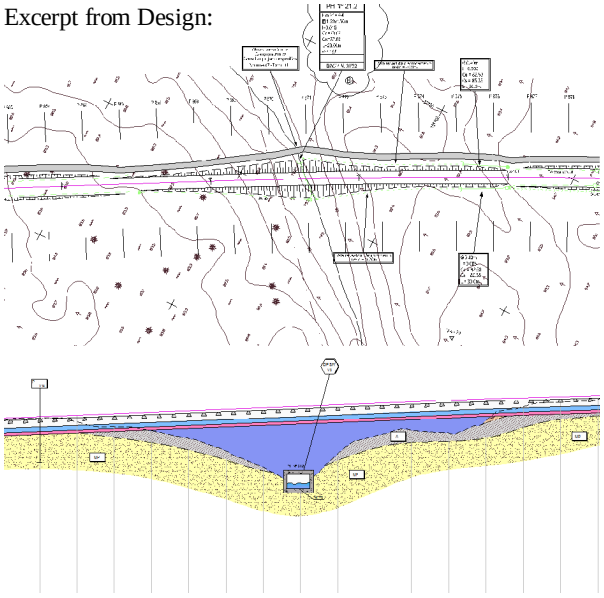

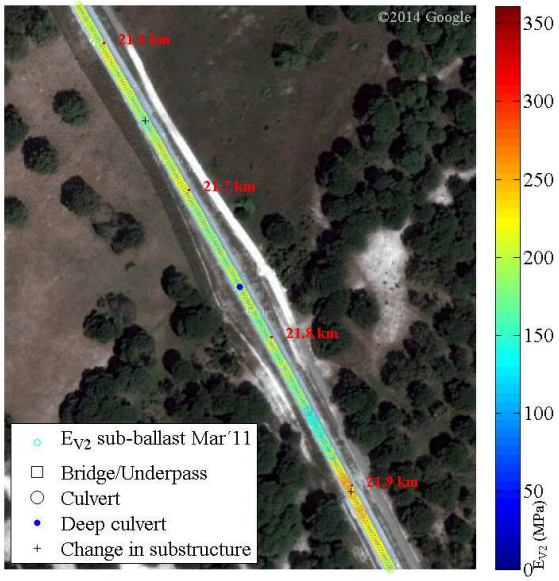

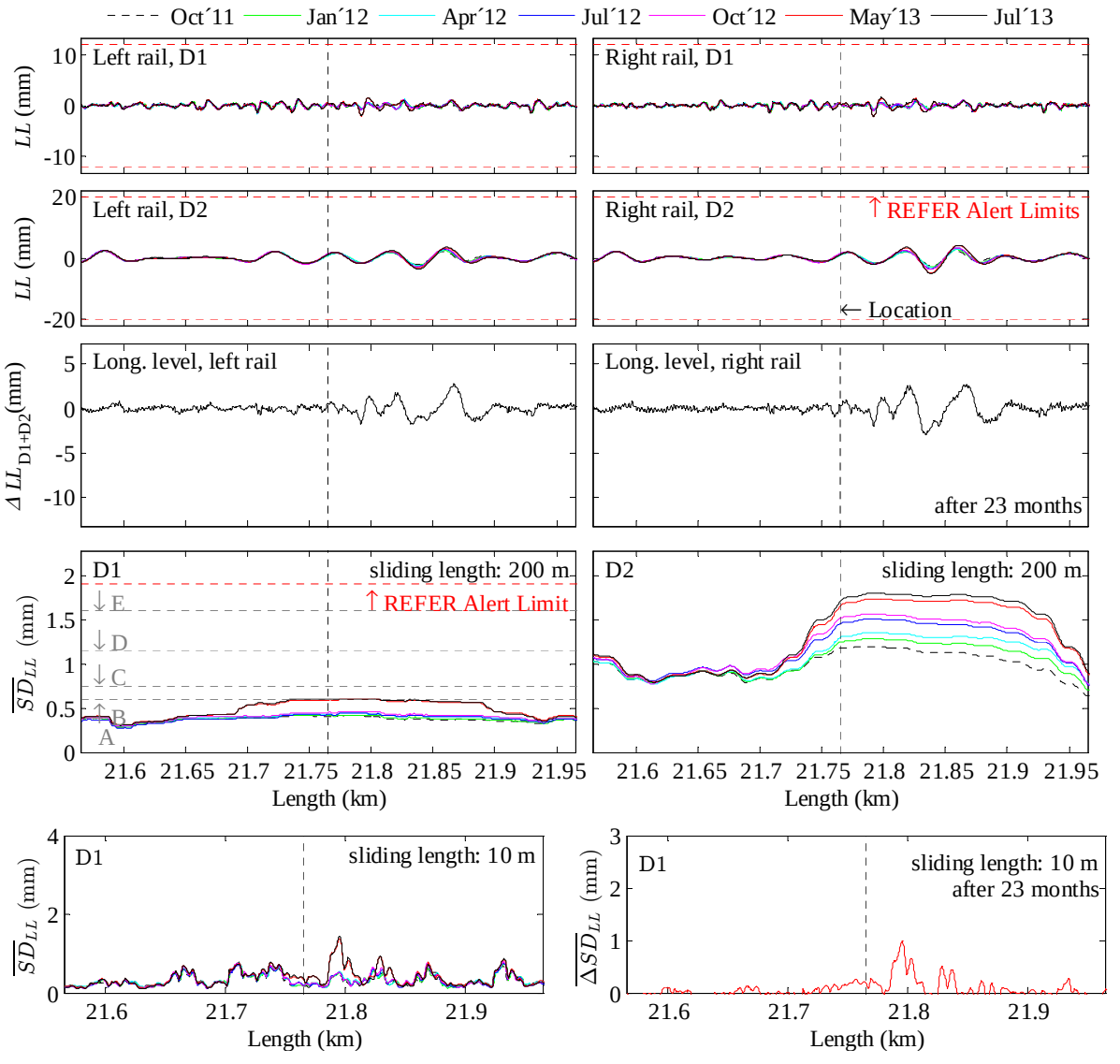

PH 23.3 at km 23.653 (deep culvert, no Technical Block), Ø=1.2m

Excerpt from Design:

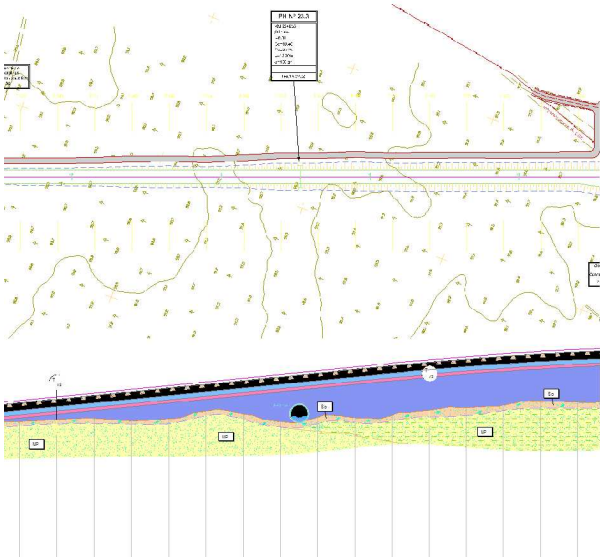

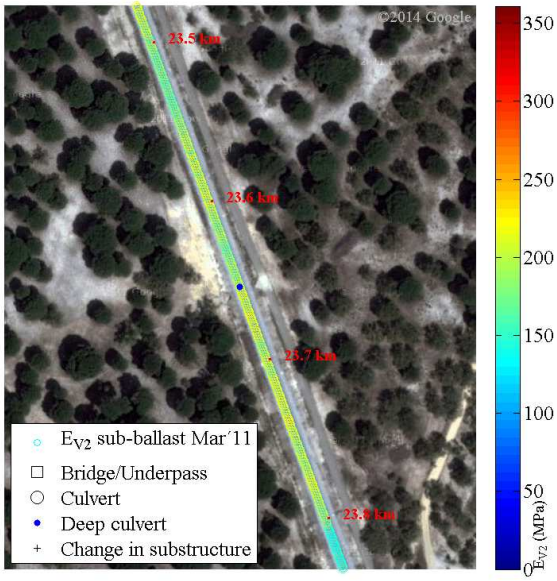

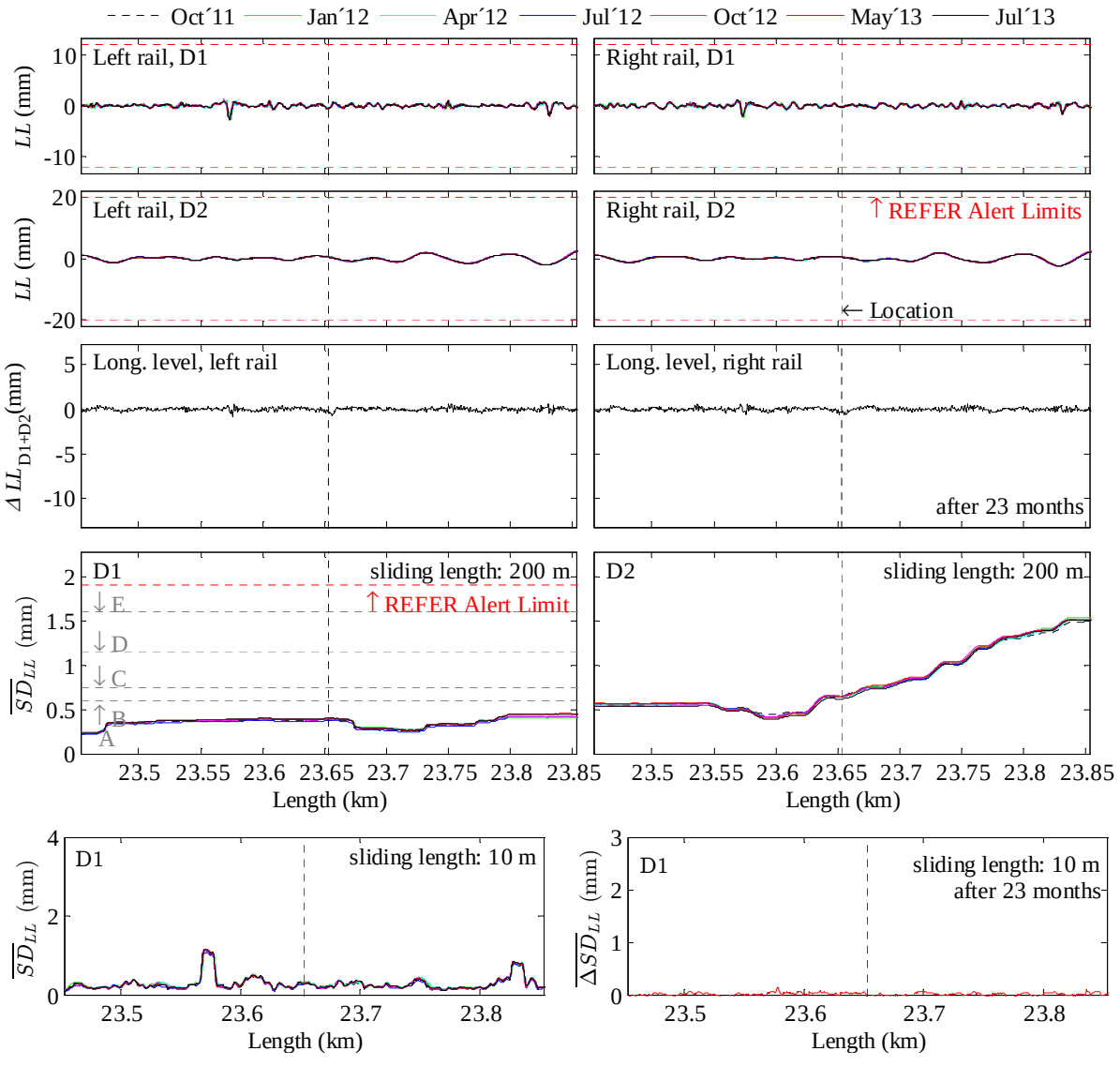

PH 25.2 at km 25.363 (deep culvert, no Technical Block), Ø=1m

Excerpt from Design:

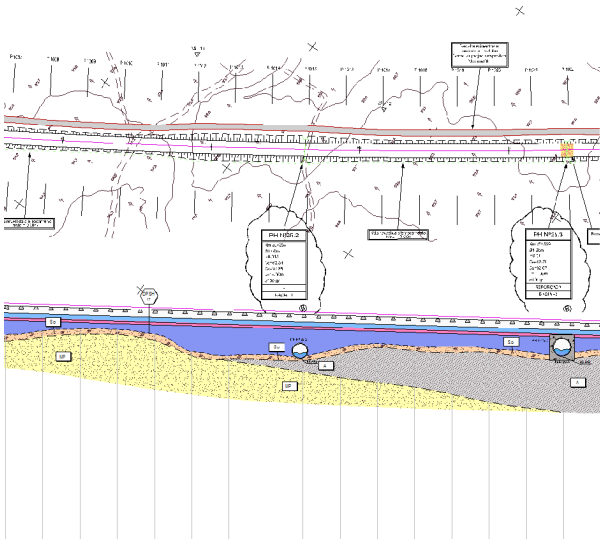

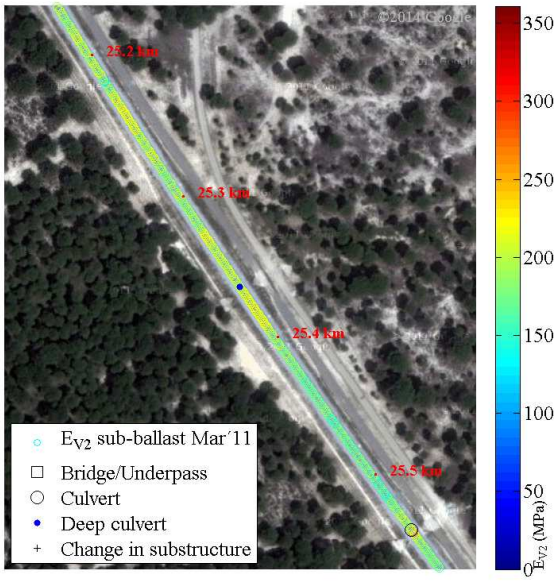

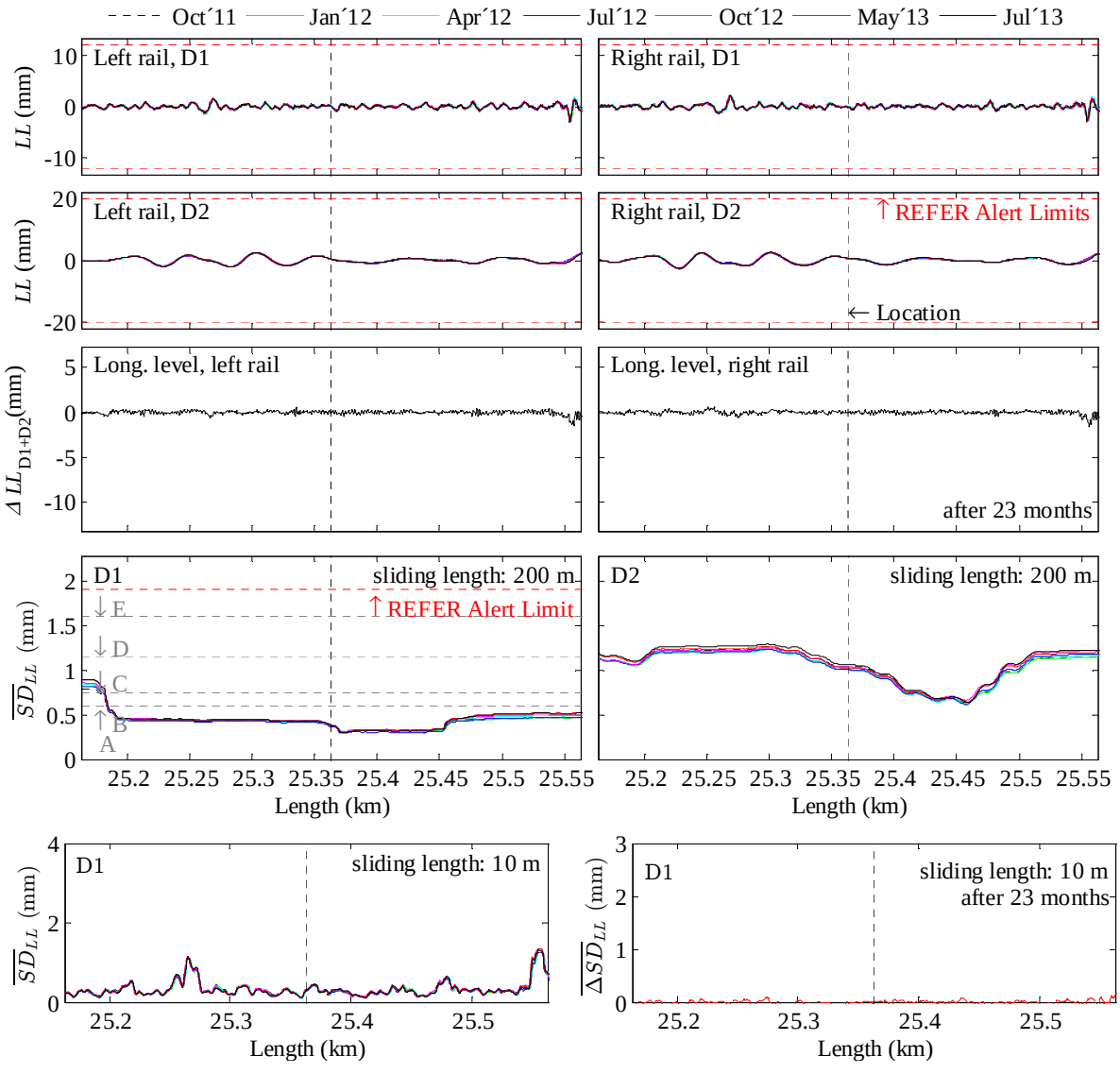

PH 25.4 at km 25.88 (deep culvert, no Technical Block), Ø=1.2m

Excerpt from Design:

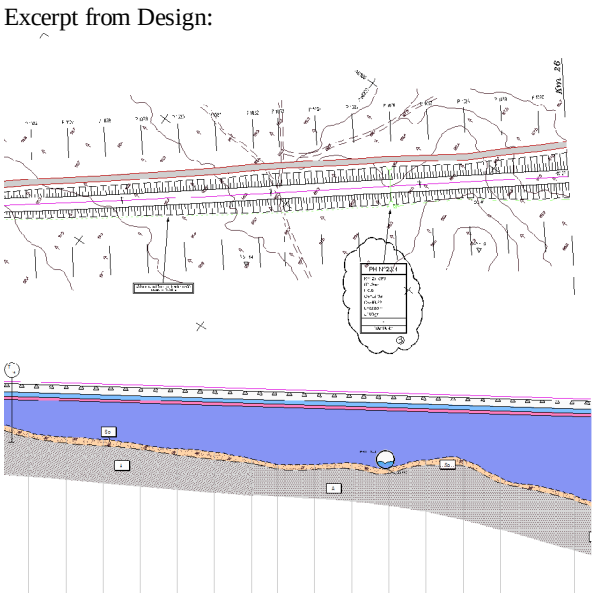

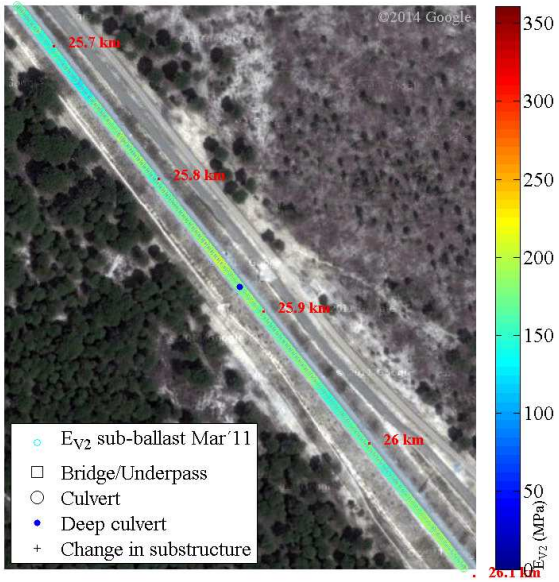

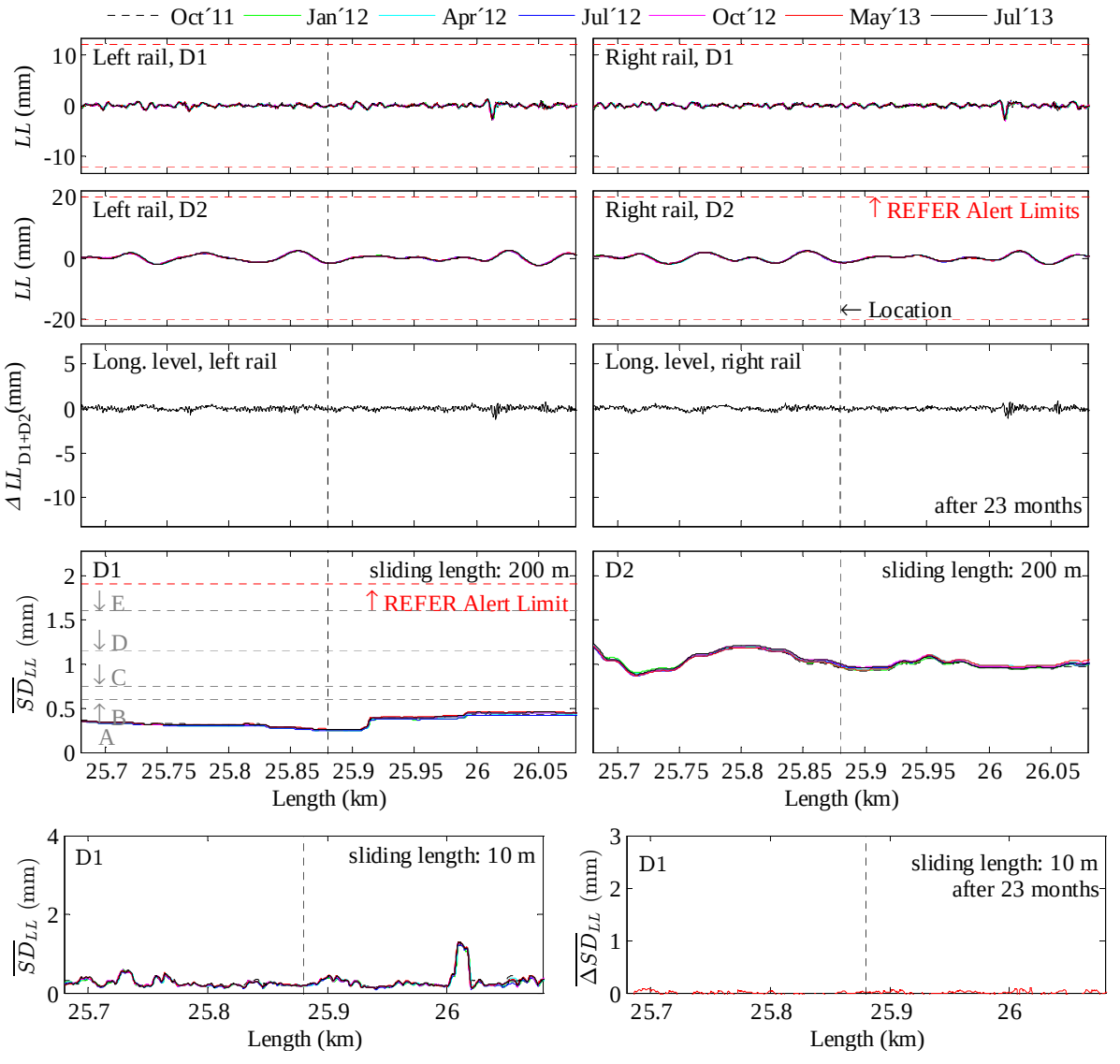

PH 26.1 at km 26.685 (deep culvert, no Technical Block), Ø=1m

Excerpt from Design:

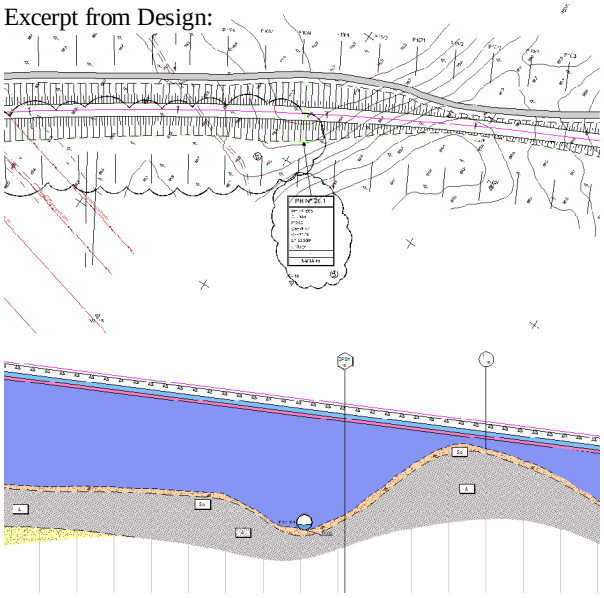

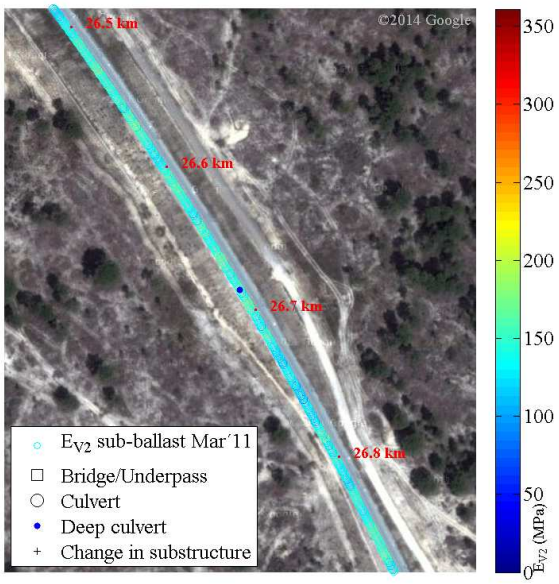

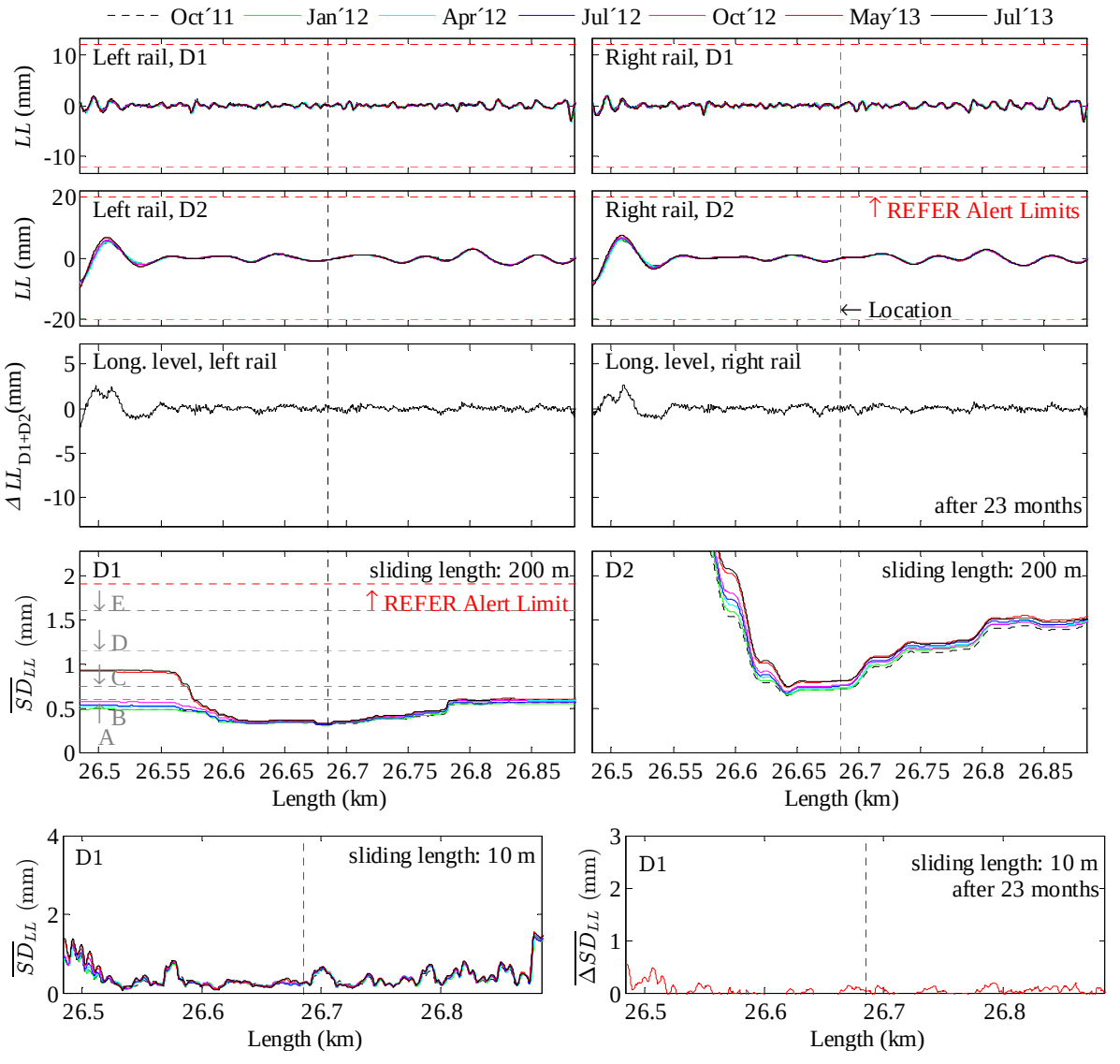

PH 27.1 at km 27.047 (deep culvert, no Technical Block), Ø=1m

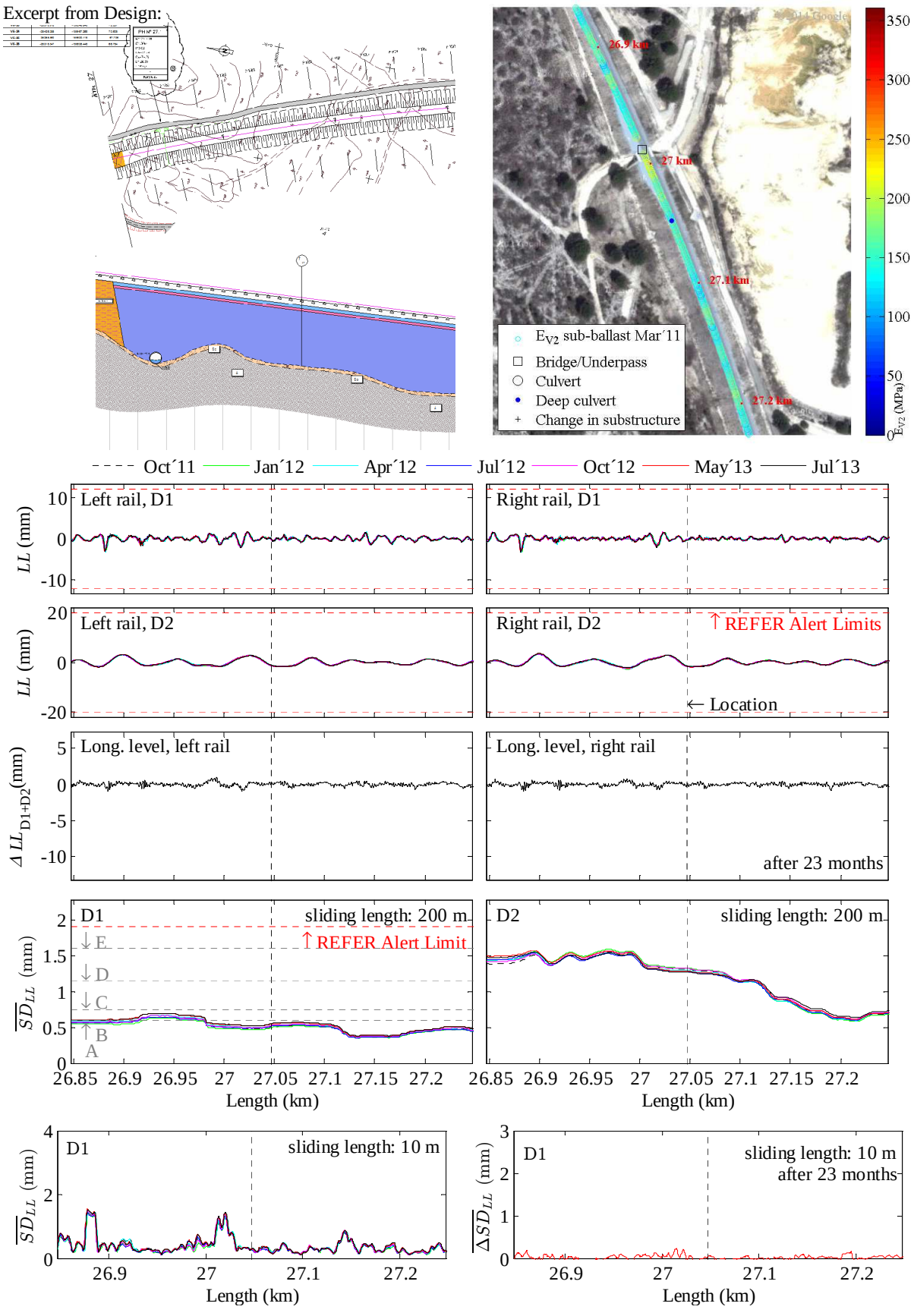

PH 27.2 at km 27.494 (deep culvert, no Technical Block), Ø=1m

Excerpt from Design:

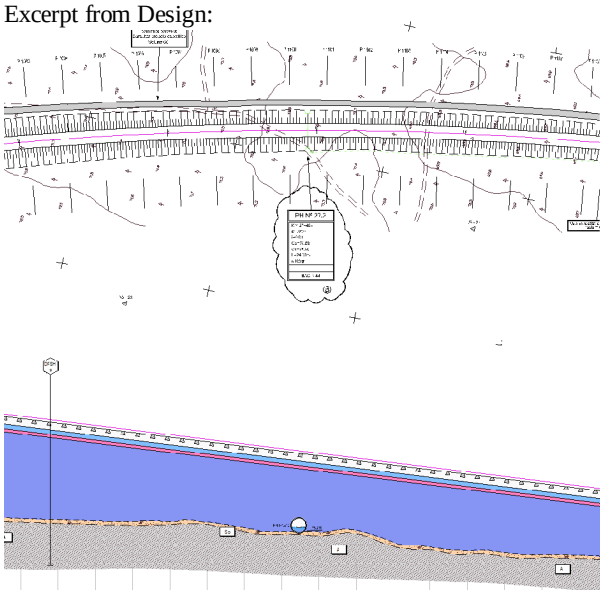

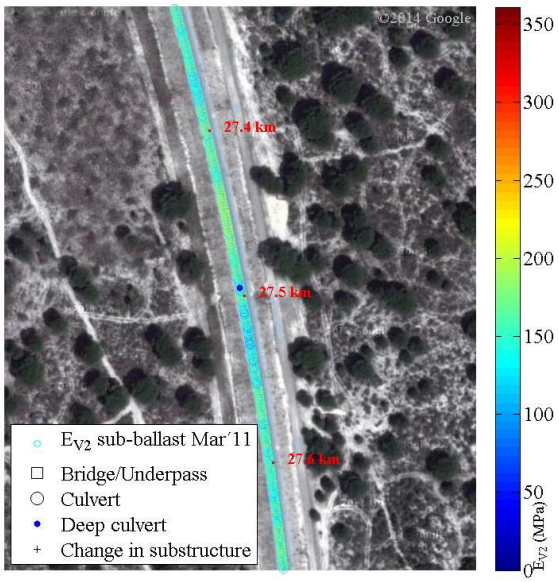

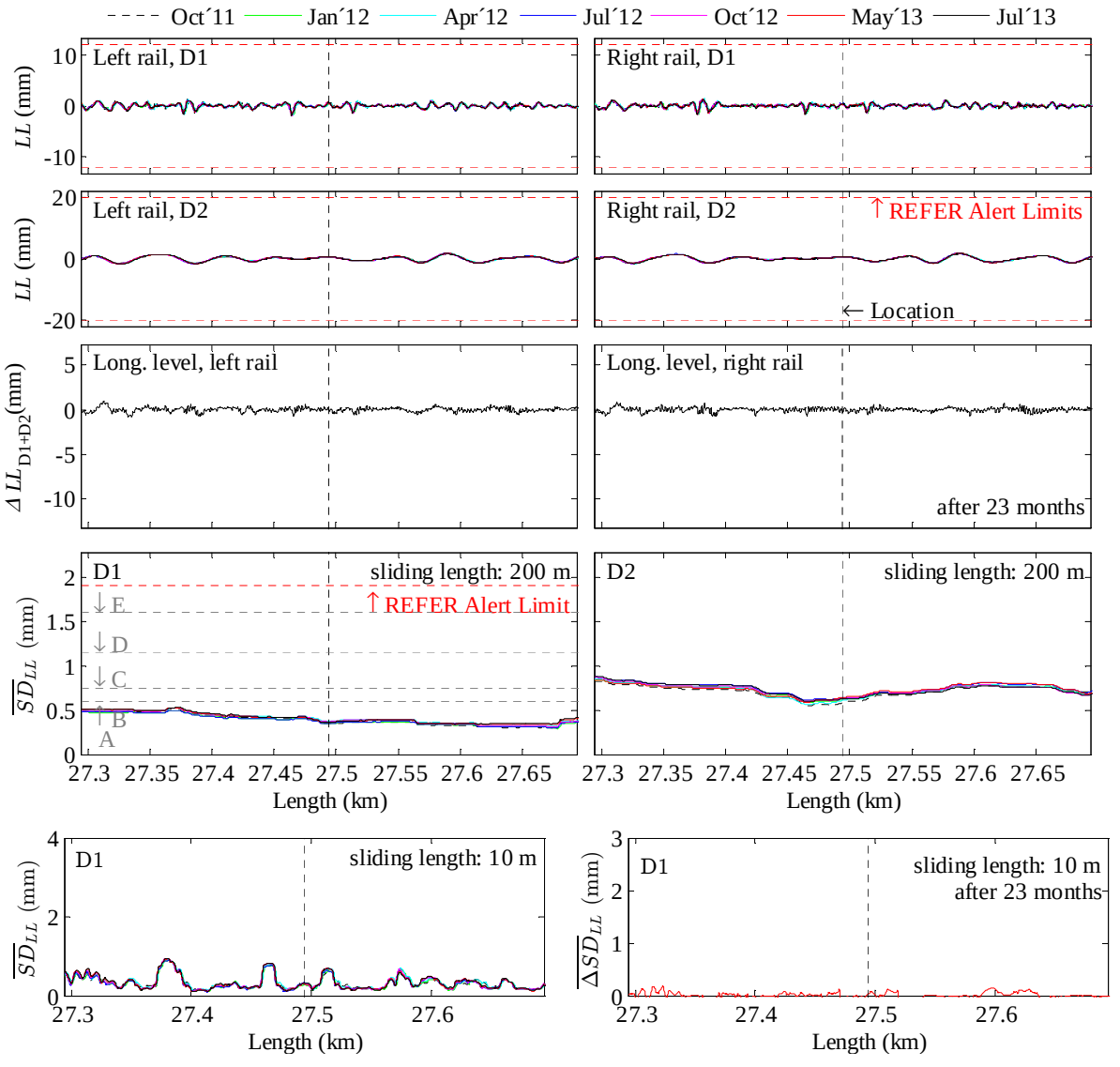

Rail expansion joint at km 8.79 (pier P7N)

Excerpt from Design:

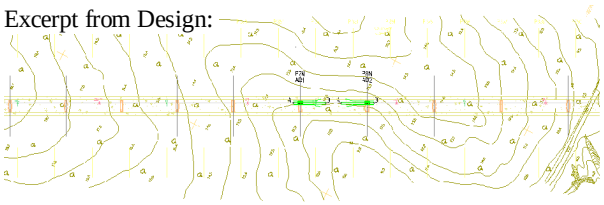

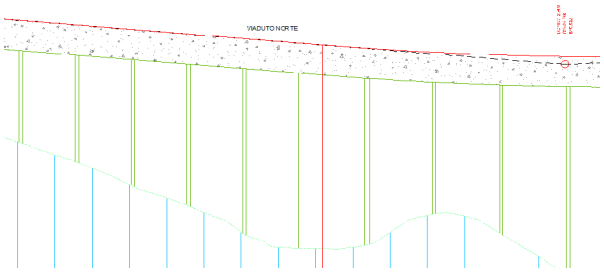

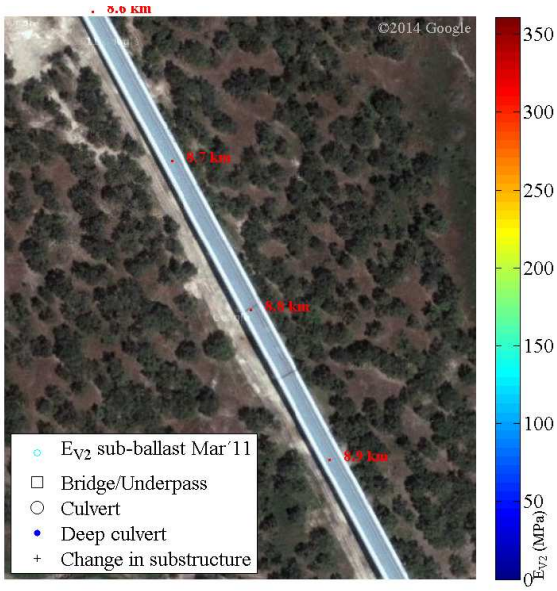

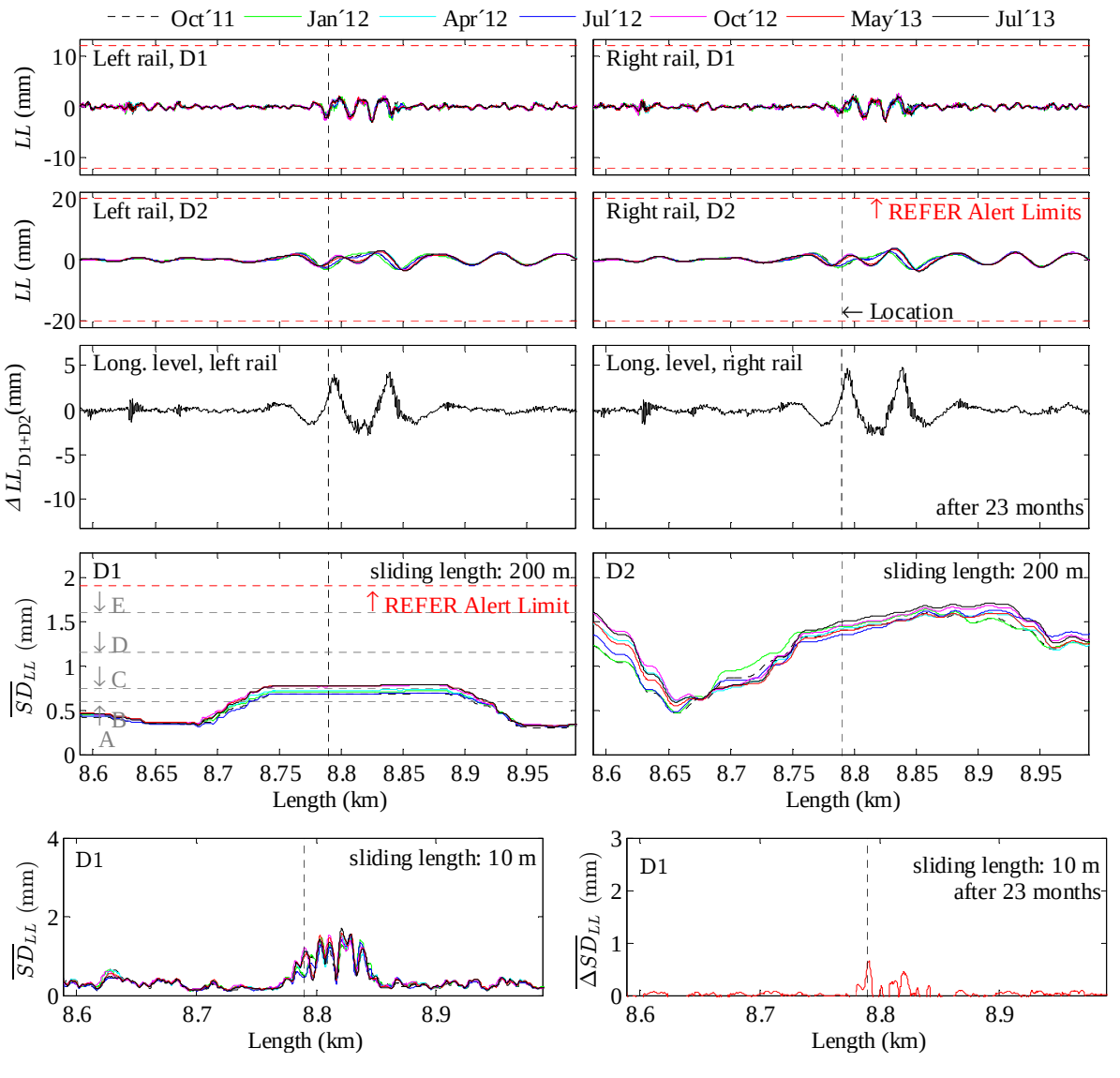

Rail expansion joint at km 8.835 (pier P8N)

Excerpt from Design:

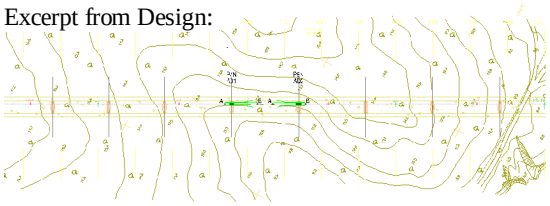

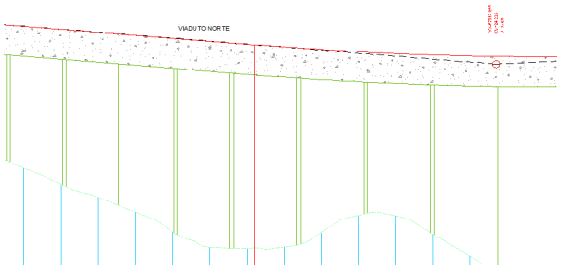

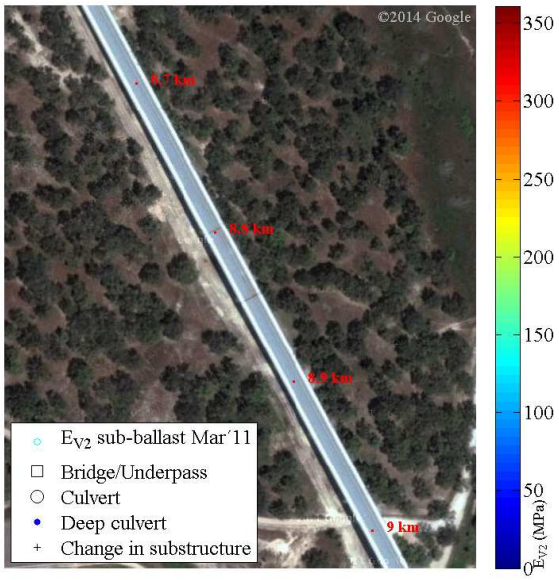

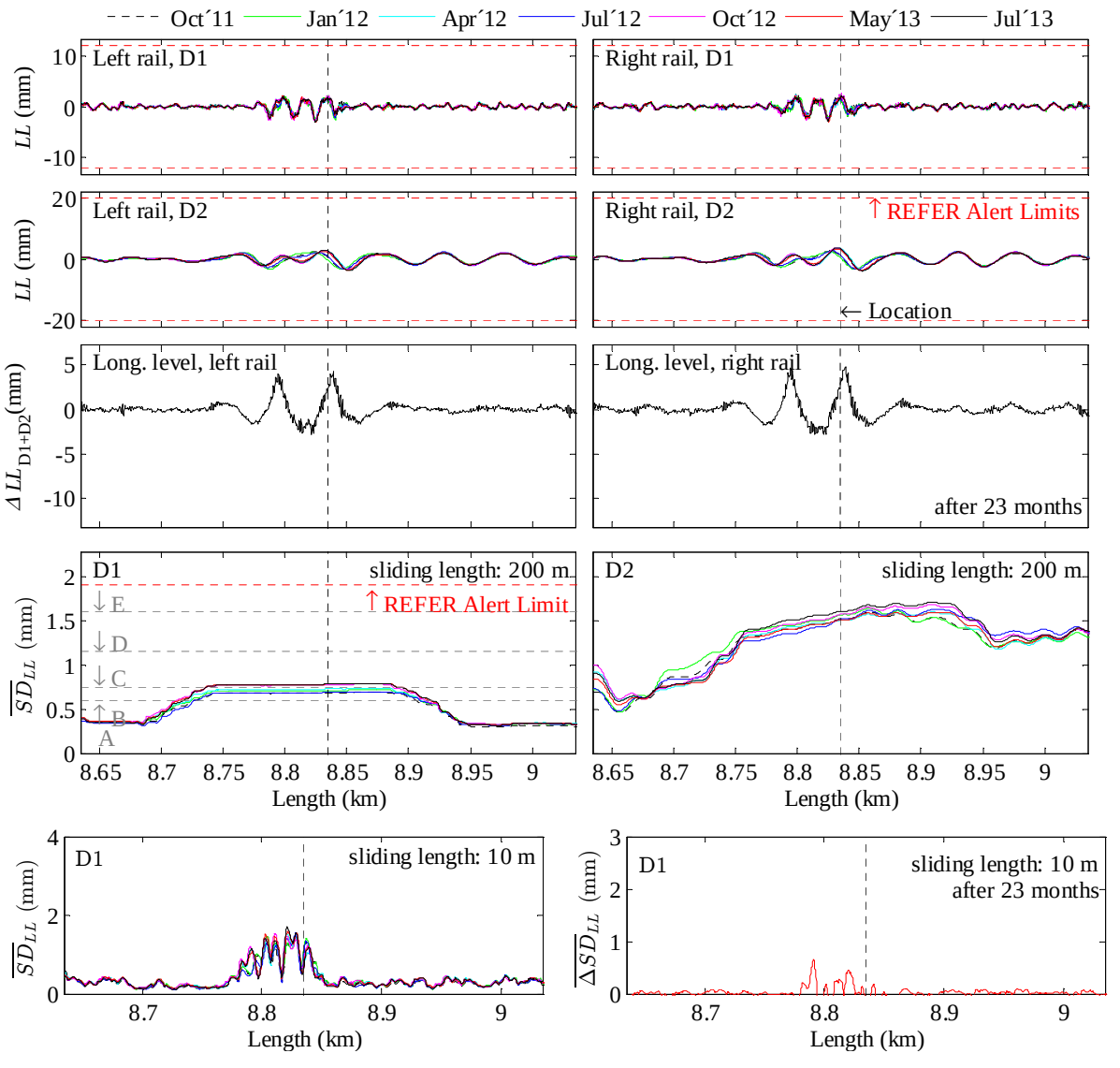

Rail expansion joint at km 9.6 (pier P25N)

Excerpt from Design:

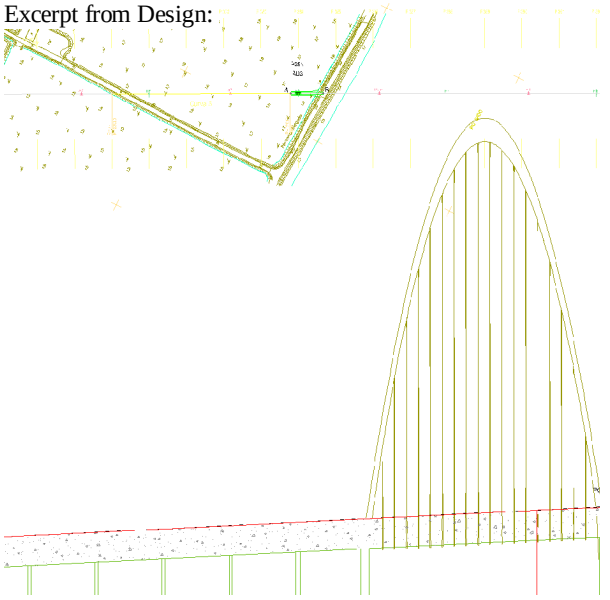

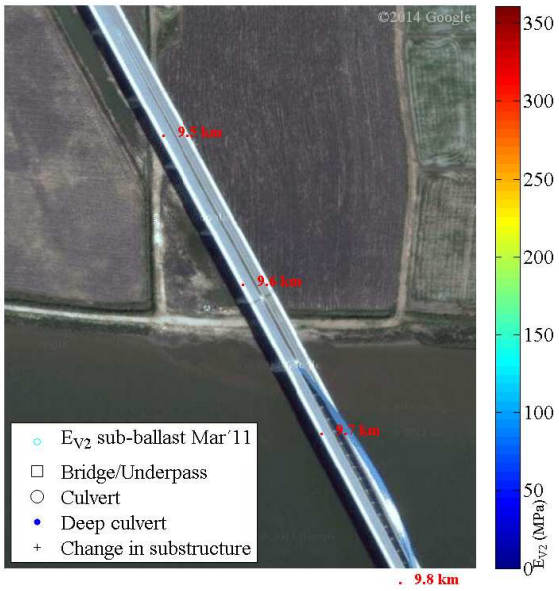

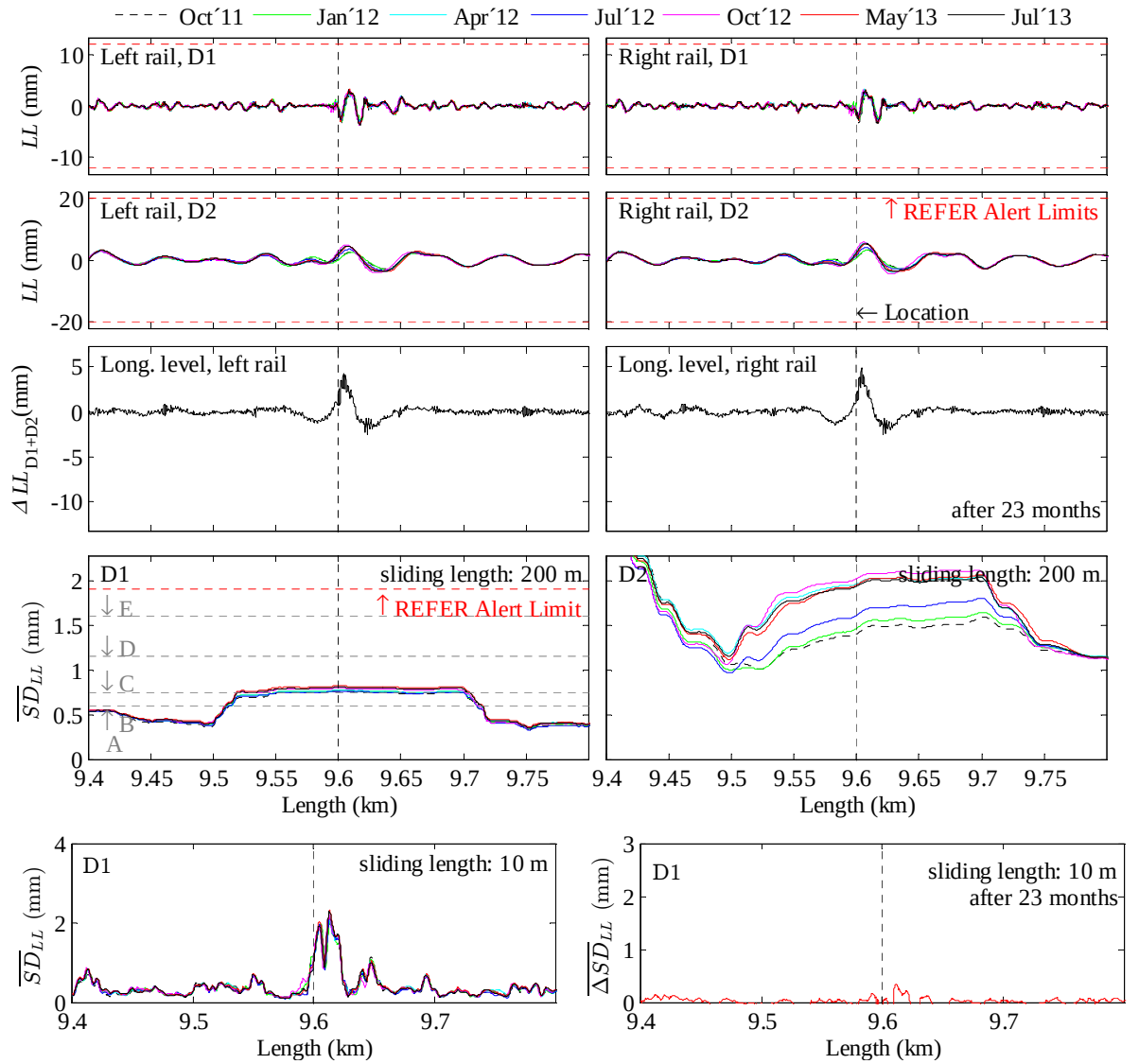

Rail expansion joint at km 10.125 (pier P4)

Excerpt from Design:

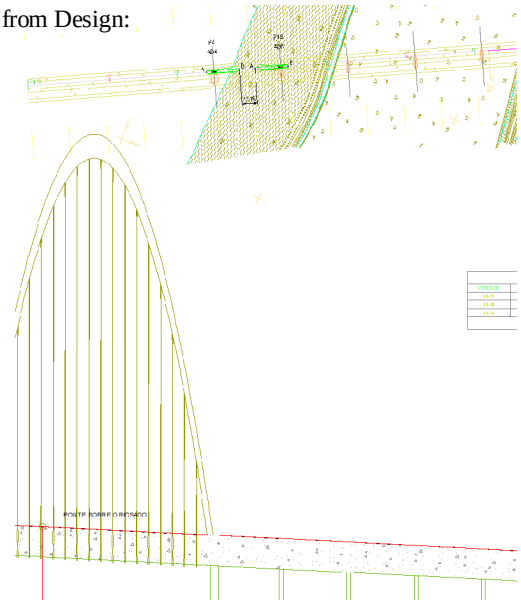

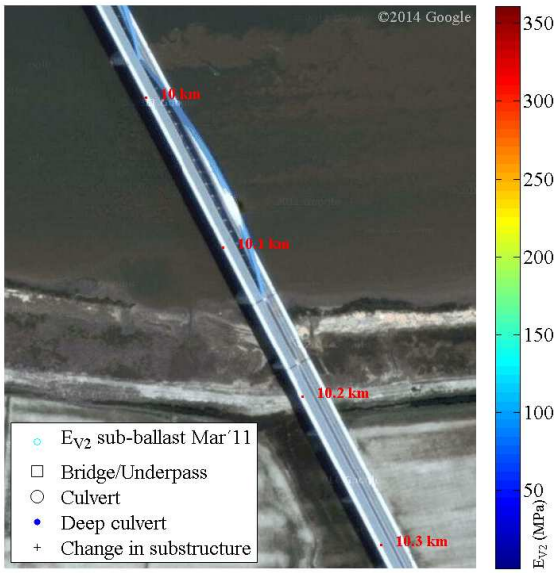

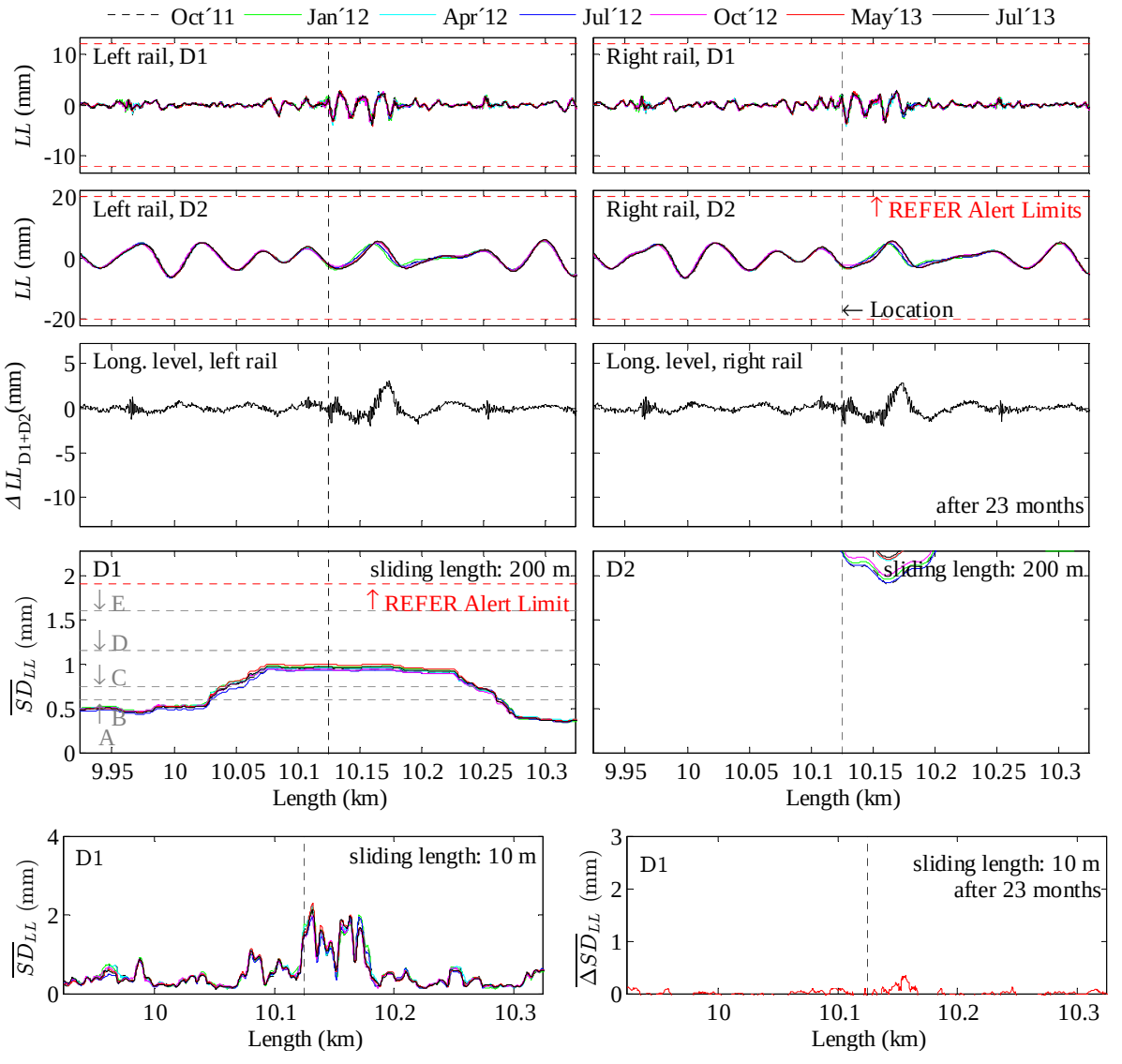

Rail expansion joint at km 10.17 (pier PIS)

Excerpt from Design:

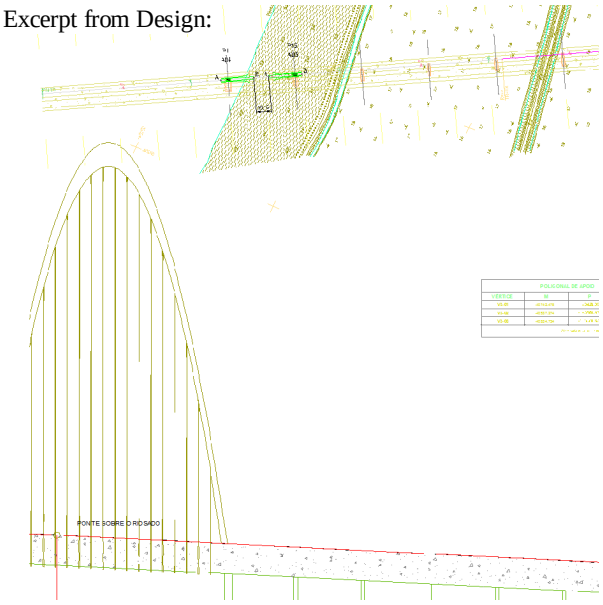

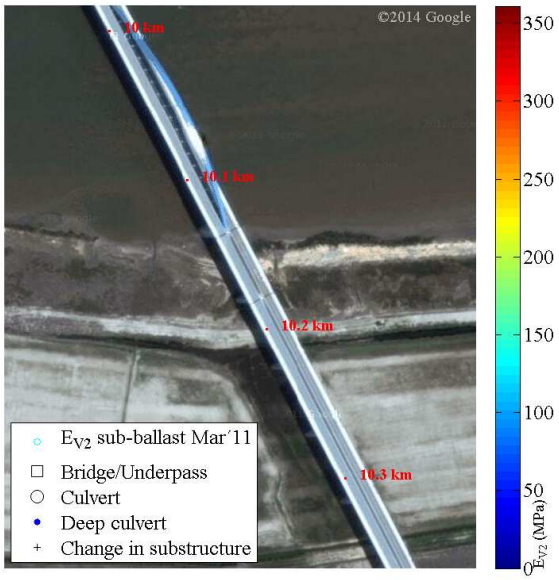

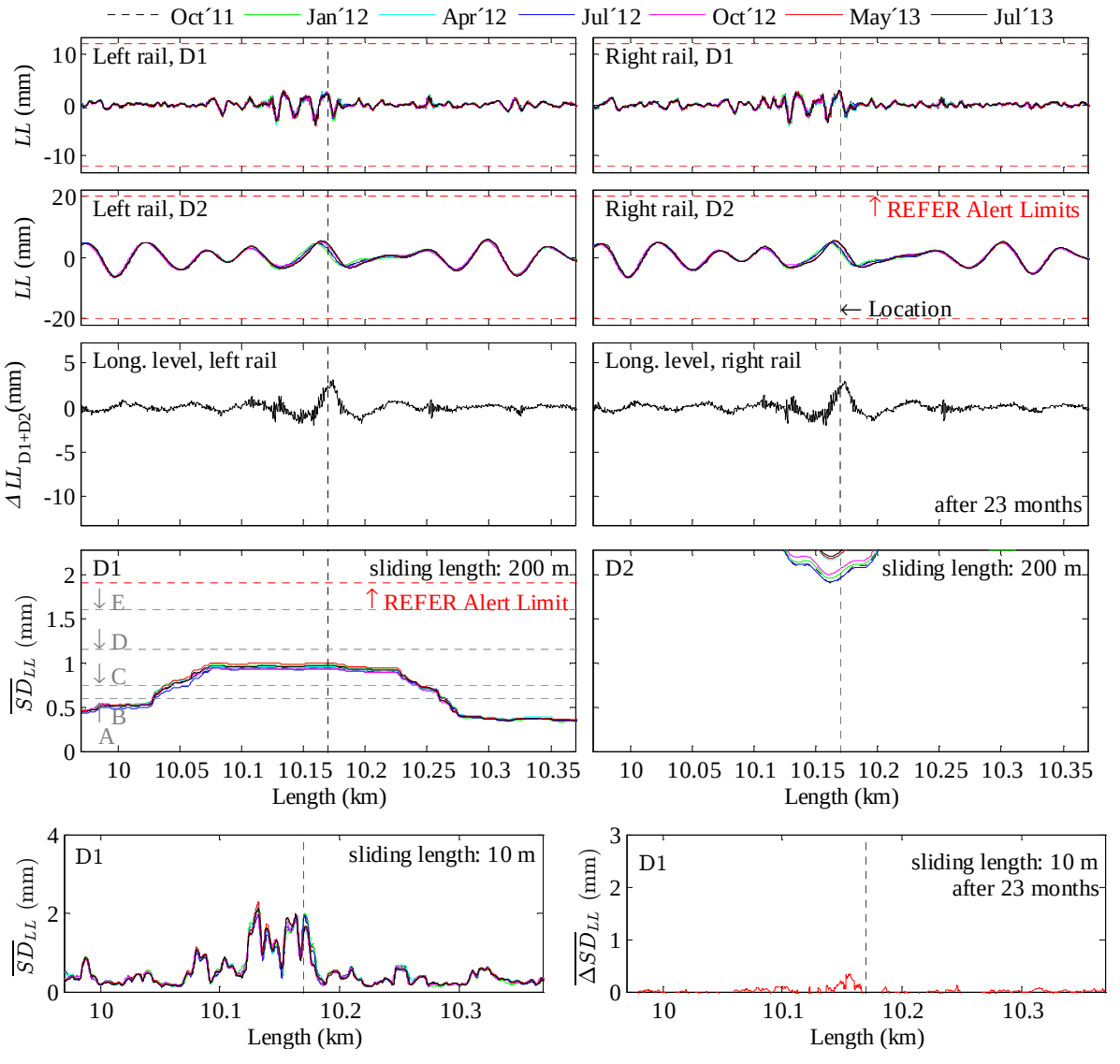

Rail expansion joint at km 10.89 (pier P17S)

Excerpt from Design:

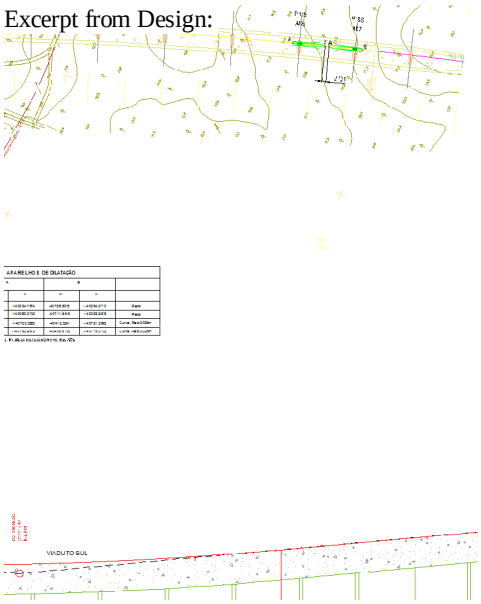

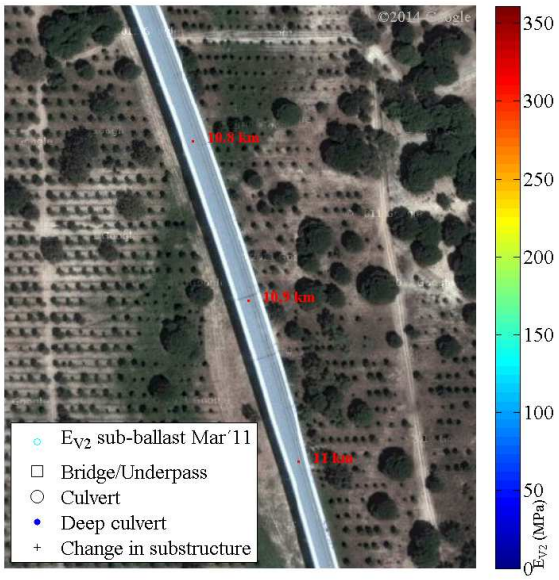

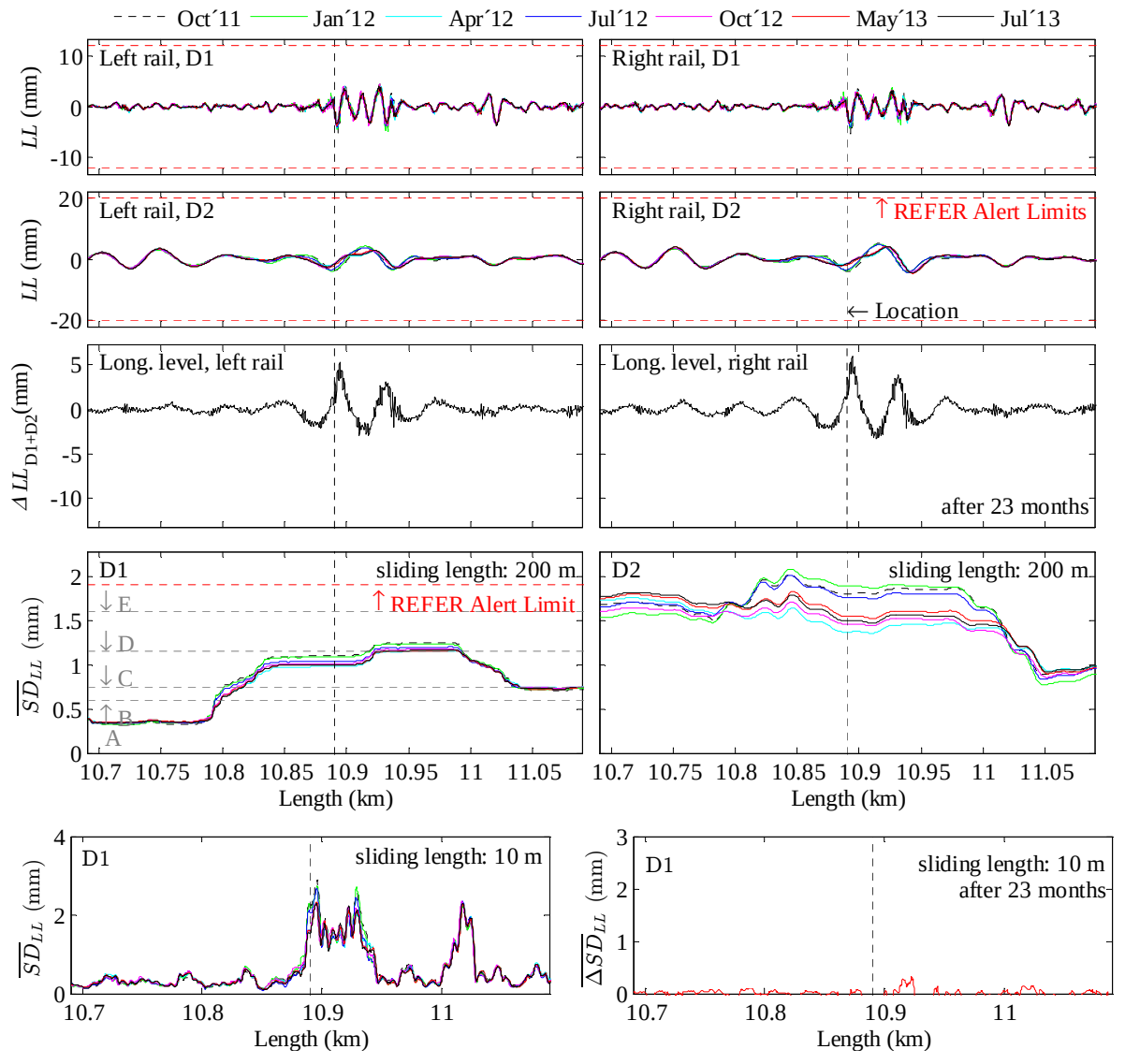

Rail expansion joint at km 10.928 (pier P18S)

Excerpt from Design: